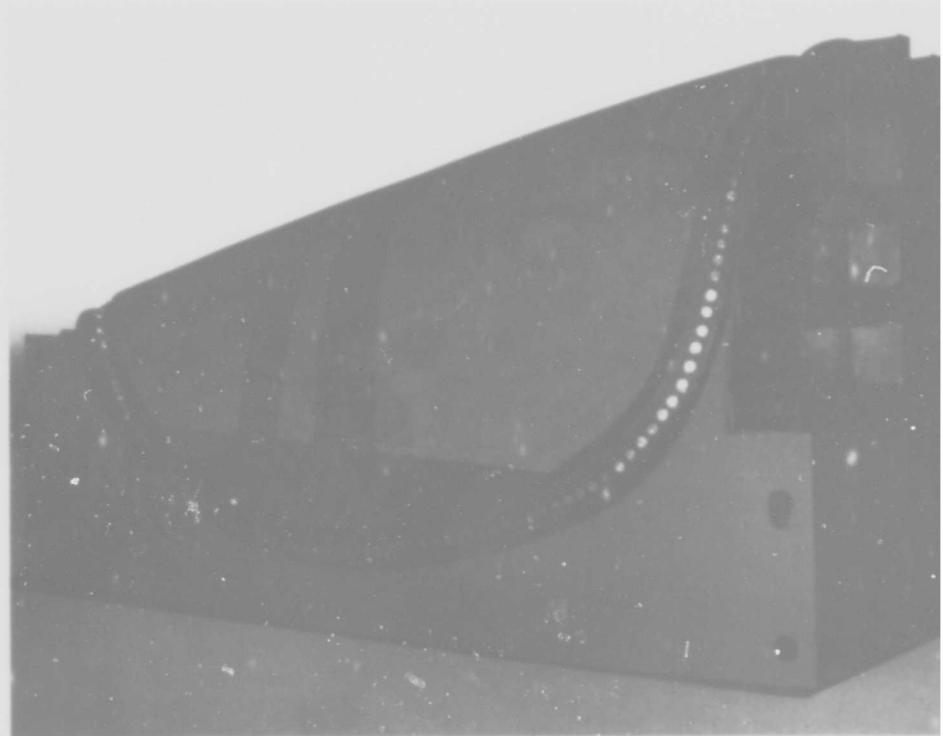




BOW DOME RUBBER ACOUSTIC WINDOW

INTERIM REPORT PHASE I, FEASIBILITY

AD610189



B.F. Goodrich Aerospace and Defense Products
a Division of The B.F. Goodrich Company
Akron, Ohio

COPY	2	00	3	R
HWID			150	
MICROFILM			220	

4548

DDC
RECORDED
JAN 25 1985
RESOLVED
DDC-IRA C

Contract NObnr 89483
Serial No. SS041-001
Task 8156

Report No. 17
Phase I Interim Report
30 September 1964

PRESSURIZED BOW DOME
OF A CABLE-REINFORCED RUBBER CONSTRUCTION
FOR USE WITH AN/SQS-26 SONAR

Interim Report for Phase I
1 March 1963 to 30 April 1964

To
Bureau of Ships
Department of the Navy
Washington, D.C.
Attn: Code 1631

Prepared by W. J. Berus
W. J. Berus
Project Leader

Approved by A. M. LaRue
A. M. LaRue
Manager, ASW

Contract NObsr 89483
Serial No. SS041-001
Task 8156

Report No. 17
Phase I Interim Report
30 September 1964

FOREWORD

This report was prepared by the ASW Engineering Department of the B.F. Goodrich Company under BuShips Contract NObsr 89483. The work was administered under the direction of Code 1631, Bureau of Ships, Washington, D. C.

This report covers work conducted from March 1963 through April 1964 in completing Phase I, Feasibility of the subject contract.

Contract NObser 89483
Serial No. SS041-001
Task 8156

Report No. 17
Phase I Interim Report
30 September 1964

ABSTRACT

This report summarizes studies of the feasibility of a pressurized, cable-reinforced, rubber acoustic window for a Sonar bow dome. The discussion includes theoretical approaches as well as descriptions of the fabrication and testing of samples.

Due to the large size of the rubber acoustic window, tooling is a special problem. This report includes results of the tooling investigation. Several other associated studies were also completed, and the results are presented herein. These include an anti-fouling paint system for the rubber acoustic window, an investigation of methods for transporting the window, and a study of design methods for adapting a universal window to four similar, but not identical, ship's hulls.

It was concluded that a rubber acoustic window is entirely feasible and, in fact, superior to an all-steel dome from the standpoint of acoustical performance.

The prototype window being designed will mate with either the DL-4, DL-5 or DIG-26 ships.

TABLE OF CONTENTS

	<u>Page No.</u>
I. Technical Discussion	
A. Purpose	1
B. General Factual Data	3
1. Introduction	3
2. List of Figures	4
3. List of Tables	7
4. Identification of Personnel	8
5. References	9
C. Detail Factual Data	10
1. Introduction	10
2. Background	10
3. Design Criteria	18
a. Contract Specification	18
b. Design Guidance	20
c. Special Equipment	22
4. Pressurization Requirements	23
a. Design Pressure	23
b. Tension Waves on Acoustic Window Construction	26
c. Effects of Slamming on Pressurized Bow Dome	30
5. General Acoustic Considerations	32
6. Evolution of Heavy Cable-Reinforced Rubber Construction	33
a. Summary	33
b. Introduction	33
c. Design Study	33
d. Conclusions	49

TABLE OF CONTENTS (Continued)

	<u>Page No.</u>
7. Analysis of Weftless Cable-Reinforced Window	50
a. Summary	50
b. Introduction	50
c. Strength Analysis	50
d. Panel Compound Studies	57
e. Acoustical Considerations	67
f. Conclusions	81
8. Acoustic Window Construction Study	83
a. Summary	83
b. Introduction	83
c. Force Distribution in an Acoustic Window	83
d. Ship Attachment	91
e. Testing of Representative Window Section Samples	97
f. Method of Window Assembly	140
g. Conclusions	146
9. Anti-Fouling Paint Study	148
a. Summary	148
b. Introduction	148
c. Discussion	148
d. Conclusions	160
10. Prototype Test Panel	161
a. Summary	161
b. Introduction	161
c. Panel Design	163
d. Tooling	179
e. Panel Fabrication	202
f. Panel Installation in Test Fixture	232
g. Panel Testing Program	234
h. Conclusions	241
11. Universal Window Study	244
a. Summary	244
b. Introduction	244
c. Discussion	244
d. Conclusions	252

TABLE OF CONTENTS (Continued)

	<u>Page No.</u>
12. Prototype Window Design	253
a. Summary	253
b. Introduction	253
c. Design Study	254
d. Conclusions	260
13. Transportation Study	261
14. Ship Modification	265
a. Summary	265
b. Introduction	265
c. Window Attachment	265
d. Pressurization System	265
e. Conclusions	272
D. Conclusions	273
E. Recommendations	274
F. Project Performance Schedule for Next Phase	275
G. Appendices	
I. Plane Wave Normally Incident on a Plane Wall Immersed in a Liquid.	
II. Ring Slot Correction for Pulse Tube	
III. Acoustic Panel Analysis	
IV. Bow Dome Acoustic Window Computer Programs	
V. Stress Calculations on Seaming Section of Panel Mold	
VI. Stress Calculations on Steel Seaming Fixture	
VII. Panel Friction Requirements	
VIII. Mathematical Analysis	
H. Errata/Points of Clarification	

BLANK PAGE

Contract Number 89483
Serial No. SS041-001
Task 8156

Report No. 17
Phase I Interim Report
30 September 1964

I. Technical Discussion

A. Purpose

The purpose of this project is to develop a rubber Bow Dome window having characteristics superior to the present steel domes when used with the AN/SQS-26 sonar. To accomplish this, a three-phase program was established.

Phase I -- Determine the feasibility of design approaches for a pressurized, cable-reinforced, rubber acoustic window. Design, fabricate and test a representative panel.

Phase II -- Design a complete rubber acoustic window for a Bow Dome. Design and procure the necessary tooling.

Phase III -- Fabricate, test and deliver the window.

This Interim Report summarizes Phase I efforts and results. It has been prepared in accordance with MIL-R-978A (Ships) dated 7 December 1960 and Amendment -2 dated 8 March 1962, except that some items, such as formulae, illustrations and measurement procedures are included in the text rather than being grouped in separate sections. This was done for clarity and continuity of presentation.

Present steel Bow Domes have evolved from several previous programs originated by the Bureau of Ships. The use of truss-reinforced steel windows has been dictated by the size and structural requirements, and compromises have been accepted in the acoustical properties. In seeking to improve sonar performance, the B.F. Goodrich Company submitted Proposal 1815-105-163 to BuShips. Therein, it was proposed that a pressurized Bow Dome window of a cable-reinforced, rubber panel construction be considered as a replacement for the steel windows in the Bow Domes for the AN/SQS-26 sonar.

The BFG Proposal was based on experience obtained by producing rubber products for sonar applications since 1938. A series of highly efficient "acoustically transparent" rubber compounds has been developed for these products. In addition, many special research and development programs, some Navy-sponsored but mostly Company funded, have been successfully completed. Since 1944, BFG has been producing "windows" or metal-reinforced rubber panels for use with various sonar systems.

The success of the early rubber windows led to the design and production of steel-reinforced, rubber domes, measuring 60" in length. Design improvements, some of which were conceived and developed by B.F. Goodrich,

have made this a very satisfactory dome and it has been in production as recently as 1963.

The satisfactory characteristics of the steel-reinforced 60" dome (and of other similar B.F. Goodrich rubber products for sonar) led to the award of Contract NObser 72595 for fabrication of a 100" pressurized rubber dome. The 100" dome was, at the outset, to be designed to collapse after the transducer had been retracted into the ship's hull. This concept was introduced to permit the ship to operate in shallow water and to dock without damage to the transducer or dome.

To accomplish this design goal, it was necessary to replace the usual steel trussed and steel-reinforced rubber skin construction by a flexible skin or membrane. A pressurized rubber dome, utilizing geodetically arranged reinforcing cables as shown in Figure 2, was conceived and fabricated. This dome, shown in Figure 3, was installed on the USS Bronson and operated for two years. It was found to be very satisfactory in all respects for which it was originally designed except the requirement that it be collapsible. This requirement was discarded when the retractable transducer did not materialize. During its service life, this 100" pressurized, cable-reinforced, rubber dome was proven superior to steel domes.

With the success of this first pressurized dome as a stimulus, thoughts were turned toward the improvement of larger domes, by utilizing the cable reinforced rubber design. It was on this basis that B.F. Goodrich proposed the use of the cable-reinforced rubber construction for the large Bow Domes. Proposal 1815-105-163 suggested that the window for the Bow Dome be constructed of a number of individual rubber panels which would be assembled during installation on the ship. This BFG Proposal led to the award of this Contract NObser 89483 for the development of a pressurized, cable-reinforced, rubber acoustic window for a sonar Bow Dome.

The advantages of a one-piece window, rather than a panelized arrangement, were recognized and efforts were immediately begun towards determining the feasibility of this concept. In order to minimize the time required to develop a one-piece acoustic window for the sonar Bow Dome, it was determined that the similarity of the operational characteristics to the 100" sonar dome should be exploited. With this basic approach determined, development of the acoustic window was initiated under Contract NObser 89483.

Contract NObsr 89483
Serial No. SS041-001
Task 8156

- 3 -

Report No. 17
Phase I Interim Report
30 September 1964

B. General Factual Data

1. Introduction

This report is prepared and assembled in accordance with the requirements of Military Specification MIL-R-978A (Ships) dated 7 December 1960 and Amendment -2 dated 8 March 1962. However, for the sake of clarity and continuity some items, such as formulae, illustrations and measurement procedures are included in the text, rather than separate sections.

2. List of Figures

	<u>Page No.</u>
Figure 1	15
2	16
3	17
4	24
5	34
6	47
7	48
8	61
9	61
10	63
11	64
12	72
13	74
14	75
15	77
16	79
17	80
18	92
19	94
20	95
21	96
22	100
23	102
24	102
25	103
26	103
27	104
28	106
29	107
30	108
31	110
32	110
33	110
34	111
35	114
36	115

2. List of Figures (Continued)		<u>Page No.</u>
Figure 37	Assembly of 6" Sample Test Equipment	116
38	6" Sample with Monitors Attached	116
39	6" Sample #1 Cross Section	119
40	Stress-Strain Graph of 6" Sample #1 (Strain gauge readings)	124
41	Stress-Strain Graph of 6" Sample #1 (Motion Transducers)	125
42	6" Sample #2 Cross Section	126
43	6" Sample #2 Stress-Strain Curve (Strain Gauges)	130
44	6" Sample #2 Stress-Strain Curve (Motion Transducers)	131
45	6" Sample #3 Cross Section	132
46	6" Sample #3 Stress-Strain Curve (Strain Gauges)	134
47	6" Sample #3 Stress-Strain Curve (Motion Transducers)	135
48	Elastic Stretch of Membrane and Clamp System- Excluding Constructional Stretch	137
49	Membrane Tension vs 1/F (Elastic Stretch Factor)	138
50	Construction Stretch of Membrane and Clamp System	139
51	Dome Segment Concepts	144
52	Pico Abrasion Test Machine	150
53	July 1963 Paint Panel @ 100% Elongation (x30 Mag)	156
54	March 1964 Paint Panel @ 100% Elongation (x30 Mag)	156
55	July 1963 Paint Panel (x30 Mag)	157
56	March 1964 Paint Panel (x30 Mag)	157
57	Anti-Fouling Paint in Direct Light @ x1200 Mag	159
58	Anti-Fouling Paint in Diffused Light @ x1200 Mag	159
59	Prototype Test Panel	162
60	Aft Section Grid Plate Contour Member	165
61	Aft Section Contour Attainment by Warp Membrane	166
62	Aft Section Contour Attainment by Double Wall Construction	167
63	Aft Section Contour Attainment by Rubber Fill	168
64	Aft Section Contour Attainment with Compression Member	169
65	Cross Section of Window Construction	171
66	Radial Frame Determination	172
67	Cross Section of Panel with Compression Member	173
68	Prototype Panel Ply Orientation	176
69	Splice Overlap Construction	178
70	Tooling Flow Program	182
71	Prototype Panel Mold Male Model - Bottom Side	184
72	Prototype Panel Mold Male Model - Top Side	184
73	Rubber Bead Extrusions for use on Model	186
74	Assembly of Prototype Panel Mold	189

2. List of Figures (Continued)		<u>Page No.</u>
Figure 75	Assembly of Prototype Panel Mold with Bead Clamps	189
76	Strong Back Seaming Structure	192
77	Prototype Panel Hydrostatic Test Fixture - Side View	194
78	Prototype Panel Hydrostatic Test Fixture - End View	194
79	BFG Dwg. 47G-27203A - Prototype Section - Hydro Test Fixture	198
80	BFG Dwg. 47G-27240A - Hydrostatic Test Fixture - Clamp Details	199
81	BFG Dwg. 47G-27237A - Hydrostatic Test Fixture - Plate Detail (Sectional)	200
82	BFG Dwg. 47G-27243A - Hydrostatic Test Fix- ture - Clamp Subassembly	201
83	Panel Cross Section - Fill Gum Application	204
84	15° Ply Lay Up and Splice Construction of Prototype Panel	209
85	Bead Wrap Around Operation of Prototype Panel	209
86	Prototype Panel with Vacuum Bag Ready for Cure	211
87	Prototype Panel Thermocouple Locations	212
88	Panel and Mold Separated After Cure	219
89	Restraint of 15° Plies during Splice Fabri- cation	219
90	Bead Cable Weld for Splicing	220
91	Thermocouple Insertion during Panel Splice Assembly	220
92	Strongback in place for Splice Cure Operations	222
93	Splice Curing Operations	222
94	Thermocouple Locations during splice cure	223
95	Bead Tongs for Handling Panel	225
96	Panel in Mold Prior to Removal	226
97	Panel Removed from Mold	226
98	Top of Panel - Exterior Surface	227
99	Bottom of Panel - Exterior Surface	227
100	X-ray Coverage of Panel	229
101	X-ray Positive of Bead Area	230
102	X-ray Positive of Splice Area	231
103	Completed Prototype Panel-80 psi-Bottom Side	233
104	Completed Prototype Panel-80 psi-Top Side	233
105	Typical Radial Frame Cross-Section of Prototype Panel	238
106	Forward Contour Comparison of Domes	249
107	Top View of Dome Model	255
108	Side View of Dome Model	255
109	Comparison of DL-5 and DLG-26 Domes	256
110	Approximate Cross-Section at Frames 16 and 17 Using Existing Attachment Locations	257
111	Approximate Cross-Section at Frames 16 and 17 Using Modified Attachment Locations	258
112	Chock Extensions for Ship Modification	267
113	Schematic of Proposed Pressurization System	271

3. List of Tables

	<u>Page No.</u>
I. Frequency vs % Energy Carried in Water	29
II. Ply Cable Adhesion Tests	52
III. 35003 Neoprene Bonding Adhesion	53
IV. Cable Break Strength After Aging	56
V. Physical Properties of Neoprene - BFG Code 35003	57
VI. Physical Characteristics of Neoprene - BFG Code 35003	57
VII. The Densities and Sound Velocities (PC) of Various RHO-C Compounds	60
VIII. Sample Window Cure Data	65
IX. Wire Cable Adhesion Test Data	66
X. Pulse Tube Reflection Measurements	71
XI. Bead Panel Tensile Test Results	101
XII. 6" Sample #1 Test Cycle	121
XIII. 6" Sample #1 Actual Data Sheet	122
XIV. 6" Sample #1 Test Results on Bead Clamp	123
XV. 5" Sample #2 Test Cycle	127
XVI. 6" Sample #2 Actual Data Sheet	128
XVII. 6" Sample #2 Determined Stress on Bead Clamps	129
XVIII. 6" Sample #3 Test Cycle	133
XIX. Cost Comparison of Dome Fabrication Concepts	145
XX. Modified Pico Abrasion Test Results on Anti- Fouling Paint Sample	151
XXI. Modified Pico Abrasion Test Results on Anti- Fouling Paint Sample Immersed 1 Month in Sea Water	152
XXII. Modified Pico Abrasion Test Results on Anti-Fouling Paint Sample Immersed 6 Months in Sea Water	153
XXIII. Coordinates of Prototype Panel	175
XXIV. Lap Splice Strength	177
XXV. Bead Cable Attachment	179
XXVI. Prototype Panel Mold Costs	181
XXVII. Prototype Panel Cure Cycle	215
XXVIII. Splice Cure Temperature Cycle (°F)	224
XXIX. Panel Test Cycle Record	234
XXX. Prototype Panel Tests - Arc Lengths and Radii	236
XXXI. Prototype Panel Tests - Arc Length Measured Along Radial Frames Between Edges of Gum Fill	237
XXXII. Prototype Panel Tests - Distance From Edge of Bead Seat to Edge of Panel	237
XXXIII. Drawings Utilized in Universal Window Study	245
XXXIV. Cost of Universal Windows	251
XXXV. Coordinates of DL-5 Acoustic Window	260
XXXVI. Railroad Maximum Oversize Shipments	262
XXXVII. Stress Diagram of Window Periphery	268

4. Identification of Personnel

Following is a list of personnel that have and currently are participating in the over-all development program.

<u>Name</u>	<u>Hours Expended</u> ¹
J. C. Barker	2
W. J. Berus	1,492
R. H. Bockbrader	1,376
Dr. E. H. Bollinger	612
J. C. Cacioppo	134
R. S. Colley	1,583
Prof. J. J. Conner	100
L. G. Gatton	37.5
H. Gibitz	27.5
Dr. R. A. Harrington	216
J. C. Hess	165
W. Johnson	123
H. F. Neff	231
R. F. Nichols	52
F. A. Pedigo	1,649.5
S. C. Sabo	296
R. M. Sandusky	1,597
R. L. Sell	735
W. C. Simons	354
R. D. Tubaugh	1,615
P. N. Wiland	1,321.5
R. C. Wise	956
E. C. Wilson	119

¹Hours expended to report date but does not include anticipatory work.

5. References

- a. "Cavitation Characteristics of SQS-26 Sonar Dome for DLG-26 Class Frigate, Model 4858-1(u), Report C-1242-4. David Taylor Model Basin.
- b. Louis A. Becker, "Experimental Determination of Pressure and Strain on the Bow Sonar Dome of USS Barry (DD933)", David Taylor Model Basin Report 1395, July 1960.
- c. Kazuo Ochi, "Model Experiments on the Effect of a Bulbous Bow on Ship Slamming," DTMB Report 1360, Oct. 1960.
- d. Margaret D. Bledsoe, "Experimental Investigation of Slam-Induced Pressures on the AN/SQS-26 Sonar Dome", DTMB Report C-950 (Confidential) Sept. 1958.
- e. L. M. Brekhovskikh, "Waves in Layered Media" Academic Press, London, 1960.
- f. Timoshenko, "Strength of Materials", 3rd Edition, Part II, P. 119.
- g. Macwhyte Wire Rope Co., Catalog G-17.

C. Detail Factual Data

1. Introduction

The efforts described herein were necessary to complete the basic requirement of this program of determining feasibility of the rubber acoustic window concept. To satisfactorily accomplish this assigned task it was necessary to review the origin of pressurized rubber domes. With this background fresh in mind a highly concentrated development effort was expended in analyzing all facets of the present task. This study culminated in the satisfactory fabrication and testing of a full size cable-reinforced prototype panel, and provided the design data required for a one piece Prototype Acoustic Window.

2. Background

In the early period of sonar needs, 1938 through 1955, the operating frequencies were in the high range extending from 20KC up to 107KC's. However, from this time development effort was directed at the creation of progressively lower frequencies, with associated longer wave lengths, resulting in larger and larger transducers and, of course, requiring greater size of domes as streamlined enclosures.

Many complex problems in the sonar system relegated, at that time, the dome to a lesser importance in total development plans. As the sonar gear improved, the dome became of paramount importance since it offered restrictions to optimum acoustical performance. Generally, speaking the domes:

- (a) Created interfering harmonics to sonar signals.
- (b) Generated or transmitted noises.
- (c) Was highly susceptible to corrosion.
- (d) Had inadequate retention of anti-fouling paints.

Analysis of the actual and potential problems with steel domes suggested that the utilization of rubber construction might improve the overall performance of the sonar system.

B.F. Goodrich participation in the field of sonar domes started about 1944 with the Submarine Signal Company. This initial effort consisted of producing "windows" or panels of a metal structure embedded in a wall of rubber. The rubber was a specially compounded rubber to furnish a good acoustic match with sea water. The strength member was a metal framework of round wire rods or

Evolution of the 60" dome continued to keep pace with the changing requirements. The 307 series were essentially CW 177 domes with steel braces on the inside for increased structural strength. Two (2) domes, the 307/U and the 307 A/U were fabricated and upon testing failed in the bow area. With the additional "blow outs" encountered, a complete redesign of the bow section was accomplished. A continuous bow was designed for the upper panels joining them about one-third back. This model was designated CW 307 B/U.

Prior to complete testing of the CW 307 B/U sonar technology made significant strides toward larger transducers, consequently, larger domes. Interest in the 60" dome was diminishing as larger domes came on the scene.

b. 120" Dome

The need for bigger domes was firmly established through the successful development of larger sonar equipment. To satisfy the requirements of larger transducers the B.F. Goodrich, in cooperation with U.S. Navy personnel, designed a punch plate reinforced rubber dome 120" long, 48" high and 25" wide. The design contour of this dome was in accordance with David Taylor Model Basin recommendations and exhibited a length to beam ratio of 5 to 1. The general design principal was similar to the 60" dome without any appreciable internal strength structure. During the initial launch of this dome, free flooding was not accomplished with sufficient speed and the dome collapsed.

Redesign and reinforcement of the dome was accomplished resulting in successful testing and service use.

This dome was produced near and during the period of larger transducers and the final movement to steel domes. As far as B.F. Goodrich participation in the field of sonar domes the education, knowledge and experience gained on the smaller domes paved the way for participation in this contract directed toward development of a pressurized sonar dome.

c. 100" Pressurized Sonar Dome

In 1959 the B.F. Goodrich completed contract NObsr 72595 for the fabrication of a sonar dome. This dome was, at the outset, to be designed so that it would collapse after the transducer had been retracted into the ship's hull. This concept was employed

punch plates. This mesh framework resulted in a construction having interstices on the order of 1-1/2 inches. The intersecting wires were "mash fused" or welded at all cross overs. Additional braces were included for structural strength either in the primary frame as molded or as a post cure, post assembly operation.

a. 60" Dome

The success of the "rubber window" concept prompted Bureau of Ships and B.F. Goodrich to proceed on the design of a rubber 60" dome. The domes, in service at that time, were covered with a .020" stainless steel window. The all steel domes failed prematurely at spot welded attachment points, as did the earlier windows. Through holes approximately 1/8" in diameter were developed which played havoc with the hydrodynamic dome design resulting in severe curtailment of sonar capabilities.

The rubber panel replacement proved vastly superior to the stainless steel, thus extreme interest was generated in a complete 60" dome fabricated of this construction. The 177 A/U dome was the beginning of a full scanning dome and was henceforth referred to as the "NRL 60". During the course of production contracts a design improvement program was omnipresent resulting in improved service life.

The main problem with the initial domes was rupturing at the bow immediately adjacent to the welded seam. Examination of the defective area showed what appeared to be blowouts that ruptured the rubber and severed the grid structure. After intensive investigation it was concluded that fatigue failure of metal under constant vibration and bombardment of sound waves was the primary cause of failure.

During this series of CW 177 domes the combination 347 stainless steel and 310 welding rod non-magnetic dome was developed. This dome, CW 177/c/u, was mounted to the ship about one-third (1/3) aft of the bow and off to one side of the keel. This was a change in the normal practice of on keel mounting. Ultimately, due to the ship's yaw and turning radius, severe forces were exerted against the dome sides, bending them severely.

Design modification included the addition of strong internal bracing and reducing the bending moment by lengthening the skirt. The improved design was designated Model CW 177 D/U and performed without casualties.

as a means of protection and would permit the ship to dock without fear of transducer or dome damage.

In order to accomplish the desired design goal, the usual steel truss and skin construction would be replaced by a flexible membrane. In the specifications of the flexible dome were requirements to improve the following factors:

- (a) Improved range and clearness of sound transmission.
- (b) Reduce self-producing noise.
- (c) Hydrodynamically streamlined.
- (d) Self-cleaning and non-fouling.
- (e) Reduce susceptibility to damage by impact.
- (f) Serve as a prototype to a 300" dome.

In essence, the requirements dictated that the flexible dome act like a rigid body, improving upon the characteristics of the steel domes and remain flexible to the point of being collapsible.

First thoughts concerning suitable constructions turned to reinforced rubber containers rigidized by internal pressurization.

Among the ideas initially pursued were fabric (nylon, cotton, glass and rayon) reinforced rubber. Research showed that acoustically those constructions were undesirable because of high attenuation factors. This phenomenon is explainable when one realizes that air pockets are trapped within the fibers. The amount of air, with the resultant increase in attenuation, cannot be predicted accurately. This variation in acoustic properties coupled with the high and continuous creep factor, in the presence of water vapor, directed the approach toward other more accurate, acceptable and predictable constructions. It should be noted, at this point, that the possibility of a fabric reinforcement should not be discarded completely. However, an extensive research and development effort is required to thoroughly analyze all facets of this approach and determine methods of controlling the variables. Time - being a critical factor in this program it was determined that the project should utilize past experiences and, in this instance, the concept of the cable-reinforcement be adopted for the 100" sonar dome.

The initial plan in this development was to interlace cable throughout the rubber dome, Figure 1, so that loads would be distributed on the cables in a predetermined manner. Geodesic paths for the cables were obtained using a full size wood mock-up, Figure 2. The interstices of this construction were reinforced with weftless wire fabric to minimize pillowing or bulging between the load bearing cables.

The method employed to attach the cables to the boundary bar, which itself attached to the hull of the ship, was through the use of pulleys. The number of cables running to each pulley varied from 1 to 3 depending upon how the dome shape affected the cable layout pattern. Each cable end was wrapped around a pulley, lapped back on itself and locked in place by a crimped sleeve.

Culmination of this study, under contract NObsr 72595, was the successful fabrication and testing of one dome. This dome, shown in Figure 3, was in operation continuously for two years and found to be very satisfactory in all respects for which it was originally designed, except the requirement to be collapsed. This original requirement for a collapsible dome was discarded when the retractable transducer did not materialize. During the service life of this pressurized dome it was proven superior to steel domes.

With the success of the first pressurized dome as a stimulus, thoughts were immediately turned toward developing improved and larger reinforced rubber domes. Utilizing the then current state-of-the-art of pressurized domes as a base line, and as a result of BFG Proposal 1815-105-163, the effort under Contract NObsr 89483 was enthusiastically and vigorously initiated. Realizing the operational characteristics of the sonar bow dome are similar to the 100" sonar dome the basic proposal concept was aimed at pursuing the wire cable-reinforced rubber dome concept and improve upon it. This was in contrast to the alternative of attempting to conduct a research program, of the magnitude indicated by earlier studies, necessary to evaluate other constructions. A major consideration for this decision was the time factor -- the desire by B.F. Goodrich and Bu Ships to obtain an acceptable end product in minimum time. This coupled with the great success of the 100" dome indicated the tried and proven construction should be exploited.

Thus with this decision, and the basic approach determined, upon award of the contract the design and development efforts of a pressurized cable-reinforced rubber acoustic window were initiated.

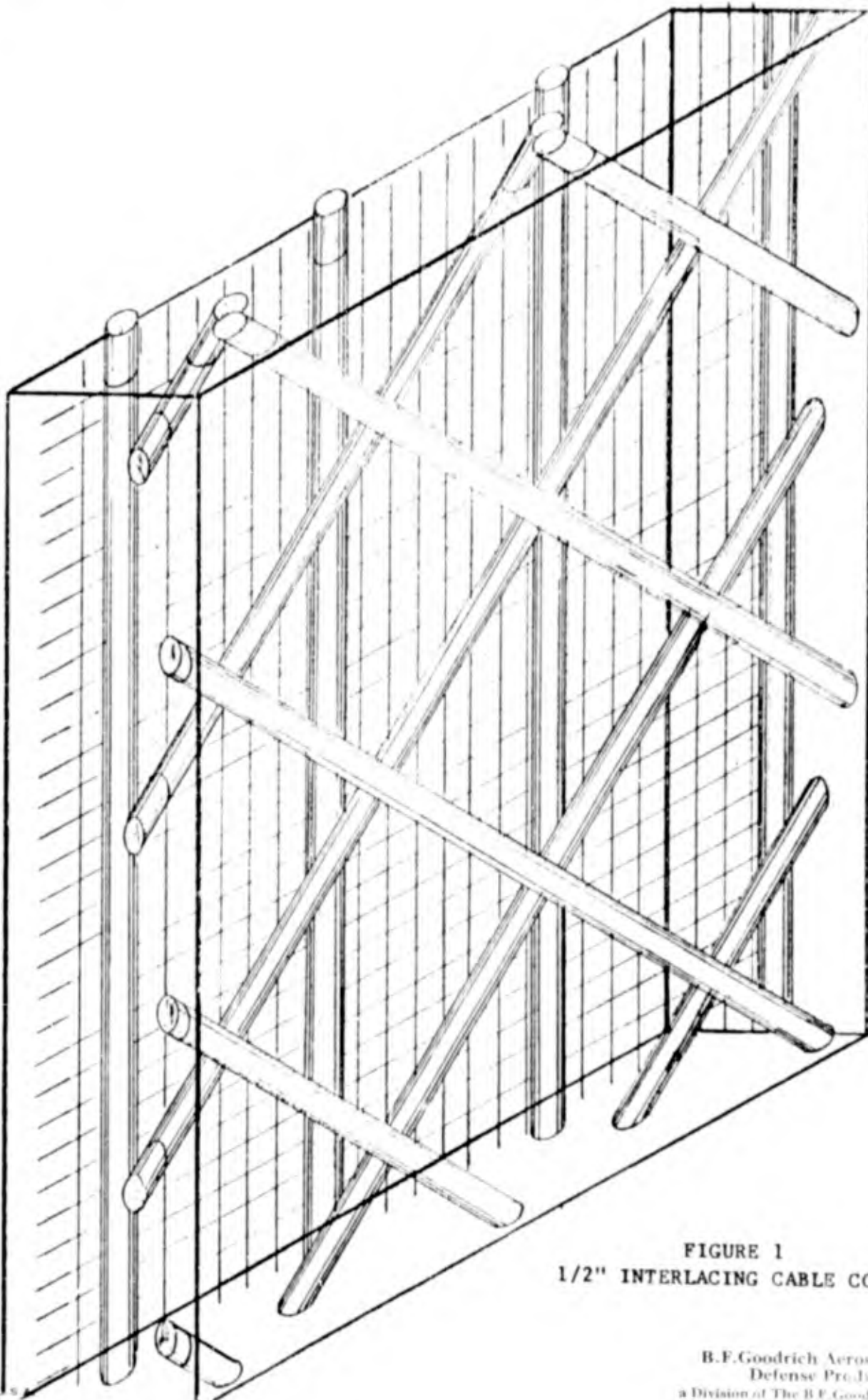


FIGURE 1
1/2" INTERLACING CABLE CONCEPT

B.F. Goodrich Aerospace and
Defense Products
a Division of The B.F. Goodrich Company

Contract NObsr 89483
Serial No. SS041-001
Task 8156

-16-

Report No. 17
Phase I Interim Report
30 September 1964

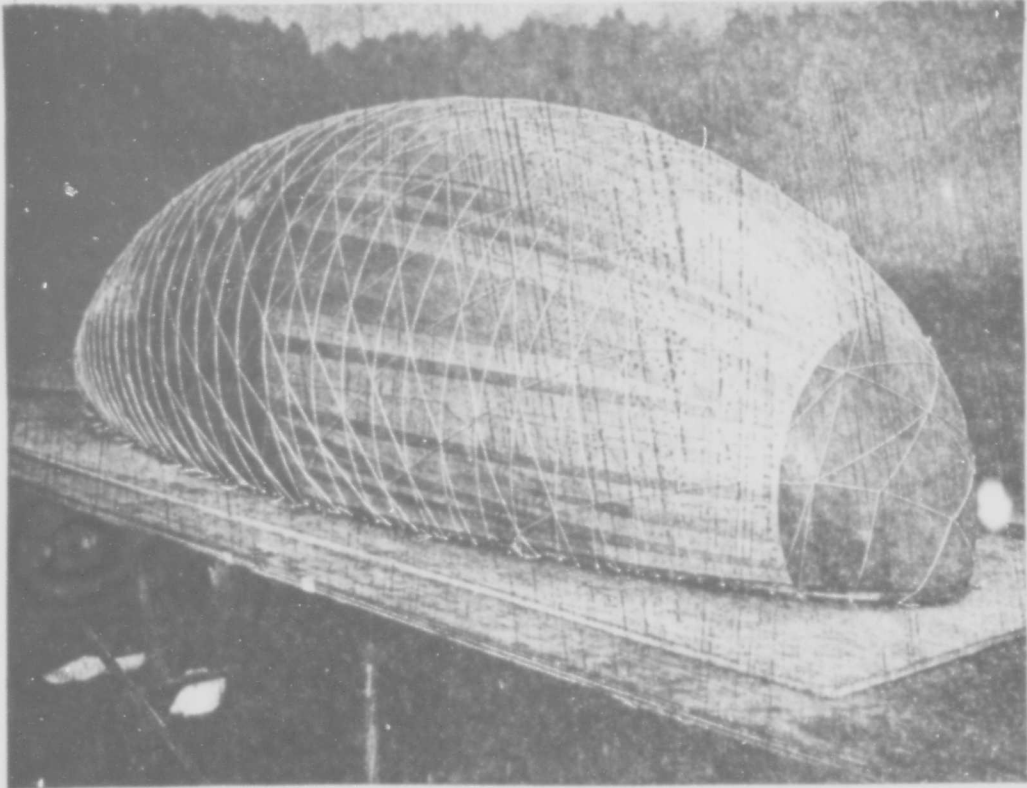


FIGURE 2
GEODESIC CABLE PATTERN, 100" DOME

Contract N0bsr 89483
Serial No. SS041-001
Task 8156

- 17 -

Report No. 17
Phase I Interim Report
30 September 1964

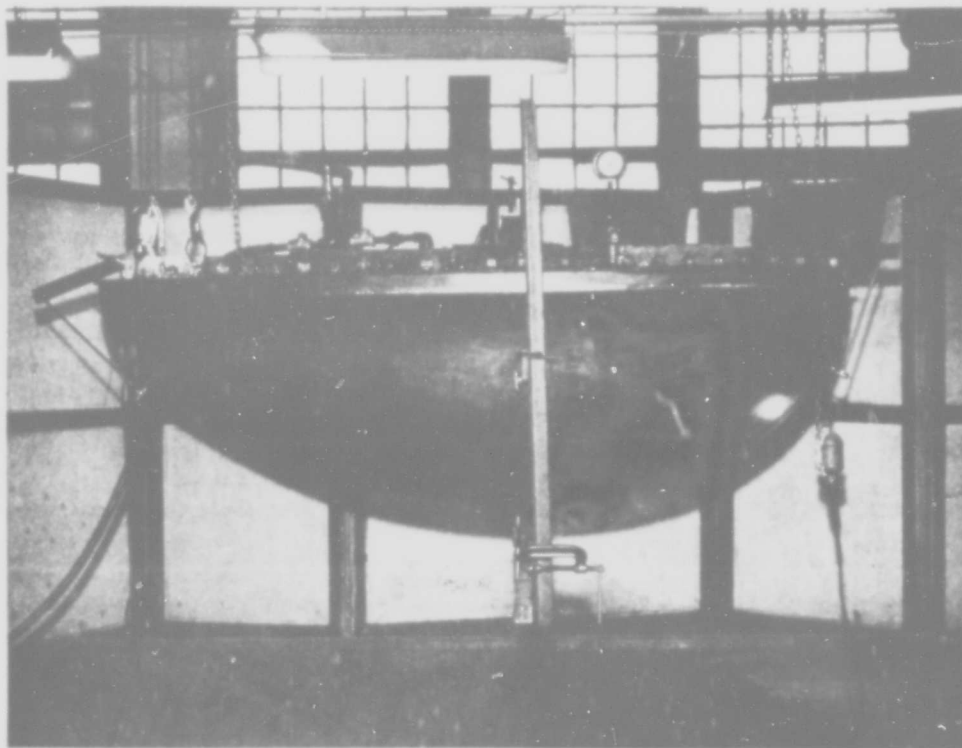


FIGURE 3
100" PRESSURIZED DOME

3. Design Criteria

In accordance with contractual requirements, the B.F. Goodrich Company initiated a research and development program for a "Pressurized Bow Dome of a Cable-Reinforced Rubber Construction for use with AN/SQS-26 Sonar". This program is based on B.F. Goodrich proposal 1815-i05-163 and encompasses guide lines outlined mutually by Bu Ships and B.F. Goodrich personnel.

The ultimate developed acoustic window is intended for eventual use on four ships: DL-5, DLG-26, DE-1040 and DE-1052. Initially, the prototype developed under this contract is to fit the DL-5. However, the desirability of a universal dome is such that additional effort was expended in attempts to make one window fit all ships.

For designing the DL-5 or universal window the following design factors were to be considered.

- a. Ships Speed = 35 knots max.
- b. Ships Yaw = 0°
- c. Sea State = Calm
- d. Ships Draft from (DL-5 = 15 ft.)
0 ft. WL to base (DLG-26 = 19 ft.)
line flat (full (DE-1040 = 14.3 ft.)
load)
- e. Sonar System = AN/SQS-26

Utilizing the aforementioned data, the general approach, listed in the contract, is presented below for reference.

a. Contract Specifications

Program continuity and progress shall be maintained using the following contract specifications:

- 1) Phase I shall include an investigation of the feasibility of providing a one piece acoustic window for the AN/SQS-26 sonar.
- 2) Should 1) above not prove feasible, determine the feasibility of directly attaching the reinforcing cables of each acoustic panel of the dome to the reinforcing cables of the adjacent acoustic panel and eliminate all vertical boundary bars of each panel and all truss support structure at each panel joint.

- 3) Should neither 1) nor 2) above prove feasible, determine the minimum size of truss support structure required at each acoustic panel joint, including elimination of these truss supports.
- 4) Should 1) above not prove feasible, investigate the method of attachment to be used at the joint between acoustic panels, with a view toward assuring improved hydrodynamic characteristics, i.e., eliminate insofar as possible any portions which might present a sharp, exposed edge to the free flow of water.
- 5) Sections aft of E-E of BFG Drawings 5S-1076 and 5S-1077 deviate from those sections taken from existing AN/SQS-26 sonar domes. In addition, a discontinuity exists in this portion of the proposed dome, at the point of attachment between dome and ship's hull. These discrepancies are considered undesirable, and efforts directed toward their elimination or considerable improvement, are required.
- 6) Should design efforts specified in (5) above indicate a solution which may necessitate a slippage in date of completion, the following course of action shall be considered:
 - a) For purposes of the prototype dome only, complete that portion of the dome forward of the vertical joint which exists in current steel domes for AN/SQS-26 (this joint is located approximately at section EE in BFG drawings 5S-1076 and 5S-1077.
 - b) Concurrently, complete the design changes necessary to overcome the objections given in 5) above, and incorporate these changes in the engineering drawings.
- 7) The above referenced proposal provides for acoustic test of sample panels by the contractor, and the furnishing of one sample panel for structural tests by the contractor to be followed by acoustic tests by the government. In addition, the contractor shall provide as a part of Phase I within one month after date of award, one 1-1/2 inch by 5 feet by 5 feet panel or the type rubber ultimately to be used in the prototype dome, painted with two coats of rubber Tie Coat, formula 133 (per Specification MIL-P-22298) followed by two coats of Rubber anti fouling, formula 134 (per specification MIL-P-22299). This panel will be

subjected to high acoustic energy levels at a Navy Laboratory to determine the adhesion characteristics of the paint under these conditions. Results of this and other tests will dictate the paint system to be used on the prototype dome.

- 8) At the earliest possible date the contractor shall furnish the Bureau of Ships with lines and offsets at 2 foot water lines and 2-foot buttock lines, taken at ship's frames (2 foot spacing). These lines and offset shall be furnished only for the acoustic window, or that portion of the dome to be manufactured under Phase III. These lines and offsets will enable the Bureau of Ships to have a model constructed and tested, the results of which will determine the advisability of proceeding with Phase III.
- 9) The contractor shall either confirm the fact that the required hydrostatic pressure within the prototype dome is 50 psig or provide the Bureau of Ships with a new hydrostatic pressure requirement. An analysis of forces assumed and the computations made in determining the required pressure shall be forwarded to the Bureau of Ships at the earliest date possible, but in no case shall it be provided later than two months after date of award.
- 10) The prototype dome shall be constructed in a manner which will allow removal and replacement of the water within the dome while the ship is afloat, without damage to the dome or to the sonar transducer within the dome.
- 11) The design calculations used to determine the method of attachment between the acoustic window and the remainder of the dome shall be forwarded to the Bureau of Ships upon their completion. These shall include the tolerance required by both the contractor and the shipbuilder and shall indicate the method proposed for fairing in any mismatches or interferences.

b. Design Guidance

The following design guidance shall be considered:

- 1) In the design of steel components, a factor of safety of two or more on the yield is desired.

- 2) The use of corrosion resistant steel should be limited to areas which are freely flushed by water, or where moisture is barred completely.
- 3) The following criteria shall be used for determining surface roughness, form and dome fairness:
 - a) Visual Check - Visual checks shall be made during construction to assure that the surface is free from irregularities such as pits, scale and dents. Welds or mechanical fasteners should be finished smooth, and be fair with the adjacent structure.
 - b) Forms -
 - (1) Mold loft offsets specified by the contractor shall be carefully faired, and shall not depart from the Bureau's values by more than $\pm 3/8$ " except with specific approval of the Bureau.
 - (2) The mold loft offsets in the actual construction shall be followed to within $\pm 3/16$ " of those specified by the contractor.
 - (3) An inspection report shall be made to the Bureau, comparing the Bureau's and contractor's mold loft offsets, and also showing construction departures from the contractor's mold loft offsets.
 - c) Smoothness -
 - (1) The overall roughness height rating shall not exceed 125 micro-inches, as defined by MIL-STD-10A. This shall be measured on three waterlines (maximum dome thickness and, as selected by the Bureau of Ships, one typical waterline above that and one below that) and three buttock lines (centerline of dome, and, as selected by the Bureau of Ships, one typical buttock plare port and one starboard.
 - (2) To assure that there is no undue waviness, a batten and feeler gages shall be used. A 36" long-batten (wood, metal, or plastic) shall be used, with stiffness suitable for the curvature of the area being checked. With the batten held tightly against the dome at batten's ends the

fairness shall be such that:

- 1 A feeler $1/16'' + .008''$ thick is excluded over the least 75% of the length.
 - 2 A feeler $1/8'' + .008''$ thick is excluded over the entire length.
- 4) The maximum cross section dimension (a diagonal, in the case of a rectangular cross section) of any metal structure within the acoustic window of the dome other than the reinforcing cables, shall be kept to a minimum consistent with structural requirements. It is desirable that this dimension not exceed 1.7 inches. The diameter of the reinforcing cables within the acoustic window shall not exceed that necessary to support the tensile loads, and in no case shall their diameter exceed 1/2 inch.

c. Special Equipment

Special tools and non-standard fasteners necessary for installation of the prototype dome shall be kept to an absolute minimum. However, should these be necessary, a sufficient quantity of tools and 10 percent excess of fasteners shall be supplied by the contractor with the prototype dome for use by the installing activity.

4. Pressurization Requirements

In order to fully assess the rigors of anticipated environmental conditions the internal pressure requirements within the acoustic window (similar to steel dome shown in Figure 4) must be determined. It is a function of the membrane rigidity and the forces acting on the window. This interrelated effort generates constructional requirements in turn dictating membrane composition.

Shape integrity and oscillatory control of the membrane are of prime importance in assuring a constant acceptable hydrodynamic shape.

a. Design Pressure

Letting all pressures be gauge pressures, with respect to atmospheric pressure, the amount of internal pressurization required is derived as follows:

The external pressure (psi) on the acoustic window because of depth in the water, is:

$$P_w = \frac{d \phi h}{144} = 11.2 \text{ psi}$$

in which d = density of water (62.4 lbs/ft³)

ϕ = specific gravity of sea water (1.03)

h = extreme draft

The maximum external pressure (psi) on the acoustic window due to speed is:

$$P(\text{max}) = \frac{.5 \rho \phi C_p (\text{max}) U^2}{144} = 24.3 \text{ psi}$$

in which ρ = density of water (1.94 slugs/ft³)

ϕ = specific gravity of sea water (1.03)

C_p = pressure coefficient (max = 1)

U = velocity (ft./sec)

Contract NObar 89483
Serial No. SS041-001
Task 8156

- 24 -

Report No. 17
Phase I Interim Report
30 September 1964



FIGURE 4
STEEL BOW DOME

The minimum external pressure (psi) on the acoustic window due to speed is:

$$P(\min) = \frac{.5 \rho C_p(\min) U^2}{144} = -12.4 \text{ psi}$$

in which $C_p(\min) = -.51$

The values of the pressure coefficient, C_p , come from the results of tow tests made at the David Taylor Model Basin¹.

To maintain a rigid structure under actual operational conditions it is recommended that initially an assurance margin of 7 psi be added. This figure is derived from existing (100") dome pressurization requirements where satisfactory service life has resulted. Thus, the required design pressure (psi) becomes:

$$P_D = P_w + P(\max) + 7$$

At a speed of 35 knots, 0° yaw and calm seas, the design pressure for the DL-5 ships, which have an extreme draft of 25 feet, is

$$P_D = P_w + P(\max) + 7 = 11.2 + 24.3 + 7 = 42.5 \text{ psi}$$

And the design pressure for the DLG-26 ships, which have an extreme draft of 29 feet, is

$$P_D = P_w + P(\max) + 7 = 13.0 + 24.3 + 7 = 44.3 \text{ psi}$$

Under rough sea conditions the speed of the ship is reduced to prevent damage. As long as the dome remains under water, the hydrodynamic forces on the dome are actually less than at the highest speeds in calm seas.

In rough seas, the transverse and vertical motion has the effect of changing the aspect angle of the dome, so that the minimum C_p might become $-.85$ instead of $-.51$. However, the forward speed of the ship would be reduced to, at most, 23 knots. This speed must be added vectorially to the speed of heave,

¹"Cavitation Characteristics of SQS-26 Sonar Dome for DLG-26 Class Frigate, Model 4858-1(u), Report C-1242-4", David Taylor Model Basin.

pitch and roll, which might become as great as 10 knots in the roughest sea, to give a maximum instantaneous speed of 25 knots.

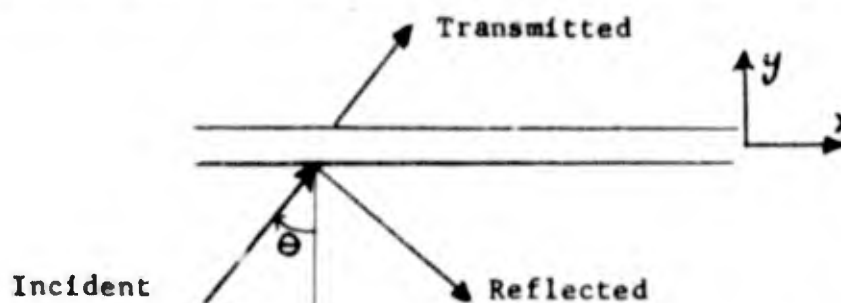
The stagnation pressure (equal to outside pressure) at 25 knots is 12.4 psi, and at $C_p = -.85$, the maximum negative hydrodynamic pressure is -10.5 psi.

Thus these values are less than the similar hydrodynamic pressures at 35 knot speeds in calm seas.

b. Tension Waves on Acoustic Window Construction

The flexural wave velocity on a rubber-wire structure is very small since the bending stiffness of the section is small; however, when tension is applied to such a system, the tension contributes a significant restoring force which gives rise to a relatively high wave velocity on this kind of system. To determine the magnitude of the effect we shall assume that a wave of fixed frequency is traveling along an infinite sheet of material whose mass per unit area (m_a) is equal to that of the bow dome wall, whose tension per unit length (T) is uniform in all directions, whose thickness is negligible since the wave lengths are large compared to thickness, and which is immersed in a fluid with specific impedance Z_0 and sound velocity C .

In analyzing such a system one assumes that a plane wave is incident upon the sheet at an angle θ , referred to the normal, and that this wave gives rise to both a transmitted and a reflected wave. The acoustic pressure and vertical component of



velocity (p and U respectively) are by standard methods.

c. Effects of Slamming on the Pressurized Bow Dome

The external pressures encountered under slamming conditions depend upon many factors, some of them random in nature, which determine the relative speed and angle at which each area element of the dome encounters the water surface. The best estimates of these pressures come from (a) measurements on the USS Barry¹ (b) model studies at DTMB^{2,3}.

Measurements on USS Barry, fitted with a metal bow sonar dome, show maximum measured pressure in a state 6 sea at about 42 psi above atmospheric, at a position on the centerline roughly eight feet forward of the lowest point of the sonar dome. Gauges aft of this position had become inoperative; they might have registered a somewhat greater pressure.

The measurements on models indicate that the maximum slamming pressure in a state 6 sea may be 120 psi (Ref. 2) to 310 psi (Ref. 3). The pressure observed on the models has to be multiplied by the scale factor of the experiment. The model in the Bledsoe report was scaled down by the factor 18.45, thus the 17 psi maximum observed pressure on the model corresponds to 17×18.45 or 310 psi.

It must be borne in mind that in the model studies the waves are probably much more regular than at sea and a wider range of speeds and angles can be tried; both factors tending to make the observed pressures high. Also in the model studies, the models tend to be more rigid than the full-scale ship. With the very non-rigid pressurized dome, we would expect the dome and its contained water to have almost exactly the same compliance as the surface of a wave, therefore, the maximum pressure at impact would be half what would be obtained with a rigid dome.

¹Louis A. Becker, "Experimental Determination of Pressure and Strain on the Bow Sonar Dome of USS Barry (DD933)", David Taylor Model Basin Report 1395, July 1960.

²Kazuo Ochi, "Model Experiments on the Effect of a Bulbous Bow on Ship Slamming", DTMB Report 1360, Oct. 1960.

³Margaret D. Bledsoe, "Experimental Investigation of Slam-Induced Pressures on the AN/SQS-26 Sonar Dome", DTMB Report C-950 (confidential) Sept. 1958.

$$K = \frac{Z_0}{\omega m a} (\omega \cos \theta) \frac{c_0 \sin \theta}{c \cos^2 \theta}$$

which reduces to

$$K = \frac{PD}{\omega m a} \left(\frac{\rho}{c} \right)^2 \left[\left(\frac{\rho}{\rho_0} \right)^2 - 1 \right]^{3/2}$$

Using the data previously determined, the ratio K and the percentage of energy carried by the water may be calculated as a function of frequency.

These values are listed in Table I.

Table I
Frequency vs % Energy Carried in Water

<u>Frequency</u> <u>cy/sec</u>	<u>K</u> <u>-</u>	<u>% Energy</u> <u>in Water</u>	<u>Velocity (c)</u> <u>m/sec</u>
.147	232.0	99.	7.5
1.47	50.0	98.	16.2
14.7	10.6	91.	35.5
147.	2.16	68.	72.
1470.	.375	27.	123.

At the very low frequencies one is concerned about standing waves which would lead to surface irregularity. However, since most of the energy is carried in the water, a high percentage will be radiated upon reflection from any boundary. Under these conditions one would not expect standing waves to be a problem.

At high frequencies, the shear damping in the rubber-steel matrix will be sufficient to prevent the formation of standing wave systems.

Thus, a wave of high frequency, set up by a local water disturbance, will lose energy rapidly through shear losses in rubber, while a low frequency wave will lose energy rapidly through reflection at dome boundaries. These energy losses will prevent the development of transverse waves of more than about 0.2" amplitude.

so that the velocity of free waves on the wall immersed in water is given in terms of known constants relative to D , the velocity of free waves in the wall when no medium is present.

The nominal tension in the bow dome wall under pressure is about 3,000 pounds/inch and the mass per unit area is 2.0 gm/cm^2 . Thus, $D \approx 162 \text{ meters/sec}$. Since the velocity of sound in water is $C = 1500 \text{ m/s}$, then the equation (4) can be written approximately as

$$\left[\left(\frac{D}{C}\right)^2 - 1\right] \frac{D}{C} \approx \frac{2PD}{Wm_A} \quad (5)$$

and it is immediately apparent that as $W \rightarrow \infty$ $C \rightarrow D$ so that at very high frequencies the velocity of free waves approaches that of the free wall, while as $W \rightarrow 0$ $C \rightarrow D \left[\frac{Wm_A}{2PD} \right]^{1/2}$ and the velocity approaches zero.

It is thus apparent that no energy can be radiated from the wall into the water since $C < C_0$ indicating that free waves occur only beyond the critical angle and total internal reflection must result. Thus, energy can only be transmitted along the wall. Effectively, a channel can be defined which runs parallel to the wall and the total energy transmitted is contained in this channel. Equation (4) can be interpreted to mean that the mass per unit area of the wall is increased by the mass of water contained in a channel about one wave-length wide, so that the velocity of waves is reduced by the increased mass loading and the energy is propagated primarily through the water.

The ratio of energy carried in the water to that carried by the wall may be easily calculated. Since the velocity amplitude on the wall is v and the wave is transverse, the average energy transmitted per unit width is

$$\Pi_0 = m_A \frac{v^2}{2} C$$

while that transmitted by water is

$$\Pi_w = 2 \int_0^{\infty} (P_r v_x) dy$$

where $(P_r v_x)$ is the product of the real parts of the transmitted pressure and x component of velocity. Performing the operations one assures at the ratio $K = \frac{\Pi_w}{\Pi_0}$

In the Bledsoe report¹, the 17 psi slamming pressure fell off to about 6 psi in .0007 sec. This length of time must be multiplied by the square root of the scale factor for interpretation to what would happen at full scale. Thus the pressure at a point on the full scale dome would fall from 310 psi to 120 psi in .003 sec.

This is because the severest high-pressure area would sweep forward at the rate of about 700 ft. per second (calculated from the Bledsoe report).

The pressure at any point on the dome window would be at most 160 psi and pressure this high would persist only .003 seconds. Because the local inside pressure for such rapidly applied loading will almost match the outside pressure, no damage to the pressurized dome window or its supports will result.

The disturbances due to slamming will be transmitted through the water inside the dome and will reach the transducer. Because of the narrowness of the high-pressure band on the outside (the region in which the pressure is greater than 60 psi as calculated from Ref. 1 is 2 ft. wide), the maximum pressure on the transducer will be about 30 psi.

¹Margaret D. Bledsoe, "Experimental Investigation of Slam-Induced Pressures on the AN/SQS-26 Sonar Dome", DTMB Report C-950 (confidential) Sept. 1958.

$$\begin{aligned}
 P_I &= P_I e^{j\omega(t - x \frac{\sin \theta}{c_0} - y \frac{\cos \theta}{c_0})} \\
 v_I &= \frac{\cos \theta}{Z_0} P_I \\
 P_R &= P_R e^{j\omega(t - x \frac{\sin \theta}{c_0} + y \frac{\cos \theta}{c_0})} \\
 v_R &= - \frac{\cos \theta}{Z_0} P_R \\
 P_T &= P_T e^{j\omega(t - x \frac{\sin \theta}{c_0} - y \frac{\cos \theta}{c_0})} \\
 v_T &= \frac{\cos \theta}{Z_0} P_T
 \end{aligned} \tag{1}$$

Examining a small area of the wall one finds that a differential equation may be written for the force equilibrium on the section:

$$\frac{T}{j\omega} \frac{\partial^2 v}{\partial x^2} + P_I + P_R - P_T = m_a \dot{v} \tag{2}$$

where v is the vertical component of velocity on the wall. From continuity conditions the vertical components of velocity in the medium must equal that of the wall at $y=0$ so that

$$v_I + v_R = v_T = v$$

Using these conditions and the equation for v

$$v = v_0 e^{j\omega(t - \frac{x}{c})}$$

where v_0 is an arbitrary velocity amplitude and c the wave velocity on the wall, one arrives at the equation.

$$\frac{D^2}{C^2} - 1 = \frac{2Z_0}{j\omega m_a \cos \theta} \tag{3}$$

for C in terms of the known parameters of the system, $D^2 = T/m_a$ by definition and $\cos \theta = j\sqrt{C^2 - 1}$ by application of Snell's Law.

Upon rearranging one finds

$$\left[\left(\frac{D}{C} \right)^2 - 1 \right] \left[\left(\frac{D}{C} \right)^2 - \left(\frac{D}{C_0} \right)^2 \right] = \frac{2PD}{\omega m_a} \tag{4}$$

Contract NObser 89483
Serial No. SS041-001
Task 8156

- 32 -

Report No. 17
Phase I Interim Report
30 September 1964

5. General Acoustic Considerations

The primary acoustic consideration is to impart no interference to transducer performance. The basic design of the cable-reinforced rubber window eliminates many undesirable characteristics found in steel dome, i.e. vibration, flow noise and reflectivity. Therefore, the main consideration is to obtain a window construction with minimum attenuation characteristics. Specific discussion of acoustic requirements will be discussed as they apply during this report.

6. Evolution of Cable-Reinforced Rubber Construction

a. Summary

The concept of a 1/2" steel cable - neoprene coated weftless wire fabric combination for a pressurized acoustic window is acceptable from a strength and acoustic standpoint. However, the use of steel boundary bars to segment the construction is undesirable because of acoustic interference, weight and contour fairing requirements. Means of splicing the adjacent panels without steel boundary bars leads to the use of massive, cumbersome connectors which are also undesirable. Therefore, it was determined other constructions should be analyzed for this application.

b. Introduction

The first considered design, as discussed briefly in the proposal, entails the use of vertical and horizontal steel boundary bars. The bars create a series of windows, Figure 5, composed of 1/2" steel cables and neoprene coated weftless wire fabric. This design eliminates all the steel truss work except at the attachment points. The boundary bar technique considered here was similar to the 100" dome concept which had already proven itself. However, things to consider are (1) degree of precision required in the ply cable lengths, (2) effect on acoustic performance, and (3) required fairing at attachment points.

In addition to the steel boundary bar concept the idea of splicing adjacent panels into a one piece window was also to be investigated. This concept, of a continuous window, is desired and mentioned in the contract.

Studies were to be taken to verify the acceptability of this concept and included (1) contour attainment, (2) strength requirements, (3) acoustical considerations and (4) cable splicing methods.

c. Design Study

Knowledge from studies made of panel reinforcing cables with regard to size, weight, strength, material and cost revealed that one family of cables laid "radially" (running vertically from boundary bar to boundary bar) would be more efficient, with less weight, cost and labor, than three families of cables laid at a crossing angle.

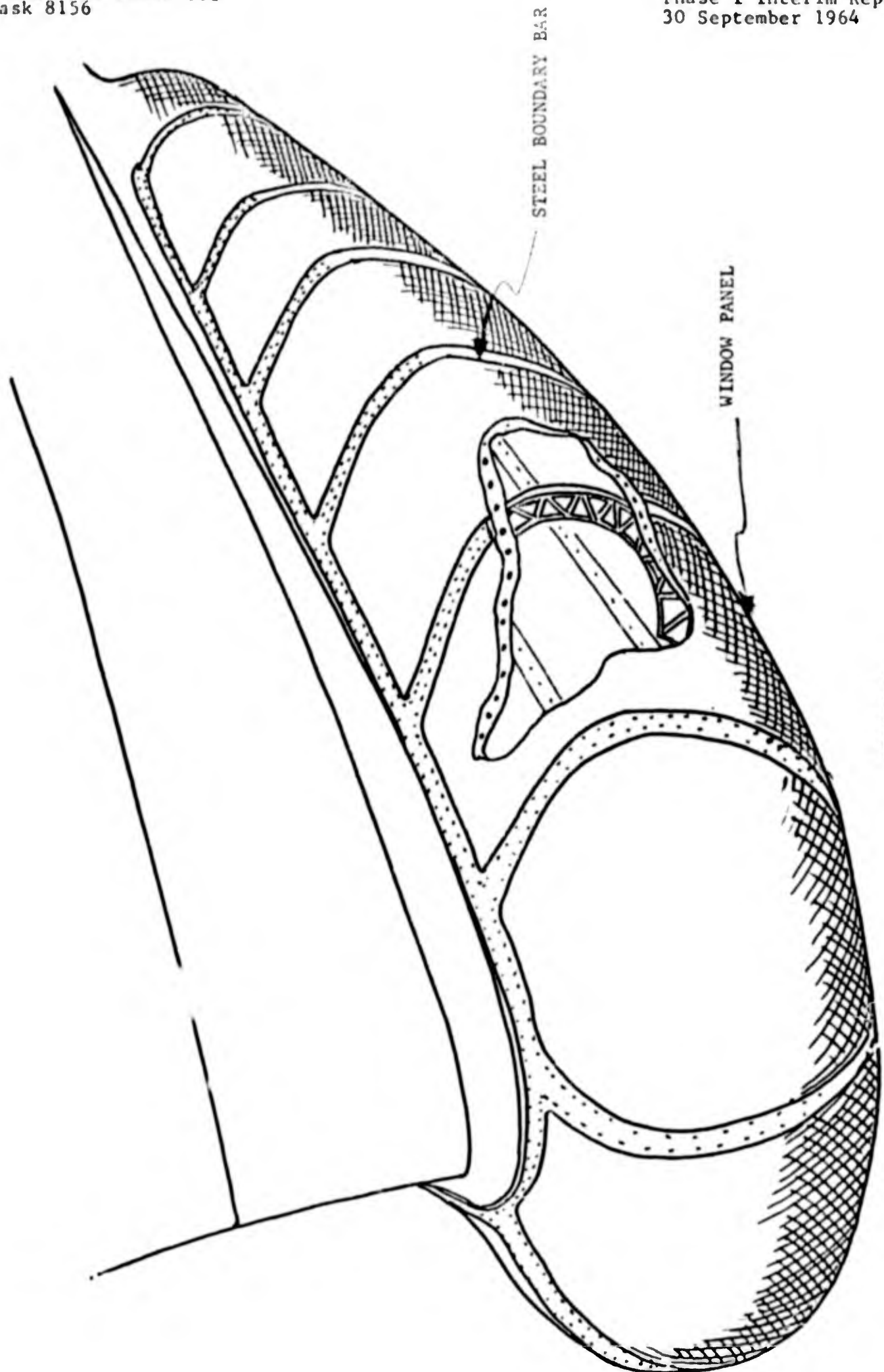


FIGURE 5

STEEL BOUNDARY BAR - WINDOW PANEL CONCEPT

1) Determination of Pillowing

With this concept of a family of spaced cables comes the problem of pillowing or bulging between cables.

Two factors are involved in the determination of the amount of pillowing between the 1/2" diameter load carrying cables. The weightless fabric which bridges the 1/2" cables and the thickness of the window between the 1/2" cables resisting stretching due to pressure. Let us consider first the amount of pillowing if only the weightless fabric is present.

In the following derivations let:

e = elastic stretch (in)

T_C = tensile load on cables in weightless fabric (lb.)

D = nominal diameter of cables in weightless fabric (in.)

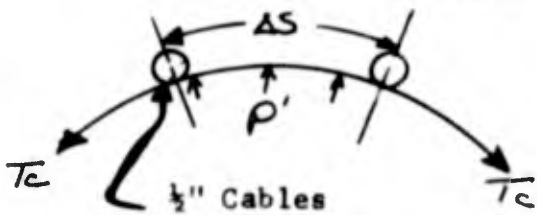
$F' = \frac{D^2}{AE}$, where A is the cross-sectional area of cables and E is its modulus of elasticity F' is a factor of elasticity and varies according to grade and construction of cable.

P = pressure load (psi)

H = pillowing between reinforcing cables caused by pressure (in.)

N = number of cables per inch in weightless fabric

n = number of plies of weightless fabric



$$P' = \frac{P \text{ lb./in.}^2}{N \text{ cables/in.}}$$

$$T_R = P' \Delta S$$

$$T_R = 2 T_C \sin 1/2 \theta$$

$$\text{For small } \theta: \sin 1/2 \theta = 1/2 \theta$$

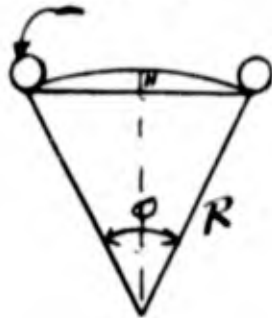
$$P' \Delta S = 2 T_C 1/2 \theta$$

$$S = R \theta$$

$$P' R \theta = T_C \theta$$

$$T_C = P' R$$

1/2" Cables



Thus we have:

$$(1) T_c = P'R = \frac{PR}{nN} \quad (\text{lbs.})$$

$$(2) R \sin 1/2 \theta = 1/2 C$$

The elongation of the chord, C, under tension is

$$e = S-C = R\theta - C$$

According to Macwhyte's formula:

$$e = \frac{T_c C}{D^2} \quad F'$$

(3) Thus:

$$e = R\theta - C = \frac{T_c C}{D^2} \quad F'$$

For small θ , a good approximation of $\sin 1/2 \theta$ is:

$$\sin 1/2 \theta = \frac{\theta}{2} - \frac{\theta^3}{48}$$

Substitute this in (2)

$$R \left(\frac{\theta}{2} - \frac{\theta^3}{48} \right) = 1/2 C$$

$$\frac{R\theta}{2} - \frac{R\theta^3}{48} = \frac{C}{2}$$

$$R\theta - C = \frac{R\theta^3}{24}$$

Substitute this in (3)

$$\frac{R\theta^3}{24} = \frac{T_c C}{D^2} \quad F'$$

which (when using the value of T_c from (1) can be written

$$\frac{R\theta^3}{24} = \frac{PRCF'}{nND^2}$$

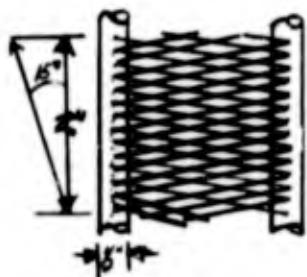
Solve for θ :

$$(4) \quad \theta = \left(\frac{24 PCF'}{ND^2} \right)^{1/3}$$

Find R from (2) using (4) when the amount of pillowing is determined by

$$(5) \quad H = R \pm \sqrt{R^2 - C^2/4}$$

As an example let us consider two (2) plies of weftless wire fabric as pictured and determined degree of pillowing under 50 psi pressure.



Let $F' = 1.2 \times 10^{-7}$ and from equation (4),

$$\theta = \left[\frac{(24)(50) \left(\frac{2}{\cos 15^\circ} \right) (1.2 \times 10^{-7})}{(2)(7 \cos 15^\circ) (.048)^2} \right]^{1/3} = .2124 \text{ rad.}$$

Using equation (2),

$$R = \frac{(1/2) \left(\frac{2}{\cos 15^\circ} \right)}{\sin \frac{.2124}{2}} = 9.7689$$

The pillowing therefore is:

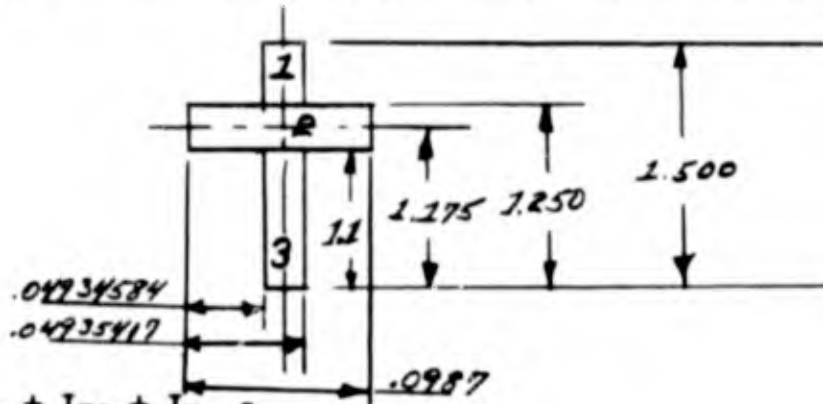
$$H = 9.7689 - \sqrt{9.7689^2 - \frac{2.071^2}{4}} = .055$$

It may be concluded that two (2) plies of weftless wire fabric so oriented are not sufficient to prevent pillowing. Let us now look at the effect of the entire 1-1/2" thick membrane including 1/2" cables in resistance to pillowing.

The method of study in this case is based on that used to study beams made up of two (2) materials -- "equivalent area method".

The neutral axis of the cross section is at the center of the wire fabric.

The moment of inertia of the area about the neutral axis is:



$$I_x = I_{x_1} + I_{x_2} + I_{x_3} = 3.24 \times 10^{-5}$$

$$\text{Section Modulus } Z = \frac{I}{C} = \frac{3.24 \times 10^{-5}}{1.175} = 2.76 \times 10^{-5}$$

Thus maximum stress is:

$$\text{Equation of Shear } V = -50X + 50$$

$$\text{Max. } V = 50 \text{ lb./in.}^2 \text{ where } X = 0$$

$$\text{Equation of Moment } M = -25X^2 + 50X + C$$

$$\text{When } X = 0, M = 0, C = 0$$

$$\text{Max. } M = 25 \text{ ft. lbs. where } X = 1$$

$$\text{Max. Stress} = \frac{\text{Max. } M}{Z}$$

$$\text{Max. } S = \frac{25}{2.76 \times 10^{-5}} = 9.06 \times 10^5 \text{ lbs/in.}^2$$

Deflection or Pillowing at $X = 1$ " where $X =$ distance between 1/2" cables:

$$y = \int \frac{Mm}{EI} dx \text{ where } M = -25X^2 + 50X$$

$$E = 30 \times 10^6 \text{ lbs./in.}^2$$

$$I = 3.24 \times 10^{-5}$$

$$m = \text{eq. of bending moment due to 1 lb. load acting vertically at } X = 1".$$

Equation of shear:

$$V = .5, 0 < X < 1$$

$$V = -.5, 1 < X < 2$$

Equation of moment:

$$M = .5X + C_1, \text{ When } X = 0, M = 0, \text{ therefore } C_1 = 0$$

$$M = -.5X + C_2, \text{ When } X = 1, M = .5, \text{ therefore } C_2 = 1$$

Therefore:

$$M = .5X, 0 < X < 1$$

$$M = -.5X + 1, 1 < X < 2$$

$$EI = (30 \times 10^6) (3.24 \times 10^{-5}) = 972$$

$$y = \int_0^1 \frac{(-25X^2 + 50X) (.5X)}{972} dx + \int_1^2 \frac{(-25X^2 + 50X) (-.5X + 1)}{972} dx$$

$$= .0107''$$

The calculated results indicate that pillowing is resisted mainly by the thickness of the window and should not be serious.

Verification of the above by empirical means was not attempted because of the change in window design which eliminated the 1/2" cables.

2) Analysis of Constructional Strength

With few load carrying cables the resultant size and strength of the members must furnish the required strength. Having only one (1) family of cables running vertically to support the loads the equation of equilibrium becomes:

$$P = \frac{T}{R}$$

Where P = Internal Pressure, psi

T = Tension in cable, lbs.

R = Radius of curvature, inches

Specifications call for a factor of safety of 2 or more on the yield of steel components be maintained in all phases of the Bow Dome construction. To maintain shape integrity it is necessary that the loads on the cables do not exceed the cable elastic limit. The elastic limit of wire cable is 55% to 65% of its yield strength. Thus, if the design of the bow dome construction is such that a minimum safety factor of 2 is maintained, then no cable will be loaded beyond its elastic limit.

During that period of the feasibility study when one family of load carrying cables was under evaluation, it was determined that the expected pressure differential would require an internal dome pressure of 50 psi. Also, the largest load carrying cable radius would be about 120". Thus, the force per inch of boundary bar would be:

$$T = PR = (50 \text{ psi}) (120 \text{ inches}) = 6000 \text{ lbs/in}$$

The size and spacing of cables, to satisfy the above conditions, together with consideration for fabrication techniques indicates 1/2 inch diameter "7 flex" cables spaced on 2 inch centers are required. This cable is rated at 26,200 lbs. strength which is satisfactory (safety factor of 2.15), considering the potential 12,000 lb. load.

3) Acoustical Considerations of Cable-Reinforced Rubber Construction

The effects of scattering and diffraction from a series of equally spaced rigid cylinders in a plane wave have been calculated. This system is analogous to the large diameter cable construction originally proposed for the acoustic window. With one half (1/2) inch cables spaced on two (2) inch centers, the transmission loss was calculated in the following paragraphs to be less than 0.1 db at angles of incidence up to eighty degrees. Also, no diffraction images are formed since the cable spacing is much less than a wave length and, thus, the phase difference between the scattered waves from successive cables is less than 2π radians at all angles of incidence.

The structure of the acoustic window membrane, as originally conceived, consisted of one half (1/2) inch diameter steel cables on two (2) inch centers for support of the high

tensions in the wall. To determine the acoustic effects of such a series of cables, imbedded in a rubber matrix, several reasonable approximations must be made to idealize the system to one for which analytic solutions exist. Since the cables are to be imbedded in a Rho-C rubber, whose acoustic characteristics are similar to water, one can reasonably assume that the cables act as if immersed in a continuous water medium. The solution to the problem of a plane wave incident upon a single rigid cylinder immersed in a infinite medium is given in the literature¹ thus the pressure distribution in the scattered wave at a distance r from the cylinder is:

$$P_s = \sqrt{\frac{4Z_0 a e}{\mu r}} e^{ik(r-ct)} \sum_{m=0}^{\infty} \epsilon_m \sin \delta_m e^{i\sigma_m \cos \theta}$$

- where P_s = acoustic pressure of scattered wave
 Z = specific impedance of medium
 a = radius of cylinder
 μ = $w a/c$ = phase radius of cylinder
 c = sound velocity in medium
 k = w/c = phase constant
 θ = scattering angle with respect to direction of incident wave
 ϵ_m, δ_m = are associated with the eigen function for this solution
 P_0 = intensity of incident plane wave

In our particular case, the radius of the cylinder is very small compared to a wave length so that,

$$\mu \ll 10, \delta_0 \approx -\delta_1 \approx \pi \mu^2/4; \delta_m = 0 \quad (m \geq 2),$$

and $\epsilon_0 = 1.0, \epsilon_m = 2.0 \quad (m \geq 1).$

¹"Vibration & Sound" by Philip Morse, McGraw-Hill Book Co., 1948.

Thus:

$$P \rightarrow \frac{\pi \mu^2}{4} \sqrt{\frac{4 \pi \gamma_0 a}{\pi \mu r}} e^{ik(r-a)} (1-2 \cos \theta)$$

and the intensity scattered in a given direction is:

$$\gamma_s = \frac{P_s^2}{2Z} = \frac{\pi a}{8\mu} \mu^3 \gamma_0 (1-2 \cos \theta)^2$$

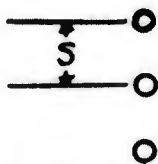
The total energy scattered in the forward direction is:

$$E_F = \int_{-\pi/2}^{\pi/2} \gamma_s r d\theta = (3\pi - 8)\pi \frac{\mu^3}{8} \gamma_0$$

and that scattered in the backward direction is:

$$E_B = \int_{\pi/2}^{3\pi/2} \gamma_s r d\theta = (3\pi + 8)\left(\frac{\pi \mu^3}{8}\right) \gamma_0$$

These apply to a single cylinder. Now let us assume that a line of these cylinders are equally spaced a distance S apart.



Then, due to symmetry, we can say that for each band of width S, there is a total incident energy $E_I = \gamma_0 S$ on a cylinder. Assuming that this represents an infinitely long line, the scattered energy for each band is E_F and E_B as previously defined. In the far field, these scattered waves must add up algebraically to produce a plane wave in both the forward and backward directions, such that the phase of the forward scattered wave reduces the energy in the plane wave to compensate for the reflected energy. Thus E_B/S is the intensity of the reflected wave and γ_0 is the intensity of the incident wave so that the transmitted wave must have an intensity

$$T = \gamma_0 - E_B/S$$

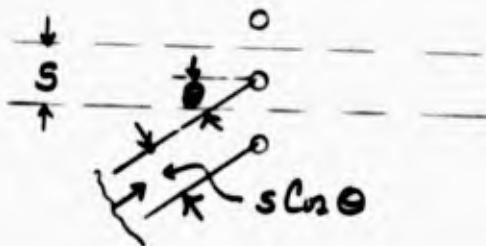
The transmission loss is then

$$T.L. = 10 \log_{10} \frac{Y_0}{T} = 10 \log_{10} \frac{1}{1 - E_0/SY_0} = 10 \log_{10} \left[\frac{1}{1 - \frac{(3\pi+8)\pi a \mu^3}{8S}} \right]$$

For the construction under consideration, the transmission loss calculated according to this analysis is less than .01 db, totally insignificant.

The secondary scattering from the field of one element by its neighbor has been neglected since the neighbor subtends an angle of less than 15° and less than 5% of the total energy is scattered in this manner.

At angles of incidence other than normal, we may modify this equation as shown in the diagram. The width of the plane wave-front



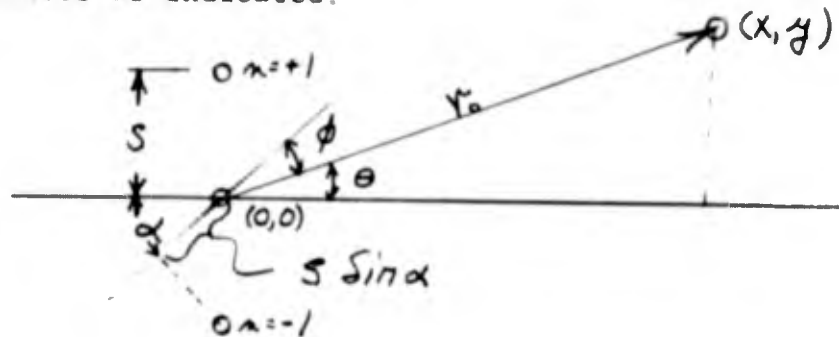
associated with each cylinder is reduced to so that the transmission loss

$$T_o L_o = 10 \log_{10} \left[\frac{1}{1 - \frac{(3\pi+8)\pi a \mu^3}{8S \cos \theta}} \right]$$

This equation indicates little change in the transmission loss until the angle of incidence approaches 90°; however, under these conditions the neighboring cylinders begin to interfere with the forward scattered beam and the equation is no longer valid. We therefore reach the conclusion that the transmission loss is less than 0.1db for angles of incidence up to at least 80°.

The next consideration is diffraction effects.

Let us now look at a plane wave incident upon a system of cylinders as indicated:



where α is now the angle of incidence and θ is a direction from the center of the array to a point of observation in the far field. It is possible to find a direction in which the scattered waves add in phase to produce a diffraction image similar to those produced by Fraunhofer diffraction in optics²?

The pressure amplitude at the point of observation (x,y) is

$$P_s \propto \sum_{n=-M}^{+N} \frac{e^{ik(r_n + nS \sin \alpha)}}{r} [2 \cos(\theta - \alpha) - 1]$$

where n is the number associated with the n -th cylinder counting from the origin $(0,0)$ and r_n is the radius vector from this cylinder to (x,y) .^{*} Since we are only interested in the phase of the separate scattered waves we can neglect all factors except the exponential function. If the argument of this function indicates an integral number of wave-length phase difference between each scattered wave, then there will be a diffraction image formed which could give a false target indication. For this to be true,

$$k [r_{n+1} + (n+1)S \sin \alpha - (r_n + nS \sin \alpha)] = 2\pi p.$$

where p is some integer.

* The summation from $-M$ to N includes all the elements in a finite array such that $(M + N)S$ (the width of the array) is less than r .

Now $r_n^2 = x^2 + (y - ns)^2$, and, since S is small
 r_n can be approximated by $r_n \sqrt{x^2 + y^2} - n S \sin \theta$
so that

$$ks (\sin \alpha - \sin \theta) = 2\pi p$$

is the phase difference of the scattered waves between two successive cylinders.

At the critical frequency and a spacing $S=2$ inches in water images are found only at $\theta = \alpha$ and $\theta = \pi - \alpha$ which corresponds to the transmitted and reflected waves, and no spurious diffraction images can be formed.

As a result of these studies it was concluded, the proposed construction incorporating 1/2" diameter cables spaced 2" apart was acceptable acoustically.

4) Cable Attachment

One basic problem of this system is that of properly anchoring the ends of the 1/2" load carrying cables. The various techniques considered were:

- (a) Wrap cable around pulley and use crimped sleeve, similar to 100" dome.
- (b) Lacing cable between sheaves and zinc ends - use grommet for splice.
- (c) Zinc filled ends - each cable
- (d) Swedged ends - each cable

The first technique was considered initially since it is similar to that used on the 100" dome. The reason it was discarded was because of the size of the cable and the swedged fitting. It would involve a special fitting rather

than an off-the-shelf item. Furthermore the cable and fitting manufacturers would only guarantee the reliability of the swaged fitting and the assurance of full cable strength if they applied the fittings. If B.F. Goodrich were to apply these fittings, a special designed tool would be necessary which would have been cumbersome with reduced reliability.

This evolved into the interlacing design. In this approach a cable would be laid continuously from one boundary bar to the other, wrapping around a sheave at each boundary. At a splice area between panels the continuous cable would be cut-off and its end positioned in a socket hole in the boundary bar and the cavity zinc filled. In the splice itself a grommet would be added between sheaves. (Figure 6)

Application of this technique, as in the previous technique, demands laying of the cable in its predetermined location in the mold in a non-distorted arrangement. Elimination of crimped sleeves on the ends made this procedure much more acceptable.

The radius of the sheaves around which the cable would wrap, together with the center-to-center distance of the sheaves presented a problem. The bending of the cable around the sheave in a consistent or precise radius was difficult, mainly due to the stiffness of the cable. This problem could be met by a method of pre-forming the cable at the point where it must wrap around a sheave, but this reduces the cable strength as shown in the following graph (Figure 7).

The greatest problem in this conception is holding the cable in its proper location so that when the rubber is being cured under pressure it would not shift or slip around the sheaves. Such movement of the cable would cause exaggerated distortions or deflections of the contour.

Thinking then returned to the individual cable concept with consideration given to a substitute for the crimped fitting. Two possible ideas came forth. The first was to use the zinc fitted socket idea, which was to be used in the splice area of the previously discussed construction concept. Special skills and experience are essential to

Contract NOber 89483
Serial No. SS041-001
Task 8156

- 47 -

Report No. 17
Phase I Interim Report
30 September 1964

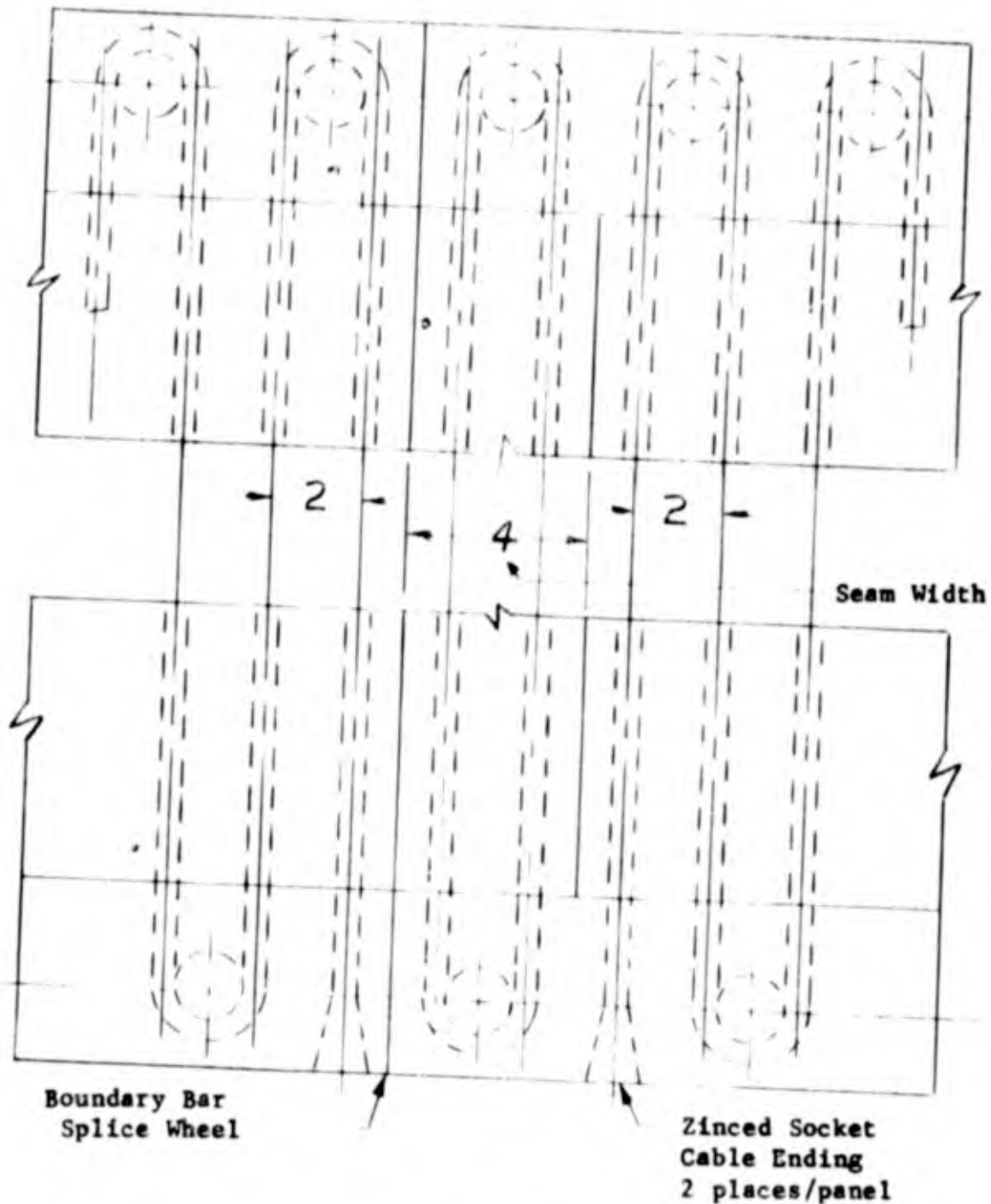
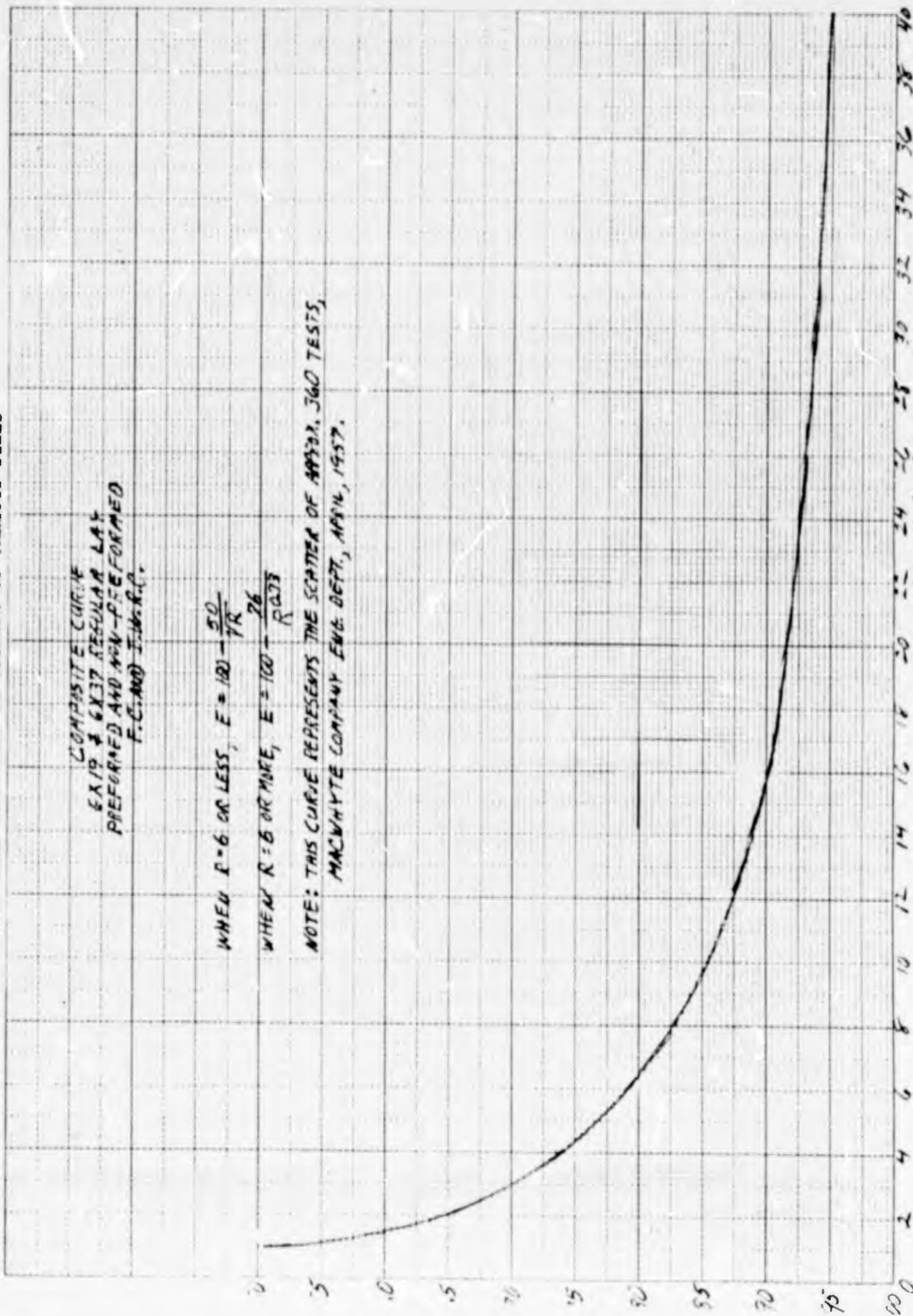


Figure 6

ZINC FILLED GROMMET ATTACHMENT
OF 1/2" CABLE TO BOUNDARY BAR

FIGURE 7
 STRENGTH EFFICIENCY OF WIRE ROPE (NEW OR USED)
 WHEN BENT OVER PINS OR SHEAVES OF VARIOUS SIZES



COMPOSITE CURVE
 EX 19 & 6X37 REGULAR LAY
 PREFORMED AND NON-PREFORMED
 F.C. 100 I.W.R.C.

WHEN R = 6 OR LESS, $E = 100 - \frac{50}{R}$
 WHEN R = 6 OR MORE, $E = 100 - \frac{76}{R}$

NOTE: THIS CURVE REPRESENTS THE SCATTER OF APPROX. 360 TESTS,
 MACWHYTE COMPANY ENG. DEPT., APRIL, 1957.

$R = \frac{\text{PIN (OR SHEAVE) DIA.}}{\text{ROPE DIA.}}$

BLANK PAGE

utilize this type of cable anchoring. Consistency within the anchor, from one cable to the next, is needed to insure meeting prescribed contours. This consistency is better met through use of a swedged fitting instead of a zinc socket. On each end of a cable, which has been cut to the prescribed length for a specific location in the dome, a fitting would be swedged. The boundary bar would require slots or key-holes into which the swedged ends could be inserted. Through the use of an adjusting mechanism or shims, the length tolerance allowed in the original pre-fabrication of the cables could be tightened up greatly, thus assuring a better matching of the desired contour. However, because of the larger size of the swedged fittings and the reliability requirements these fittings can be put on only by the fitting supplier. Special equipment is required for this function which is available only at the supply source.

In general the problems involved in a construction as previously discussed are considerable with a resultant negative effect on window installation and performance.

d. Conclusions

- 1) The weftless wire plies will resist the pillowing tendency between the 1/2" cables.
- 2) Cables 1/2" in diameter, spaced on 2" centers would support the loads resulting from a 50 psi internal pressure.
- 3) The construction, utilizing 1/2" cables, is acceptable acoustically yielding a calculated transmission loss of .1 db for angles of incidence up to 80 degrees.
- 4) Attachment of the 1/2" cable panel construction to the ship cannot be accomplished without a resultant negative affect on acoustical performance, weight and ease of attachment and fairing.
- 5) Investigations should be undertaken to eliminate the 1/2" cable and to simplify the attachment and splicing hardware.

7. Analysis of Weftless Cable-Reinforced Window

a. Summary

Following a thorough investigation strength analysis and acoustical study it was determined that a superior acoustic window for a bow dome could be fabricated from a multi-ply weftless wire fabric construction. This is a fabric which has cable (14 ends per inch) running only in one direction. Consequently, all strength is in the direction of the cables with the gum coating holding the cables together along the width. These plies oriented properly yield a construction of proper strength to withstand expected service conditions.

b. Introduction

After determining the limitations of constructions reinforced with heavy cables, other methods were sought for obtaining the required wall strength.

The most obvious approach, which was pursued, was to utilize only the weftless wire fabric as the strength members. This was studied with respect to acoustical performance, strength and fabrication ease.

In lieu of the combination of 1/2 inch diameter radial cables as strength members and weftless wire fabric as shear plane members, the membrane will be constructed of plies of weftless wire fabric. They will lay at prescribed angles, to produce a window of equivalent strength as the 1/2" cable design and superior acoustic characteristics. Advantages of this design include:

- (1) simplified ply lay up and boundary bar attachment technique,
- (2) a more homogeneous cross-section, which will be more conducive to uniform acoustical transmission, and
- (3) a more flexible structure which will reduce the problems of transportation, handling and damage during service.

c. Strength Analysis

Mathematical calculations predict that this concept is feasible from a strength standpoint. Three (3) plies of weftless wire fabric, each having .048 inch diameter carbon

steel cables, brass coated, spaced 14 ends per inch, laid radially (running vertically from boundary bar to boundary bar) will be equivalent to the strength of 1/2 inch cables running radially and spaced on approximately two inch centers. The minimum breaking strength for 1/2" diameter "7 Flex" cable is 26,200 lbs. This cable was to take the load over a 2" width. With the weftless wire construction each of 14 cables per inch has a minimum 355# breaking strength. Three plies of this construction yields a breaking strength over a 2" width of 29,820 lbs. As in the 1/2" cable design it is planned that shear plane forces be taken by a number of weftless wire fabric plies laid at 75° angles to the main reinforcement plies.

In addition to the cable tensile strength consideration, the ultimate strength of the construction is dependent upon the strength of the adhesives.

The first consideration will be the constructional adhesive evaluation. In essence this evaluatory phase is concerned with determining proper adhesives for bonding: (1) steel cables to Neoprene, (2) Uncured Neoprene to Uncured Neoprene, and (3) Cured Neoprene to Uncured Neoprene. Many adhesive systems are available for each situation mentioned; therefore, this study is necessary to determine the best system for incorporation into the window construction.

In determining structural strength of the window construction, it is desirable that the full strength of the wire cable be utilized. Adhesive failure of the Neoprene bond to the cable or the Neoprene to Neoprene bond at the splice is not considered satisfactory. Consequently, it is necessary to attain adhesive bond strengths of such a value that failure would not occur in these areas.

- 1) Cable Adhesion - Relative cable adhesion of potential primers was determined using the standard American Society for Testing Materials V-186 Adhesion Block Test. The procedure outlined in this test requires priming with the desired adhesives, then curing the cables in a one (1) inch square bar of the appropriate compound. Subsequent to cure, the cables are pulled from the block in an appropriate testing machine. This value, in pounds, is recorded and gives an indication of the relative bond strengths.

The best system, as determined from this evaluation, is further tested in the Bead-Panel Tensile Testing phase of this program.

Test data obtained from this program are recorded in Table II.

TABLE II
PLY CABLE ADHESION TESTS

<u>Com- pound No.</u>	<u>Dip No.</u> ⁴	<u>Load in Pounds</u>							<u>Remarks</u>
		<u>1</u>	<u>2</u>	<u>3</u>	<u>4</u>	<u>5</u>	<u>6</u>	<u>Av.</u>	
16148 ¹	018615	59	68	70	71	67	72	68	Cable Clean
16148	220	78	102	96	118	113	100	101	10% Gum on Cable
16148	203-220	130	129	125	167	133	145	138	50% Gum on Cable
35001 ²	018615	46	48	42	56	43	45	64	Cable Clean
35001	220	78	97	95	74	98	81	87	20% Gum on Cable
35001	203-220	160	166	170	189	150	102	156	20% Gum on Cable
35003 ³	018615	25	24	24	21	20	16	22	Cable Clean
35003	220	120	118	125	124	89	110	114	50% Gum on Cable
35003	203-220	133	112	113	118	110	96	113	85% Gum on Cable

1. Natural Rubber Compound.
2. Rho-C type Natural Rubber Compound.
3. Rho-C type Neoprene Compound.
4. Dip applied to brass coated carbon steel cable.

The intended compound for dome construction is 35003 Neoprene. This material is a RHO-C Neoprene compound used in many other sonar applications. It is preferred over Natural Rubber in that greater splice bonding strengths can be attained.

Due to the ready availability of material, the original test samples and panels were constructed with the Compound 16148 - Dip 018615 System. However, upon completion of this test program, and the acceptability of the combination 35003 Neoprene - 220 dip material proven, subsequent samples were fabricated from this material and tested as discussed later.

- 2) Compound Adhesion - As mentioned previously, there are many adhesive systems available for bonding Neoprene to itself, either cured or uncured, whatever the construction might dictate. The purpose of this program phase is to evaluate several acceptable adhesives and determine which is more acceptable for use. During this program, the ultimate goal was to obtain an adhesive system which would require Neoprene stock shearing for sample failure to occur.

Samples were fabricated and tested with resulting data in Table III, "Bonding Adhesion",

TABLE III

35003 NEOPRENE BONDING ADHESION¹ (lbs/in)
CURE 30' @ 300°F

<u>Adhe- sive</u>	<u>Peel Test²</u>			<u>Shear Test³</u>								
	<u>1</u>	<u>2</u>	<u>Ave.</u>	<u>3" Lap</u>			<u>5" Lap</u>			<u>7" Lap</u>		
				<u>1</u>	<u>2</u>	<u>Ave.</u>	<u>1</u>	<u>2</u>	<u>Ave.</u>	<u>1</u>	<u>2</u>	<u>Ave.</u>
1024	58	68	63	1160	1275	1217	1590	1595	1593	1900	2000	1950
369	65	75	70	1000	1000	1000	1510	1560	1535	2155	2410	2282

1. Data in pounds pull per inch of sample width.
2. Stock sheared in all cases.
3. Stock shear in all cases except 3" lap.

This data coupled with considerable experience using 369 cement indicates this cement is acceptable for this application.

- 3) Constructional Strength - The sample testing program conducted during ship attachment design studies, Section C.8.e.1, further verified the acceptability of the strength characteristics. During those studies as shown in Table XI thru XVII the ultimate strength of the chosen construction was found to be 11,000 to 14,000 lbs/inch. This yields an ultimate strength safety factor of approximately 4 to 1 in the panel area.
- 4) Effect of Salt Water on Ply Cable

The purpose of this study was to determine the effect of salt water corrosion on brass-plated wire cable cord, code W-70100, currently used in the construction of the prototype panel. Secondly, to evaluate wire cables of various compositions and other materials capable of performing a similar function.

The results to date disclosed that there was no deleterious effect on tensile strength, of W-70100 wire after four months immersion in salt water at 80 psig, of a segment representing the standard window construction.

When the bare wire was immersed in salt water under controlled conditions, the tensile strength was reduced approximately 50% after 14 days exposure. Bare wire tested concurrently with the above in an atmosphere of salt water fog deteriorated completely within 14 days.

The attached data showed stainless steel had very good resistance to salt water spray.

Galvanized wire appeared to lose no strength, but it was postulated that this was due to the large wire size and plating thickness. A smaller wire having a thinner plating would be more susceptible to corrosion.

The presence of moisture in glass cord has a severe effect on tensile strength resulting in a shearing stress on the individual filaments in the cord. The degree of degradation was not fully exemplified in these results, primarily because the samples were partially dry at the time of tensile testing.

The procedure consisted of applying a hydrostatic pressure on a single ply of wire cables coated with .020" neoprene, totaling an over-all thickness of .075". Actually, the window construction is 1" thick with $\frac{1}{2}$ " of neoprene over the outside of the 5 wire plies. Permeation of the sea water thru the $\frac{1}{2}$ " of neoprene furnishes a filtering action, thus when it reaches the wire it is relatively free of salts. This, coupled with the absence of air, considerably reduces and may eliminate the problem of wire corrosion.

The single ply samples were immersed in salt water to simulate the window in its use environment. The test fixture used to contain the sample and water was a section of pipe 30" long x 3" in diameter and capped at each end, one of which was equipped with a $\frac{3}{8}$ " orifice used to pressurize the system to 80 psig with air. The test segment was 15" long x 1" (14 cables) wide.

Various uncoated materials were immersed in the salt solution reservoir of a salt spray cabinet and/or suspended in the salt spray fog in such a position that they did not overlap or shield each other. The salt spray apparatus included the following:

- a) An exposure chamber with attachments for supporting samples which would not affect the corrosiveness of the salt spray nor cause electrolytic corrosion.
- b) A salt solution reservoir with a solution consisting of iodine-free NaCl and distilled water, and adjusted to a specific gravity of between 1.14 and 1.15.
- c) An atomizer consisting of an air arrangement so that it will blow across a glass tube immersed in the salt solution, and spray against a baffle plate forming a fog throughout the chamber.
- d) A heater element immersed in the salt water solution which maintained the temperature between 94 - 98°F within the chamber.

At specific intervals, samples were removed from their environment, examined for corrosion, and the resulting strength or break load determined as indicated in Table IV.

TABLE IV
CABLE BREAK STRENGTH AFTER AGING

<u>Data:</u> <u>Material</u>	<u>Ultimate tensile strength psi- Control</u>	<u>Aging in Weeks</u>	<u>Ultimate tensile strength psi after aging</u>	<u>% Tensile Strength Retained</u>
Control-Code W-70100 (5 x 7) Brass plated Steel Dia. 0.048"	325			
Code W-70100 coated and immersed @ 80 psig air	325	4	325	100
		8	332	100
		12		
		16		
Code W-70100 immersed salt water	325	1	305	94
		2	172	53
Code W-70100 salt spray	325	1	78	24
		2	15	5
Code W-40007 Stainless steel-Type 302 Dia. 0.012"	37	4	36	97
Code W-31- (7.1) Stainless steel-Type 18-8 Dia. 0.039	120	4	104	87
Code W-609 Galvanized steel-Dia. 0.148"	1635	4	1660	100
Fiberglas Cord-RFL Dipped 150/10/4 Dia. 0.045"	176	4	134	76
Code 8363 (150/3/10) Fiberglas Cord - Neoprene Dipped - Dia. 0.040"	124	4	103	83

Continued testing of the materials are planned, specifically the window samples, to determine effective life of the materials.

The stock described is classified as a "Rho - C rubber". The term "Rho-C" rubber was coined to describe rubber compounds developed especially by The B.F. Goodrich Company for use in sonar devices. The density and the sound velocity of the rubber closely matches the same properties of sea water. To obtain maximum transmission and minimum reflection of sound passing through two adjacent media, it is necessary to match their acoustic impedance.

The normal classical acoustic impedance equation can be applied to determine the approximate intensity of surface reflections. As the sound beam passes through the interfaces between media the intensity of the reflection is given by:

$$R = \frac{P_1 C_1 - P_2 C_2}{P_1 C_1 + P_2 C_2} = \frac{Z_1 - Z_2}{Z_1 + Z_2}$$

R = Percent of sound power reflected

$P_1 C_1$ = Acoustic impedance of first medium (density x sound velocity)

$P_2 C_2$ = Acoustic impedance of second medium (density x sound velocity)

$Z = PC$ = Acoustic impedance

The equation above assumes a loss free media. However, in the case of rubber, there is some hysteresis loss. This fact makes it impossible to obtain reflection - free transmission through rubber due to the reactive component present in the acoustic impedance of a "lossy" medium. The impedance is shown by:

$$Z_2 = \frac{PC}{1+r^2} + \frac{ir PC}{1+r^2}$$

Where

Z_2 = Acoustic impedance of "lossy" material

P = Density of material

C = Sound velocity in the material

$r = \frac{\alpha C}{\omega}$ = loss parameter

α = Sound attenuation in material (Nepers / cm)

$\omega = 2\pi f$

d. Panel Compound Studies

The basic elastomer utilized in the proposed bow dome acoustic window is neoprene, a chloroprene polymer. This is a compounded stock which exhibits the physical properties and characteristics noted in Tables V and VI.

TABLE V

PHYSICAL PROPERTIES OF NEOPRENE BFG CODE 35003

<u>Property</u>	<u>Value</u>	<u>ASTM Reference</u>
Tensile	2900 psi	ASTM D412-51T
300% Modulus	400 psi	ASTM D412-51T
Shore A Durometer	45	ASTM D676-49T
Compression Set	59%	ASTM D395-53T
Tear Resistance	200 lbs./in.	ASTM D624-54
Water Absorption 481-RS @ 25°C	1.63%	ASTM D471-54T

TABLE VI

PHYSICAL CHARACTERISTICS OF NEOPRENE BFG CODE 35003

<u>Characteristic</u>	<u>Resistance</u>
Tear	Fair to Good
Abrasion (Dry)*	Fair
Ozone	Good
Mineral Oil	Good
Castor Oil	Excellent
Sunlight	Excellent
Weather	Excellent

*Resistance to abrasion while wet is excellent since the water acts as a lubricant.

The attenuation, α , is very low in most elastomers at frequencies below 100 kilocycles. However, α increases with increasing frequency, and becomes appreciable in some materials at frequencies above 500 Kilocycles.

Although the slight mis-match is of little concern to sonar design engineers, it does point up the reason for some surface reflection even though a perfect ρc match has been obtained.

The densities and sound velocities (ρc) of the various RHO-c compounds are listed in Table VII.

Also, Figure 8 and 9 present graphs of Sound Velocity Vs. Temperature and Sound Absorption Vs. Temperature.

TABLE VII
 THE DENSITIES AND SOUND VELOCITIES (ρ C) OF
 THE VARIOUS RHO-c COMPOUNDS

Material	Density (ρ)	Sound Velocity (c) (Meters/Second)										*Reflec- tivity T = 25°C
		5	10	15	20	25	30	35	40	45	50°C	
Natural Rubber Gum (35000)	.98 g/cc	1578	1570	1552	1535	1518	1502	1488	1469	1452	1427	-34 db
Natural Rubber Black (35001)	1.10	1588	1578	1554	1548	1525	1502	1480	1471	1455	1427	-25
GR-S	1.11	1630	1590	1572	1550	1530	1505	1495	1475	1460	1438	-22
Neoprene (35003)	1.32	1640	1602	1570	1542	1525	1502	1485	1469	1460	1427	-12
Hycar 1001	1.12	2190	2070	2005	1905	1815	1780	1655	1640	1575	1550	-14
Butyl Gum	.97	1985	1840	1732	1731	1630	1575	1575	1540	1522	1490	-25
Butyl Black	1.04	1925	1850	1800	1750	1700	1640	1585	1575	1536	1510	-22
Sea Water	1.03	1510	1530	1546	1560	1570	1580	1587	1592	1597	1602	-

* Referred to incident beam

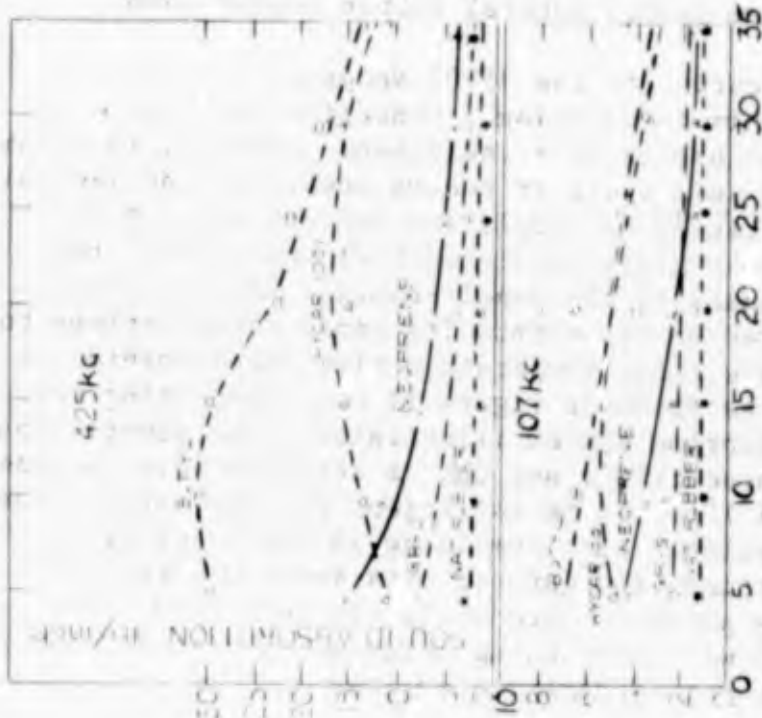


Figure 9
 SOUND ABSORPTION VS. TEMP.

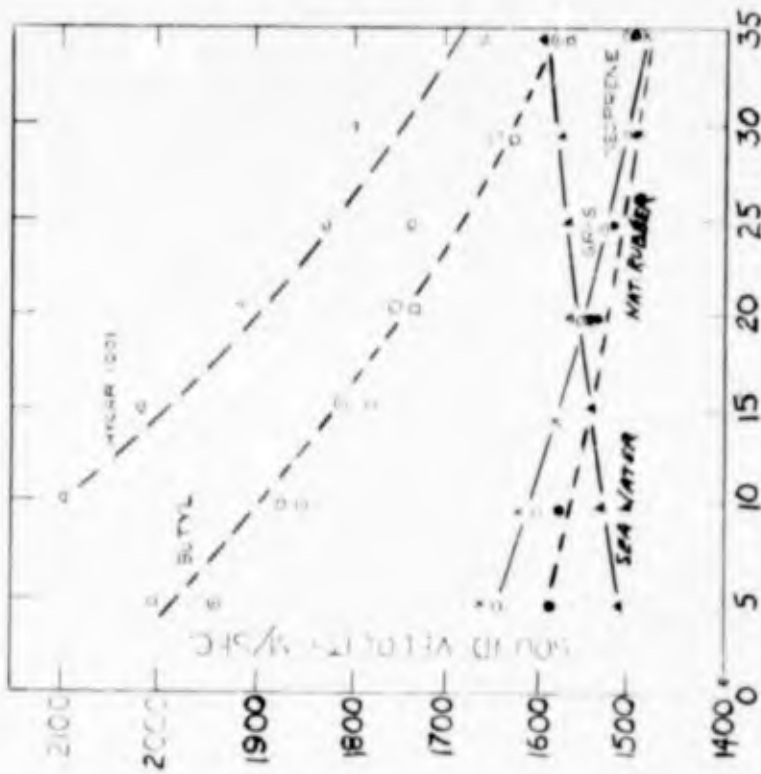


Figure 8
 SOUND VELOCITY VS. TEMP.

Analysis of the information presented indicates other materials listed appear to be more desirable than the chosen neoprene stock. Two primary considerations prompted the decision to use neoprene: (1) the greater level of durability exhibited by neoprene with respect to ozone resistance, oil resistance and life span and (2) the great increase of reliability of a neoprene bonded seam versus natural rubber bonded seam.

The stress strain curve for the 35003 Neoprene is shown in Figure 10. With this information a tentative cure cycle for the prototype panel had to be established. However, in attempting to establish a cure cycle it became apparent that several unique situations tended to complicate the picture. First, the size of the Epoxy-glass laminated tool and second, the variation in thickness of the panel itself. Several sample cures were conducted on representative panel constructions to investigate the cure cycle temperature time relationship. A sample fabricated as shown in Figure 11 was cured using the thermo couple monitoring system illustrated. The general concept pursued in these trials was that a standard cure for the panel thickness of 1" would be sufficient for the entire panel thickness. The residual heat remaining in the heavy fill sections would continue the cure of this section after the normal temperature phase of cure cycle was completed. The sample illustrated was cured using this technique and Table VIII presents temperature data accumulated.

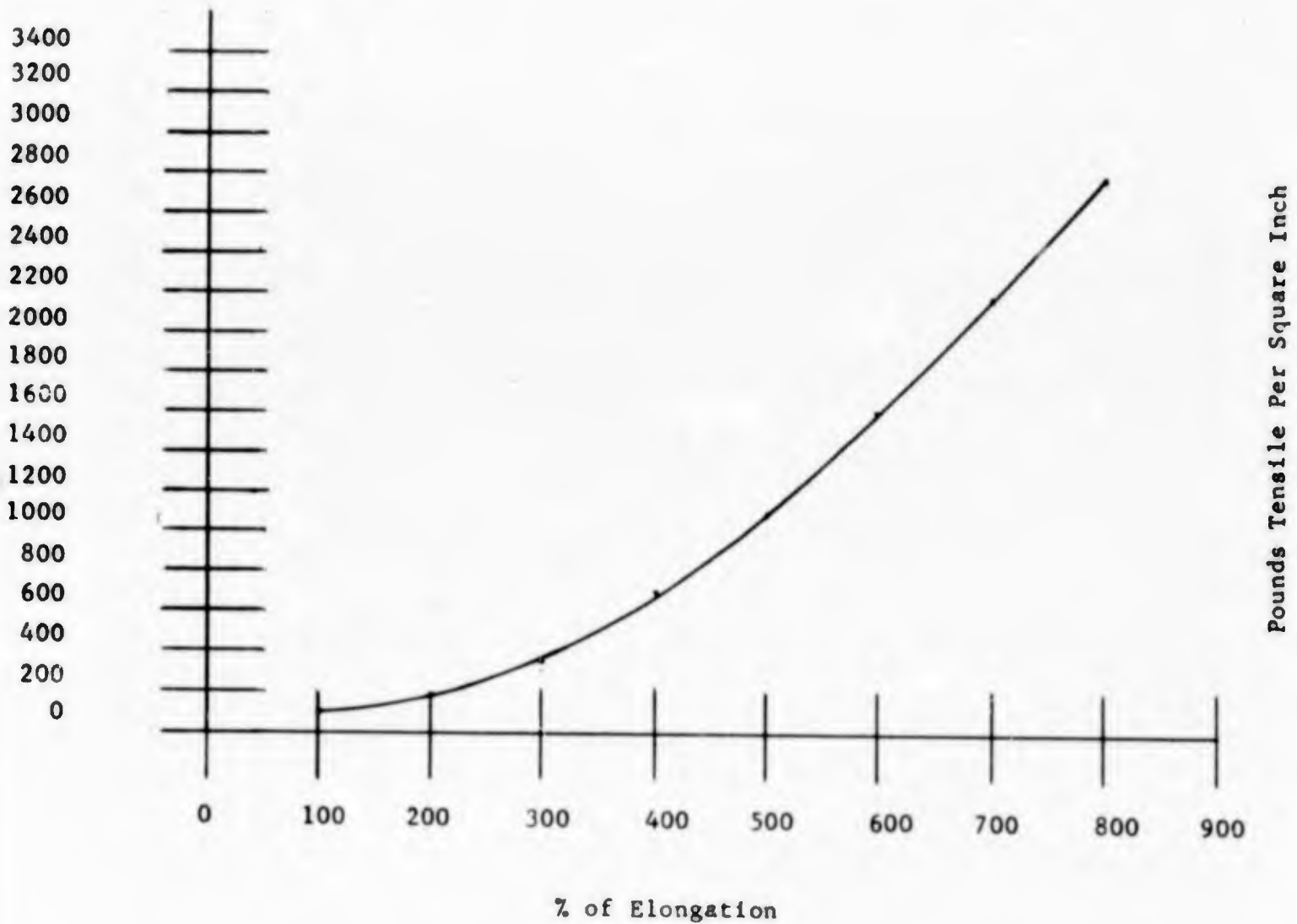


FIGURE 10
35003 NEOPRENE STRESS-STRAIN CURVE

Contract N0bsr 89483
Serial No. SS041-001
Task 8156

- 64 -

Report No. 17
Phase I Interim Report
30 September 1964

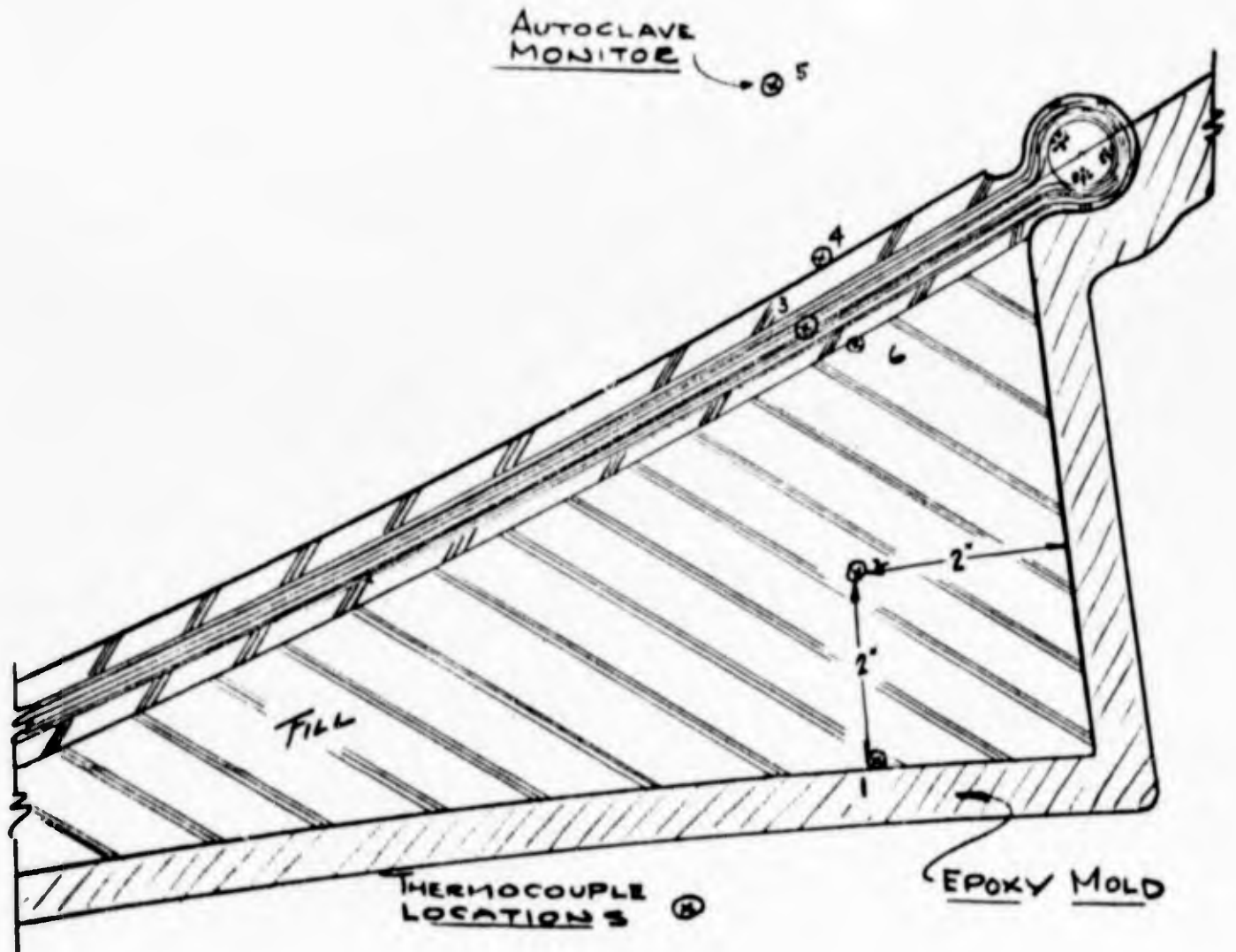


FIGURE 11
SAMPLE WINDOW CURE SECTION

TABLE VIII
SAMPLE WINDOW CURE DATA

Time	Thermocouple Temperature °F						Remarks
	1	2	3	4	5	6	
Start	-	-	-	-	-	-	
1/4 hr.	187	-	126	219	300	90	
1/2	233	-	166	258	290	113	
3/4	251	98	200	270	299	146	
1 hr.	259	113	220	276	298	170	
1/4	265	132	234	280	298	189	
1/2	269	145	243	280	292	202	
3/4	266	162	249	277	292	217	
2 hrs.	278	175	256	289	303	226	
1/4	285	178	264	295	305	236	
1/2	283	200	269	290	297	245	
3/4	282	201	271	288	291	252	
3 hrs.	281	221	273	286	290	257	
1/4	283	230	274	289	297	260	
1/2	290	239	278	296	304	265	
3/4	299	249	286	304	311	272	Start cure cycle.
4 hrs.	299	257	291	303	304	278	
1/4	297	262	292	297	300	281	Start water cool-down.
1/2	221	267	253	130	110	278	
3/4	170	269	195	95	-	250	Shut off water - drain autoclave with door closed.
5 hrs.	160	259	169	132	156	215	
1/4	165	248	172	158	158	199	Door opened.
1/2	155	239	175	159	116	194	

Analysis of these data indicate that all areas of the section, including the deep fill area, received an adequate cure. Also, heat transfer through the proposed mold-bag structure was determined and was utilized in establishing the optimum prototype panel cure.

In a panel of this thickness variation, the possibility of over cure in thin sections is very good. Over curing of neoprene stock itself for the time expected has no effect on the physical properties as seen in the Stress-Strain Curve (Figure 10) previously presented.

A more vulnerable trouble spot on over cure is wire cord adhesion to compound 35003. A study was established with the primary purpose of determining the effects of prolonged curing temperatures on the adhesion of neoprene to W-70100 brass-plated wire cable with the standard Number 220 metal primer cement system.

The adhesion samples were prepared and tested according to ASTM D-1871 - 61T procedure, except that the wire was pulled from a 1" block in place of a 2" block. The processed material was obtained by dipping the wire once in the metal primer then calendar coating with .020" (each side) 35003 neoprene. The results of this study are shown in Table IX.

TABLE IX
WIRE CABLE ADHESION TEST DATA

Cure Cycle	Load (lbs.)						Ave.	Remarks
	1	2	3	4	5	6		
20' @ 292°F	100	105	102	88	112	90	99.5	
40' @ 292°F	116	95	108	116	90	125	108.3	
60' @ 292°F	85	93	110	94	116	105	100.5	85.90% Gum on Cable
80' @ 292°F	95	100	105	112	105	89	101.0	
100' @ 292°F	90	87	103	111	100	95	97.7	
120' @ 292°F	110	95	97	107	86	-	99.0	
140' @ 292°F	100	89	91	100	90	87	92.8	75% Gum on Cable
160' @ 292°F	86	82	96	97	90	105	92.7	

The results of the wire adhesion tests disclose the ultimate adhesion was obtained in 40' @ 292°F.

Progressive exposure of the specimens at curing temperature reduced the adhesion proportionately to a maximum of 14% after 160 minutes @ 292°F. It was further determined that for a "safe" level of adhesion of the neoprene to wire in the finished part, the curing cycle of the panel will be adjusted so that an equivalent cure at the wire-elastomer interface will not exceed 120' @ 292°F.

e. Acoustical Considerations

Substitution of three plies of weftless wire fabric for the 1/2 inch diameter main reinforcing cables reduces the amount of average metallic cross-sectional area about 40%. This fact coupled with the homogeneity of the resulting cross section improves the sound transmission properties of the dome over previous designs.

The transmission loss of the pressurized acoustic window membrane of both 5 and 8 ply systems were evaluated. The 5 ply duplicates the normal panel construction and the 8 ply the maximum overlap situation adjacent to the beads. Theoretical calculations were completed and the results compared with pulse tube data, taking into consideration all the corrections required. Excellent agreement was found and thus the basis established for calculating the transmission loss of a large panel in the free field.

1) Sound Velocity in the Wall

The window wall consists of a series of closely spaced cables embedded in a neoprene compound. At the frequencies under consideration, the wave length of sound is far greater than the diameter and spacing of the wires in the matrix. Under these conditions, one would expect that the effect of the steel cables would be conveniently described as increasing the bulk modulus and increasing the density of the composite material, and that the sound-transmission properties of the composite could be calculated, using these modified properties, in the following manner.

In the homogeneous medium the sound velocity (longitudinal waves) $C_0^2 = B_0/\rho_0$ where B_0 is the bulk modulus and ρ_0 is the density. If, to this medium, a specified volume percent (v) of incompressible material of density (d) is added, then the modified bulk modulus $B' = B_0/(1-v)$ and the modified density $\rho' = \rho_0 + (d-\rho_0)v$. Thus the velocity of longitudinal waves (C') and density (ρ') in the matrix combination are:

$$C' = C_0 \sqrt{\frac{\rho_0}{(1-v)\rho'}}$$
$$\rho' = \rho_0 \left[1 + \left(\frac{d}{\rho_0} - 1 \right) v \right]$$

(1)

where

c' = longitudinal wave velocity in wire-rubber-wall

ρ' = density of wall

c = sound velocity in rubber

ρ = density of rubber

d = average density of incompressible filler cables

V = volume percent of filler

2) Transmission

When a plane wave is normally incident upon a plane wall of non-absorbing material, the energy is both reflected and transmitted such that $R^2 + T^2 = 1$ (where R and T are the absolute values of the reflection and transmission coefficients).

Also:

$$R/T = 1/2 \left(\frac{Z_1 - Z_0}{Z_0 + Z_1} \right) \sin \frac{\omega a}{c_1} \quad (\text{Appendix I}) \quad (2)$$

where Z_0 = Specific impedance of medium

Z_1 = Specific impedance of wall

c_1 = Longitudinal wave velocity in wall

ω = angular frequency

a = wall thickness

In the bow dome at frequencies below 10kc the properties of the wall are such that $\omega a/c < .15$ and thus $\sin \omega a/c \sim \omega a/c$.

Thus (2) becomes

$$R/T = \frac{\omega a \rho}{2Z_0} \left[1 - \left(\frac{Z_0}{Z_1} \right)^2 \right] \quad (3)$$

Since the neoprene compound used in the bow dome wall has less than 0.1db/inch absorption at frequencies less than 10kc/sec, we may consider the wall to be of a non-absorbing material. We may then measure the reflection coefficient from such a wall (this can be done far more accurately than measuring transmission).

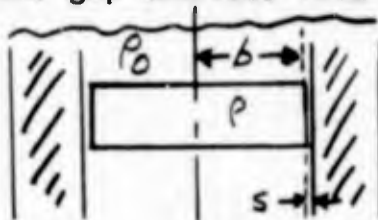
Since $R/T = R / \sqrt{1-R^2}$, a plot of (R/T) versus frequency gives a straight line passing through the origin with a slope (m) and;

$$m = \frac{\rho_a}{\rho_0} \rho_1 \left[1 - \left(\frac{z_0}{z_1} \right)^2 \right] \quad (4)$$

or

$$m = \frac{\rho_a}{c_1} \left[\frac{z_1}{z_0} - \frac{z_0}{z_1} \right]$$

The measurements of reflection coefficient are made with a disc of the material suspended half way down a fourteen-foot vertical pulse tube. Thus, the first front surface reflection is received at the transducer, mounted at the bottom of the tube, before the return pulse from the air-water interface at the top of the tube. In this way, accurate measurements of reflection coefficients are possible. The disc samples are molded to precise dimensions, but there is still a small gap between the periphery of the disc and the tube wall. This gap modifies both the



sound velocity and the density of the medium in accordance with the following equations (See Appendix II).

$$c_1' = c' \left[1 + \frac{d}{2} \left(1 - \frac{c_1'^2}{c_0'^2} \right) \right] \quad (5)$$

$$\rho_1 = \frac{\rho_0'}{A + \frac{\rho_0'(1-A)}{\rho_0}}$$

C_1 is the effective wave velocity

C' the velocity in a free field

ρ_1 the effective density

ρ' the actual density

A the fractional area of the tube that is filled with absorber (.9662 for our system) and $\theta = 2\sigma\rho/\rho_0$

In the window construction C'/C_0 is approximately 1.0 and $\ll 1.0$ so that $C_1 \approx C'$ and the longitudinal wave velocity is not changed. Therefore, only the density ρ must be modified.

3) Analysis of the Wall Structure

The wall structure in our present design consists of neoprene rubber (density, $\rho = 1.32\text{g/cm}^3$ and velocity of sound $C = 1.602 \times 10^5$ cm/sec at 10°C .) and steel cable with an equivalent diameter of 0.122 cm and an average weight per unit length of 0.05305 gm/cm. The strands are so tightly packed that the cable is practically incompressible. There are 14 cables/inch in a single ply, thus each ply contains $14 \times 0.05305/2.54 = 0.2925$ gms/cm² of steel. For the five-ply sample, whose measured density (ρ') was 2.66 gm/cm^3 and thickness 0.785 cm, the volume fraction of steel (ν) is 0.40, and from (1);

$$C_1 = C' = 1.602 \times 10^5 \sqrt{\frac{1.32}{(1-0.40)2.66}} = 1.458 \text{ m/sec.}$$

$$\text{and (5) } \rho_1 = 2.66 / [0.9662 \times 0.0338 \times 2.66/1.00] = 2.52 \text{ gm/cm}^3$$

At 10°C the velocity of sound in water (C_0) is 1.431×10^5 cm/sec and $\rho_0 = 1.000$. Using these values in (4);

$$m_s = \pi \frac{0.785 \times 2.52}{1.431 \times 10^5} \left[1 - \left(\frac{1.431 \times 10^5}{2.52 \times 1.458 \times 10^5} \right)^2 \right]$$
$$= 0.0367 \times 10^{-3} \text{ /sec.}$$

Table X gives the measured values of R for various frequencies for both a 5 ply and an 8 ply sample.

TABLE X

PULSE TUBE REFLECTION MEASUREMENTS

Frequency kc/sec	<u>5 ply</u>		<u>8 ply</u>	
	<u>R</u>	<u>$R/\sqrt{1-R^2}$</u>	<u>R</u>	<u>$R/\sqrt{1-R^2}$</u>
2.52	0.087	0.088	0.150	0.151
3.15	0.125	0.126	0.188	0.191
3.94	0.148	0.149	0.225	0.230
5.01	0.175	0.177	0.281	0.292
6.32	0.212	0.216	0.350	0.373
7.96	0.281	0.292	—	—

These values are plotted in Figure 12. A best-square line fit to the data gives a slope of $0.0361 \times 10^{-3}/\text{sec}$ for the 5-ply sample. A similar calculation for an 8-ply sample with density $\rho = 2.58$ and a thickness of 1.30 cm gives an experimental value of $m = 0.0589 \times 10^{-3}/\text{sec}$. compared to the calculated value of $0.0590 \times 10^{-3}/\text{sec}$. Thus we see that the method of calculating the longitudinal wave velocity for this structure gives excellent agreement with experimental values. These values, when used to calculate transmission loss of this structure in a free field will be quite accurate.

4) Transmission of Acoustic Window Wall as a Function of Angle of Incidence

The analysis of a plane wave incident upon a thin plate immersed in a fluid is discussed in many places in the literature¹. This detailed analysis indicates that the shear components of the waves have a negligible effect when the shear wave velocity in the plate is much less than the longitudinal wave velocity and when the plate thickness is small compared to a shear wave-length.

¹ The most complete analysis is given in "Waves in Layered Media", L. M. Brekhovskikh, Academic Press, London, 1960.

ME 10 X 10 TO THE CM. 200-14
REPRODUCED BY THE CM. 200-14

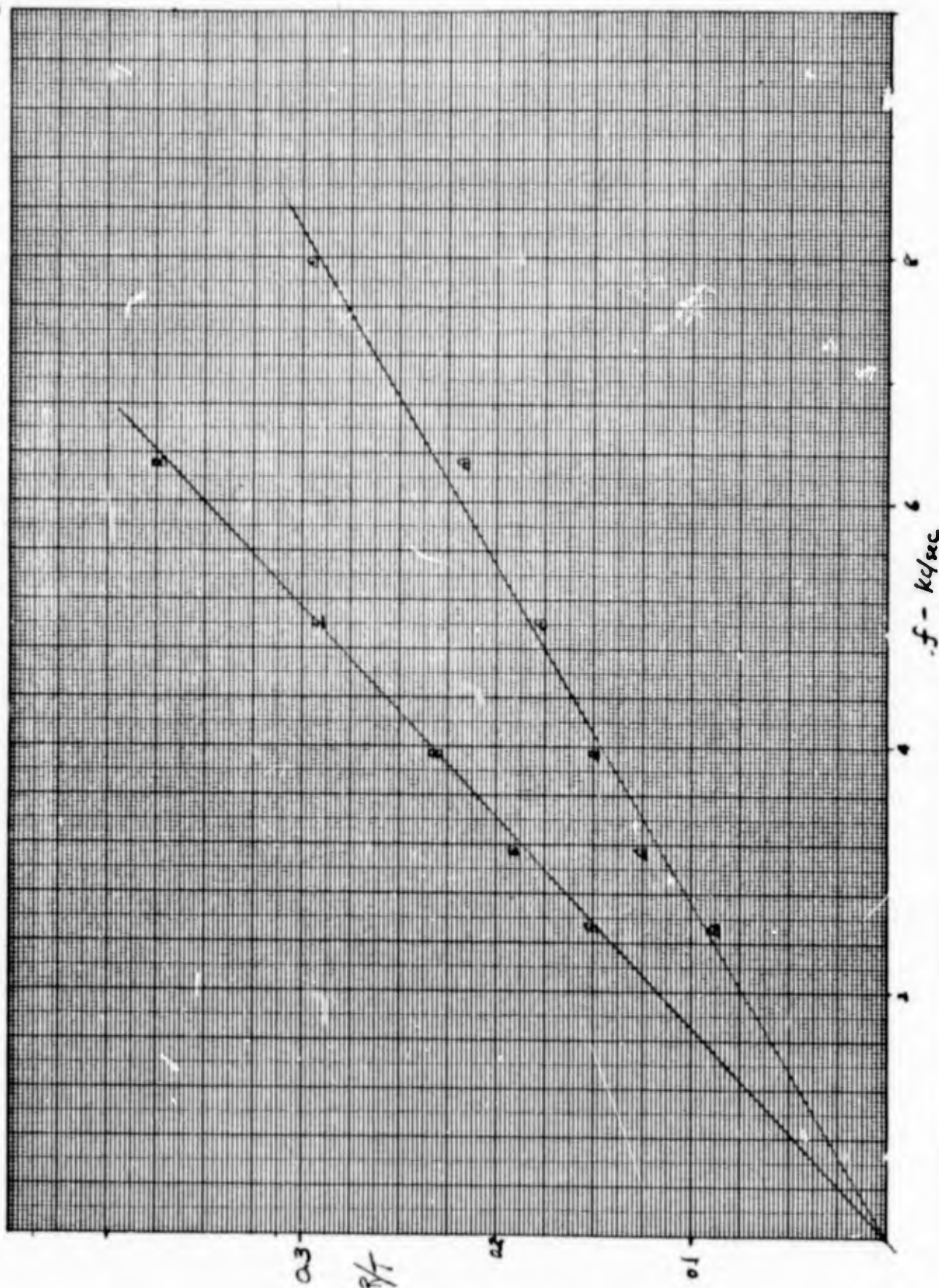


FIGURE 12
REFLECTION/TRANSMISSION VS FREQUENCY OF PULSE TUBE TESTS

Under these conditions, the transmission loss through the plate is given by

$$T.L. = 10 \log_{10} \left\{ 1 + \left[\frac{Z_0^2 (1 - C_1^2 \sin^2 \theta / C_0^2)}{Z_1^2 \cos^2 \theta} - 1 \right]^2 \left(\frac{w a \rho_1 \cos \theta}{2 Z_0} \right)^2 \right\}$$

where

- Z_0 - specific impedance of fluid
- Z_1 - specific impedance of plate
- C_0 - longitudinal wave-velocity in fluid
- C_1 - longitudinal wave-velocity in plate
- a - plate thickness
- ρ_1 - density of plate
- θ - angle of incidence

As noted earlier the sound velocity in the rubber-steel matrix is given at 10°C as 1460 m/sec with the density taken as 2.66 gm/cm³. Using a value of 1520 m/sec and a density of 1.03 gm/cm³ for sea water at 10°C, the transmission loss (db) at the critical frequency for a 5-ply wall ($a = .785$ cm) may be calculated and will be found to be insignificant.

When additional rubber is added to the wall symmetrically to make the entire thickness one inch, there is an additional mass impedance added to the wall which will increase the transmission loss. If a number of layers exist, as shown in the diagram, the overall equation for transmission loss is

$$T.L. = 10 \log_{10} \left\{ 1 + \left(\sum_{k=1}^n \left[\left(\frac{Z_0}{Z_k} \right)^2 - 1 \right] \frac{w a_k \rho_k}{2 Z_0} \right)^2 \cos^2 \theta \right\}$$

This calculation shows that the additional rubber has a very minor effect.

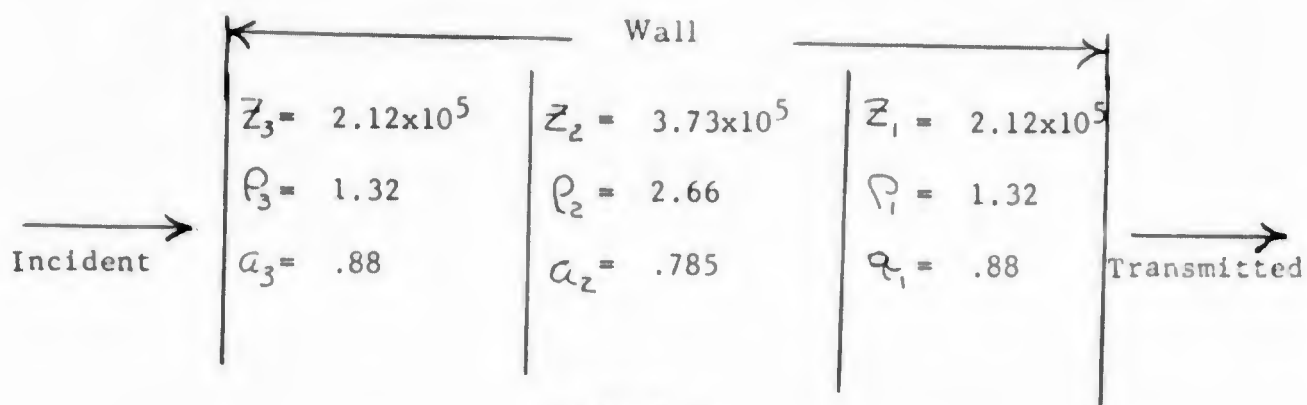


Figure 13

Acoustic Schematic of Five Ply Sample

5) Fabrication and Testing of Sample Acoustic Window Panel

As a means of verifying theoretical and pulse tube results a sample panel of the proposed construction was fabricated and submitted to the Underwater Sound Laboratory, New London, Connecticut, for acoustical testing.

The panel, 1" thick x 5' square, consisted of 8 plies of weftless wire fabric with .290" of neoprene on one side and .150" of neoprene on the other. Wire ply orientation was as shown in Figure 14. This resulted in 4 plies of wire laid vertically, 2 plies laid 15° above the horizontal

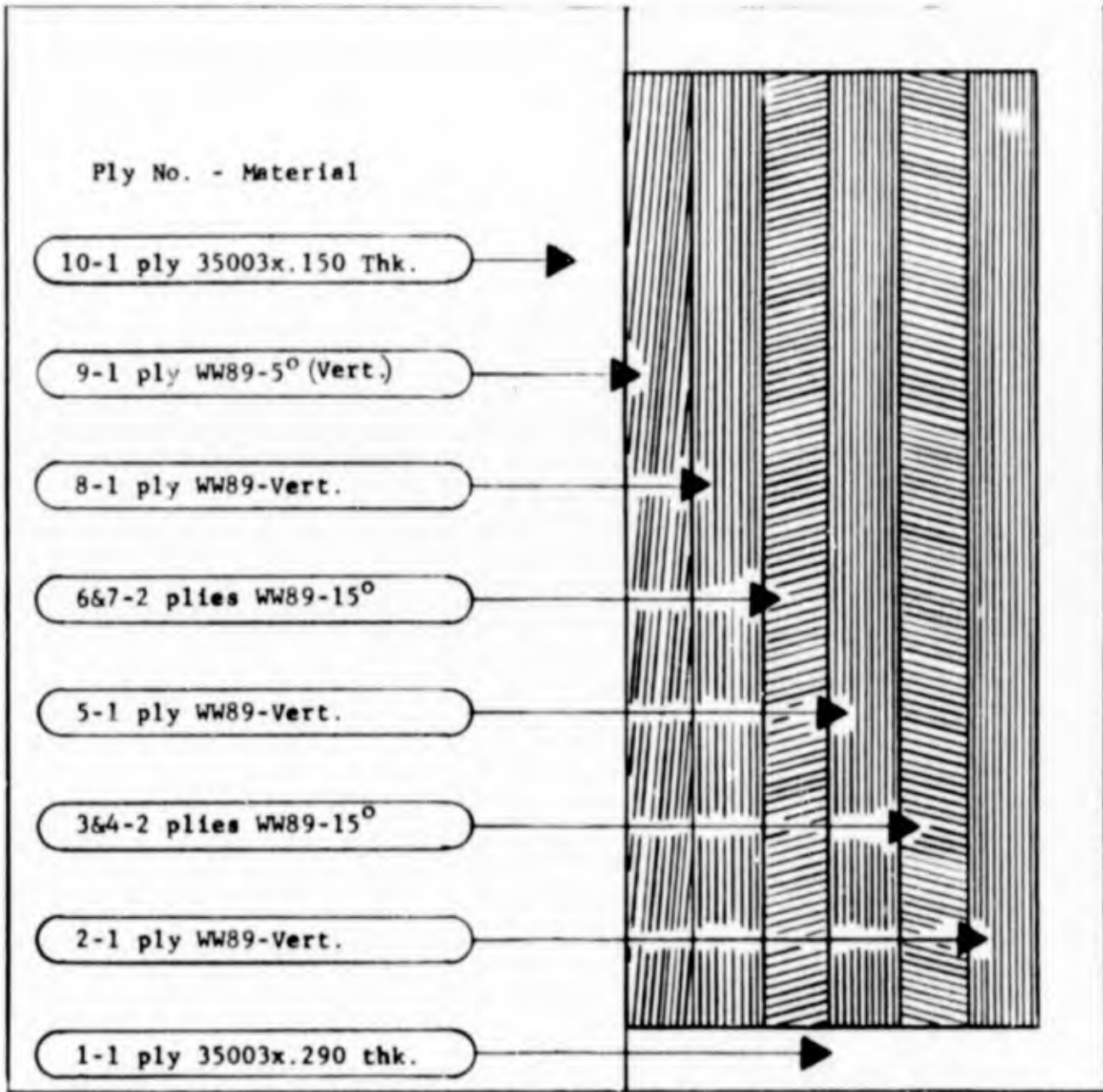


Figure 14

5' x 5' x 1" ACOUSTIC TEST PANEL, PLY ORIENTATION

and 2 plies laid 15° below the horizontal. The net result, 8 plies, simulated the most extreme case of Ply overlap anticipated in the acoustic window. This overlap situation is expected in the forward area, adjacent to the bead. Plies wrapping around the bead, in addition to overlap from normal ply lay, when traversing the distance from the dome - 4' WL (large window circumference) to the bead (small window circumference) will result in this situation.

Panel fabrication was accomplished by building the panel to the proper dimensions then inserting the construction in a steel mold. A soap mold release was sprayed on the surface of the mold to insure ease of panel removal. The loaded mold was placed in a 2000 psi, hydraulic ram, 5' platen press and the panel cured @ 300°F for 2 hours.

Subsequent to cure and prior to the final finish operations a complete x-ray analysis was made. Figure 15 depicts the panel, with the grid denoting the pattern. Viewing of the film did not uncover any defects such as voids, delaminations or broken wires.

Final finish and cleaning of the panel was accomplished to remove processing decontamination and molding marks.

Initially minor surface depressions on both sides of the panel were filled with B.F. Goodrich adhesive 429348. This is a high solids, rubber base, waterproof adhesive. It is resistant to fresh and salt water, ages well and remains resilient to withstand impact and vibration.

The bottom surface of the panel possessed several flow marks and mold lines and it was considered desirable to buff them smooth. A skill belt sander with 80, then 120 grit sandpaper was used for this operation.

Buffing was accomplished only on the bottom surface since the top appeared to be acceptable, with only minor mold imperfections.

The panel was washed thoroughly with Methyl Ethyl Ketone and Petroleum Naphtha and then stenciled with necessary information.

The panel was completed and shipped to the Underwater Sound Laboratory, New London, Connecticut on August 19, 1963. This panel was tested by Hazeltine Corporation

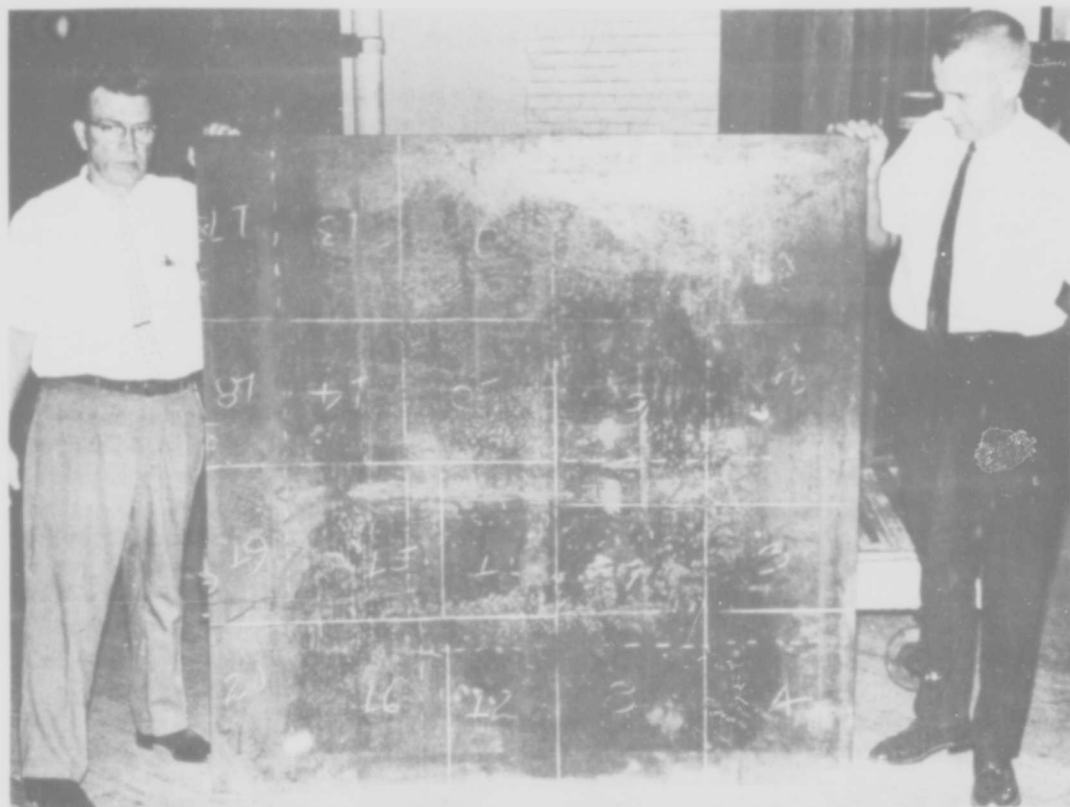


FIGURE 15
5'x5'x1" ACOUSTIC PANEL, SUBSEQUENT TO X-RAY ANALYSIS

with results recorded in Test Report, No. EASL-AS-5 dated November 5, 1963, entitled "Acoustic Characteristics of Material". In essence this report states that no acoustical absorption or reflection was detectable in the frequency range of interest.

Upon completion of testing by Hazeltine additional testing of the panel was accomplished by the Underwater Sound Laboratory. Basically, this test was to determine if exposure to high power sonar transmission degrades the panel in any way. After the first 65 hours of test a cracking and discoloration was noticed. An additional 163 hours of testing was accomplished without an increase in severity of the defects noted.

A segment of the 5' square panel was returned to The B.F. Goodrich Company for examination and an explanation of noted discrepancies.

Upon receipt of the panel segment, it was immediately examined by project personnel, a consulting microscopist, and photographs taken. Figures 16 and 17 depict the specific areas in question as indicated by the Underwater Sound Laboratory. The detailed description and explanation of defects as discovered by microscopist is included in Appendix III. It was ascertained that the surface condition noticed was a result of a combination of conditions.

- (a) Rubber flow lines - The surface neoprene plies were added in sections during construction of the panel. The resulting joint is not always perfect and rubber flow during cure is expected to fill the gap and knit adjacent plies together. The flow lines may be visible after cure because of materials on the surface, such as mold release agents or soapstone, which are carried along by the movement of the rubber. The rubber flows into a gap until it is stopped by the opposing flow. This line where the flow stops may also be visible because of flow patterns on the surface. This results in visible lines which for all practical purposes have no depth.
- (b) Mold impressions - Rubber ridges and depressions apparent on the panel surface are a result of machining marks on the insert plate used in the molding operation. The mold utilized was originally designed for a 1-1/2" thick panel, thus a 1/2" thick steel insert had to be used to obtain the desired 1" thickness. In addition, other slight mold surface irregularities, i.e., pits, gouges, weld droplets, etc., were also transferred to the panel.

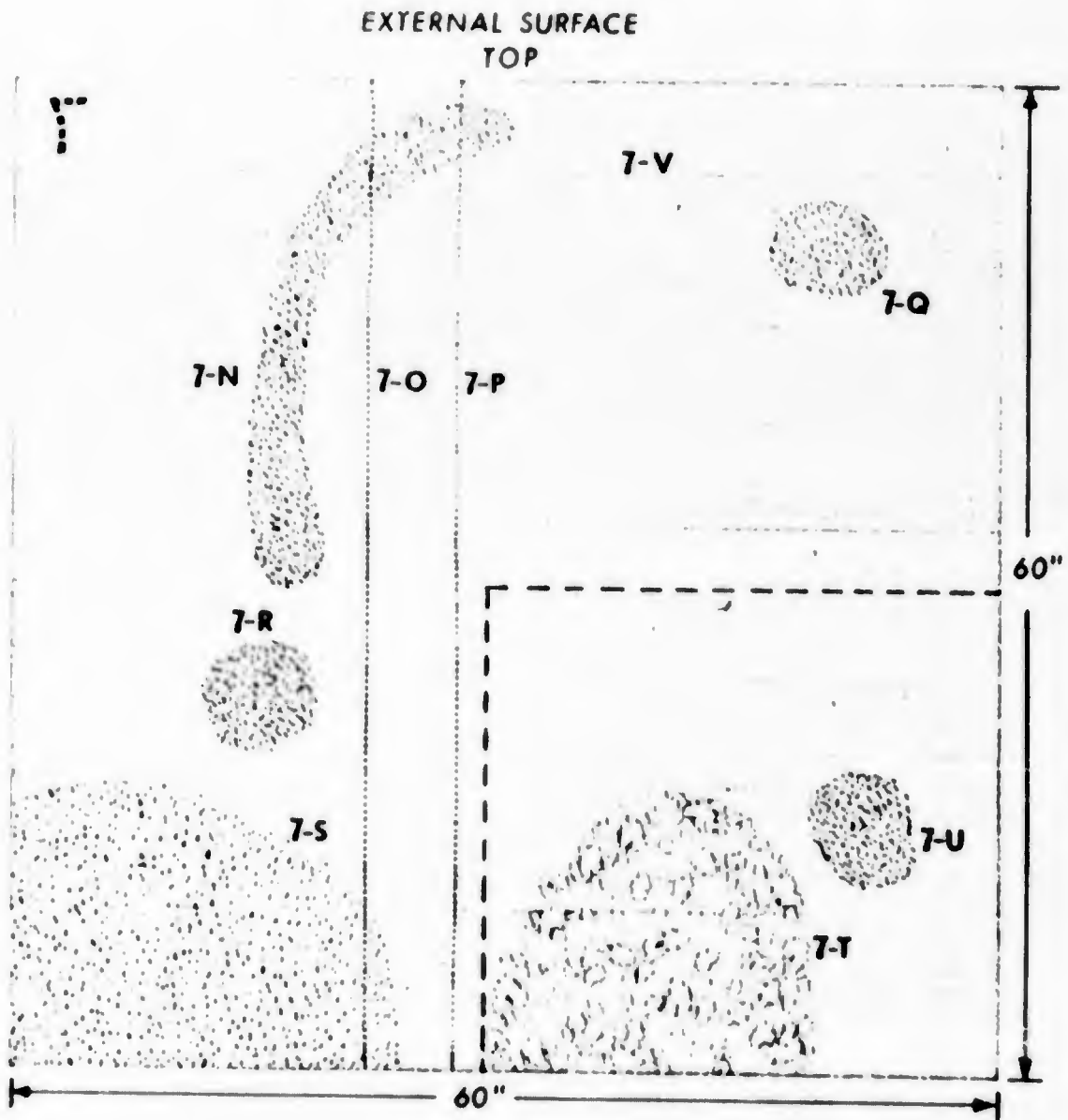


FIGURE 16
POSSIBLE EXTERNAL AREAS AFFECTED
BY HIGH POWER SONAR TRANSMISSION

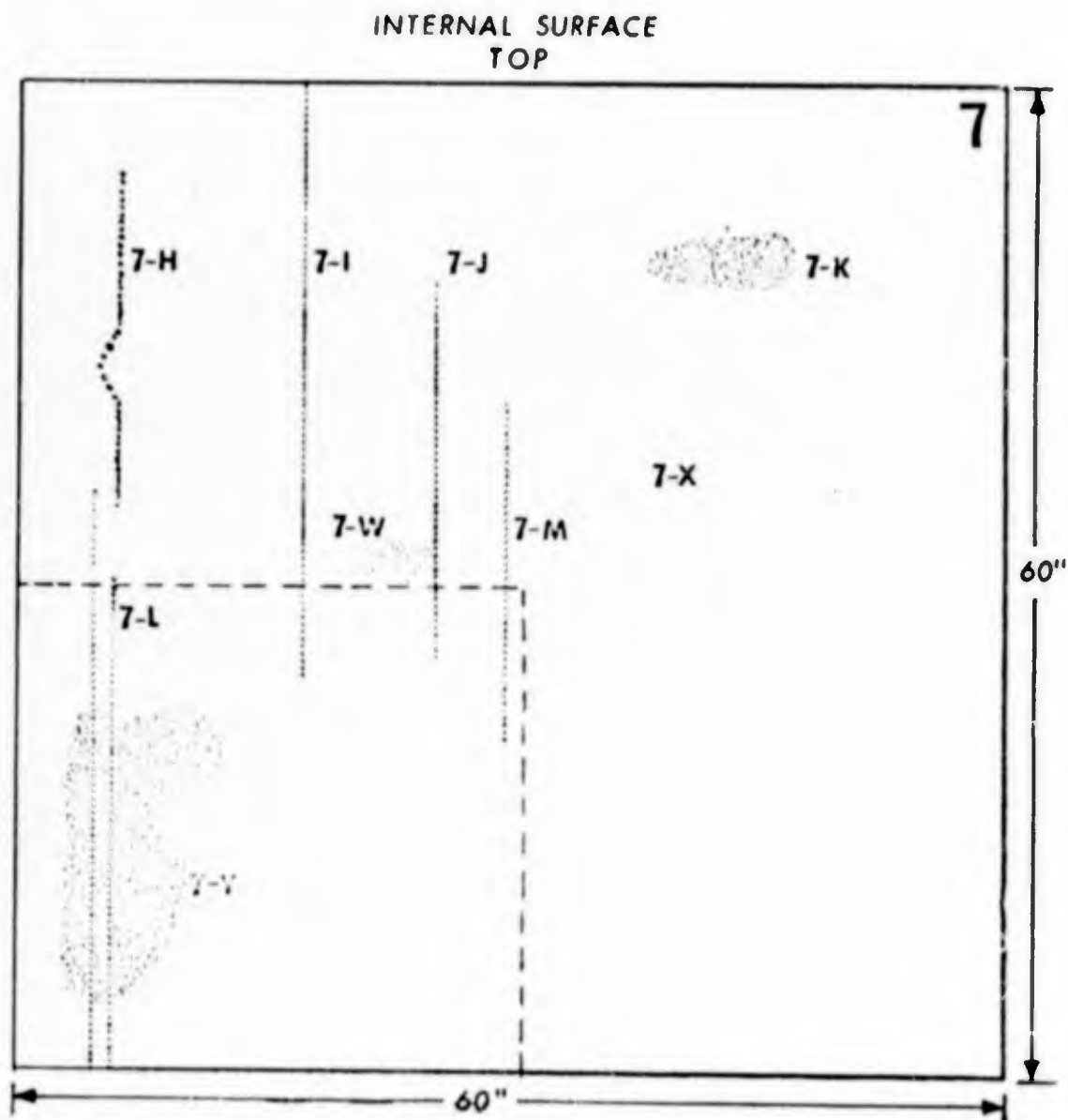


FIGURE 17
POSSIBLE INTERNAL AREAS AFFECTED
BY HIGH POWER SONAR TRANSMISSION

- (c) Discoloration of filler 429348 - Surface voids were filled with the heavy rubber filler, previously discussed, which is dark gray in color. During the subsequent cleaning operation these irregularities were seemingly masked. The solvent, Methyl Ethyl Ketone, used for cleaning, becomes black from buffing dust and dissolved neoprene and acts like a paint, furnishing a uniform color to the panel surfaces. Subsequent handling, immersion in water and etc., washed this cover off the filler yielding the original gray color.

This was accomplished without degradation to the filler.

Thorough examination of this test panel, including microscopic study resulted in the conclusion that the existing irregularities were seemingly masked during the cleaning phase and then uncovered again during subsequent handling and testing. Also, during this examination it was not possible to discover any defects such as ply separation, voids, cable migration, or other general degradation which could be construed as a direct result of acoustical energy bombardment.

f. Conclusions

- 1) Five plies of weftless wire fabric properly oriented, will furnish the required strength for withstanding anticipated service conditions.
- 2) Metal Primer 220 furnishes the best adhesion between the 35003 Neoprene and the brass plated steel wire.
- 3) Adhesive 369 yields the best degree of adhesion for Neoprene to Neoprene bonding.
- 4) There are no deleterious effects on the tensile strength of a single ply of W-70100 wire stock after 4 months immersion in sea water at 80 psig when coated with .020" 35003 Neoprene.
- 5) The standard cure for a 1" panel thickness would be sufficient for the entire panel; residual heat will cure the fill sections.

Contract N0bsr 89483
Serial No. SS041-001
Task 8156

- 82 -

Report No. 17
Phase I Interim Report
30 September 1964

- 6) Testing of representative acoustic window panels showed that there was no acoustical absorption or reflection detectable in the frequency range of interest.
- 7) Utilizing information obtained about these materials efforts can continue on determining actual ply sequence, seaming techniques and ship attachment method.

8. Acoustic Window Construction Study

a. Summary

The most reliable and operationally acceptable acoustic window was found to be constructed of five plies of weftless wire fabric wrapped around a bead cable. The window should be constructed of four panels ultimately spliced together to form a continuous one piece window. Attachment to the ship will be accomplished using a bead seat (welded to the ship) - bead clamp retention-sealing system.

b. Introduction

With the acceptability and desirability of the weftless wire concept proven, a program was established to determine the exact construction of the acoustic window. For this study several separate theoretical and analytical fabrication and testing programs were conducted. These included:

- 1) Determination of the optimum number and orientation of the weftless wire plies
- 2) Method of wrapping ply cables around bead cable
- 3) Method of attachment to the ship
- 4) Means of fairing acoustic window to ship
- 5) Procedure, techniques and cement to be used in fabricating the window.

In performing these studies, with the utilization of representative small scale samples, certain limitations were recognized. These, arising primarily from small sample end and edge effects, would furnish somewhat erroneous results. However, realizing this, data analysis was directed toward ultimately testing a full size prototype panel. In turn, testing of this prototype panel would furnish accurate test data and permit finalization of membrane characteristics thus permitting completion of the full size prototype acoustic window design.

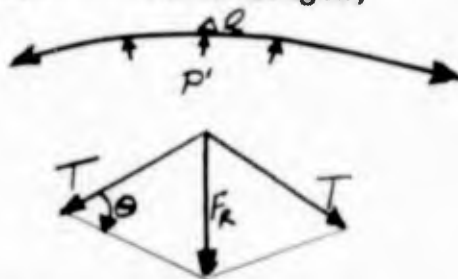
c. Force Distribution in the Acoustic Window

A study of the force distribution in the rubber window membrane was necessary to accurately predict its performance under normal service conditions and permit fabrication and testing of representative sample sections.

ΔT_{11} and ΔT_{22} result from the movement of the dome thru the water, from cables seeking the true geodesic curve and from any changes affecting cable tension. For our purposes they are insignificant since the flexible nature of the membrane will cause them to reach a state of equilibrium.

R_1 and R_2 are radii of curvature.

To develop the formulas for pressure distribution on the cables, consider an element of cable length,



where F_R = Resultant Force

T is the force at each end of Δl (tangential action)

P' = pressure acting on a cable, $P' = \frac{P \text{ lbs./in}^2}{N \text{ cables/in}}$

$$F_R = 2T \sin \frac{1}{2} \theta = P' \Delta l$$

for small θ ,

$$\sin \frac{1}{2} \theta = \frac{1}{2} \theta$$

Substitute this in (2) we get

$$T\theta = P' \Delta l$$

$$T\theta = P' R\theta,$$

$$P' = \frac{T}{R} \quad (\text{lbs/in})$$

where R is the radius of curvature taken by Δl .

The equation for expressing the state of equilibrium for a pressurized flexible membrane such as the acoustic window is,

$$(1) \quad P_{diff} = \frac{T_{11}}{R_1} + \frac{T_{22}}{R_2} \quad {}^{1,2}$$

¹Timoshenko, "Strength of Materials", 3rd Edition, Part II, P 119.

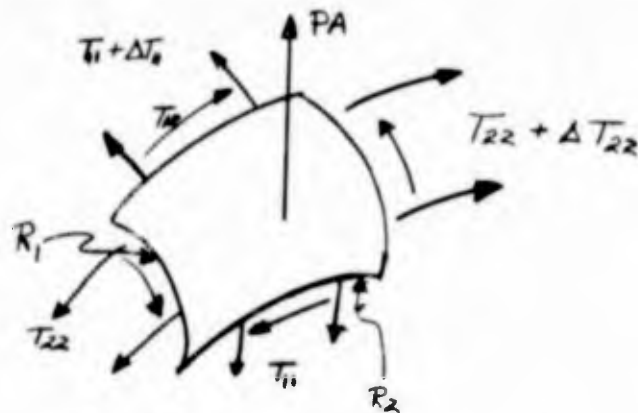
²Equation 1 obtained by multiplying Timoshenko's expression by thickness and converting to this notation.

To derive the formulas from which strength and deflections are determinable it shall be assumed that a cross-section taken vertically or horizontally and perpendicular to the surface of the membrane shall approximate an arc of a circle.

The deflection of the membrane due to the pressure differential between the inside and outside of the dome is dependent upon the pressure coefficient factor. Although this factor varies from the top to the bottom of the dome, an average value will be taken for each vertical cross-section.

Because of the dome curvature, gathering or lapping of each ply of wire fabric stock as it is laid from the top to the bottom of the dome, is necessary for proper fit. The resulting additional build-up at the membrane boundaries will be neglected in the calculation of deflections.

If an increment of the acoustic window, as depicted, is considered, the total force (lbs. acting on the increment) is:



$$F = PA$$

where: $P =$ is pressure (lbs/in²)
 $A =$ is area of increment (in²)

T_{11} is defined as the cable force per inch (lbs/in) along X-direction acting vertically, T_{22} as the cable force per inch (lbs/in) along y-direction acting horizontally and T_{12} and T_{21} are the cable shearing stresses which can be considered negligible. The nearly symmetrical construction and loading of the membrane causes the shearing stresses to be negligible in calculations of strength and deflection. The resultant of the total cable forces balance the hydrodynamic forces.

where, P_{diff} is the differential pressure between the inside and outside of the dome (psi)

T_{11} is the force per inch of horizontal direction acting in the vertical direction (lb/in);

T_{22} is the force per inch of vertical direction acting in the horizontal direction (lb/in);

R_1 is the radius of curvature of the membrane in the vertical plane (in);

R_2 is the radius of curvature of the membrane in the horizontal plane (in).

The differential pressure between the inside and outside of the dome at any location is,

$$P_{diff} = P_I - P_O$$

$$P_I = P_D - f(\text{depth})$$

where, P_D is the design pressure of the dome,

$f(\text{depth})$ is defined below.

$$P_O = P_W - f(\text{depth}) + P$$

where, P_W is the hydrostatic pressure at the dome draft extreme (psi);

P is the hydrodynamic pressure due to the speed of the ship (psi).

The expression $f(\text{depth})$ is a correction factor for the hydrostatic pressure at a point on the dome located above the maximum hydrostatic pressure point.

$$f(\text{depth}) = \frac{d \cdot \sigma}{144} h_1$$

where, h_1 is the distance of a point above the draft extreme point of the dome (ft);

d is the density of standard water, (62.4lb/ft³);

g is the acceleration due to gravity (32.17 ft/sec²);

σ is the specific gravity of sea water (1.03).

The hydrodynamic pressure is given by,

$$P = \frac{1/2 \rho C_p U^2}{144g}$$

where, C_p is the average pressure coefficient at a point on the dome;

U is the speed of the ship (ft/sec).

Therefore,

$$P_{diff} = P_D - f(\text{depth}) - [P_W - f(\text{depth}) + P]$$

or (1)
$$P_{diff} = P_D - P_W - P$$

The effect of the sea state upon P_{diff} is discussed in other sections of this report.

With perspective normal to the membrane, choose the horizontal axis as X and the vertical axis as Y. The typical dome construction consists of families of cables; n_V families making angle β_1 and n_H families making angle β_2 and $-\beta_2$, respectively with the X-axis. Let the number of cables per inch for each family be N. The total number of cables per X-inch is

$$n_V N \sin \beta_1 + n_H N \sin \beta_2$$

The total number of cables per Y-inch is

$$n_V N \cos \beta_1 + n_H N \cos \beta_2$$

Let T_V be the tension in each vertically directed cable and T_H be the tension in each horizontally directed cable.

Then the Y-force in each cable of a family making angle β_1 and $\pm \beta_2$ is,

$$T_V \sin \beta_1 \text{ and } T_H \sin \beta_2 \text{ respectively.}$$

The X-force in each cable is,

$$T_V \cos \beta_1 \text{ and } T_H \cos \beta_2 \text{ respectively.}$$

Therefore,

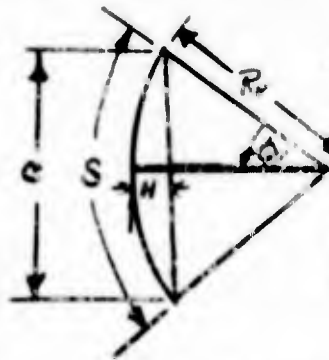
$$T_{11} = T_V \sin \beta_1 (n_V N \sin \beta_1) + T_H \sin \beta_2 (n_H N \sin \beta_2)$$

$$T_{22} = T_V \cos \beta_1 (n_V N \cos \beta_1) + T_H \cos \beta_2 (n_H N \cos \beta_2)$$

Equation (1) can now be written as,

$$(2) \quad P_{diff} = \frac{n_V N T_V \sin^2 \beta_1 + n_H N T_H \sin^2 \beta_2}{R_V} + \frac{n_V N T_V \cos^2 \beta_1 + n_H N T_H \cos^2 \beta_2}{R_H}$$

At a point on the dome the cable tensions are related to the deflection of the membrane caused by the differential pressure at that point.



The figure shown here represents a vertical cross-section. It is a plane perpendicular to the membrane surface. Before a pressure differential is developed the dimensions as shown represent those for a membrane increment strip. The ends of the strip are anchored.

anchored (both ends)

When a pressure differential is developed:

S	changes to S + dS
ϕ_V	changes to $\phi_V + d\phi_V$
R_V	changes to $R_V + dR_V$
H	changes to H + dH
C	remains constant

The problem is to find the elongation, e, of the strip with respect to its original length,

$$\frac{e}{S} = \frac{dS}{S}$$

The following relations are true:

$$\begin{aligned} S &= R_V \phi_V \\ C &= R_V \sin \phi_V \\ H &= R_V (1 - \cos \phi_V) \end{aligned}$$

By differentiating, solving for dS and dividing by S we get:

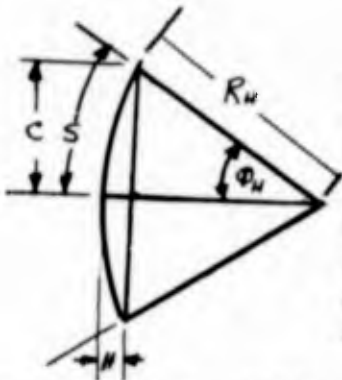
$$\frac{dS}{S} = \frac{(\sin \phi_V - \phi_V \cos \phi_V) dH}{R_V \phi_V (1 - \cos \phi_V)}$$

or

$$\frac{e}{S} = \frac{\Delta}{R_V} \left[\frac{\sin \phi_V - \phi_V \cos \phi_V}{\phi_V (1 - \cos \phi_V)} \right] \approx \frac{T F^1}{D^2}$$

where $\Delta = dH$, the deflection of the strip (in);
 $F =$ elastic stretch factor (in²/lb);
 $D =$ nominal diameter of cable (in).

(3) It follows that $T \approx \frac{\Delta D^2}{R_V F} \left[\frac{\sin \phi_V - \phi_V \cos \phi_V}{\phi_V (1 - \cos \phi_V)} \right] \approx T_V$



The figure shown here represents part of a horizontal cross-section. It is a plane perpendicular to the membrane surface. Before a pressure differential is developed the dimensions as shown represent those for a membrane increment strip. The ends of the strip are not anchored.

When a pressure differential is developed:

S	changes to S + dS
ϕ_H	remains constant
R_H	changes to $R_H + dR_H$
H	changes to H + dH
C	changes to C + dC

The problem is to find the elongation, e, of the strip with respect to its original length,

$$\frac{e}{S} = \frac{dS}{S}$$

The following relation is true:

$$S = R_H \phi_H$$

¹Supposing that the strip is a single cable - Macwhyte Wire Rope Co., Catalog G-17.

By differentiating, solving for dS and dividing by S we get:

$$\frac{dS}{S} = \frac{dR_H}{R_H}$$

or

$$\frac{e}{s} = \frac{\Delta}{R_H} \approx \frac{I F}{D^2}$$

where $\Delta = dR_H$, the deflection of the strip. Note that dR_H of this equation equals dH of equation (3).

$$(4) \text{ It follows that } I \approx \frac{\Delta D^2}{R_H F} \approx T_H$$

Divide (4) by (3)

$$(5) \quad \frac{T_H}{T_V} = \frac{R_V}{R_H} \left[\frac{\phi_V (1 - \cos \phi_V)}{\sin \phi_V - \phi_V \cos \phi_V} \right] \left(\frac{F_V}{F_H} \right)$$

$$\begin{aligned} \text{From (2)} \quad P_{diff} &= T_V \left[\frac{n_V N \sin^2 \beta_1 + n_H N \frac{T_H}{T_V} \sin^2 \beta_2}{R_V} + \frac{n_H N \frac{T_H}{T_V} \cos^2 \beta_2}{R_H} \right] \\ &= T_V \left\{ \frac{n_V N \sin^2 \beta_1}{R_V} + \frac{T_H}{T_V} \left[\frac{n_H N \sin^2 \beta_2}{R_V} + \frac{n_H N \cos^2 \beta_2}{R_H} \right] \right\} \end{aligned}$$

Substitute for $\frac{T_H}{T_V}$ from (5) and solve for T_V :

$$(6) \quad T_V = \frac{P_{diff}}{\frac{n_V N \sin^2 \beta_1}{R_V} + \frac{R_V}{R_H} \left[\frac{\phi_V (1 - \cos \phi_V)}{\sin \phi_V - \phi_V \cos \phi_V} \right] \left(\frac{F_V}{F_H} \right) \left[\frac{n_H \sin^2 \beta_2}{R_V} + \frac{n_H N \cos^2 \beta_2}{R_H} \right]}$$

$$(7) \quad T_H = \left(\frac{T_H}{T_V} \right) T_V ; \quad \frac{T_H}{T_V} \text{ is determined by (5)}$$

(8) From (3):

$$\text{The deflection, } \Delta = \frac{T_V R_V F_V}{D^2} \left[\frac{\phi_V (1 - \cos \phi_V)}{\sin \phi_V - \phi_V \cos \phi_V} \right]$$

Appendix IV presents the development of a computer program utilizing the previous discussion to analyze the stretch of the membrane when subjected to internal pressurization. A case example is given. In addition this program was used to predict pressurized prototype panel contours as discussed in Section I.C.J.

The value of F , the factor of elastic stretch for the cable is obtainable, however, the cables in the window are not permitted to react to pressure independently. This is a result of the membrane construction. It is therefore necessary to find what the elastic characteristics of the membrane are. This was accomplished by fabricating and testing a series of tension samples duplicating the design membrane.

In the design of the membrane the following boundaries were set:

- 1) The maximum load to be put on a ply cable would be 110 lbs.
- 2) Cable plies wrapping around bead. Cable would be properly oriented so that approximate symmetrical loading of the bead would result.
- 3) In extreme bead contour areas additional plies will be added such that the cables will uniformly distribute the loads to the bead and add strength to the membrane.

With these stipulations a minimum factor of safety of 3 is maintained for normal operational conditions. The effect of this rule places range of loading present in the dome such that the value of F , elastic stretch, is a variable, in fact, it is a function of the cable tension.

d. Ship attachment

One of the main problems involved in this design is determining the method of attaching the acoustic window to the ships structure. During the first phase of the design study several potential methods were reviewed and the optimum method determined.

1) Bolting-Bonding

One (1) possible idea examined is illustrated in Figure 18. In this instance, depending on the shear modulus and elasticity of the stock a non-uniform load would be applied

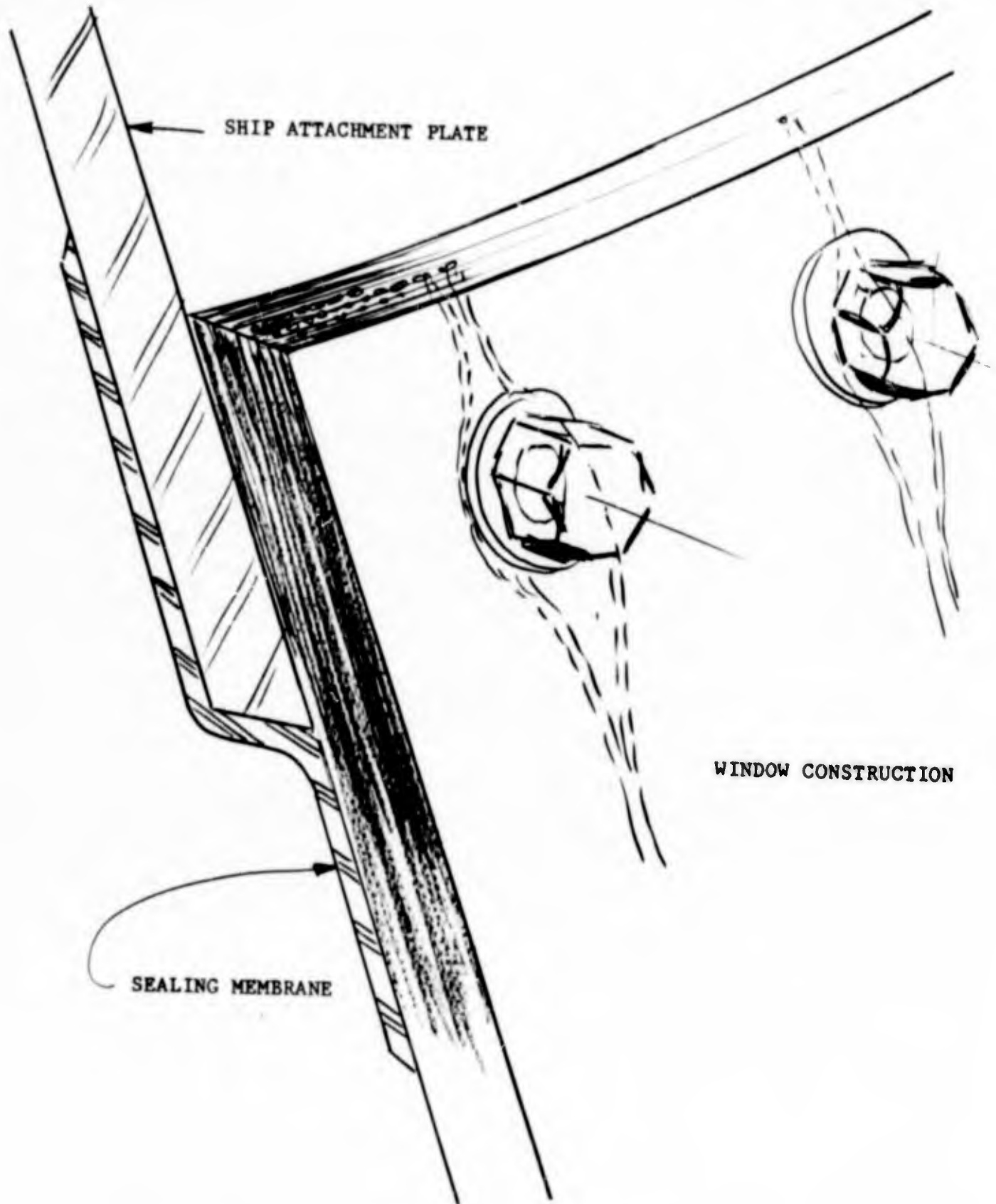


FIGURE 18

BAR BONDING - THRU HOLE BOLTING ATTACHMENT

to the cables. This arises from the necessity of spreading ply cables to permit bolt penetration. The distorted cables would take the initial loads, possibly rupturing before the other cables fully participated. In addition to this undesirable affect, under loads the thru hole would tend to elongate and impair the seal. Also the possibility of the bolt shearing thru the end of the construction negated the use of this concept.

2) Bolt-Shim Bonding

To eliminate the necessity of inserting bolts thru the construction a modification was accomplished as shown in Figure 19. A series of steel shims are bonded to the individual rubber plies and, in turn, bolted to the ships structure. In this instance retention of the acoustic window relies solely on an adhesive bond. The reliability of such a system is questionable when considering length of service, environment and loads. The complex curvature of the window would require segmented shims which in turn would present a sealing problem. The undesirable features of this system prompted a further look into this area.

3) Wrap-Bolting Technique

This concept, Figure 20, was conceived as a means of eliminating the undesirable elements of a bonding technique. An increase in mechanical retention was accomplished by wrapping the construction around a bar and then locking them together with bolts. Attachment to the ship is accomplished at the bolting point. The load as applied to the membrane attempts to pull the bar and shear the bolts. This system again requires holes thru the construction resulting in the properties previously discussed. In addition the wrap around the bar would yield a non uniform loading with the inner plies breaking before all the cushion (layers of rubber between plies) was eliminated from the outer plies.

4) Bead Design

Experienced obtained in pressure sealing tires indicated a successful attachment system could be patterned after a tire bead. This system (Figure 21) would furnish adequate retention and sealing characteristics. However, the idea of wrapping around a bar or "bead wire" was somewhat

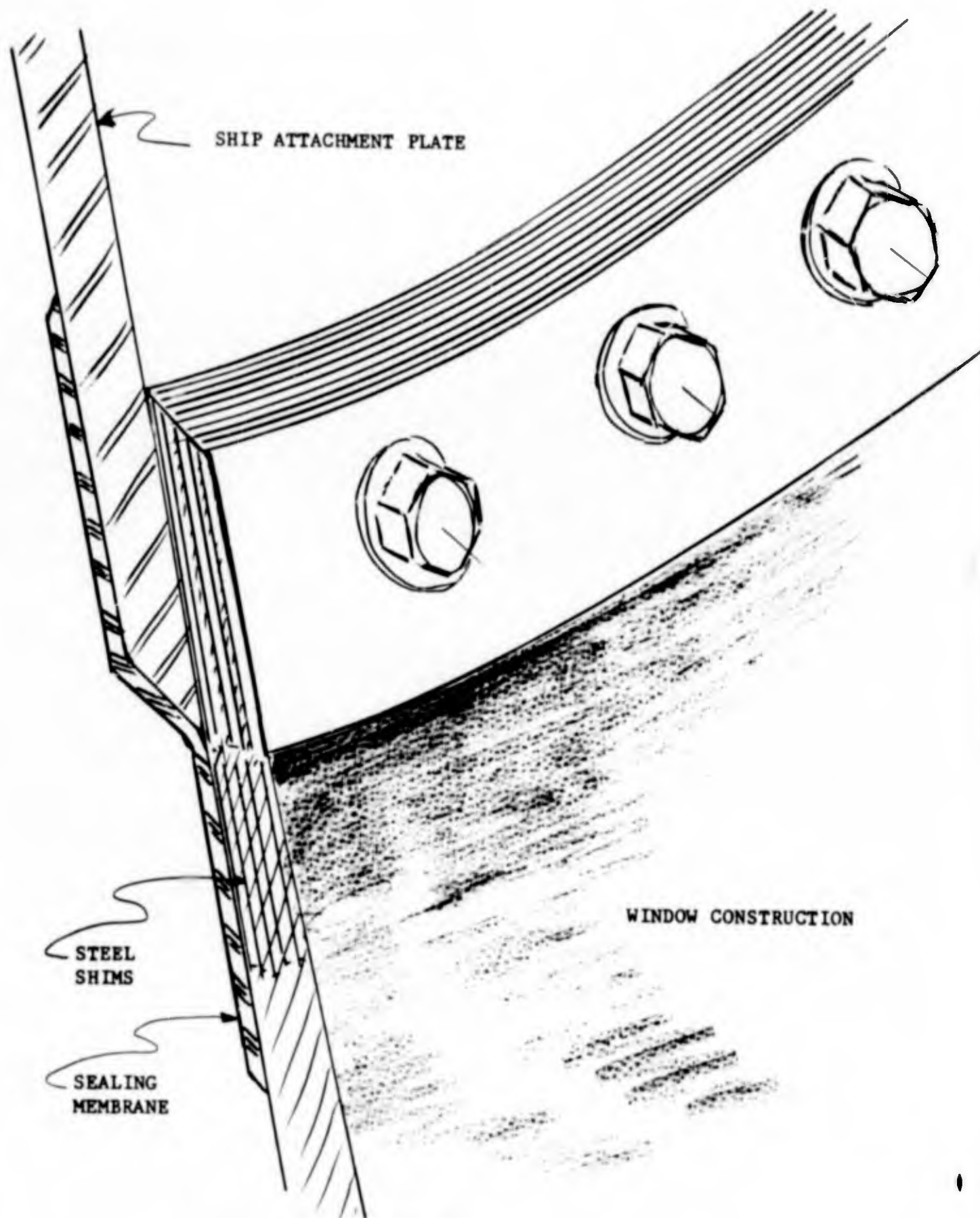
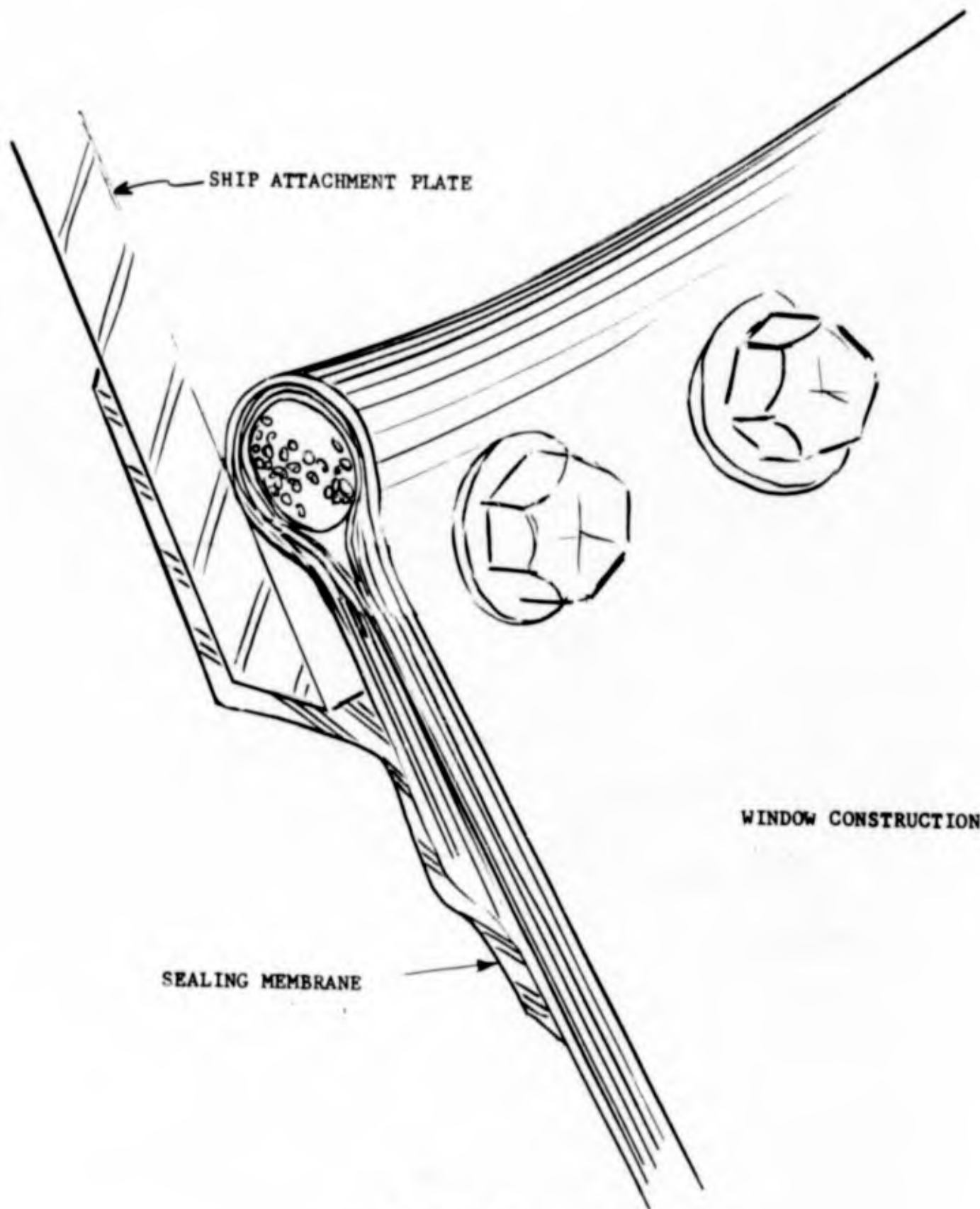


FIGURE 19

STEEL SHIM BONDING - BOLTING ATTACHMENT



SEALING MEMBRANE

WINDOW CONSTRUCTION

FIGURE 20

CONSTRUCTIONAL WRAP - BOLTING ATTACHMENT

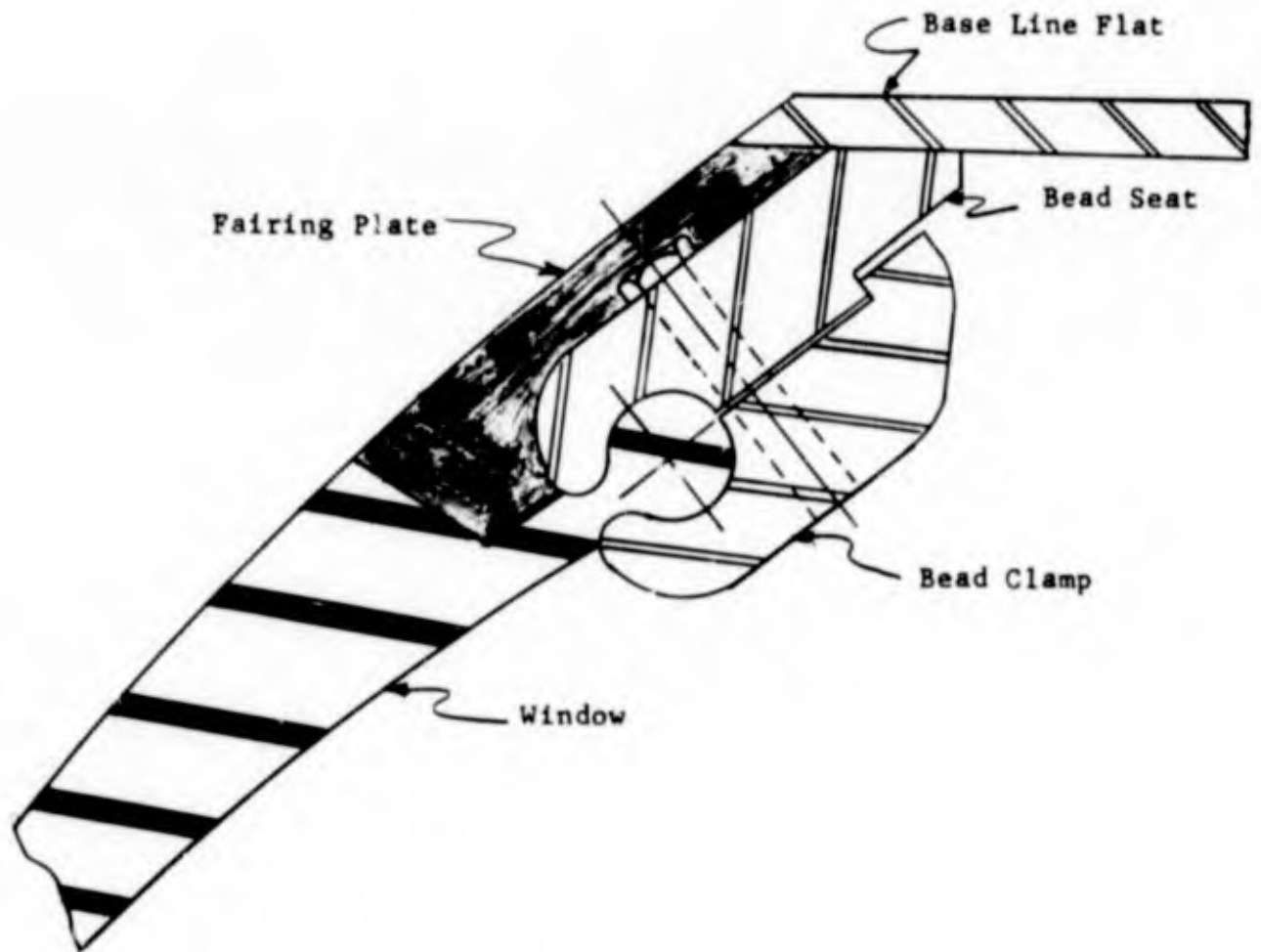


FIGURE 21
BEAD CLAMP RETENTION SYSTEM

distasteful due to non-uniform loading as previously discussed. A large part in perfecting the now tried and proven bead retention system was in perfecting an acceptable ply bead wrap around overlap system. With indications of a successful retention system design, fabrication and testing of samples was immediately undertaken.

e. Testing of Representative Window Section Samples

Determination of a satisfactory design for panel construction opened the door for a thorough investigation of the bead-panel composite. As mentioned previously the complete validity of sample testing was considered somewhat questionable due to end effects of small samples. However, it was considered advantageous to proceed and obtain this test data which would be subject to a comparison with data obtained during full size prototype panel testing. Once compiled and analyzed all the data would serve to indicate membrane characteristics.

Knowledge of the physical properties of the membrane and clamping system is important in determining their behavior when under the influence of forces which cause a pressure differential. To gain this knowledge a series of tests have been conducted. Specific characteristics sought were:

- 1) Membrane moduli of elasticity in the vertical and horizontal directions.
- 2) Constructional stretch of the membrane-bead system.
- 3) Ultimate strength of the membrane.
- 4) Fatigue characteristics.
- 5) Stabilization characteristics and the procedure for attainment.
- 6) Torque required on clamp bolts.
- 7) Bead-clamp design evaluation.

Consideration was first given to the characteristics of the reinforcing members of the membrane, that is, the .048 diameter 5 x 7 IWRC carbon steel cables. Test results, as discussed, confirm the ratings published by cable manufacturers and also supply pertinent information for the proper construction design of the dome. The cable data are:

Ultimate Breaking Strength	355 lb (min)
Yield Point	337 lb
Elastic Limit	220 lb
Elastic Modulus (based on metal cross-section)	20×10^6 psi

Window deflection is proportional to cable tension after all constructional stretch has been removed and under loads within the elastic limit of the cable. Since the elastic limit of the cable is 220 lbs., it is deemed advisable to construct the membrane such that the cables are not loaded beyond 50% of this value at 35 knots, 0° yaw and calm sea conditions. This loading stipulation, therefore, assures a safety factor of 3 with respect to the yield point.

Various tests were made to obtain data relating to the above dome characteristics.

1) 2-3/4" Bead Panel Samples:

Extensive testing was performed on representative samples of various conceived acoustic window constructions.

Determination of the most acceptable adhesive system for fabrication of the panel construction, permitted a concentrated design effort on actual construction problems.

One area of prime importance is the bead-panel attachment area extending around the periphery of the panel. The function of this area is to furnish a means of clamping the panel in place and furnish a satisfactory seal to permit dome pressurization to the design pressure.

Mathematical analysis of stresses expected in the dome construction, during specified operating conditions (35 knots, 0° yaw and calm seas), indicate that maximum tensions expected in the radial (vertical) cables are in the vicinity of 3100 lbs/inch of bead. Considering a minimum safety factor of 2, equivalent constructional strengths of at least 6200 lbs/inch of bead must be obtained.

With the previously stipulated requirements in mind, a study was initiated to investigate the most promising bead constructional concepts. These concepts were conceived through investigation and analysis of possible methods, consultation with tire bead design experts, and the theoretical and mathematical analysis of stresses in various proposed constructions.

The series of constructions outlined in Figure 22, Construction Concepts, were evaluated with respect to their ultimate strength, stress equalization tendency and producibility. This series of samples was built using the radial ply build-up only. Actual ply layup is illustrated in Figure 22 with test data and descriptive terminology shown in Table XI Bead-Panel Tensile Tests. Figure 23 shows a sample of this construction with an in process test shown in Figure 24. Figure 25 shows a second bead sample being tested and Figure 26 presents the entire Tinius Olsen Test Machine.

Analysis of the test data indicates the undesirability of a simple lap splice (Sample A) and the necessity of a complex composite overlap system (Sample H). In most instances, the necessary strength was attained from the samples; however, considering the types of failures, adhesive or bond breaks were considered unsatisfactory. Although configurations C and D yielded adequate strength characteristics, the ply layup pattern make their production use impossible. Configurations E, F, G and H, although appearing quite complex, actually are easy to fabricate.

Review and analysis of pertinent test data indicates configuration H, detailed in Figure 27, yields the necessary strength and constructional characteristics without excessive material buildups.

Considerable effort was expended on fabricating and testing 2-3/4" wide samples to determine proper bead ply lay-up as well as general panel ply construction. During the initial phase, necessary sample strength was of paramount importance.

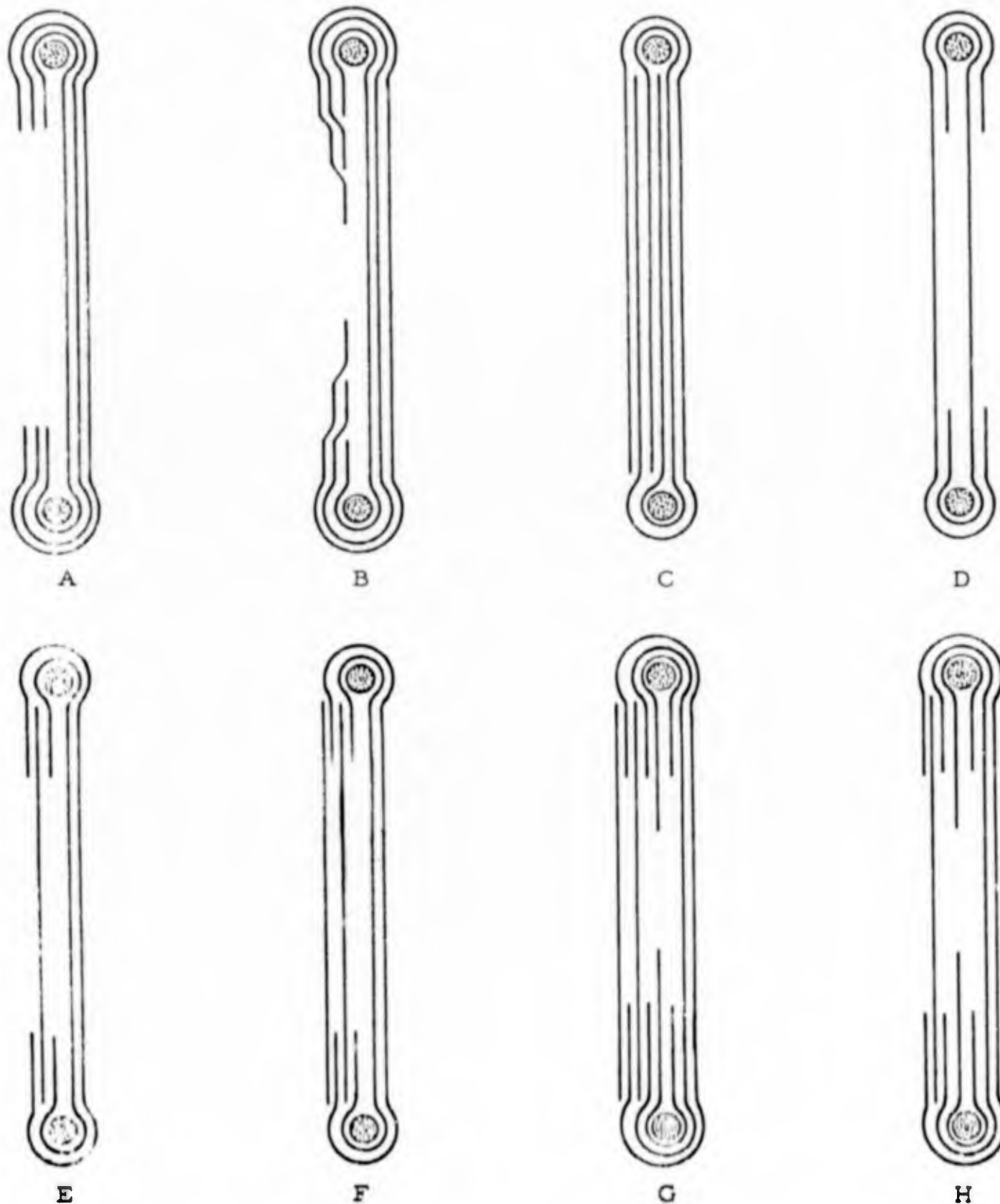


FIGURE 22
SCHEMATIC OF BEAD PANEL TEST SAMPLES

TABLE XI
BEAD-PANEL TENSILE TEST RESULTS

<u>Sample No.</u>	<u>Sample Conf.¹</u>	<u>Bead Size</u>	<u>Splice Overlap, in.</u>	<u>Total Load lbs/in.</u>	<u>Remarks</u>
1	A	1" Dia. 6x37 IWRC	1.75	3,250	Cable distorted and squeezed through retaining plates.
2	A	1" Dia. 6x37 IWRC and 1" Dia. Rod	4.6	5,090	Adhesive failure.
3	B	1" Rod	15	9,830	Adhesive failure.
4	C	1" Rod	30	12,810	Cable failure bead-plate contact area.
5	D	1" Rod	6	10,540	Panel failure.
6	E	1" Rod	6	10,980	Inner ply cable failure bead-plate contact area.
7	F	1" Rod	6	11,820	Cable failure bead-plate contact area.
8	F	1" Rod	6	11,930	Cable failure bead-plate contact area.
9	F	1-1/4" Rod	6	14,100	Cable break bead-plate contact.
10	G	1-1/4" Rod	6	14,550	3 ply break in panel area - 1 ply adhesive failure.
11	H	1-1/4" Rod	6	13,990	Panel failure.

1. Sample configuration as illustrated in Figure 2.
2. Panel failure is a Tensile failure of cables in panel.

Contract NObsr 89483
Serial No. SS041-001
Task 8156

- 102 -

Report No. 17
Phase I Interim Report
30 September 1964



FIGURE 23
BEAD-PANEL TEST SAMPLE

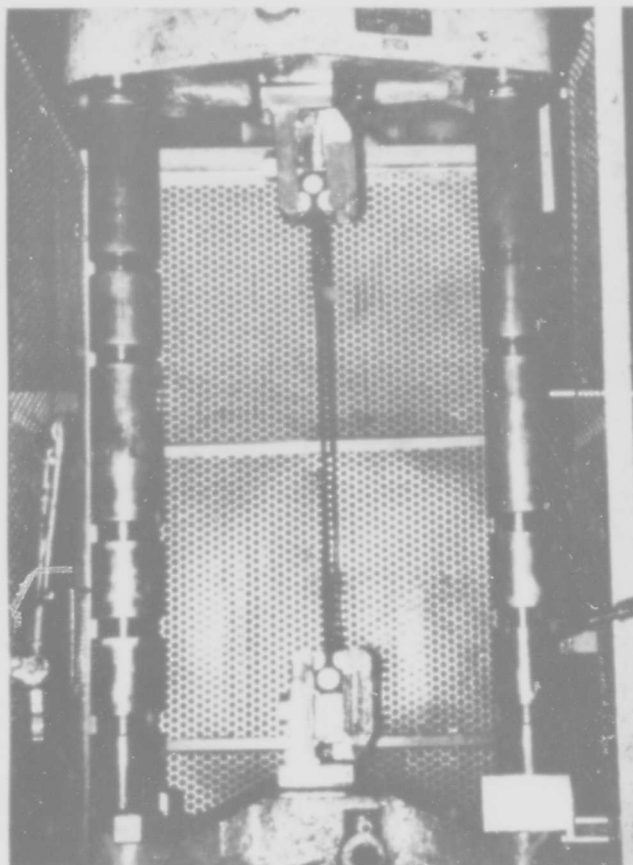


FIGURE 24
BEAD-PANEL TEST SAMPLE DURING TEST

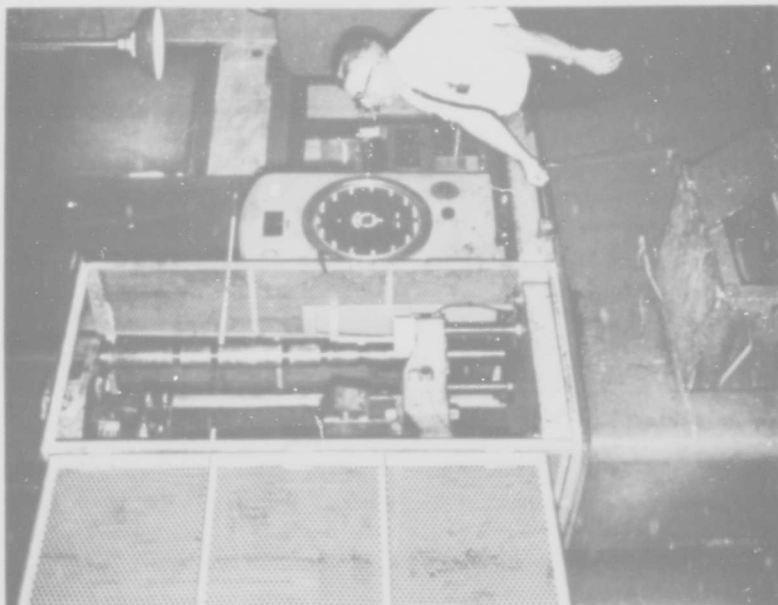


FIGURE 26
TINIUS OLSEN TEST MACHINE

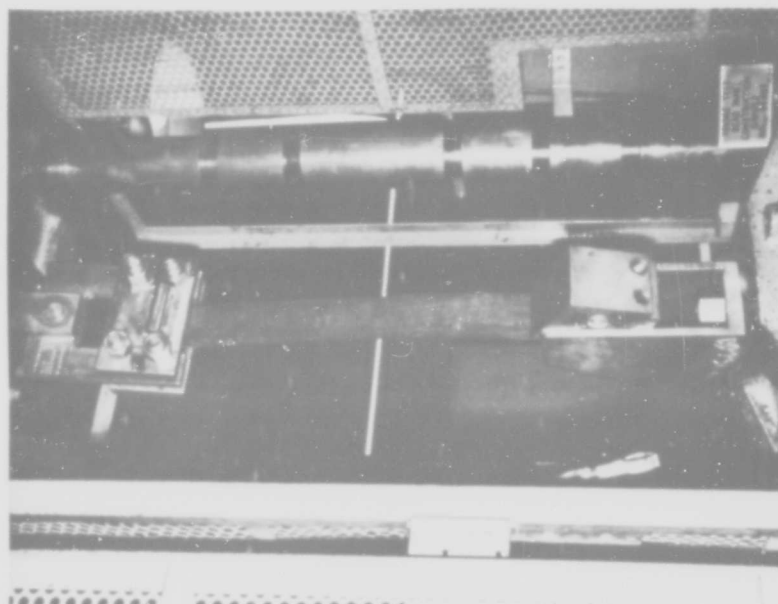
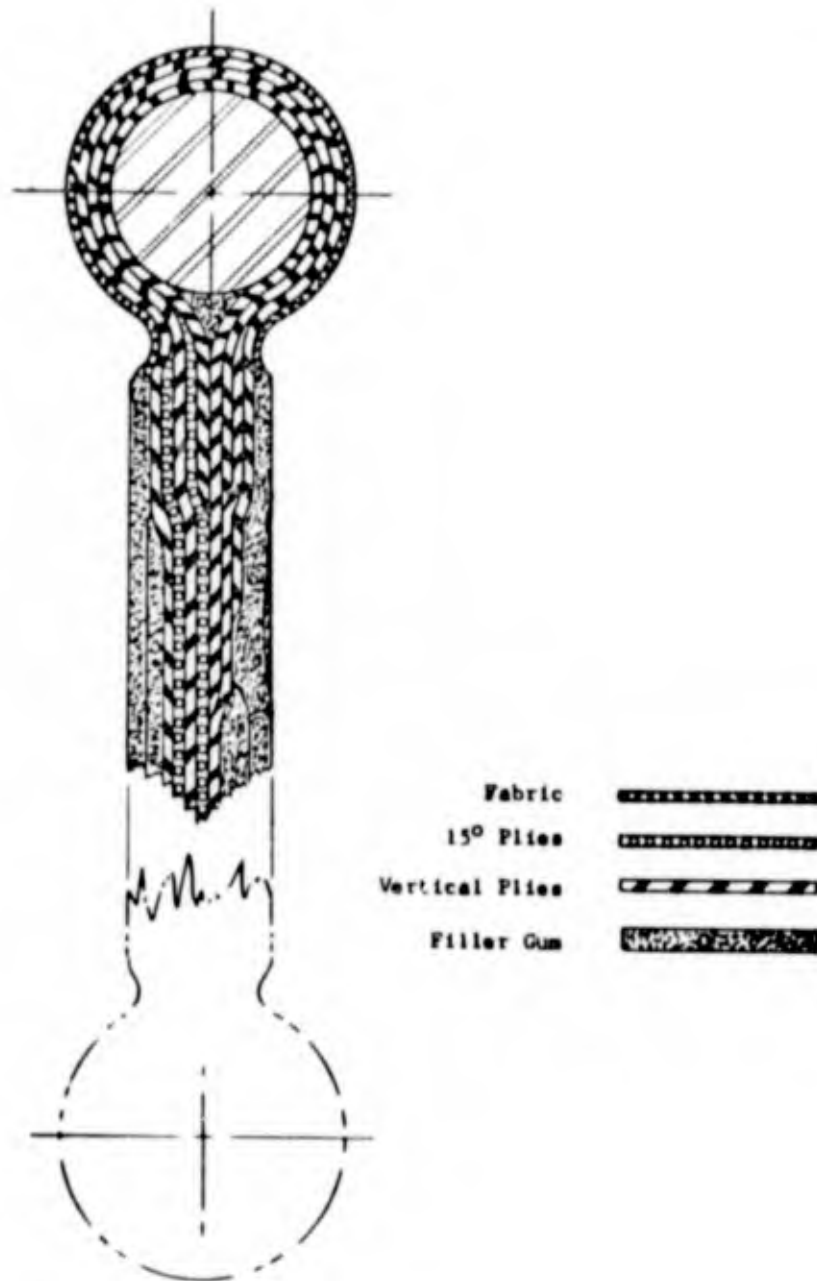


FIGURE 25
BEAD-PANEL (ANGULAR PULL)
SAMPLE DURING TEST

Contract NObser 89483
Serial No. SS041-001
Task 8156

- 104 -

Report No. 17
Phase I Interim Report
30 September 1964



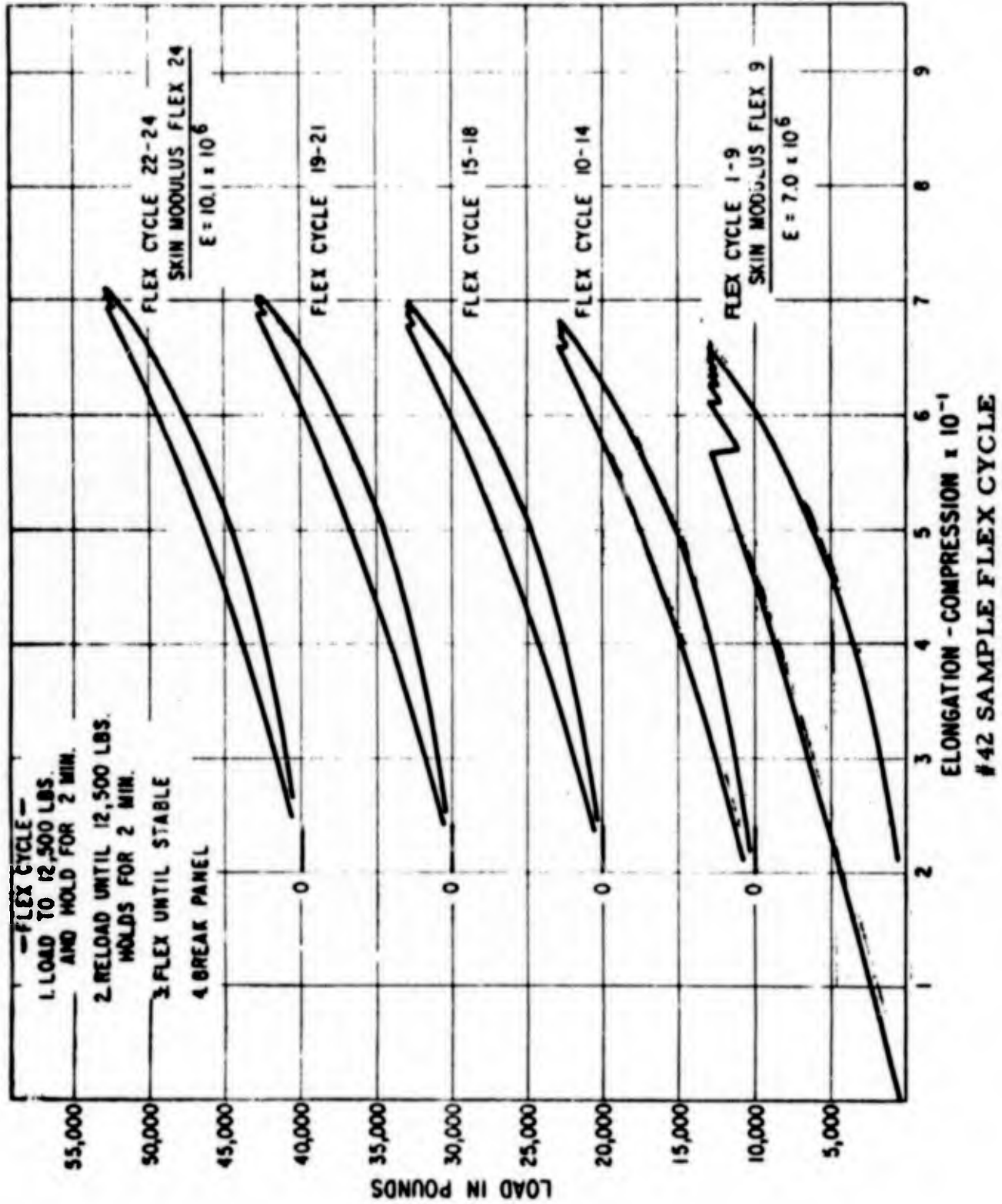
COMPOSITE OVERLAP PANEL CONSTRUCTION
FIGURE 27

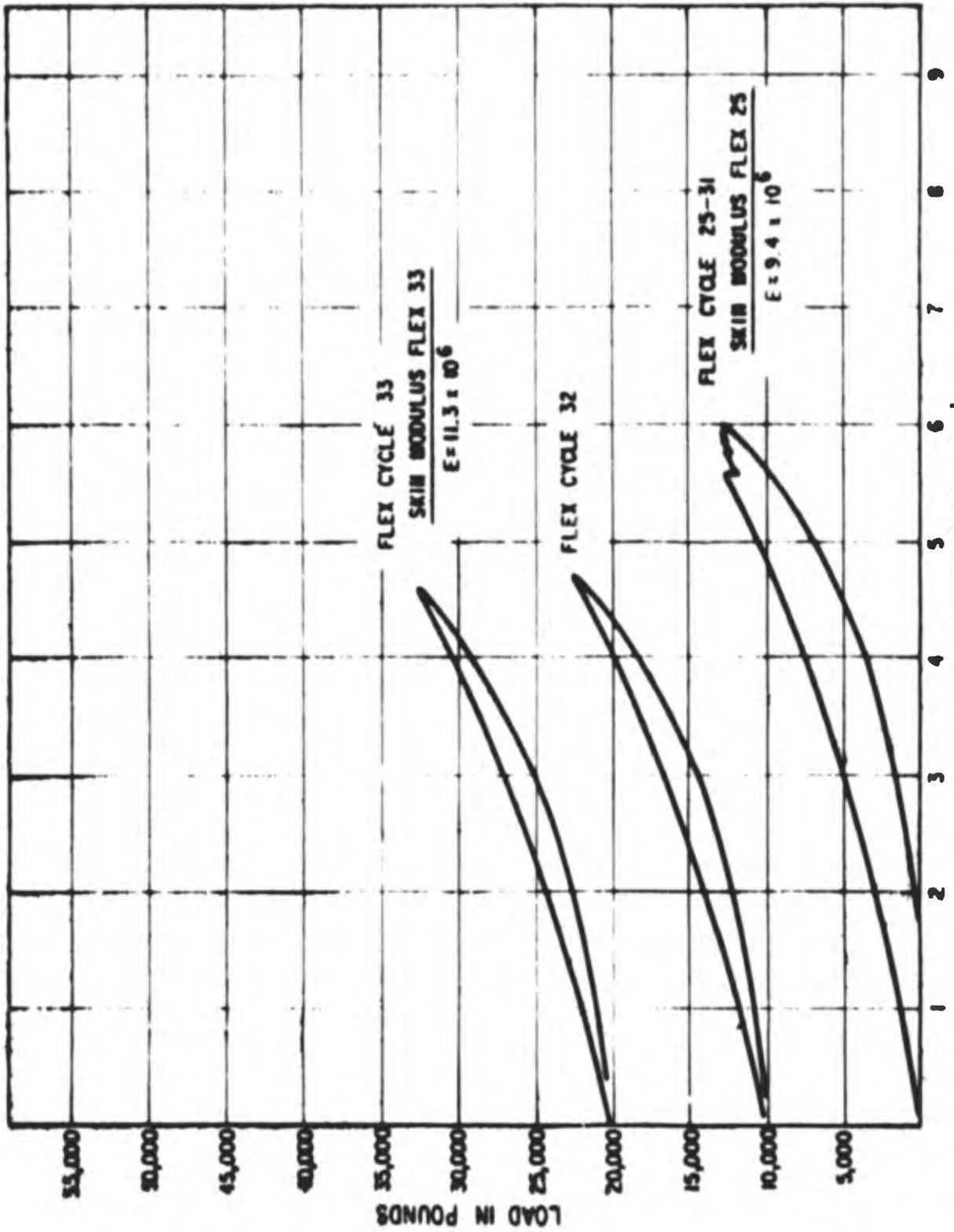
This early study phase was considered completed with the successful testing of the present panel construction concept shown in Figure 27. Subsequent to finalization of this cross sectional design, sample tests were resumed in an attempt to determine constructional stretch and fatigue strength on a short cycle basis. Samples of the construction illustrated in Figure 27 were subjected to flex cycle tests and ultimately to burst loads.

A sample of the data accumulated during this program is shown in Figures 28, 29, and 30. Measurement of the exact sample elongation was found to be difficult due to the test system, however, these data were comparable to those obtained later on the 30" x 48" panel testing program. By studying the charts it can be seen that the cycle consisted of pulling the sample to a tension of 12,500 lbs., reloading the sample at two minute intervals until there was no load loss over the two minute span. This sample required a total of 31 flex cycles to eliminate the constructional stretch and bead slippage components. On cycle 34 the panel was burst reaching a total load of 35,850 lbs. or 2.8 times the maximum allowable design load. The modulus of elasticity of the sample based on metal cross-section varies somewhat from the 7.0×10^6 noted at the first flex to 11.3×10^6 noted after the 33rd flex. The variance cannot be completely explained due to the limited number of data sensors utilized.

The most important problem discovered during this sample program involves rubber shear in the bead-bead clamp contact area. At high sustained loads of 7000#/inch or cycle loads of 5300#/inch the rubber tends to peel off the panel cables in the opposite direction of load application. This has occurred primarily in the 2-3/4" samples where the rubber is essentially unimpeded in distorting or squeezing out from under the bead clamp. This was analyzed further during later testing.

The inclusion of metal shim stock or high impact plastics has been evaluated for protecting the Neoprene in this area. However, a more accurate assessment of the situation was made during the 6" sample testing program.





ELONGATION - COMPRESSION in in.
#42 SAMPLE FLEX CYCLE
FIGURE 29

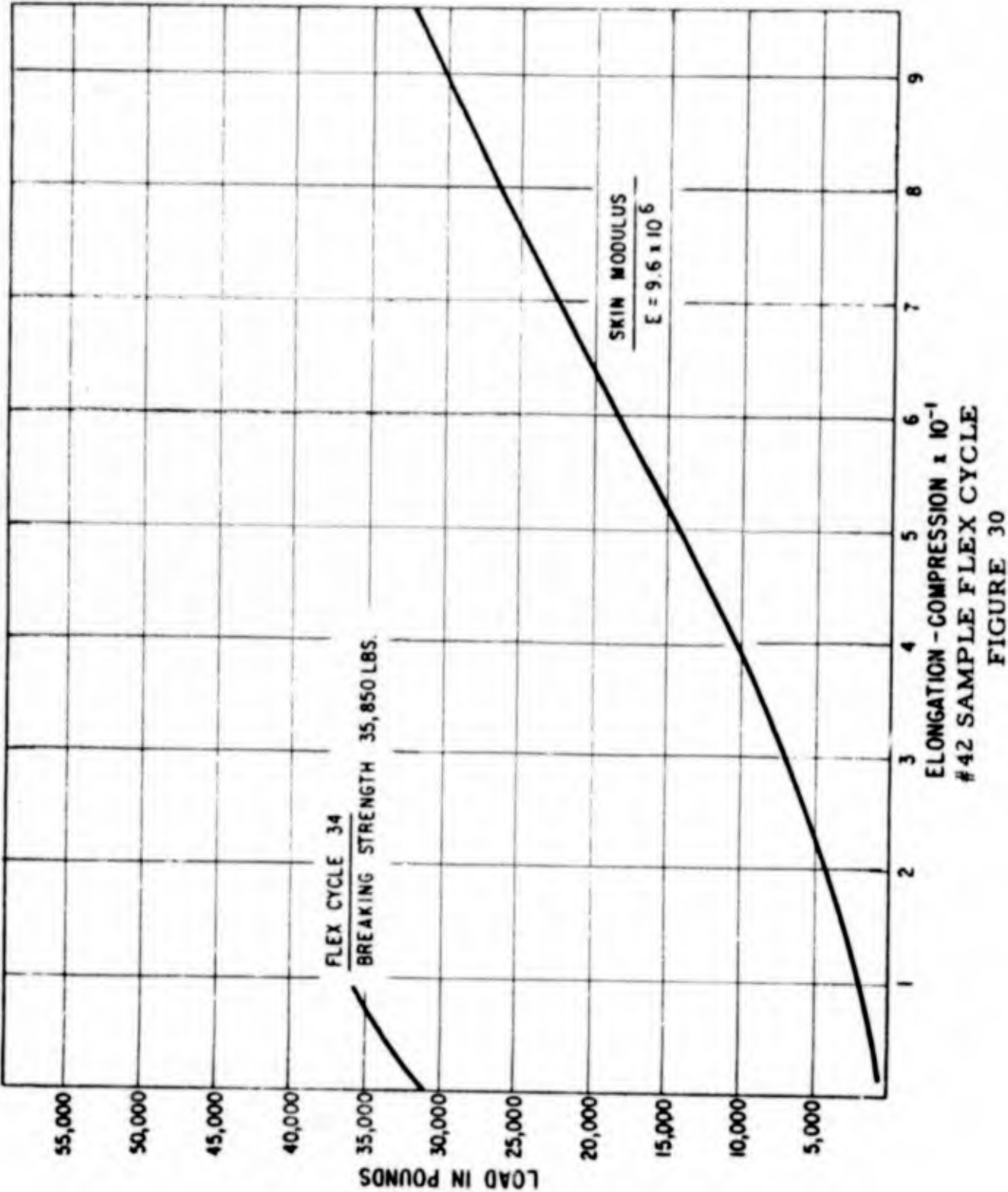


FIGURE 30

2) 30" x 48" Flat Panel Sample Testing

A mold and a pressure test fixture was designed for testing 30 inch by 48 inch experimental flat panels. These panels were fabricated in the mold after the bead construction, boundary bar attachment configuration and skin cross-section were evaluated in the 2-3/4 inch samples described above. After curing, the panel was placed in the test fixture and subjected to uniform pressure distribution by means of a pressure bag. Deflections of the panel, under progressive pressure loadings were measured.

This part of the testing program was an intermediate step between 2-3/4" sample testing and prototype panel testing. A 30" x 48" flat panel, attached at the long ends with the bead design previously discussed, was utilized to obtain strength and elongation data on the proposed dome construction.

The hydrostatic test fixture, with end support only, is designed to furnish uniform pressure against the panel without the undesirable reinforcing side effects of a fully supported panel. The water used for pressurization is contained by a lightweight Neoprene coated Nylon bag. This bag, in turn, is restrained by metal surfaces on all sides except the top constructional surface. As the system is pressurized, the panel will deflect and the deflections will be measured and recorded. Figures 31, 32 and 33 show the panel at various stages.

Three (3) 30" x 48" flat panels were fabricated and tested. These panels were:

- (a) A panel with the three (3) vertical plies extending from bead to bead.
- (b) A panel with the two (2) 15° plies extending to the bead.
- (c) A panel identical to the first except a 3" splice extends from bead to bead.

Many tests were performed on the first panel in an attempt to determine the modulus of elasticity. Figure 34 illustrates the stress-strain relationship of the various panel pressurization cycles.



FIGURE 31
30"x48" FLAT PANEL OF WINDOW CONSTRUCTION

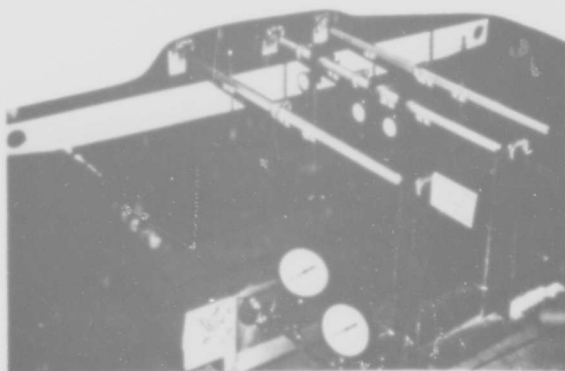


FIGURE 32
30"x48" FLAT PANEL-MOUNTED IN TEST FIXTURE

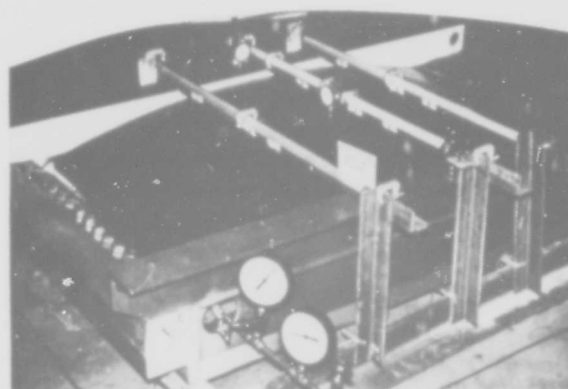
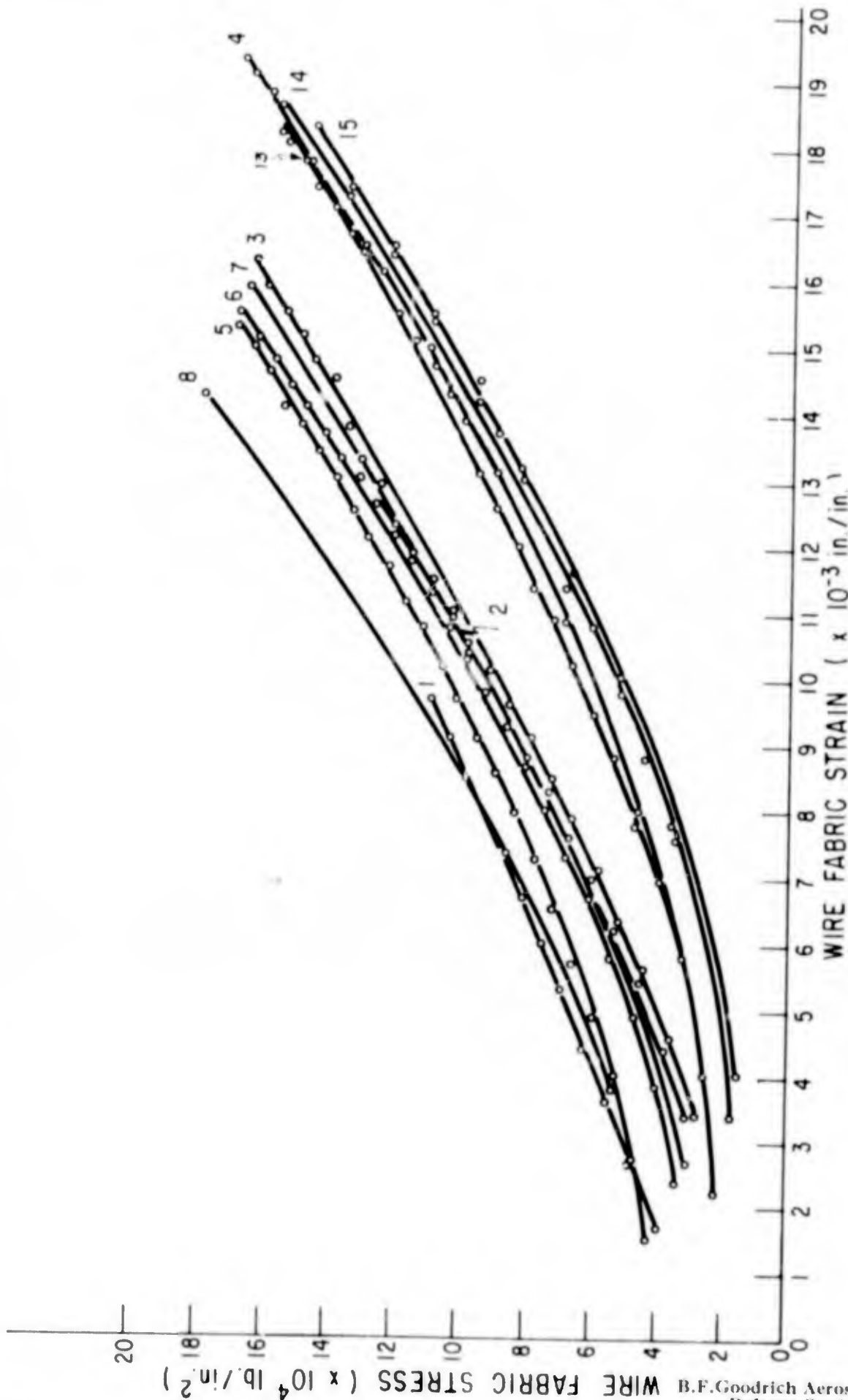


FIGURE 33
30"x48" FLAT PANEL DURING TEST

STRESS-STRAIN (METALLIC CROSS-SECTIONAL AREA) BASED ON TOTAL
MEASURED DEFLECTION - 30 x 48 PANEL-NUMBER ONE



STRESS STRAIN RELATIONSHIP OF 30" x 48" PANEL #1
FIGURE 34

Review of the test data and the subsequent plotting of the curves as shown indicate certain inherent inaccuracies. These can be attributed primarily to the early bead design used in this fixture and difficulty in measuring to the desired degree of accuracy on deflection measurements which were used to calculate strain.

It was found early in the test program that the designed bead clamp, utilizing a 3" Snub, introduced a large potential variable in panel elongation. Specifically, as the bead clamp is tightened, tension is applied to the panel construction. After considerable experimentation it was determined this tension, as applied, was not constant. Therefore, the results obtained were somewhat inconclusive. This, in addition to the potential error resulting from the inability to read to five (5) significant figures, made this entire program an indication rather than a determination of panel modulus of elasticity.

Testing of the first panel with the vertical plies extending over the beads resulted in the curves plotted in Figure 34. It is evident from the variation that an explanation of these curves is necessary. Tests 1 through 4 were conducted concurrently without changes in the panel or test fixture. The plotted curves progress in the direction of increased strain. This can be attributed to a combination of constructional stretch and accumulative bead slippage. Loads in tests 1 and 2 were equivalent to 52 psig, test 3 to 100 psig and test 4 to 111 psig. Test 5 and 6 were conducted after removal and re-installation of the test panel. The fact that test 5 and 1 are not duplicates is concluded to be the result of permanent constructional stretch and variable clamp tensions. Test 7 was conducted rapidly from 0 to 100 psig and data taken at 8 and 100 psig. The curve itself was approximated. Notice that the curve representing test 8 is to the extreme left of previous tests. This can be attributed to bead clamp re-tightening after the previous test. Tests 9 through 12 were discarded because of an error in the test set-up. Tests 13, 14 and 15 were run concurrently subsequent to panel re-installation. Increased strain noted here is due to an attempt to keep premature tension off the panel by leaving the bead clamps loose. These tests were taken to 100 psig and deflection data recorded.

It was discovered in testing the 15° panel that deflection at 25 to 30 psig was beyond the physical limits of the test fixture. Several tests as shown in Figure 35 were conducted to obtain the modulus at lower pressure ranges. The excessive deflection can be attributed to the fact that only two (2) strength plies are used and the strength plies ran at 15° to the load. The theoretical calculated modulus was in the same range as that determined from this test.

The splice panel, was installed in the test fixture and a test attempted. However, due to the incompatible design of this test fixture bead clamp a slight protuberance in the seam area prevented acceptable clamping action. Due to this severe problem no data were accumulated during this test. A subjective test cycle was conducted which was inconclusive since the clamping problem magnified a contour deviation. Splice characteristics were investigated further with 6" samples.

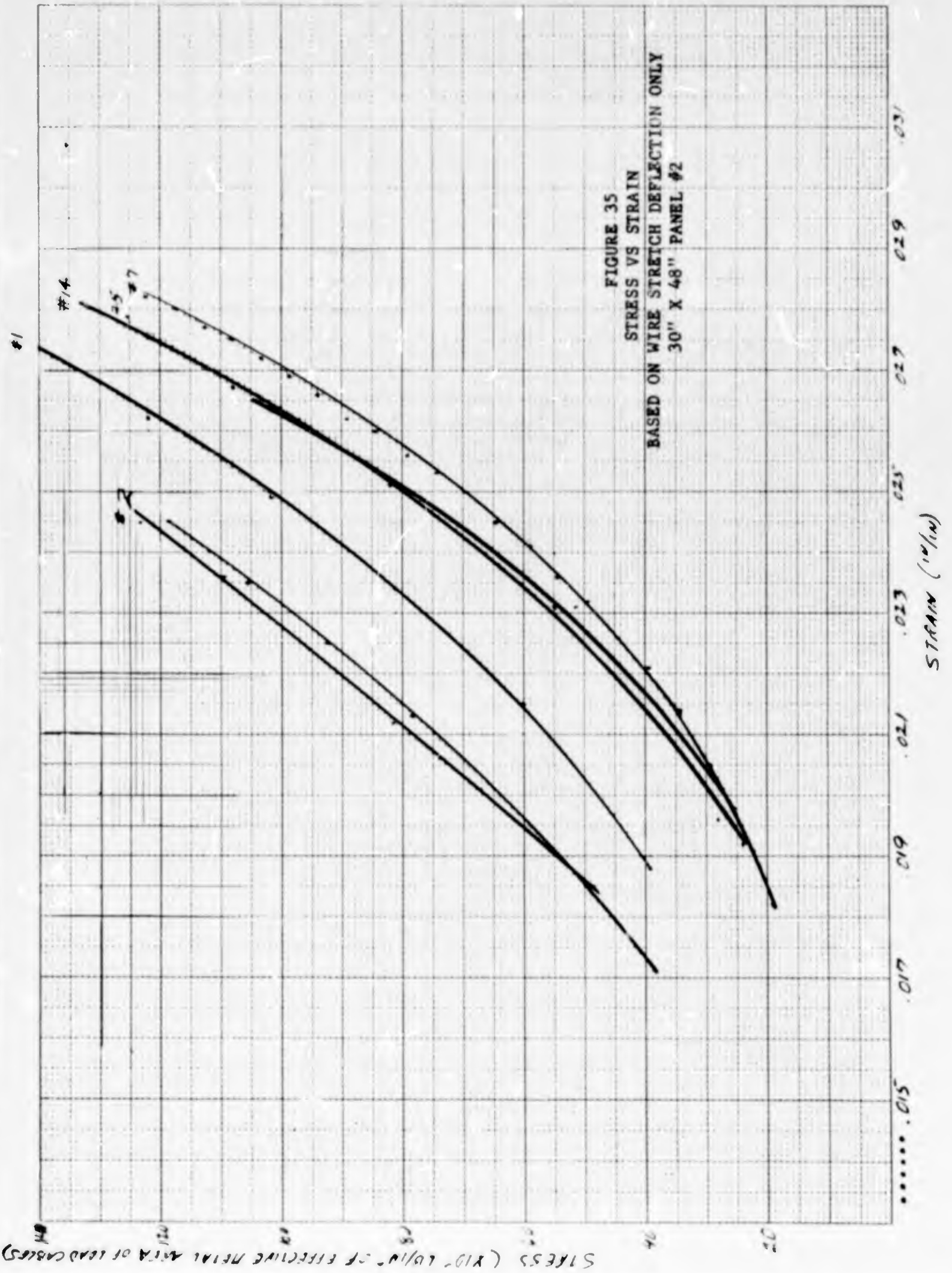
3) 6" Bead-Panel Samples

In order to increase the accuracy of the determination, a 6" wide sample testing program was initiated. Each sample tested was monitored with displacement transducers and strain gauges. With this system each distinctly different panel area was independently evaluated permitting variables and errors experienced in other tests to be eliminated or minimized.

These samples, through more thorough monitoring, furnished additional, necessary data for use in determining panel deflection during pressurization.

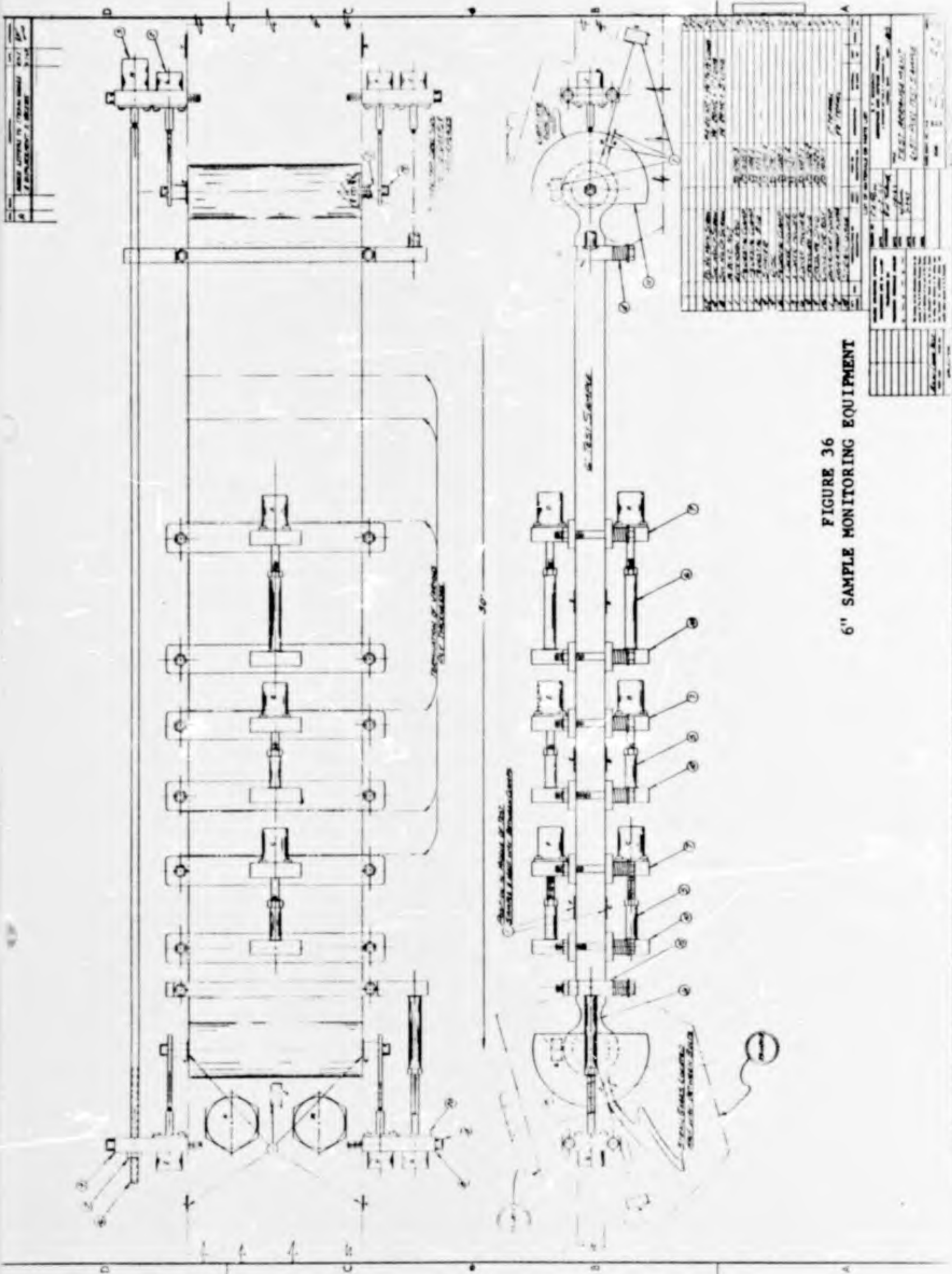
The monitoring was accomplished through use of motion transducers and strain gauges. They were located such that detailed breakdown of the sample into study-areas was obtained.

A schematic of this monitoring system is shown in Figure 36. The complete test setup including recording equipment is shown in Figure 37. A sample ready for test is shown in Figure 38.



Contract NObser 89483
Serial No. SS041-001
Task 8156

Report No. 17
Phase I Interim Report
30 September 1964



Contract NObsr 89483
Serial No. SS041-001
Task 8156

- 116 -

Report No. 17
Phase I Interim Report
30 September 1964

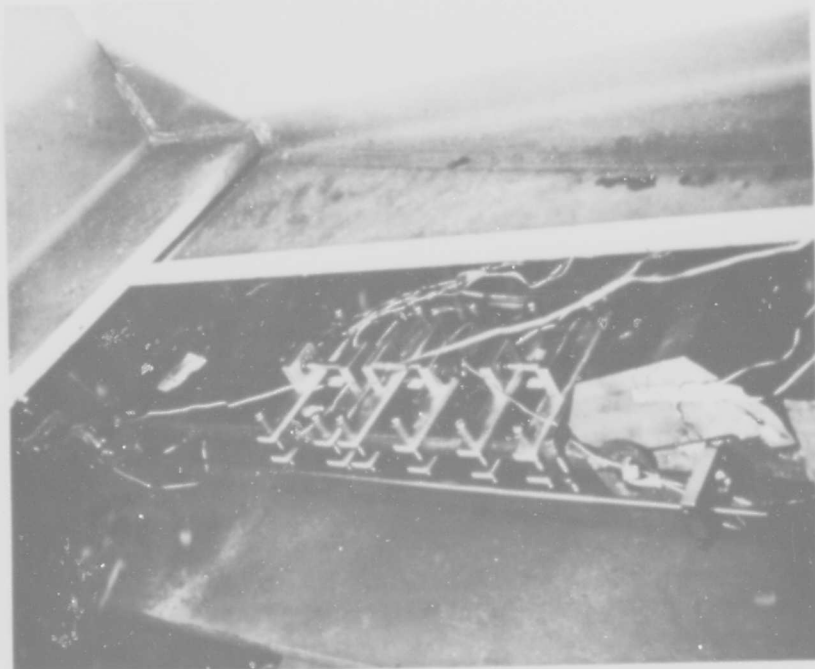


FIGURE 38
6" SAMPLE WITH MONITORS ATTACHED



FIGURE 37
ASSEMBLY OF 6" SAMPLE TEST EQUIPMENT

a) Test Equipment

The Recording Equipment used during these studies included:

System No. 1 - The system is manufactured by Minneapolis-Honeywell Co.

Conditioning Equipment

- A. 6 channels, Model No. 119 Amplifier System
- B. 2 channels, Model No. 130-2C Amplifier System
- C. 12 channels, Model No. HS-CS4 Gauge Control Units
- D. 13 channels of Potentiometers for Motion Transducers
- E. 1 channel for 3 Cox & Stevens Load Cells to read total force.

Recording Equipment

- A. One 24 channel Model No. 1108 Visicorder Oscillograph

System No. 2

Conditioning Equipment - The conditioning equipment is manufactured by B & F Instruments, Inc.

- A. One 24 channel Model No. 24-202 Bridge balancing unit.
- B. One 0 to 24 volt D.C. power supply.

Recording Equipment

- A. One 24 channel Model No. 1108 Visicorder Oscillograph manufactured by Minneapolis-Honeywell Co.

During these tests the following test procedure was followed. Specimens were instrumented as shown in Figure 36 with variations as described for each sample. The specimens were cycled numerous times at various loads ranging from zero to ultimate strength and all data was continuously recorded on the above listed equipment.

As mentioned above the main objectives of the 6" sample tests were to get more accurate physical property data of the acoustic window clamp system. An additional objective of these experiments was to determine the feasibility of using strain gauges for monitoring the acoustic window during service tests.

To check the results of strain gauges, corrolative data must be known. It was determined that the strain gauge data would be compared with data obtained from motion-transducers measuring elongation over a specified length.

When starting the testing it was assumed that the steel wire would transmit its strain through the thin layer of rubber and the rubber would be acting as an adhesive layer. Upon completion of the initial tests inconsistent data were obtained. Rubber has a very low modulus compared to the foil strain gauge. Therefore there is not enough shear stress in the rubber to transmit the strain from the steel cable to the strain gauge. If a strain gauge acoustic window monitoring system is desired for service tests additional work will be required.

Due to the fact that the 6" specimens were not completely symmetrical instrumentation was placed on both sides. When analyzing the data it was evident that the specimen was bending, thus giving some tension and compression readings on opposite sides.

b) Sample Testing

A specific report of each 6" sample tested is discussed in the following sections.

(1) Sample #1

Sample #1, shown in Figure 39, consisted of two (2) plies of WC775 weftless wire fabric wrapped around the bead. In this instance, to investigate seam strengths, a 9" splice was included. The purpose of these tests was to determine 2 ply, 4 ply, clamp and bolt, and splice characteristics.

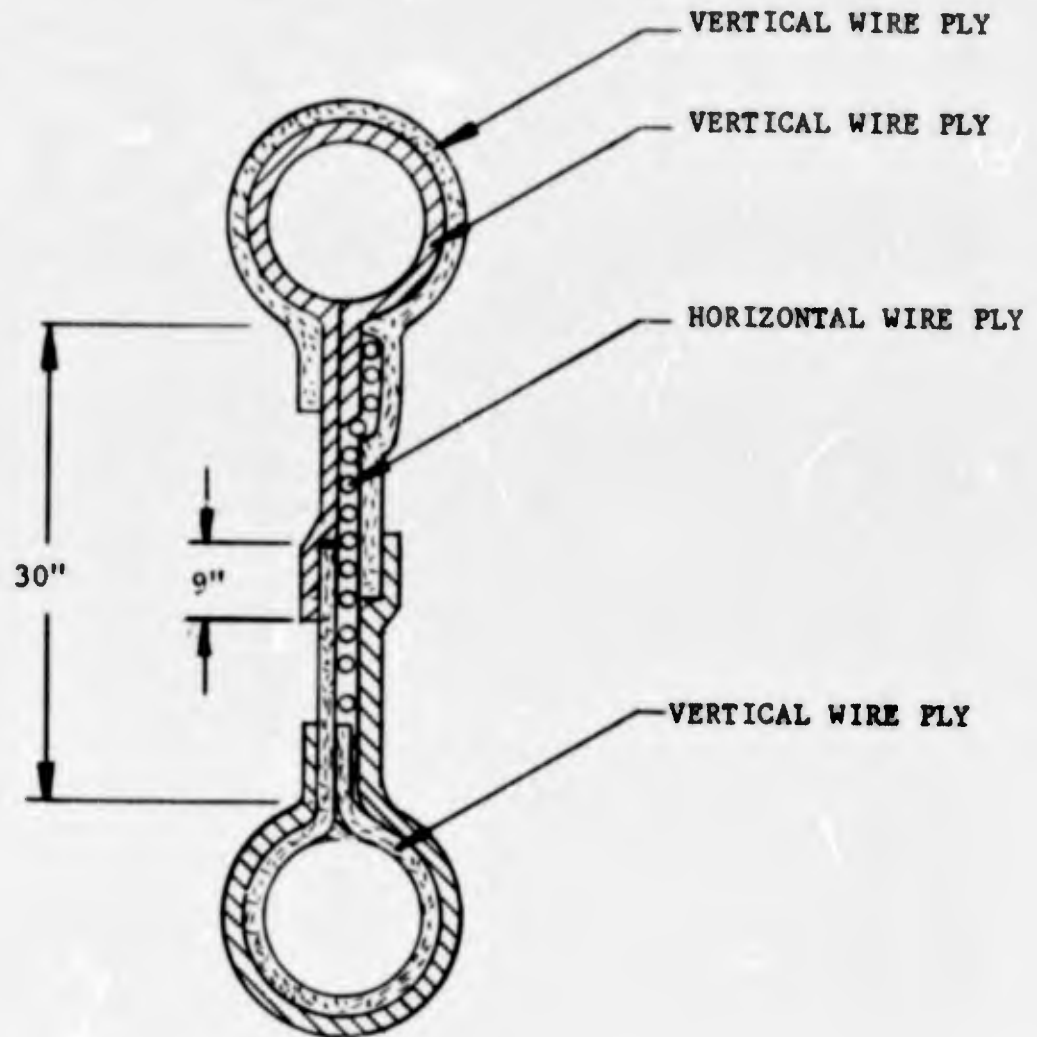


FIGURE 39
6" SAMPLE #1 CROSS SECTION

The sample was instrumented according to Figure 36 except the following sensors were eliminated: MT(G,H,I,J,K,L,M). The test cycle is shown in Table XII. The loads, in accordance with Table XII were attained, held momentarily, then released to zero. Test data accumulated during this test are shown in Table XIII. Table XIV shows the resulting theoretical clamp stresses compared to the predicted. Figure 40 and 41 present the panel results in graphical form.

Analysis of the test data and observations made are discussed at this time as a means of presenting results. During this test cycle the ply cables cut through the neoprene at the bead clamp pressure point. The side in contact with the bead clamp was more severe than the bead seat side. It appears this condition was exaggerated by the bead end retainers bending during test permitting the construction to spread and the cables nestling in between sub-layer cables. The motion transducer readings were questionable and one transducer (#8) was found after test to have its shaft forced against the adjacent clamps. The strain gauge data recorded reflected consistency of information. Bead slippage, or movement of the bead with respect to the clamp, due to constructional and elastic stretch was $3/16$ ". Membrane characteristics in the splice area are similar to those of other areas when compared on the basis of metal cross-sectional area.

(2) Sample #2

Sample #2 shown in Figure 42, was of the standard composite overlap construction. The purpose of this test was to determine 3 ply, 4 ply, 7 ply, clamp, bolt, bead and overall length characteristics. The sample was instrumented according to Figure 36 except the following sensors were eliminated: SS-J,Q,R and MT-H,I,K,L. The following were added: SR on either side of SR-D. The test cycle is shown in Table XV. The loads were attained, held momentarily then released to zero. Test data accumulated are shown in Table XVI. Theoretical vs. Actual stress on the bead clamp is shown in Table XVII.

Contract NOber 89483
Serial No. SS041-001
Task 8156

- 121 -

Report No. 17
Phase I Interim Report
30 September 1964

TABLE XII
6" SAMPLE #1 TEST CYCLE

<u>Cycle #</u>	<u>Lb./Sample</u>	<u>Lb./Cable</u>
1	2914	17
2	3311	20
3	8212	49
4	8344	50
5	12980	77
6	12848	77
7	12980	77
8	15629	93
9	16159	96
10	20795	124
11	20927	125
12	25430	151
13	24901	148
14	27947	166
15	29007	173
16	33510	200
17	35497	211
Break	50463	300

Bolts were not torqued to any specific tightness.

B.F. Goodrich Aerospace and
Defense Products
a Division of The B.F. Goodrich Company

BLANK PAGE

TABLE XIV

6" SAMPLE #1 TEST RESULTS ON BEAD CLAMP

	<u>Maximum Stresses During Test</u>		
	<u>Theoretical</u>	<u>Experimental</u>	<u>Comments</u>
Fixed Clamp - Side G-H	26,000	14,850	
Fixed Clamp - Side O-P	26,000	19,440	
Fix. Clp. \angle bolt ϕ , J	22,800	5,640	
Movable Clp, \angle bolt ϕ , I	24,400	9,600	
Fixed clp, Straight bolt ϕ , R	22,800	6,000	
Mo Clp, Str Bolt ϕ , Q	24,400	14,400	
Clamp Hook - bending stress K-L	33,600	- 1,800	Friction force caused by bolt tightness prevented load from transferring to hook.
Clamp Hook - bending stress S-T	33,600	3,270	
\angle bolt M	30,000	22,080/20°	
\angle bolt N	30,000	27,720/60°	

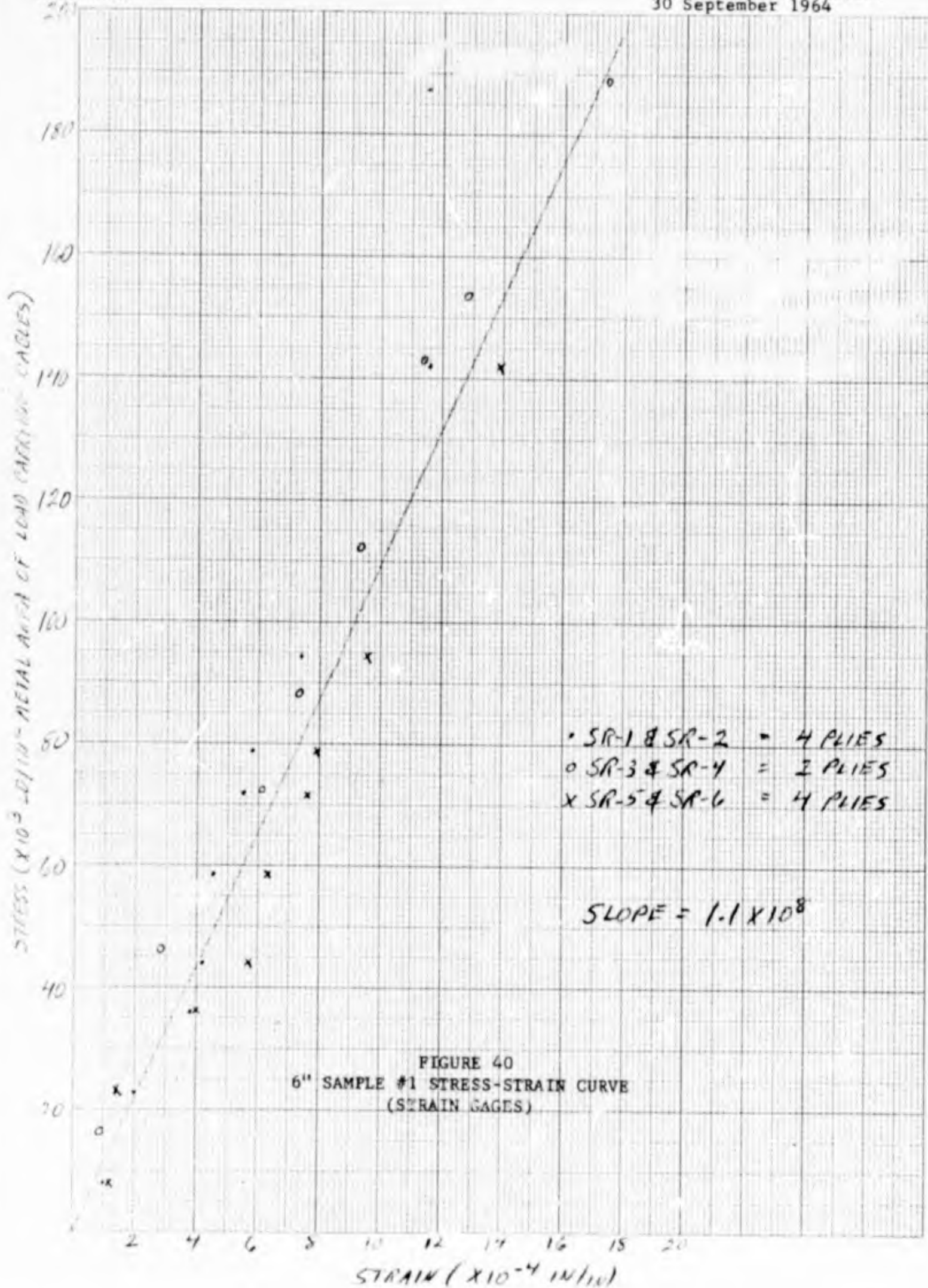
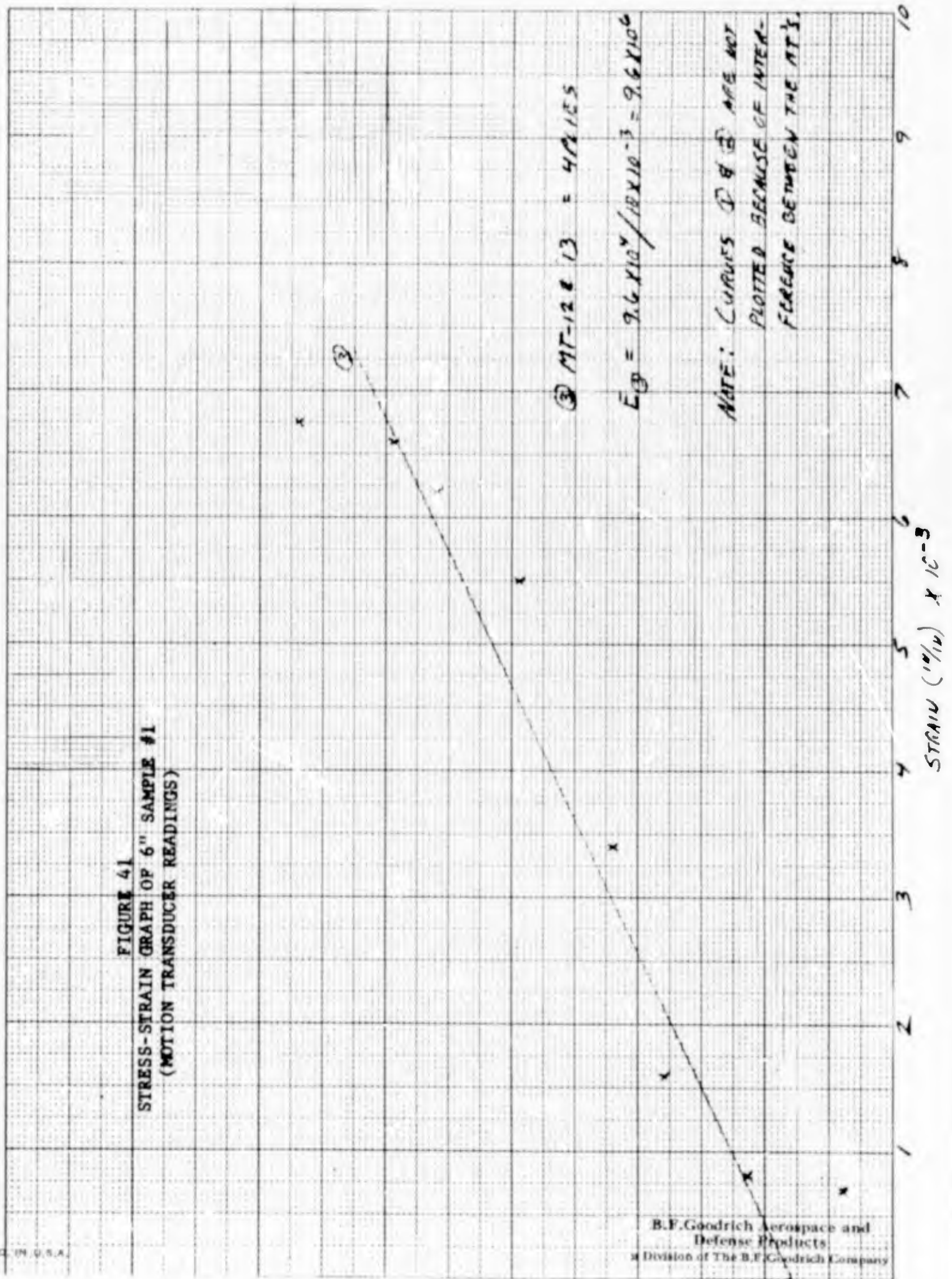


FIGURE 41
STRESS-STRAIN GRAPH OF 6" SAMPLE #1
(MOTION TRANSDUCER READINGS)



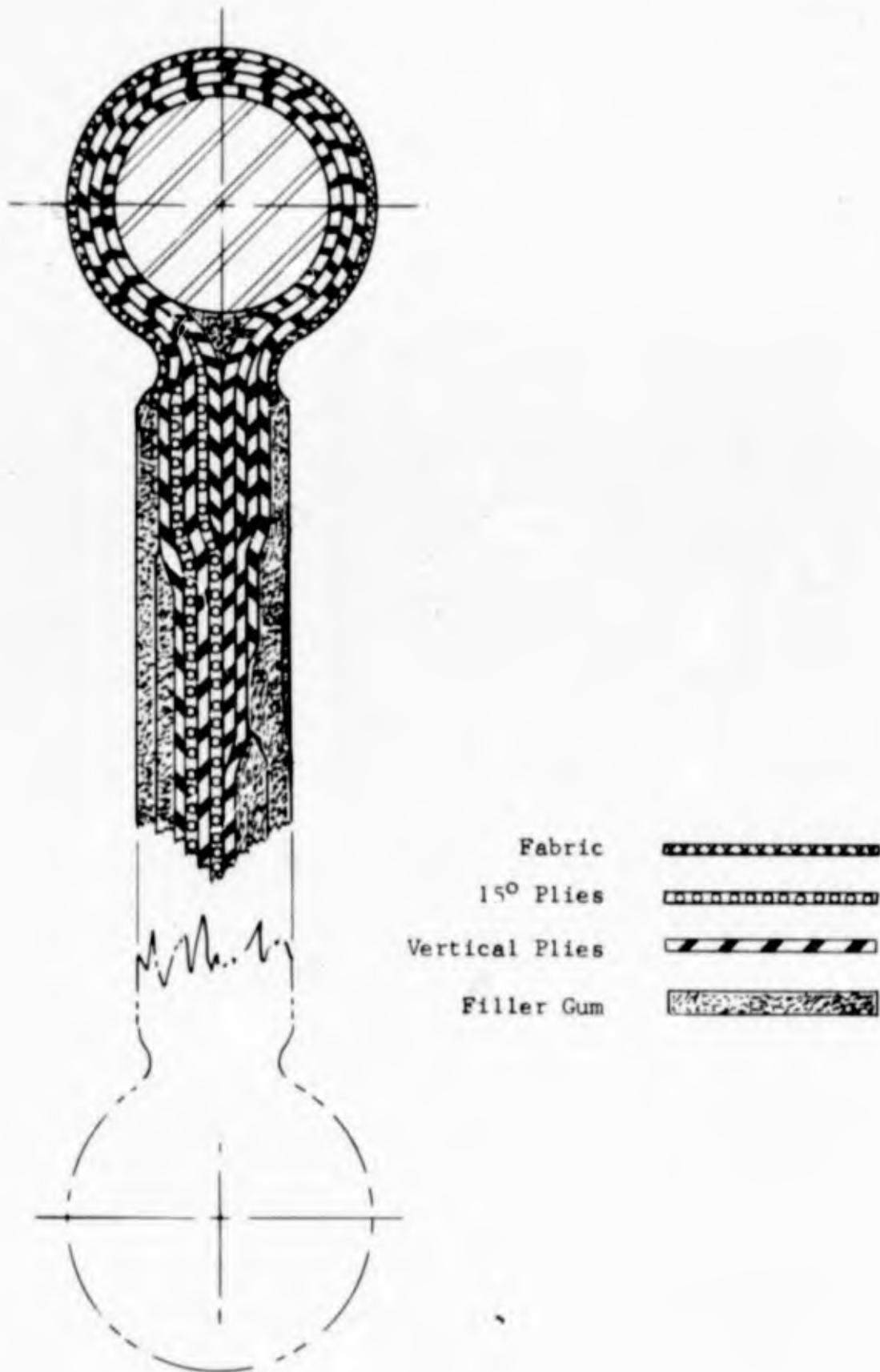


FIGURE 42
6" SAMPLE #2 CROSS SECTION

Contract NObsr 89483
Serial No. SS041-001
Task 8156

- 127 -

Report No. 17
Phase I Interim Report
30 September 1964

TABLE XV
6" SAMPLE #2 TEST CYCLE

<u>Cycle #</u>	<u>Lb/Sample</u>	<u>Lb/Cable</u>
1	6627	26
2	6362	25
3	12459	49
4	12989	51
5	18821	75
6	19218	76
7	25448	101
8	25315	100
9	31810	126
10	31545	141
11	37244	148
12	38702	154
13	37509	149
14	25183	100
15 (held 15 min.)	25183	100
16	32870	130
17	31810	126
18 (held 16 hrs.)	33135	131
19	32200	128
20	31200	124
21	31677	126
22 (no load for) (6 days prior) (to this cycle)	25978	103
23	26110	104
24	25315	100
25	25580	101

Bolts were torqued to 200 ft.-lbs. each.

B.F. Goodrich Aerospace and
Defense Products
a Division of The B.F. Goodrich Company

Contract NObr 89483
Serial No. SS 041-001
Task 8/56

Report No. 1/
Phase I Interim Report
30 September 1964

128

Main data table with columns for various parameters and a large grid of numerical values.

TABLE XVI
6" SAMPLE # 2 ACTUAL DATA SHEET

Summary table with columns for STRAIN CELL, COMPRESS CELL, and numerical data.

BLANK PAGE

TABLE XVII

6" SAMPLE #2 DETERMINED STRESS ON BEAD CLAMPS

	<u>Maximum Stresses During Test</u>	
	<u>Theoretical</u>	<u>Experimental</u>
Fixed Clamp - Side G-H	26,000	9,360
Fixed Clamp - Side O-P	26,000	10,800
Clamp Hook - Bend Stress K-L	33,600	NG
Clamp Hook - Bend Stress S-T	33,600	NG
∠ bolt M	30,000	18,600/70°
∠ bolt N	30,000	24,480/110°

In analyzing the test data and the sample several observations and conclusions were reached. The cables again cut through the rubber at the bead clamp pressure point. The side in contact with the bead seat was more severe than the bead clamp side. The bead, end retainers bent also indicating a seating or nestling of cables between those of under layers was in process. This sample was not loaded to failure and the motion transducers gave consistent readings. Constructional strain in the bead-clamp area was .185 in./in. whereas the panel area yielded 9.4×10^{-4} in./in. Stabilization of the construction was reached after the 7th cycle.

The accumulated data was plotted and is presented in Figures 43 and 44. It indicates further that minor bending was in evidence, but the sample membrane behaved properly and was duplicated later in Sample #3.

(3) Sample #3

Sample #3 duplicated the proposed construction for areas of extreme bead contour change. This test analyzed 3 ply, 6 ply, 9 ply, bead, overall length and bond strength characteristics. This sample (Figure 45) was instrumented according to Figure 36 except the following were deleted: SS all, and MT-H,I,K,L.

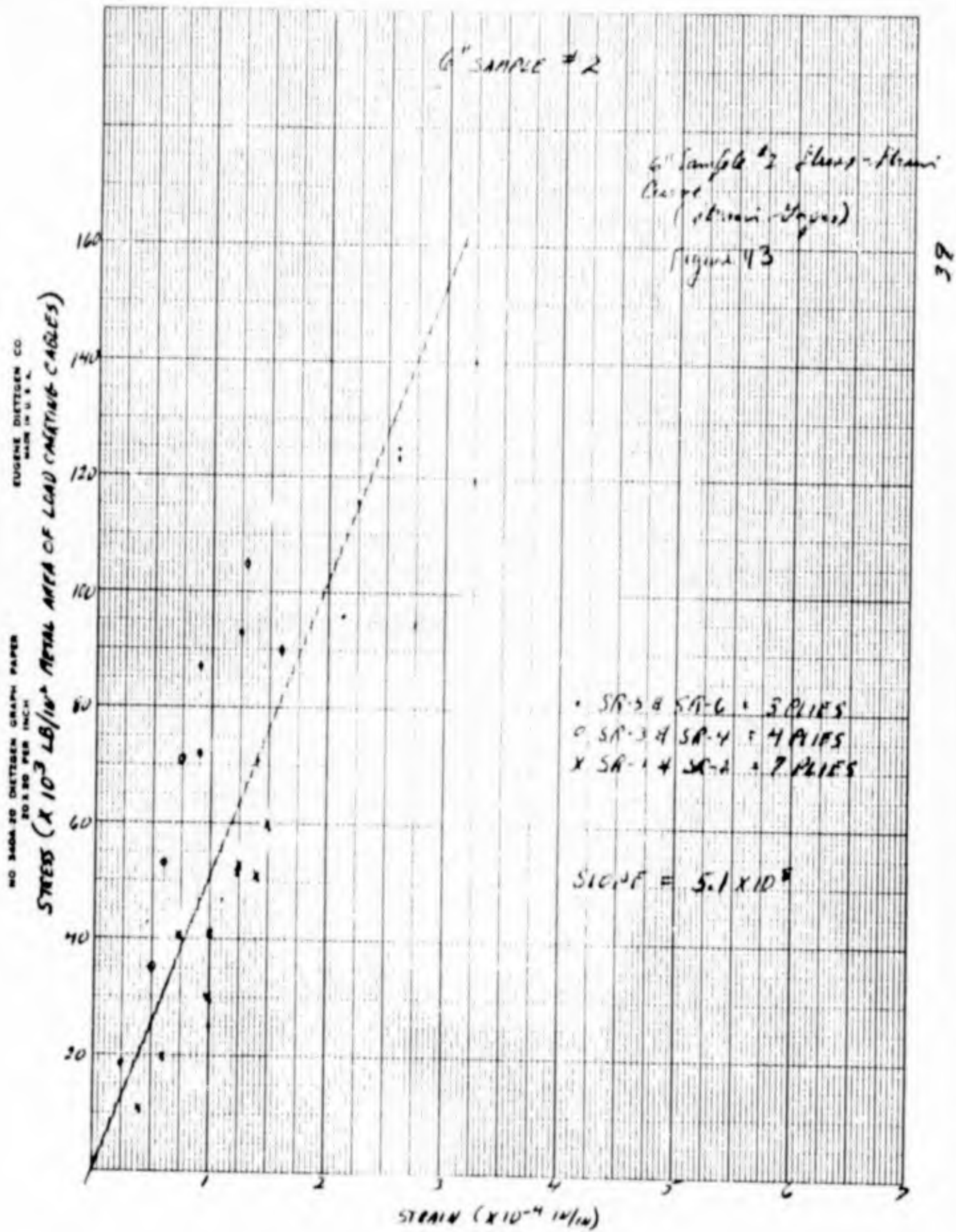


FIGURE 43
 6" SAMPLE # 2 STRESS-STRAIN CURVE
 (STRAIN GAGES)

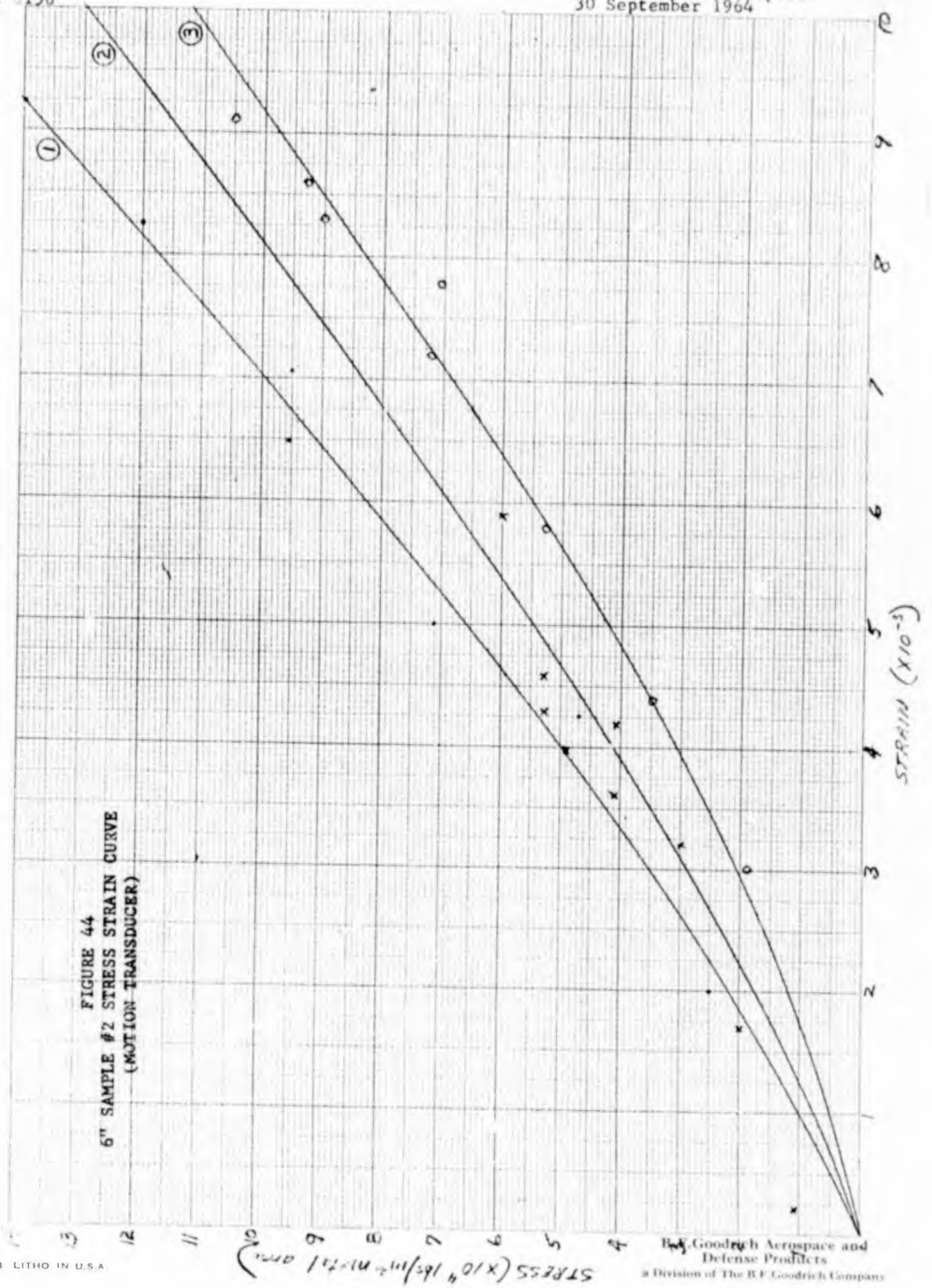


FIGURE 44
6" SAMPLE #2 STRESS STRAIN CURVE
(MOTION TRANSDUCER)

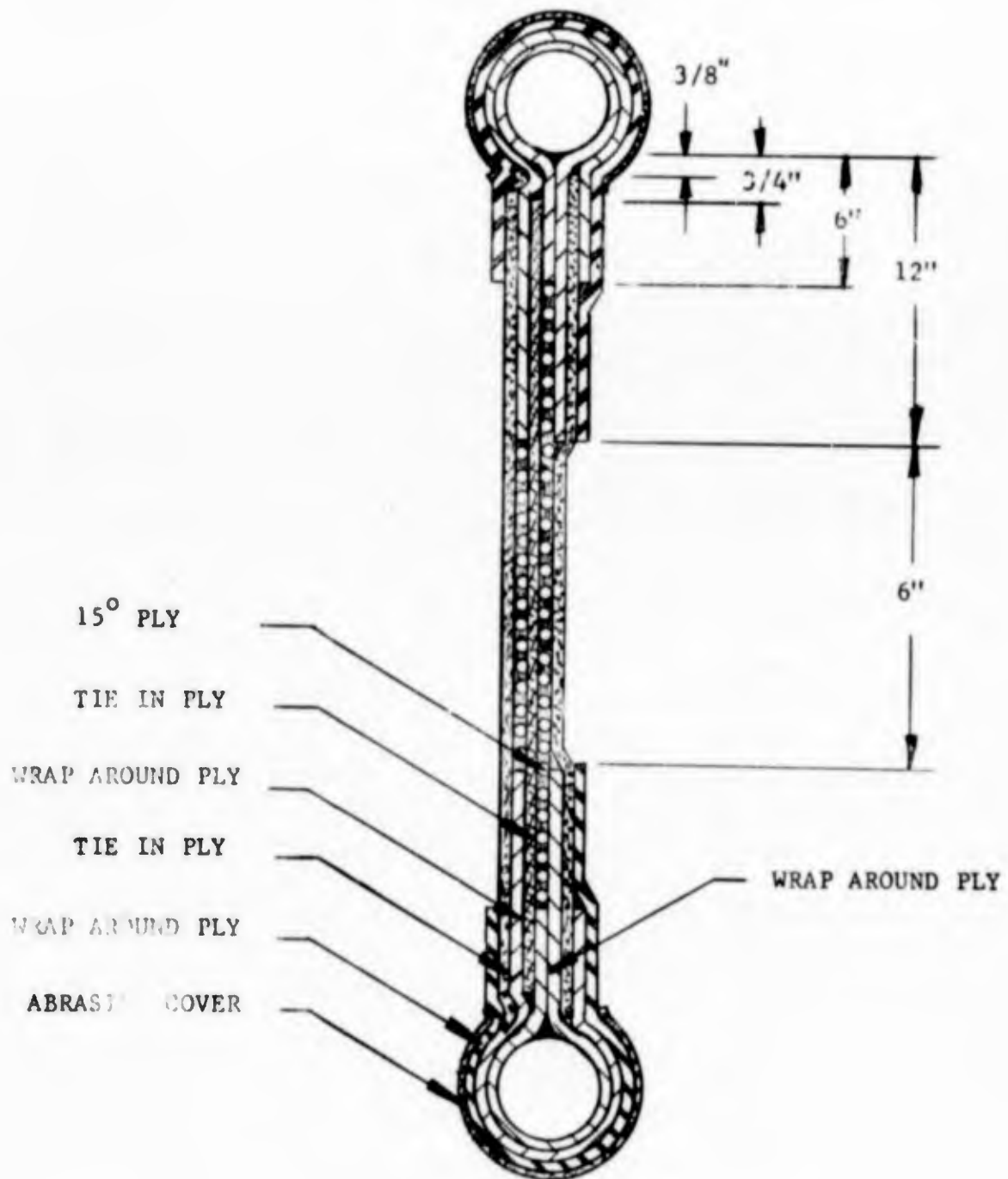


FIGURE 45

6" SAMPLE #3 CROSS SECTION

Contract NObsr 89483
Serial No. SS041-001
Task 8156

- 133 -

Report No. 17
Phase I Interim Report
30 September 1964

This sample was subjected to the same test cycle as Sample #2 (Table XV) except for the additional 7 cycles shown in Table XVIII.

TABLE XVIII

6" SAMPLE #3 TEST CYCLE

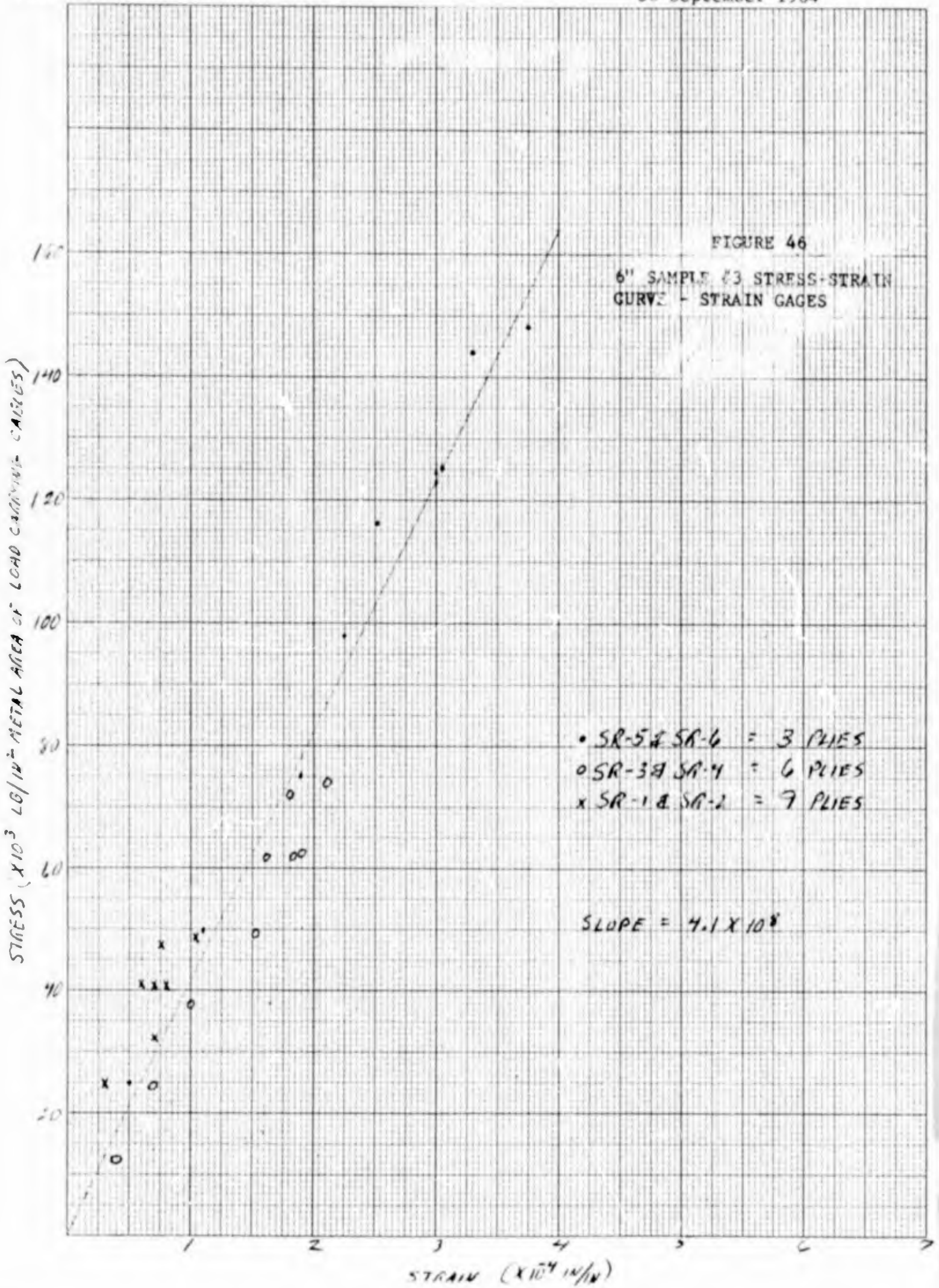
(Same as Sample #2 through Cycle #18 then)

<u>Cycle #</u>	<u>Lb./Sample</u>	<u>Lb./Cable</u>
19	33,100	131
20	32,600	129
21	33,100	131
22	33,100	131
23	33,100	131
24	33,100	131
Break	65,200	259

Bolts were torqued to 200 ft.-lbs. each.

The same cable migration through neoprene was prevalent at the bead clamp pressure points. The bead end retainers were also bent again indicating a nestling action. Sample failure occurred in the tie in ply of the 5 ply area. The motion transducers and strain gauges gave very consistent readings. The constructional strain in the bead clamp area was .222 in./in. and in the panel was 12.8×10^{-4} in./in. Stabilization was reached after cycle number 9.

The data graphed are shown in Figures 46 and 47.



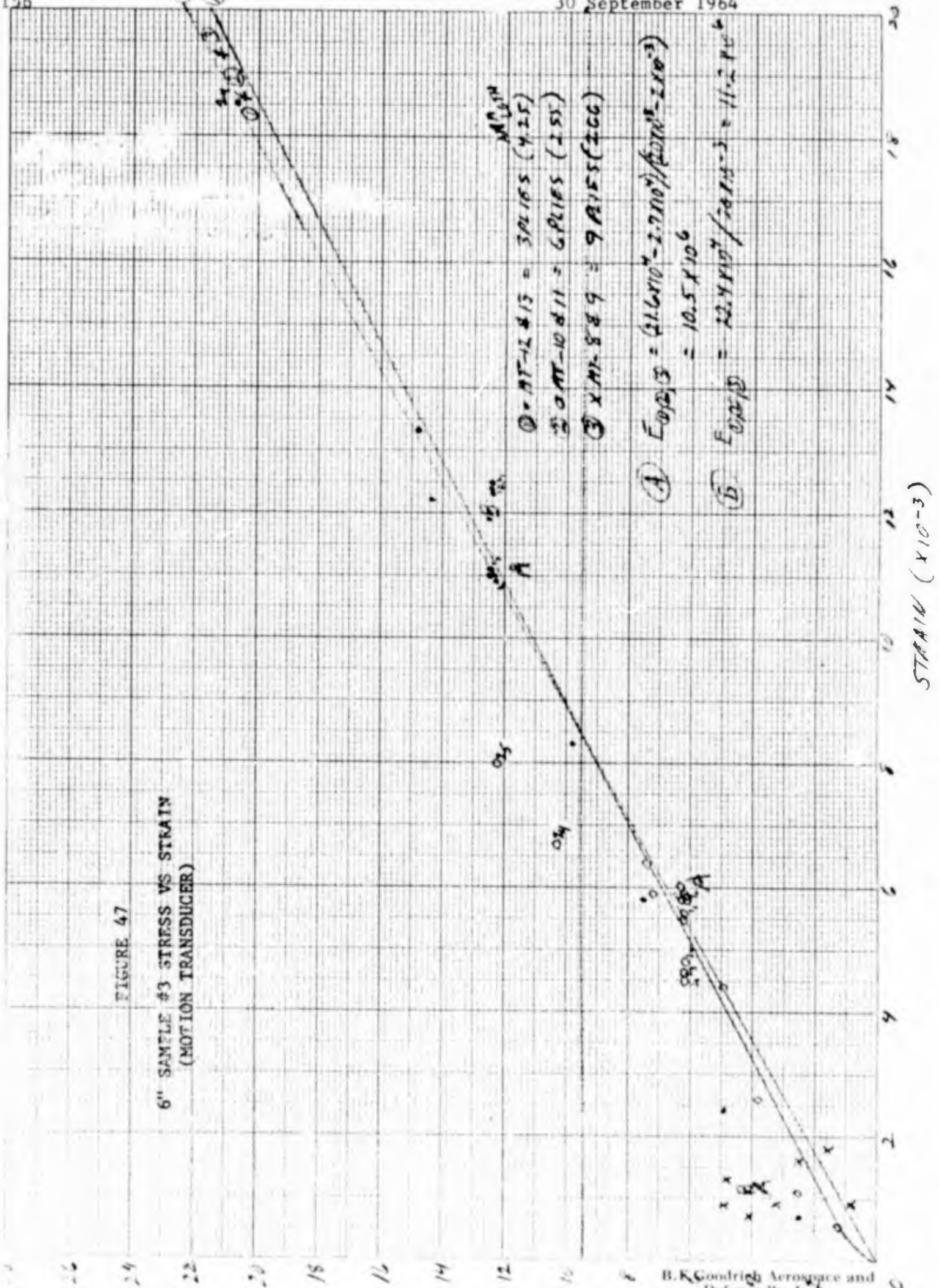


FIGURE 47
 6" SAMPLE #3 STRESS VS STRAIN
 (MOTION TRANSDUCER)

4) Conclusions:

From the data collected during the various tests the following is apparent:

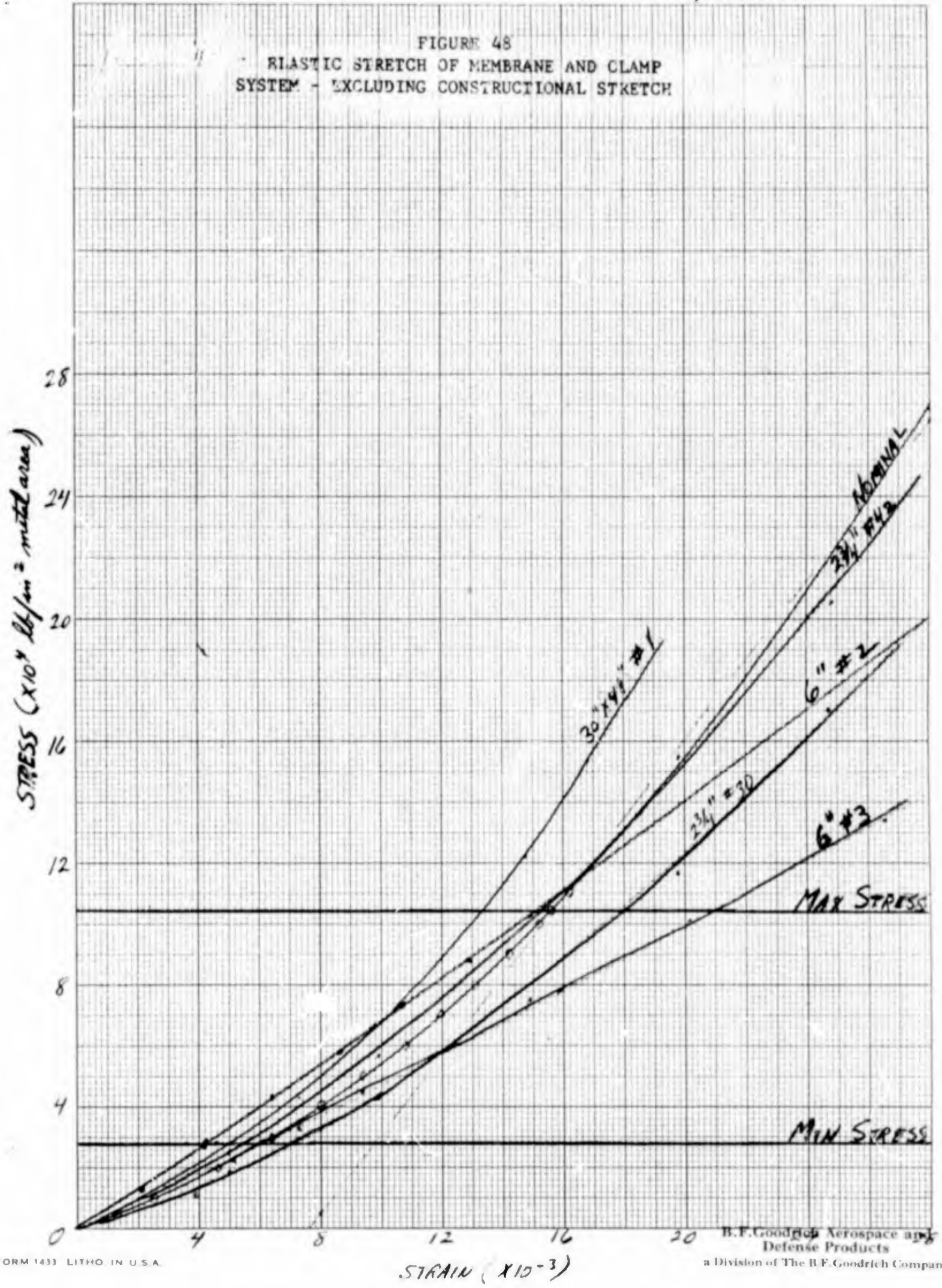
- (a) There is some degree of correlation between results obtained from motion transducers and strain gauges. This is observed by comparison of the graphs depicting the stress-strain characteristics of the 6" samples. Taking account of the explanations given for the deviations from consistency it has been concluded that a rough estimate of the adjustment factor for converting strain gauge readings into actual strain dimensions is $.029 \pm .003$. This is true providing the amount of rubber separating the strain gauge from the load carrying cables is in the range of $5/32"$ to $5/16"$. Further experimentation is desirable and recommended before much confidence in the reliability of this factor can be assumed.
- (b) The elastic stretch modulus of the membrane-clamp system, with respect to the metal cross-sectional area of the load carrying cables, is $13 \times 10^6 \pm 3 \times 10^6$ lbs./in.². This modulus is applicable only after the membrane has been loaded beyond 31% of its theoretical ultimate strength but less than the elastic limit of the membrane. Because the loads placed upon the cables during normal operating conditions will be less than 31% of their ultimate strength, the modulus or slope of the stress-strain curve will be variable, depending upon the stress. (Figure 48)

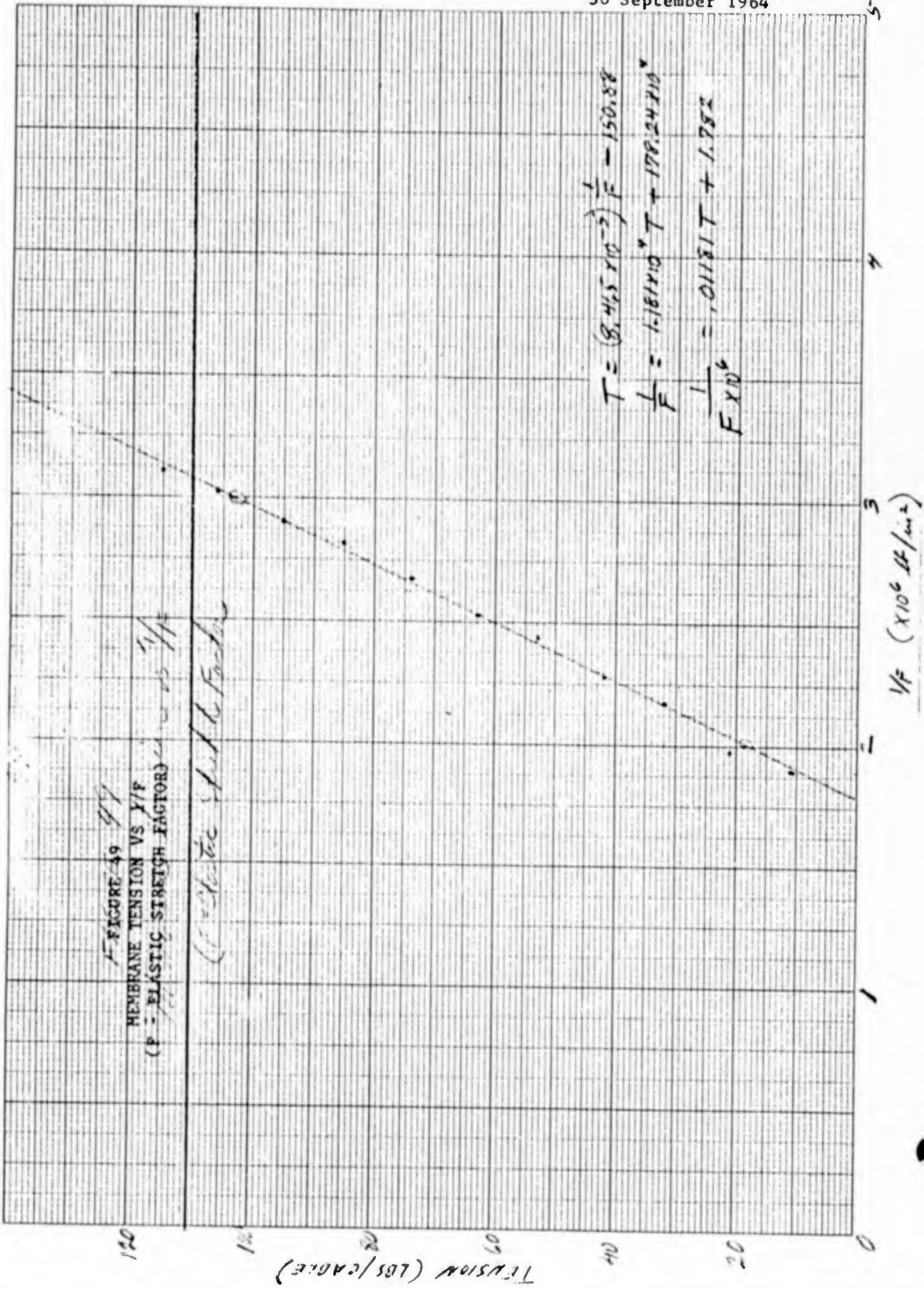
The variable becomes linear when expressed in terms of cable tension, T, and the reciprocal of the factor of elastic stretch for cables, 1/F. It is this linear relationship that is used in the formulas for calculating cable tensions and deflections. Its equation is $\frac{1}{F \times 106} = .01181 T + 1.782$

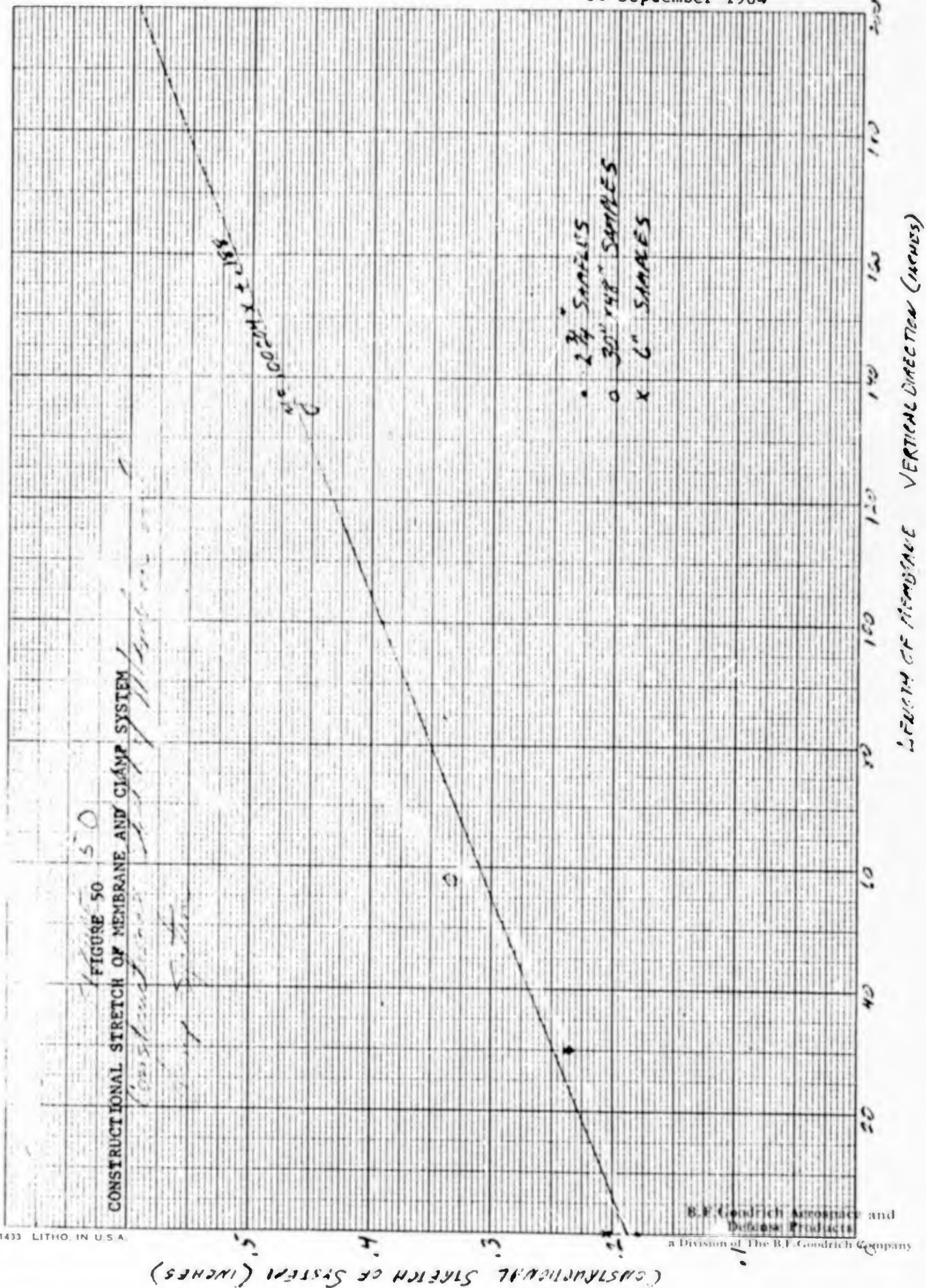
Figure 49 represents a graphic presentation of this.

- (c) Constructional stretch of the entire bead-panel system was found to be linear and is given by the equation: $e_c = .00204 \chi + .188$ where χ is the length of the membrane from one bead to the opposite bead. Figure 50 gives these data.

FIGURE 48
ELASTIC STRETCH OF MEMBRANE AND CLAMP
SYSTEM - EXCLUDING CONSTRUCTIONAL STRETCH







The steam piping for the panels should be redundant piped to insure against valve, steam traps, etc. type of malfunction.

As the outside surface is the one the diaphragms press against during the cure, it is anticipated that some surface irregularities will occur. These surface blemishes would be smoothed out by grinding with belt sanders or drum sanders.

The cost of such a combination jig would amount to at least \$500,000 to attain the desired degree of accuracy and reliability necessary in such a system. This cost figure is purely an estimate.

Another possibility is to procure a large vulcanizer capable of handling the entire part and a one price mold.

(b) Advantages of One Piece Construction

- 1) Scheduling of work and materials should be simplified.
- 2) One central location for all work effort.
- 3) Centralization of supervision.
- 4) No seams in rubber parts.
- 5) No seams in attachment beads.
- 6) No special handling and transportation problems during manufacture.
- 7) May alter design to completely incapsulate "banjo" area reducing attachment points and fairing requirements.

(c) Disadvantage of One Piece Construction

- 1) Massive, expensive and non-transportable tooling.
- 2) Faulty cure spoils entire dome instead of only a segment.
- 3) Damage to tooling would shut-down all manufacture until repaired.
- 4) Increased complexity of construction since 15° plies would extend possibly 30'. These long plies would be difficult to handle and would require intermediate splicing.
- 5) Time required to build may permit partial stock cure resulting in flow problems during heat cure.
- 6) Smooth surface would be on inside requiring considerable buffing of outside to meet contour requirements.

- (d) Strength of the bead-panel system for the bow dome acoustic window yields approximately a 3 factor of safety.
- (e) Except for crushing of rubber in the area where the clamp comes in contact with the bead there were no fatigue characteristics observed throughout all tests. This condition will be improved as a result of additional bead design.
- (f) Procedures for removing constructional stretch from the membrane were evaluated. The most effective was to cycle the system about 9 times at the equivalent load of 100 lbs./cable.
- (g) Bead clamp bolt torque necessary was determined to be about 400 ft.-lbs. This torque is proper without damaging effects upon the bead and was confirmed by tests.
- (h) Verification that the strength of the bead clamp is sufficient was also accomplished. Furthermore actual stresses were within those theoretically determined.

f. Method of Window Assembly

The general philosophy of rubber products manufacture dictates designs, minimizing and eliminating if possible seams or attachment joints. Of course, adherence to this principle must be tempered with due consideration for the part to be manufactured. In this instance the size of the total part indicates that it would be more desirable to fabricate in smaller sections.

1) One Piece, Non-Segmented Dome Construction

In analyzing the possibility of fabricating a one piece dome, the following factors must by necessity, be considered:

- (a) Size of Part
- (b) Complexity of Construction
- (c) Reliability of Part
- (d) Acoustical Considerations
- (e) Degree of Stabilization Required
- (f) Acceptability of Air Cure Concept

The overall size of the prototype acoustic window is 37.5 long, 20' wide and 9' high with a general contour similar to a horseshoe. There is approximately 1059 square feet of panel surface area and 156 feet of bead peripheral length. The size of the part indicates considerable time will be required for fabrication.

The degree of quality and reliability required in this window is extremely high. Therefore, to insure an optimum construction a heat-pressure-vacuum cure should be utilized. This can be accomplished by obtaining a large combination building, curing and testing jig.

(a) Combination Building and Curing

A full size building and curing form may be constructed from concrete and steel with internal piping for steam.

The method of construction would consist of making male building forms from sheet metal (probably from stainless steel) as if making individual panels, but joining the individual panel molds together to make a full size form. On the back side of the forms piping for steam and water would be attached by welding. When all the forms are positioned and proper cross bracing and tie-rods are installed, the cavity in the center of the "horse-shoe" is cast full of concrete. The completed assembly will serve as the building form, the curing form - when the outside steam jacket is in place and as the hydrostatic test stand for the proof pressure testing of the complete acoustic window.

The outside steam jacket for the building form would be constructed of bolt-on panels made in the manner of the present steel bow dome panels with bridge like reinforcing members. The 1/4 inch outside skin would be on the inner surface instead of the outside. Attached to the inside skin surface at the perimeters would be a diaphragm made from resin cured butyl stock approximately 3/8 inch thick. The panels would be piped for steam between the diaphragm and the inside steel skin. When in place, the steam jacket panels would operate very much like a diaphragm press.

2) One Piece, Segmented Dome

The alternative to fabrication of a non-segmented window, of course, is to build a one piece, segmented window. This can be accomplished in a multitude of sections as shown in Figure 51. The primary limiting factor to the individual segment size is the capabilities of existing facilities.

Female building forms would be procured of either steel or plastic construction of the exact part contour. They would be simple in design in that they need only contain the part during cure. Subsequent to cure, which occurs in existing facilities the panel would be removed from the molds and assembled to the Hydrostatic Test Fixture. This structure is made primarily of concrete with a steel reinforcing structure and bead clamp to contain the panel. Upon installation of the separate panels on the test fixture they would be seamed in place, the complete window tested and prepared for shipment.

The outside surface of the panel is molded smooth and rework should be minimized.

The cost of basic tooling for this complete job would amount to approximately \$175,000.

(a) Advantages of this system are:

- (1) Minimization of expense for tooling.
- (2) Faulty cure would scrap only 1 panel, and because of the control of cure in vulcanization being more reliable, this possibility should be minimized.
- (3) Tooling damage would slow effort on only a limited part of project.
- (4) Smaller panels would simplify handling of materials and construction procedures.
- (5) Time to build one panel is relatively short and stock problem would be minimized.
- (6) Outer surface molded with resurfacing effort minimized.
- (7) Actual construction time should be reduced since several sections of the window can be fabricated simultaneously.

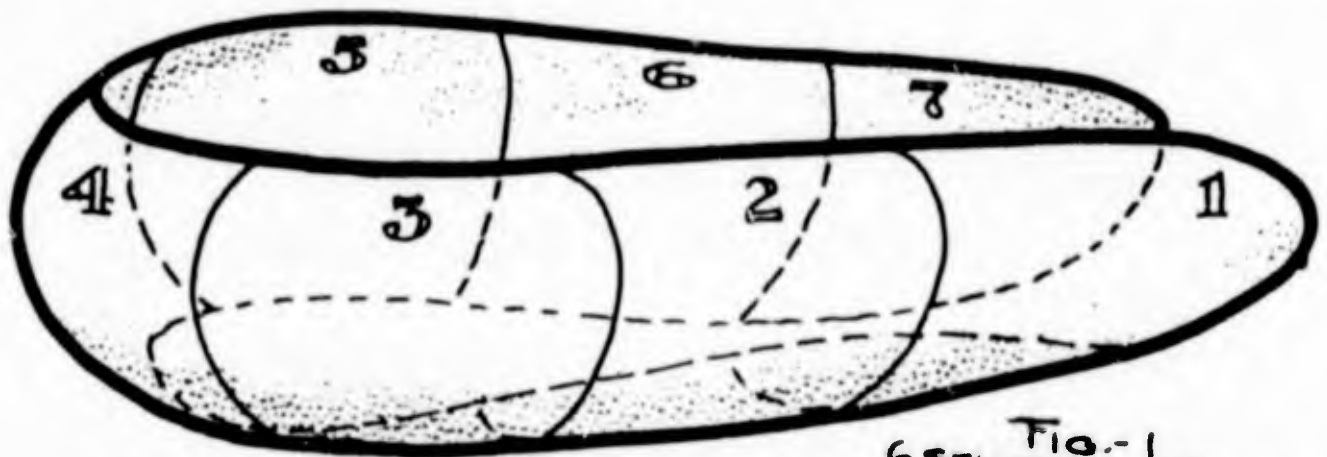


FIG.-1
6 SPLICES - 7 PANELS

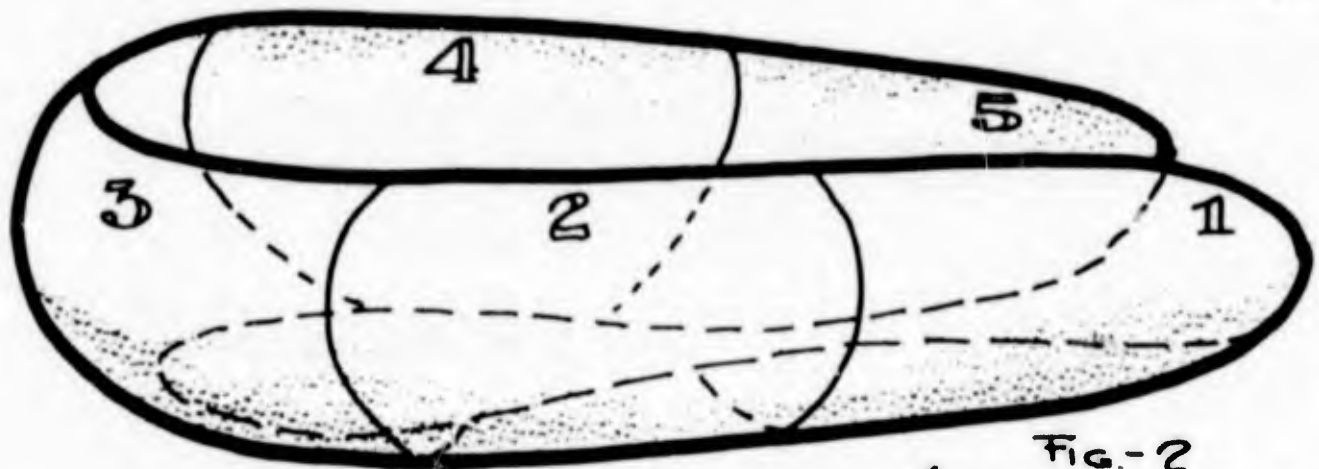


FIG.-2
4 SPLICES - 5 PANELS

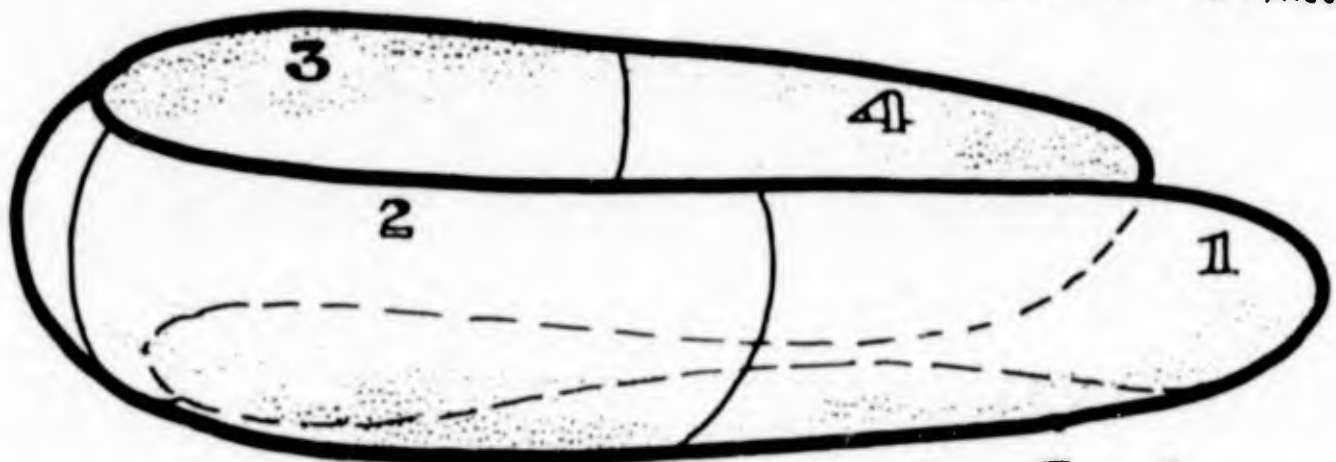


FIG.-3
3 SPLICES - 4 PANELS

FIGURE 51
DOME SEGMENT CONCEPTS

(b) Disadvantages:

- (1) Seams to assemble entire part requires additional operations.
- (2) More actual pieces of tooling to accomplish job.

3) Cost Analysis

One major consideration in this analysis is the cost of building, a non-segment versus a segmented one piece acoustic window. Table XIX presents briefly estimated figures of what costs are involved in both systems. The one price, non-segmented costs consider the use of a vulcanizer since costs associated with it are more accurate.

TABLE XIX

COST COMPARISON OF DOME FABRICATION CONCEPTS
 (Hydrostatic Test Equipment Not Included)

<u>Item</u>	<u>1 Piece Non-Segmented</u>	<u>1 Piece 4 Segments</u>	<u>1 Piece 7 Segments</u>
Vulcanizer (25' Dia. 40' Long (350 PSI)	\$800,000	-	-
Molds (Est)	80,000	\$100,000	\$110,000
Seaming Molds	-	9,000	15,000
Building Area	40,000	20,000	20,000
Track for Mold	2,000	-	-
Splice Fabrication	-	3,000	6,000
Total	<u>\$922,000</u>	<u>\$132,000</u>	<u>\$151,000</u>
100 Windows	922,000	429,000	745,000
200 Windows	922,000	729,000	1,345,000

Note: Costs compared only in those areas listed since other efforts would be comparable.

Considering the various influencing factors analyzed and discussed previously it can be seen that, in this instance, a segmented construction is more desirable.

From that discussion it can be seen that a one (1) piece mold would require exacting surface contours and bead areas, heat sources for curing, vacuum sources for curing, and some means of exerting external pressure against the panel surfaces to insure the end product is devoid of blisters, delaminations and general porosity. Means of accomplishing this will add considerable cost and complexity to the one piece tooling, with the control of this much less sensitive than a vulcanizer.

The use of a 25' diameter vulcanizer adds considerably to the cost and complexity of the operation rendering it undesirable.

On the basis of the foregoing discussion and conclusions the final recommendation of this study is to utilize the segmented concept, in this case four (4) pieces, and fabricate the complete dome, joining the panels at a later time.

The segmented four (4) piece dome concept is being utilized in the current development program. It has been determined that panels of the sizes intended can be cured in existing vulcanizer facilities with resulting high quality products. The seaming or splice attachment mechanisms have been evaluated and found to furnish strength levels equivalent to the panel when a 9" overlap is utilized.

g. Conclusions

- 1) The most reliable window retention system is a bead clamp-bead seat combination on the ship which clamps the panel bead.
- 2) A complex composite overlap system is necessary for wrapping ply cables around the bead cable to obtain complete ply strength.
- 3) A method must be devised to prevent cable migration and gum shearing.
- 4) The elastic stretch modulus of the membrane-clamp system, with respect to metal cross-sectional area of the load carrying cables is approximately 13×10^6 lbs/in². Further data concerning this value is presented in the later section on prototype panel testing.

- 5) Strength of the bead-panel system for the bow dome acoustic window yields approximately a safety factor of 3.
- 6) Fabrication of the acoustic window in one piece is not economically feasible at this time.
- 7) Acoustic window fabrication in 4 sections and then spliced together to form a one piece construction is the most desirable approach.
- 8) Additional work is required to determine whether a system can be devised to permit utilizing strain gages during later testing phases.
- 9) Previous studies have determined design criteria for the prototype panel thus permitting actual panel design to proceed.

9. Anti-Fouling Paint Study

a. Summary

Tests show that B.F. Goodrich's adhesive 423552 satisfactorily bonds the polyisobutylene anti-fouling paint to the acoustic window neoprene wall structure. The resultant system remains intact after 6 months exposure to sea water and 139½ hours of acoustical energy bombardment.

b. Introduction

An investigation and development program was undertaken to obtain a suitable adhesive system for use with a polyisobutylene anti-fouling paint system. This would permit utilization of the recently developed, outstanding, polyisobutylene anti-fouling paint on the acoustic window to be developed under this contract.

In essence this system required bonding neoprene to polyisobutylene with a suitable, serviceable tie coat cement.

c. Discussion

A survey of potential, available materials for the assigned task resulted in the following materials being utilized in this investigation:

- (1) Adhesive R 575 T
- (2) Adhesive R 1078 T
- (3) Adhesive A 851 B
- (4) Adhesive A 625 B
- (5) Adhesive A 862 B
- (6) Adhesive 423552

Sample panels of the appropriate Neoprene compound were washed thoroughly to remove all contamination. Separate sample panels were primed with two (2) spray coats of each tie-in cement. After the prescribed drying time two (2) spray coats of black Polyisobutylene paint (Formula No. 133) per MIL-P-22298 (Ships) were applied to each panel. Then, two spray coats of Polyisobutylene anti-fouling paint (Formula No. 134), per Mil-P-22299 (Ships) were applied to each panel.

Contract NObsr 89483
Serial No. SS041-001
Task 8156

- 149 -

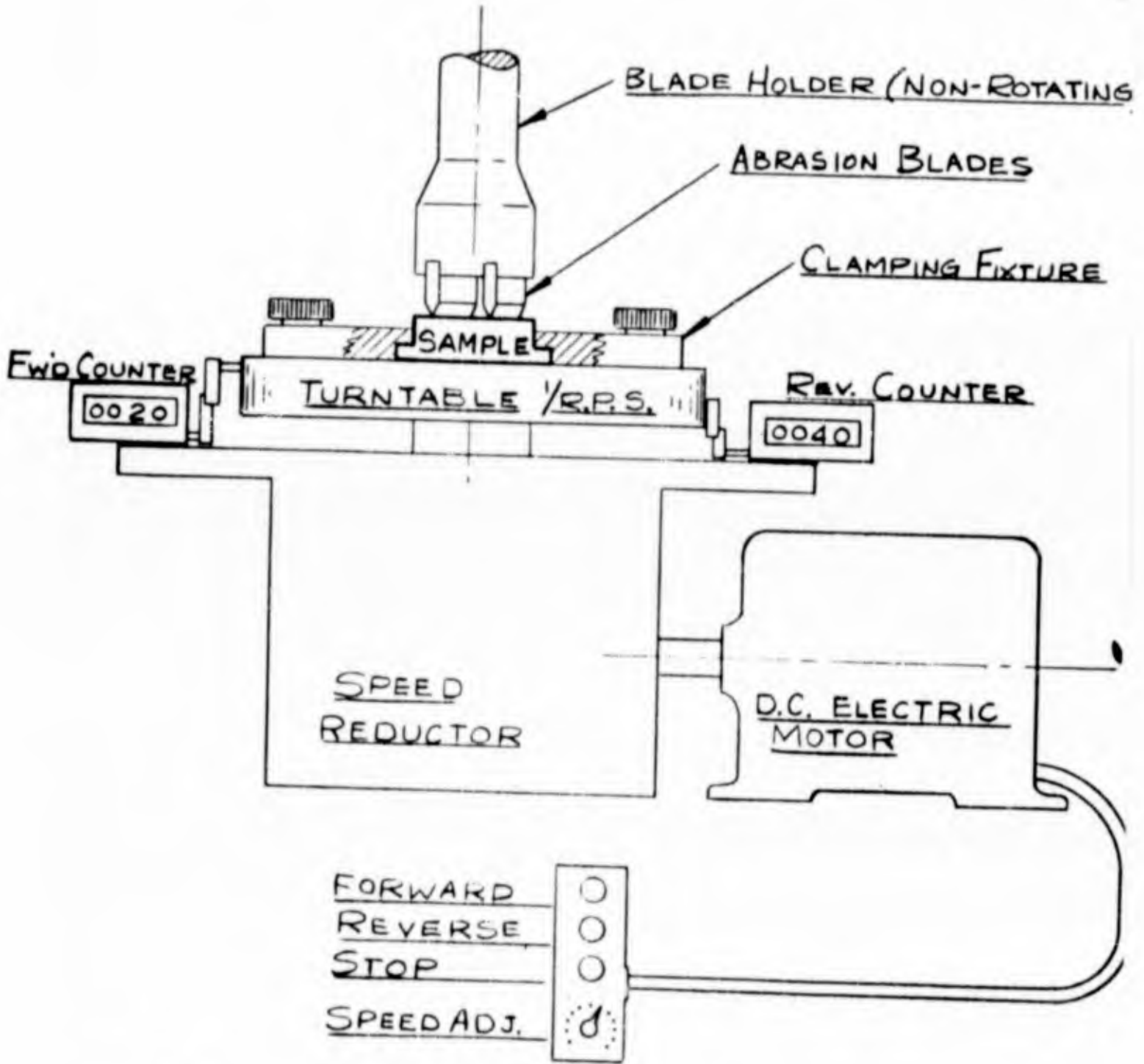
Report No. 17
Phase I Interim Report
30 September 1964

General spraying and handling characteristics of all tie-coat adhesives were satisfactory. However, samples A 862 B, R 1078 T and R 575 T, when completed and dry, resulted in an alligatoring or checking condition in the outer anti-fouling paint coating. This may be attributed to an incompatibility between the tie-coat and Polyisobutylene phases of the system.

Determination of the relative effectiveness of the various potential systems was accomplished utilizing a modified Pico Abrasion test method, Figure 52.

Essentially this procedure consists of inserting a suitable test specimen in a rotatable retention fixture and position the knife blades against the sample with a specific force. Four (4) revolutions of the sample constituted this test with weight loss and surface condition recorded.

Initial data derived from this test are presented in Table XX, "Modified Pico Abrasion Test Results".



PICO ABRASION MACHINE

FIGURE 52

PICO ABRASION TEST MACHINE

TABLE XX

MODIFIED PICO ABRASION TEST RESULTS
ON ANTI-FOULING PAINT SAMPLE

<u>Sample</u>	<u>Revo- lutions</u>	<u>Initial Weight</u>	<u>Final Weight</u>	<u>Weight Loss</u>	<u>Remarks</u>	<u>Rating</u>
*Control	4	15.7525	15.7320	.0205	Surface Abraded Clean	7
A625B	4	14.4990	14.4742	.0248	30% Coating Re- mained	3
A851B	4	15.9117	15.8897	.0220	Surface Abraded Clean	6
A862B	4	16.0310	16.0154	.0156	50% Coating Re- mained	2
R575T	4	15.1616	15.1340	.0276	5% Coating Re- mained	5
R1078T	4	16.2178	16.1994	.0184	5% Coating Re- mained	4
423552	4	16.0053	15.9883	.0170	50% Coating Re- mained	1

* Neoprene panel painted directly with Polyisobutylene coating.

Segments of the panels tested, as indicated in Table XX, were subjected to water soakage in artificial sea water and at the end of one (1) month the abrasion test rerun. The difference derived from a comparison of the data obtained before and after water soakage would indicate synergistic, deleterious effects, if any, of the composite system when exposed to simulated environmental service conditions. Data obtained from the second test are recorded in Table XXI and indicate the effect of a one (1) month exposure to artificial sea water.

TABLE XXI

MODIFIED PICO ABRASION TEST RESULTS
ON ANTI-FOULING PAINT SAMPLE
IMMERSED ONE MONTH IN SEA WATER

<u>Sample</u>	<u>Revo- lutions</u>	<u>Initial Weight</u>	<u>Final Weight</u>	<u>Weight Loss</u>	<u>Remarks</u>	<u>Rating</u>
Control	4	16.5265	16.5043	.0222	Surface Abraded Clean	6
A625B	4	16.7550	16.7350	.0200	10% Coating Re- mained	5
A851B	4	16.8430	16.8300	.0130	Surface Abraded Clean	2
A862B	4	16.3030	16.2870	.0160	50% Coating Re- mained	3
R575T	4	16.4740	16.4510	.0230	Surface Abraded Clean	7
R1078T	4	16.9550	16.9370	.0180	Surface Abraded Clean	4
423552	4	17.3150	16.3020	.0130	50% Coating Re- mained	1

Table XXII presents data on samples tested after 6 months exposure to artificial sea water.

TABLE XXII

MODIFIED PICO ABRASION TEST RESULTS
ON ANTI-FOULING PAINT SAMPLE
IMMERSED 6 MONTHS IN SEA WATER

<u>Sample</u>	<u>Revo- lutions</u>	<u>Initial Weight</u>	<u>Final Weight</u>	<u>Weight Loss</u>	<u>Remarks</u>	<u>Rating</u>
Control	4	16.6586	16.6440	.0226	Surface Abraded Clean	7
A625B	4	15.2443	15.2310	.0133	20% Coating Re- maining	4
A851B	4	16.6030	16.5910	.0120	Surface Abraded Clean	2
A862B	4	16.3018	16.2850	.0168	50% Coating Re- maining	5
R575T	4	16.0720	16.0550	.0170	Surface Abraded Clean	6
R1078T	4	16.4840	16.4710	.0130	5% Coating Re- maining	3
423552	4	16.2212	16.2110	.0102	50% Coating Re- maining	1

NOTE: Examination of samples did not uncover any signs of flaking, peeling, cracking and delamination or other types of environmentally initiated and propagated degradation.

In all instances, except the control and A862B samples, weight loss after water exposure was less than before. As the exposure time increased to 6 months the weight loss was further reduced except as noted where it increased. It appears that the water exposure is not detrimental in all instances, except the control and A862B samples, and that the additional aging time actually improves system capabilities.

Adhesive 423552 furnishes the most desirable system and shall be utilized, when necessary, during this program.

As a result of the Polyisobutylene Anti-Fouling Paint Study a 1½" x 5' x 5' paint panel was submitted to the Underwater Sound Laboratory for evaluation. This panel utilizes B.F. Goodrich Adhesive 423552 as the tie-coat for adhering the anti-fouling paint to the 35003 neoprene gum stock. The basic panel was a molded sheet press cured in a steel framework.

Upon completion of 139½ hours of acoustical energy bombardment, the paint panel was thoroughly examined by personnel of the Underwater Sound Laboratory. Under 40 x magnification, minor surface eruptions or bubbles were noticeable.

The test panel was returned to the B.F. Goodrich Company and subsequently examined by a consulting microscopist. This analysis entailed examination of several specially prepared panels and comparing them to the returned paint panel. Those included were:

- (1) Return paint panel originally processed July, 1963.
- (2) Control panel processed with paint panel July, 1963 but not subjected to test.
- (3) Panel with only BFG Adhesive 423552.
- (4) Panel with BFG Adhesive 423552 and Rubber Tie Coat, Formula 133 (per Mil-P-22298).
- (5) Panel as (4) with Rubber Anti-Fouling Formula 134 (per Mil-P-22299).

The primary concern in examining the quality of the paint on the tested panel was to study the protuberances and cracking present. This examination disclosed that:

- (1) There are no blisters or bubbles originating on the surface of the returned panel. The stock protuberances are solid particles of black adhesive substratum - either the adhesive tie coat or the polyisobutylene primer.

- (2) The cracking condition noticed on the returned panel extends through the paint layers. This condition was not indicative of a general degradation of the adhesive system. Moreover, the adhesive bond between the layers of paint was extremely good. No indication of delamination, peeling, or flaking was noticed throughout the panel surface or adjacent to the cracks.
- (3) The B.F.Goodrich Adhesive, 423552, used as a tie coat for adhering Polyisobutylene Anti-Fouling paint to the neoprene stock, forms a smooth continuous film when applied.
- (4) The black, Polyisobutylene paint (Formula No. 133) Mil-P-22298 (Ships) also forms a smooth, continuous film when applied over B.F.Goodrich tie-coat adhesive, 423552.
- (5) The red, Polyisobutylene anti-fouling paint (Formula No. 134) per Mil-P-22299 (Ships) appears to crack as the applied film begins to dry. These cracks, initially, resemble alligatoring or mud cracking and appears to be a thinning of the paint rather than a complete separation.
- (6) When specimens with the complete system applied, were bent over a 1/2" diameter essentially no change in the surface occurred. Figures 53 and 54 presents samples, photographed at x 30 magnification during elongation in the order of 100%.
- (7) The quality of recent specimens photographed at x 30 magnification and compared in Figures 55, July 1963 Sample and 56 March 1964 Sample, is excellent and greatly superior to the returned panel.

In searching for any factors which could contribute to the poor quality of the paint exhibited particularly by the samples of July, 1963, the large particle size of the cuprous oxide was observed. Actually there is little or no difference between the cuprous oxide of July, 1963 and March, 1964. In both cases the material is too coarse to be a good rubber reinforcing segment.

The cuprous oxide has an average particle size of about 8 microns (estimated on the basis of weight). The particles range from 1 to 12 microns in size and there is a high concentration in the 4 to 8 micron range. These sizes are well under the 325 sieve size which has an opening of 44 microns, but it would be classed

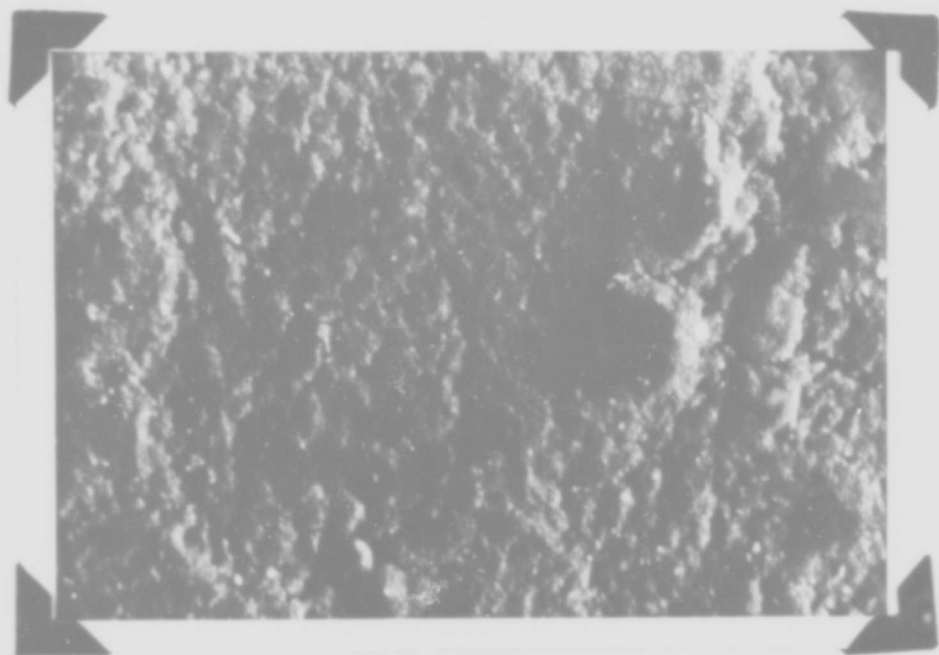


FIGURE 53
JULY 1963
PAINT PANEL @ 100% ELONGATION (X30 MAG)

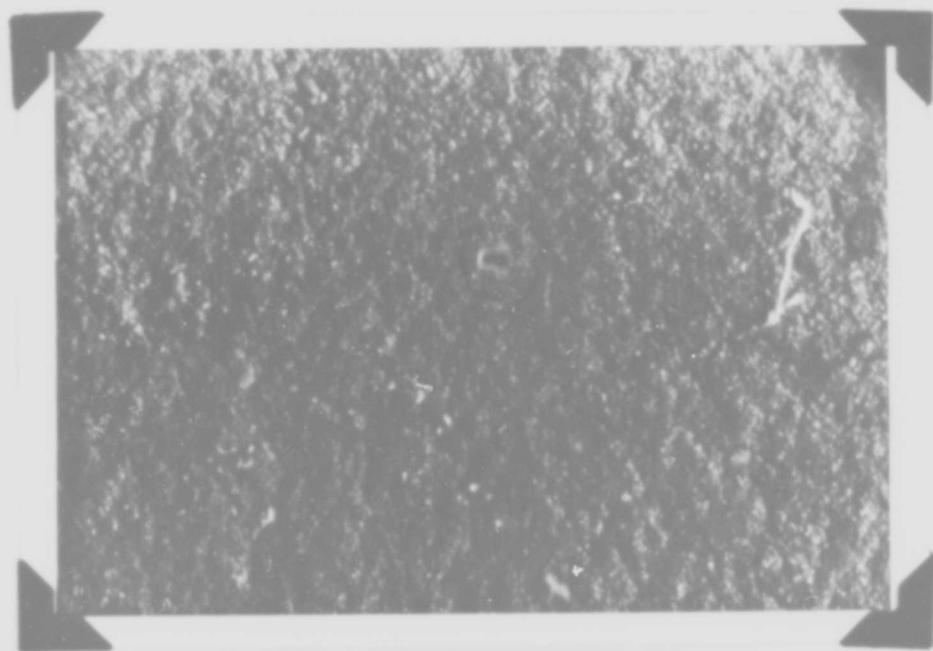


FIGURE 54
MARCH 1964
PAINT PANEL @ 100% ELONGATION (X30 MAG)

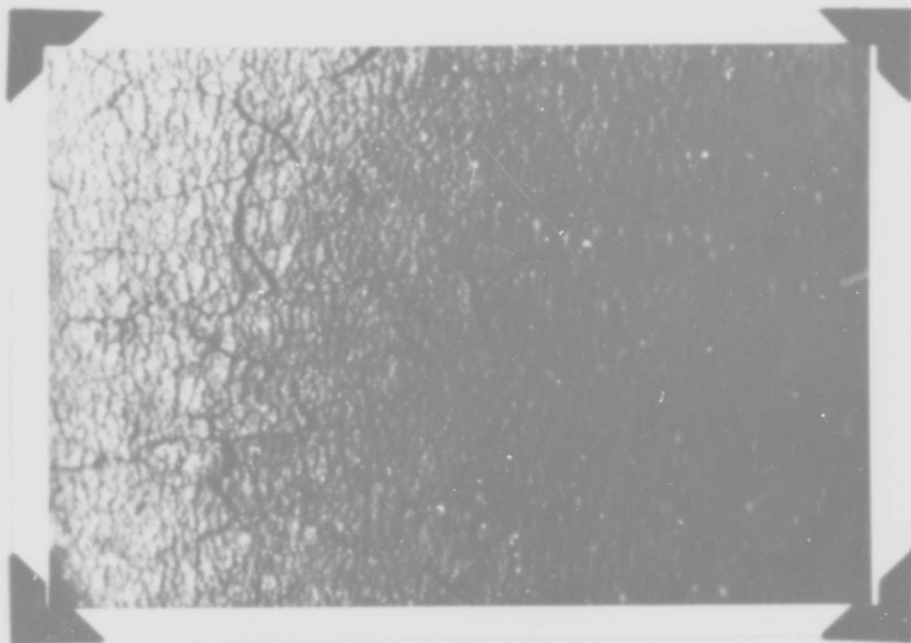


FIGURE 55
JULY 1963
PAINT PANEL (X30 MAG)

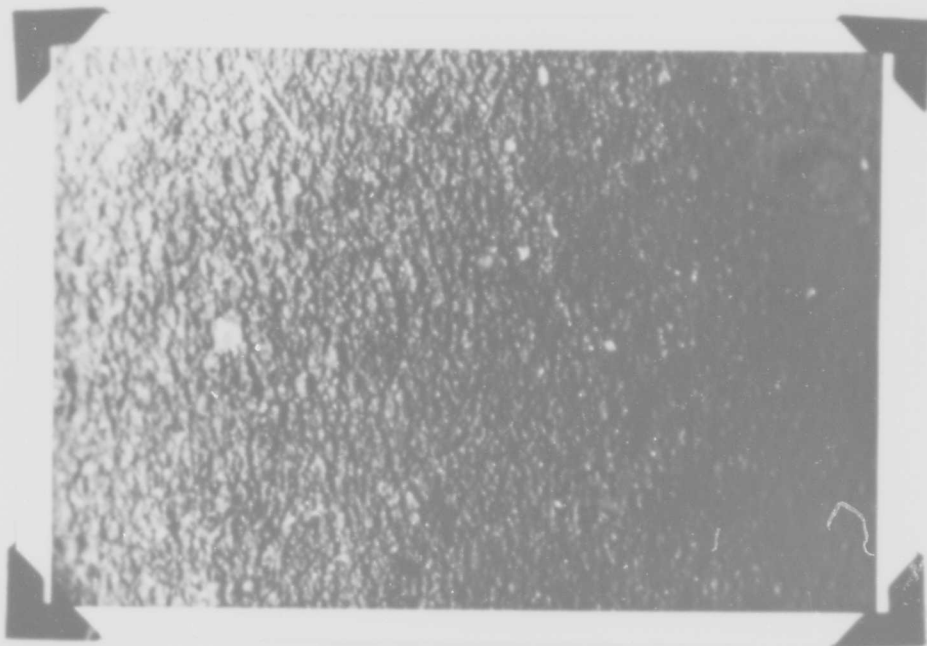


FIGURE 56
MARCH 1964
PAINT PANEL (X30 MAG)

as a "filler" rather than as a reinforcing material. Thus if the maximum physical properties, such as a strong film, are required, it would be desirable to have a cuprous oxide substantially free from these large particles. It is assumed that the electrical properties or any other required property would be either enhanced or at least not degraded by the use of a smaller particle size cuprous oxide.

The accompanying darkfield photomicrographs, at a magnification of xl200, show the cuprous oxide in this paint. The preparations were made by a method used to prepare thin sections of a rubber compound¹. Fig. 57 is an area which is typical of the compound, showing both the smallest particles, range of sizes and those which approach the maximum. The elastomeric binder is present in about the normal quantity in this area. This was taken with direct light on the material in question.

In some other areas of the preparation, the large particles predominate because they have been literally shoved out, separated from the elastomer, by the techniques of making the preparation; actually this phenomenon is an indication of what may be called the lack of coherence of the large particles to the elastomer. One of these areas is shown in Fig. 58. This was taken by diffused light where the large particles have been pushed out of the binder and are on the surface reflecting the light.

General conclusions resulting from this specific study were:

- (1) The Cuprous Oxide particle size is larger than that desired for a good rubber reinforcing segment.
- (2) Improved application technique has increased the uniformity of the paint layers to an acceptable level.
- (3) Future procurement of anti-fouling paint will be followed closely to insure adherence to pertinent specifications.

¹ ANAL. Chem. JIEC. 2, 311 (1930)

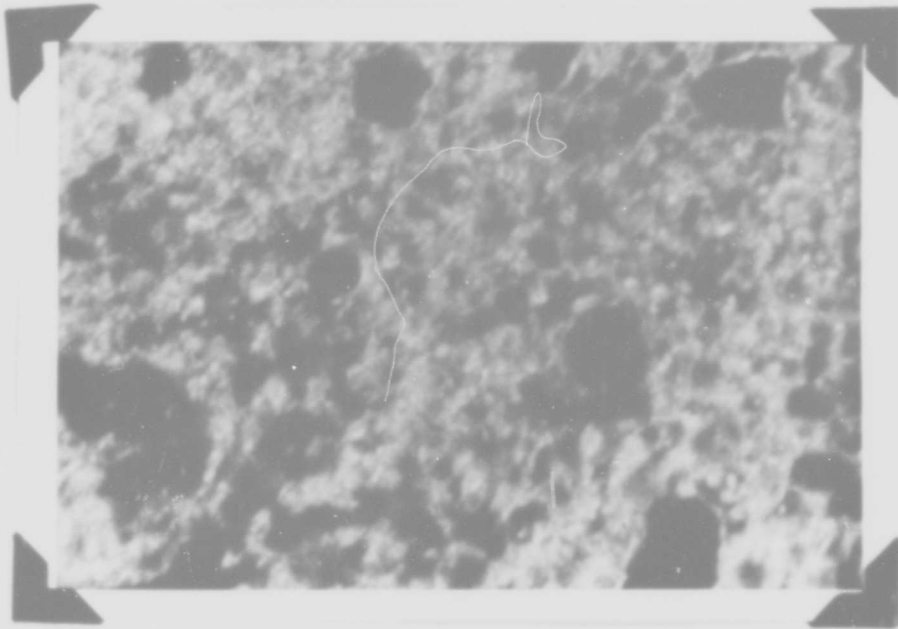


FIGURE 57
ANTI-FOULING PAINT IN DIRECT LIGHT @ X1200 MAG.

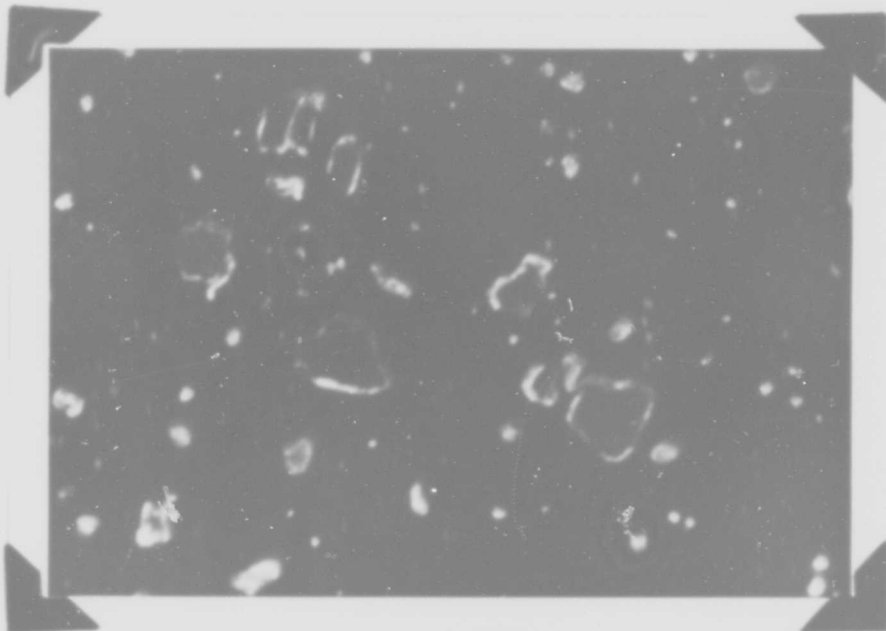


FIGURE 58
ANTI-FOULING PAINT IN DIFFUSED LIGHT @ X1200 MAG.

d. Conclusions

Final conclusions resulting from this program were:

- (1) B.F. Goodrich adhesive 423552 furnishes an excellent bond between the acoustic window neoprene wall and the polyisobutylene anti-fouling paint.
- (2) Extended artificial sea water soakage (6 months) does not deteriorate the anti-fouling paint-tie coat system.
- (3) Acoustical energy bombardment up to 139½ hours does not affect the coatings.
- (4) Specific application procedures for the anti-fouling paint must be followed to insure uniformity of coating.
- (5) B.F. Goodrich adhesive 423552 and the Polyisobutylene anti-fouling paint should be used on the prototype acoustic window for protection purposes.

10. Prototype Test Panel

a. Summary

The net result of this program was the fabrication and testing of a complete, full size, acoustic window test panel. This panel represents the aft, most complex, section of the dome and includes a splice for adjacent panel attachment. Successful testing of this panel verified the acceptability of the pressurized cable-reinforced rubber acoustic window concept.

b. Introduction

Completion of Phase I, "Determination of Feasibility" was to include the satisfactory testing of a full size prototype panel. It was desirable from this standpoint that:

- (1) Test results would verify sample test data and provide precise data for design of the prototype acoustic window.
- (2) Proposed construction would be tested in the best simulated condition short of full dome window evaluation.
- (3) Degree of contour attainment would be determined.
- (4) Attainment of smoothness requirements could be evaluated.
- (5) Design and fabrication procedures could be determined prior to the prototype acoustic window program.

In considering what segment of the complete window to fabricate it was determined an aft section would be most desirable from the standpoint of beneficial results to B.F. Goodrich and the U.S. Navy. This area is the most complex of the entire acoustic window, possessing a non symmetry as well as a slight reverse curvature. To attain this configuration would surely indicate the remainder of the window can be correctly fabricated.

This panel, Figure 59, representing the aft, starboard section of the window, includes a full size panel, a seam for attaching adjacent panels and a panel extension to remove jig reinforcing effects from the immediate seam area. With this concept it then becomes possible to test simultaneously the complete panel and splice area and obtain the necessary test data.

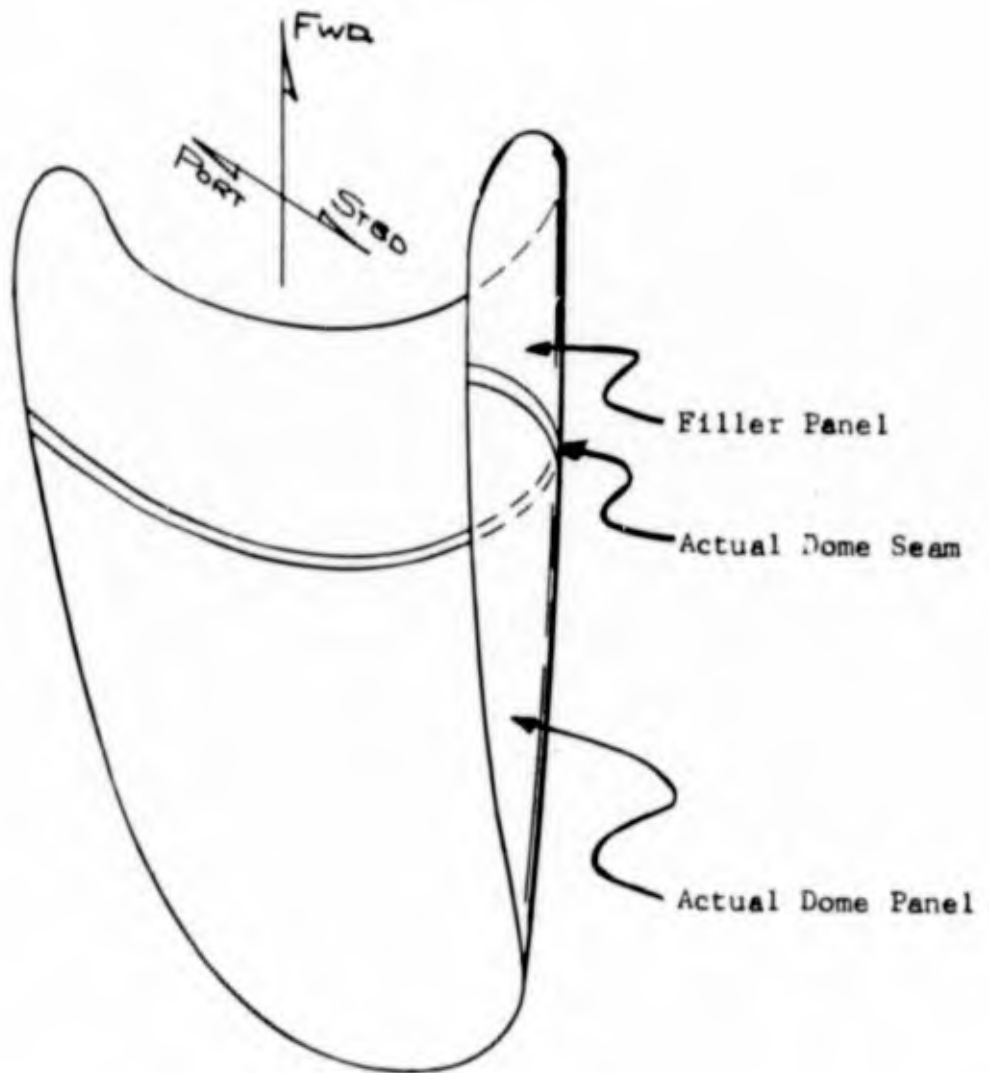


FIGURE 59
PROTOTYPE TEST PANEL

During fabrication of the panel, separator material will be placed in the critical splice area to permit complete separation of the segments after cure. Thus, fabrication of the splice will duplicate the procedure intended for production.

c. Panel Design

(1) Contour Determination

Drawings of the DE-1040, DLG-26 and DL-4 ships were received from Bu Ships on July 26, 1963. Immediately upon receipt of these drawings maximum effort was expended in the design of the cable-reinforced rubber window for replacement of the steel plate - steel ribbing structure of the current Bow Domes. Initial plans called for completing the final design of the acoustic window (requested to use DL4 drawings for DL-5) for the DL-5 dome and then utilize an aft segment for the prototype test panel. However, during the course of this endeavor it was determined that a more expeditious approach would be to utilize an arbitrary contour for the prototype panel and necessary tooling and complete Phase I in minimum time. The fact that the forward contour is relatively simple to attain, prompted the decision to concentrate on the aft, starboard panel.

Coordinates of the DLG-26 steel dome were layed out with water lines, frames and buttock lines. Once complete these drawings were utilized in laying out the rubber window and determining the contour for tooling design.

In the rear section of the dome, commencing at approximately the sound absorbing baffle area and aft, the curvature of any cross section becomes a composite of curves and generally not circular. A pressurized vessel, flexible in nature, such as the acoustic window, will tend to assume the maximum volume shape of a sphere. The problem then is one of taking a vessel that wants to assume spherical characteristics and constrain it to satisfy the desired contour. This problem had to be resolved prior to panel tooling design.

Several initial schemes were considered:

- (a) Built-in grid plates - This approach, Figure 60, requires contoured grid plates fabricated into or attached to the construction. The complexity of this operation would be severe with an impairment of acoustics.
- (b) Warp Membrane by Anchoring. - This concept, Figure 61, requires attachment of restraints to the membrane wall, with resultant buckling in some areas. This would require additional fill and possibly sculpturing to contour. Penetration of the wall for anchoring is undesirable with the internal cable structure possibly acting like a tuning fork.
- (c) Double Construction. - This system, Figure 62, requires a separate pressurization source for contour. Also, a multi-cavity construction would add complexity to fabrication and impede acoustic transmission.
- (d) Rubber Fill. - The rubber fill idea, Figure 63, has considerable merit in that internal support structures are eliminated. The main detriment is magnitude of fill which might affect acoustics. Future study is planned to minimize the amount of fill required, determine affects on acoustics and obtain optimum fabrication techniques.
- (e) Compression Member. - This concept, Figure 64, requires the use of an internal contour support suitably reinforced to prevent collapse. This idea is not desirable acoustically, however, it minimizes alterations necessary to the acoustic window. On this basis and as a means of continuing progress, it was decided this concept would be utilized in the prototype panel. Additional effort was planned to further investigate potential methods for a more desirable approach.

With the method of contour attainment determined for the prototype panel efforts were initiated to determine fabrication contour. Originally, plans called for determining the complete acoustic window contour, shrinking the tooling for expected stretch of the membrane during pressurization, thus ending up with the exact steel dome contour when fully inflated. Problems encountered during

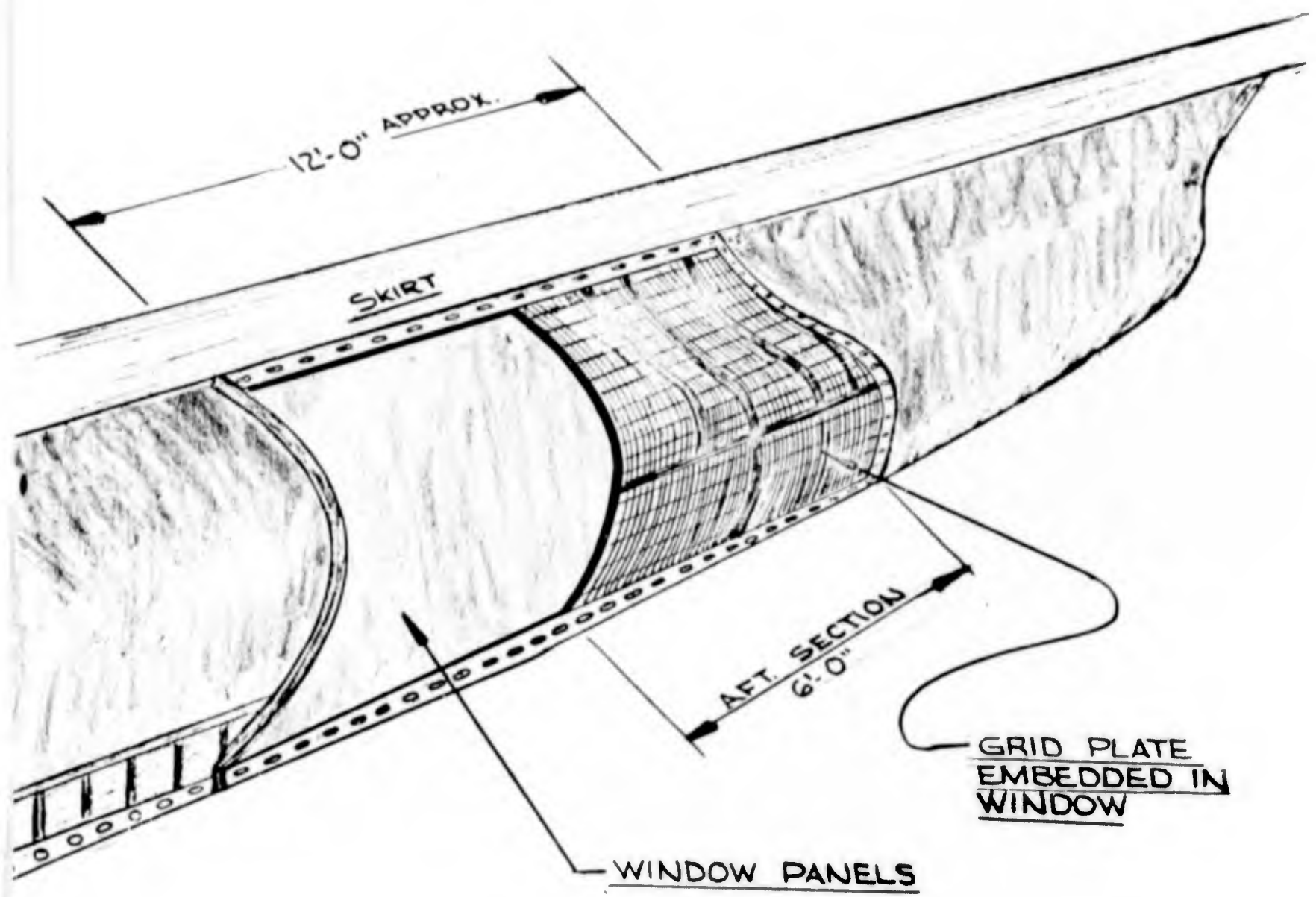


FIGURE 60
AFT SECTION GRID PLATE CONTOUR MEMBER

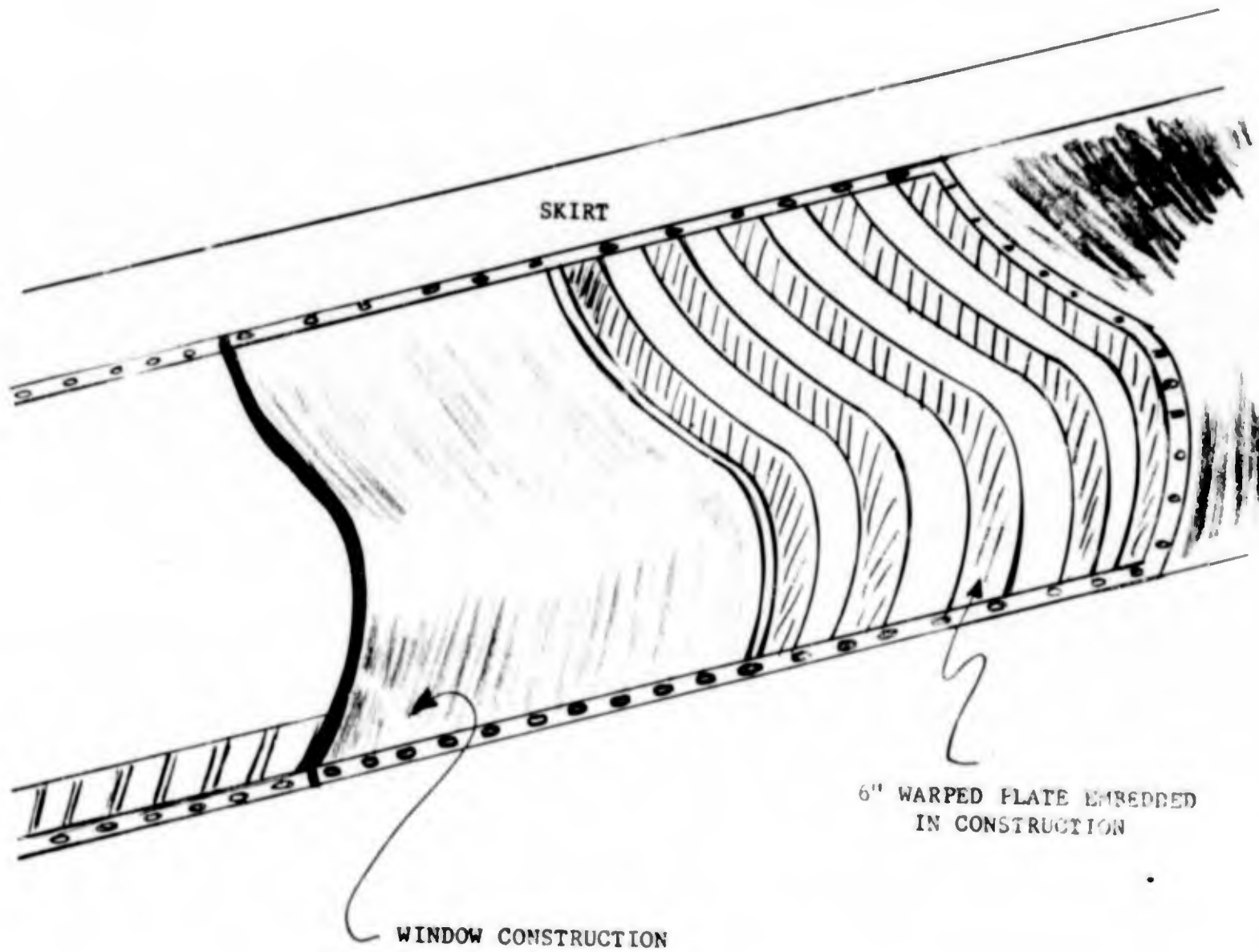
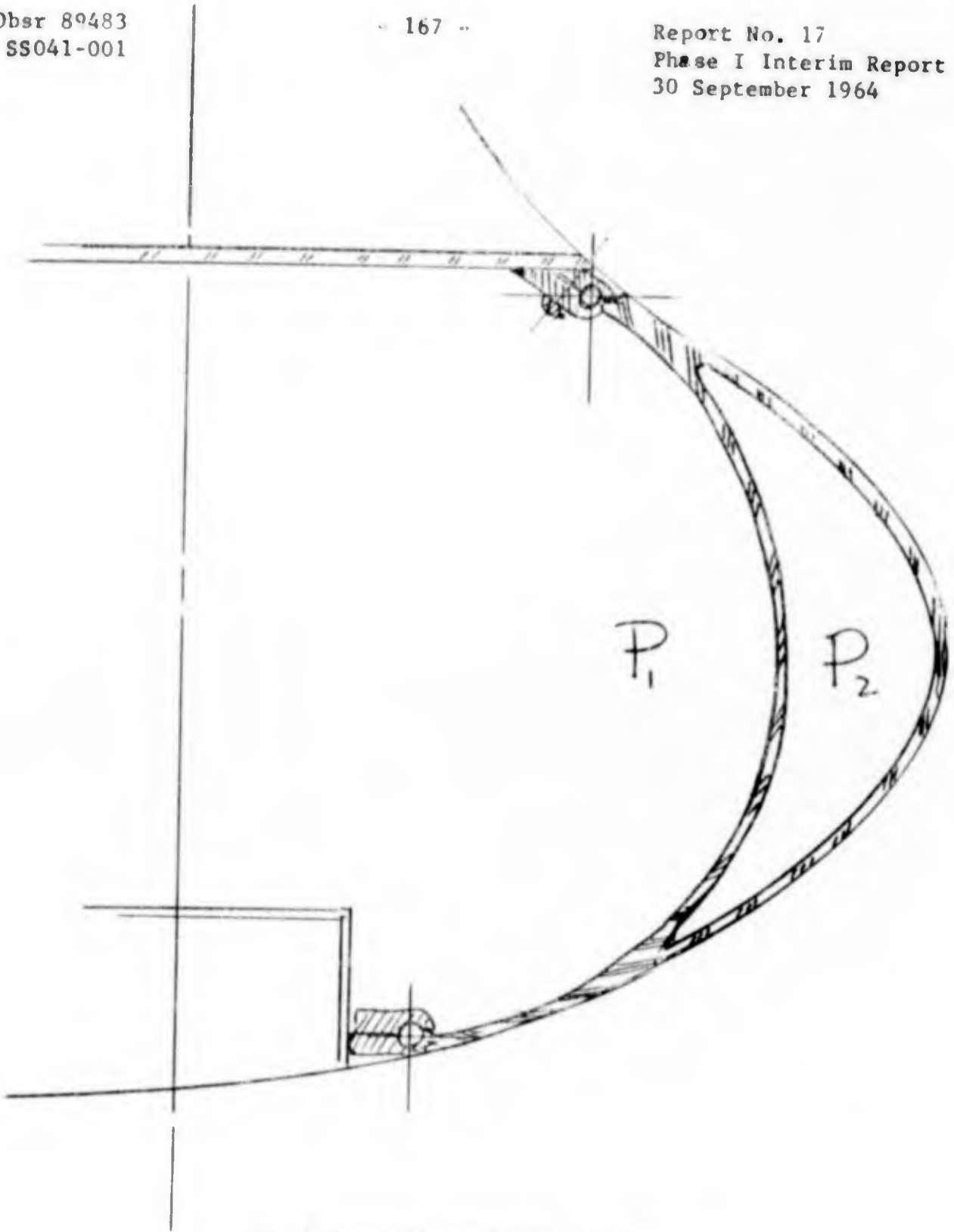


FIGURE 61
AFT SECTION CONTOUR ATTAINMENT BY WARP MEMBRANE



P_1 = INTERNAL PRESSURE IN DOME
 P_2 = CAVITY PRESSURE APPROACHING
BUT NOT EQUAL TO P_1

FIGURE 62
AFT SECTION CONTOUR ATTAINMENT BY DOUBLE WALL CONSTRUCTION

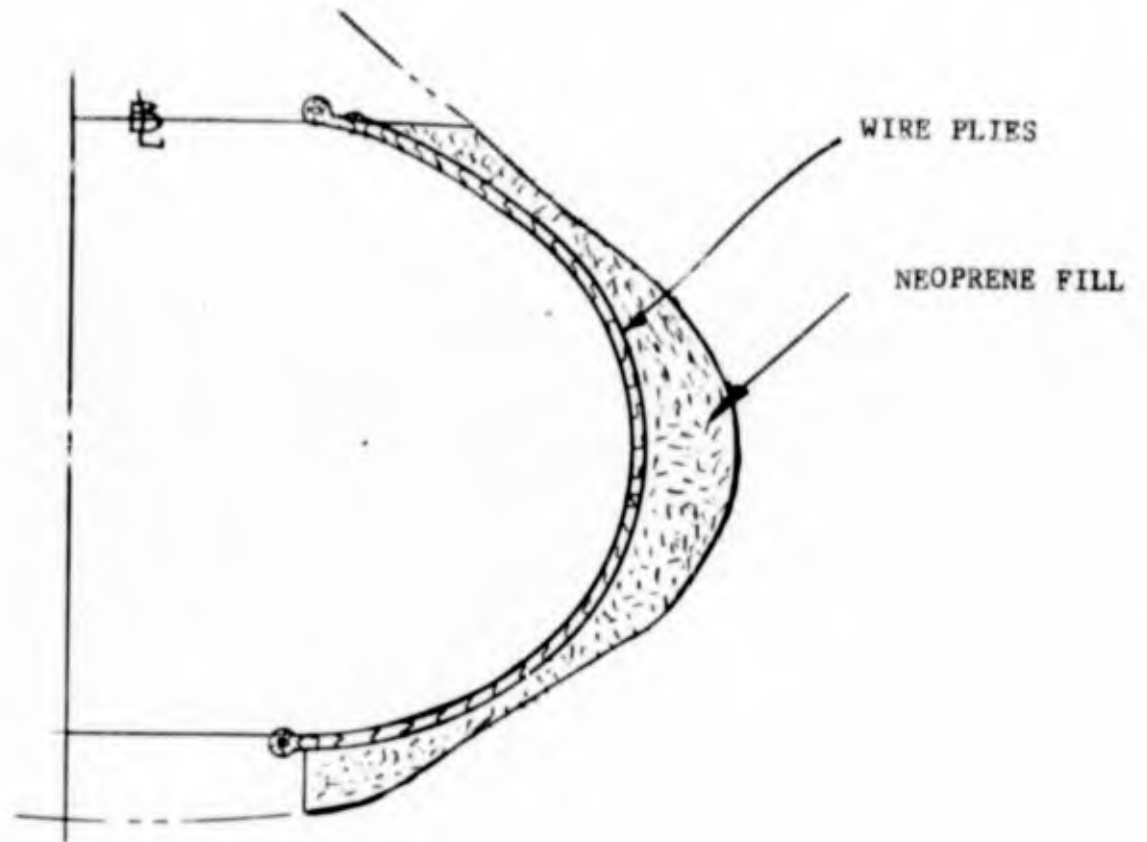


FIGURE 63

AFT SECTION CONTOUR ATTAINMENT BY RUBBER FILL

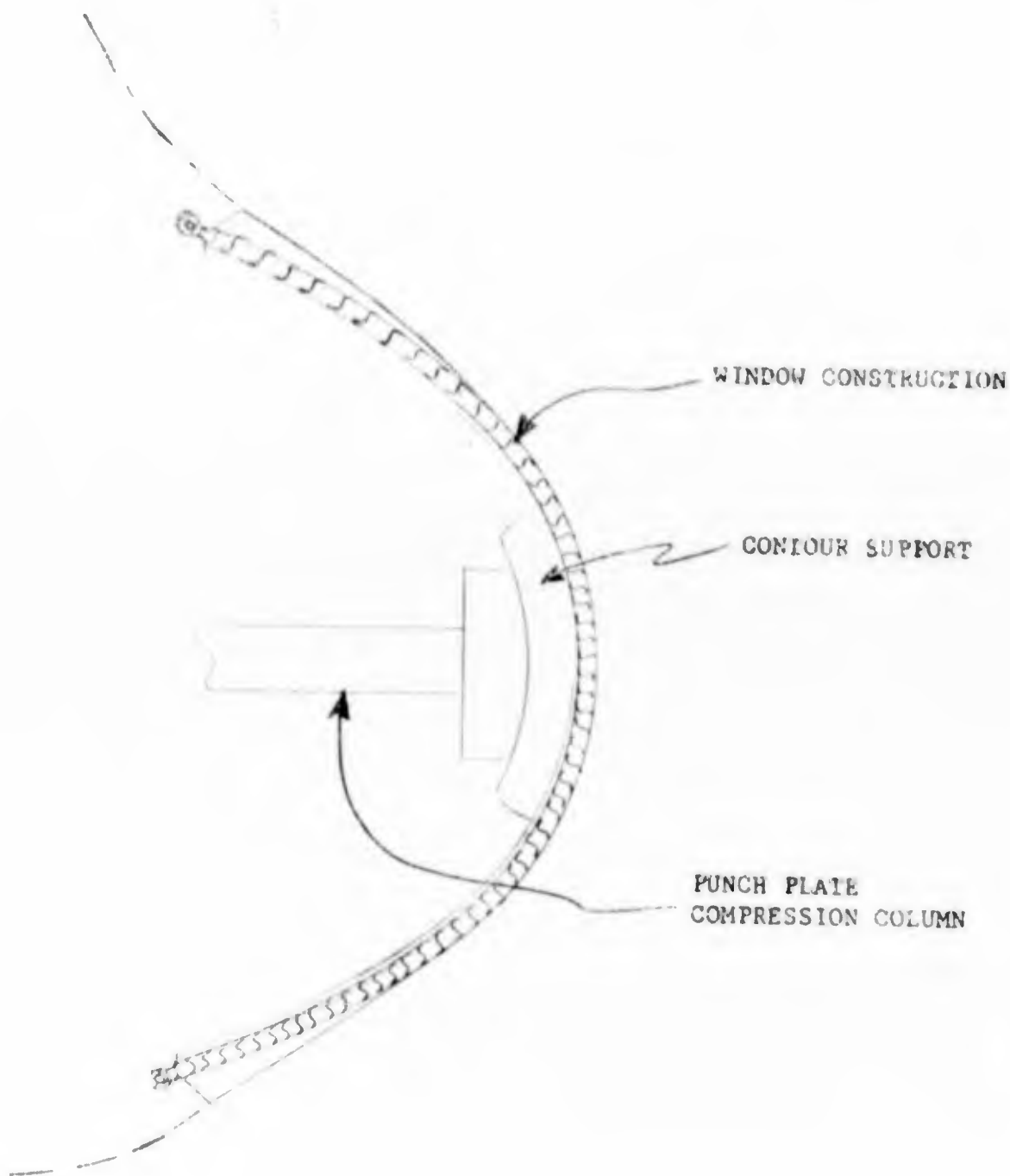


FIGURE 64
AFT SECTION CONTOUR ATTAINMENT WITH COMPRESSION MEMBER

testing, as discussed, delayed determining the stretch of the panel and obtaining necessary shrink factors. Because of this it was decided that the steel dome contour would be utilized as the base prototype panel contour. During pressurization change of panel length and radii would be monitored from the base or initial contour and additional shrink factor data obtained.

In designing a pressurized acoustic window the means and placement of the attachment mechanism is extremely important. The radius of the window, upon pressurization, would be determined by the attachment points. For proper hydrodynamic flow any mismatch of the window and ships structure must be properly faired using a gum fill. A cross section of the panel is shown in Figure 65. It can be seen that the strength members are arcs and the contour is attained by the gum fill.

The specific drafting procedure utilized can be outlined as thus:

- (a) Lay out steel dome contour in frames, water lines and buttock lines.
- (b) Determine general location of bead centerline with respect to the steel structure.
- (c) Transpose transverse frames to radial frames with respect to the -4' WL. (Figure 66)
- (d) Lay in arc depicting strength plies of rubber window and locate exact bead centerline.
- (e) Determine amount of fill necessary for proper fairing.
- (f) Fair final contour during each applicable step so that fairness is maintained in frames, waterlines and buttock lines.

In this design of the aft panel we were required to obtain something other than a true arc. Therefore, our approach was to incorporate a compression member and utilize three (3) separate arcs as shown in Figure 67. The separate arcs blend, resulting in a smooth uniform curvature on the outside surface.

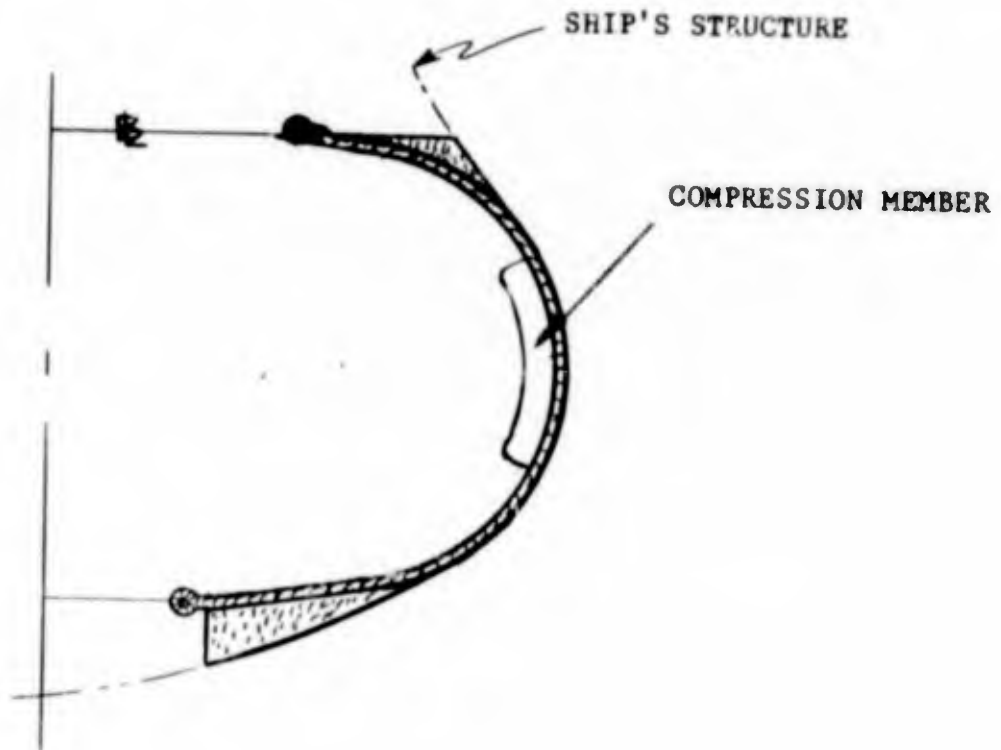


FIGURE 67
CROSS SECTION OF PANEL WITH COMPRESSION MEMBER

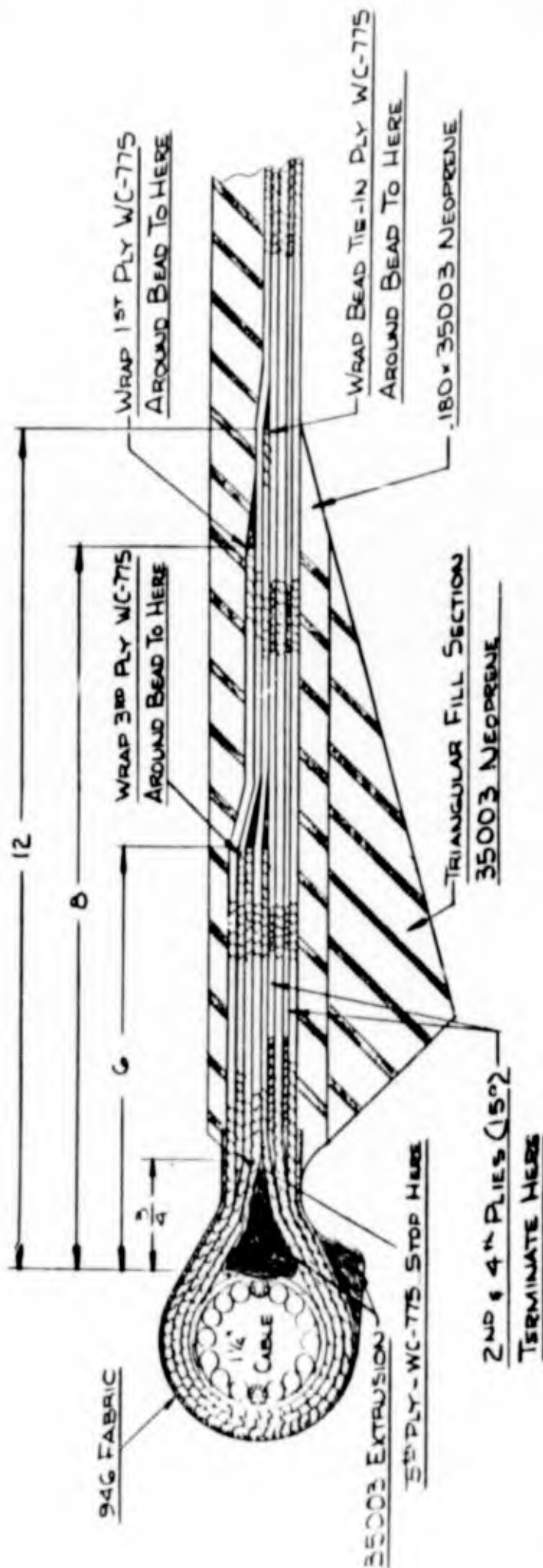


FIGURE 65
 CROSS SECTION OF WINDOW CONSTRUCTION

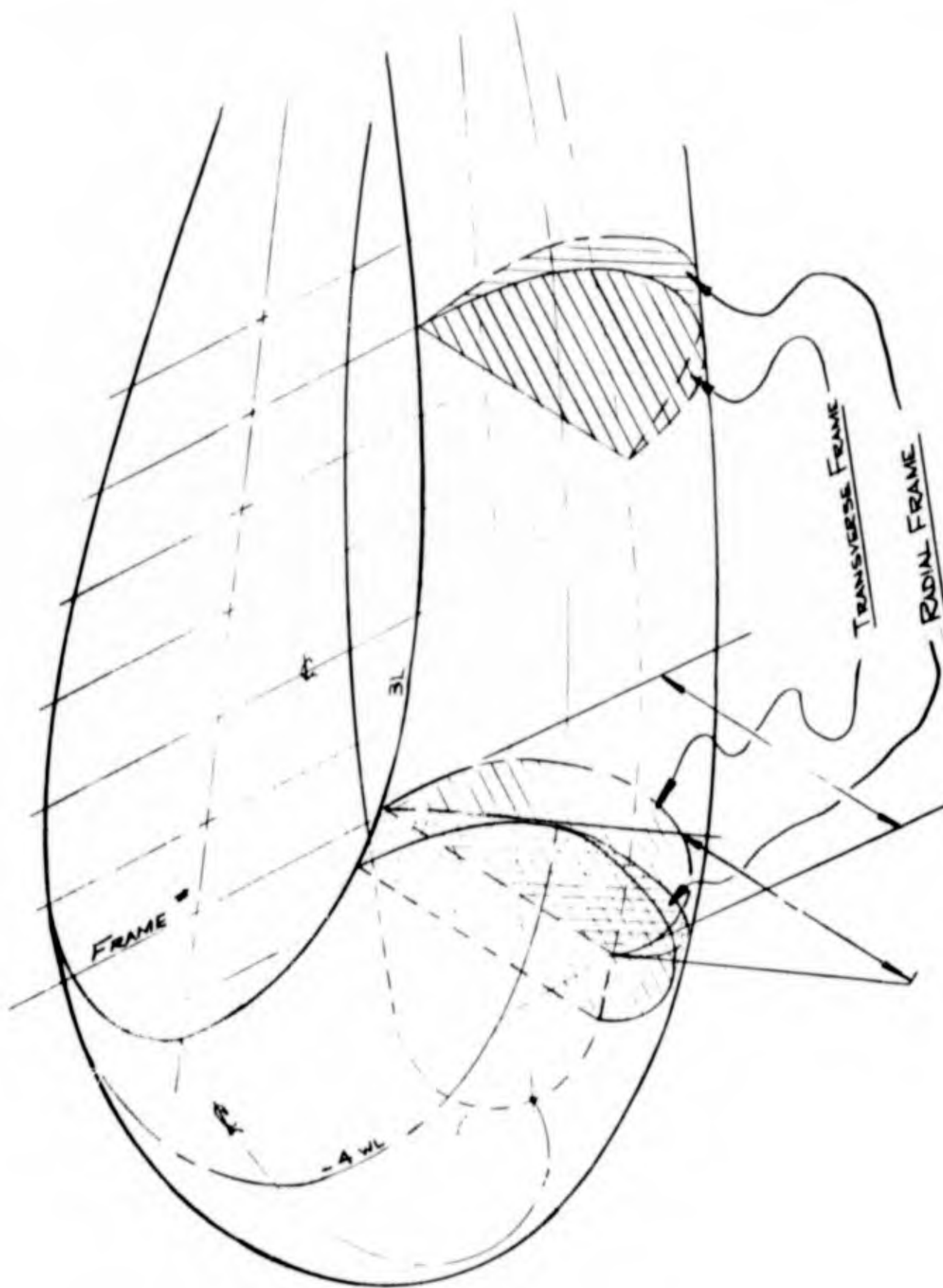


FIGURE 66
RADIAL FRAME DETERMINATION

To actually document the panel contour for tooling design and fabrication a coordinate system was established. This system utilizes frames, waterlines and a "d" dimension. A reference plane was established parallel to the panel - 4" WL and 15° off the ship's center line. Dimension taken from this plane are "d" dimensions.

Dimensions determined from this coordinate system are illustrated in Table XXIII and were utilized in tooling design.

(2) Panel Construction

Utilizing the knowledge obtained from the sample fabrication and testing program the panel construction was finalized. It was determined the build up should consist of basically 5 wire plies and 4 neoprene plies laminated together to yield a 1" thickness. Actual ply orientations are shown in Figure 68. Three (3) plies are oriented vertically and two (2) plies 15° off the horizontal. In addition two (2) short 38° plies were added at each end to distribute stress concentrations at transition points. Transition points can be defined as areas where the panel ply wrap around the bead is changed from the vertical to 15° cables. This permits the load bearing cables at the panel ends, 15° plies, to tie into the bead directly.

A 1-1/4" wire rope will be utilized as the bead core. Around this core will be wrapped, using the composite design, the layers of wire fabric comprising the panel strength plies.

(3) Panel Seam Fabrication

Fabrication of the complete prototype acoustic window, utilizing available autoclaves for curing the neoprene depends on the acceptability of the seams used to attach adjacent sections together. Therefore it was considered important that the initial panel be fabricated in two (2) pieces and spliced together. Thus, testing of the completed panel would not only furnish strength and contour characteristics but the acceptance of the seaming technique.

BLANK PAGE

Table XXIII
 Coordinates of Prototype Panel

RADIAL FRAME 7		RADIAL FRAME 8		RADIAL FRAME 9		RADIAL FRAME 10	
Z	Y	Z	Y	Z	Y	Z	Y
6.000	29.625	6.000	29.312	6.000	29.00	6.000	28.687
6.250	33.687 <i>Bd</i>	6.250	33.687 <i>Bd</i>	6.250	33.437 <i>Bd</i>	6.250	33.250 <i>Bd</i>
12.00	24.375	12.000	23.875	12.000	23.375	12.000	22.937
24.000	13.343	24.000	12.75	24.000	12.275	24.000	11.781
36.000	4.625	36.000	4.312	36.000	4.125	36.000	4.10
48.000	1.437	48.000	1.406	48.000	1.343	48.000	1.437
60.000	5.032	60.000	4.468	60.000	4.093	60.000	3.906
72.000	16.500	72.000	15.406	72.000	14.312	72.000	13.00
84.000	40.250	84.000	36.437	84.000	32.750	84.000	30.00
84.375	57.875 <i>Bd</i>	87.187	65.625 <i>Bd</i>	89.906	70.968 <i>Bd</i>	92.062	75.500 <i>Bd</i>
87.750	53.00	91.125	61.687	94.312	67.750	96.000	68.375
						96.750	71.500

RADIAL FRAME 11		RADIAL FRAME 12		RADIAL FRAME 13		RADIAL FRAME 14	
Z	Y	Z	Y	Z	Y	Z	Y
6.000	28.312	6.000	28.00	6.000	27.687	6.006	27.437
6.250	32.937 <i>Bd</i>	6.250	32.625 <i>Bd</i>	6.250	32.437 <i>Bd</i>	6.250	32.313 <i>Bd</i>
12.000	22.437	12.000	22.062	12.000	21.750	12.000	21.500
24.000	11.531	24.000	11.250	24.000	11.125	24.000	11.187
36.000	4.10	36.000	4.125	36.000	4.250	36.000	4.563
48.000	1.812	48.000	2.062	48.000	2.375	48.000	2.812
60.000	3.968	60.000	4.00	60.000	4.250	60.000	4.375
72.000	11.687	72.000	10.875	72.000	10.343	72.000	9.812
84.000	27.00	84.000	25.30	84.000	23.718	84.000	22.00
94.000	76.656 <i>Bd</i>	96.000	54.312	96.000	49.750	96.000	45.812
96.000	60.437	96.125	78.187 <i>Bd</i>	97.906	79.000 <i>Bd</i>	99.437	79.000 <i>Bd</i>
98.875	73.625	100.312	75.062	101.750	76.000	103.875	75.937

RADIAL FRAME 15		RADIAL FRAME 16		RADIAL FRAME 17	
Z	Y	Z	Y	Z	Y
6.000	27.375	6.000	27.250	6.750	26.437
6.250	32.125 <i>Bd</i>	6.250	32.125 <i>Bd</i>	6.940	30.500 <i>Bd</i>
12.000	21.375	12.000	21.250	12.000	21.250
24.000	11.125	24.000	11.500	24.000	11.937
36.000	5.125	36.000	5.812	36.000	6.437
48.000	3.218	48.000	4.00	48.000	4.750
60.000	4.625	60.000	5.250	60.000	5.875
72.000	9.781	72.000	9.906	72.000	10.437
84.000	20.875	84.000	19.812	84.000	19.687
96.000	42.437	96.000	39.125	96.000	38.437
100.937	77.750 <i>Bd</i>	102.000	75.000 <i>Bd</i>	101.562	68.375 <i>Bd</i>
105.500	74.812	106.375	72.125	105.625	64.875

NOTE:
 1. Radial Frame 13 at center of splice
 2. *Bd* notation designates bead centerline

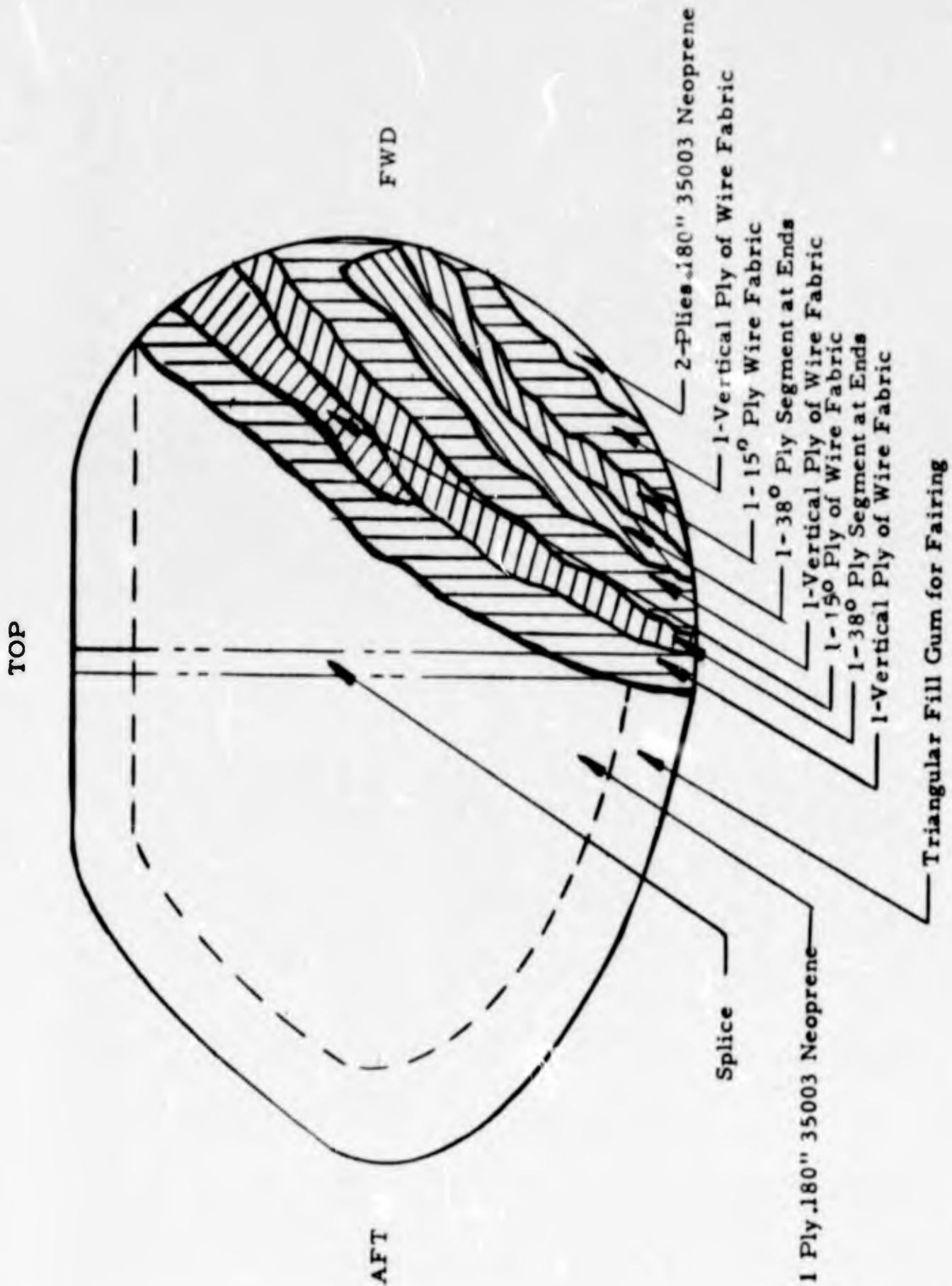


FIGURE 68
PROTOTYPE PANEL PLY ORIENTATION

The cable-reinforced rubber bow dome window will be fabricated in sections and spliced together to form the complete unit. This splicing operation has been the subject of a separate study to insure sufficient strength is obtained to maintain dome integrity during service.

Representative splice sections furnishing 6", 9", and 12" overlaps, as illustrated in Figure 69, have been investigated as part of the 2-3/4" sample test program. The data obtained are shown in Table XXIV, Lap Splice Strength.

TABLE XXIV

LAP SPLICE STRENGTH

<u>Splice Length</u>	<u>Strength (#/in.)</u>	<u>Remarks</u>
6" Lap	5545	Neoprene stock failed.
9" Lap	6370	Neoprene stock failed.
12" Lap	9410	Tensile failure of cables in panel.

Development of the computer program, Appendix V permits the computation of maximum expected tension in both the horizontal and vertical ply cables. The program output is available at B.F. Goodrich and because of its volume will not be included in this report. From this the maximum expected tension on a splice is 504 lbs./inch.

All splice sections tested furnish the desired strength and with the 9" lap exhibiting approximately a 120 safety factor and the 12" lap a 18 safety factor. Analysis of conditions to be encountered and possible variation of strength in a full size lap indicates a 9" lap will suffice for this panel.

- (1) Meet contour within requirements of the contract, $\pm 3/8"$ of design coordinates.
- (2) Smoothness of mold to be within requirements of contract when 3 ft. batten is used and $1/8"$ feeler is excluded over 100% and $1/16"$ feeler over 75% of length.
- (3) Mold structure to be strong enough to permit builders to fabricate panel.
- (4) Mold to be capable of cure cycles of 300°F , 90 PSI, open steam - 10 hour duration.
- (5) Life of mold to be at least 10 complete parts.

With these requirements in mind and the contour and coordinates of the panel available, final tooling design was the major outstanding effort prior to panel fabrication.

During the time panel contour was being determined, mold design was in process. The first hurdle to pass was the question of steel versus plastic tooling. In each instance either the size or shape and intent of the tool was making this a novel item. Reliability of steel tooling is its greatest asset. However, when considering the contour of the part, with the corresponding tolerances, the cost and delivery of such an item are adversely affected. Plastic tooling of this size for use in an open steam autoclave is non-existent up to the present time. Therefore, the reliability and extended production use of such an item has not been determined to date.

Vendors for plastic and steel tooling were approached, the tooling discussed, and a quotation requested. When all bids were received (as noted in Table XXVI) the plastic tooling was quoted at half the price of steel with delivery in about half the time. On this basis, and satisfactory testing of segments of glass-epoxy laminate, it was decided the purpose of the project could best be served by using plastic tooling.

In addition to bonding adjacent membrane plies the bead cable will have to be attached together. This attachment will not be subjected to any extreme tension load, but will restrain the ply cables from slipping thru. This action will result in a compression force from the tension exerted by the ply cables.

Samples of 1" diameter IWRC cable were ground at 45° and welded together. Test results are shown in Table XXV.

TABLE XXV
BEAD CABLE ATTACHMENT

<u>Cable</u>	<u>Attachment</u>	<u>Tensile Loads</u>	<u>Remarks</u>
1" Dia. IWRC	Welded W/55310 Rod	42,000	Cable broke adjacent to weld.
1" Dia. IWRC	Brazed W/Silver Solder	17,600	Cable pulled away from braze.

Cable tensile strength is 74,400 lbs. so that at least 56% of the original strength was attained by welding. This is more than adequate for the intended purpose.

d. Tooling

To accomplish the task of building and testing a prototype panel three basic pieces of tooling were required: (1) building mold, (2) seaming fixture and (3) test fixture.

(1) Fabrication of Panel Mold

The prototype panel size, 15' x 10' x 5' draft, and configuration dictates the use of a large, complex tool capable of furnishing the characteristics necessary for proper panel fabrication. In analyzing the requirements of such a tool the following were considered essential.

TABLE XXVI

PROTOTYPE PANEL MOLD COSTS

	<u>Portage Mold Co.</u>	<u>Consolidated Welding</u>	<u>Mandrels Inc.</u>	<u>Latrobe Plastics</u>
Cost	\$27,000	\$34,000	\$10,000	\$24,445
Delivery	8 weeks	12 weeks	8 weeks	8 weeks

The general concept of tooling for this project changed periodically as our knowledge of plastic tooling increased.

The developed procedure consisted of a complex interchange of tooling use resulting in procurement of the entire set of tooling in less time, for less money and being dimensionally more accurate. The tooling utilized in the female building mold sequence were:

- (1) Male model of mold
- (2) Bead seat patterns
- (3) Compression member contour mold
- (4) Seaming fixture heating element mold
- (5) Female building mold
- (6) Master bead

An interlaced effort was accomplished utilizing one type of tooling to fabricate a second. This can be seen in Figure 70 which is a flow diagram of this effort.

(a) Male Model of Mold

Fabrication of plastic mold tooling requires the use of a full scale model as a pattern. In this instance, Mandrels Inc. of Louisville, Ohio was the vendor accomplishing the work. A slab of concrete 20' x 20' square, which was level, furnished the base for the model. Templates furnished by B.F. Goodrich were cut out of plywood and dimensionally checked prior to use. During template fabrication, a rough, undersize and approximate steel angle iron, steel rod, wire and plastic backing was assembled on site. Over this structure were placed the female

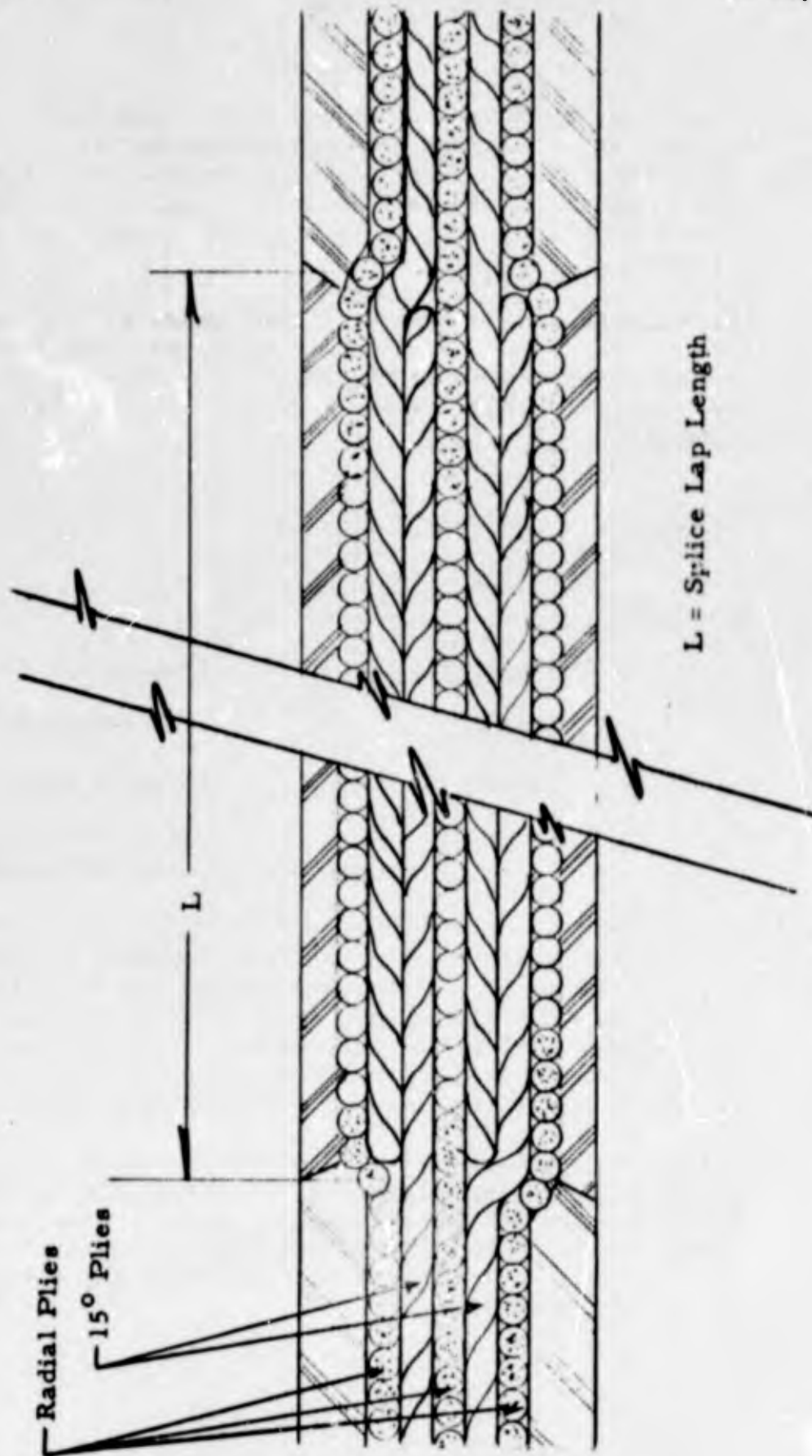


FIGURE 69
SPlice OVERLAP CONSTRUCTION

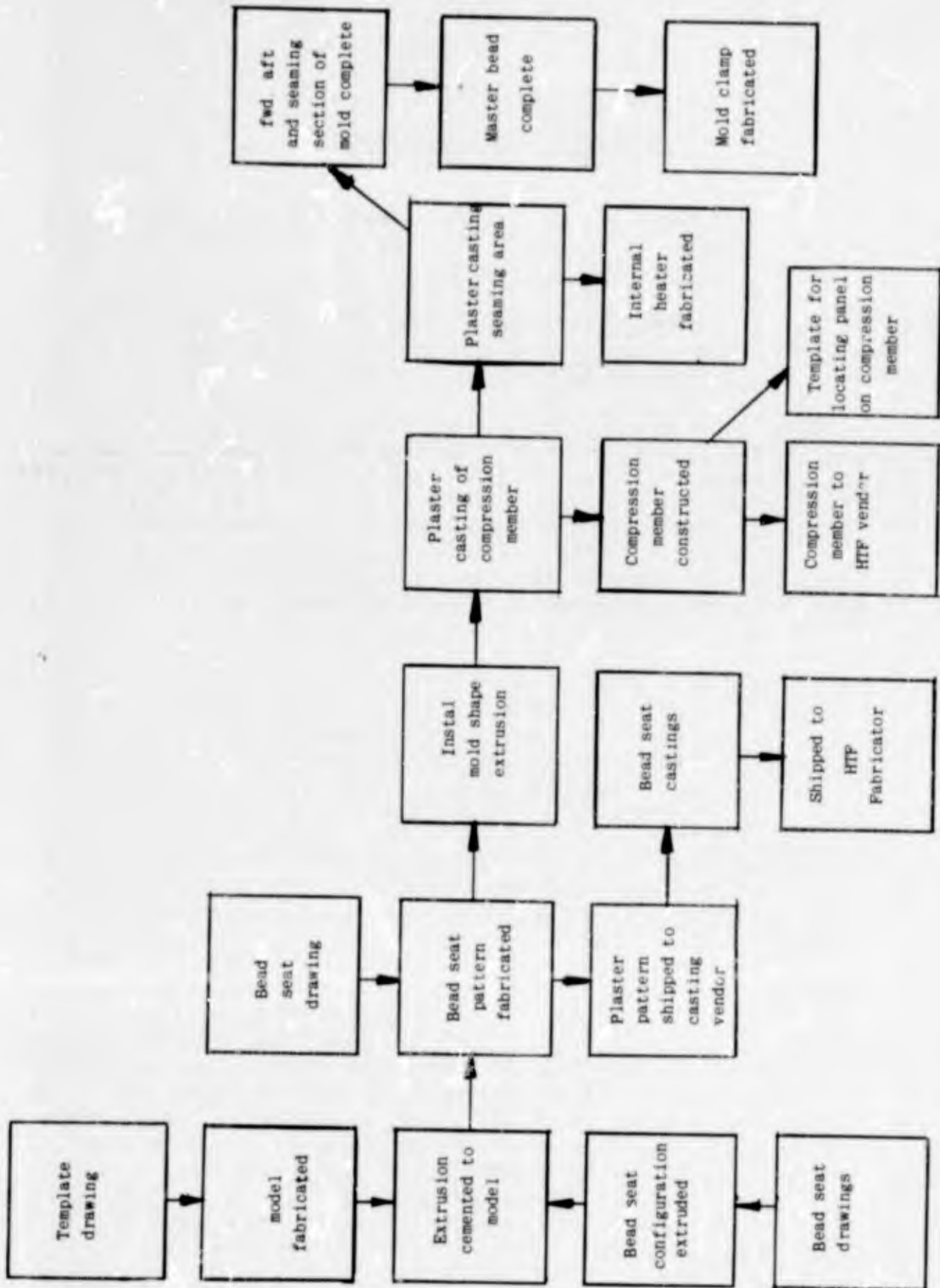


FIGURE 70
TOOLING FLOW DIAGRAM

Contract NOber 89483
Serial No. SS041-001
Task 8156

- 183 -

Report No. 17
Phase I Interim Report
30 September 1964

templates and Ultracal, a form of hard plaster, was forced between the template and the rough model surface. When the Ultracal hardened, the templates were removed resulting in a series of ribs of correct height and contour. Finish plaster was then screeded in the areas between the ribs furnishing the complete smooth model shown in Figure 71 & 72.

In the bead area a rubber extrusion of the exact size of the cavity was cemented and used for fabrication of the bead seat patterns.

(b) Bead Seat Pattern

The rubber extrusion placed in the bead cavity was of the exact size required for bead seat fabrication. Plaster patterns were constructed of an appropriate length, about 2', on the model. They included a tension rod for added strength and an added 1/4" per linear foot which compensated for shrinkage anticipated during casting. When complete, the patterns were shipped to Massillon Casting Company of Massillon, Ohio. These models furnish the exact contour necessary to obtain the continuous, smooth surface necessary for adequate retention and sealing. These models were made of the entire panel periphery and finished to a high degree of accuracy.

(c) Compression Member Contour Mold

Contour of this prototype panel is highly dependent upon the compression member. Therefore, to insure the desired shape is obtained, the upper contour portion of the compression member was cast of Epoxy to the exact surface contour of the panel. The mold for this casting was obtained by taking a plastic impression of the model surface, then filling with a 1" thickness to simulate the panel construction. This resulted in the internal panel contour against which the compression member will rest.

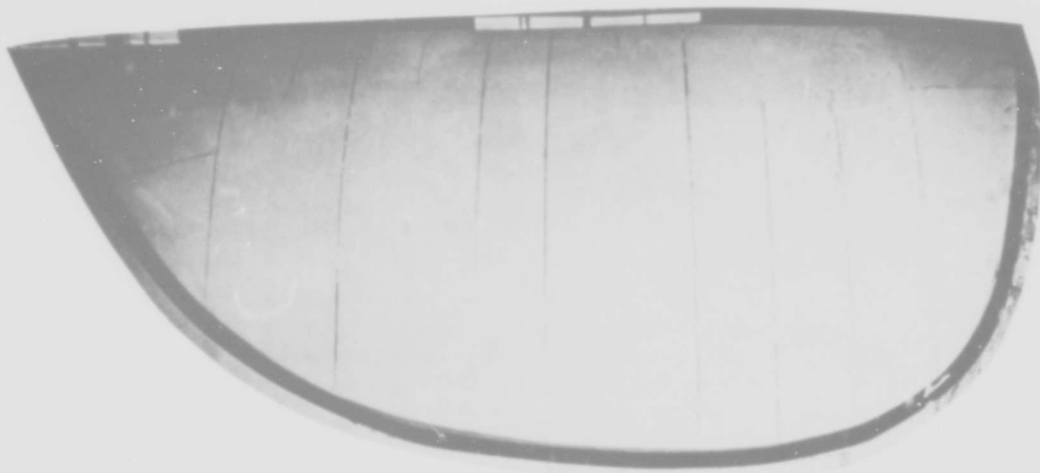


FIGURE 71

PROTOTYPE PANEL MALE MODEL - BOTTOM SIDE

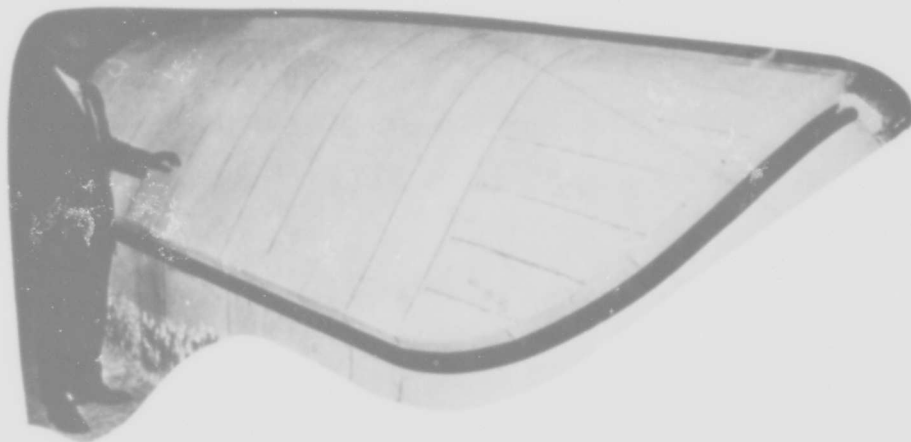


FIGURE 72

PROTOTYPE PANEL MALE MODEL - TOP SIDE

(d) Seaming Fixture Heating Element Mold

During seaming of the panels a heat source will be furnished on the inside of the part. In this instance, since the heater is rigid, contour is critical. A reinforced plaster cast was taken of the seam area and this, in turn, was used as the mold for the heater build up. This consisted of iron wire mesh 3/8" opening and .105 dia. wire embedded in an epoxy build up.

(e) Female Building Mold

Upon completion of the aforementioned castings the rubber extrusion in the bead was replaced with a second extrusion which was of the panel bead configuration. The difference in the two (2) extrusions is shown in Figure 73. The decrease of the clamp cavity furnishes a compression action when the clamp is in position. This compression facilitates the initial sealing of the system.

The surface of the model was divided into distinct sections per mold design, a forward section, a aft section and a seaming mold section. The plaster model surface was then coated with wax and a layer of aluminum foil. The end sections of the mold were constructed by laminating layers of high strength glass fabric and high temperature, low shrinkage epoxy resin.

Upon completion of the lay up operation the system was cured using heat lamps to the B stage, about 180° - 190° F. It was interesting to note that virtually no shrinkage was measurable from the time of initial lay up until the mold was cured later at B.F.Goodrich.

The center section of the mold or seaming fixture was then fabricated. This build up used the same resin-glass system but required a considerably heavier section.

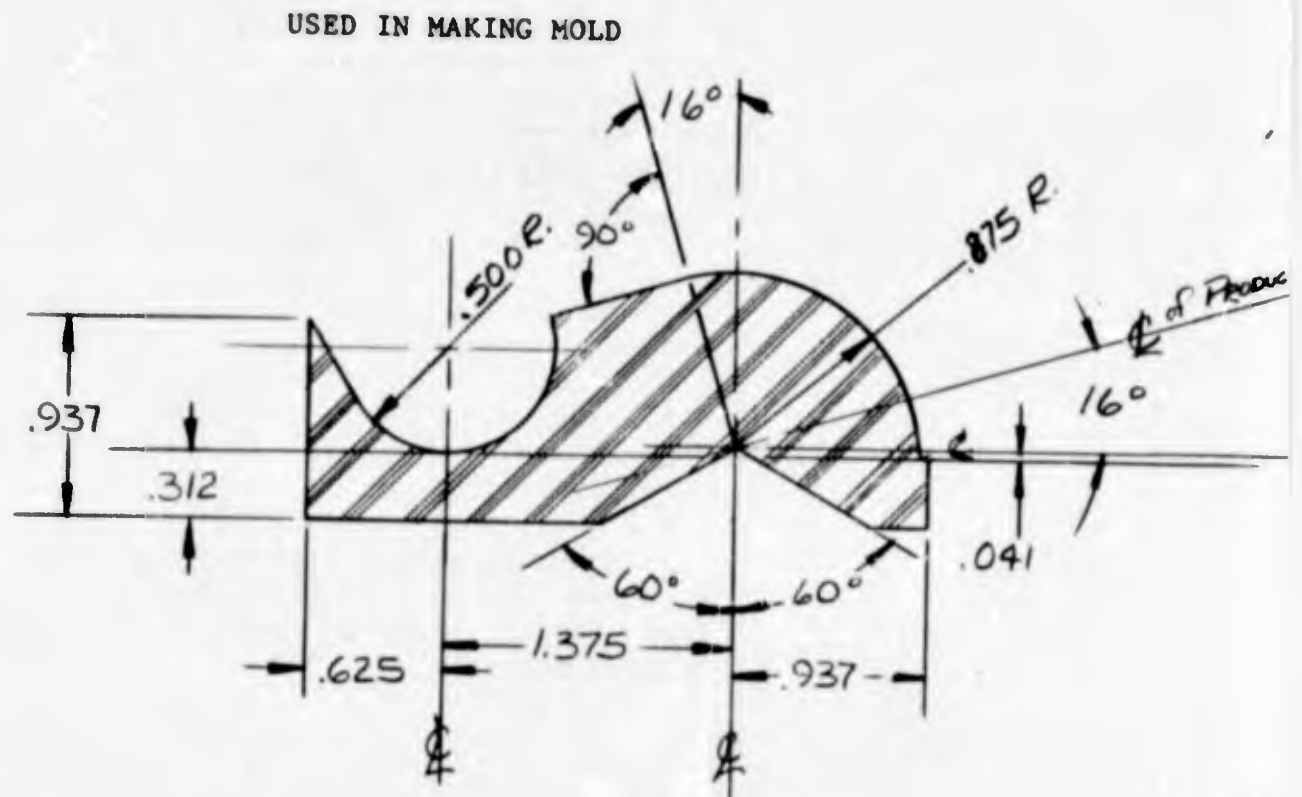
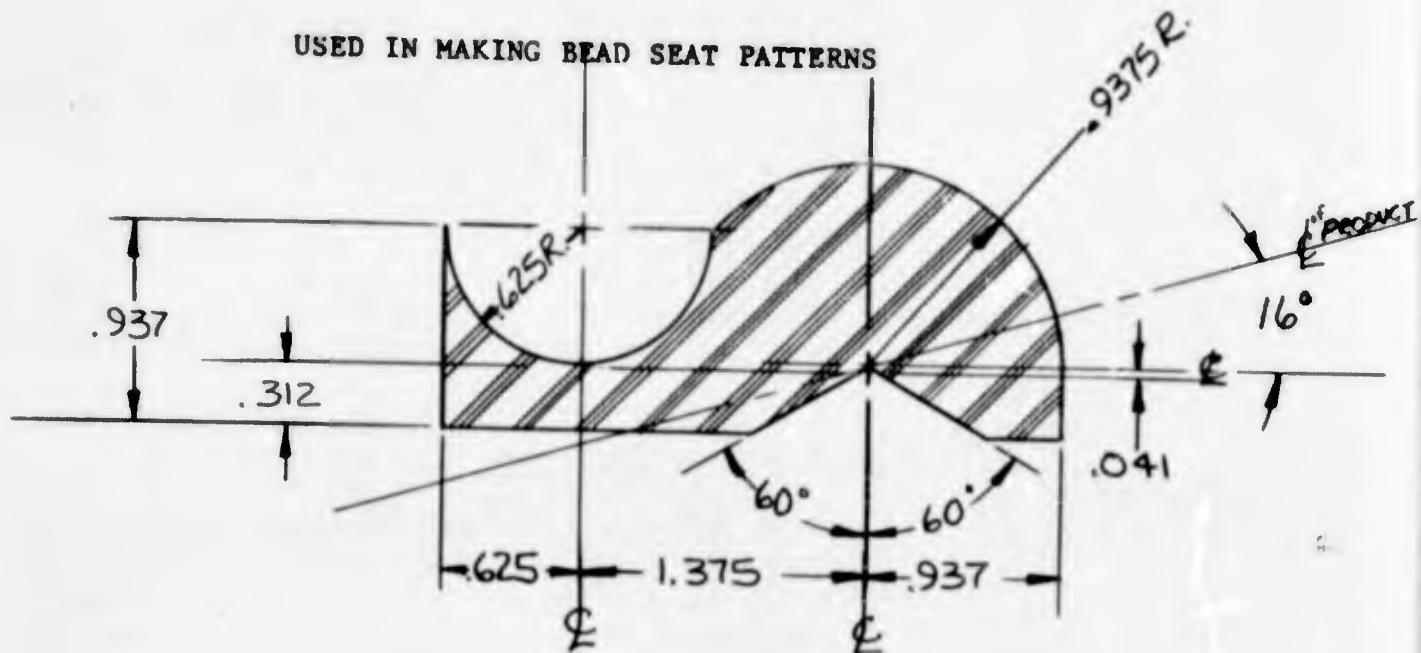


FIGURE 73
RUBBER BEAD EXTRUSIONS FOR USE WITH MODEL

Determination of the actual section of the seaming mold which would be subjected to additional stresses from the pressures encountered during splice curing, was accomplished as a separate structural analysis. It is presented as Appendix VI to show the actual calculations.

In this analysis the flexural and normal stresses were checked. The analysis shows that the maximum flexural stress is 25% of the ultimate flexural strength of the material and the normal tensile strength is 50% of the ultimate tensile strength of the material. Therefore it is concluded that the external flange of the mold splice section possesses a safety factor of about 2 for the anticipated internal, seaming, pressure.

Also built into the seaming section were provision for the heat source to be used during the seaming operation. The entire system was obtained from the Hanco International, Division of Hannon Electric Company, Canton, Ohio. It includes a Model FL-60, 20KVA, 550 Volt, single phase, Flex Power Heating transformer with a variable heating tap switch. From the transformer the current is carried via a woven copper lead to the actual heating elements. These elements consist of two (2) pieces of standard iron wire mesh with 3/8" openings and .105" diameter wire. The bottom element was laminated into the mold surface below the top two (2) glass layers. The element emerged on each end of the mold with sufficient length for bus bar attachment. The upper element was embedded in a separate laminated structure as previously discussed which is positioned over the panel for curing.

During the lamination process tapped inserts, for attaching mold clamps to the mold, were integrated. Also, vacuum taps, for bleeding from a channel exposed on the bottom side of the mold clamps, were built into the construction. Matching holes were located in the adjacent flanges of the forward-seaming mold and seaming mold - aft sections for bolting the sections together. An "O" ring type channel was built in to the seaming section and a silicon seal inserted. As the sections were bolted together the seal became effective.

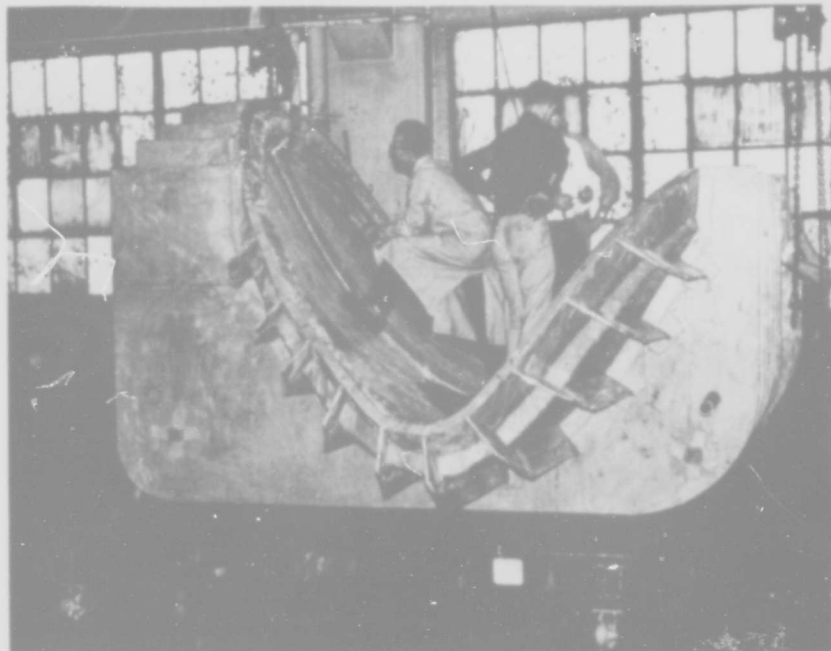


FIGURE 74

ASSEMBLY OF PROTOTYPE PANEL MOLD



FIGURE 75

ASSEMBLY OF PROTOTYPE PANEL MOLD WITH BEAD CLAMPS

Upon completion of the final lay up, the "egg-crate" support structures, which were fabricated as a separate sub-assembly, were bonded to the external surface of the mold. The complete construction was then removed from the model. During removal it was necessary to destroy the model because of back draft of contour.

Subsequent to removal from the model the mold was reassembled and an extrusion simulating the panel bead was inserted in the bead cavity. The bolts, to be used for attaching the clamps, in addition to metal clearance sleeves and washers were installed. Around this complex the mold clamps were laminated, the length of each varying from 12 to 16 inches depending on the curvature and location of the threaded inserts. Using heat lamps the clamps were cured to the B stage, removed from the mold and buffed smooth to obtain a finished surface. The completed mold was delivered to B.F. Goodrich and assembled on site; Figures 74 and 75.

(f) Master Bead

Proper mating of the panel with the test fixture was insured through the use of a master bead. This item was obtained directly from the mold, thus minimizing potential differences between the molded part and the test fixture.

Plaster was screeded into the bead cavity reducing it by 5/16". This meant that the resultant cast bead would clear all theoretical surfaces of the bead cavity when it is installed in the test fixture. This spacing was chosen such that when the bead seat castings are positioned using the master bead and maintaining proper tolerance of $\pm 1/4$ " the two would not contact each other. A flange was also designed into this item to assist in proper orientation of the bead seat during fabrication of the test fixture. The tool was simply a rigid duplication of the panel bead.

The master bead was then built using glass fabric and epoxy resin and steel reinforcement to obtain and maintain the desired configuration. A two (2) piece structure was built to permit installation and removal in the test fixture.

(g) Stabilization Cycle of Mold

Up to this time, or the B-stage of cure, the dimensions of the mold had remained virtually constant. However, the final curing cycle of the epoxy structure had not been accomplished. This final stabilization cycle was necessary to obtain maximum dimensional stability with minimum residual stresses. The entire mold assembly, including in place clamps, was placed in a 12' diam. vulcanizer and the stabilization cycle started. Initially the temperature was raised to 175°F. which is just below the original pre-cure temperature, of 180-190°F. The temperature was held at this level until the entire mold temperature was uniform. Thermocouples had been mounted on the surface of the part and embedded in the heavy seaming mold section. Upon completion of this 4 hour heat soak period the heater temperature was raised in 25°F increments every two (2) hours. This cycle continued until the heater temperature reached 325°F. This upper limit is 25°F. above the maximum panel curing temperature (300°F.) and will permit the use of the mold without fear of deformation.

Upon completion of the cycle the heater temperature reduced slowly minimizing the possibility of residual stresses remaining in the mold.

In checking dimensional stability of the mold during pre cure, post cure and all subsequent cures two (2) types of checks are necessary, warpage and shrinkage. These were determined using a series of six (6) points around the mold periphery. These points were checked and showed a maximum shrinkage to be an insignificant 1/16". The actual arc lengths along the mold surface were measured and found to range from 0 to 1/16" change.

(2) Seaming Fixture

The concept pursued for the splice tooling was designed to make maximum use of other necessary equipment, specifically the building mold. The mold in the seam area was reinforced sufficiently (as discussed) to withstand the forces encountered during seaming.

With the mold capable of taking splicing forces, a top supporting structure, or strong-back had to be designed. This separate strength member would attach to the mold via two 2" diameter steel pins. The structure designed is shown in Figure 76. This includes a steel structure capable of retaining a 100 psi pressure, a cavity for the pressure hose and an attachment mechanism for coupling the mold and the strong-back. In designing the structure for sufficient strength the maximum operational pressure was considered to be 100 psi.

Calculation for designing this structure are shown in Appendix VII.

This structure was determined to be structurally sound with a minimum safety factor of 2.5.

The strong-back was fit checked in the mold and a trial pressure cycle conducted prior to the actual panel seaming operation. The water pressure in the hose was increased in 5 psi increments until 80 psi was attained. The mold seaming structure was visually examined during this cycle. During and subsequent to this cycle, examination did not uncover any type of degradation and the system was considered acceptable for panel seaming.

(3) Hydrostatic Test Fixture

In order to adequately and accurately assess the relative merits of the prototype panel a suitable test fixture had to be designed. During this design program the following objectives were established.

1. Permit maximum test pressure of 150 psi.
2. Possess adequate rigidity to insure changes in panel were not a result of fixture deflection.
3. Closely simulate ship's structure to permit evaluation of boundary bar mounting method.
4. Panel oriented on vertical and horizontal components to aid in measurements.
5. Minimum cost commensurate with function.

Contract No. 801
Serial No. 100, 101
Task 8158

Phase 1, 2, 3, 4, 5, 6, 7, 8, 9, 10
30 Sep. aber 1964



FIGURE 76

STRONG BACK SEAMING STRUCTURE

The early design effort was involved in determining what basic concept should be pursued. Basically, three systems were looked at: (1) Parasite attachment to an existing pressure vessel, (2) Concrete structure with steel reinforcement, and (3) Steel structure with concrete reinforcement.

The use of an already designed or fabricated pressure vessel, either cylindrical or conical, was initially considered desirable from a cost and time standpoint. Reasoning was that the necessary boundary bar system would be welded directly to the basic structure after minor reinforcing. However, after delving into this superficially it was seen that the diameter structure required with reinforced construction would increase the cost many fold. This, coupled with the fact that the complex curvature of the panel made mating of the panel extremely difficult indicated other approaches should be investigated.

A second method looked into was the use of a concrete structure suitably reinforced to take necessary tension loads. The basic concrete block would easily absorb the hydrostatic compression forces, but tension loads would have to be handled with a steel reinforcing structure. The cost of the concrete and steel necessary to hold the unbalanced forces acting on the structure became prohibitive thus ruling out this concept.

The final design examined and ultimately utilized, was that of a basic steel structure as depicted in Figures 77 and 78. The basic box consists of steel I beam, channels and plates for containing the pressurizing medium. Three basic units of the ships structure were duplicated in this fixture: (1) Diagonal Bulkhead, (2) Base plate and (3) Catwalk area. A flat plate end cap was utilized to cap off the end of the cavity formed by the three ships plates. To this structure the bead seat was welded utilizing the master bead for location purposes.

To insure satisfactory performance of the test fixture a specification was written detailing the requirements as closely as possible. Following is a detailed list of the specification requirements.

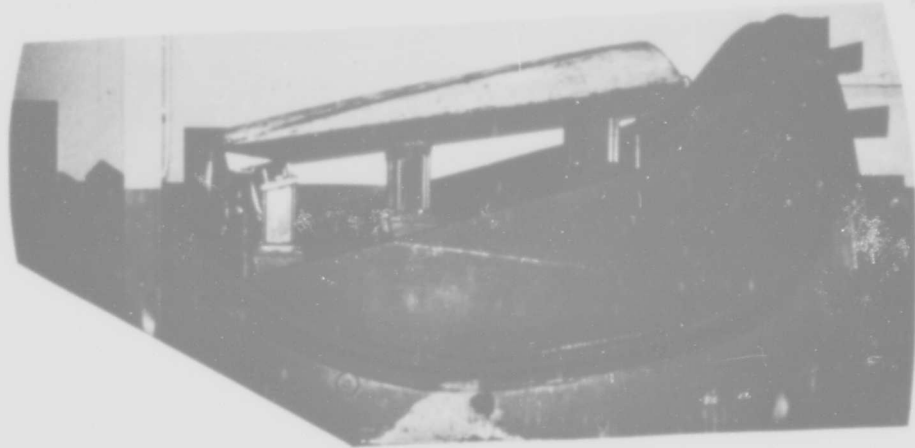


FIGURE 77

PROTOTYPE PANEL HYDROSTATIC TEST FIXTURE

SIDE VIEW

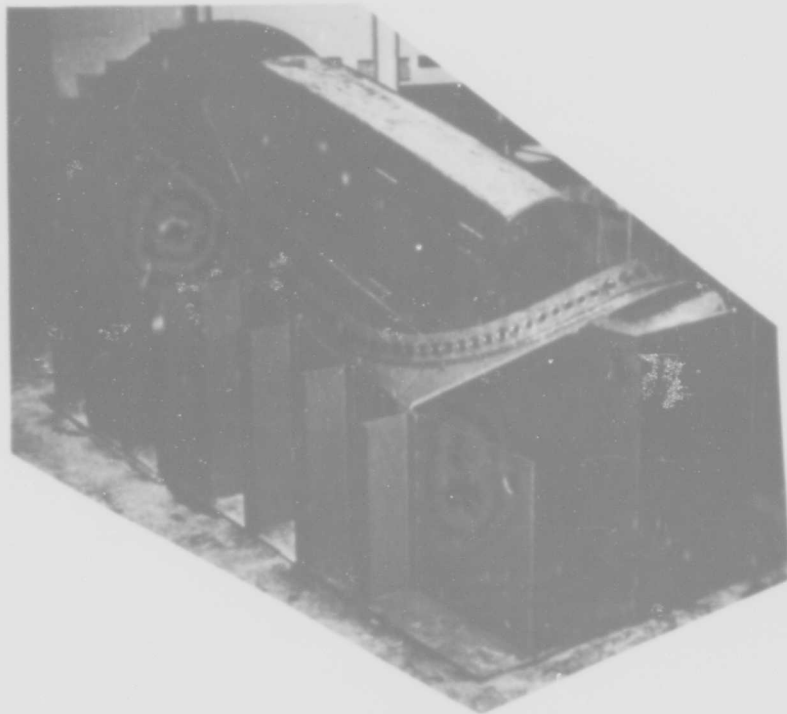


FIGURE 78

PROTOTYPE PANEL HYDROSTATIC TEST FIXTURE

END VIEW

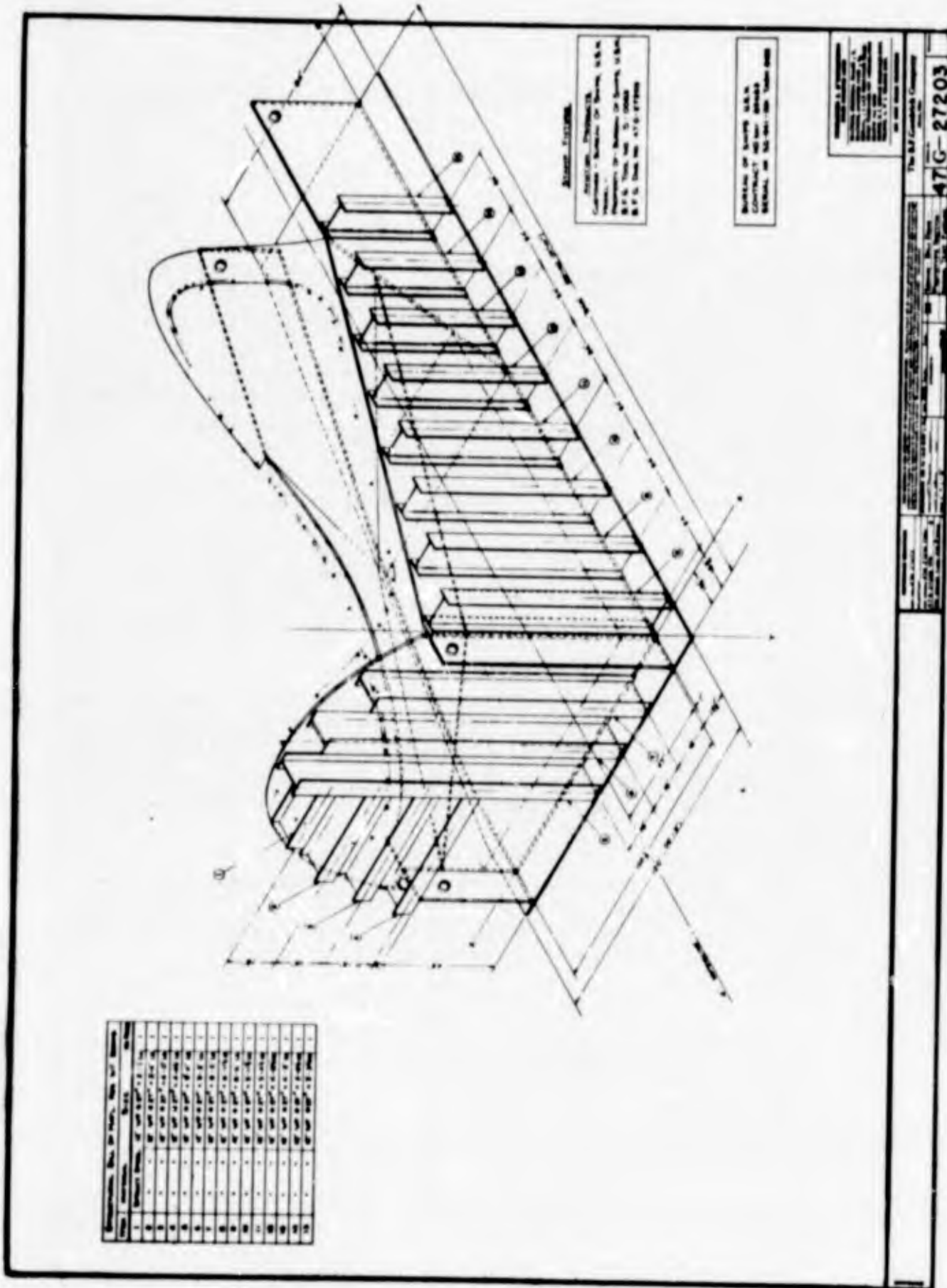
1. The fixture must be capable of accommodating the bead of the bow dome section, clamping it to form a pressure tight seal, and securing it in the required contoured position within the specified limits when the dome is subjected to the test pressures.
2. Maximum test pressure of 150 psi water to be applied to the fixture one time only for a period of not more than five minutes.
3. Normal pressure is 50 psi water to be applied to the fixture for extended periods and occasionally increased to 100 psi for several hours.
4. Maximum force acting perpendicular to the bead core and tangent to the curvature of the tensile elements of the dome is 15,000 lbs. per linear inch of bead when the test pressure is 150 psi.
5. Maximum leakage not to exceed five cubic inches per minute at pressure of 50 psi exclusive of seal along bead of dome section.
6. All welding to be equal in quality to that required for pressure vessels.
7. Primary fixture structure to be per assembly drawing 47G-27203-A. (Figure 79)
8. The peripheral bar to which the dome bead will be clamped is to be a continuous member with a cross-section as shown on drawing Figure 80 and so shaped and positioned that the groove for the dome bead will follow the contour of a bead template, furnished by B.F.Goodrich Co., within a maximum tolerance of 1/4" in any direction. Further, the included angle between the side plate of the fixture and the principle face of the bar at any particular point of determination is to be within plus or minus 2 degrees of the angle specified or otherwise indicated as required for that point.

Also, the periphery of the bead groove must be equal to or not more than 1/2 inch longer than the length of a gage cable to be furnished by B.F.Goodrich Co. Any adjustment needed for this length requirement may be made along the upper curved edge of end plate Figure 81, item 2, by a departure from the normal bead contour in an amount to be approved by a B.F.Goodrich Co. engineer at the time.

See drawings Figure 80 and Figure 82 for typical sections representing relative positions between the peripheral bar and the side plates of the fixture. The bar is to be supported by and tied to the fixture side plates by a tension plate suitably contoured and positioned to be in line with the direction of the force applied to the clamp by the dome section. An indefinite number of gusset braces (not shown) will also be required to stabilize the bar position when it is subjected to forces not in line with the tension plate due either to initial misalignment of the plates or a change in the direction of the applied force when the dome section is deflected by the internal test pressure.

9. The peripheral bar may be made from segments of any convenient length obtained as steel castings, plaster patterns for which will be furnished by B.F. Goodrich Co., or, as formed lengths of premachined rectangular steel bar, or any combination of both. Such alternatives to be subject to the following limitations -
 - a. Adjacent segments to be so shaped and positioned to give a smooth curve across the joint with no radius of curvature to be less than 3". Maximum initial misalignment may not exceed 1/16" and such step must be faired out over a minimum length of 1" subject to the 3" radius of curvature limitation.
 - b. Welds joining adjacent segments to be continuous around the periphery of the section and pressure tight to 150 psi where subject to the test pressure. Such welds to be at least 1/4 inch deep.
 - c. Joint welds to be so positioned that they will not pass thru a clamp bolt hole.
 - d. Joint welds and casting surfaces in contact with dome bead to be hand smoothed to a surface finish of 125 or better.
10. The tension plates may be of any convenient length and shape with all joining welds to be full strength and pressure tight.

11. Loose clamp segments are to be shaped substantially per item 1, shown in Figure 80. They may be individual steel castings for which a pattern will be furnished by B.F.Goodrich Co. Segments are to be so located along the peripheral bar that the gap between segments is $1/8$ " plus or minus $1/16$ " when measured at the centerline of the cable. Material is to be removed from one or both edges of the segments as required to obtain such positions. Clamp segments may be cut to approximately half length when required to fit positions where bar has greatest curvature. Surfaces in contact with the dome bead to be hand smoothed to a surface finish of 125 or better. Segments and bar to be match marked with painted numerals to indicate proper position along bar.
12. Steel castings to have a minimum yield strength of 35,000 psi.
13. Clamp bolt heads to be closely parallel with the surface of the bar to effect a pressure seal with the bar and copper gasket. The bar surface may be spotfaced if required.
14. Inspection to be made by B.F.Goodrich Co. engineer at Suppliers Shop with suppliers gauging and measuring equipment prior to shipment of fixture. Final acceptance of fixture to be subject to satisfactory performance during pressure tests after installation.
15. Variations of design or construction from any of the above specifications or issued drawings will be considered upon presentation by the supplier. Such variations may not be used, however, until specifically accepted in writing by B.F.Goodrich Co.



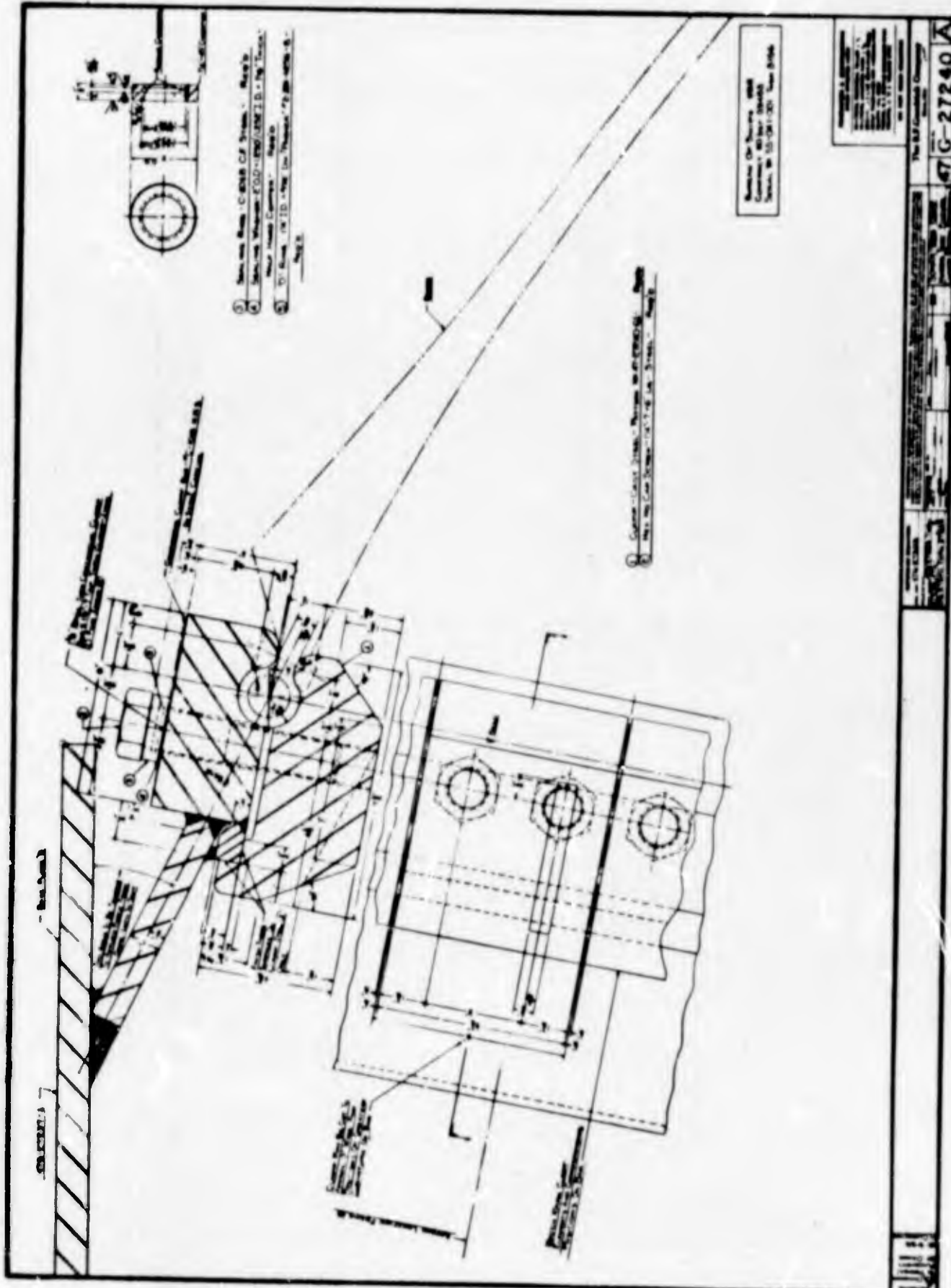


Figure 80
B. F. Goodrich Drawing 47G-27240A

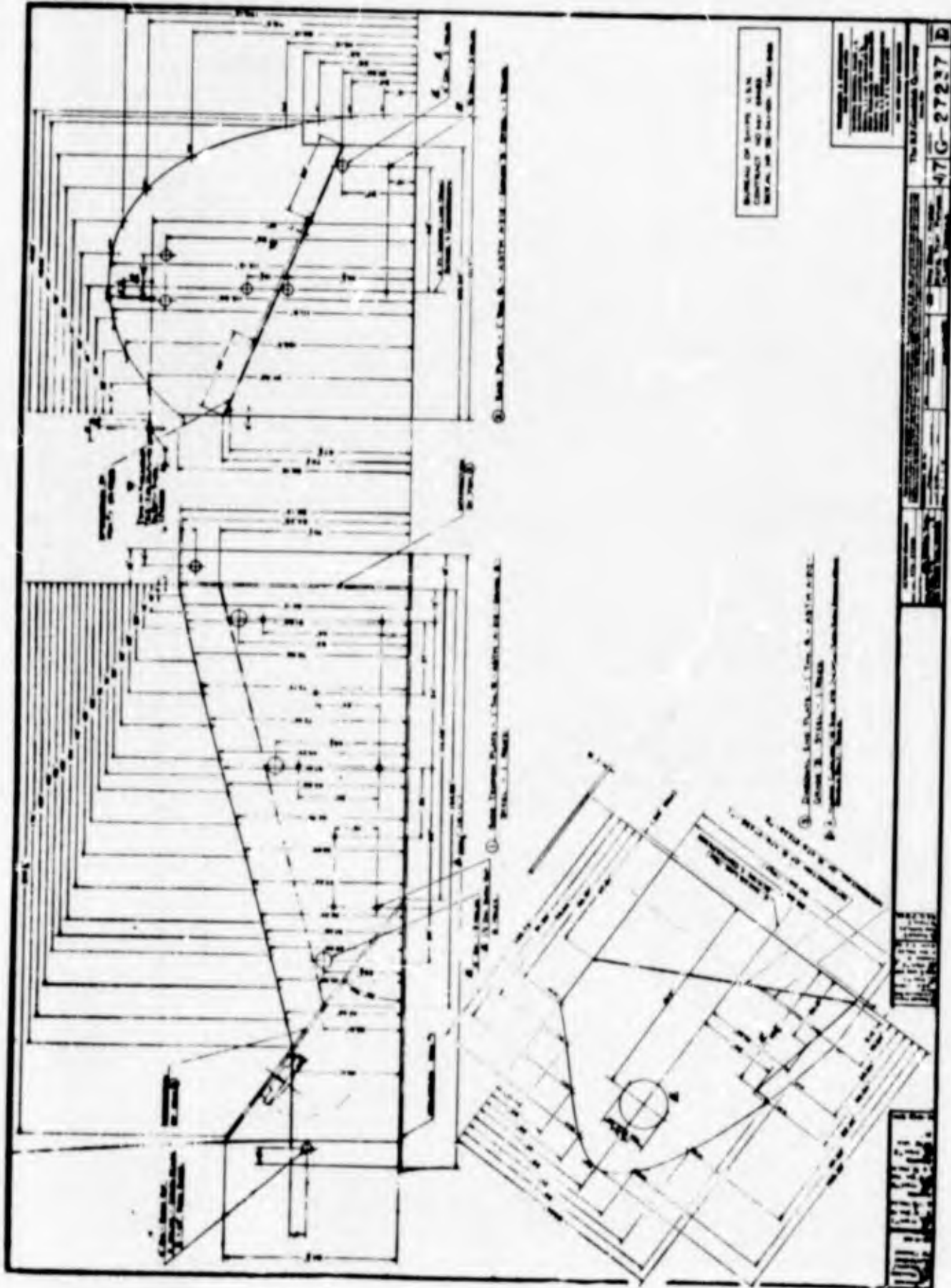


Figure 81
B. F. Goodrich Drawing 47G-27237A

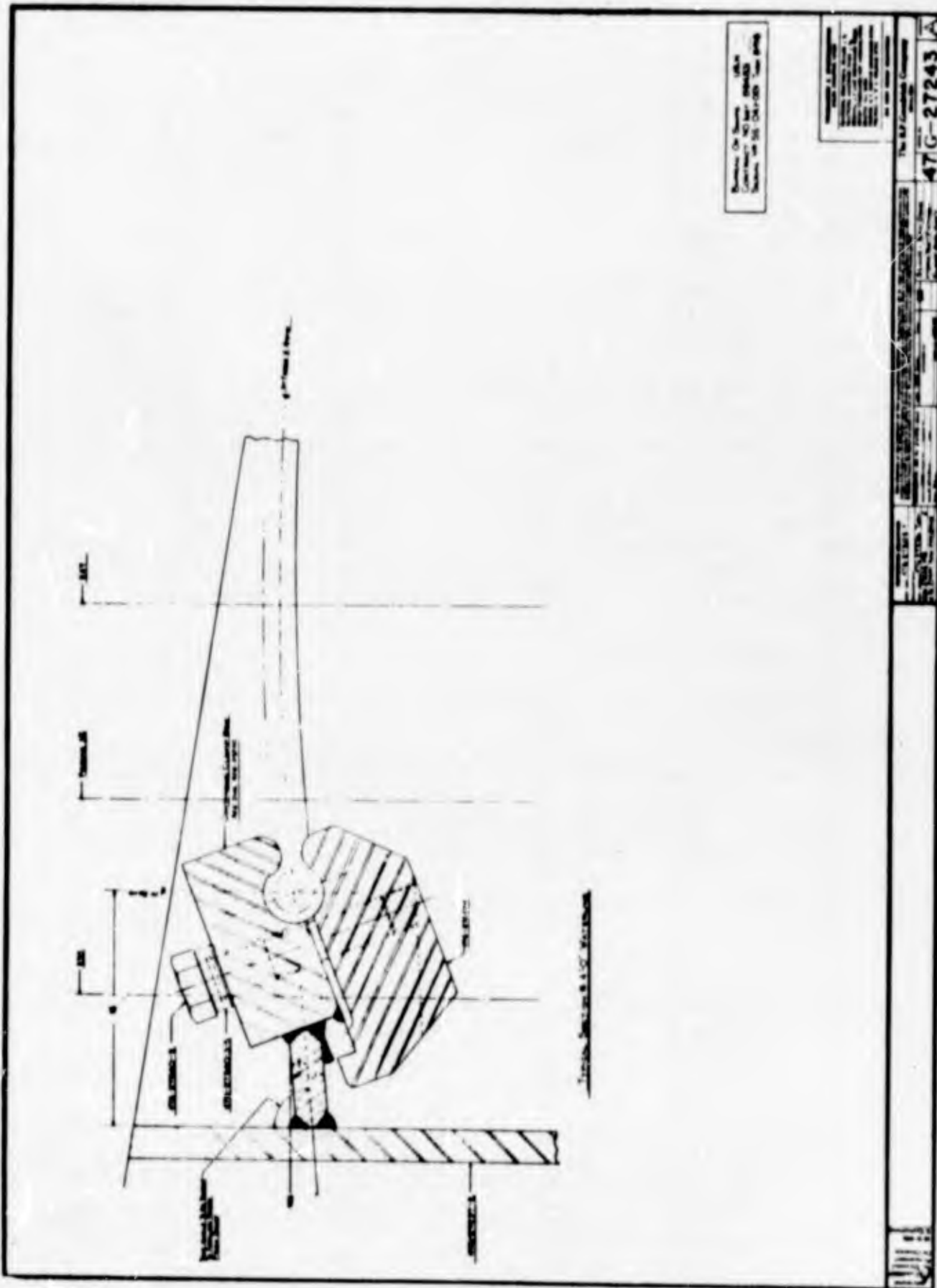


Figure 82
 B. F. Goodrich Drawing 47G-27243A

e. Panel Fabrication

Prior to initiation of the fabrication operation a vacuum test cycle was conducted on the mold. This consisted of isolating the mold surface, drawing a vacuum in the resultant cavity and subjecting the entire complex to a sample cure cycle.

The vacuum bag had a series of vacuum lines which fed into an overall 2" diameter line. This in turn leads to a Water Seal Wash Pump capable of holding 24 inches of Mercury vacuum at a flow rate of 100 CFM. During the course of this cure cycle vacuum was maintained at the 24 inch (Hg) level.

Examination of a fabric bleeder structure within the cavity, subsequent to cure, indicated a slight introduction of water vapor around several edges of the bag. These leaks were attributed to seam leakage where the vacuum bag was spliced. The amount of leakage was well within the source pump capabilities of maintaining the ultimate vacuum level. It was concluded that special care should be taken in bagging the fabricated panel to minimize this condition although no real damage would occur if it happened during panel cure.

(1) Preparation of Mold

The mold surface was thoroughly smoothed eliminating all protuberances of either epoxy or rubber in nature. Once this was completed the surface was cleaned and degreased using Methyl Ethyl Ketone. A layer of carnuba wax was applied to all surfaces in which the neoprene would be in contact during cure. Over the wax, a layer of Fluorocarbon Mold Release S-122 was applied. The wax-teflon system was applied as a mold release to insure the panel could be easily removed from the mold subsequent to cure.

A layer of B.F. Goodrich Code 935, 1.5 oz./yd.², nylon twill fabric was cemented in place over the surface of the mold. This material further facilitates removal of the part, in addition to impressing the surface of the panel. During application of this fabric care was taken to keep the wrinkles and bridging to a minimum.

The nylon was extended approximately eight (8) inches beyond the bead cavity for eventual wrap around the bead buildup. Also, since the mold-panel combination would be split, a two (2) inch overlap was maintained in the center

of the splice area. A layer of natural rubber cement, incompatible with the neoprene panel gum, was applied over the fabric to hold it in place during panel fabrication and to permit release after cure.

(2) Fill Gum Application

The thick fill section shown in Figure 83 was applied in three (3) separate operations. First, a layer of gum was applied to the entire mold surface directly over the nylon impressing fabric. Then, in the maximum volume area, using a series of contour templates, layers of .180" neoprene gum were applied in a step sequence. Building cement was used between plies of the build up, both gum and wire. Extreme care was taken during this lay up to eliminate all trapped air between plies. All gum splices were of the angle-skive variety to insure void free integrity of the fill areas.

The fill was accomplished in two (2) sections, first the forward panel area, then the aft panel area. A vertical separator was placed between the sections, in the fill area, to permit separation of the panel for splicing.

In the forward section of the mold a method of expediting fill installation was attempted. In this instance blocks of rubber 1" thick, 18" long, and varying depths depending on location were utilized. These sections were contoured to the curvature of the panel and laid in place using the same template procedure previously discussed. This method did not prove more efficient and in some instances may prove less effective. The larger sections presented greater problems in insuring the absence of trapped air.

Upon completion of the fill with both techniques a second .180" ply of neoprene was laid over the entire surface and firmly cemented to the substrate.

Thermocouples were placed, at the splice area, in the center of the heaviest gum section for monitoring temperatures during cure. Thermocouples were also placed between the mold surface and the first layer of gum.

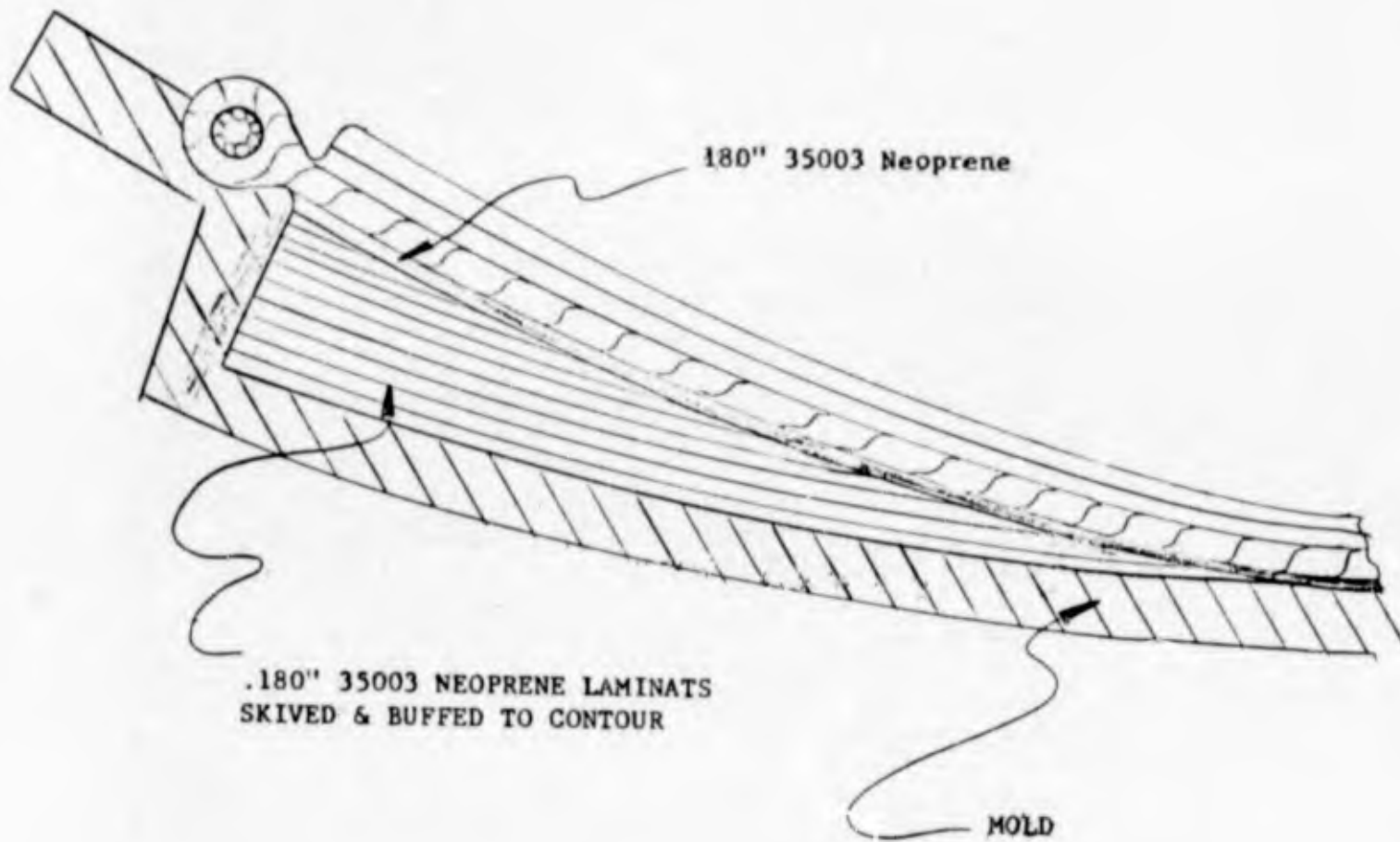


FIGURE 83
PANEL CROSS SECTION - FILL GUM APPLICATION

(3) Chafing Strip Attachment

The bead chafing strip of neoprene coated BFG Code 946 Nylon twill fabric, 4.9 oz/yd², was applied in the bead cavity. The component is used to protect the wire fabric from abrasion by the bead clamps. The neoprene coating is a high abrasion resistant stock BFG Code 65014. The actual position of this strip is shown in Figure 83. This strip extended 1/2" past the bead clamp recess and terminates at the splice section.

(4) Wire Fabric Application

Actual ply orientation is shown in Figure 68 of section D.C.2. The first vertical ply was laid in strips which varied from six inches wide at the center to one inch wide at the extreme end. The reason for this variation in width was the extreme complex curvature of the panel.

The first vertical ply was allowed to extend past the bead cavity approximately eighteen inches to permit wrap around the bead.

This extension was terminated at the point where the vertical ply, when wrapped around the bead cable, formed a 15° angle to the four foot water line. This is known as the "transition point".

Outboard of the four (4) transition points the vertical ply was cut on a line 1-3/4 inches from the bead cable. A strip of extruded fillet (BFG Number 2S-1037 and compound 59380) was cemented along the cut edge as shown in sketch, Figure 83. In all instances where the fabric ply terminated, a fillet was installed to smooth the transition.

The section of this ply which covered the splice area was applied with a nylon separator to permit removal after cure. The ply was cut off approximately 1-3/4 inches from the edge of the bead cable.

The first 15° ply was applied with the cables running from the lower bottom-forward edge area to the upper aft edge. The forward section was applied first and allowed to extend to the aft edge of the splice section of the mold. Nylon separators were used as shown on the drawing. The aft section was then applied and allowed to extend over the

forward section nine inches. This would be one series of lapped 15° plies in the completed panel.

Outboard of the transition points this ply was allowed to extend approximately eighteen inches beyond the bead cavity.

The remainder of the ply on the bottom and top edge was cut off 1-3/4 inches from the bead cable.

At this point in the fabrication the extensions of both the vertical ply and the 15° ply were stitched into the bead cavity and held there with sections of rod and eight inch "C" clamps. The extending surfaces were covered with polyethylene film to prevent inadvertent adhesion to each other.

To permit proper load distribution to the bead cable a ply mid-way between vertical and 15°, i.e., 38° applied twelve inches beyond what was determined to be the critical lines would suffice to distribute load perpendicular to the beads. These plies were to be applied over the first 15° ply and the second 15° ply after the second bead turnover to best centralize the additional build up and impart the most strength to the panel.

A ply, as explained above, was applied to each end of the panel over the first 15° ply. The tapered fillet extrusion was applied around the entire periphery of each section of this ply.

The second vertical ply was applied following virtually the same procedure as the first vertical ply. There were, however, some exceptions as follows. The transition points were different owing to the 30° different angle between the first and second 15° ply, and the plies were extended only about twelve inches beyond the bead cavity. The extending ends were stitched into the bead cavity and held in place with sections of rod and "C" clamps.

A thermocouple was placed twelve inches from the bead cable on both the top and bottom of the panel in the center of the splice section over the second vertical ply.

The second 15° ply was applied 30° from the first 15° ply and the edges were allowed to extend about 12" beyond the bead cavity fore and aft of the transition points.

The bead tie-in ply is installed in all cases at 90° to the bead cable and extending six (6) inches inboard of the cable. Considerable difficulty was experienced in applying this ply around the extreme curvatures.

The outer edge was allowed to extend fifteen inches for future lapping.

The bead cable was cut into two (2) pieces, each long enough to extend from the center of the splice section around the periphery of the fore or aft mold and back to the center of the splice. The ends of the cable were tapered to facilitate welding at a later date when the two panels were ready for splicing.

After cutting and tapering, the cable was degreased in trichloroethylene vapor for approximately six hours. The cable was then laid on a holland covered table, supported by wood blocks and a heavy coat of 220 adhesive (a metal primer) was applied. After allowing one half hour (1/2 hour) drying time the cable was coated with Code 369 neoprene cement. In the meantime the bead cavity was prepared by laying in strip of .030" x 35003 neoprene stock.

The cable was then wrapped in stock liner fabric and placed in the bead cavity. Clamps were used to press the cable into position such that the tapered ends would just meet at the center of the splice section. A nine inch long 1-1/4 I.D. x 1-3/4 O.D. rubber hose was split lengthwise, covered with nylon at the splice area and used as a filler in the bead cavity. An extruded fillet, BFG No. 2S-1022 was cemented in place. White cotton gloves were used to handle the cable during all steps after degreasing. Cable length was determined by installing a 1-3/4" O.D. rubber hose in the bead cavity prior to beginning fabrication of the panel.

It was found during this operation that, what was a relatively simple operation during sample fabrication, was a difficult operation on the full scale panel. The cause of the difficulty arose from two (2) sources; (1) the curves which had to be negotiated and (2) the position that a person had to attain to correctly turn the cable. It is of extreme importance that the cable plies be tight around the bead cable in order to sustain the forces that will be present when the panel is pressurized. This tight wrapping required extreme effort to accomplish.

The extension beyond the bead, on the bead tie-in ply, was cemented and turned at right angles to the cable at all times. Even in this case considerable ply overlapping was present at the extreme aft section in order to keep the ply cables in a straight line.

Turning the next ply was somewhat more difficult than the bead tie-in ply since the ply cables crossed the bead cable at an angle. This caused the plies to "pile up" in the areas of extreme panel curvature. The plies were turned always keeping them tight against the cable.

The second turn over was trimmed to six inches, (the bead tie-in ply was cut to length prior to installation) after turning. "C" clamps and pieces of rod were used to assist in tightening the turn over.

The second set of 38° plies was applied approximately the same as the first set. The ply cables were oriented 76° from the first 38° plies and the area covered was only 12 to 16 inches wide.

The third vertical ply was applied exactly like the first two except that it was cut off 1-3/4 inches from the bead cable around the entire periphery of the panel. The splice section was handled the same as before with separators being installed. Figure 84 depicts lay up of the 15° plies in the panel aft section. Figure 85 depicts the bead wrap around being accomplished.

The final ply turnover was accomplished the same as the second one, but with less effort, since we received an education on the earlier one. This ply was also cut after turnover and held in place with rods and "C" clamps.

The bead chafing strip was also turned at this time.

(5) Inner Neoprene Plies

The edge of this ply was skived to the shape of the panel and the ply terminated at either edge of the splice. The reason for stopping this ply at the edges of the splice was the excess splice thickness caused by lapping of plies. A .080" gum covering was laid over the ply resulting in a flush inside surface.



FIGURE 84
15° PLY LAY UP AND SPLICE CONSTRUCTION OF PROTOTYPE PANEL



FIGURE 85
BEAD WRAP AROUND OPERATION OF PROTOTYPE PANEL

The inside mold clamps were then installed with .005 sheet stainless steel shims used to bridge the gaps between adjacent clamps and provide cross section continuity. The clamps were torqued down until they bottomed which resulted in the desired bead cross-section.

In several cases it was necessary to add rubber to the surface of the wire fabric or patch the ply itself with wire fabric. In the case where the surface rubber was patched the exposed cables were primed with primer 220, cemented with 369 cement and .010, sheet 35003 applied over the exposed area.

In the other case a lap of at least six inches was required to provide equivalent strength. This procedure was used in several places and should not have any detrimental effect on the panel strength.

(6) Preparation for Cure

"To bag" is a vernacular phrase meaning, in this case, to place in a sealed envelope. This procedure must be accomplished to provide insurance that any trapped gasses will literally be pulled from the panel.

In a practical sense the mold acts as one side of the envelope and a heavy rubber sheet as the other. An escape route for gasses and vapors is provided by layers of corofelt (pressed wood fibers) and fiberglass or burlap fabric. Valves are provided in the rubber sheet to draw the vacuum. Figure 86 presents the panel ready for cure with the vacuum harness in position.

The procedure used in this case was as follows:

- (a) Cover the panel with BFG Code 935 Nylon impressioning fabric.
- (b) Cover the entire product with two plies of heavy fiberglass fabric BFG Code 994.
- (c) Cut holes in the glass fabric and install the necessary thermocouples per Figure 87.
- (d) Cover the product with one ply of corofelt to the edge of the mold clamp.

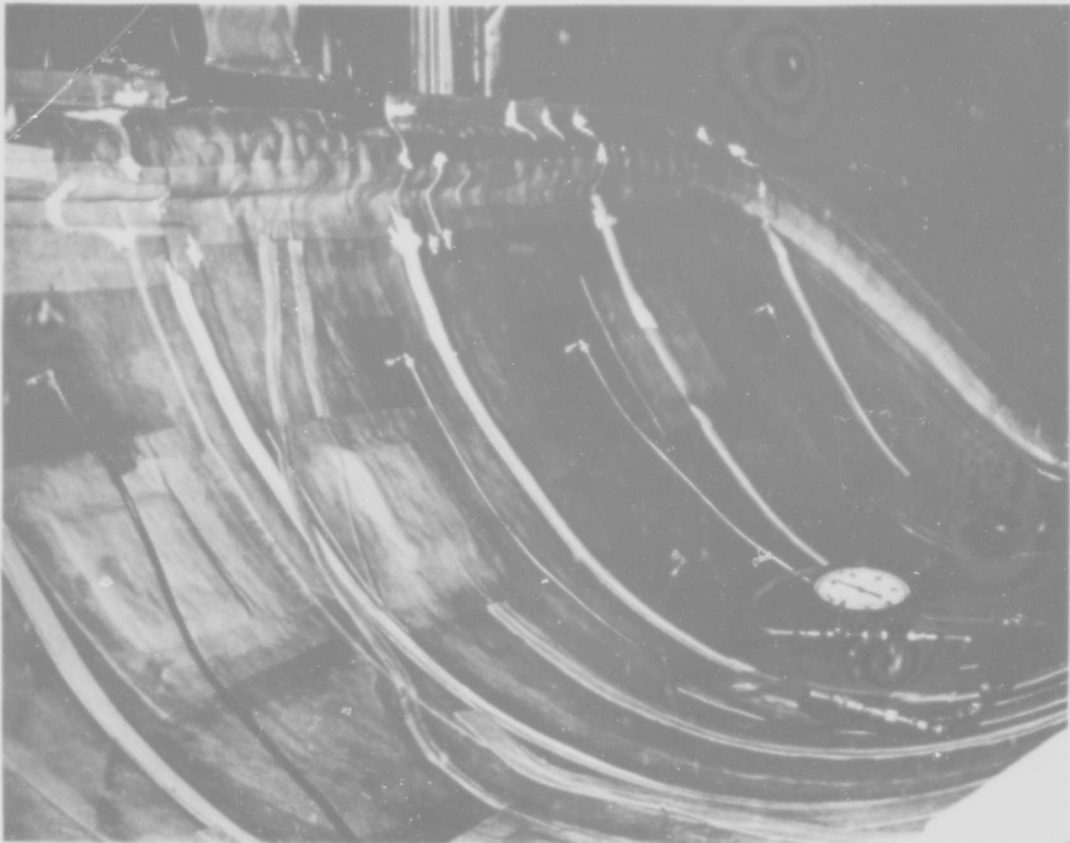


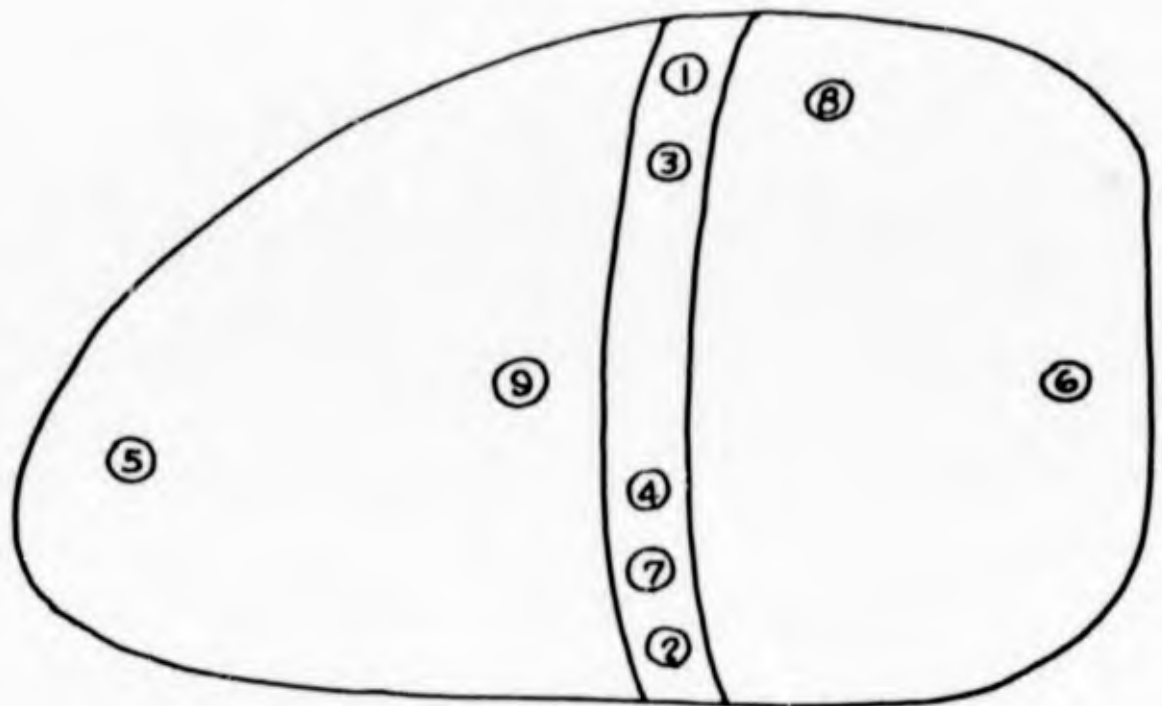
FIGURE 86

PROTOTYPE PANEL WITH VACUUM BAG READY FOR CURE

Contract NObsr 89483
Serial No. SS041-001
Task 8156

Report No. 17
Phase I Interim Report
30 September 1964

CONTROL THERMOCOUPLE LOCATIONS



1 & 2 CENTER OF GUM FILL

3 & 4 CENTER OF CONSTRUCTION

5 THRU 9 SURFACE OF PANEL

FIGURE 87

PROTOTYPE PANEL THERMOCOUPLE LOCATIONS

- (e) Cover the corofelt with two plies of heavy fiber-glass fabric BFG code 994.
 - (f) Fill all exposed bolt holes and other cavities with rubber.
 - (g) Apply cured .060" bagging stock over mold clamp.
 - (h) Cement bagging rubber, BFG Code 139EP2 on bag sealing surface around mold periphery using appropriate cement.
 - (i) Install ten valves appropriately spaced on the bag surface. Two are to be used to monitor the vacuum.
 - (j) Apply vacuum to the bag.
 - (k) When the bag has been sufficiently evacuated apply a redundant ply of bag stock to insure all leaks are sealed and minimize the possibility of pulling holes during cure.
 - (l) Several leaks were repaired and the mold installed in the autoclave and vacuum recorders attached.
 - (m) Bag integrity was checked by placing the mold in the autoclave and pressurizing. The vacuum level should be maintained at least at 10 inches of mercury with 90 psig on the vulcanizer.
 - (n) Thermocouples were attached to the temperature recorder and the cure begun.
- (7) Prototype Panel Cure

As determined earlier the prototype panel cure would be completely monitored and the actual cycle determined as the cure progressed. Once the unit was in the heater, with the proper level of vacuum and all thermocouples operating air pressure was introduced into the vulcanizer. With pressure increase the initial vacuum level of 28" of mercury held until about 40 psi was reached. At this point the vacuum level began dropping so heat was introduced as a means of softening the bag and permit elongation without tearing as it seated itself against the mold. The vacuum level continued to drop until it reached about 10" of mercury. As the cure progressed the bag sealed and the vacuum level attained 22" of mercury where it remained during the actual cure time.

The heater temperature was raised to 300°F gradually within a one (1) hour period. From this point the internal thermocouples governed the cure with the following cycle established. (Refer to Figure 87)

- (a) Monitor temperature at the center of the construction (No. 3 & 4 thermocouples) and when this temperature reaches 275° start cure period.
- (b) Total cure time shall be two and one half (2½) hours.
- (c) Following cure, cool part until thermocouples 3 & 4 register 250°F. This may be done with an intermittent water cool down.
- (d) When 250° is reached allow, or force, the part to drift to 200° at the center of the fill (Thermocouples #1 & 2) in three (3) to four (4) hours. Water may be used to assist this cool down but maintain at least 40 psi and full vacuum.
- (e) When 200° is reached the cure cycle may be considered complete and the heater opened.

The actual cure cycle is shown in Table XXVII following. In analyzing this data it was realized that a wide variation of temperatures would be noticed. However, realizing a time-temperature relationship is critical the data was analyzed to insure that all areas received a proper cure cycle. A proper cure for B.F. Goodrich Code 35003 neoprene in the construction is either: (1) 45' @ 292°F, (2) 90' @ 275° and 150' @ 250°F. Analysis of the cure data indicates all areas received a satisfactory cure.

TABLE XXVII

PROTOTYPE PANEL CURE CYCLE

<u>Time</u>	<u>Heater Temp</u>	<u>1</u>	<u>2</u>	<u>3</u>	<u>4</u>	<u>5</u>	<u>6</u>	<u>7</u>	<u>8</u>	<u>9</u>
Start	-	74								
10		74								
20		73								
30		78					90	109	109	
40		82		86			100	128	128	
50		86		94	113	113		141	146	
1 hr.	248°F	91		103				154	164	
10		96	150	121	141	142		166	181	
20		101	168	130	160	156	154	179	197	
30		108	176	139	178	169	160	190	212	
40		112	180	149	196	185	167	205	229	165
50		120	188	158	207	198	175	216	243	174
2 hrs.	300°F	127	198	167	215	211	184	225	253	182
10		136	200	176	222	222	194	234	265	190
20		145	202	184	224	231	203	239	271	199
30		153	203	191	228	240	211	244	277	208
40		162	205	198	231	253	218	248	280	214
50		169	207	204	234	258	225	251	282	221
3 hrs.	300°F	177	213	211	236	261	230	256	285	228
10		184	216	217	236	261	236	261	287	233
20		191	219	224	241	263	241	266	290	238
30		198	226	230	242	266	246	269	292	242
40		204	236	235	250	268	250	271	292	249
50		210	234	240	258	270	254	270	290	251
4 hrs.	298°F	215	234	244	254	272	256	274	292	254
10		220	234	248	254	273	259	278	293	256
20		226	240	253	260	274	262	280	294	260
30		231	244	256	264	274	264	282	295	263
40	296°F	236	249	260	268	276	266	282	295	265
pm 50.		240	255	262	271	277	268	282	294	268
5 hrs.	296°F	244	259	264	274	279	270	283	293	270
10		248	262	267	274	280	271	283	292	271
20		251	261	269	274	280	272	284	292	272
30		255	266	271	278	281	273	284	292	274
40		258	266	271	276	281	274	287	294	275
50		258	262	274	278	282	276	289	295	276
6 hrs.	300°F	261	266	275	278	282	276	289	295	278
10		263	271	277	280	284	278	290	295	278
20		265	273	279	282	284	279	289	294	280
30		268	275	280	284	284	280	289	294	280
40		269	276	281	284	284	280	289	294	281
50.		271	277	281	285	285	281	289	293	282

TABLE XXVII (Continued)

Time	Heater Temp	<u>1</u>	<u>2</u>	<u>3</u>	<u>4</u>	<u>5</u>	<u>6</u>	<u>7</u>	<u>8</u>	<u>9</u>
50		272	278	282	284	285	282	289	293	282
7 hrs.	300°F	274	278	283	283	286	283	291	295	283
10		275	279	284	283	287	284	292	295	284
Start		276	280	284	282	284	284	288	290	284
Cool Down		278	279	280	281	278	268	281	282	277
40		280	279	279	280	262	252	277	279	264
50		278	278	278	278	248	238	273	276	252
8 hrs.	248°F	278	278	278	278	236	225	268	268	240
10		277	268	277	268	223	212	262	251	229
20		276	272	275	267	220	200	256	243	218
30		276	270	271	265	199	188	252	239	207
40		274	269	269	262	190	177	246	228	197
50		272	265	266	258	180	168	241	218	189
9 hrs.	200°F	271	263	262	255	171	161	239	218	180
10		269	260	259	251	165	155	236	219	175
20		267	257	256	248	160	150	234	218	169
30		265	255	254	245	155	145	231	217	165
40		263	251	251	241	150	141	228	215	160
50		262	248	248	237	145	138	226	212	157
10 hrs.	186°F	260	246	246	234	144	134	224	210	154
10		258	242	244	231	140	132	220	207	151
20		256	240	241	228	136	129	218	203	148
30		254	237	239	225	135	126	215	200	146
40		252	234	236	221	132	124	212	198	143
50		250	231	234	218	130	122	200	196	140
11 hrs.	168°F	247	228	232	214	127	120	206	192	137
10		245	224	229	211	124	116	203	190	134
20		243	222	226	208	122	114	220	181	132
30		240	219	224	204	120	112	198	179	129
40		238	216	221	202	118	110	196	177	127
50		236	212	219	198	116	110	194	176	124
12 hrs.	154°F	234	210	216	196	115	108	192	173	123
10		231	207	214	193	113	108	190	171	121
20		229	204	212	191	113	107	189	169	120
30		227	203	210	190	112	106	185	166	118
40		224	200	207	188	111	105	182	163	118
50		222	198	204	185	110	105	178	160	116
13 hrs.	136°F	220	196	202	183	108	102	175	157	114
10		217	172	199	170	106	100	172	145	111
20		214	185	196	175	103	97	171	144	109
30		212	186	193	175	101	95	168	142	106
40		210	185	190	174	100	94	166	141	105
50		207	184	188	173	101	94	163	140	104

Contract NObsr 89483
 Serial No. SS041-001
 Task 8156

Report No. 17
 Phase I Interim Report
 30 September 1964

TABLE XXVII (Continued)

<u>Time</u>	<u>Heater Temp.</u>	<u>1</u>	<u>2</u>	<u>3</u>	<u>4</u>	<u>5</u>	<u>6</u>	<u>7</u>	<u>8</u>	<u>9</u>
14 hrs.	122°F	204	182	186	171	101	94	162	138	104
10		200	180	183	170	101	93	160	136	104
Total Start		5:20	4:50	4:20	3:30	2:40	3:30	2:40	1:50	3:40
Time End		10:50	9:40	9:40	9:10	7:40	7:40	8:40	8:10	7:50
250°F Total		5-30	4-50	5-20	5-40	5-00	4-10	6:00	6-20	4-10
275°F Start		7:10	6:20	5:50	5:00	4:30	5:40	4:00	2:20	5:30
End		8:30	8:00	8:20	8:00	7:30	7:20	7:40	7:50	7:30
Total (hrs- min)		1-20	1-40	2-30	3-00	3-00	1-40	3-40	5-30	2-00

NOTE: Vacuum maintained above 20" Hg during actual cure cycle

#1 & 2 Center of Fill
 3 & 4 Center of Construction
 5 - 9 Surface of Part

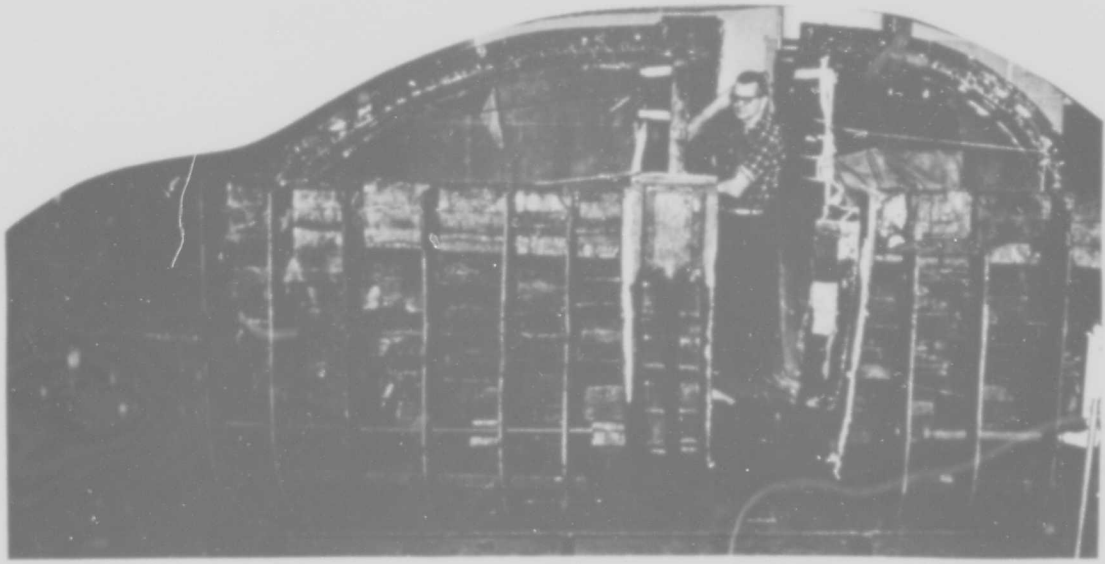


FIGURE 88
PANEL & MOLD SEPARATED AFTER CURE



FIGURE 89
RESTRAINT OF 15° PLUS DURING SPLICE FABRICATION



FIGURE 90
BEAD CABLE WELD FOR SPLICING

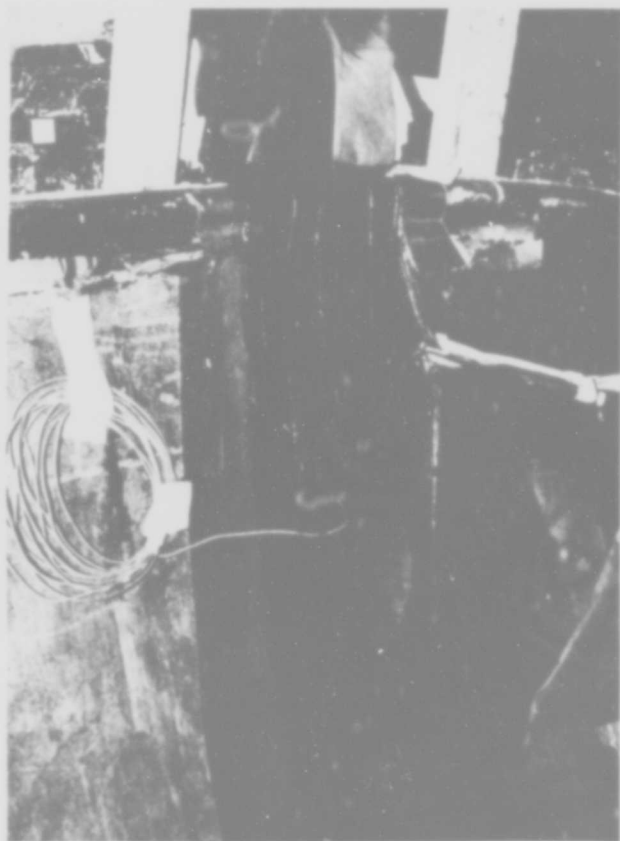


FIGURE 91
THERMOCOUPLE INSERTION DURING PANEL SPLICE ASSEMBLY

(8) Panel Splicing

One main reason for building the prototype panel was to determine the feasibility and strength of the splice construction.

Subsequent to cure the bag was removed and the panel separated (Figure 88) in preparation for the seaming operation. This was accomplished and the nylon and teflon fabric separators and the vertical plies removed. Figure 89 shows the 15° plies being restrained. Uncured neoprene was cemented to the exposed vertical rubber fill edges, the horizontal plies were cleaned and the panel repositioned together. The uncured gum at the edges of the fill was positioned together and put into compression during the joining operation because of the added gum thickness. Thermocouples positioned against the mold surface were installed prior to bolting the mold together.

The bead cables were electric welded together with the part being protected with asbestos sheeting. It was impossible to completely weld the cable at once without burning the panel so alternate welding and quenching was accomplished. The bead cable weld is shown in Figure 90. Due to the time factor and heat build up in the panel, it was decided, in order to reduce cost and improve design, a pre-welded mechanical cable joining method would be used in the future.

After the cables were welded the part was cleaned and allowed to dry (several small fires had to be extinguished during welding and water was still present).

The same fabrication procedure was followed during splice assembly as during panel building. The only difference was replacement of separator material with cement. Also, the fabric was installed in two to four inch strips to assist in passing it under the cable. Appropriate thermocouples as depicted in Figure 91 were installed during building.

The top gum layer used was only .080 thick due to the extra ply build up resulting from the horizontal ply overlaps.

Nylon impressioning fabric was applied to the surface, thermocouples installed and a preformed electric heating element positioned over the surface.

Two layers of asbestos sheeting and two layers of uncured butyl rubber .180" thick were used as insulation between the heating element and the pressure hose. The strongback Figure 92, was installed. Water was introduced into the hose until 80 psig was attained and the transformer turned on to start the induction heaters.

This cure Figure 93 was essentially designed to be identical to vulcanizer cure. Thermocouples were built in and pressure monitored during the entire cure. Figure 94 shows the thermocouples locations and again the center of the construction monitors were most critical and controlled the cure. Table XXVIII presents temperature data collected during this cure. Two pickups were apparently not recording, therefore, the readings were discarded. The remainder of the pickups varied considerably depending upon the size of the panel or heat sink. Heat dissipation was expected into the adjacent panel areas so the entire splice fixture was made 4" wider than the actual seam. To insure a satisfactory cure throughout the critical parts of the panel it was necessary to slightly over cure some areas. Generally speaking the splice cure was considered to be very satisfactory.

(9) Final Finish

Special tongs as illustrated in Figure 95 were used to remove the panel from the mold and generally assist in the handling operation. Actual panel release from the mold was accomplished by peeling the panel, i.e., pulling one bead toward the opposite bead.

This was accomplished from one side then the other eventually breaking the entire panel free. Once free the panel Figure 96 was removed from the mold, Figure 97, and was inverted and positioned over several cylindrical objects. The panel at this stage can be seen in Figures 98 and 99.

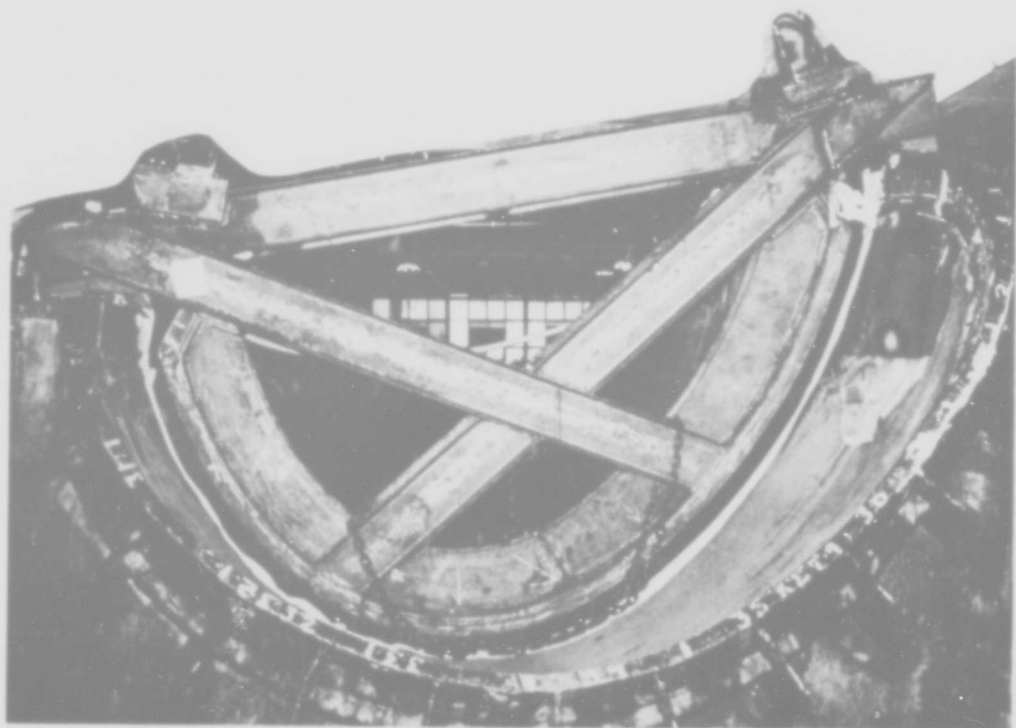


FIGURE 92
STRONG BACK IN PLACE FOR SPLICE CURE OPERATIONS

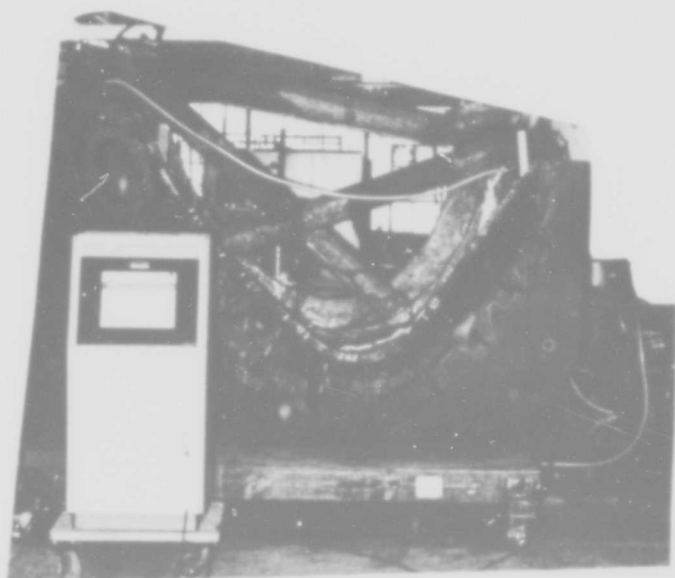
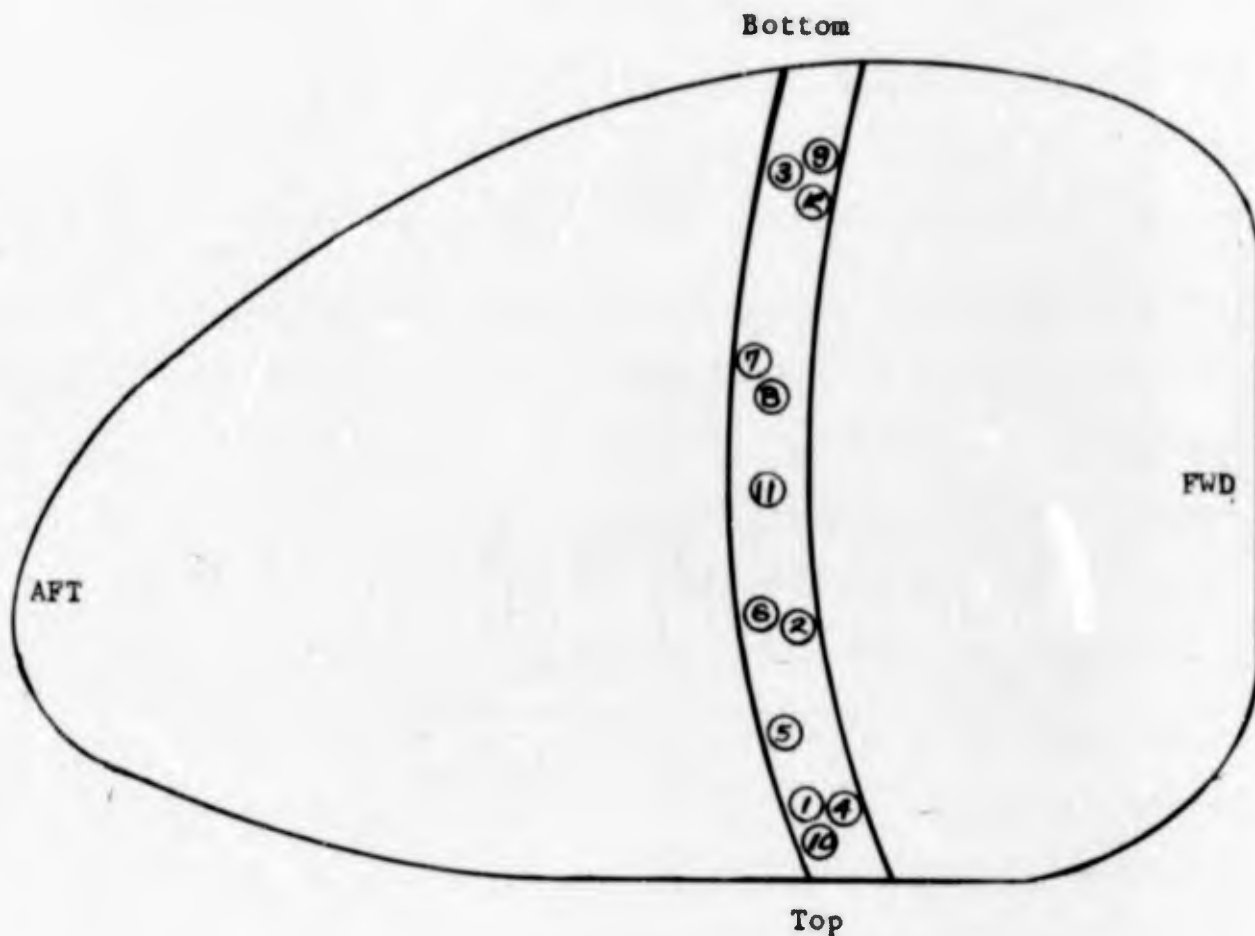


FIGURE 93
SPLICE CURING OPERATIONS



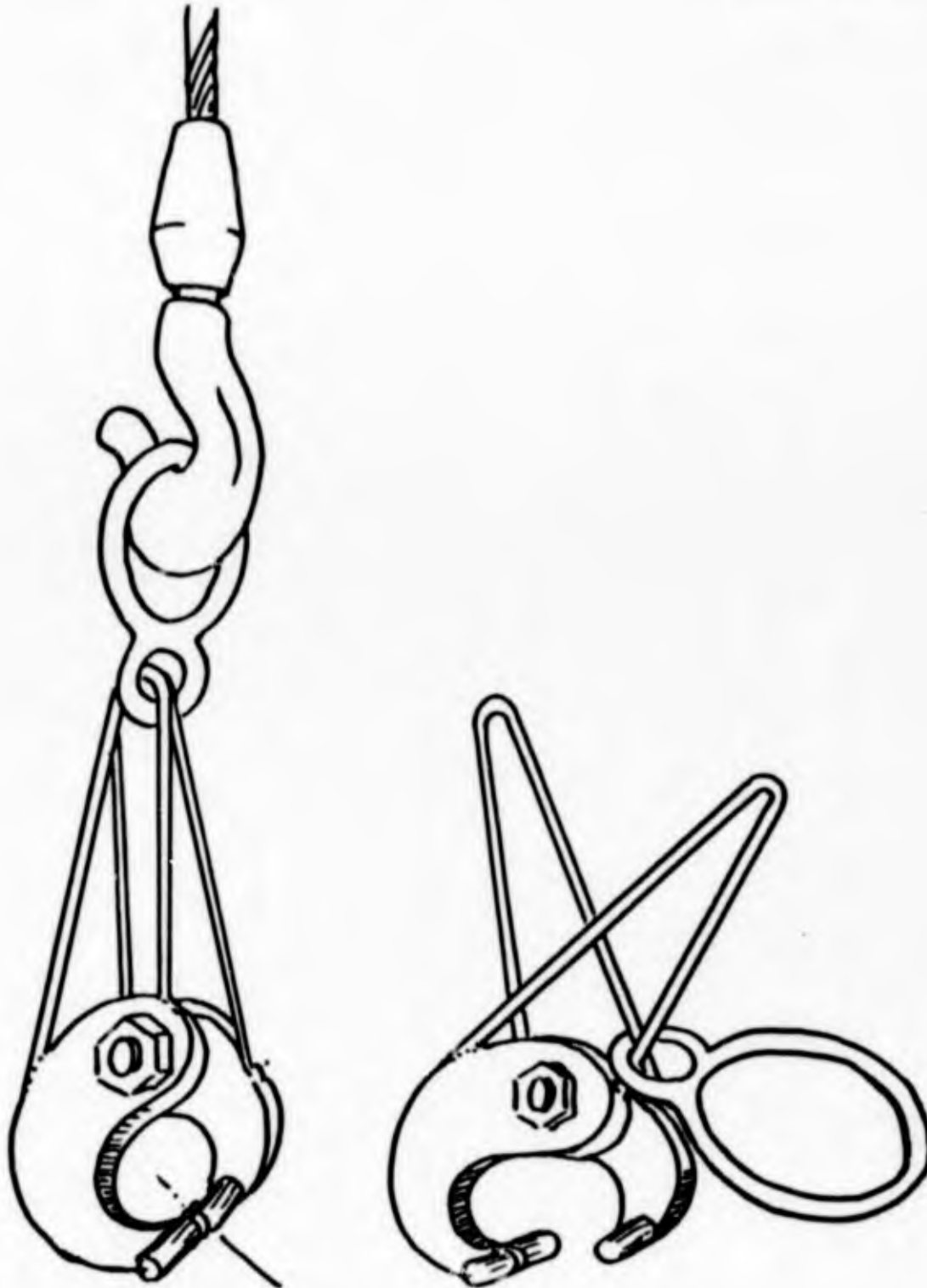
- 1, 2 and 3 - On Surface of Panel
- 4, 5, 6, 7, 8 and 9 - Center of Wire Plies
- 10, 11 and 12 - Between Mold and Panel

Figure 94
Thermocouple Locations During Splice Cure

Contract NObnr 89483
Serial No. SSO41-001
Task 8156

- 225 -

Report No. 17
Phase I Interim Report
30 September 1964



CLOSED

OPEN

FIGURE 95

BEAD TONGS FOR HANDLING PANEL

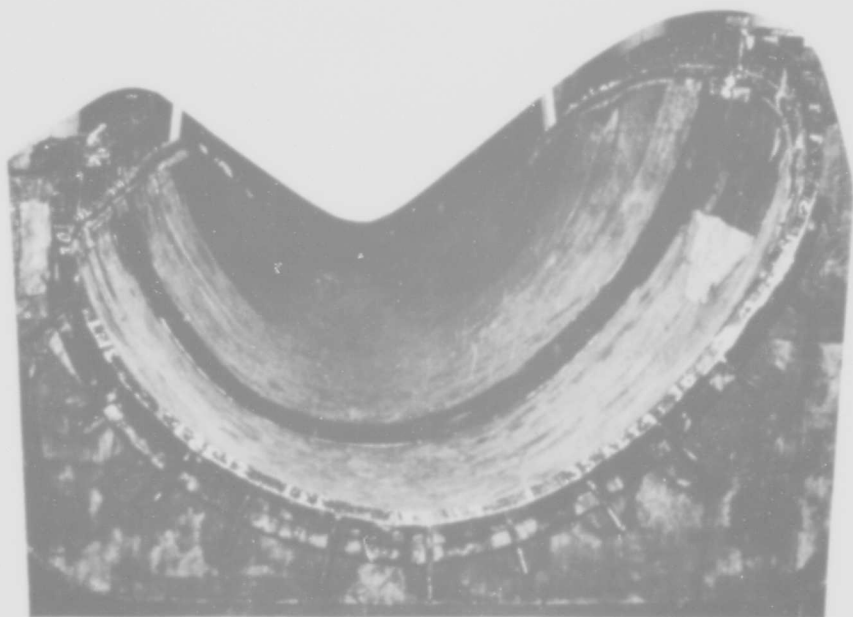


FIGURE 96 - PANEL IN MOLD PRIOR TO REMOVAL

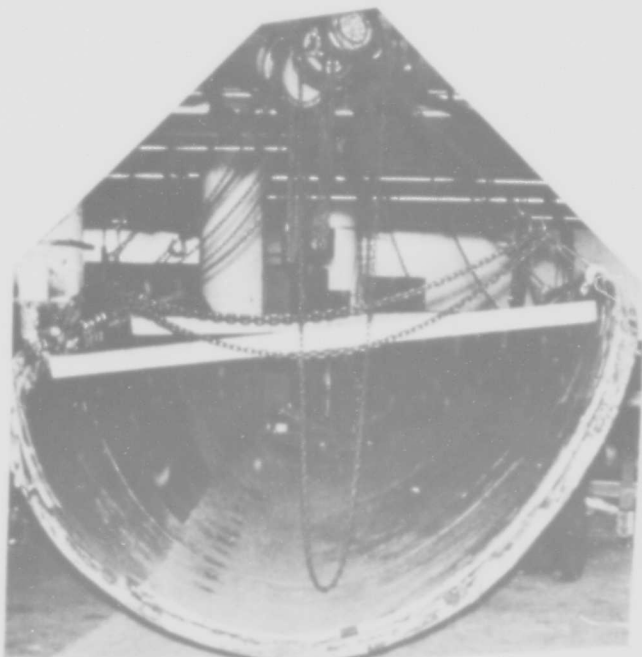


FIGURE 97 - PANEL REMOVED FROM MOLD

Contract N0bsr 89483
Serial No. SS041-001
Task 8156

- 227 -

Report No. 17
Phase I Interim Report
30 September 1964



FIGURE 98 - TOP OF PANEL-EXTERIOR SURFACE



FIGURE 99 - BOTTOM OF PANEL EXTERIOR SURFACE

Contract NObser 89483
Serial No. SS041-001
Task 8156

- 228 -

Report No. 17
Phase I Interim Report
30 September 1964

The condition of the panel after removal was considered to be excellent even though it had undergone severe handling during removal. However, several surface blemishes were present which apparently stemmed from porous sections of the plastic mold tooling.

In these areas during cure the air and moisture forced its way through the mold forming a cavity between the panel and the mold. Areas approximately 30 inches square by 1/8" to 1/4" deep were present. The shallow depressions were buffed to contour while the larger were filled with an Epoxy 820 - Versamide, flexible, air-curing resin system and then buffed to contour.

(10) Panel Inspection

Subsequent to assembly and splicing of the panel a thorough examination was made. This includes a check for delamination, blisters, voids and etc. Several voids along the edges of the fill were buffed and smoothed over with a putty type epoxy base material. This was then buffed smoother to blend with the panel surface.

Measurement of the water line and station marks on the outside of the panel indicated the measurements were virtually the same as those in the mold.

The prototype panel was dropped over two cylindrical supports approximately two feet apart at their closest point. The weight of the panel and necessary supports prevented 100% X-Ray coverage, however, the most important areas, the bead periphery and the splice section were completely examined. The extent of panel coverage can be seen in Figure 100.

The actual technique utilized employed a 260 kVP Holger Andreason Andrex SMA continuous cycle portable unit mounted on a mobile hoist. Figures 101 and 102 present representative pictures obtained from the X-Ray program. Figure 101 presents a bead area with the wire pattern and Figure 102 presents a panel area including part of the splice. The wire pattern is readily distinguishable and was found to be extremely uniform. A slight void 1/2" from the bead measuring approximately 4" x 1/8" can be seen in Figure 101. There were only three isolated areas of this type of void picked up during this X-Ray process.

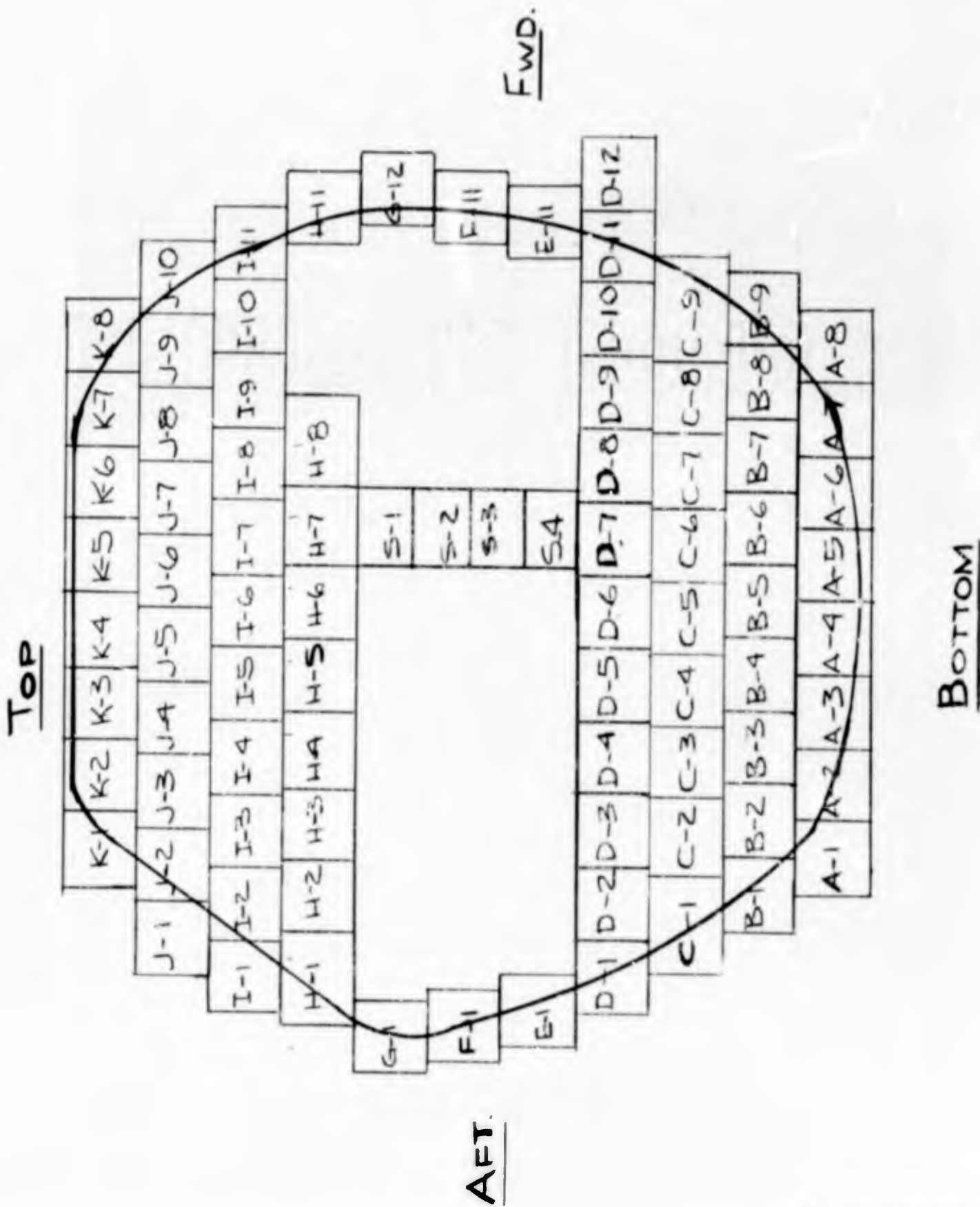


FIGURE 100
 X-RAY COVERAGE OF PANEL

Contract N0ber 89483
Serial No. SS041-001
Task 8156

- 230 -

Report No. 17
Phase I Interim Report
30 September 1964



FIGURE 101
X-RAY POSITIVE OF BEAD AREA

Contract NObsr 89483
Serial No. SS041-001
Task 8156

- 231 -

Report No. 17
Phase I Interim Report
30 September 1964

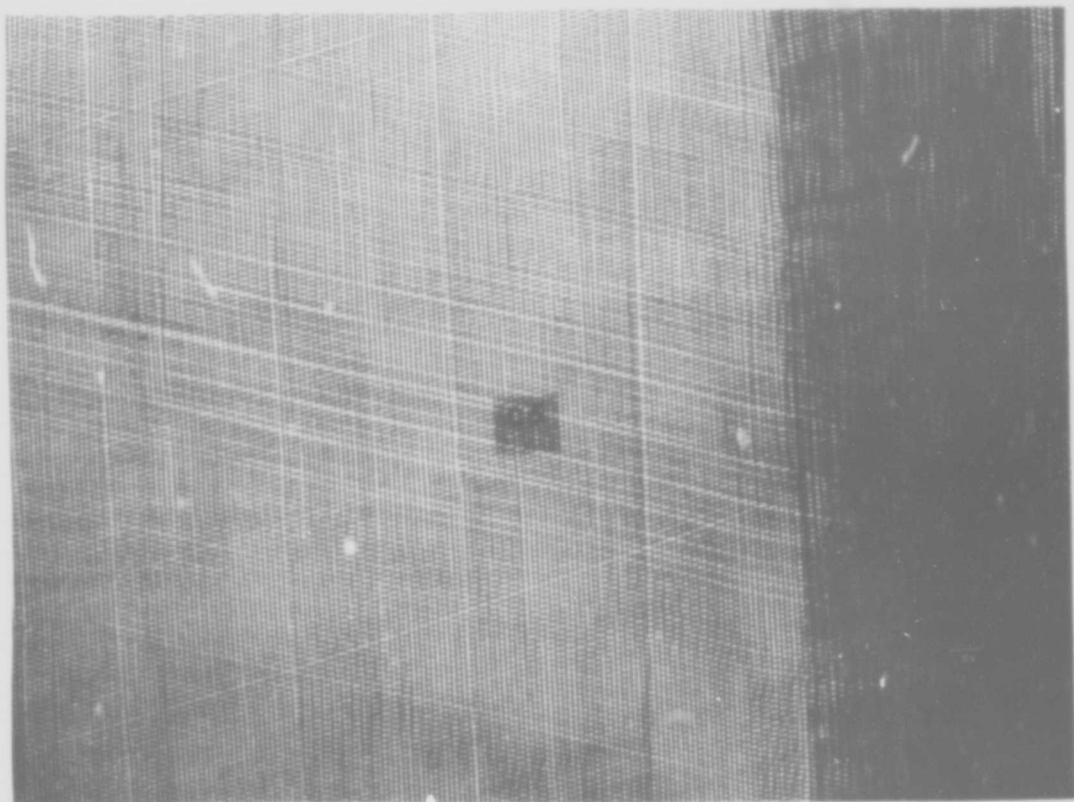


FIGURE 102
X-RAY POSITIVE SPLICE AREA

f. Panel Installation in Test Fixture

The panel was transported to the test area on several "field expedient" type handling cradles. From the cradle, using a combination of handling tongs, spreader bar and lifting lugs, the panel was hoisted into position on the test fixture. Location of the lugs on the panel surface was determined to permit lifting over the center of gravity. Considerable maneuvering of the panel was required to insert the bead inside the bead seat and nestled into the cavity.

The bead clamps had been placed inside the fixture prior to panel installation. Once panel positioning was accomplished the clamps were bolted in place.

Also, prior to panel positioning the compression member was lowered to facilitate this operation. Upon final positioning and clamping of the panel movement of the compression member into final position was accomplished.

To insure adequate retention of the panel and prevent slippage over the compression member a combination restraint system was utilized. A single line of rubber biscuits 2" dia. and 1/2" high were utilized to position the panel accurately over the compression member. A layer of Code 369 cement was applied to both the compression member surface and the inner panel surface. When the cement reached the proper tack the compression member was raised into position and the biscuits guided into their respective recesses. After completion of installation the panel surface was painted with the anti-fouling system previously discussed. The completed panel is shown in Figures 103 and 104. The black strips are areas (1) devoid of cement and (2) with black primer cement to determine effect of panel elongation on each system phase.

Upon complete installation and clamping of the panel in place, a wrinkle appeared at the forward end of the panel just off the compression member. The main cause of this condition is attributable to the hydrostatic test fixture being shorter than the panel mold. During final welding of the bead seat to the basic pressure structure, the heat generated from the weld caused shrinkage, warpage and other distortions in excess of those anticipated. The net result of these actions was a forward to aft measurement reduction of 3/4" from center of bead to center of bead.

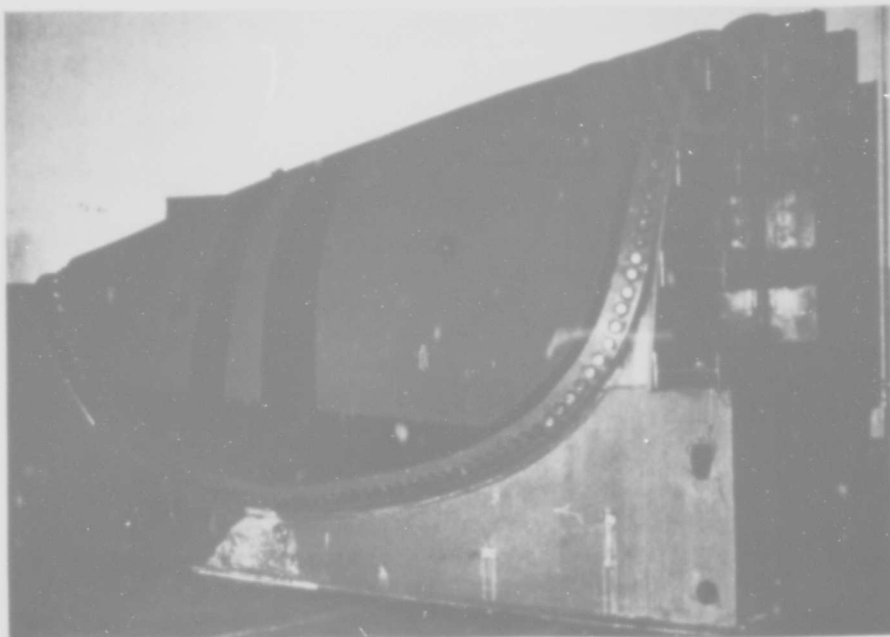


FIGURE 103
COMPLETED PROTOTYPE PANEL-80 PSI - BOTTOM SIDE



FIGURE 104
COMPLETED PROTOTYPE PANEL-80 PSI - TOP SIDE

Contract NObsr 89483
 Serial No. SS041-001
 Task 8156

Report No. 17
 Phase I Interim Report
 30 September 1964

g. Panel Testing Program

The prototype panel was subjected to a series of test conditions during a three (3) week period. In essence, pressure has been maintained on the panel from April 11, 1964 through April 30, 1964. Table XXIX presents the actual cycles performed on the panel during this time interval.

TABLE XXIX
PANEL TEST CYCLE RECORD

Cycle No.	Date	Time		Pressure	Measurements Taken	Remarks
		From	To			
	4/11/64		10:00 a.m.	Empty	ARC Length-Radius of Curvature	
1	4/11/64	10:00 a.m.	4:00 p.m.	Fill to 40 psi	"	
	4/11/64	4:00 p.m.	5:30 p.m.	80 psi	"	
	4/11/64	5:30 p.m.	6:30 p.m.	40 psi	"	
	4/11/64	7:00 p.m.		Drain		
	4/13/64	1:30 p.m.		Fill to 40 psi		
2	4/14/64			40 psi		
	4/15/64			40 psi		
	4/16/64			40 psi		Buships and USL USL personnel observance of panel
3	4/17/64	1:00 p.m.	2:00 p.m.	80 psi		" "
	4/17/64	2:00 p.m.	3:00 p.m.	40 psi	ARC Length-Radius of Curvature	
4	4/17/64	3:00 p.m.	4:00 p.m.	80 psi	"	
	4/17/64		4:00 p.m.	Drain		Check and re-torque bolts
5	4/22/64	9:30 a.m.	3:30 p.m.	Fill to 40 psi	"	
6	4/23/64	12:55 p.m.		(Conduct 0-50		
26	4/24/64		2:00 p.m.	psi cycle	"	
	4/24/64		2:00 p.m.	Drain		
27	4/28/64	3:00 a.m.	11:30 a.m.	Fill to 10	} (Wave Study conducted by BFG & USN/USL personnel	
	4/28/64	11:30 a.m.	4:45 p.m.	Fill to 40		
	4/29/64	7:30 a.m.		21 psi		
28	4/29/64	7:30 a.m.	9:15	40 psi	} (Wave Study conducted by BFG & USN/USL personnel	
	4/30/64	7:45 a.m.	10:30 a.m.	25 psi		
29	4/30/64	7:45 a.m.	10:30 a.m.	40 psi	} (Wave Study conducted by BFG & USN/USL personnel	
	4/30/64	10:30 a.m.	1:30 p.m.	80 psi		
	4/30/64		4:30 p.m.	60 psi		
	4/30/64			Drain		

Prior to the test sequence all bead clamp bolts were tightened to 550-600 ft.-lbs. of torque. Strain gages were mounted on the bead clamps and on both the inside and the outside of the panel.

The fixture was then filled with water and the instruments calibrated for recording automatically the internal pressure of the panel and the strain on its various components. The internal pressure was increased to 40 psi and held for measuring arc lengths and radii, then to 80 psi and back to 40 psi; maintaining each pressure for data gathering. Tables XXX through XXXII list data collected during this program. Figure 105 gives the description of the measurements. The strain gages, although an attempt was made to waterproof them, shorted out.

The surface area of the panel was buffed and blended - in part while under pressure and in part while not under pressure. Defect and blemish areas were repaired. Where necessary for contour preservation, an epoxy repair material was used to fill. During the panel testing, flexing of the surface caused crazing (alligatoring) of the anti-fouling paint over these materials. The epoxy-amine compound became brittle and cracked under the blow of a metal mallet. Consequently the development of a flexible, compatible neoprene compound for repair purposes is being expeditied.

The fixture was drained and specified clamp bolts were checked for their torque. Readings varied from 375 ft.-lbs. to 650 ft.-lbs. for two-thirds of the perimeter and from 100 ft.-lbs. to 600 ft.-lbs. for the remaining one-third. Upon evaluation of these results, it was discovered that for the one-third section of the bead the bolts had been tightened and torque tested individually in succession without returning to recheck the torque on the previously tightened bolt. It is concluded, therefore, that for the section having readings ranging from 100 ft.-lbs. to 600 ft.-lbs. of torque, the wide range of variance was due mainly to incorrect bolt tightening procedure and not entirely to the panel pressure cycle.

Several clamps were removed for inspection of the bead. No detrimental effects to the bead were found during this examination.

The clamps were replaced and bolts tightened. All bolts were checked for a minimum of 400 ft.-lbs. Then a stabilization test was performed in which the panel was cycled ten times from 10 psi to 50 psi pressure and measurements of arc lengths and radii taken. It was found that after the second series of ten cycles, the measurements repeated themselves which indicated that the panel had stabilized.

TABLE XXX
 PROTOTYPE PANEL TESTS
ARC LENGTHS & RADII

Cycle	Pressure	RADIAL FRAMES										
		7	8	9	10	11	12	13	14	15	16	
1	0	T	14.938	14.594	14.625	15.063	14.250	17.032	14.000	13.688	13.500	13.375
		M	25.375	25.250	40.625	39.313	38.938	38.375	38.125	38.032	53.875	52.938
		B	16.625	16.313	21.938	20.687	19.562	18.688	17.500	16.718	24.750	22.531
		R ₂	102	89	85	72	69	65	62	60	53	51
		R _H	23	26	27	29	34	37	40	44	44	48
	R _B	61	69	75	79	78	83	85	87	86	79	
	40		15.000	14.625	14.625	15.063	14.250	14.000	13.969	13.688	13.500	13.375
			25.375	25.219	40.750	39.344	39.031	38.500	38.250	38.156	54.000	53.000
			16.750	16.406	22.156	20.812	19.594	18.719	17.563	16.750	24.875	22.750
			75	67	61	68	65	59	68	59	W*	W
			23	26	27	29	34	37	40	44	44	48
	80		15.000	14.625	14.656	15.125	14.250	14.000	13.969	13.688	13.500	13.375
		25.375	25.250	40.750	39.375	39.094	38.500	38.313	38.188	54.063	53.063	
		16.813	16.438	22.156	20.781	19.594	18.750	17.625	16.750	24.937	22.750	
		66	61	59	64	61	57	66	57	W	W	
		23	26	27	29	34	37	40	44	44	48	
40		14.938	14.625	14.625	15.063	14.250	13.938	13.969	13.719	13.500	13.344	
		25.375	25.188	40.688	39.313	39.000	38.438	38.250	38.125	54.000	53.063	
		16.719	16.375	22.187	20.750	19.563	18.687	17.563	16.750	24.938	22.625	
		79	69	64	70	67	60	63	61	W	W	
		23	26	27	29	34	37	40	44	44	48	
6	40		14.938	14.625	14.375	15.094	14.250	13.969	13.969	13.719	13.438	13.313
			25.312	25.156	41.000	39.312	38.969	38.469	38.219	38.062	53.968	52.968
			16.938	16.375	22.125	20.782	19.719	18.812	17.750	17.282	24.875	22.750
			71	66	60	68	67	59	68	60	W	W
			23	26	27	29	34	37	40	44	44	48
	80		14.969	14.688	14.375	15.125	14.281	14.000	14.000	13.719	13.469	13.375
			25.344	25.125	41.125	39.406	39.157	38.563	38.281	38.219	54.094	53.031
			16.968	16.500	22.125	20.844	19.656	18.812	17.844	17.312	24.937	22.813
			66	61	57	62	62	57	64	57	W	W
			23	26	27	29	34	37	40	44	44	48
		60	57	69	73	75	72	81	76	76	W	

* "W" means that a wrinkle prevented measurement of the radius.

TABLE XXX (Continued)

Cycle	Pressure	RADIAL FRAMES									
		7	8	9	10	11	12	13	14	15	16
16	50	14.938	14.656	14.375	15.094	14.250	14.031	13.969	13.719	13.469	13.375
		25.343	25.125	41.000	39.342	39.094	38.469	38.219	38.094	53.969	52.938
		16.907	16.469	22.125	20.812	19.594	18.750	17.781	17.281	24.906	22.750
		75	66	60	67	66	59	68	61	W	W
		23	26	27	29	34	37	40	44	44	48
		60	66	75	76	76	73	88	82	71	W
26	50	15.000	14.625	14.313	15.094	14.250	13.938	14.031	13.719	13.438	13.406
		25.313	25.219	41.000	39.344	39.063	38.562	38.219	38.094	54.000	52.969
		16.937	16.406	22.156	20.812	19.625	18.719	17.781	17.281	24.906	22.781
		70	66	61	66	66	59	68	60	W	W
		23	26	27	29	34	37	40	44	44	48
		62	66	63	76	76	73	75	79	71	W
30	0	14.906	14.594	14.281	15.094	14.281	14.063	13.906	13.719	13.375	13.313
		25.313	25.125	40.969	39.219	38.969	38.343	38.094	37.969	53.875	52.812
		16.875	16.344	21.969	20.750	19.625	18.719	17.719	17.250	24.750	22.688

TABLE XXXI
ARC LENGTH MEASURED ALONG RADIAL FRAMES BETWEEN EDGES OF GUM FILL

4	40	121.125	131.000	138.250	143.000	146.125	148.813	150.000	150.500	149.750	146.375
	80	121.500	131.250	138.500	143.250	146.375	149.000	150.375	150.750	151.000	147.750
30	0	120.563	130.250	137.438	142.375	145.438	148.188	149.438	150.063	149.250	146.250

TABLE XXXII
DISTANCE FROM EDGE OF BEAD SEAT TO EDGE OF PANEL

STATION	PRESSURE				
	40	80	50	50	0
10	2.219	2.188	2.250	2.250	2.250
18	2.219	2.156	2.188	2.250	2.500
23	1.969	1.938	1.938	2.000	2.313
31	2.875	2.844	2.875	2.875	3.000
38	3.313	3.344	3.375	3.375	3.375
43	3.344	3.344	3.375	3.375	3.219
53	1.563	1.594	1.563	1.500	1.656
60	2.688	2.469	2.094	2.531	2.750
78	2.031	2.031	2.063	2.031	2.125
92	2.594	2.688	2.750	2.750	3.000
102	2.531	2.563	2.594	2.563	2.813
112	3.281	3.313	3.313	3.250	3.375
Cycle	6	6	16	26	30

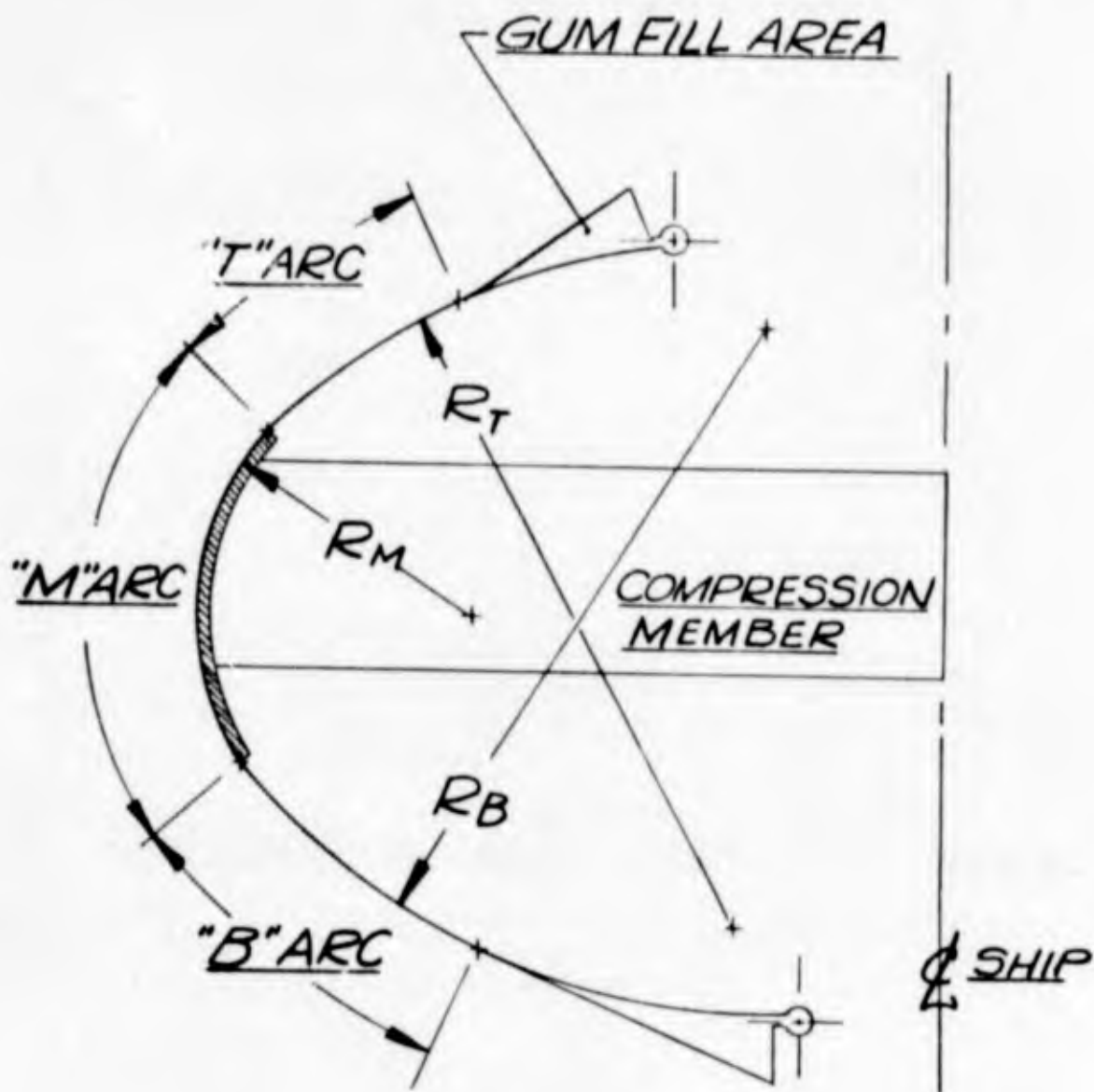


FIGURE 105
TYPICAL RADIAL FRAME CROSS SECTION OF PROTOTYPE PANEL

During draining of the fixture after the initial test, the breather valve was not opened. As the water drained out, a negative pressure was created which caused the sides of the panel to partially collapse. This confirms the belief that the bow window will flex inward when evacuated of water for purposes of repairing the transducer.

Strain gages and accelerometers were then mounted on the panel and acoustical equipment was set up by Underwater Sound Laboratory and B.F. Goodrich personnel. The intent was to study waves in the panel as induced by internal and external excitation. In particular the vibration decay rate or damping characteristics of the panel was of interest.

The panel was forced to oscillate by external blows with a mallet. Measurements of the dissipation of energy causing the membrane to vibrate normal to the surface of the panel were accomplished through accelerometers. It was found that the decay rate was significantly better than that found on steel domes.

The decay rate of reverberations induced by a transducer suspended inside the test fixture was next attempted. The pressure waves induced by the transducer vibrations imposed oscillations in the panel. Results indicated that the transducer had a slower rate of decay than the panel, thus no useful information was attained.

An attempt was made to determine the decay factor of the panel through use of strain gages. If this would be successful, then strain gages could be used instead of accelerometers at a substantial savings in cost and ease of gathering data would be enhanced. However, no success was experienced. The strain gages did not react to the vibrations induced externally or internally. Furthermore, the internal strain gages were shorting out somewhat through the water.

Within the limits of the testing procedure and instruments, the following conclusions were made:

- (1) The rubber window exhibited a 5% to 6% critical damping factor in contrast to a .2% factor for the 100 inch steel dome at the critical frequency.
- (2) The percent critical damping was uniform over a frequency range of 100 cycles to 16 kilocycles.

Throughout all the testing to date, there has been no leakage of water through the bolt retention system, around the bead, or through the panel itself.

The next test planned for the prototype panel is a fatigue test. During this test the panel will be flexed 1000 cycles or more by automatically varying the pressure from 30 psi to 50 psi. Periodically, measurements will be taken for later analysis.

After the fatigue test, a 60-day stand test at 40 psi will be performed followed by a strength test. The panel will be loaded with forces created by 125 psi internal pressure during this strength test.

According to the final design concept, the bow dome window will not utilize a compression member. It is desirable to know how the membrane will react in the tail section without it. Therefore a test without the compression member restraining the prototype panel is scheduled.

Evaluation of repair techniques on a full scale application is also deemed necessary. This will be achieved also on the prototype test panel.

Finally, it is significant to know the safety factor of the panel. The hydrostatic test fixture has been designed to withstand short term loads of 150 psi. Withstanding loads at this pressure magnitude will reflect a panel safety factor of 3.7.

The stretch characteristics of the acoustic window, which were derived from samples tested, were applied to predict the contour of the prototype panel when subjected to various internal pressures. However, the panel did not react exactly as predicted and the constructional stretch was approximately 1/2 of that expected.

An explanation of this result is that the constructional and elastic stretch curves which were used to estimate the contour of the window were developed from samples which did not reflect true full-scale conditions. Most of the information for these curves was obtained from 2-3/4" & 6" wide samples. At these widths the 15° horizontal plies do not help support loads, while in actual practice they do. Furthermore, the cables in the plies of these samples had a tendency to migrate and nestle inbetween each other. This was made possible because of the limited width of the sample and the somewhat

BLANK PAGE

unrestrained condition of the wrap-around at the bead. While the existence of this circumstance was known, its affect upon the stretch characteristics as derived from the samples could not be determined.

Another factor of undetermined magnitude was the elastic properties of the panel. That area of the panel which is in contact with the compression member was treated as a fixed and rigid section. To insure this condition, the compression member surface was sandblasted to produce a better frictioned surface, biscuits of rubber were bonded to the inside surface of the panel such that they would register in pre-located holes of the compression member, and further, the contact surface of the panel and compression member were cemented and bonded together. Nevertheless, this portion of the panel did not react as a fixed body nor was it rigid. Consequently, some strain was experienced in that part of the panel in contact with the compression member.

Another influencing factor, because of end effects, compression member influence and the gum fill areas, it was impossible to acquire accurate radius readings.

In spite of the relatively rough measurements, it is possible to derive the elastic properties of the prototype panel. This can be accomplished by the collecting, comparing and examining an abundance of data from future testing.

h. Conclusions

- (1) A test panel representing the aft most section of the complete window should be built. It is the most useful for confirming the feasibility of the proposed window.
- (2) A compression member, to hold the panel out to the desired contour, is acceptable and desirable for use on the prototype test panel. However, additional work should be done to improve this system, acoustically and structurally, for use with the prototype acoustic window aboard ship.

- (3) A panel constructed of 5 wire plies, properly oriented, and 4 neoprene plies laminated together to form a 1" thickness will withstand the stresses expected during service.
- (4) A cured splice 9" wide with an interlacing of 15⁰ plies, will hold adjacent panels together to form a one piece window.
- (5) Plastic tooling will be procured for use in building the prototype panel. Contour attainment, cost and delivery indicated that the use of epoxy-fiberglass laminated tooling would be more advantageous than steel.
- (6) A two piece panel will be built and spliced together, using a reinforced seaming section in the mold and a steel strong back splicing jig over the panel.
- (7) A steel-concrete hydrotest fixture will be fabricated for testing the panel. This fixture will contain the bead seat-bead clamp system proposed for use on the ship.
- (8) Extreme caution must be exercised in panel fabrication to insure uniformity and smoothness of wire lay.
- (9) The cure cycle as described in Section 10.c. resulted in very satisfactory cure of the panel.
- (10) Welding of the bead cable for splicing is difficult to accomplish and this procedure should be replaced with a pre-welded mechanical cable joint.
- (11) A more acceptable surface repair gum must be developed to assist in panel finishing operations.
- (12) X-Ray examination of the panel indicated that the wire pattern was good and only 3 voids, adjacent to the bead, were present.
- (13) The panel construction is structurally sound and can withstand an 80 psi internal positive pressure.
- (14) The bead seat-bead clamp retention and sealing system performed successfully and can be used on the prototype window.

Contract NObsr 89483
Serial No. SS041-001
Task 8156

- 243 -

Report No. 17
Phase I Interim Report
30 September 1964

- (15) Damping characteristics (5-6%) of the rubber panel are better than either steel or plastic domes.
- (16) Contour and smoothness of the panels indicates the prototype acoustic window can be fabricated well within the requirements of the program.

11. Universal Window Study

a. Summary

It is not practical to build one acoustic window to fit the DL-5, DLG-26, DE-1040 and DE-1052 ships. The additional effort required to accomplish fairing operations makes this concept economically unfeasible. However, semi-universal windows, one for the DL-4 and DLG-26, and one for the DE-1040 and DE-1052 combination are practical and feasible. This concept will be incorporated into the DL-5 acoustic window design program.

b. Introduction

Currently there are four (4) classes of ships which incorporate a Sonar Bow dome. These are: (1) DE-1040, (2) DE-1052, (3) DLG-26, and (4) DL-2 (DL-4 and 5 of this class). It was considered desirable, from a cost and logistics standpoint, to fabricate windows of one design for all of these ships. Consequently, a Universal program aimed at that end was established.

c. Discussion

Initial considerations were concerned with how such a comparison could best be made and a resultant design program initiated. To accurately and correctly tackle this program a complete set of drawings were requested for each of the ships. The drawings received are listed in Table XXXIII following:

TABLE XXXIII
DRAWINGS UTILIZED IN UNIVERSAL DOME STUDY

Class of Ship	BuShips Drawing Number	Origin of Drawing	Drawing Number	Title of Drawing
DLG-26	100-1994101 Rev. E	Gibbs & Cox for Bath Iron Works	DLG-26-1001-1	Outside Plating Stem to FR 44 1/2
DLG-26	101-1994112 Rev. H	Gibbs & Cox for Bath Iron Works	DLG-26-1011-7	CVK & STGR Nos. 1/2 -13 3/4 FWD FR 44 1/2
DLG-26	101-1994113 Rev. B	Gibbs & Cox for Bath Iron Works	DLG-26-1011-8	STGR No. 14-21 FWD FR 44 1/2
DLG-26	101-1994116 Rev. B	Gibbs & Cox for Bath Iron Works	DLG-26-1011-11	TRANSV FRG FR 1/2 to 4 1/2
DLG-26	101-1994117 Rev. D	Gibbs & Cox for Bath Iron Works	DLG-26-1011-12	TRANSV FRG FR 5 1/2 to 19 1/2 & Web FR 8, 11,13,16 & 18
DLG-26	101-1994118 Rev. C	Gibbs & Cox for Bath Iron Works	DLG-26-1011-13	TRANSV FRG FR 20 1/2 -31 1/2 Web FR 23, 26 & 29
DLG-26	101-1994119 Rev. C	Gibbs & Cox for Bath Iron Works	DLG-26-1011-14	TRANSV FRG FR 33 to 46 & Web FR 35 & 38
DLG-26	114-1994286 Rev. F	Gibbs & Cox for Bath Iron Works	DLG-26-1141-2	TRANSV BHD 5, 8, 11, 13 & Chain LKR BHD
DLG-26	145-1994360 Rev. HH	Gibbs & Cox for Bath Iron Works	DLG-26-1451-5	Mold Loft Offsets (the following sheets)
			1	
			1a	Revisions
			2	Index
			2a	Index
			3	General Information
			7	Bow Profile 4'0" WL to 0
			7a	Bow profile 6'0" WL to 9'0" WL
			8	Bow Plan, Stem to Frame 13
			8a	Bow Plans Between Frames 13 & 27
			12	Waterline Half Breadths Baseline & Below
			12a	Waterline Half Breadths
			12b	Waterline Half Breadths
			19	Buttock Heights
			19a	Buttock Heights
			20	Buttock Heights
			31	Shell Knuckle Fwd And Half Siding Fwd
			34	Decks & Platforms
			35	Decks & Platforms

TABLE XXXIII (Continued)

Class of Ship	BuShips Drawing Number	Origin of Drawing	Drawing Number	Title of Drawing
DLG-26	145-1994369 Rev. C	Gibbs & Cox for Bath Iron Works	DLG-26-1451-14	Deck Sup. Compt. & Access Inboard Profile
DLG-26	404-1994384 Rev. D	Gibbs & Cox for Bath Iron Works	DLG-26-4041-3	Sonar Dome AN/SQS-26 Sonar Equipment
DLG-26	404-1994385 Rev. C	Gibbs & Cox for Bath Iron Works	DLG-26-4041-4	Sonar Dome Details AN/SQS-26 Sonar Equip.
DLG-26	404-1994386 Rev. B	Gibbs & Cox for Bath Iron Works	DLG-26-4041-5	Sonar Turntable Arr. & Details
DE-1040	100-2093623 Rev. D	Bethlehem Steel Company	5496-123-1	Outside Plating & Long'l Framing FWD FR 78
DE-1040	100-2093624 Rev. E	Bethlehem Steel Company	5496-123-2	Outside Plating & Long'l Framing AFT FR 78
DE-1040	100-2093625 Rev. J	Bethlehem Steel Company	5496-123-3	Sonar Dome & Framing
DE-1040	101-2093613 Rev. F	Bethlehem Steel Company	5496-122-1	Center Keel
DE-1040	101-2093614 Rev. E Sheet 1 of 2	Bethlehem Steel Company	5496-122-3	Bow Framing FR 14 & FWD
DE-1040	101-2093614 Rev. E Sheet 2 of 2	Bethlehem Steel Company	5496-122-3	Bow Framing FR 14 & FWD
DE-1040	101-2093616 Rev. C	Bethlehem Steel Company	5496-122-5	Web Frames, Floors & Intermediate Transv. Frames - FR 30-37 Incl.
DE-1040	101-2093617 Rev. C	Bethlehem Steel Company	5496-122-6	Web Frames - FR 31-44 Incl. & Intermediate Transv. Frames - FR 30-37 Incl.
DE-1040	114-2093635 Rev. D	Bethlehem Steel Company	5496-125-5	BHD's 14 53 & Chain LKR Below 1st Platform
DE-1040	404-2093652	Bethlehem Steel Company	5496-123-7	Sonar Dome Baffle
DE-1040	404-2093653 Rev. A	Bethlehem Steel Company	5496-123-8	Sonar Dome Transducer Turntable, Arrangement & Details
DE-1040	800-2093601 Rev. E 88 sheets	Bethlehem Steel Company	5496-11-41	Mold Loft Offsets
DE-1040	114-2093635 Rev. A	Bethlehem Steel Company	5496-125-1	Transv BHD's 29, 38 & 53

TABLE XXXIII (Continued)

Class of Ship	BuShips Drawing Number	Origin of Drawing	Drawing Number	Title of Drawing
DE-1040	800-2094116 Rev. F	Bethlehem Steel Company	5496-11-4	Deck Supports & Compartment & Access Hold & Second Platform
DL-4	102-1340425 Rev. D	New York Naval Shipyard	BuShips No.	Bow Modification Hold & Baseline Flat Pltg. & Beams
DL-4	113-1340429 Rev. B	New York Naval Shipyard	BuShips No.	Bow Modification Foundations for Transducer
DL-4	145A-1340452 Rev. D Sheet 1 of 3	New York Naval Shipyard	BuShips No.	Compartment & Access Third Platform - Hold & Inner Bottom
DL-4	404-1340415 Rev. E	New York Naval Shipyard	BuShips No.	Bow Modification Sonar Dome Framing & Details, Sheet 2
DL-4	404-1340415 Rev. E (Reproducible)	New York Naval Shipyard	BuShips No.	Bow Modification Sonar Dome Framing & Details Sheet 2
DL-4	404-1340428 Rev. B	New York Naval Shipyard	BuShips No.	Bow Modification Sonar Dome Framing & Details
DL-4	404-1340428 Rev. B (Reproducible)	New York Naval Shipyard	BuShips No.	Bow Modification Sonar Dome Framing & Details
DL-4	845-1340411 Rev. A	New York Naval Shipyard	BuShips No.	Bow Modification Body Plan & Offsets
DL-4	845-1340412 Rev. A	New York Naval Shipyard	BuShips No.	Bow Modification Faired Lines From Offsets
DL-4	Encl. (4) to BuShips Ser. 688E-970	Boston Naval Shipyard	No Number	Offset Readings taken on Bow Sonar of "Lee" DL-4 By Shop 64 on Docking Period of 2/5/63 at Boston Naval Shipyard - Dry Dock #4
DL-5	1987146 Rev. F	Long Beach Naval Shipyard	BuShips No.	AN/SQS 26 Sonar-Sonar Turntable Arrgt. & Details
DL-5	13 pages of Half Breadths lifted from actual dome of "Wilkinson", DL-5			
DE-1052	800-2120649	BuShips	BuShips No.	Sonar Dome Plating & Framing

Using the furnished drawings frames, waterlines and buttock lines were drawn comparing the contour and size of the four units in question. During this study the drawings were discussed with BuShip, Hull Design personnel to insure assumptions being made were within the allowable limits of the program. Also full scale drawings of the base plate and chocks, at the frames were layed out to get a better perspective of what fairing problems had to be handled.

At first an attempt was made to fit the DL-5 window, on which the greatest effort had been placed up to this time, to each of the other three ships. In attempting this it became apparent that several basic design concepts should be kept in mind.

- (1) The bead location and size would have to remain constant whether 2, 3 or 4 ships were included in the study.
- (2) The bead location would have to fit the smallest ship's dome and have a fairing member for matching other ships contours.
- (3) The chocks along the "banjo" and "cat walk" would have to be standardized.

Conclusion resulting from this program indicate that the one (1) universal dome concept is not feasible. However, this study also indicates that a two (2) universal dome concept is feasible and practical. Reason for the preceeding statements are:

- (1) The contours of the four (4) classes of ships classify themselves into two (2) basic groups as seen in Figure 111. The DL-5 and DLG-26 dome contours appear to be similar as do the DE-1040 and DE-1052 domes. The maximum difference between the largest and the smallest critical fairing point of all four (4) domes is approximately eight (8), whereas between the domes of each pair is less than two (2) inches.
- (2) The acoustic window area of the DLG-26 dome is approximately twelve (12) inches shorter than the other three (3) ships. Therefore, if it is included in the universal analysis, all other domes will have to be shortened and their corresponding ship's structure reworked to project the diagonal bulkhead forward the required distance or

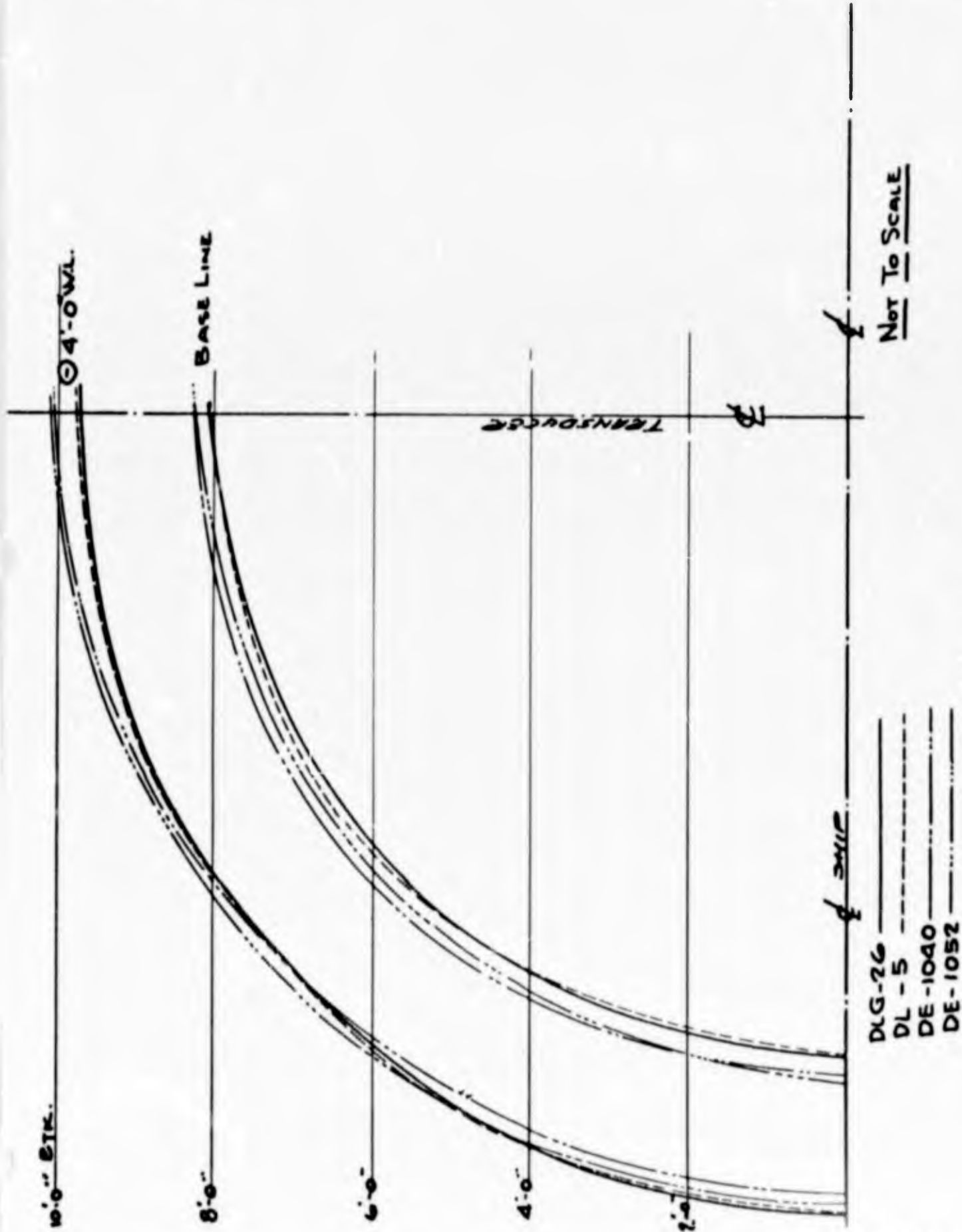


FIGURE 106
FORWARD CONTOUR COMPARISON OF DOMES

Contract NOber 89483
Serial No. SS041-001
Task 8156

- 250 -

Report No. 17
Phase I Interim Report
30 September 1964

the DLG bulkhead back the required distance. With two (2) universal domes, as previously discussed, the diagonal bulkhead need only be moved on the one DL-5 currently planned as the prototype dome.

To fully realize the economic aspects of this study with respect to individual domes Table XXXIV was generated.

Thus from an economic, and technical standpoint the feasible approach is the combination or semi-universal dome concept. With this knowledge additional effort is being expended to convert the DL-5 window contour to permit its use with the DLG-26.

TABLE XXXIV
 COST OF UNIVERSAL DOMES

	FOUR INDIVIDUALLY TAILORED WINDOW DESIGNS				48 INSTALLATIONS OF A UNIVERSAL WINDOW				24 INSTALLATIONS SEMI UNIVERSAL				24 INSTALLATIONS SEMI UNIVERSAL			
	1 PIECE DL-5	9 PIECES DLG-26	13 PIECES DE 1040	25 PIECES DE-1052	DL-5	DLG-26	DE 1040	DE-1052	DL-5	DLG-26	DE-1040	DE-1052	DL-5	DLG-26	DE-1040	DE-1052
TOOLING	\$150,000	\$125,000	\$125,000	\$125,000	\$170,000	\$170,000	\$170,000	\$170,000	\$450,000	\$150,000	\$150,000	\$150,000	\$150,000	\$150,000	\$150,000	\$150,000
BPG SELLING PRICE OF WINDOW PLUS HARDWARE	150,000	150,000	150,000	150,000	170,000	170,000	170,000	170,000	450,000	150,000	150,000	150,000	450,000	150,000	150,000	150,000
HYDROSTATIC TEST FIXTURE	75,000	75,000	75,000	75,000	20,000	10,000	20,000	20,000	20,000	10,000	10,000	10,000	20,000	10,000	10,000	10,000
REWORK OF SHIP	10,000	10,000	10,000	10,000	20,000	10,000	20,000	20,000	20,000	10,000	10,000	10,000	20,000	10,000	10,000	10,000
WINDOW INSTALLATION & FINISH	STD	STD	STD	STD	15,000	15,000	5,000	5,000	15,000	15,000	5,000	5,000	15,000	15,000	5,000	5,000
DOCK TIE UP	8 WKS	8 WKS	8 WKS	8 WKS	10 WKS	10 WKS	9 WKS	9 WKS	10 WKS	10 WKS	9 WKS	9 WKS	9 WKS	9 WKS	9 WKS	9 WKS
	168,000	168,000	168,000	168,000	210,000	210,000	189,000	189,000	210,000	210,000	189,000	189,000	189,000	189,000	189,000	189,000
TOTAL	553,000	350,221	343,376	326,000	419,687	409,687	388,687	368,687	386,500	366,500	359,921	349,921	386,500	366,500	359,921	349,921
TOTAL INDIVIDUAL COSTS		3,151,989	4,463,888	8,150,000		3,508,083	5,052,931	9,217,175		3,388,500	4,678,273	8,748,025		3,388,500	4,678,273	8,748,025
TOTAL COST TO NAVY FOR 48 INSTALLATIONS	3,704,989	16,318,877				4,307,770	18,177,876				3,744,500	17,111,498				

*1DL5 + 9DLG 26 + 13DE 1040 + 25DE 1052

d. Conclusions

The following conclusions were reached:

- (1) Due to the variation in contour a single Universal window will not mate with the contours of the four classes of ships in question.
- (2) Two semi-universal windows will fit all classes of ships. One will fit the DL-5 and DLG-26 and one the DE-1040 and DE-1052.
- (3) The prototype window designed under this contract will be the semi-universal for the DL-5/DLG-26 combination.
- (4) Additional effort will be required later in the program to design the second semi-universal window for the DE-1040/DE-1052 combination.

12. Prototype Window Design

a. Summary

The prototype acoustic window will be of a semi-universal design capable of fitting ships of the DL-5 or DLG-26 contour. Minor compromises, i.e. (1) moving the diagonal bulkhead attachment point of the DL-5 forward to match the DLG-26 bulkhead location, have been accepted. Also buffing of excess gum on each ship as necessary must be accomplished to render this concept workable.

b. Introduction

In order to accurately determine the final contour of the prototype acoustic window, as with the prototype panel, several decisions were necessary and certain data obtained. Additional information, as well as an upgrading of sample test data, was obtained from prototype panel testing and will be utilized. Basically finalization of the following is required:

- (1) Panel Construction - Number and type of fabric-rubber plies.
- (2) Bead Construction - Size and type of bead cable and wrapping sequence of panel plies around bead wire.
- (3) Panel Elongation Data - Elongation of panel construction under specific loads.
- (4) Bead Construction Compressibility - Degree of compression of fabric wrapped plies as bead clamp retains bead construction.
- (5) Bead Clamp Design and Location - Firm design of clamp and exact location with respect to ship's structure.
- (6) Dome Operating Condition - Internal and external forces acting on dome skin.

A slight alteration in any one of these areas will result in a configuration or contour change. Therefore, it was imperative that these areas be investigated thoroughly and all data possible be accumulated.

c. Design Study

Early in the program, in the interests of compressing time, and with a majority of the data available, a preliminary contour coordinate determination was initiated. These efforts were concerned with placing an acoustic window on a steel dome of the DLG-26 class ship. The model shown in Figures 107 and 108 was built to assist in this program.

Basically, the task of contour determination consists of using the coordinates of the steel dome, as furnished by Bu Ships, and transposing them from perpendicular to the dome centerline to perpendicular to the dome wall at specific points along the -4' waterline. With the radial frame cross-sections it becomes a matter of determining; (1) bead centerline, (2) radius of curvature for strength members and (3) the amount of gum necessary to furnish desired contour. The task quickly listed entail considerable, painstakingly accurate work. Each point placed or changed on the dome required lay out in the three basic dimensions - frames, waterlines and buttock lines.

Accomplishment of this task was initially (prototype panel) extremely frustrating, however, with this past experience work on the prototype window progressed much faster.

During work on designing a DLG-26 acoustic window a change was introduced making a DL-5 ship the test vehicle. The two (2) steel domes are different as seen in Figure 109, therefore, the entire procedure was re-initiated using the DL-5 steel dome coordinates. The ultimate goal of this program was to build a rubber acoustic window which would match the steel dome exactly.

One major problem area is the aft sections, as discussed in the prototype panel section. The concept employed in the test panel, using a compression member, was discarded because of structural and acoustical considerations. Additional verification of the fill concept feasibility had been done. It was determined the idea of filling the center of the aft panels can be accomplished by laminates, extrusions or castable materials. These are being investigated without any significant results to date.

Attempting to design the dome for attachment to existing ships contours requires the inclusion of a maximum 10" (Figure 110) center fill at frames 16 and 17. However, an alternate approach as depicted in Figure 111 was determined to be desirable and reduces the maximum fill to 6". The system

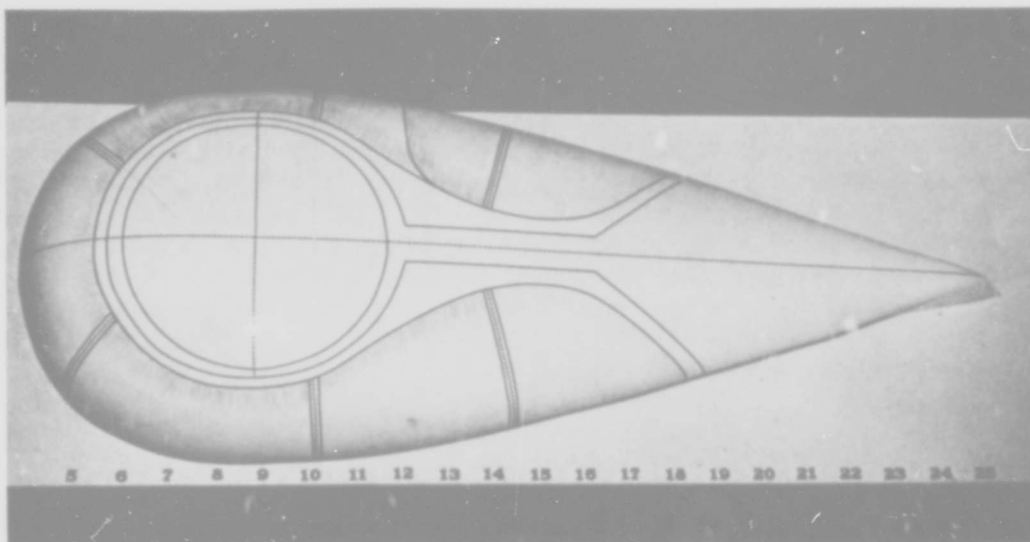


FIGURE 107
TOP VIEW OF DOME MODEL

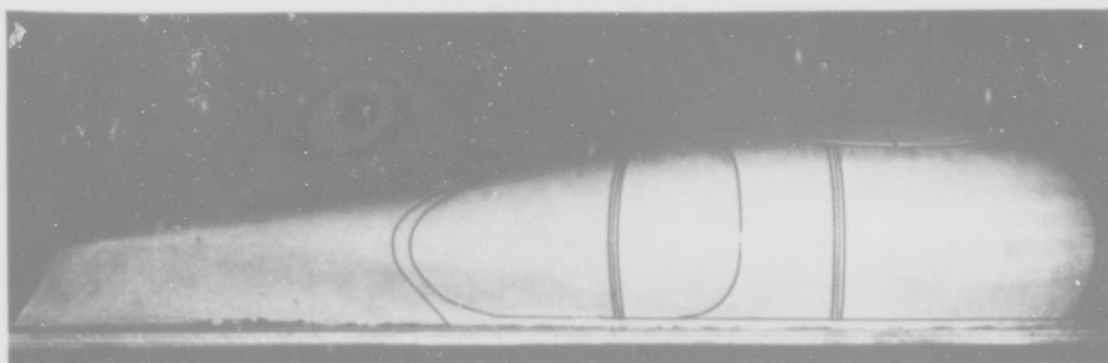
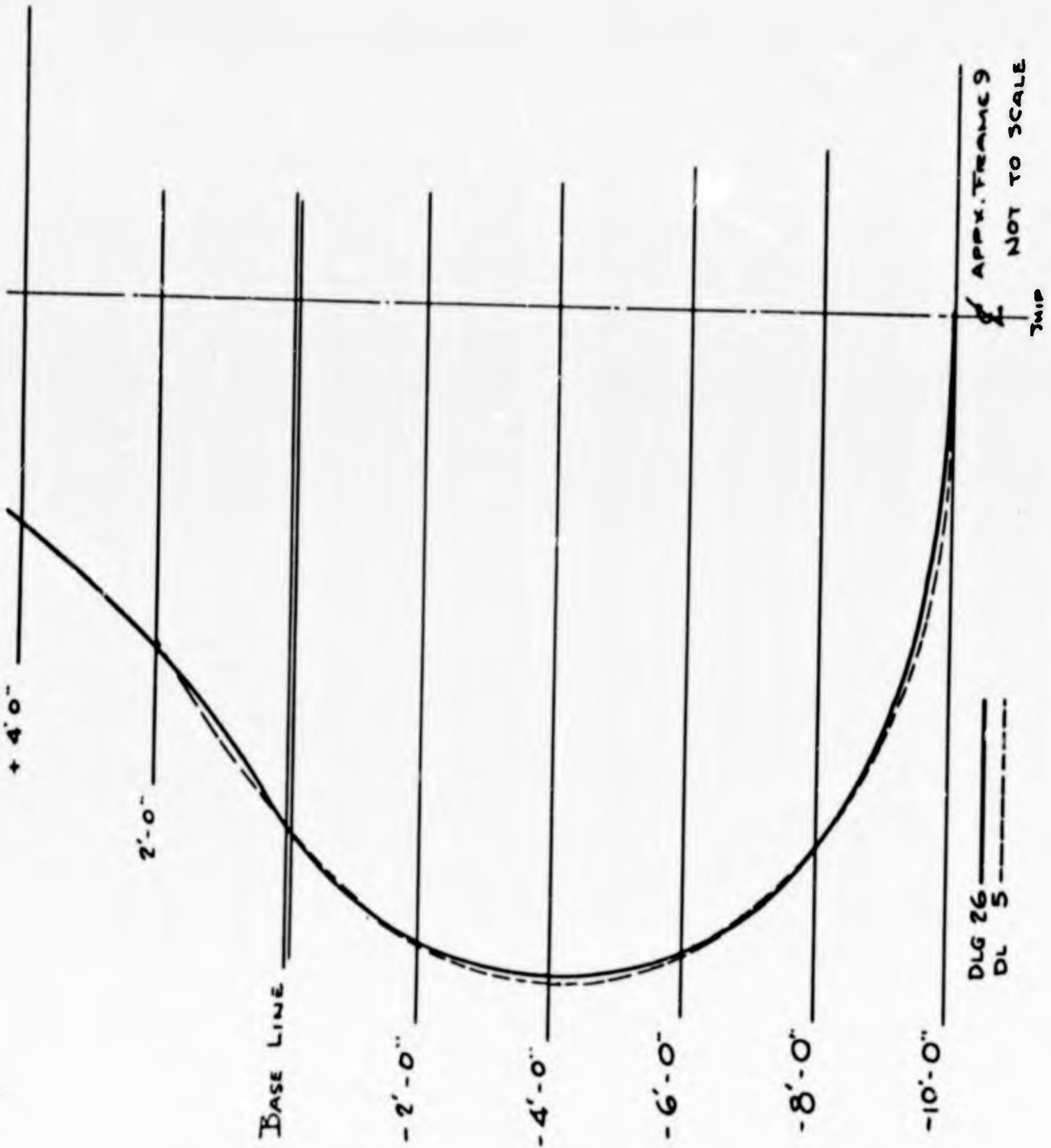


FIGURE 108
SIDE VIEW OF DOME MODEL

FIGURE 109
COMPARISON OF DL-5 + DLG-26 DOMES



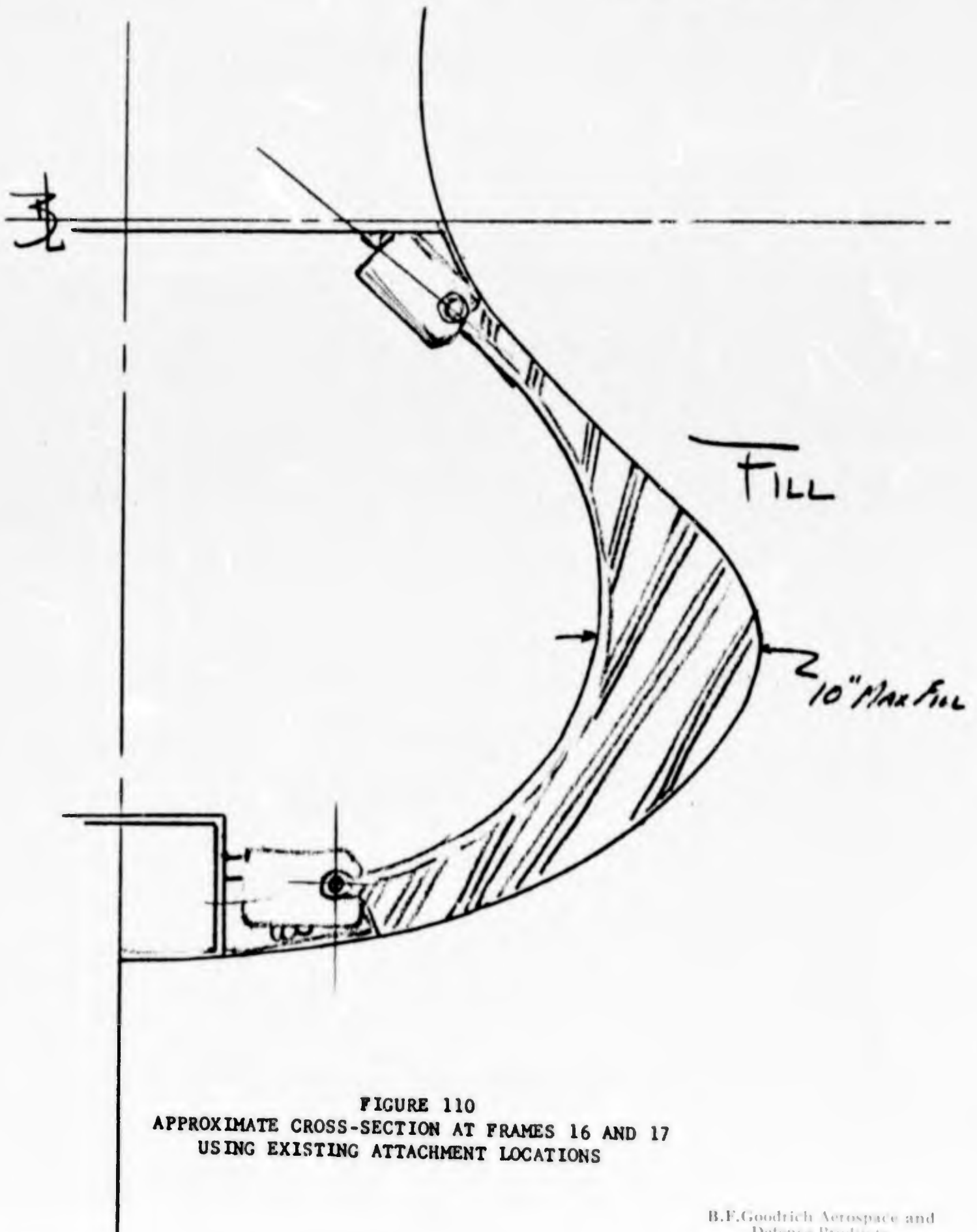


FIGURE 110
APPROXIMATE CROSS-SECTION AT FRAMES 16 AND 17
USING EXISTING ATTACHMENT LOCATIONS

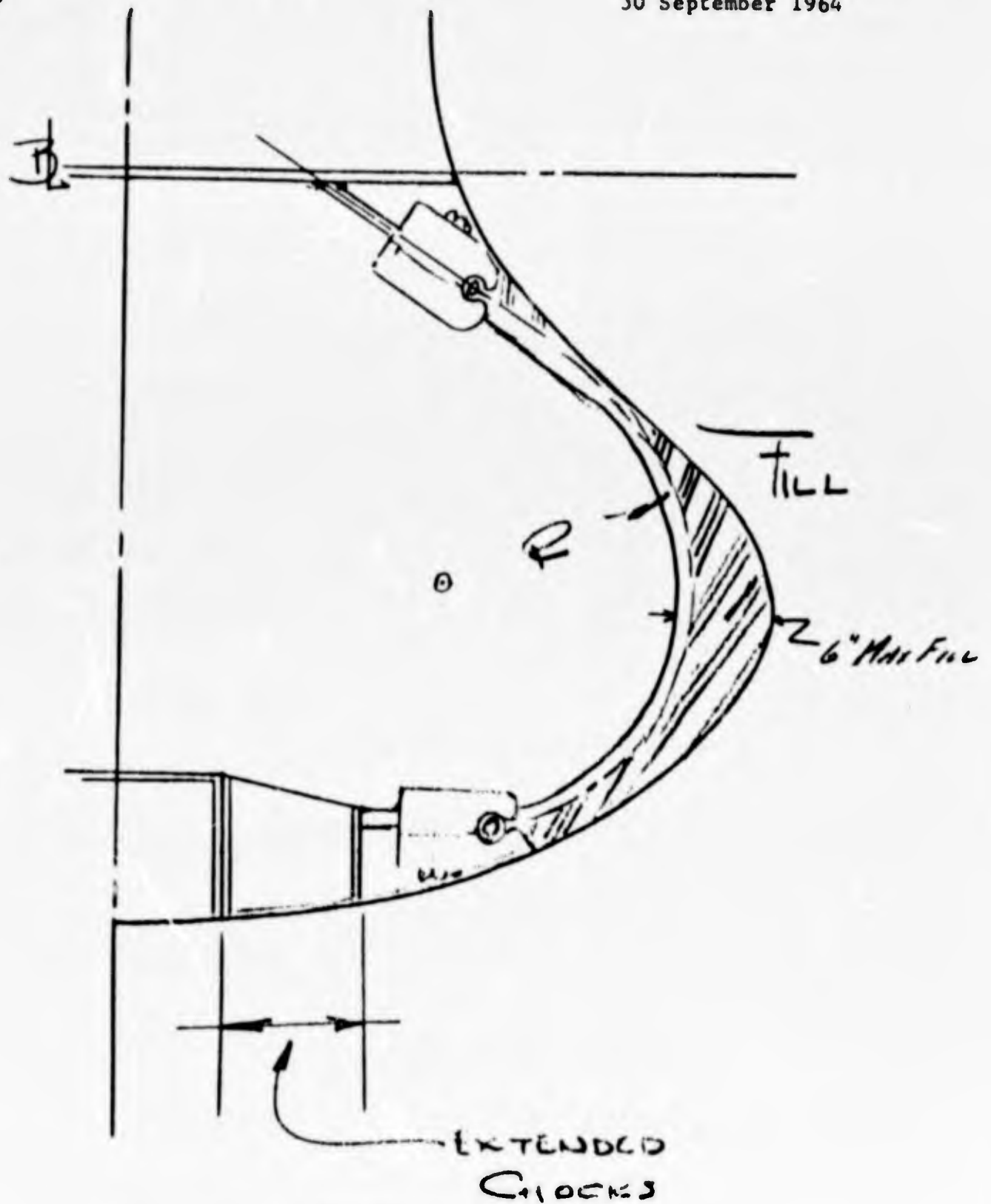


FIGURE 111
APPROXIMATE CROSS-SECTION AT FRAMES 16 AND 17
USING MODIFIED ATTACHMENT LOCATIONS

requires a 6"-12" extension to the chocks along the cat walk from frames 12 to 19. Reduction of this fill as much as possible will certainly improve acoustic properties and reduce fabrication time and cost. Acoustical testing of a sample exhibiting an 8" gum fill will be accomplished by USN/USL.

The net result of this program was a set of coordinates for the outside of the window and determination of the bead centerline. These coordinates are listed in Table XXXV.

As mentioned in the "Universal Window Study" a window can be fabricated to fit both the DL-5 and DLG-26 ships. Therefore, the set of coordinates listed in Table XXXV will be revised at a later date to reflect this change.

d. Conclusions

- (1) The combination DL-5/DLG-26 Window will be designed for use as the prototype acoustic window under the contract.
- (2) Actual design of the window and necessary tooling for fabrication will proceed during Phase II utilizing information and data obtained during Phase I of this contract.
- (3) The rubber fill concept for contour attainment is more desirable to use on the prototype window than the compression member. Additional work is required to finalize this design.
- (4) The rubber window will not identically match the steel dome contour. Therefore, when available, coordinates of the new contour will be given to the David Taylor Model Basin for evaluation with their computer program, "Three Dimensional Potential Flow". Output from this program, determining the hydro dynamic acceptability of the window contour, will then be presented to BuShips for their approval.

13. Transportation Study

a. Summary

All possible means of transporting the rubber acoustic window have been analyzed. This study included air freight, rail shipment, rail-water combination, truck transportation and helicopter assist in transit. After analysis it was determined that truck transportation is the most efficient and economical means of moving the window.

b. Introduction

A study was initiated to determine the most feasible and desirable method of transporting the prototype window from the fabrication facility to the installation facility. Realizing the true package size cannot be determined until the rubber window itself is built, the maximum non-compressed size was considered for this study.

c. Air Freight

Personnel at Wright Patterson Air Force Base, Dayton, Ohio were contacted relative to this problem. It was concluded that the dimensions of this unit are too great to transport by either the C-124 Globemaster or the C-133. There is one (1) aircraft, owned by Aero Spacelines, Inc. of California, that is capable of near the capacity required. The aircraft is the modified Boeing 377 which has an effective internal dimension of 19.5 ft. The aircraft is currently under contract to NASA. The rate for this carrier is \$6.80 per mile on the basis of round trip from home base. Considering the destination of the window is the Boston Naval Shipyard this concept appears to be economically unfeasible.

d. Rail Shipment

Another possible method of shipment is by rail. Regulation regarding the mode of movement is strict with maximum dimensions established as listed in Table XXXVI.

TABLE XXXVI
RAILROAD MAXIMUM OVERSIZE SHIPMENTS

<u>Railroad</u>	<u>Height Above Rail</u>	<u>Width Permissible</u>
Erie Lackawana	17' 5"	0. 0"
	10' 5"	14' 0"
	9' 5"	14' 0"
	3' 5" (Car Floor)	10' 4"
New York, New Haven and Hartford	15' 5"	10' 0"
	8' 11"	11' 8"
	3' 5" (Car Floor)	10' 4"

The extra wide loads can only be handled in a special train which will entail special train charges. These charges cannot be fully determined until the time of the move. However, on an estimated basis it appears the cost would be between \$2,500.00 to \$3,500.00. The size restriction outlined in the table, being considerably smaller than the rubber window, makes this means of transportation unusable.

e. Rail-Water Combination

The concept utilizes Erie rail shipment, with the size restrictions previously mentioned, to Pier #1, Marian Dock, Jersey City, New Jersey. From this point commercial boat hauling to Boston via either Jones or Hughes, Inc. or McAllister Light-Weight Line, Inc. The estimated charges for this system are \$7,000 to \$10,000.

f. Truck Transportation

The most feasible approach in transporting the window is by truck. Fishback Trucking Company of Akron has estimated the total cost of such a shipment to be approximately \$1,700.00 per unit shipped.

The cost presented was broken down in general and special charges. They were:

- (1) Heavy and Specialized carriers Tariff 100-D, 14F-I.C.C. #19, Item 120, 2.39 CWT based on 20,000# minimum weight.
- (2) Oversize charges based on 2¢ per foot per mile for the first two feet over eight feet in width; 5¢ per foot per mile for the next five feet; 10¢ per foot per mile over 15 feet.
- (3) Two escort vehicles would probably have to be furnished at a rate of 20¢ per mile on the round trip. Household guide mileage Akron to Boston is 669 miles and this can vary depending on each states routing of the carrier.
- (4) Ohio will not issue a permit for any load in excess of 13 feet wide and other states have similar restrictions. In order to move a load over 13 feet in width a government priority would be needed and cleared through the department of Highways, State Capitol of each state involved. This would include Ohio, Pennsylvania, New York and Massachusetts. Permit charges range from \$50.00 to \$100.00. To insure the necessary permits would be obtainable when necessary the Eastern Traffic Region of the Military Traffic Management Agency, Pittsburgh, Pennsylvania was contacted. Personnel there were certain that when necessary the permits would be forthcoming.

The commander, Boston Naval Shipyard has been contacted, via letter, questioning whether this size load can enter that installation. A reply indicates that the entrance gates at the shipyard are adequate to handle the load, being thirty-six (36) and thirty-two (32) feet respectively. However, the access highways leading into the shipyard are heavily traveled and congested. Travel on the highways would have to be cleared with the department of Public Works, Nashua St., Boston, Massachusetts.

Also the transportation division of that shipyard has in the past encountered considerable difficulties in transporting loads of much smaller dimensions in the Boston and peripheral areas.

g. Helicopter Assist in Transit

To expedite certain phases of the move it appeared desirable to investigate the possibility of helicopter assistance. A B.F Goodrich representative contacted personnel at Fort Rucker, Alabama to ascertain the capability of large army helicopters. Information received indicated Army helicopters are not capable of handling the rubber window payload. However, we were referred to the Sikorsky Company. They possess a helicopter known as the "Flying Crane". It is based in New York and may be available if necessary. Arrangements were made to contact Sikorsky and it was determined the approximate cost would be \$14.50 per flight hour away from their plant, plus cost of living expenses for their crew. An estimate 15 to 20 hours would be required resulting in a rather large expense. Sikorsky is delivering four (4) S-64 cranes to the U.S. Army at Fort Benning, Ga. in the fall of 1964. If considered desirable at that time, the Army will be contacted for assistance.

The net result of the transportation study indicates the most feasible and economical means of movement will be by truck. This conclusion is based on the full non-compressed size of the dome, 40' x 20' x 10'. Handling of the prototype panel indicates the flexibility of the construction is considerable and the shipping volume should be reduced considerably from the full size. In any case it would still appear that truck transportation is the means by which the window will be shipped to the Boston Naval Shipyard.

h. Conclusions

Actual ease of loading and movement cannot be determined until the window has been built and the minimum transportation volume determined. However, from available information it was concluded the most efficient and economical means of moving the complete prototype acoustic window is by truck.

14. Ship Modification Study

a. Summary

Per discussions with the Structural Branch of BuShips it was determined the ship's structure is capable of taking the loads generated by the approximate 40 psi internal dome pressure. Reinforcement of the diagonal bulkhead and the cylindrical bulkhead inside the transducer will be required and is under study by BuShips.

Modification to the pressurization system must be accomplished to meet the requirements of a cable-reinforced rubber window. This is planned for study under Phase II of this program.

b. Introduction

The major change which necessitates modifying the ship's structure is the increase of operating pressure from 15 PSI in the all steel domes to 40PSI in the rubber window domes. Because of this the following structural considerations must be analyzed:

- (1) Effect of 40 PSI on remaining steel structure
- (2) Effect of tension loads at bead seat attachment points around the window periphery.
- (3) Modification of chocks along "Banjo" to permit window fit.
- (4) Acceptability of pressurization system.

c. Window Attachment

BuShips personnel have and are resolving the questions involved in item (1). In discussions with persons from the Structural Branch of BuShips this problem was discussed. A survey of the structural strength of the dome has been made and it was concluded with two (2) exceptions the structure was capable of 40 PSI with a safety factor of 2. It was also ascertained that the diagonal bulkhead and the transducer cylinder must be reinforced to withstand the expected load. This problem has been given to the Boston Naval Shipyard for ironing out the details.

During this same gathering the tensions expected on the bead seat attachment point was introduced into the conversation. The maximum normal operating tension expected at the bead clamps is 3,100 lbs./inch. Considering the strength of the

construction the maximum tension prior to panel rupture would be in the 17,000 lb./inch range. In the past BuShip structural personnel informed us that these loads in the 3100 lbs./in. range were within the capabilities of the structure and special precautions were not required. However, additional effort will be required to analyze the affect of the higher peak loadings.

The contour of the rubber window periphery in the aft, bottom area is that of a series of arcs. This was chosen as a means of reducing stress concentrations in the window and thus increasing its reliability. As a result of this change, as part of this program, a series of chock extensions will be designed and discussed with the shipyard. These extensions, shown in Figure 112, will in essence move the ships structure out to meet the window. It shall be comparable to the existing design and will include steel plate covering.

Table XXXVII presents necessary tensions and angles of approach to the ship's structure of load bearing members.

d. Pressurization System

The pressurization system currently employed with steel domes utilizes a stand pipe with an inert gas atmosphere for additional pressure.

As with the structural considerations the main difference is that of pressure. It is desirable from a retrofit standpoint to utilize as much existing equipment as possible. With this in mind and the thought of the necessity of additional reliability required in a rubber pressurized dome this program was initiated.

Basically it appears the existing system is satisfactory in principal. However, some means of pressure compensation internally for the change of dynamic pressure outside must be included. In addition the reservoir tank must be enlarged to compensate for stretch of the window during pressurization and relaxation during depressurizing. These two (2) considerations plus increasing the strength of each to accept the pressures are the basic tasks of this study.

A pressure control system has been conceived to maintain the internal pressure of the dome to that prescribed for proper pressure differential with respect to the outside static and dynamic pressures.

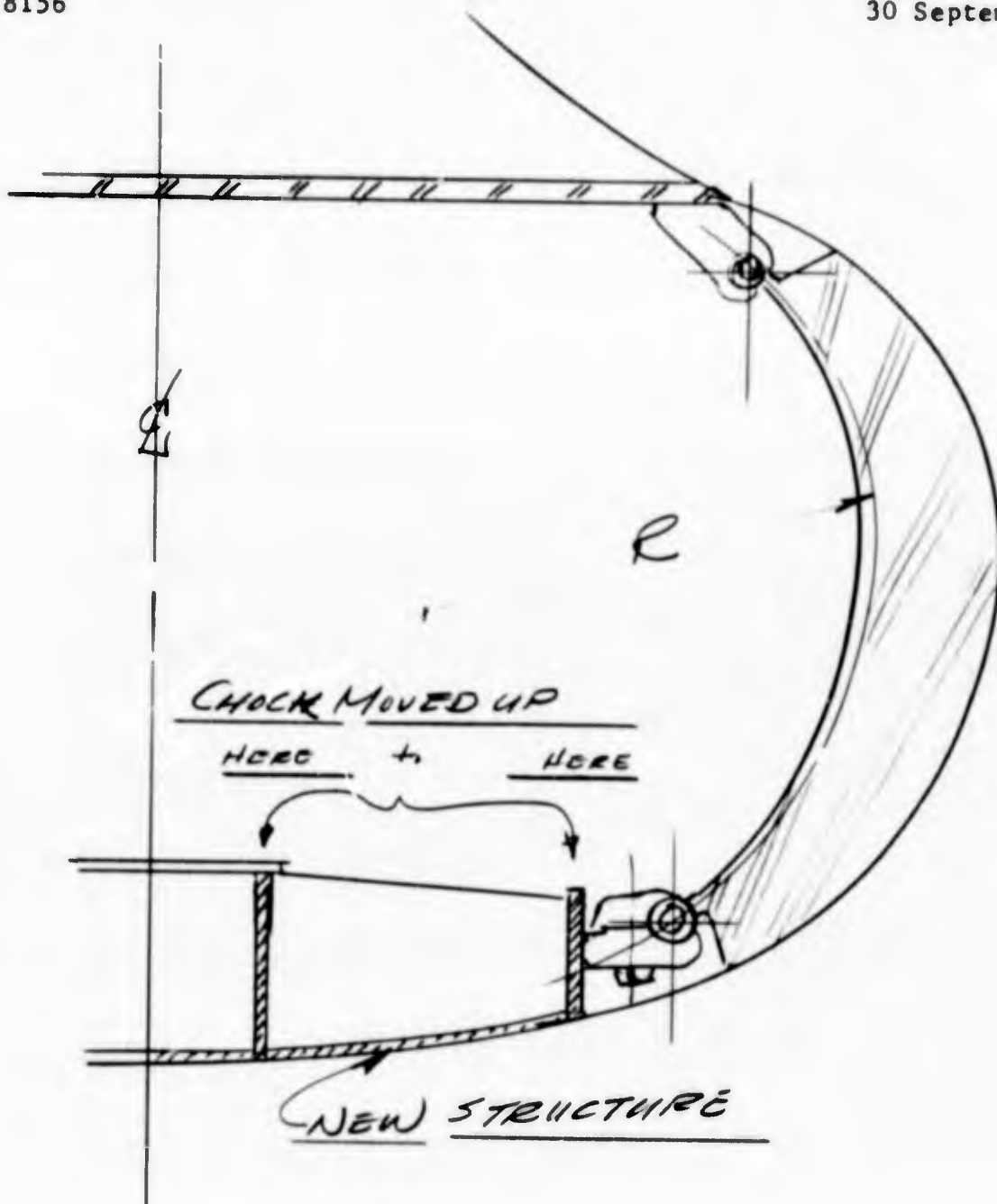


FIGURE 112
CHOCK EXTENSION FOR SHIP MODIFICATION

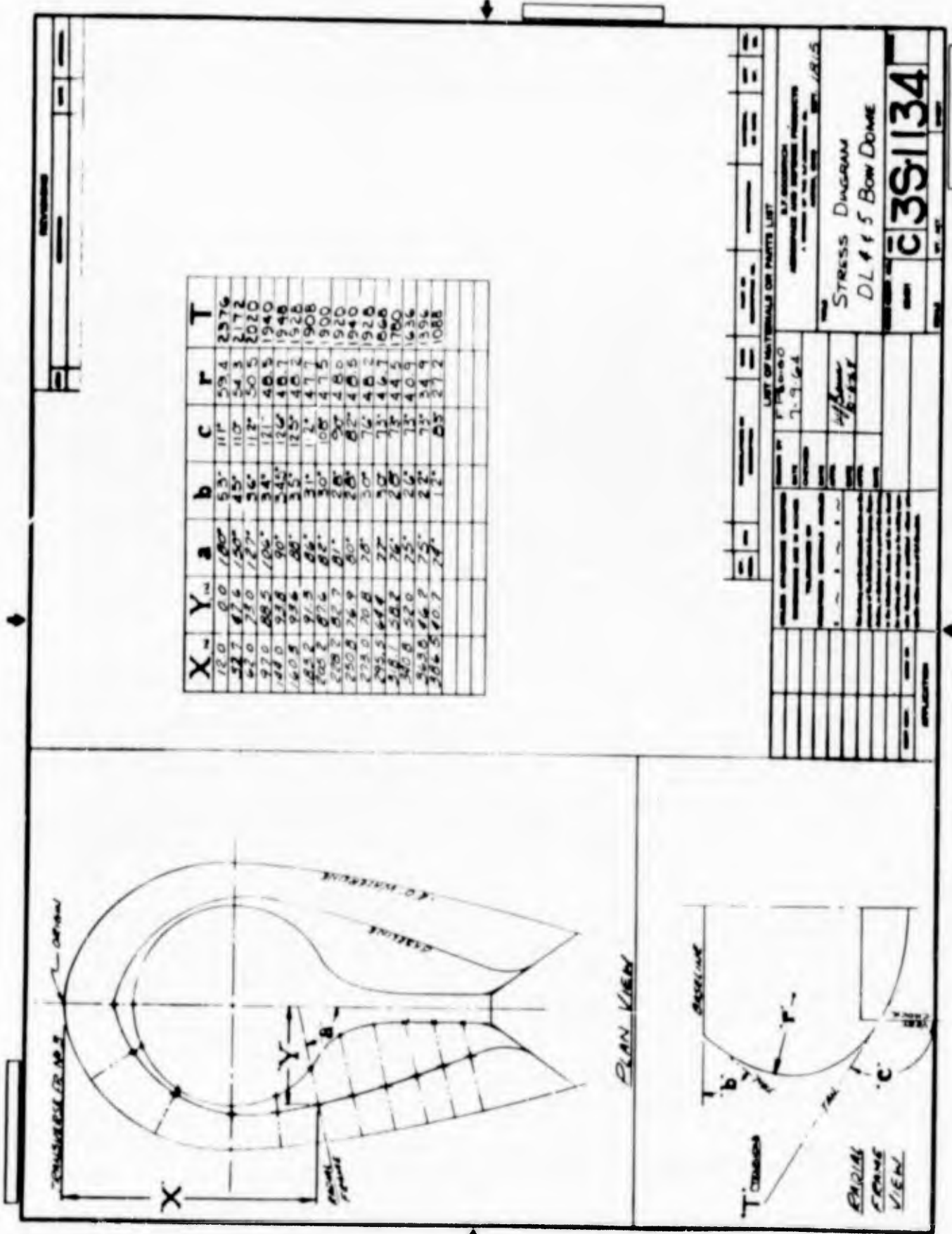


Table XXXVII
 Stress Diagram of Window Periphery

Calculations have shown that the pressure in this case should be 40 PSI at the negative four (4) foot water line.

This pressurization system should be designed to provide:

- (1) Filling of dome in two (2) hours from ship or shore with fresh or salt water.
- (2) Sufficient strength to withstand at least 80 PSI at base line flat.
- (3) A positive pressurization source with a minimum possibility of failure.
- (4) An automatic pressurization system.
- (5) A manual override and emergency pressure system.
- (6) A capability for handling 100 gpm leakage from dome with no pressure loss.
- (7) Units to be corrosion resistant.

(a) System Description

A system which will accomplish the foregoing specifications is described in the following paragraphs. In many instances the system description is that of the existing pressurization system wherever it can be used.

The dome will be filled with a 3" inch fire hose from ship or shore in 2 hours or less. A connection to such a hose will be provided aboard the ship in such a way that it could be connected to an on shore fire hydrant or to the fire control system aboard the ship. It will be necessary for emergency leakage control, to provide a permanent connection to the shipboard fire control system while underway.

Standard fittings and pipe are of sufficient strength to withstand 80 PSI. The filling and pressurization tank will be designed to eliminate sloshing of water within the tank while the ship is underway.

It is intended that the pressurization source be an inert gas. The gas will be stored in a pressurized cylinder and transferred, through a regulator, to the filling tank to provide the extra head of pressure necessary to accomplish 40 PSI. A safety pop off valve will be located above the water line in the tank to vent excess gas pressure. Water level in the tank would be maintained by an electronic system and a solenoid operated valve. A manual valve and a sight gauge will be provided and checked periodically to be sure the system is operating correctly.

Maintaining water level in the filling tank is an important task with this system since, if the water level were to be lowered enough the dome pressure might be decreased to a critical level.

(b) System Operation

A hose will be connected to the provided fitting and filling would take place through the manual valve. The automatic valve will be turned off and a vent valve in the tank opened.

As soon as the water level reached a predetermined level in the filling tank, as shown on the sight gauge, the manual valve will be turned off.

The automatic system should be turned on and the gas pressure inserted into the tank. Pressure may be read at the filling tank and through a remote system to the bridge.

In the event a leak is experienced the level in the tank will go down and gas will fill to maintain pressure. When a predetermined low level is reached the automatic valve will open and the tank will refill. During this filling the pop off valve will open venting off excess pressure caused by gas volume decrease. This cycle will repeat until the leak is repaired. If the system should fail a man could manually operate the filler valve and change gas tanks if necessary.

Figure 113 presents a schematic diagram of the proposed system.

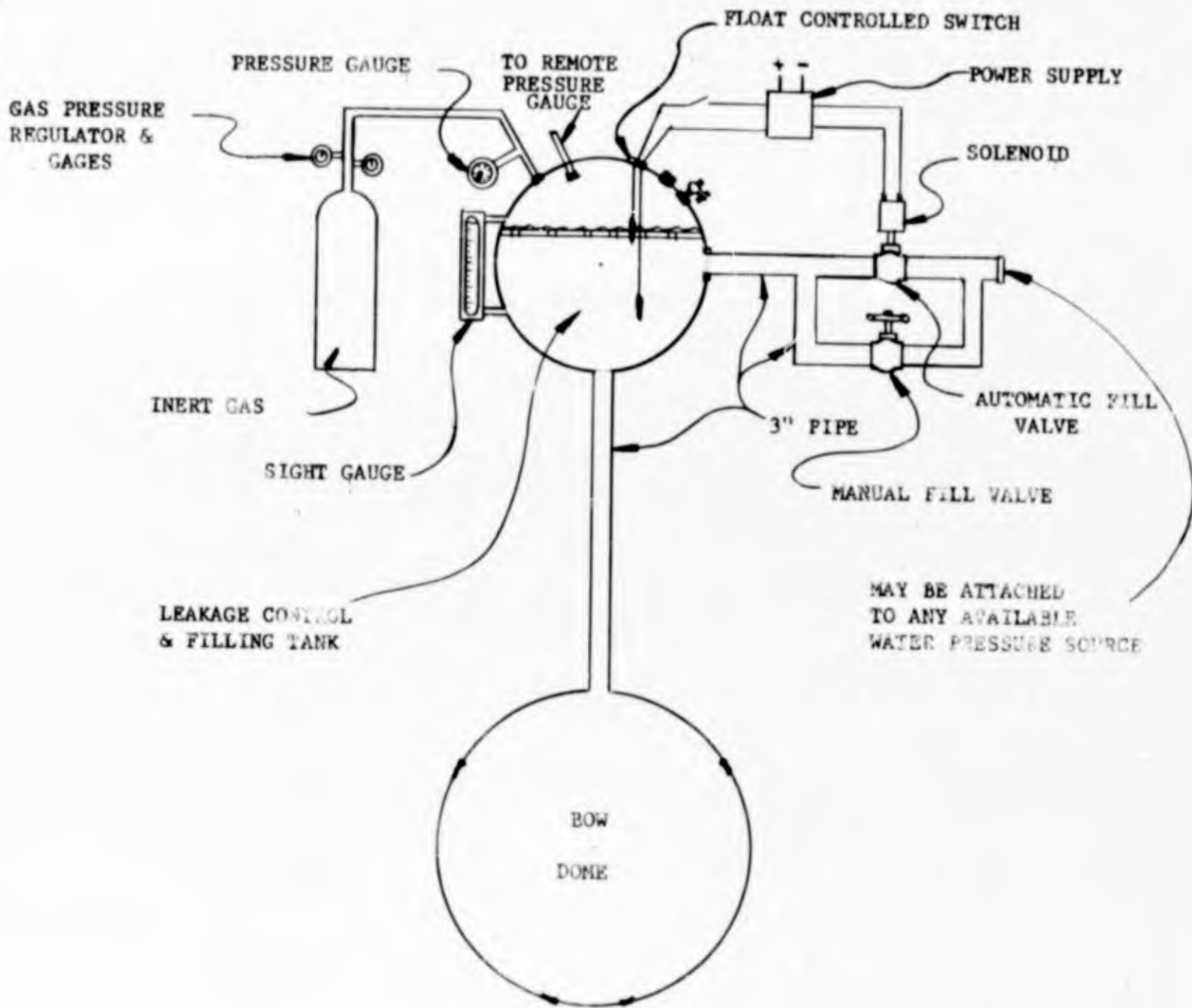


FIGURE 113
SCHEMATIC OF PROPOSED PRESSURIZATION SYSTEM

D. Conclusions

As a result of satisfactory, design, fabrication and testing of the prototype panel the feasibility of the pressurized cable-reinforced rubber acoustic window for the AN/SQS-26 sonar has been firmly established. In addition the following conclusions were reached.

1. The pressurization requirement for this acoustic window is 40.2 psi at the -4' water line.
2. A structure of five (5) plies of wire fabric will furnish sufficient strength to withstand all expected operating conditions.
3. A bead type retention system furnishes the most desirable and reliable means of attachment to the ship.
4. The rubber acoustic window will be furnished to the Navy in one piece.
5. The acoustical interference of the window construction, as verified by testing of a 5' square acoustical panel of the proposed construction, is less than .5db at the critical frequency.
6. The damping characteristics (5-6%) of the cable-reinforced rubber window are far superior to those of plastic or steel domes.
7. The acoustic window should be fabricated in four pieces and spliced together to form a single unit.
8. The polyisobutylene anti-fouling paint, as verified by testing of the 5' square paint panel, adheres well to the Neoprene of the window construction when applied over 1177 tie coat adhesive. This system should be used to cover the prototype rubber acoustic window.
9. A rubber fill of varying thickness is acceptable as a means of obtaining the necessary shape in all areas deviating from the normal pressurized contour.
10. The prototype window can be shipped by truck to the Boston Naval Shipyard for installation.

e. Conclusions

1. Bu Ships structural people will analyze the steel structure of the bow dome and determine what modifications are necessary to make it strong enough for use with the rubber acoustic window.
2. The maximum normal operating tension expected at the bend clamps is 3100 lbs./inch with panel rupture occurring about 17,000 lbs./inch.
3. Modification of the existing pressurization system will be required to make it usable with the rubber acoustic window.
4. Additional work, including consultation with the shipyard, will be required to finalize this study and is planned in the future.

Contract NObsr 89483
Serial No. SS041-001
Task 8156

- 275 -

Report No. 17
Phase I Interim Report
30 September 1964

F. Project Performance Schedule

With the completion of Phase I the future efforts involved in prototype fabrication and testing can be initiated. The second phase of this program is concerned with tooling design. The attached "Pert Control Network" is included to display the effort planned in this area.

E. Recommendations

1. With feasibility of the concept proven, it is recommended the project continue into Phase II and III, prototype window fabrication, testing and service evaluation.
2. Concurrent with these subsequent phases, testing of the prototype test panel should continue in order to obtain all information possible.
3. Additional development programs should continue to finalize the window construction and fabrication procedures.
4. An evaluation be conducted on the plastic tooling and determine its suitability for production use.
5. The David Taylor Model Basin study be continued to determine the acceptability of the semi-universal window contour.

A

Contract NOB sr. 89483
Serial No. SS 041-001
TASK 8156

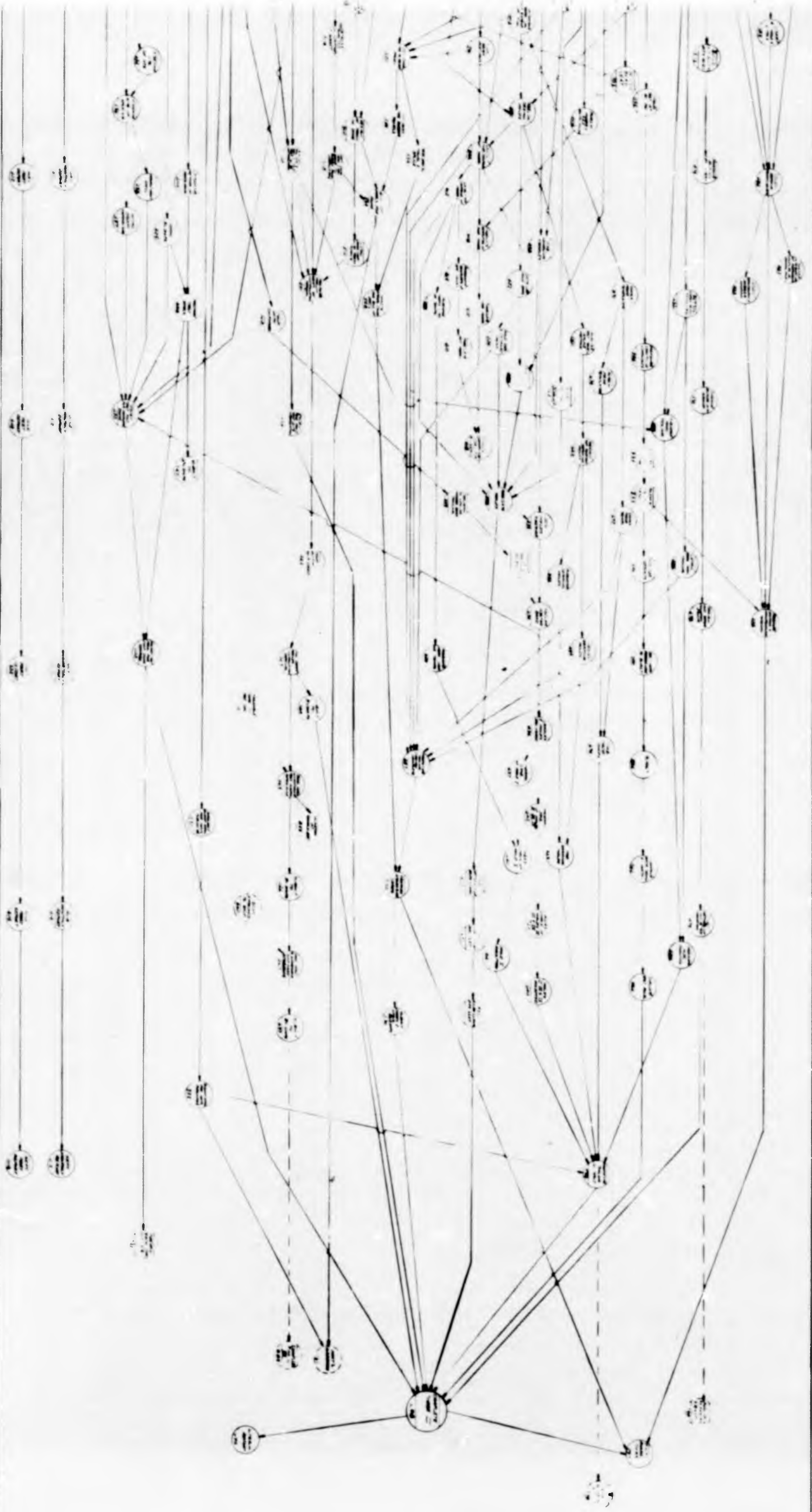
-276-

Report No. 1
Phase I m.p.
30 September



PHASE II PERT NETWORK

B



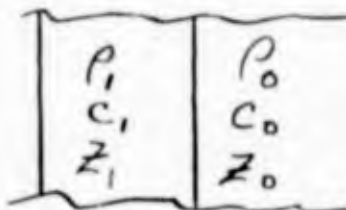
PHASE II PERT NETWORK

BLANK PAGE

Contract NObser 89483
 Serial No. SS041-001
 Task 8156

Report No. 17
 Phase I Interim Report
 30 September 1964

APPENDIX I
PLANE WAVE NORMALLY INCIDENT ON A
 PLANE WALL IMMERSSED IN A LIQUID



When a plane wave is normally incident on a plane sheet of material immersed in a fluid, the impedance Z at the front surface is given by the equations

$$Z = z_1 \text{Coth}(\varphi + j\eta)$$

$$z_1 \text{Coth} \varphi = z_0$$

where $\eta = \omega a / c_1$, z_1 is the specific impedance of the sheet, c_1 the velocity of longitudinal waves in the sheet, and a its thickness. These equations may be rearranged to give

$$Z = z_1 \frac{z_0 + z_1 \text{Tanh} j\eta}{z_0 \text{Tanh} j\eta + z_1} = z_1 \frac{z_0 + j z_1 \text{Tan} \eta}{z_1 + j z_0 \text{Tan} \eta}$$

Now the reflection coefficient at the front surface is

$$\bar{R} = (Z - z_0) / (Z + z_0)$$

so that

$$\bar{R} = j(z_1^2 - z_0^2) \text{Tan} \eta / [2z_0 z_1 + j(z_1^2 + z_0^2) \text{Tan} \eta]$$

APPENDIX I (continued)

If the transmitted coefficient is \bar{T} , then by simple energy balance, since there is no absorption, $|\bar{R}|^2 + |\bar{T}|^2 = 1$, $R^2 + T^2 = 1$ so that $T^2 = 1 - R^2$ and the transmitted energy is

$$T^2 = 1 - \frac{(z_1^2 - z_0^2)^2 \tan^2 \eta}{[4z_0^2 z_1^2 + (z_1^2 + z_0^2)^2 \tan^2 \eta]}$$

and since

$$R^2 = \frac{(z_1^2 - z_0^2)^2 \tan^2 \eta}{[4z_0^2 z_1^2 + (z_1^2 + z_0^2)^2 \tan^2 \eta]}$$

then

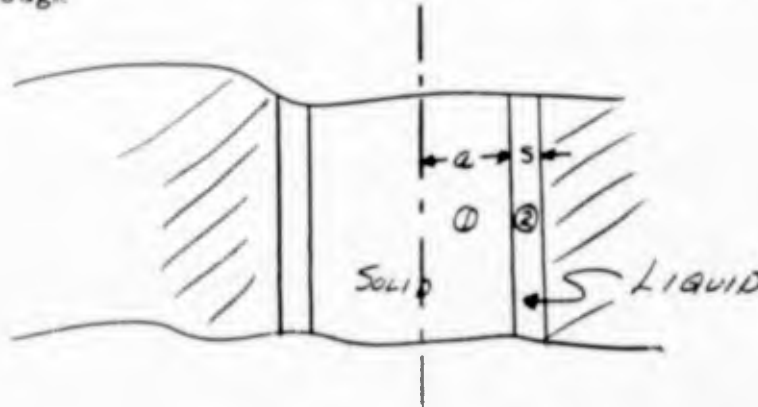
$$\begin{aligned} \left(\frac{R}{T}\right)^2 &= \frac{(z_1^2 - z_0^2)^2 \tan^2 \eta}{[4z_0^2 z_1^2 + 4z_0^2 z_1^2 \tan^2 \eta]} \\ &= \frac{(z_1^2 - z_0^2)^2 \sin^2 \eta}{4z_0^2 z_1^2} \end{aligned}$$

and

$$\frac{R}{T} = \frac{(z_1^2 - z_0^2) \sin \eta}{2z_0 z_1} = \frac{1}{2} \left(\frac{z_1}{z_0} - \frac{z_0}{z_1} \right) \sin \frac{\omega a}{c}$$

APPENDIX II
RING SLOT CORRECTION FOR PULSE TUBE

Let a cylindrical solid be surrounded by a rigid wall with a liquid filling a small gap between the solid and wall as shown in the figure. If a wave is transmitted through



the solid material parallel to its axis, then the solution of the wave-equation in both the two media yield, for the acoustic pressure,

$$P_1 = E J_0(ka) e^{j(\omega t - Bz)} \quad k^2 + B^2 = \omega^2 / c_1^2 \quad (1)$$

$$P_2 = F \cosh m(s-x) e^{j(\omega t - Bz)} \quad -m^2 + B^2 = \omega^2 / c_2^2$$

where c_1 and c_2 are the velocity of longitudinal waves in each media. Since we assume that the gap is small, we approximate the pressure in it by the hyperbolic function rather than the Bessel functions, a valid operation as long as $s \ll a$; and adjust the constants so that the radial particle velocity is zero at the wall. Thus the coordinate x is zero at $r = a$ and s at the wall.

At the interface between the solid and liquid the pressures and radial velocity are continuous. These conditions yield two equations in terms of A , E and B :

$$k E \frac{J_1(ka)}{P_1} = \frac{F m \sinh m s}{P_2} \quad (2)$$

$$E J_0(ka) = F \cosh m s$$

APPENDIX II (continued)

Since δ is very small so that $\text{Cosh } m\delta < 1.0$ and $\text{Sinh } m\delta \approx m\delta$

$$(ka)^2 J_1 / J_0(ka) \approx m^2 a^2 \delta P_1 / a P_2 \quad (3)$$

This equation may now be solved for B since k and m are defined in terms of B by (1). If a wave is to be propagated B must be real and since $B^2 = \omega^2 k^2 - k^2 = \omega^2 / c_2^2 + m^2$, k^2 must be less than ω^2 / c_1^2 which is small. Thus k^2 is a small number $k^2 \ll 1.0$. Referring back to (3), one sees that the right hand side of the equation is much less than 1.0 since $\delta/a \ll 1.0$ and thus, the only possible solution of (3) which will give a real propagation constant is when $ka \ll 1.0$. Since $J_1(x)/x J_0(x) \rightarrow 1/2$ as $x \rightarrow 0$; (3) gives

$$(ka)^2 \approx (ma)^2 \varphi; \quad \varphi = 2 \delta P_1 / a P_2$$

and therefore, replacing k and m in terms of B ,

$$B^2 = \left(\frac{\omega^2}{c_1^2} + \frac{\varphi \omega^2}{c_2^2} \right) / (1 + \varphi) \quad (4)$$

Since the propagation constant is equal to ω/k' where c' is the actual wave velocity,

$$c' = c_1 \sqrt{(1 + \varphi) / (1 + \frac{\varphi c_1^2}{c_2^2})}$$

and when $\varphi \ll 1$

$$c' \approx c_1 \left[1 + \frac{\varphi}{2} \left(1 - \frac{c_1^2}{c_2^2} \right) \right] \quad (5)$$

APPENDIX II (continued)

Since $ka \ll 1$, the pressure distribution across the cross-section is constant and a plane wave is propagated through the solid liquid combination. However, since the densities of liquid and solid are different, the particle velocity in the axial direction is different in each of the two media. Referring to (1), since $ka \ll 1, 0$ at $ma \ll 1$

$$P_1 = P_2 \approx E e^{j(\omega t - \beta z)} \quad (6)$$

and, defining v_i as the velocity in the z direction in the i medium,

$$v_i = \frac{1}{j\omega\rho_i} \frac{\partial P_i}{\partial z}$$

so that, from (6)

$$\begin{aligned} v_1 &= \frac{\beta}{\omega\rho_1} A e^{j(\omega t - \beta z)} = \frac{1}{\rho_1 c'} P \\ v_2 &= \frac{\beta}{\omega\rho_2} A e^{j(\omega t - \beta z)} = \frac{1}{\rho_2 c'} P \end{aligned} \quad (7)$$

Since the effective specific impedance of the combination is the quantity that is measured in the pulse tube, we must calculate the quantity. It is necessarily equal to the acoustic pressure P divided by the velocity average over the cross-section of the tube. If A is the fraction area of tube filled with the solid cylinder then the average velocity

$$\bar{v} = Av_1 + (1-A)v_2$$

which becomes, substituting from (7)

$$\bar{v} = \left[\frac{A}{\rho_1} + \frac{(1-A)}{\rho_2} \right] \frac{P}{c'}$$

APPENDIX II (continued)

and the effective specific impedance

$$Z_c = \frac{P}{\sigma} = \rho_1 c' / [A + (1-A)(\rho_1/\rho_2)]$$

We, therefore, define the effective density

$$\rho' = \rho_1 / [A + (1-A)(\rho_1/\rho_2)]$$

Contract NObar 89483
Serial No. SS041-001
Task 8156

Report No. 17
Phase I Interim Report
30 September 1964

APPENDIX III
ACOUSTIC PANEL ANALYSIS

This report summarizes a study of several areas on the External Surface of the B.F. Goodrich Rubber Dome Panel Which Had Been Subjected To High-Power Sonar Transmission.

The specific areas appeared on Official Photographs from the U.S. Navy Underwater Sound Laboratory External Surface Internal Surface.

Approximately half, the top half, of the panel was available for study in Akron. The panel was examined microscopically and by other means in the production area of the B.F. Goodrich Aerospace Plant.

Considering first the external surface, it was observed that the spotted areas 7-N and 7-Q were most obvious. The horizontal striations, 7-V, were much less conspicuous; these were observed under the microscope, to be slightly raised parallel ridges, (the order of 0.0005" in the "rubber reproduction") of the marks of the cutting tool on the mold surface. The marks at 7-O and 7-P were rather indistinct small scratches of an unknown origin.

The areas of 7-N and 7-Q received the most detailed study, because the areas were large and in these areas the surface appeared to be affected most. The deviation from the normal smooth surface in these areas was a spotty condition wherein the spots appeared either darker or lighter than the surrounding surface depending on the angle of the incident light. A close inspection in a stereo microscope disclosed that the spots consist of a multitude of irregular microscopic pits each capable of reflecting the incident light in a slightly different way from the surrounding stock.

The character of the spots having been disclosed, a technique was next employed which made it possible to examine the spots in great detail and in an easily controlled fashion; an exact reproduction was made of a portion of the surface by means of a special air-curing rubber compound. With this method, the surface details are reproduced with accuracy. The surface of one of these vulcanized rubber impressions is shown in fig. 1 and 2 at a magnification of approximately x4. It is known already that the spots appear either dark or light, depending on the lighting; this same phenomenon shows on the rubber reproduction.

APPENDIX III (continued)

In fig. 1 the lighting is arranged to show the spots as dark spots on a light surface; in fig. 2 the same spots, by a slight change in the lighting, appear lighter than the surrounding surface, thus behaving exactly as they behave on the panel itself.

One of the spots, at the lower center, was encircled in ink on the panel before making the rubber impression; some of this ink came off on the rubber, thus making it possible to identify this specific spot. In fig. 3 this area is observed as it appears on the panel in a glancing light at x20; the microscopic spots are seen as pits. In fig. 4 the same areas as reproduced in rubber is seen; here the tiny craters are observed as raised spots. These points should be noted:

1. Fig. 4 is a mirror image of fig. 3 and therefore all features should be reversed but in order to match the features more easily, fig. 4 has been reversed in enlarging so that the left of fig. 4 corresponds to the left of fig. 3 and so on.
2. The large panel itself is difficult to move; this was one good reason for making the rubber impressions. To use any variation in the angle of lighting on the panel is difficult; the small rubber impression, in contrast, makes it possible to make any desired change in lighting; thus it is easily possible to make the craters and other features more pronounced as shown in fig. 4.
3. The vertical striations at the left side of the circle of figs. 3 and 4 are an example of the tool marks which cause the surface feature identified as 7-V in Figure 16.

Proceeding now with a more detailed study of this spot, figs. 3 and 4, fig. 5 shows an area close to the center of the circle at a magnification of x50; here the craters are shown vividly. Observing these craters in this picture, one immediate question is this: how deep are these microscopic pits in the panel? On the rubber impression, it is a simple matter to measure the depth by using suitable objectives and the fine adjustment on a high power microscope. The microscopic pits are thus found to have a nominal depth of 10 to 15 microns (0.0005"); the maximum found was 25 microns (0.001"). From these depths it would be concluded that these are not very serious surface defects.

Contract NObsr 89483
Serial No. SS041-001
Task 8156

- 3 -

Report No. 17
Phase I Interim Report
30 September 1964

APPENDIX III (continued)

The next question concerns the origin of these microscopic pits. These pits have been examined in several ways in order to study their character; for example they have been observed with glareless surface lighting (the Ultrapack Illuminator) using high power objectives, as in fig. 6 at a magnification of x150. At this magnification, these spots look very bad but actually the largest one is only about 0.01".

APPENDIX III (continued)

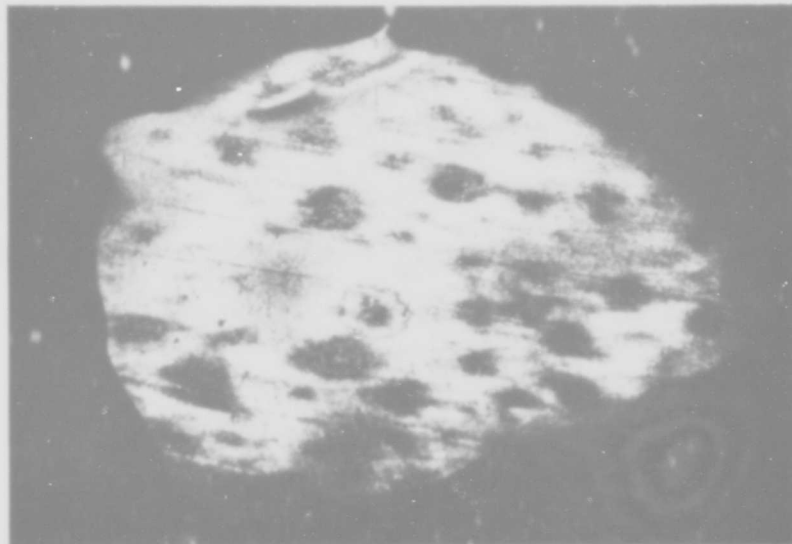


FIGURE 1
RUBBER IMPRESSION OF PANEL AREA 7N and 7Q

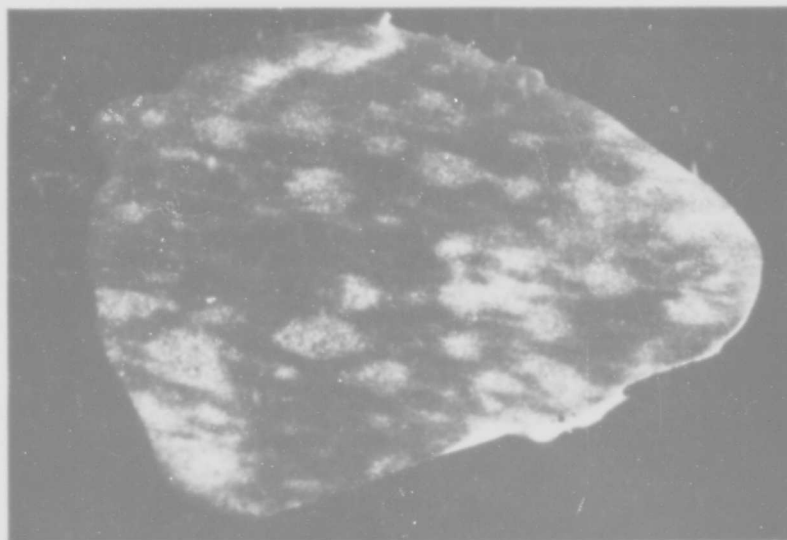


FIGURE 2
RUBBER IMPRESSION OF PANEL AREA 7N and 7Q
(LIGHTING DIFFERENT THAN FIGURE 1)

APPENDIX III (continued)



FIGURE 3
X20 MAGNIFICATION OF AREA SHOWN IN FIGURE 1 and 2



FIGURE 4
RUBBER COAT OF AREA SHOWN IN FIGURE 3

APPENDIX III (continued)



FIGURE 5
X50 MAGNIFICATION OF AREA IN FIGURE 3

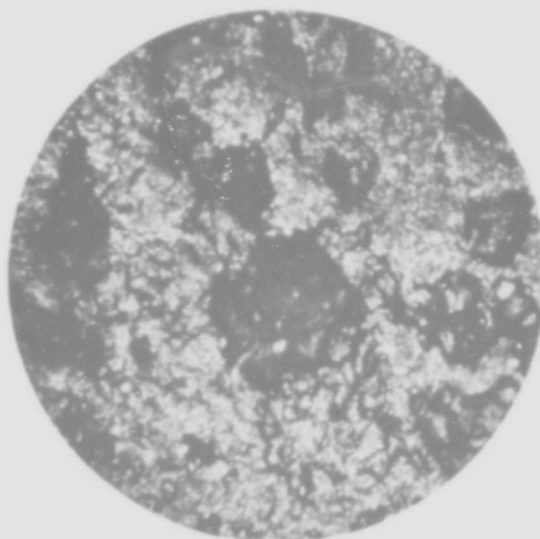


FIGURE 6
X150 MAGNIFICATION OF AREA IN FIGURE 5

APPENDIX III (continued)

Considering the distribution of the spotted areas on the panel and the shape and character of the microscopic pits, it is concluded that they were probably produced during molding because of a local overabundance of droplets of mold lubricant.

The other side of this panel, the internal surface, shown in Figure 17 presents different features from the external surface. The internal surface was buffed after curing and before the panel was shipped. The buffing appears to be a satisfactory and uniform job.

The most conspicuous marks on the internal surface are those labelled 7-J and 7-Z. The vertical line above 7-J and the horizontal line 7-X have the same cause; they consist of a thin film of rubber cement on the surface. This thin film can be rubbed off and underneath the buffing marks are uniform and good. The origin of this thin film of cement was final finish operations.

The dotted vertical line, more or less indistinct on the panel, below the mark 7-J is caused by a number of scratches in the rubber. It is possible that these were produced by a few grains dislodged from the buffing wheel. The scratches in general are in the direction of buffing but some of them lie at a slight angle. The depth of these scratches is in general around 25 microns (0.001"); the deepest part of the largest crack was found to be 90 microns (approx. 0.004").

This summary of the conditions on the internal surface is based on the examination of the panel itself and on the several rubber reproductions which were cast on the surface. These impressions are still available for further study if required.

It may be concluded from this study that the surface conditions on this panel are strictly superficial; it seems very unlikely that they originated from the testing operation.

BLANK PAGE

APPENDIX IV
BOW DOME ACOUSTIC WINDOW COMPUTER PROGRAMS

DETERMINATION OF CIRCLE CENTERS
 FROM TWO GIVEN POINTS AND A RADIUS
 BFG-ASD-0070

PROGRAM NO. 06964911
 ABSTRACT

This program determines the centers of the two circles which can be drawn through two given points with a given radius.

It was written for use in the Sonar Bow Dome prototype panel project.

METHOD

The following diagram is useful in understanding the formula derivations.

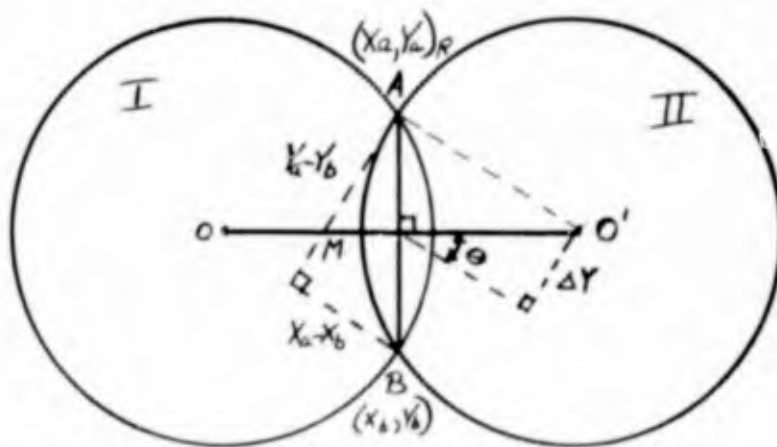


FIGURE 1.

Given are X_a , Y_a , X_b , Y_b , and R .

$$\overline{AB} = \sqrt{(X_a - X_b)^2 + (Y_a - Y_b)^2} \dots \dots \dots (1)$$

APPENDIX IV (continued)

$$\overline{AM} = 1/2\overline{AB} \text{ ----- (2)}$$

$$\overline{MO} = \overline{MO'} = \sqrt{R^2 - \overline{AM}^2} \text{ ----- (3)}$$

The slope of \overline{AB} is given by the following:

$$m_{AB} = \frac{Y_a - Y_b}{X_a - X_b} \text{ ----- (4)}$$

The slope of OO' is given by the following:

$$m_{OO'} = -\frac{1}{m_{AB}} \text{ ----- (5)}$$

Therefore, from (4) and (5),

$$m_{OO'} = -\frac{X_a - X_b}{Y_a - Y_b} \text{ ----- (6)}$$

$$\Theta = \tan^{-1}(m_{OO'}) \text{ ----- (7)}$$

$$\Delta X = \overline{MO'} \cos \Theta \text{ ----- (8)}$$

$$\Delta Y = \overline{MO'} \sin \Theta \text{ ----- (9)}$$

$$X_M = 1/2 (X_a - X_b) \text{ ----- (10)}$$

$$Y_M = 1/2 (Y_a - Y_b) \text{ ----- (11)}$$

APPENDIX IV (continued)

The equations for the circle centers as derived from the previous equations are the following:

$$\text{Circle I} \quad \begin{cases} X_0 = Y_M - \Delta X \\ Y_0 = Y_M - \Delta Y \end{cases}$$

$$\text{Circle II} \quad \begin{cases} X_0' = X_M + \Delta X \\ Y_0' = Y_M + \Delta Y \end{cases}$$

An error message will print out when $\underline{Y}_a = Y_b$ or $X_a = X_b$. In the first case, slope m_{00}' is infinite; therefore, $\overline{00}'$ is a vertical line. In the second case the slope is zero and the line is horizontal. However, the validity of the output is not affected in either case.

MACHINE REQUIREMENTS

This program is written in FORTRAN I and uses the IBM 1620 computer with card reader-punch.

APPENDIX IV (continued)

CIRCLE THROUGH THREE POINTS
BFG-ASD-0074

PROGRAM NUMBER 07964927
ABSTRACT

This program finds the radius and center of a circle which passes through three given points. It was written for use in the Sonar Bow Dome Prototype Panel Project.

METHOD

Given three points, we are to find the center and radius of the unique circle through these three points.

Let the three points be denoted by $P_1(x_1, y_1)$, $P_2(x_2, y_2)$ and $P_3(x_3, y_3)$. Denote the center by $O(h, K)$ and the radius by r . The equation of the circle is:

$$(x - h)^2 + (y - K)^2 = r^2 \quad (1)$$

Expanding and rearranging this equation gives us

$$\begin{aligned} x^2 - 2xh + h^2 + y^2 - 2yK + K^2 &= r^2 \\ (h^2 + K^2 - r^2) - 2xh - 2yK &= -(x^2 + y^2) \\ \text{let } Z = h^2 + K^2 - r^2 & \\ Z - 2xh - 2yK &= -(x^2 + y^2) \end{aligned} \quad (2)$$

Each of the x-y coordinates of the three points must satisfy this equation. Substitute the coordinates of the 3 points in (2)

$$\begin{aligned} Z - 2hx_1 - 2Ky_1 &= -(x_1^2 + y_1^2) \\ Z - 2hx_2 - 2Ky_2 &= -(x_2^2 + y_2^2) \\ Z - 2hx_3 - 2Ky_3 &= -(x_3^2 + y_3^2) \end{aligned} \quad (3)$$

h , K , and Z can be found by solving the above set of three simultaneous linear equations. The radius can then be found by

$$r = \sqrt{h^2 + K^2 - Z}$$

Contract NObsr 89483
Serial No. SS041-001
Task 8156

- 5 -

Report No. 17
Phase I Interim Report
30 September 1964

APPENDIX IV (continued)

MACHINE REQUIREMENTS

The Program was written in FORTRAN II for the IBM 7074. Floating point hardware and three tape units are required.

Contract NObsr 89483
Serial No. SS041-001
Task 8156

- 6 -

Report No. 17
Phase I Interim Report
30 September 1964

APPENDIX IV (continued)

BOW DOME MATERIAL
STRESS AND STRAIN PROPERTIES

PROGRAM NO. 06906901
ABSTRACT

This report describes a program for calculating stress and strain properties of the material to be used for the Bow Dome Project.

INTRODUCTION

This program was written to assist in calculating results of tests run on the material to be used for the acoustic window of the bow dome. A rectangular section of the material was secured along two ends and stressed by means of water pressure from a water bag under the test section. The pressure tended to raise the material in the form of an arc of a circle while the chord length remained constant.

The data recorded during the test was the water pressure and the sagitta, or height of the arc.

METHOD

The equations for the radius and the angle ϕ are found from trig relations involving a chord of constant length and the known sagitta.

MACHINE OPERATION

The IBM 1620 is used for this program.

APPENDIX IV (continued)

PREDICTING ARC LENGTH OF SONAR
BOW DOME PROTOTYPE PANEL
BFG-ASD-0065

PROGRAM NO. 07904916
ABSTRACT

This program computes the arc length between any two points on an arc of a circle before and after expansion due to pressure, providing that the ends of the arc are fixed.

INTRODUCTION

This program was written specifically for the Sonar Bow Dome prototype panel. It was used to find the amount of arc expansion between two fixed points on the dome due to various pressures.

The program is useful for finding arc lengths on any circle which expands between two fixed points on its surface.

METHOD

The diagram in this section is useful in following the derivation of the formulas used in this program.

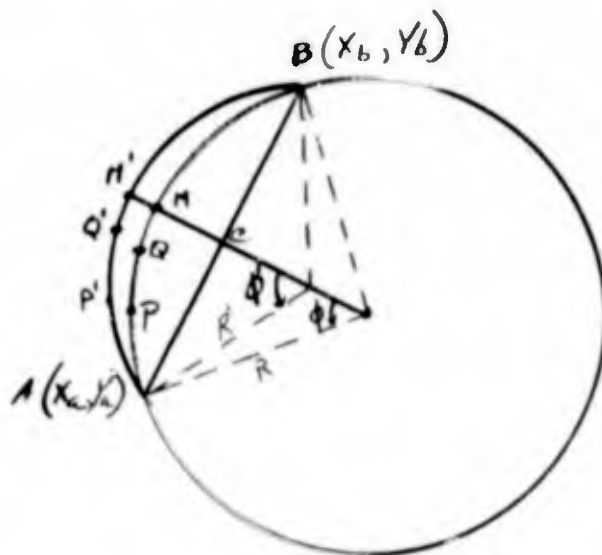


FIGURE 1.

APPENDIX IV (continued)

Symbols Used:

- $A(X_a, Y_a)$ - Fixed point on circle arc.
 $B(X_b, Y_b)$ - Fixed point on circle arc.
 $P(X_p, Y_p)$ - Point on original unexpanded portion of circle arc.
 $Q(X_q, Y_q)$ - Point on original unexpanded portion of circle arc.
 $P'(X_{p'}, Y_{p'})$ - Point on expanded portion of circle arc.
 $Q'(X_{q'}, Y_{q'})$ - Point on expanded portion of circle arc.
 \overline{MC} - Original sagitta.
 $\overline{M'C}$ - Expanded sagitta.
 R - Original circle radius.
 R' - Expanded circle radius.
 \emptyset - 1/2 of included angle of arc \widehat{AMB} .
 \emptyset' - 1/2 of included angle of arc $\widehat{AM'B}$.
 \overline{AB} - Chord length of arc \widehat{AB} .
Given: Point $A(X_a, Y_a)$
Point $B(X_b, Y_b)$
Point $P(X_p, Y_p)$
Point $Q(X_q, Y_q)$
Radius R
Radius R'
Sagitta MC
Sagitta $M'C$

The following is a general proof of the formulas used in predicting the arc length. Refer to Figure 1.

Let, $h = \overline{MC}$, $h' = \overline{M'C}$
 $L = \widehat{AMB}$, $L' = \widehat{AM'B}$
 $S = \widehat{PQ}$, $S' = \widehat{P'Q'}$

APPENDIX IV (continued)

$$C = \overline{AB},$$

$$L = R(2\phi) \text{-----} (1)$$

From triangle ACO;

$$\tan \phi = \frac{\overline{AC}}{\overline{OC}} \text{-----} (2)$$

But, $\overline{AC} = 1/2C; \overline{OC} = R - h \text{-----} (3)$

Therefore, From (2) and (3),

$$\tan \phi = \frac{C}{2(R - h)}$$

Therefore, $\phi = \tan^{-1} \frac{C}{2(R - h)} \text{-----} (4)$

From (1) and (4),

$$L = 2R \tan^{-1} \frac{C}{2(R - h)} \text{-----} (5)$$

Similarly, $L' = 2R' \tan^{-1} \frac{C}{2(R' - h')} \text{-----} (6)$

$$\frac{S}{L} = \frac{S'}{L'}$$

$$S' = \left(\frac{S}{L}\right) L' \text{-----} (7)$$

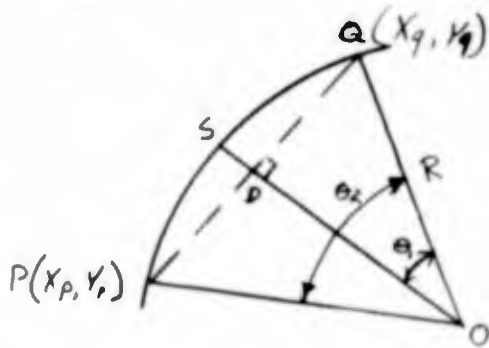


FIGURE II.

APPENDIX IV (continued)

$$\overline{PQ} = \sqrt{(X_q - X_p)^2 + (Y_q - Y_p)^2} \dots \dots \dots (8)$$

$$\overline{PD} = 1/2 \overline{PQ} \dots \dots \dots (9)$$

From (8) and (9),

$$\overline{PD} = 1/2 \sqrt{(X_q - X_p)^2 + (Y_q - Y_p)^2} \dots \dots \dots (10)$$

$$(\overline{PD})^2 = 1/4 \left[(X_q - X_p)^2 + (Y_q - Y_p)^2 \right] \dots \dots \dots (11)$$

$$(\overline{DO})^2 + R^2 - (\overline{PD})^2 \dots \dots \dots (12)$$

From (11) and (12),

$$(\overline{DO}) = \sqrt{R^2 - 1/4 \left[(X_q - X_p)^2 + (Y_q - Y_p)^2 \right]} \dots \dots \dots (13)$$

$$\theta_1 = \tan^{-1} \frac{\overline{PD}}{\overline{DO}} \dots \dots \dots (14)$$

$$\theta_2 = 2 \theta_1 \dots \dots \dots (15)$$

From (10), (13), (14) and (15);

$$\theta_2 = 2 \tan^{-1} \frac{\sqrt{(X_q - X_p)^2 + (Y_q - Y_p)^2}}{2 \sqrt{R^2 - 1/4 \left[(X_q - X_p)^2 + (Y_q - Y_p)^2 \right]}} \dots \dots \dots (16)$$

$$S = R \theta_2 \dots \dots \dots (17)$$

From (16) and (17),

$$S = 2R \tan^{-1} \frac{\sqrt{(X_q - X_p)^2 + (Y_q - Y_p)^2}}{2 \sqrt{R^2 - 1/4 \left[(X_q - X_p)^2 + (Y_q - Y_p)^2 \right]}} \dots \dots \dots (18)$$

APPENDIX IV (continued)

Therefore, From (5), (6), (7) and (18)

$$S' = 2R' \tan^{-1} \frac{\sqrt{(X_q - X_p)^2 + (Y_q - Y_p)^2}}{2 \sqrt{R^2 - 1/4 [(X_q - X_p)^2 + (Y_q - Y_p)^2]}} \cdot \frac{\tan^{-1} \frac{C}{2(R' - h')}}{\tan^{-1} \frac{C}{2(R - h)}} \quad (19)$$

Where

$$C = \sqrt{(X_b - X_a)^2 + (Y_b - Y_a)^2}$$

Equation (19) is the formula used for finding the expanded arc length.

The arc length formula is valid only for values of $\theta_2 < 180^\circ$.

MACHINE REQUIREMENTS

This program is written in the FORTRAN language and uses the IBM 1620 computer.

APPENDIX IV (continued)

ARC LENGTH MEASUREMENT
BFG-ASD-0066

PROGRAM NO. 06968917
ABSTRACT

This program finds arc lengths for any circle and sums successive arc lengths when given the circle radius and the end coordinates of each arc.

INTRODUCTION

This program was written for the purpose of finding arc lengths of a prototype panel of the Sonar Bow Dome.

METHOD

The diagram in this section is useful in following the derivation of the arc length formula.

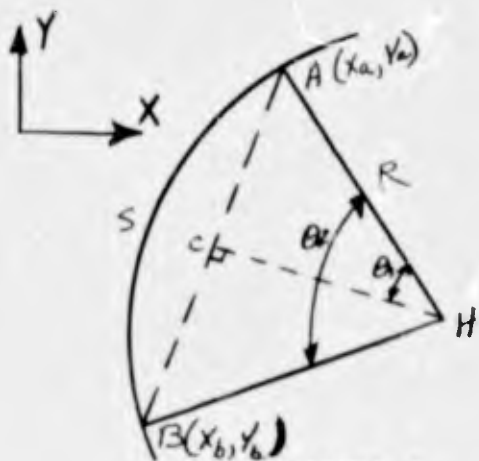


FIGURE 1.

Symbols Used:

- $A(x_a, y_a)$ - Position at one end of arc.
- $B(x_b, y_b)$ - Position at other end of arc.
- R - Circle radius.
- H - Circle center.

BLANK PAGE

APPENDIX IV (continued)

- C - Midpoint of chord AB.
- S - Arc length.
- θ_2 - Included angle of arc S.
- θ_1 - $1/2 \theta_2$

Given are the points $A(X_a, Y_a)$ and $B(X_b, Y_b)$ and the radius R.

Following is the proof of the arc length formula. Refer to Figure 1.

From isocoles triangle AHB:

$$\overline{AB} = \sqrt{(X_a - X_b)^2 + (Y_a - Y_b)^2} \quad \text{--- (1)}$$

$$\overline{AC} = 1/2 \overline{AB} \quad \text{--- (2)}$$

From (1) and (2):

$$\overline{AC} = 1/2 \sqrt{(X_a - X_b)^2 + (Y_a - Y_b)^2} \quad \text{--- (3)}$$

$$(\overline{AC})^2 = 1/4 \left[(X_a - X_b)^2 + (Y_a - Y_b)^2 \right] \quad \text{--- (4)}$$

$$(\overline{CH})^2 = R^2 - (\overline{AC})^2 \quad \text{--- (5)}$$

From (4) and (5):

$$\overline{CH} = \sqrt{R^2 - 1/4 \left[(X_a - X_b)^2 + (Y_a - Y_b)^2 \right]} \quad \text{--- (6)}$$

$$\theta_1 = \tan^{-1} \frac{\overline{AC}}{\overline{CH}} \quad \text{--- (7)}$$

APPENDIX IV (continued)

$$\theta_2 = 2 \theta_1 \text{ ----- (8)}$$

From (3), (6), (7), and (8)

$$\theta_2 = 2 \tan^{-1} \frac{\sqrt{(X_a - X_b)^2 + (Y_a - Y_b)^2}}{2 \sqrt{R^2 - 1/4} \left[(X_a - X_b)^2 + (Y_a - Y_b)^2 \right]} \text{ (9)}$$

$$S = R \theta_2 \text{ ----- (10)}$$

From (9) and (10):

$$S = 2R \tan^{-1} \frac{\sqrt{(X_a - X_b)^2 + (Y_a - Y_b)^2}}{2 \sqrt{R^2 - 1/4} \left[(X_a - X_b)^2 + (Y_a - Y_b)^2 \right]}$$

The above formula is the one used for finding the arc length.

The arc length formula is valid only for values of $\theta_2 < 180^\circ$.

MACHINE REQUIREMENTS

This program is written in the FORTRAN language and uses the IBM 1620 computer.

APPENDIX IV (continued)

EFFECTS OF WINDOW STRETCH
AND HYDRODYNAMIC FORCES
UPON THE SONAR BOW DOME CONTOUR

BFG-ASD-0076
PROGRAM NO. 07904911

ABSTRACT

This program calculates the tensions and changes in contour of the sonar bow dome. It takes into account the effects of the stretch characteristics and hydrodynamic forces.

INTRODUCTION

The sonar bow dome is a "rain-drop"-shaped rubber housing which is fastened on the bow of a ship. It houses a sonar transducer.

The contour of the dome is changed by the stretch of the wires it contains and by the hydrodynamic forces upon it while it is in use. This program predicts the changes in contour and the tensions upon the wires.

SUMMARY

Data concerning the parameters of the dome are first read in. This includes the number of plies, ships velocity, properties of the wire strands and other data.

Geometric properties of each radial frame are then read in. A radial frame is a vertical section of the dome taken such that it is perpendicular to the water level of maximum breadth of the dome.

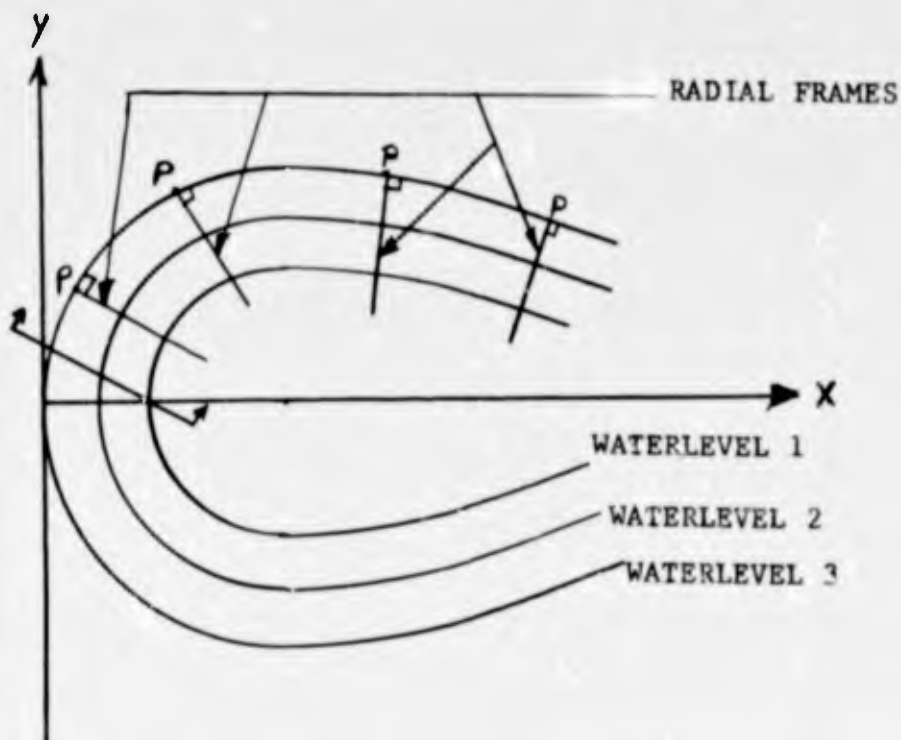


Figure 1. (Plan View of Dome)

APPENDIX IV (continued)

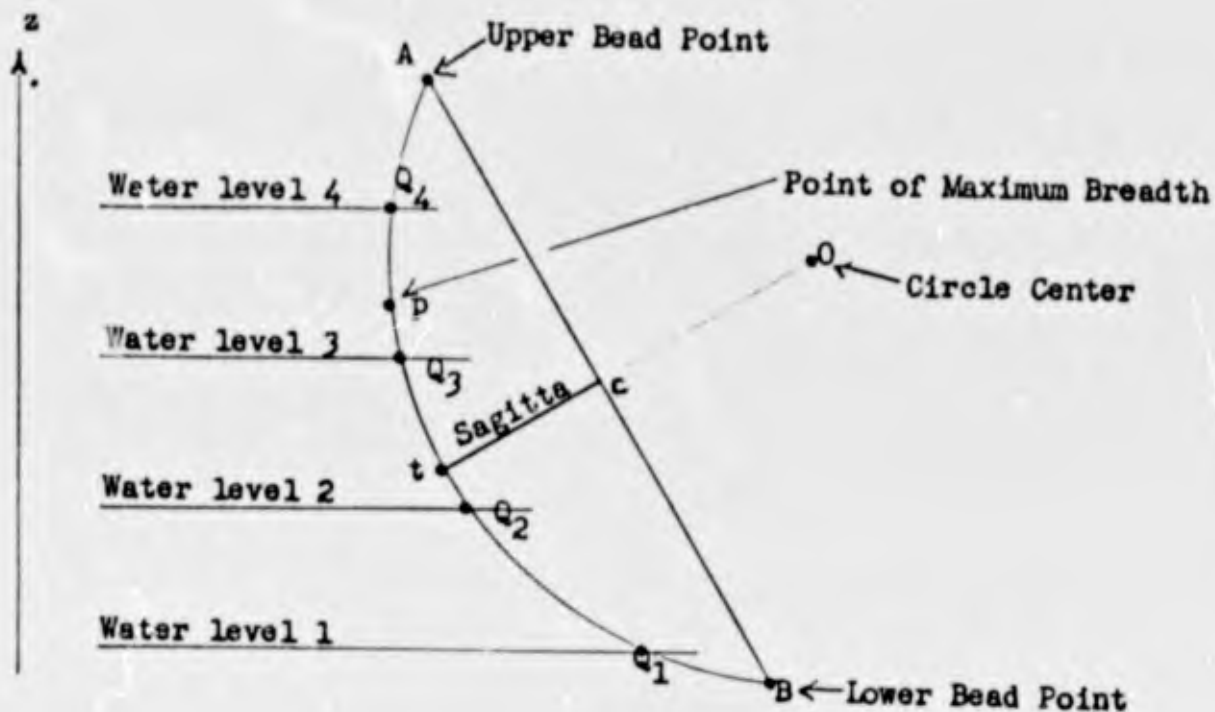


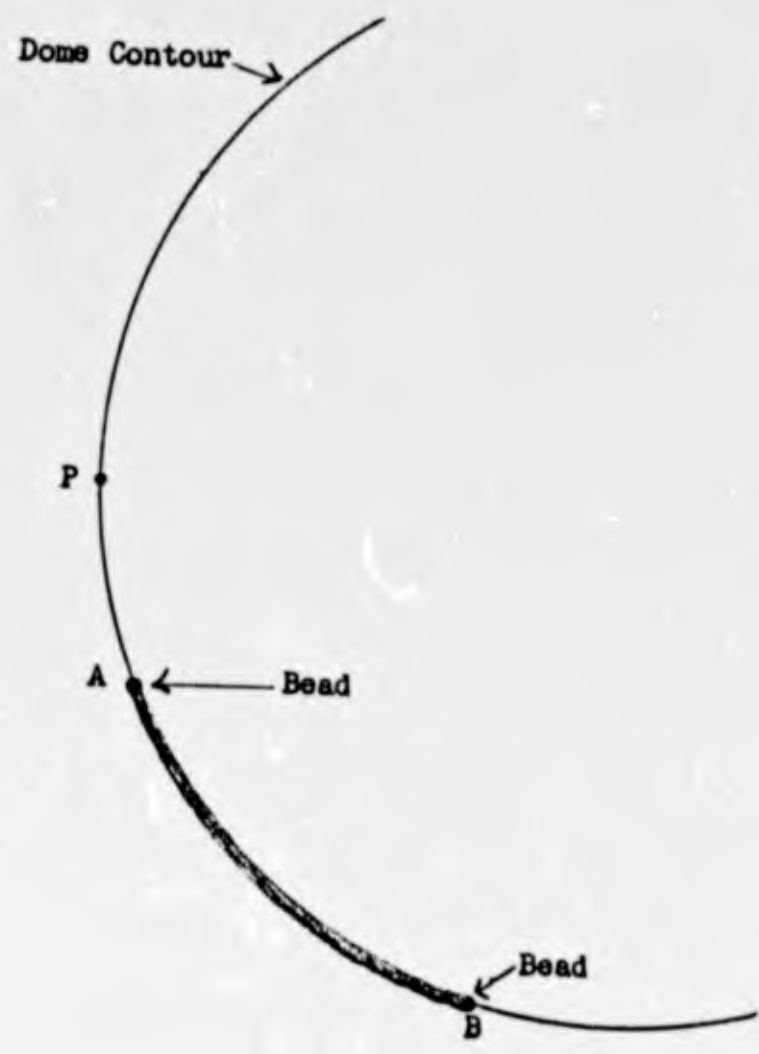
Figure 2. (A radial frame, Section A-A' of figure 1)

The geometric properties of each frame which are read in are:

1. The x, y and z coordinates of the upper and lower bead points.
2. The length of the sagitta (see figure 2).
3. The horizontal radius (radius of curvature of the water level of maximum breadth; that is, at point P) at the frame being studied.
4. X_p , the x-coordinate of point P, the point of maximum breadth of the radial frame (See figures 1 and 2).

APPENDIX IV (continued)

We exclude from analysis arcs of radial circles which do not contain the point of maximum breadth. It is not permissible to use the program to study arc AB below, since it does not contain point P, the point of maximum breadth.



APPENDIX IV (continued)

The z-coordinate must be a measure of water level, that is, the Z-axis is perpendicular to the plane of the water. The z-coordinate may be either positive or negative.

The x-y axes must determine a plane parallel to the plane of the water. The x-and y-coordinates may be positive or negative.

The origin need not be at the nose of the dome as shown in Figure 1. The coordinate system could, for example, be set up in the following manner:

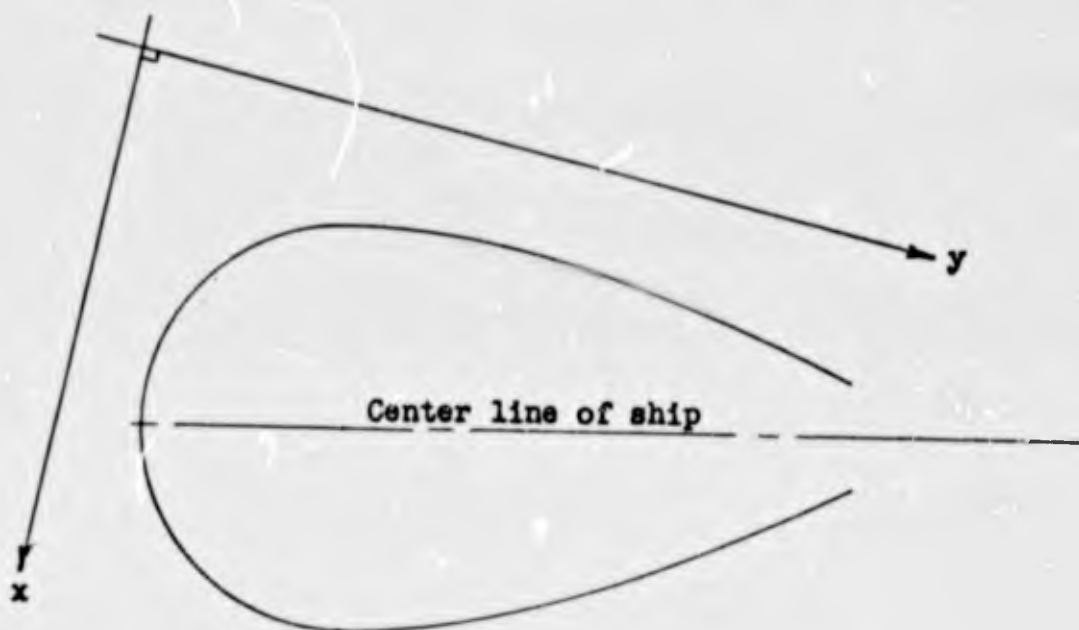


Figure 3.

The dome is symmetric about the center line of the ship, so it is only necessary to study one of the symmetric halves of the dome.

Data is read in for each frame to be studied. The program deals with one radial frame at a time. The following computations, which are broken up into "sections," are performed upon each radial frame.

Section A

The bead points and sagitta for the original radial circle are given from input data. This original radial circle is the shape the dome should take under actual operating conditions. The center and radius of this circle are found.

APPENDIX IV (continued)

Section F

The coordinates of the points on each water level are found. These are the coordinates of the points labeled Q in Figure 2.

Section C

The radial circle expands outwardly due to the constructional stretch of the window. The amount the sagitta increases is called the deflection. The water level coordinates are found for the points on the constructionally stretch circle.

Section D

Hydrodynamic forces cause the constructionally stretched circle to expand further. The amount the (new) sagitta increases is called the additional deflection or velocity deflection. The water level coordinates are found on this radial circle which reflects construction stretch and the effect of hydrodynamic forces. The tensions upon the wires are computed.

Section E

The dome will be constructed such that each radial circle will be smaller than the original radial circle. It will expand, approximately, into the shape of the original circle. The radial circle to which the dome is constructed will be called the "shrunk" circle or the "corrected" circle.

The sagitta of the shrunk circle is given by

$$\text{Sagitta}_{\text{shrunk}} - \text{Sagitta}_{\text{original}} - (\text{deflection} + \text{additional deflection})$$

Figure 4 illustrates the 4 circle discussed above, and two more circles which will be discussed after the figure.

APPENDIX IV (continued)

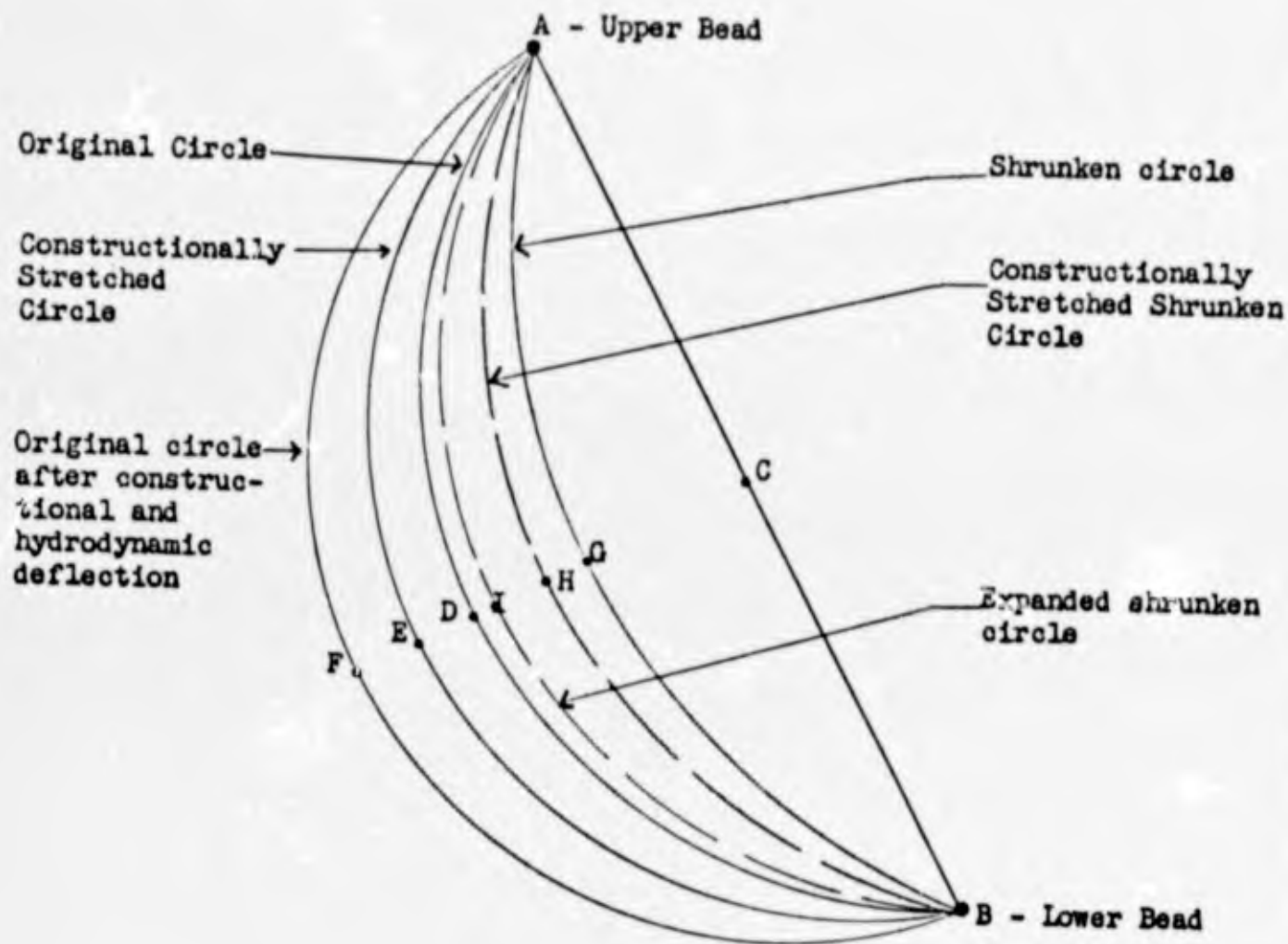


Figure 4

- AB Circle chord
- CD Original sagitta
- DE Deflection due to constructional stretch
- EF Addition deflection due to hydrodynamic forces
- CG Shrunken sagitta

NOTE: DF = DG

APPENDIX IV (continued)

Section F

The constructional stretch of the shrunken circle is found. This gives the circle with arc AHB in Figure 4. Water level coordinates are found on this circle.

Section G

The hydrodynamic forces will cause the above radial circle to expand, giving the circle with arc AIB. This should be approximately the shape of the original circle. Water level coordinates are found for this circle, which is called the expanded shrunken circle.

This can all be summed up as follows:

1. The shape of a radial frame of the dome under operating conditions should be arc ADB.
2. The radial frame will be constructed to arc AGB, which will expand to arc AIB.
3. Arcs ADB and AIB are almost identical.

The control card allows the user to omit certain sections above which might not be of interest to him.

The water level coordinates of the shrunken circle and expanded shrunken circle may be punched out. This will serve as input to other programs such as the one which computes the difference in volume between the shrunken dome and expanded shrunken dome.

APPENDIX IV (continued)

METHOD

Section A

Find the center of the radial circle.

The following data is given for each radial frame.

Upper Bead Coordinates $A(x_a, y_a, z_a)$

Lower Bead Coordinates $B(x_b, y_b, z_b)$

Sagitta h

x-coordinate of point P, x_p
 the point of maximum
 breadth on the radial
 frame

The radial line, 1, is the
 line in the x-y plane determined
 by the radial frame.

The equation of 1 is

$$y = mx + b$$

$$\text{where } m = \frac{y_b - y_a}{x_b - x_a}$$

$$\text{Then } b = y - mx$$

$$= y_a - mx_a$$

Thus m and b are determined.

Difficulties arise when line 1 is parallel to the y-axis. In this special case

$$x_a = x_b$$

$$x = x_a - x_b$$

$$= 0$$

and the slope, m, become infinite.

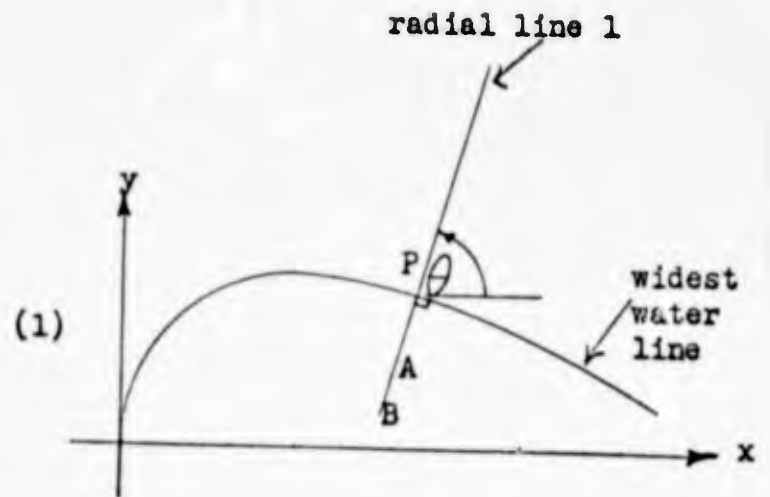


Figure 5

APPENDIX IV (continued)

If line 1 is vertical, or nearly so, a message is printed instructing the user to interchange the x and y coordinates. This will then make the slope be zero. The problem must then be run again for this frame. Note that a new value must be entered for x_p .

Line 1 is considered "vertical, or nearly so" if

$$x_a - x_b \leq 0.1$$

We also assume that the x and y coordinates of the two beads are not the same, because if that were the case, line 1 would not be determined.

The angle θ is found next.

$$\theta = \tan^{-1} m \tag{2}$$

Let g = chord of the arc of the radial circle.

$$g = \sqrt{(x_a - x_b)^2 + (y_a - y_b)^2 + (z_a - z_b)^2} \tag{3}$$

Let r = radius of circle

$$\begin{aligned} r^2 - (\frac{1}{2}g)^2 &= (r - h)^2 \\ r^2 - \frac{1}{4}g^2 &= r^2 - r - 2rh + h^2 \\ 2rh - \frac{1}{4}g^2 &= h^2 \\ r &= \frac{g^2 + 4h^2}{8h} \end{aligned} \tag{4}$$

The circle center, $O(x_o, y_o, z_o)$ will not be found.

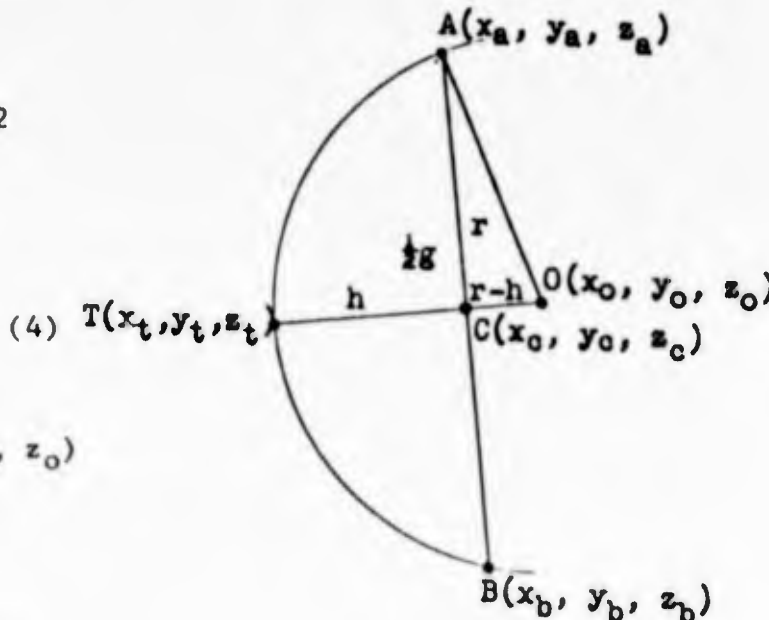


Figure 9 follows from figures 7 and 8.

Figure 6.

APPENDIX IV (continued)

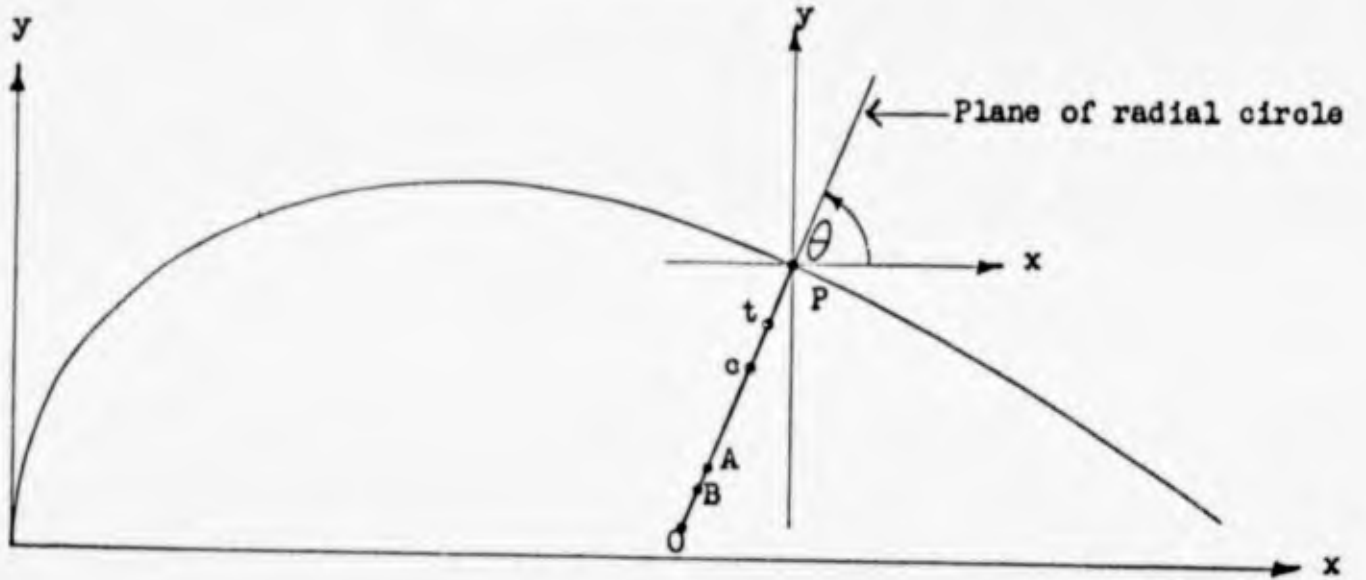


Figure 7

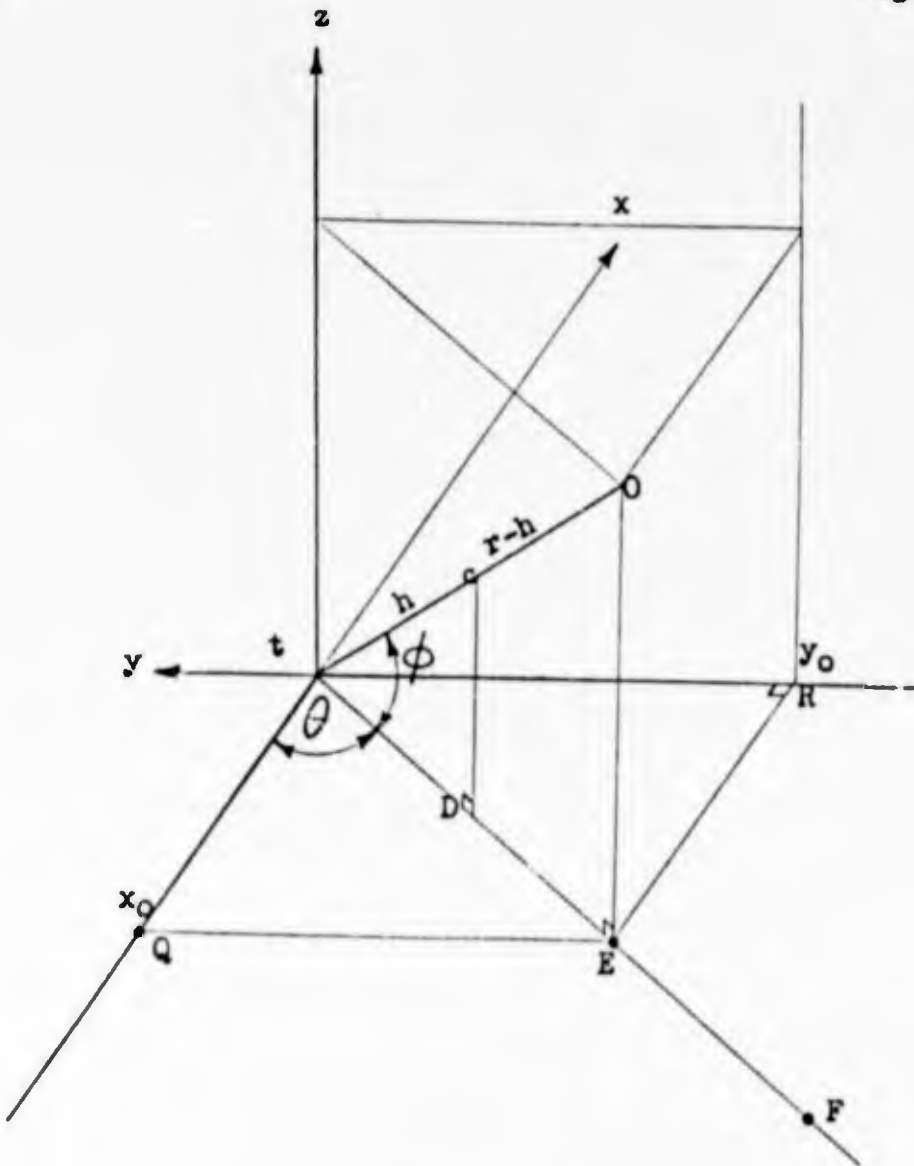


Figure 9

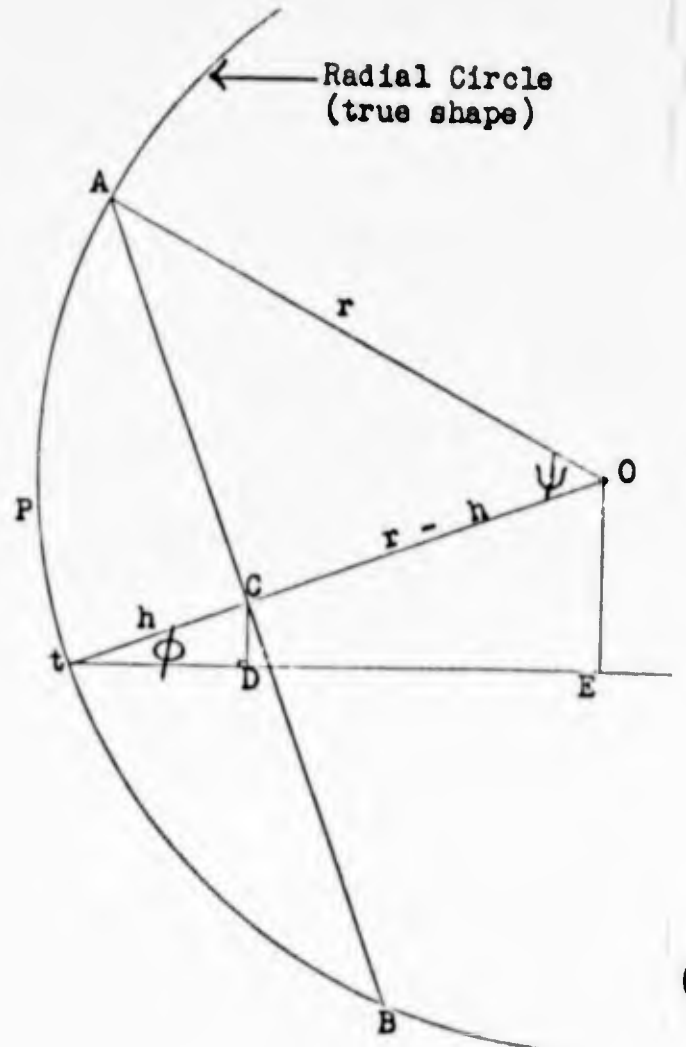


Figure 8

APPENDIX IV (continued)

Find the coordinates of $T(x_t, y_t, z_t)$. T is the intersection of the radial circle with the perpendicular bisector of chord AB .

Points A, B, C, T , and O all lie in the plane of the radial circle, (see figure 7), which along with (1) implies:

$$\begin{aligned} y_a &= mx_a & b \\ y_b &= mx_b & b \\ y_c &= mx_c & b \\ y_t &= mx_t & b \\ y_o &= mx_o & b \end{aligned} \tag{5}$$

C is the midpoint of chord AB , therefore,

$$\begin{aligned} x_c &= \frac{1}{2}(x_a + x_b) \\ y_c &= \frac{1}{2}(y_a + y_b) \\ z_c &= \frac{1}{2}(z_a + z_b) \end{aligned} \tag{6}$$

and

$$h = \sqrt{(x_o - x_t)^2 + (y_o - y_t)^2 + (z_o - z_t)^2} \tag{7}$$

Considering vectors,

$$CT = (x_c - x_t)i + (y_c - y_t)j + (z_c - z_t)k$$

$$AB = (x_a - x_b)i + (y_a - y_b)j + (z_a - z_b)k$$

The dot product of CT and AB is zero since the vectors are perpendicular.

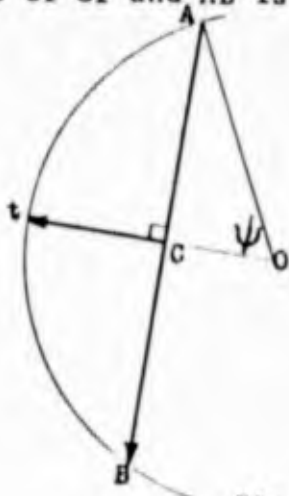


Figure 10.

APPENDIX IV (continued)

$$AB \quad CT = (x_a - x_b)(x_c - x_t) \quad (y_a - y_b)(y_c - y_t) \quad (z_a - z_b)(z_c - z_t) = 0 \quad (8)$$

The coordinates of T can be determined from (5), (7) and (8). We start with (7).

$$\begin{aligned} h &= (\underline{x_c} - x_t)^2 - (y_c - y_t) - (z_c - z_t)^2 \\ h^2 &= (x_c - x_t)^2 - (mx_c - b) - mx_t - b)^2 - (z_c - z_t)^2 \\ h^2 &= (x_c - x_t)^2 - m^2(x_c - x_t)^2 - (z_c - z_t)^2 \\ h^2 &= (1 - m^2)(x_c - x_t)^2 - (z_c - z_t)^2 \\ h^2 &= (1 - m^2)(x_c^2 - 2x_c x_t - x_t^2) - (z_c^2 - 2z_c z_t - z_t^2) \\ 0 &= (1 - m^2)x_t^2 - 2x_c(1 - m^2)x_t - z_t^2 - 2z_c z_t - (1 - m^2)x_c^2 - z_c^2 - h^2 \end{aligned}$$

Substitutions will be made to simplify the algebra. These capital letters do not represent points here. The numerical value of all these letters are known from previous results.

$$Ax_t^2 - Bx_t - z_t^2 - Cz_t - D = 0 \quad (9)$$

It follows from (8) that

$$\begin{aligned} (x_a - x_b)(x_c - x_t) - (y_a - y_b)(y_c - y_t) - (z_a - z_b)(z_c - z_t) &= 0 \\ E(x_c - x_t) - F(y_c - y_t) - G(x_c - z_t) &= 0 \\ E(x_c - x_t) - F(mx_c - b) - (mx_t - b) - G(z_c - z_t) &= 0 \\ E(x_c - x_t) - mF(x_c - x_t) - G(z_c - z_t) &= 0 \\ (E - mF)(x_c - x_t) - G(z_c - z_t) &= 0 \\ H(x_c - x_t) - G(z_c - z_t) &= 0 \\ Hx_c - Hx_t - Gz_c - Gz_t &= 0 \\ Gz_t = Hx_c - Hx_t - Gz_c \\ z_t = \frac{Hx_c - Hx_t - Gz_c}{G} \end{aligned}$$

APPENDIX IV (continued)

$$z_t = \frac{Hx_c - Gz_c}{G} - \frac{H}{G} x_t$$

$$z_t = M - Nx_t \quad (10)$$

Substitute (10) in (9)

$$Ax_t^2 - Bx_t - (M - Nx_t)^2 - C(M - Nx_t) - D = 0$$

$$Ax_t^2 - Bx_t - M^2 - 2MNx_t - N^2 x_t^2 - CM - CNx_t - D = 0$$

$$(A - N^2) x_t^2 - (B - 2MN - CN)x_t - (M^2 - CM - D) = 0$$

$$A_2 x_t^2 - A_1 x_t - A_0 = 0 \quad (11)$$

Solve (11) by Newton-Raphson Method.

$$\text{Let } f(x) = A_2 x^2 - A_1 x - A_0$$

$$f'(x) = 2A_2 x - A_1$$

$$\text{and } x_{i+1} - 1 = x_i - \frac{f(x_i)}{f'(x_i)}$$

Use x_i for the initial estimate of x_t . (See figures 7 and 8 to locate point P) The y and z coordinates of T follow immediately from (5) and (10).

$$y_t = Mx_t - b$$

$$z_t = M - Nx_t$$

Find the angle between TC and TD (see figure 9).

$$TC = h$$

The coordinates of D are

$$x_d = x_c$$

$$y_d = y_c$$

$$z_d = z_t$$

$$CD = z_c - z_d$$

APPENDIX IV (continued)

$$\begin{aligned} \sin \phi &= \frac{z_c - z_d}{h} \\ &= \frac{z_c - z_t}{h} \\ \therefore \phi &= \sin^{-1} \left(\frac{z_c - z_t}{h} \right) \end{aligned}$$

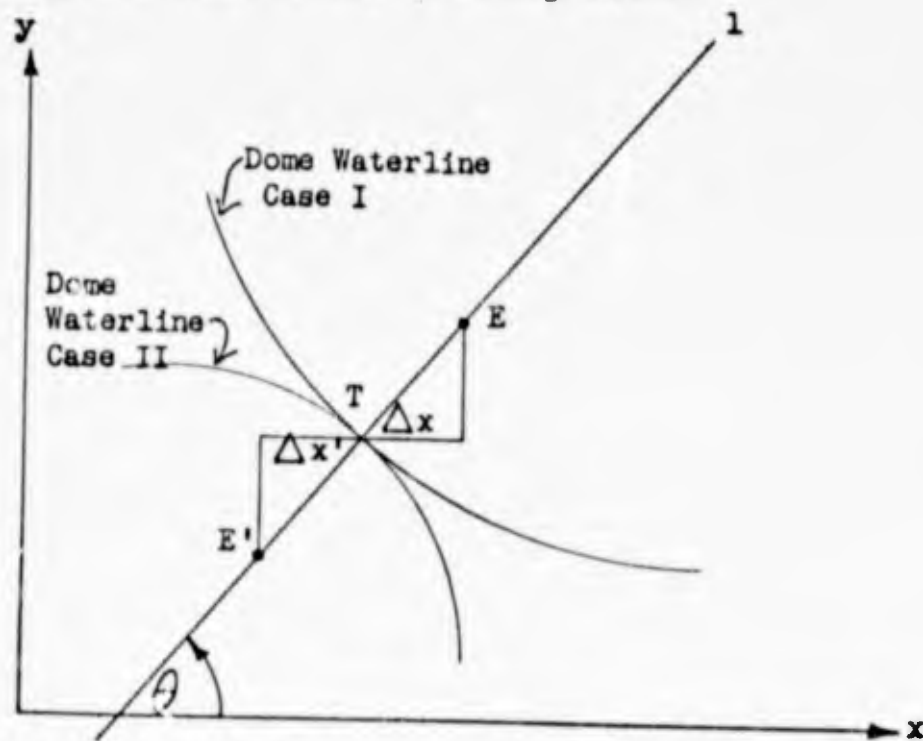
The center of the circle, point $O(x_0, y_0, z_0)$ can now be found. Referring to figure 9.

$$\begin{aligned} z_0 &= z_t - EO \\ &= z_t - r \sin \phi \end{aligned}$$

The "plus or minus" in the first equation is accounted for in the second equation since $\sin \phi$ takes on both positive and negative values. $E\theta$ is added if $\phi > 0$; subtracted if $\phi < 0$.

x_0 will be found next. Refer to figure 9 and notice that $ET = r \cos \phi$ and that $x_e = x_0$.

Assume $\theta > 0$ and refer to the following sketch:



The dome water line can be either concave up (Case I) or concave down (Case II).

APPENDIX IV (continued)

Consider first Case I. In this situation, the bead points must be to the right of the point of maximum breadth. Let x_a be the x-coordinate of the bead point A, x_p be the x-coordinate of the point of maximum breadth.

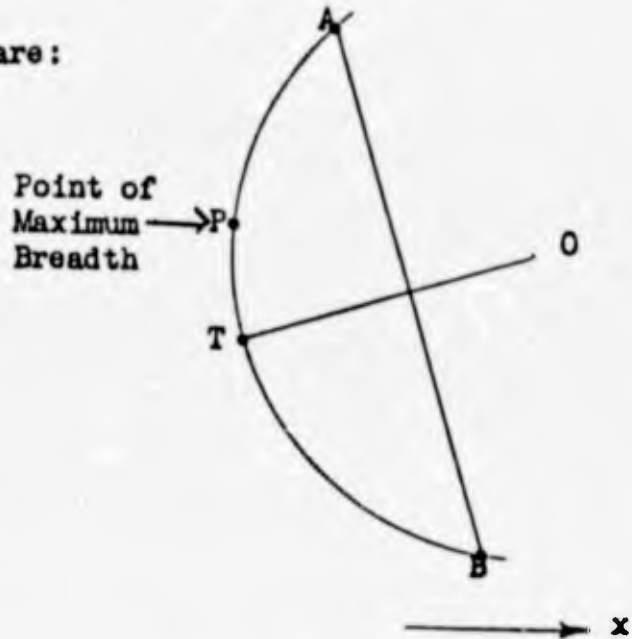
The conditions for Case I above are:

$$\theta > 0$$

$$x_a > x_p$$

Then:

$$\begin{aligned} x_e &= x_t + \Delta x \\ &= x_t + ET \cos \theta \\ &= x_t + r \cos \phi \cos \theta \\ \therefore x_o &= x_t + r \cos \phi \cos \theta \end{aligned}$$



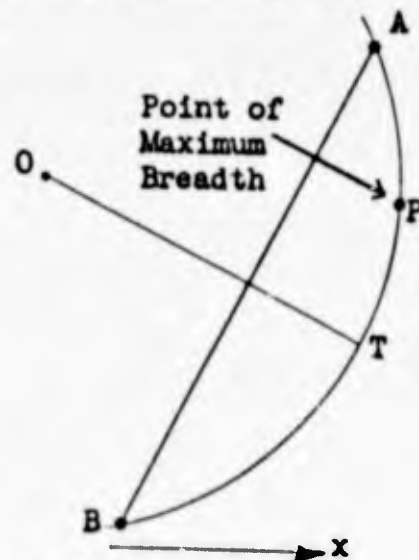
Now, consider Case II. By similar reasoning, the conditions are

$$\theta > 0$$

$$x_a < x_p$$

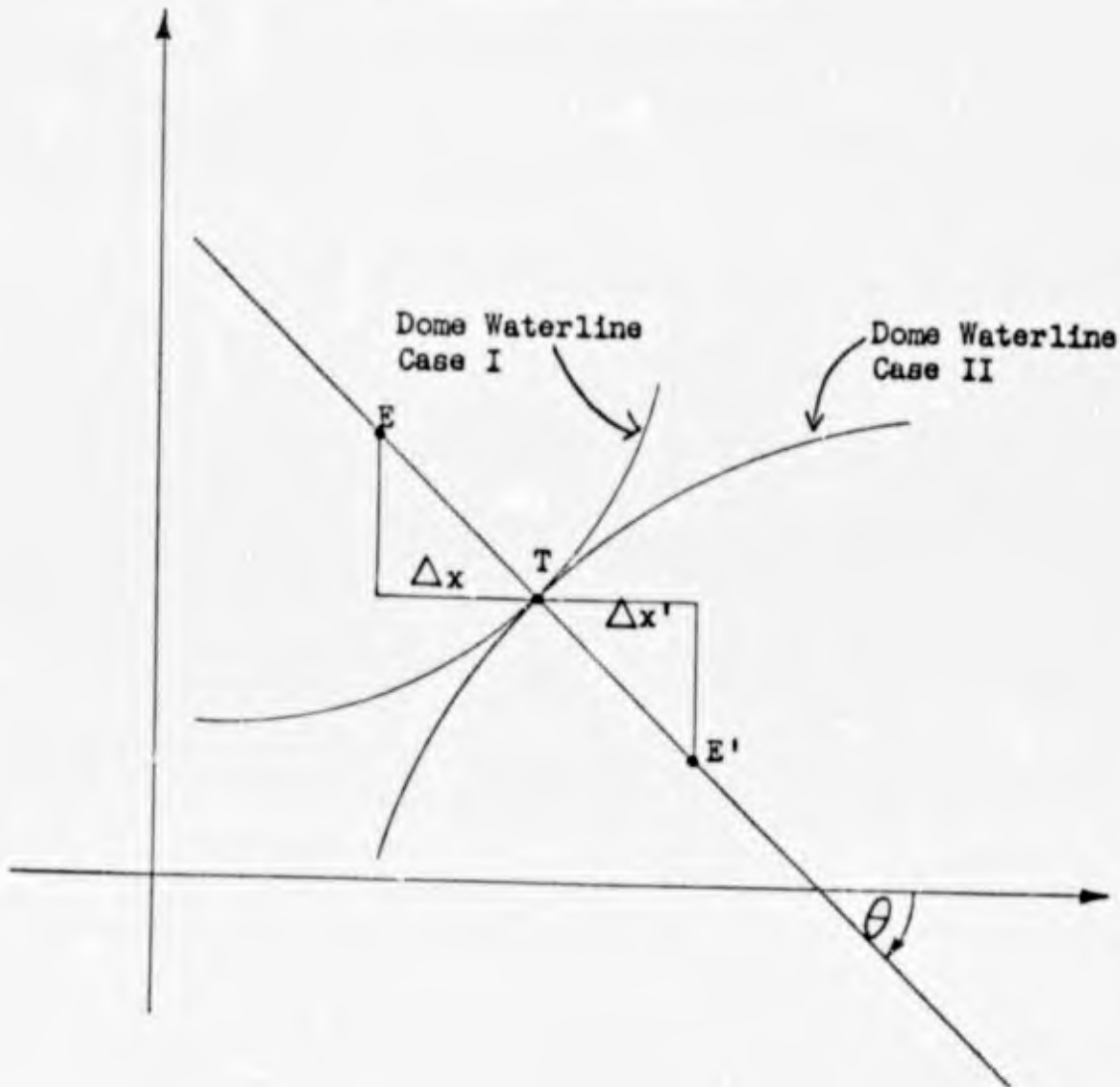
Then:

$$\begin{aligned} x_{e'} &= x_t - \Delta x' \\ &= x_t - E'T \cos \\ &= x_t - r \cos \phi \cos \theta \\ \therefore x_o &= x_t - r \cos \phi \cos \theta \end{aligned}$$



Now assume $\theta < 0$. This case is represented in the following diagram:

APPENDIX IV (continued)



If we reason in the same manner as before we arrive at the following:

Case I: $\theta < 0$
 $x_a < x_p$
 $x_o = x_t - r \cos \theta \cos \phi$

Case II: $\theta < 0$
 $x_a > x_p$
 $x_o = x_t + r \cos \theta \cos \phi$

APPENDIX IV (continued)

To sum up, x_0 can be found by one of the following equations:

If $x_a > x_p$

$$x_0 = x_t + r \cos \theta \cos \phi,$$

or if

$$x_a < x_p,$$

$$x_0 = x_t - r \cos \theta \cos \phi$$

The y-coordinate of the center can be found easily by using equation (3)

$$y_0 = Mx_0 + b$$

Thus the circle center has been found.

APPENDIX IV (continued)

Section B

Finding the points on the radial circle at various given water levels. The points are the "Q's" in Figure 2.

The circle is determined by the intersection of a sphere, with center O and radius r, and a plane containing points A, B, and P. P is a point on the radial circle at a given water level, L. P can be thought of as one of the Q points in Figure 2, or as point P in figure 8.

Equation of sphere:

$$(x - x_0)^2 + (y - y_0)^2 + (z - z_0)^2 = r^2$$

Equation of plane:

$$y = mx + b \quad (z \text{ arbitrary})$$

Therefore, the equation of the radial circle is:

$$(x - x_0)^2 + [(mx + b) - y_0]^2 + (z - z_0)^2 = r^2 \quad (12)$$

where the variables are x and z.

To find a point, P, on the circle at water level L, set $z = L$ and solve for x. The y-coordinate follows from

$$y = mx + b$$

Setting $z = L$ in equation (12)

$$(x - x_0)^2 + [(mx + b) - (mx_0 + b)]^2 + (L - z_0)^2 = r^2$$

$$(x - x_0)^2 + m^2(x - x_0)^2 + (L - z_0)^2 = r^2$$

$$(1 + m^2)(x - x_0)^2 + (L - z_0)^2 = r^2$$

$$(x - x_0)^2 + \frac{(L - z_0)^2 - r^2}{1 + m^2} = 0$$

$$x^2 - 2x_0x + \left[x_0^2 + \frac{(L - z_0)^2 - r^2}{1 + m^2} \right] = 0$$

$$x^2 + Rx + S = 0 \quad (13)$$

APPENDIX IV (continued)

Note that there are two roots to equation (13), but only one of them is a solution to our problem. Care must be taken to insure that the correct root is found. Equation (13) is solved by the Newton-Raphson method, in which originally an estimate of the desired root is made. If the estimate is near the desired root, then it will usually converge to that root. A good estimate of the desired root will be found by a linear interpolation so the method will find the desired root of (13).

Let Q_1 and Q_2 be points on the circle at water levels L_1 and L_2 , whose x-coordinate we wish to estimate. Q_1 is on a higher water level than T , while Q_2 is on a lower one. (See Figure 11). It is assumed that the upper bead is on a higher water level than the lower bead, that is, $z_a > z_b$.

Consider Q_1 , where $L_1 > z_t$.

Approximate Q_1 by Q'_1 ,

$$x_{q1} \approx x'_{q1}$$

It follows, by similar triangles,

$$\frac{x_a - x'_{q1}}{z_a - L} = \frac{x_a - x_t}{z_a - z_t}$$

$$x_a - x'_{q1} = (z_a - L) \left(\frac{x_a - x_t}{z_a - z_t} \right)$$

$$x'_{q1} = x_a + (L - z_a) \left(\frac{x_a - x_t}{z_a - z_t} \right)$$

$$x_{q1} \approx x_a + (L - z_a) \left(\frac{x_a - x_t}{z_a - z_t} \right)$$

(14)

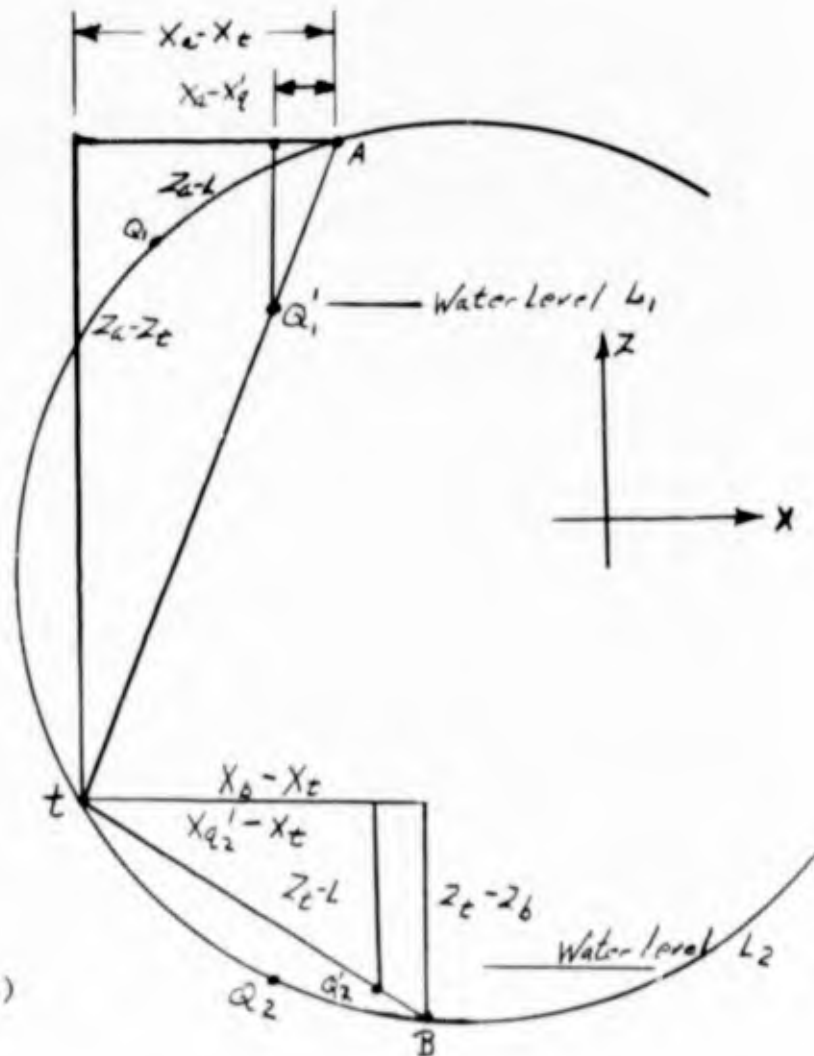


Figure 11

APPENDIX IV (continued)

Now consider Q_2 where $L_2 < z_t$.

Approximate Q_2 by Q'_2

$$x_{q_2} \approx x'_{q_2}$$

$$\frac{x'_{q_2} - x_t}{z_t - L} = \frac{x_b - x_t}{z_t - z_b}$$

$$x'_{q_2} = x_t + (L - z_t) \left(\frac{x_t - x_b}{z_t - z_b} \right)$$

$$x_{q_2} \approx x_t + (L - z_t) \left(\frac{x_t - x_b}{z_t - z_b} \right)$$

(15)

It is necessary to find angle ψ (Figure 10) for the constructional stretch calculations.

$$\tan \psi = \frac{AC}{CO}$$

$$\tan \psi = \frac{1/2 g}{\sqrt{(x_c - x_o)^2 + (y_c - y_o)^2 + (z_c - z_o)^2}}$$

$$\psi = \tan^{-1} \left[\frac{g}{2 \sqrt{(x_c - x_o)^2 + (y_c - y_o)^2 + (z_c - z_o)^2}} \right]$$

(16)

APPENDIX IV (continued)

$$\text{Let } f(r) = \sin\left(\frac{s}{2r}\right) = \frac{g}{2r}$$

$$\therefore f'(r) = \left[\cos\left(\frac{s}{2r}\right) \right] \left(-\frac{s}{2r^2}\right) - \left(-\frac{g}{2r^2}\right)$$

$$= \frac{g}{2r^2} - \frac{s}{2r^2} \cos\left(\frac{s}{2r}\right)$$

$$= \frac{1}{2r^2} \left[g - s \cos\left(\frac{s}{2r}\right) \right]$$

$$\text{and } r_1 - 1 = r_1 = \frac{f(r_1)}{f'(r_1 - 1)}$$

For the initial estimate of r , use the radius of the original circle previously found in Section A.

It follows immediately that

$$\psi = s/2r$$

$$\text{and } h = r - oc$$

$$= r - r \cos \psi$$

$$= r(1 - \cos \psi)$$

The constructionally stretched circle has been essentially found. The center and points on various water levels can be found using methods outlined in Sections A and B.

APPENDIX IV (continued)

Section C

Constructional Stretch Calculations

The equations of construction stretch in this section are empirical.

The constructional stretch is a linear function of the length of the radial circle arc AB.

$$\text{Construction Stretch} = a \widehat{AB} + b \quad (17)$$

a and b are constants which depend upon the type of wire used.

Let s' represent the length of the new arc after constructional stretch.

$$s' = \widehat{AB} + (a \widehat{AB} + b)$$

$$s' = \widehat{AB} (1 + a) + b \quad (18)$$

where

$$\widehat{AB} = 2r \psi$$

It is now necessary to find the radius of the constructionally stretched circle. Using Figure 12, the following equations arise:

$$\begin{cases} s' = 2r' \psi \\ \sin \psi = 1/2g/r' \end{cases} \quad (19)$$

The system of equations (19) will be solved simultaneously. The primes will be dropped to simplify notation.

$$\psi = s/2r$$

$$\sin \left(\frac{s}{2r} \right) = \frac{g}{2r}$$

$$\sin \left(\frac{s}{2r} \right) - \frac{g}{2r} = 0 \quad (20)$$

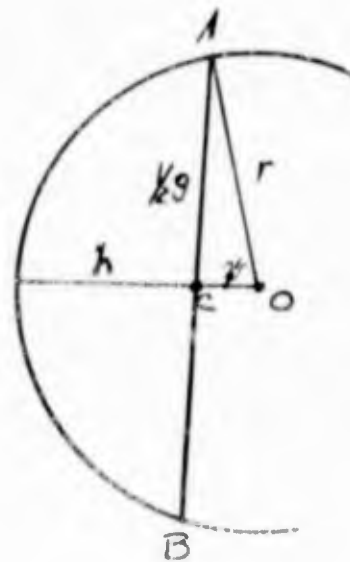


Figure 12

Equation (20) will be solved for r by the Newton-Raphson Method.

APPENDIX IV (continued)

Section D

Find the deflection of the dome due to hydrodynamic forces. (This is a function of the ship's velocity and is sometimes referred to as the "velocity deflection.")

The water pressure on the dome, P_w , is given by

$$P_w = \frac{(62.4) (SG) (\text{depth})}{144}$$

where

depth = depth of dome

SG = specific gravity of the fluid in which the dome is immersed.

P_v , the pressure on the dome due to the ship's movement through the water, is

$$P_v = \frac{1/2 \left(\frac{62.4}{32.17} \right) (SG) C_p V^2}{144}$$

where

C_p = coefficient of pressure

V = velocity of ship (ft/sec)

and

$$P_{diff} = P_d - P_w - P_v$$

P_d = Design Pressure

P_{diff} = Differential Pressure

An iteration method was derived to solve for the tensions. The deflection can then be found.

The three basic equations are:

APPENDIX IV (continued)

$$P_{diff} = \frac{\eta_v N T_v \sin^2 \beta_1 + \eta_H N T_H \sin^2 \beta_2}{r_v} + \frac{\eta_H N T_H \cos^2 \beta_2}{r_H} \quad (21)$$

$$T_v = \frac{d D^2}{r_v F_v} \left[\frac{\sin \psi_v - \psi_v \cos \psi_v}{\psi_v (1 - \cos \psi_v)} \right] \quad (22)$$

$$T_H = \frac{d D^2}{r_H F_H} \quad (23)$$

Where:

- η_v = number of vertical plies.
- η_H = number of horizontal plies.
- N = number of cables per inch of ply.
- β_1 = angle vertical cables make with horizontal.
- β_2 = angle horizontal cables make with horizontal.
- D = cable nominal diameter.
- r_v = vertical radius.
- r_H = horizontal radius.
- $\psi_v = \psi$, one-half the central angle of the frame (see figure 12)
- T_v = vertical tension.
- T_H = horizontal tension.
- F_v = elastic stretch factor, vertical.
- F_H = elastic stretch factor, horizontal.
- d = deflection (denoted by Δ in other sections of Phase I Report)

APPENDIX IV (continued)

Divide (23) by (22)

$$\frac{T_H}{T_V} = \frac{r_V}{r_H} \left[\frac{\psi_V(1 - \cos \psi_V)}{\sin \psi_V - \psi_V \cos \psi_V} \right] \frac{F_V}{F_H} \quad (24)$$

Let $C_\psi = \frac{\psi_V(1 - \cos \psi_V)}{\sin \psi_V - \psi_V \cos \psi_V}$

and $F^* = F_V/F_H$

Then, from (24)

$$\frac{T_H}{T_V} = \frac{r_V}{r_H} C_\psi F^* \quad (25)$$

From (21)

$$\begin{aligned} P_{diff} &= T_V \left\{ \frac{\eta_V N \sin^2 \beta_1 + \eta_H N \frac{T_H}{T_V} \sin^2 \beta_2}{r_V} + \frac{\eta_H N \frac{T_H}{T_V} \cos^2 \beta_2}{r_H} \right\} \\ &= T_V \left\{ \frac{\eta_V N \sin^2 \beta_1}{r_V} + \frac{T_H}{T_V} \left[\frac{\eta_H N \sin^2 \beta_2}{r_V} + \frac{\eta_H N \cos^2 \beta_2}{r_H} \right] \right\} \quad (26) \end{aligned}$$

Substitute for T_H/T_V from (25) and solve for T_V

$$T_V = \frac{\eta_V N \sin^2 \beta_1}{r_V} + \frac{r_V}{r_H} C_\psi F^* \left[\frac{\eta_H N \sin^2 \beta_2}{r_V} + \frac{\eta_H N \cos^2 \beta_2}{r_H} \right] \quad (27)$$

$$T_H = \left(\frac{T_H}{T_V} \right) T_V \quad (28)$$

The elastic stretch factors F_V and F_H are functions of the tensions

APPENDIX IV (continued)

$$\frac{1}{F_v \times 10^6} = M_f T_v + b_f$$

$$\frac{1}{F_H \times 10^6} = M_f T_H + b_f$$

$$\therefore F^* = \frac{F_v}{F_H} = \frac{M_f T_H + b_f}{M_f T_v + b_f} \quad (29)$$

The iteration process is begun by setting $F^* = 1$. T_H/T_v is then found from (25), which is then substituted in (27) to find T_v . T_H is found from (28), using the above value of T_H/T_v . A new value for F^* is calculated from the values of T_v and T_H by use of equation (29). The process then repeats itself with this new value of F^* .

The process repeats itself until it converges. The process is considered to be converged when the difference between two successive values of T_v is less than 1/10. The deflection, d , is then found by rearranging equation (22).

$$d = \frac{T_v r_v F_v}{D^2 \left[\frac{\sin \psi_v - \psi_v \cos \psi_v}{\psi_v (1 - \cos \psi_v)} \right]}$$

$$d = \frac{T_v r_v \left[\frac{1}{(M_f T_v + b_f) \times 10^6} \right]^{C \psi}}{D^2}$$

The new sagitta is equal to the length of the previous sagitta plus the deflection d .

The center of the radial circle is then found by methods outlined in sections A and B.

APPENDIX IV (continued)

Section E

The sagitta of the shrunken circle is found by subtracting the sum of the deflections due to constructional stretch and hydrodynamic forces from the original sagitta. The center and points of the shrunken circle are then found by methods outlined in Sections A and B.

Section F

The construction stretch of the shrunken circle is found by methods outlined in Section C. The center of this constructionally stretched shrunken circle is found by methods outlined in Sections A and B.

Section G

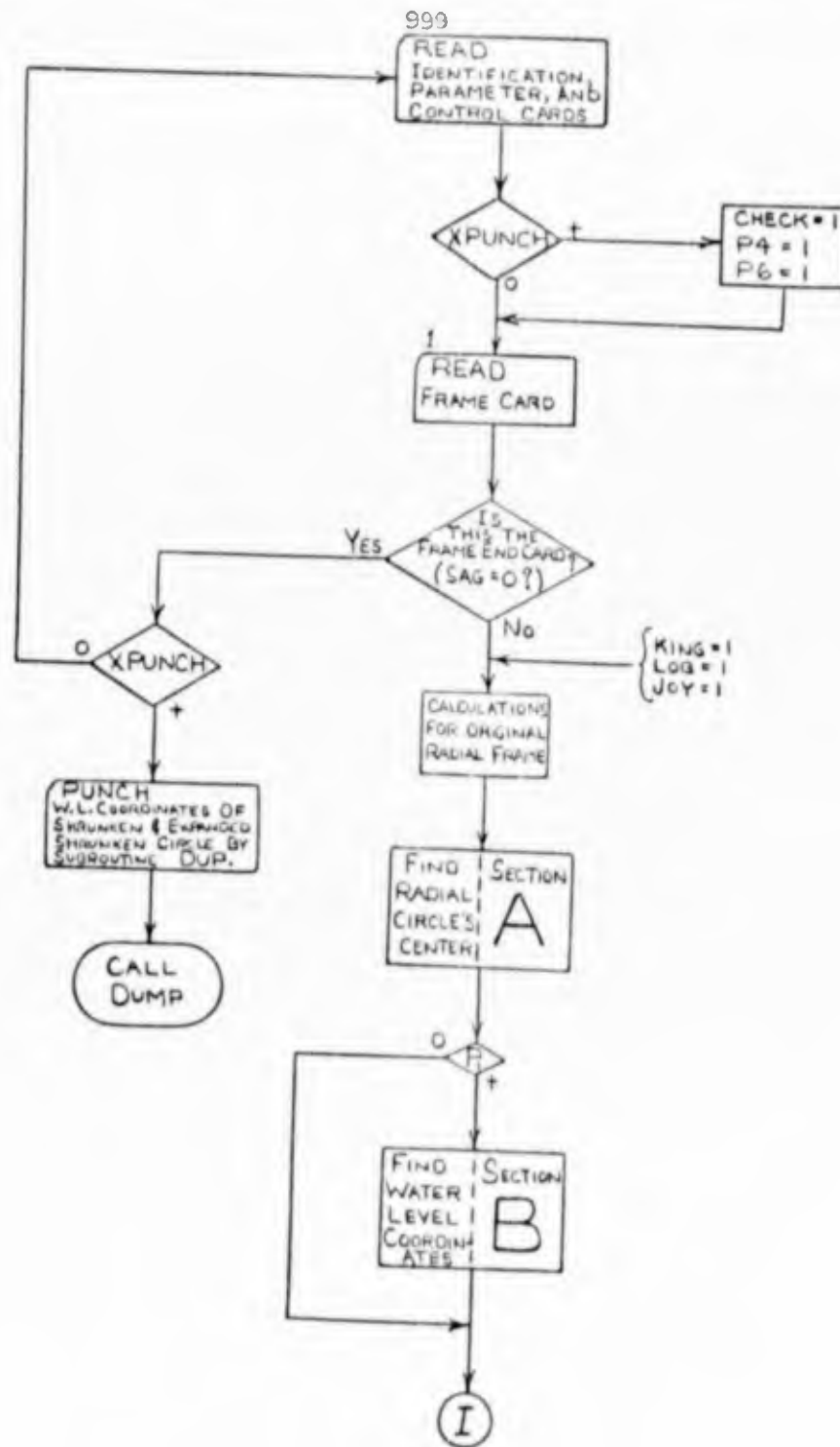
The defection due to hydrodynamic forces upon the constructionally stretched circle is found by the methods outlined in Section D. Then the center and points on this expanded shrunken circle are found by methods outlined in Sections A and B.

MACHINE REQUIREMENTS

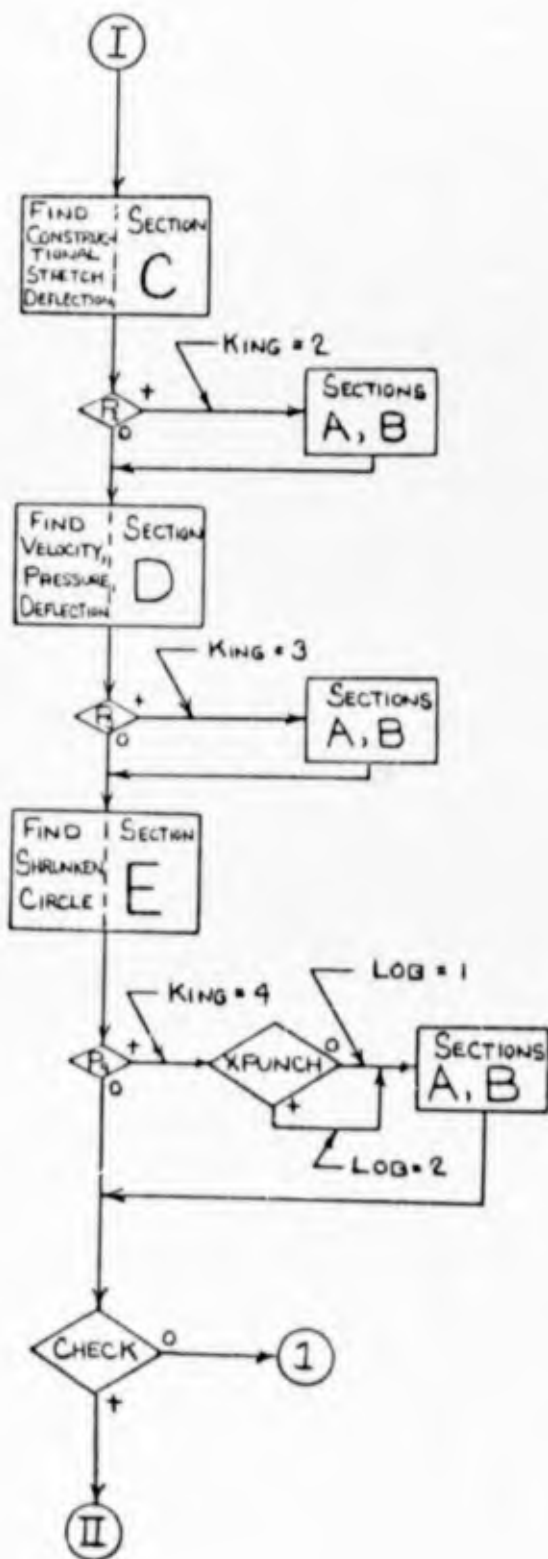
The program was written in FORTRAN II for the IBM 7074. Floating point hardware and three tape units are required.

APPENDIX IV (continued)

SIMPLIFIED FLOW CHART



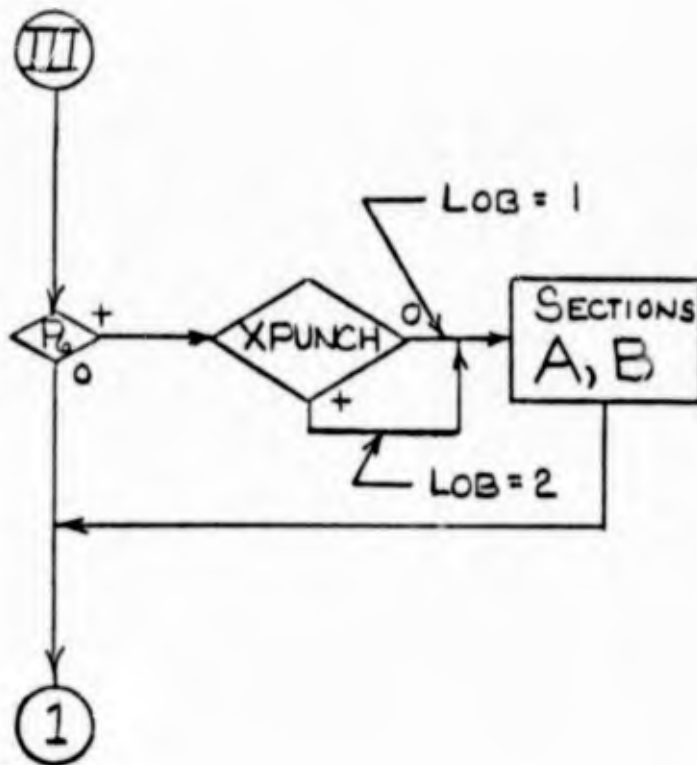
APPENDIX IV (continued)



APPENDIX IV (continued)

<u>Card Number</u>	<u>Card Type</u>	<u>Columns</u>	<u>Symbol</u>	<u>Description</u>
1	Identifi- cation	2-72	---	Any alphanumeric description of the problem.
2	Parameter Card #1			NOTE: All numbers must have decimal points.
		1-10	DEPRES	Design pressure (p.s.i.)
		11-20	DEPTH	Depth of dome (ft.)
		21-30	VEL	Ship's velocity (knots)
		31-40	VPL	Number of vertical plies.
		41-50	HPL	Number of horizontal plies.
		51-60	BETA1	Angle of vertical cables with horizontal (degrees).
		61-70	BETA2	Angle of horizontal cables with horizontal (degrees).
3	Parameter Card #2			NOTE: All numbers must have decimal points.
		1-10	CPI	Number of cables per inch of ply.
		11-20	DIA	Cable nominal diameter (inches).
		21-30	ACON	Slope } Constructional stretch factors
		31-40	BCON	
		41-50	FM	Slope } Elastic stretch factors
		51-60	FB	
		61-70	DELWL	Distance between water levels on radial frames coordinates which are desired in the out- put (inches). (See Note I at the end of this section for further explanation.

APPENDIX IV (continued)



APPENDIX IV (continued)

INPUT DESCRIPTION

The input for each problem consists of five types of cards placed in the order listed below:

<u>Type</u>	<u>Number of Cards</u>	<u>Description</u>
Identification Card	1	The user may place any comment on this card. It is usually used to identify the particular problem being run.
Parameter Cards	3	These cards contain information about the dome being studied, such as design pressure, cable diameter, specific gravity of fluid, etc.
Control Card	1	The control numbers placed on this card determine the type of output desired by the user. It will let the user decide, for example, whether or not he wants the points on the constructionally stretched circle printed out, or just that circle's center and radius.
Frame Card(s)	One card for each frame studied.	Information about a frame is contained on this card, such as the coordinates of its bead points.
Frame End Card	1	This card is placed after the last frame card. It contains zeros in columns 1-5.

If a second problem is to be run, for example on the dome at a different pressure, the cards for the second problem follow directly behind the cards of the first problem. All five types of cards must be used in the second problem.

Additional problems may be run by placing the cards behind the cards of the preceding problems.

The input data is placed on the cards in the following manner:

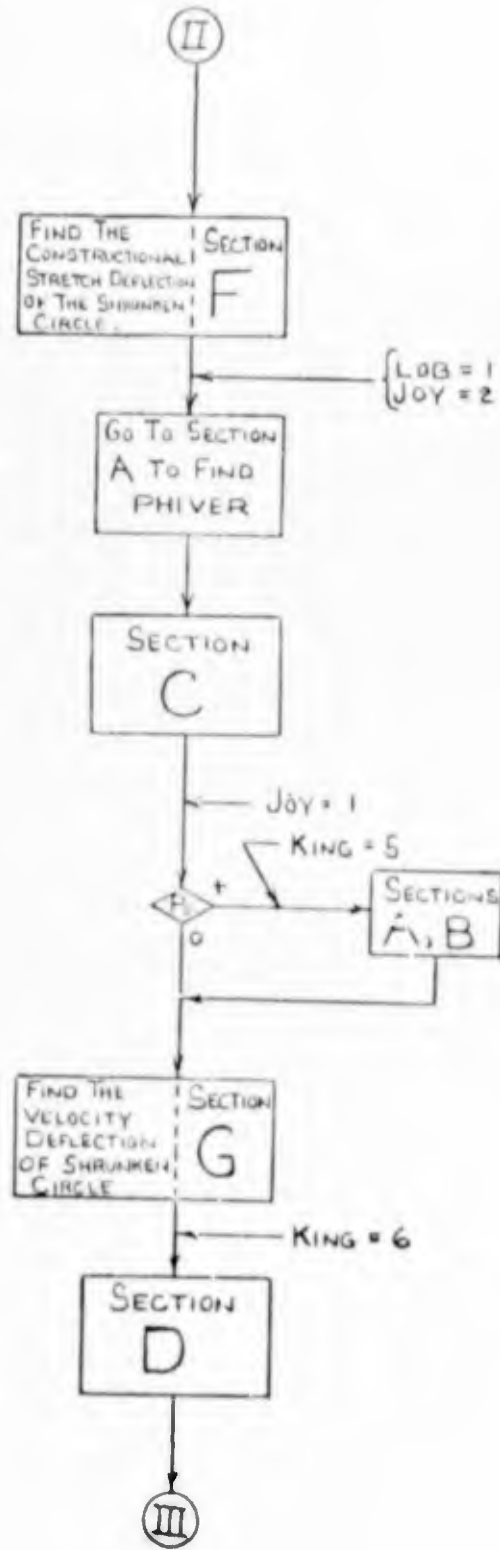
APPENDIX IV (continued)

<u>Card Number</u>	<u>Card Type</u>	<u>Columns</u>	<u>Symbol</u>	<u>Description</u>
		35	CHECK	Place a 1 in this column to expand the shrunken circle, that is, to find the constructionally stretched shrunken circle and the expanded shrunken circle; zero otherwise.
		40	XPUNCH	Place a 1 in this column to punch out points on the shrunken circle and the expanded shrunken circle; zero otherwise. (See Note II at the end of this section for restrictions).
<hr/>				
6 thru n + 5	Frame			NOTE: All numbers have decimal points except the number placed in columns 1-3.
(n is the num- ber of frames studied.)		1-3	NO	The frame number (no decimal point, right justified).
		4-10	XP	The x-coordinate of point P, the point of maximum breadth on the radial frame (inches).
		11-17	XA	x-coordinate of upper bead (inches). (See Note III at the end of this section for the definition of "upper" and "lower" bead and restrictions.) (See Note IV for description of and restrictions on the x-y-z coordinate system.)
		18-24	YA	y-coordinate of upper bead (inches).
		25-32	ZA	z-coordinate of upper bead (inches).
		33-39	XB	x-coordinate of lower bead (inches).

APPENDIX IV (continued)

<u>Card Number</u>	<u>Card Type</u>	<u>Columns</u>	<u>Symbol</u>	<u>Description</u>
4	Parameter Card #3			NOTE: All numbers must have decimal points.
		1-10	WLBEG	The begging (lowest) water level on a radial frame, (inches). (See Note I at the end of this section for further explanation.)
		11-20	SG	The specific gravity of the fluid in which the dome is immersed.
<hr/>				
5	Control Card			NOTE: No decimal points are punched on this card.
		5	P1	Place a 1 in this column to print out points on the original radial circle; zero otherwise.
		10	P2	Place a 1 in this column to print out points on the constructionally stretched radial circle; zero otherwise.
		15	P3	Place a 1 in this column to print out points on the circle expanded by hydrodynamic forces; zero otherwise.
		20	P4	Place a 1 in this column to print out the points on the shrunken circle, zero otherwise.
		25	P5	Place a 1 in this column to print out the points on the constructionally stretched shrunken circle; zero otherwise.
		30	P6	Place a 1 in this column to print out the points on the expanded shrunken circle; zero otherwise.

APPENDIX IV (continued)



APPENDIX IV (continued)

<u>Card Number</u>	<u>Card Type</u>	<u>Columns</u>	<u>Symbol</u>	<u>Description</u>
		40-46	YB	y-coordinate of lower bead (inches).
		47-54	ZB	z-coordinate of lower bead (inches).
		55-61	SAG	Frame sagitta (inches). (See Note V for definition of sagitta).
		62-66	COE	Coefficient of pressure.
		67-72	HORAD	Horizontal radius (inches).
n + 6	Frame End Card	1-5	--	Zeros in columns 1-5.

(n is the number of frames studied.)

APPENDIX IV (continued)

Identification Card

Column	Format	Comments
CARD 1		
2-72 71H....		
PROBLEM IDENTIFICATION (Any title may be written in these columns, such as, for example, "DL-5 Coordinates when under pressure")		
Symbol		

Parameter Card 1

Column	Format	Comments
CARD 2		
1-10	F10.0	Design Pressure (p.s.f.)
11-20	F10.0	Depth of Doms (ft.)
21-30	F10.0	Ship's Velocity (knots)
31-40	F10.0	Number of vertical piles
41-50	F10.0	Number of horizontal piles
51-60	F10.0	Angle of vertical cables with horizontal (degrees)
61-70	F10.0	Angle of horizontal cables with horizontal (degrees)
DEPRES	DEPTH	VEL
		VPL
		HPL
		VERTAL
		HRTAL
Symbol		

Parameter Card 2

Column	Format	Comments
CARD 3		
1-10	F10.0	Cables per inch of ply
11-20	F10.0	Cable nominal diameter (inches)
21-30	F10.0	Constructional Stretch Factors
31-40	F10.0	Stretch Intercept
41-50	F10.0	Elastic Stretch Factors
51-60	F10.0	Stretch Intercept
61-70	F10.0	Distance between rated levels in grid (inches)
CPI	DIA	ADN
		BCN
		EL
		ER
		DELVL
Symbol		

APPENDIX IV (continued)

Parameter
 Card 3

Column	1-10	11-20	CARD 4	
Format:	F10.0	F10.0		
Comments	Beginning (lowest) water level (inches)	Specific Gravity of fluid		
Symbol	1125G	2G		

Control
 Card

Column	1-5	6-10	11-15	16-20	21-25	26-30	31-35	36-40
Format:	F5.0	F5.0	F5.0	F5.0	F5.0	F5.0	F5.0	F5.0
Comments	P1 to P5 print punch points on original in order of punch, zero otherwise.	P6 to P10 print punch points on original in order of punch, zero otherwise.	P11 to P15 print punch points on original in order of punch, zero otherwise.	P16 to P20 print punch points on original in order of punch, zero otherwise.	P21 to P25 print punch points on original in order of punch, zero otherwise.	P26 to P30 print punch points on original in order of punch, zero otherwise.	P31 to P35 print punch points on original in order of punch, zero otherwise.	P36 to P40 print punch points on original in order of punch, zero otherwise.
Symbol	P1	P2	P3	P4	P5	P6	P7	P8

Prime
 Card(s)
 (n = num-
 ber of
 traces)

Column	1-3	4-10	11-17	18-24	25-32	33-39	40-46	47-54	55-61	62-66	67-72
Format:	I3	F7.0	F7.0	F7.0	F8.0	F7.0	F7.0	F8.0	F7.0	F5.0	F6.0
Comments	Prime no., x-coor- dinate of right max. break- point (inches)	Prime no., x-coor- dinate of right max. break- point (inches)	Upper East Coordinates (inches)	Upper East Coordinates (inches)	Upper East Coordinates (inches)	Lower East Coordinates (inches)	Lower East Coordinates (inches)	Lower East Coordinates (inches)	Sagitta (inches)	Coeff- ficient of pressure	Horizon. radius at midpoint of trace (inches)
Symbol	N0	XP	XA	YA	ZA	XB	YB	ZB	SAG	COE	HRAD

CARD 6 through CARD (n + 5)

Contract NObsr 89483
 Serial No. SS041-001
 Task 8156

Report No. 17
 Phase I Interim Report
 30 September 1964

APPENDIX IV (continued)

Prase
 End
 Card

Column	1-5	CARD n + 6
Format		
Comments	Place zeros in these columns.	
Symbol		

Column	CARD
Format	
Comments	
Symbol	

Column	CARD
Format	
Comments	
Symbol	

APPENDIX IV (continued)

NOTES ON INPUT

NOTE I

Explanation of "distance between water levels" and "beginning water level."

The program finds the coordinates of points on the radial frame. These two variables, denoted by "DELWL" and "WLBEG" respectively, determine the z-coordinates or "water levels" of the points which will be found.

Example: Assume the upper and lower bead points are at water levels 9.8 and 1.7 feet respectively, and we want the points on the radial frame $1\frac{1}{2}$ feet apart, beginning at water level 1. That is, we want points at the following water levels:

1, $2\frac{1}{2}$, 4, $5\frac{1}{2}$, ... (feet)

All measurements are in inches, so the desired water levels would be

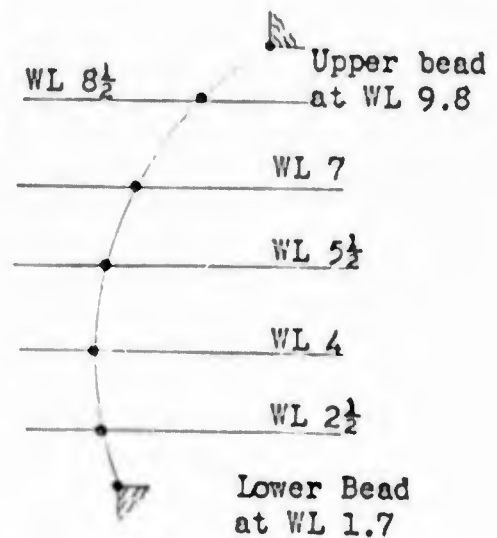
12, 30, 48, 66, ... (inches)

Therefore, we use the following values for the variables:

WLBEG = 12.

DELWL = 18.

The coordinate of the first point to be printed out would be of the point whose water level is $2\frac{1}{2}$. The 1 foot water level point would not print out since it is below the lower bead. The last point to print out would have a water level of $8\frac{1}{2}$.



NOTE II

Restrictions on program when results are to be punched out (XPUNCH = 1).

If the results of a problem are to be punched out, it is not permissible to run another problem after this problem.

NOTE III

Distinction between upper and lower beads and restriction.

The bead with the greatest water level (greatest z-coordinate) is the upper bead.

APPENDIX IV (continued)

NOTE III (Continued)

Examples:

- a) If the water levels of the beads are + 10.3 and + 1.3, the bead at water level + 10.3 would be the upper bead since $10.3 > 1.3$.
- b) If the water levels of the beads are - 10.3 and - 1.3, the bead at water level -1.3 would be the upper bead since $- 1.3 > - 10.3$.

Restriction: The x and y-coordinates of the beads may not be equal.

NOTE IV

Description of the coordinate system.

The x-y plane is parallel to the plane of the water. The z-axis is perpendicular to the plane of the water.

NOTE V

Definition of sagitta.

The distance between the mid-point of an arc and the mid-point of its chord in a circle. (Line CT in Figure 6)

APPENDIX IV (continued)

OUTPUT DESCRIPTION

A list of the output from the program follows. Note the optional print-outs which depend upon the values entered on the control card.

1. The input data - which was placed on the parameter cards.

The following is printed out for each frame.

2. The original radial frame (circle) - The frame number, coefficient of pressure, horizontal radius, sagitta, and the upper and lower bead coordinates, which were read from the frame card, are printed. The circle radius and coordinates of the circle center, which were calculated, are printed.

Optional print out if P1 = 1 - The coordinates of the points on the radial circle at water levels determined by variables WLBEQ and DELWL. (See input description)

3. The circle after constructional stretch - The frame number, deflection, sagitta and horizontal and vertical radii are printed.

Optional print out if P2 = 1 - The coordinates of the center and points on the circle.

4. The circle after constructional stretch and velocity deflection (hydrodynamic force deflection) - The frame number, additional deflection, sagitta, vertical radius, and the horizontal and vertical deflections are printed.

Optional print out if P3 = 1 - The coordinates of the center and points on the circle.

5. The shrunken circle (the corrected circle) - The radius and sagitta are printed out.

Optional print out if P4 = 1 - The coordinates of the center and points on the circle (Note: - This is punched if XPUNCH = 1).

Option - The program prints the output described below if CHECK = 1; otherwise it will do the calculations for the next frame.

6. The shrunken circle after constructional stretch - The frame number, deflection, sagitta, and horizontal and vertical radii are printed.

Optional print-out if P5 = 1 - The coordinates of the center and points of the circle.

APPENDIX IV (continued)

7. The shrunken circle after constructional stretch and velocity deflection (hydrodynamic force deflection), the expanded shrunken circle - The frame number, additional deflection, sagitta, vertical radius, and the horizontal and vertical tensions are printed.

Optional print-out if P6 = 1 - The coordinates of the center and points on the circle (Note: This is punched if XPUNCH = 1).

SAMPLE PROBLEM

The input and output of a sample problem follows.

Note that for this problem only one frame was studied, so there is only one frame card. In practice there are usually many frames to be studied, which would mean that there would be many frame cards.

All variables were given a value of 1 on the control card, so the example gives the maximum amount of print-out and in addition, the punch-out.

SAMPLE INPUT

SAMPLE PROBLEM

40.	30.	20.	3.	2.	90.	15.
14.	.048	.00204	.188	.01181	1.782	6.
-96.	1.03					
1	1	1	1	1	1	1
12 67.437	76.875	85.50	-9.000	80 750	77.25	-95.312 25.9375 -.28 2300.
00000						

Contract NObsr 89483
Serial No. SS041-001
Task 8156

- 58 -

Report No. 17
Phase I Interim Report
30 September 1964

APPENDIX IV (continued)

ILSI RUN PRIOR PROGRAM DICK BECK 219
21 MAY 1964 DATE THURSDAY 9.00 RUN
SAMPLE PROBLEM

INPUT DATA

DESIGN PRESSURE # 40.000
DEPTH # 30.000
VELOCITY %KNOTS # 20.000
VERTICAL PLIES # 3.000
HORIZONTAL PLIES # 2.000
BETA1 %DEGREES # 90.000
BETA2 %DEGREES # 15.000
CABLES PER INCH # 14.000
CABLE DIAMETER # 0.048

CONSTRUCTIONAL STRETCH FACTORS

SLOPE # 0.002
INTERCEPT # 0.185

T VS. $1/\%F \cdot 10^{+6}$

SLOPE # 0.012
INTERCEPT # 1.782

SPECIFIC GRAVITY OF FLUID # 1.030

Contract NObsr 89483
Serial No. SS041-001
Task 8156

- 59 -

Report No. 17
Phase I Interim Report
30 September 1964

APPENDIX IV (continued)

ORIGINAL RADIAL CIRCLE NO. 12

COEF. OF PRESSURE # -0.280

HORIZONTAL RADIUS # 2300.000

VERTICAL RADIUS # 49.272

SAGITTA # 25.938

	X	Y	Z
UPPER HEAD	76.875	85.500	-9.000
LOWER HEAD	80.750	17.250	-95.312
CIRCLE CENTER	88.678	60.371	-49.705

POINTS ON
RADIAL CIRCLE

76.623	86.037	-90.000
73.638	92.393	-84.000
71.529	96.882	-78.000
69.998	100.142	-72.000
68.909	102.459	-66.000
68.193	103.984	-60.000
67.310	104.799	-54.000
67.143	104.942	-48.000
67.088	104.420	-42.000
68.557	103.208	-36.000
69.479	101.247	-30.000
70.807	98.418	-24.000
72.644	94.509	-18.000
75.194	89.080	-12.000

APPENDIX IV (continued)

EFFECT OF CONSTRUCTIONAL STRETCH, CIRCLE NO. 12

DEFLECTION	#	0.286
SAGITTA	#	26.224
VERTICAL RADIUS	#	49.018
HORIZONTAL RADIUS	#	2300.286

	X	Y	Z
CIRCLE CENTER	88.450	60.857	-49.762
	76.548	86.196	-90.000
	73.536	92.608	-84.000
	71.415	97.123	-78.000
	69.278	100.397	-72.000
	68.787	102.720	-66.000
	68.070	104.246	-60.000
	67.688	105.059	-54.000
	67.624	105.156	-48.000
	67.873	104.665	-42.000
	68.448	103.440	-36.000
	69.279	101.459	-30.000
	70.720	98.603	-24.000
	72.577	94.651	-18.000
	75.162	89.146	-12.000

APPENDIX IV (continued)

CIRCLE NUMBER 12
EFFECT OF VELOCITY DEFLECTION PLUS CONSTRUCTIONAL STRETCH

ADDITIONAL DEFLECTION#		0.502
SAGITTA	#	26.725
VERTICAL RADIUS	#	42.595
VERTICAL TENSION	#	33.591
HORIZONTAL TENSION	#	0.903

	X	Y	Z
CIRCLE CENTER	88.058	61.691	-49.859
	76.414	36.481	-90.000
	73.357	92.991	-84.000
	71.215	97.550	-78.000
	69.668	100.844	-72.000
	68.572	103.178	-66.000
	67.854	104.707	-60.000
	67.474	105.515	-54.000
	67.414	105.643	-48.000
	67.(7)	105.096	-42.000
	68.257	103.842	-36.000
	69.203	101.834	-30.000
	70.567	98.930	-24.000
	72.458	94.903	-18.000
	75.107	89.265	-12.000

Contract NObsr 89483
Serial No. SS041-001
Task 8156

- 62 -

Report No. 17
Phase I Interim Report
30 September 1964

APPENDIX IV (continued)

CORRECTED ~~W~~STRUNKEN ~~D~~ CIRCLE NO. 12

RADIUS # 50.016
SAGITTA # 25.149

CORRECTED ~~W~~STRUNKEN ~~D~~ COORDINATES

	X	Y	Z
CIRCLE CENTER	89.226	58.992	-49.545
	76.823	85.611	-90.000
	73.913	91.807	-84.000
	71.839	96.222	-78.000
	70.326	99.443	-72.000
	69.246	101.742	-66.000
	68.532	103.262	-60.000
	68.147	104.082	-54.000
	68.072	104.241	-48.000
	68.306	103.744	-42.000
	68.857	102.571	-36.000
	69.793	100.663	-30.000
	71.045	97.913	-24.000
	72.825	94.123	-18.000
	75.277	88.902	-12.000

APPENDIX IV (continued)

-U/-

EFFECT OF CONSTRUCTIONAL STRETCH UPON SHRUNKEN CIRCLE NO. 12

DEFLECTION H 0.292
SAGITTA H 25.440
VERTICAL RADIUS H 49.732
HORIZONTAL RADIUS H 2299.503

	X	Y	Z
CIRCLE CENTER	89.083	59.509	-49.605
	76.750	65.766	-90.000
	73.812	92.022	-64.000
	71.725	96.465	-78.000
	70.205	99.701	-72.000
	69.122	102.007	-66.000
	68.407	103.529	-60.000
	68.022	104.347	-54.000
	67.951	104.500	-48.000
	68.188	103.994	-42.000
	68.746	102.806	-36.000
	69.652	100.870	-30.000
	70.957	98.099	-24.000
	72.758	94.265	-18.000
	75.247	88.967	-12.000

APPENDIX IV (continued)

EFFECT OF VELOCITY DEFLECTION PLUS CONSTRUCTIONAL STRETCH
UPON SPRUNGEN CIRCLE 12

ADDITIONAL DEFLECTION#	0.515
SAGITTA #	25.956
VERTICAL RADIUS #	49.255
VERTICAL TENSION #	34.080
HORIZONTAL TENSION #	0.927

	X	Y	Z
CIRCLE CENTER	88.663	60.402	-49.709
	76.618	86.047	-90.000
	73.631	92.406	-84.000
	71.522	96.897	-78.000
	69.590	100.158	-72.000
	68.902	102.476	-66.000
	68.185	104.001	-60.000
	67.803	104.815	-54.000
	67.736	104.958	-48.000
	67.981	104.435	-42.000
	68.550	103.223	-36.000
	69.473	101.260	-30.000
	70.802	98.430	-24.000
	72.439	94.518	-18.000
	75.192	89.034	-12.000

APPENDIX IV (continued)

THE FOLLOWING OUTPUT WAS PUNCHED.

CORRECTED (SHRUNKEN) COORDINATES

76.823	85.611	-90.000
73.913	91.807	-84.000
71.839	96.222	-78.000
70.326	99.443	-72.000
69.246	101.742	-66.000
68.532	103.262	-60.000
68.147	104.082	-54.000
68.072	104.241	-48.000
68.306	103.744	-42.000
68.857	102.571	-36.000
69.753	100.663	-30.000
71.045	97.913	-24.000
72.825	94.123	-18.000
75.277	88.902	-12.000

EFFECT OF VELOCITY DEFLECTION PLUS CONSTRUCTIONAL STRETCH UPON SHRUNKEN
CIRCLE 12

70.618	86.047	-90.000
73.631	92.406	-84.000
71.522	96.897	-78.000
69.990	100.158	-72.000
68.902	102.476	-66.000
68.185	104.001	-60.000
67.803	104.815	-54.000
67.736	104.958	-48.000
67.981	104.435	-42.000
68.550	103.223	-36.000
69.473	101.260	-30.000
70.802	98.430	-24.000
72.639	94.518	-18.000
75.192	89.084	-12.000

kg

BLANK PAGE

APPENDIX V
STRESS CALCULATION ON SEAMING SECTION OF PANEL MOLD

The center line of the mold splice section shown in B.F. Goodrich Drawing No. 1009 is plotted in Figure 1; the cross section and its properties are shown in Figure 2.

To expedite the analysis the exterior flange of the mold splice section is assumed to be an arch and is considered in two portions. Refer to Figure 3. Portion AD is approximated by small straight line segments and portion DBC is approximated by a portion of circular arc. Also two further assumptions are made. (1) The structure is a hinged end arch with frictionless hinges which prevent lateral deformation. (2) The structure is made of a material which follows Hook's Law. The lateral component of the hinge reaction is found by using Castigliano's Theorem. This theorem is mathematically stated as follows:

$$\delta_h = \frac{\partial U}{\partial H}$$

$$U = \int_L \frac{N^2 ds}{2EA} + \int_L \frac{M_B^2 ds}{2EI} + \int_L \frac{V^2 ds}{2e_7 A} + \int_L \frac{M_T^2 ds}{2GJ}$$

U is the strain energy stored in the structure. The first term in U is the normal deformation contribution. The second term is the bending deformation contribution. The third term is the shear deformation contribution, and the fourth term is the twisting deformation contribution.

δ_h is the horizontal deformation of the hinge which is assumed to be zero and H is the lateral reaction component of the hinge.

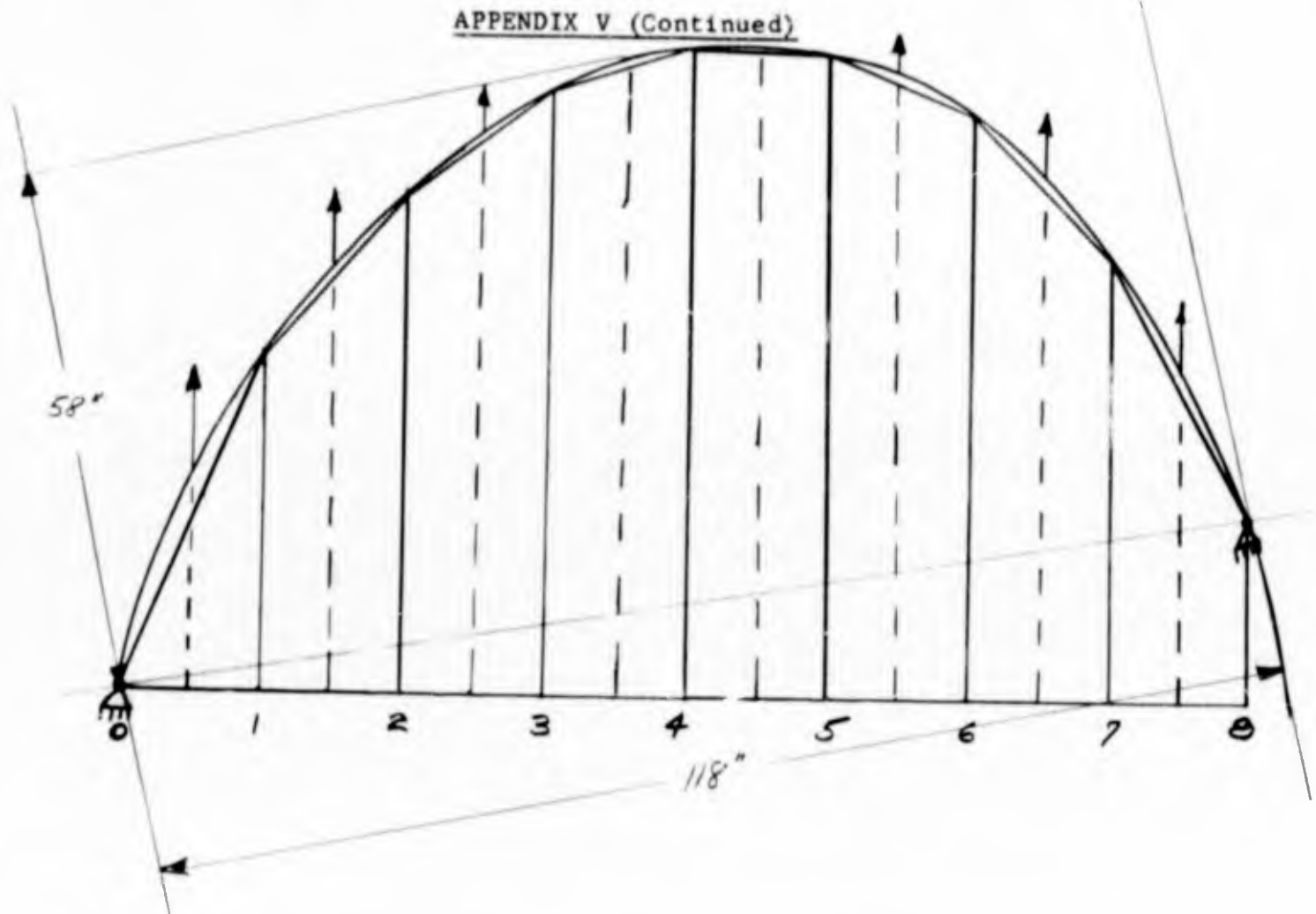
The structure is not subjected to torque, therefore

$$\int_L \frac{M_T^2 ds}{2GT} = 0; \quad \text{and} \quad \int_L \frac{V^2 ds}{2GA} \text{ is neglected}$$

because its contribution for this type of structure is in the order of 1%. Then the theorem reduces to:

$$\delta_h = 0 = \frac{\partial U}{\partial H} = \frac{\partial}{\partial H} \left[\int_L \frac{N^2 ds}{2EA} + \int_L \frac{M_B^2 ds}{2EI} \right]$$

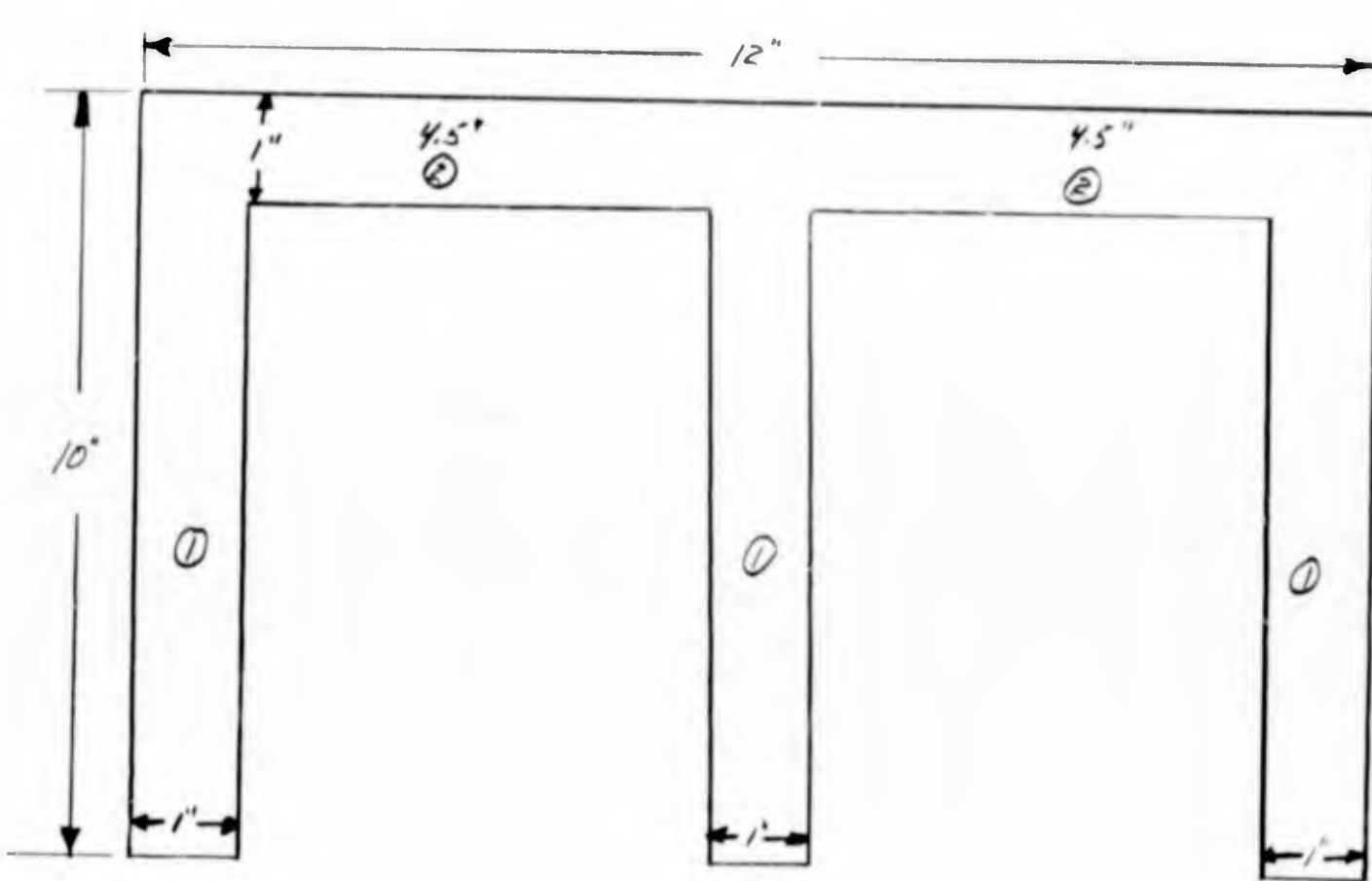
The details for the above calculation are given below.



STATION	X	Y ₁	Y ₂	\bar{Y}	ds
0-1	15	0	35.5	17.8	38.5
1-2	30	35.5	53.5	44.5	23.5
2-3	45	53.5	64.5	59.0	18.5
3-4	60	64.5	69.5	67.0	16.0
4-5	75	69.5	68.5	69.0	15.0
5-6	90	68.5	62.0	65.3	16.5
6-7	105	62.0	49.5	53.3	23.0
7-8	116	44.5	21.	32.5	26.5

FIGURE 1
ARCH CENTER LINE GEOMETRY AND COORDINATES

APPENDIX V (Continued)



SEGMENT	DIMENSION	A	Y	AY	d	d ²	Ad ²	I _{oo}
①	3 x 10 x 1	30	5	150	1.04	1.08	32.5	83.3
②	2 x 4.5 x 1	9	.5	4.5	3.46	12.0	108.0	0.8
Σ		39		154.5			140.5	84.1

$$\bar{Y} = \frac{\sum AY}{\sum A} = \frac{154.5}{39} = 3.96; \quad I = \sum Ad^2 + \sum I_{oo} = 140.5 + 84.1 = 224.6 \text{ in}^3$$

$$Y_{top} = 6.04"; \quad Y_{bot} = 3.96"; \quad S_{top} = \frac{I}{Y_{top}} = 37.3 \text{ in}^2; \quad S_{bot} = \frac{I}{Y_{bot}} = 56.8 \text{ in}^2$$

$$r = \sqrt{\frac{I}{A}} = 2.4 \text{ in}$$

FIGURE 2
 SECTION AND PROPERTIES

APPENDIX V (Continued)

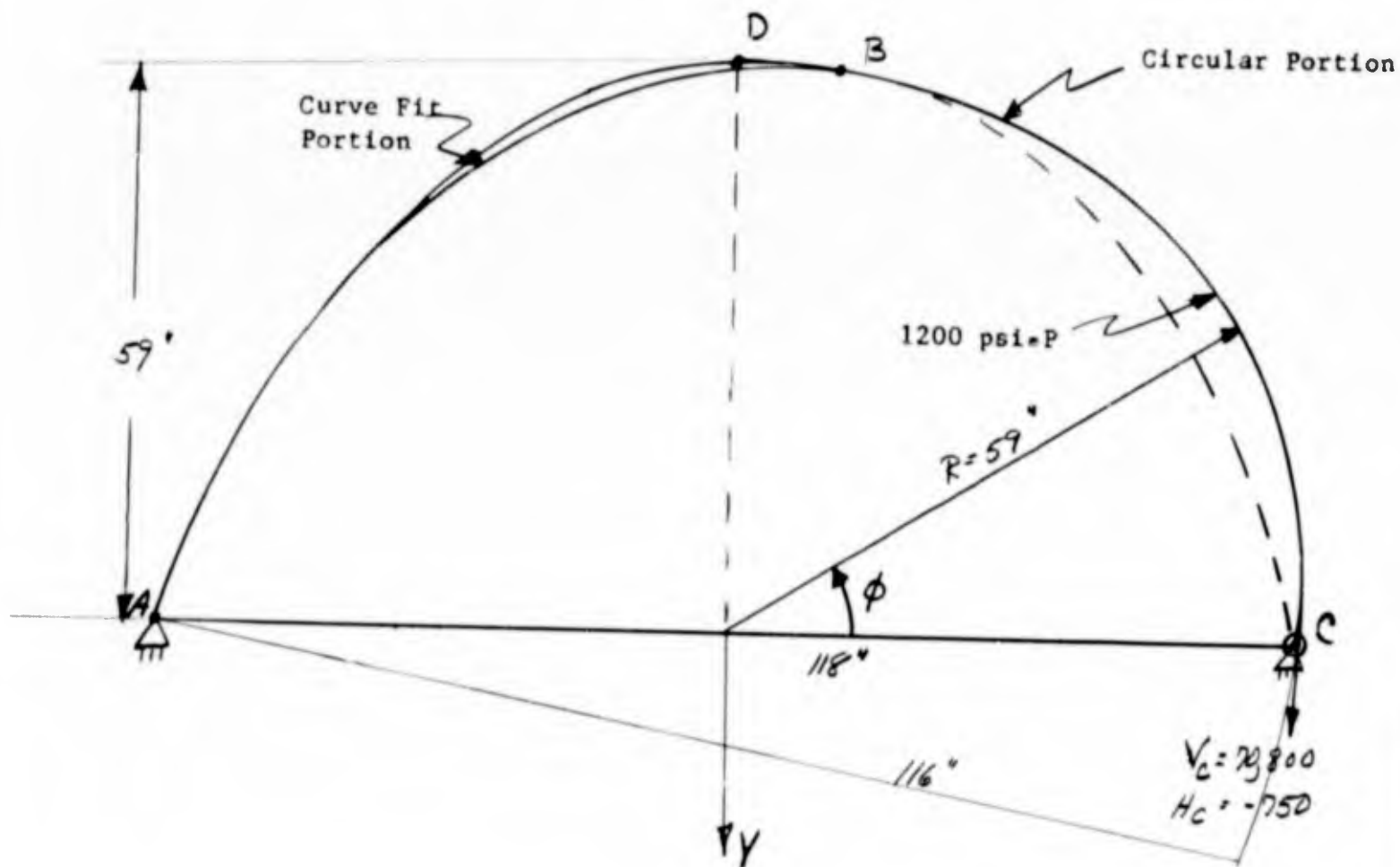


FIGURE 3
APPROXIMATIONS FOR ANALYSIS

APPENDIX V (Continued)

For Portion DBC (Figure 3)

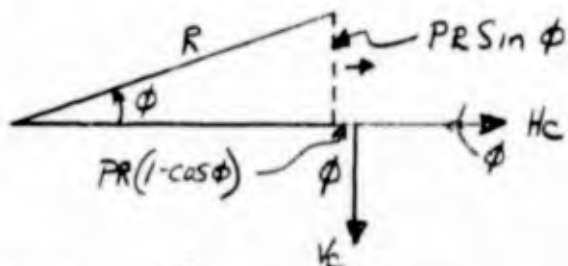
Geometry $R \approx 59$; $\theta \approx 90^\circ$

Vertical Reactions:

$$V_A \approx V_C \approx \frac{118 \times 1200}{2} = 70,800 \text{ lbs.}$$

Choose Redundant Force H. As Shown in Figure Below.

Moment At θ :



$$\begin{aligned} M_\theta &= V_C R(1 - \cos\theta) - PR^2(1 - \cos\theta) - H_C R \sin\theta \\ &= R(1 - \cos\theta)(V_C - PR) - H_C R \sin\theta \\ &= -H_C R \sin\theta \end{aligned}$$

Normal Force At θ :

$$\begin{aligned} N_\theta &= (V_C - PR(1 - \cos\theta)) \cos\theta + (H_C + PR \sin\theta) \sin\theta \\ &= V_C \cos\theta + PR(-\cos\theta + \cos^2\theta + \sin^2\theta) + H_C \sin\theta \\ &= PR + H_C \sin\theta \end{aligned}$$

Shear Force At θ

$$\begin{aligned} Q_\theta &= -[V_C - PR(1 - \cos\theta)] \sin\theta + [H_C + PR \sin\theta] \cos\theta \\ &= [-V_C + PR] \sin\theta - PR \cos\theta \sin\theta + PR \sin\theta \cos\theta + H_C \cos\theta \\ &= H_C \cos\theta \end{aligned}$$

APPENDIX V (Continued)

Summary of equations for portion DBC:

$$M_{\theta} = -HR \sin \theta$$

$$N_{\theta} = PR + H \sin \theta$$

$$Q_{\theta} = H \cos \theta$$

H Assumed pulling away from the hinge.

Portion AD (Figures 3 and 4)

At Section 1-1.

$$\sum F_y = 0:$$

$$V_A - p(a-x) - N_{\theta} \sin \theta - Q_{\theta} \cos \theta = 0$$

$$\sum F_x = 0:$$

$$H_A + P(h-y) - N_{\theta} \cos \theta + Q_{\theta} \sin \theta = 0$$

Eliminate Q_{θ} from the above equations:

$$[V_A - P(a-x)] \sin \theta - N_{\theta} \sin^2 \theta + Q_{\theta} \cos \theta \sin \theta = 0$$

$$[H_A + P(h-y)] \cos \theta - N_{\theta} \cos^2 \theta + Q_{\theta} \sin \theta \cos \theta = 0$$

$$- N_{\theta} (\sin^2 \theta + \cos^2 \theta) + [V_A - P(a-x)] \sin \theta + [H_A + P(h-y)] \cos \theta = 0$$

$$N_{\theta} = V_A \sin \theta - p a \sin \theta + P x \sin \theta + H_A \cos \theta + p h \cos \theta - p y \cos \theta = 0$$

$$= H_A \cos \theta + p(x \sin \theta - y \cos \theta + h \cos \theta)$$

$$= H_A \cos \theta + p [x \sin \theta + (h-y) \cos \theta]$$

Shear Force At Section 1-1.

$$V_A - p(a-x) - N_{\theta} \sin \theta + Q_{\theta} \cos \theta = 0$$

$$H_A + p(h-y) - N_{\theta} \cos \theta + Q_{\theta} \sin \theta = 0$$

APPENDIX V (Continued)

Eliminate N_o From The Above Equations:

$$[V_A - p(a-x)] \cos\theta - N_o \sin\theta \cos\theta + Q_o \cos^2\theta = 0$$

$$[H_A + p(h-y)] \sin\theta - N_o \cos\theta \sin\theta + Q_o \sin^2\theta = 0$$

$$[V_A - p(a-x)] \cos\theta - [H_A + p(h-y)] \sin\theta + Q_o (\cos^2\theta - \sin^2\theta) = 0$$

$$(V_A - pa) \cos\theta - p [\chi \cos\theta - (h-y) \sin\theta] - H_A \sin\theta + Q_o (\cos^2\theta - \sin^2\theta) = 0$$

$$Q_o = \frac{1}{\cos^2\theta} \left\{ H_A \sin\theta - p [\chi \cos\theta - (h-y) \sin\theta] \right\}$$

Also

$$Q_o = H_A \csc\theta + N_o \tan\theta - p(h-y) \csc\theta$$

Moment at Section 1-1.

$$\sum M = M_o = V_A (a-x) - H_A (h-y) - \int_0^2 (pd) ds.$$

Summary of Equations Portion AD (Curve fit approx.)

$$M_o = V_A (a-x) - H_A (h-y) - \int_0^2 (pd) ds$$

$$N_o = H_A \cos\theta + p [\chi \sin\theta + (h-y) \cos\theta]$$

$$Q_o = \sec^2\theta \left\{ H_A \sin\theta - p [\chi \cos\theta - (h-y) \sin\theta] \right\}$$

$$Q_o = H_A \csc\theta + N_o \tan\theta - p(h-y) \csc\theta$$

(Measured From D)

APPENDIX V (Continued)

The Energy Stored in The Structure is

$$U = \int_A^D \frac{1}{2EI} M_o^2 ds + \int_A^D \frac{1}{2EA} N_o^2 ds + \int_D^C \frac{1}{2EI} M_o^2 ds + \int_D^C \frac{1}{2EA} N_o^2 ds$$

$$\frac{\partial U}{\partial H} = \int_A^D \frac{1}{EI} M_o \frac{\partial M_o}{\partial H} ds + \int_A^D \frac{1}{EA} N_o \frac{\partial N_o}{\partial H} ds + \int_D^C \quad \text{(Circular Portion)}$$

$$\frac{\partial M_o}{\partial H} = -(h-y)$$

$$\frac{\partial N_o}{\partial H} = \cos\theta$$

$$\frac{\partial U}{\partial H} = \frac{1}{EI} \int_A^D \left[V_A (a-x) - H_A (h-y) - \int_0^x p dds \right] [-(h-y)] ds$$

$$+ \frac{1}{EA} \int_A^D \left\{ H_A \cos\theta + p [x \sin\theta + (h-y) \cos\theta] \right\} \cos\theta ds$$

$$+ \frac{\pi R^3}{EI} H_A + \frac{\pi R}{EA} H_A + \frac{2PR^2}{EA} = 0$$

The first two integrals are evaluated numerically using Figures 4 and 5 and Table I.

From the circular portion DBA substituting numerical values we obtain:

$$\frac{\pi R^3}{EI} H_A + \frac{\pi R}{EA} H_A + \frac{2PR^2}{EA}$$

$$= \frac{645,000}{EI} H_A + \frac{185}{EA} H_A + \frac{6940 P}{EA}$$

APPENDIX V (Continued)

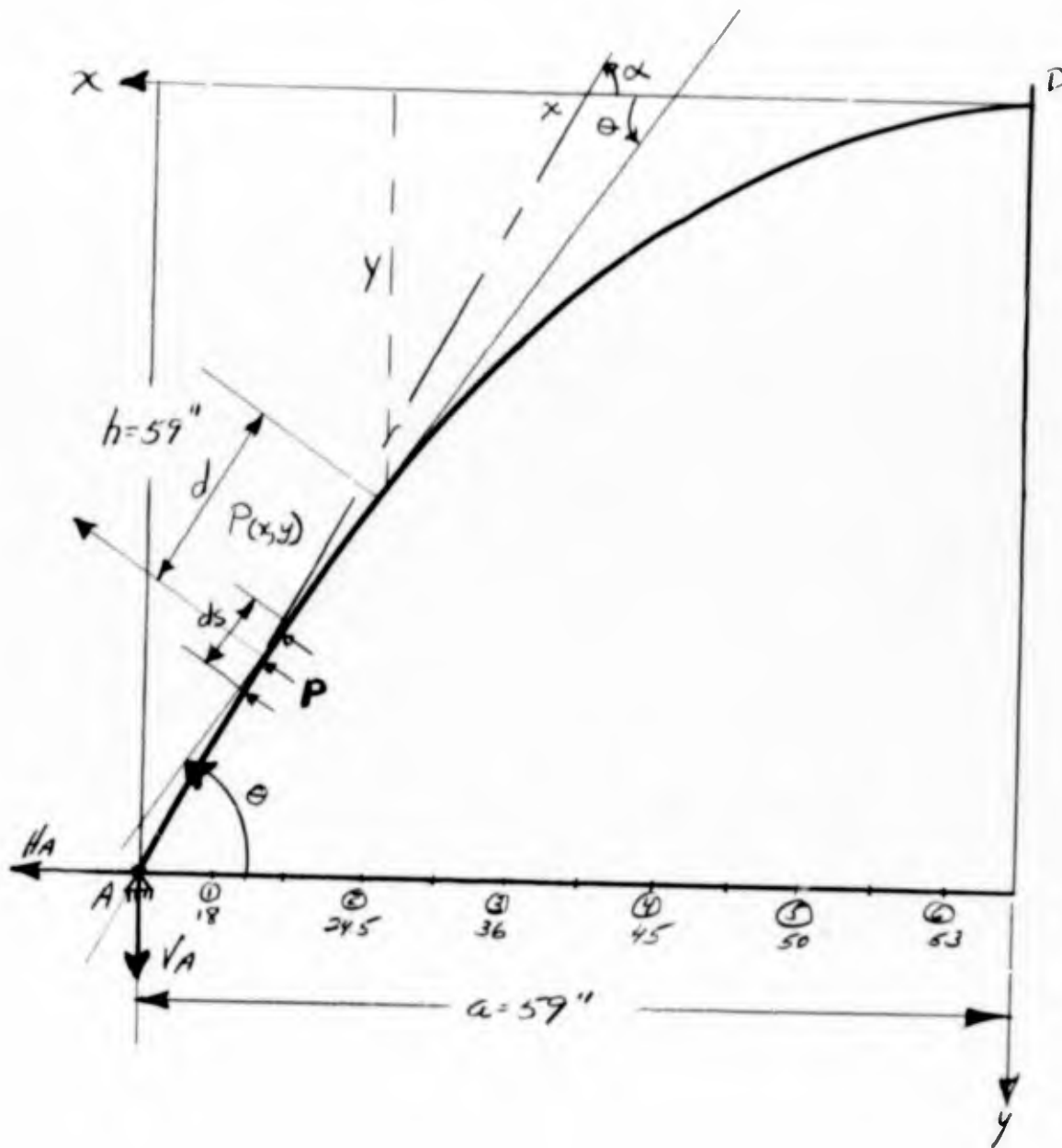
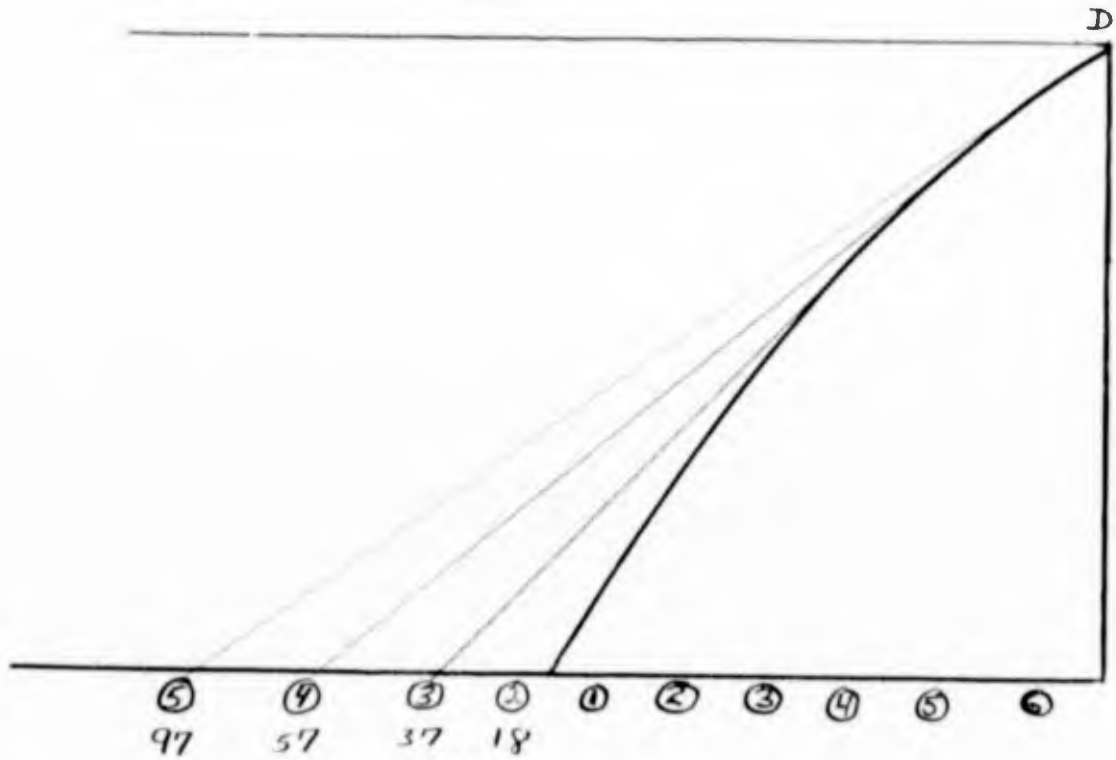


FIGURE 4
 FORCE EQUILIBRIUM PORTION AD

APPENDIX V (Continued)



	①		②		③		④		⑤		⑥		$\sum dds$
	d	ds	d	ds	d	ds	d	ds	d	ds	d	ds	
1	10	10											100
2	18	20	8.5	8.5									432
3	33.5	20	16.	17.	7.5	7.5							998
4	47	20	30.	17.	15.0	15	6.5	6.5					1717
5	58.5	20	41.5	17.	26.5	15	13.	13.	5.5	5.5			2473
6	68.0	20	51.	17.	37.	15	23.	13.	12.0	11	5	5	3240

FIGURE 5
FIGURE AND TABLE TO AID NUMERICAL INTEGRATION

APPENDIX V (Continued)

TABLE I
NUMERICAL INTEGRATION CALCULATIONS

<i>Station</i>	x	a-x	h-y	y	ds	COSθ	SINθ	(h-y)ds	COSθds
①	54	4.5	8.5	50.5	20	0.507	0.86	170	8.5
②	44	14.0	23.5	35.5	17	0.607	0.794	400	10.3
③	34	24.0	35.	24	15	0.728	0.686	525	10.9
④	24	34.0	46.	13	13	0.776	0.630	600	10.1
⑤	14	44.	53.	6	11	0.876	0.480	583	9.6
⑥	4.5	54.	57.	2	10	0.936	0.350	570	9.4

	$(a-x)(h-y)ds$	$(h-y)^2 ds$	$\cos^2 \theta ds$	$(h-y)\cos^2 \theta ds$	$x \sin \theta \cos \theta ds$	$\int_0^x ds$	$\int_0^x \frac{ds}{(h-y)}$	$V_A(a-x)$	$\int_0^x (rd) ds$	$H_A(h-y)$
①	765	1450	3.60	30.7	402	100	17000	318,000	120,000	12,300
②	5400	9400	6.25	144.	360	432	173000	980,000	518,000	34,100
③	12600	18400	7.94	278.	254	998	519000	1,700,000	1,200,000	50,800
④	20400	27600	7.84	361.	153	1717	703000	2,400,000	2,060,000	66,000
⑤	25600	30900	8.40	446.	64	2473	1440000	3,120,000	2,970,000	76,900
⑥	30800	32500	8.80	502.	15	3420	1850000	3,900,000	3,890,000	82,600
	95565	120250	42.83	1762.	1248		4702000			

APPENDIX V (Continued)

Combine these with those of Table I we obtain:

$$\frac{\partial U}{\partial H} = \frac{1}{EI} \left[-95,560 V_A + 120,250 H_A + 645,000 H_A + 4,702,000 P \right] \\ + \frac{1}{EA} \left[43H_A + 185H_A + 3000p + 6940p \right] = 0$$

Solving for H

$$\left[\frac{765,250}{EI} + \frac{228}{EA} \right] H = \frac{95,560}{EI} V_A - \left[\frac{4,702,000}{EI} + \frac{9950}{EA} \right] P$$

$$I = 224.6 \text{ in}^4; \quad A = 39 \text{ in}^2$$

Substituting these values in the equation for H_A

$$\left[3400 + 6 \right] H = 425 V_A - \left[20,900 + 255 \right] P$$

$$3406 H = 425 V_A - 21155 P$$

$$H = \frac{425}{3410} V_A - \frac{21155}{3410} P = 0.125 V_A - 6.20 P$$

$$H = 0.125 \times 70,800 - 6.20 \times 1200$$

$$= 8850 - 7400$$

$$= 1450 \text{ lbs. (as assumed)}$$

Substituting this values of H into equations for N_o and M_o for portions AD and DCB, we can calculate N_o^A and M_o at any section of the structure. These calculations are shown on Table II and are represented graphically in Figure 5. From this figure we can pick up the maximum conditions at about 20" and 60" from A.

BLANK PAGE

APPENDIX V (Continued)

The maximum condition stresses are (20" from A.)

Inner Fibers

$$\begin{aligned}\sigma &= - \frac{M_o}{S_r} + \frac{N_o}{A} \\ &= - \frac{460,000}{37.3} + \frac{62,000}{39} \\ &= - 12,300 + 1,600 \\ &= - 10,700 \text{ psi} \quad \text{Compression}\end{aligned}$$

Outer Fibers

$$\begin{aligned}\sigma &= + \frac{M_o}{S_r} + \frac{N_o}{A} = + \frac{460,000}{56.8} + 1600 \\ &= + 8100 + 1600 \\ &= 9700 \text{ psi} \quad \text{Tension}\end{aligned}$$

60" From A.

$$\begin{aligned}\text{Inner Fibers } \sigma &= + \frac{82,500}{37.3} + \frac{72,300}{39} = + 2110 + 1816 \\ &= 3930 \text{ psi} \quad \text{Tension}\end{aligned}$$

$$\begin{aligned}\text{Outer Fibers } \sigma &= - \frac{82,500}{56.8} + \frac{72,300}{39} = - 1450 + 1820 \\ &= 370 \text{ psi} \quad \text{Tension}\end{aligned}$$

All of the above stresses are well within the ultimate stresses-43,000 psi flexure, 18,600 psi tension.

APPENDIX V (Continued)

TABLE II
MOMENT AND NORMAL FORCE CALCULATIONS

Segment	M_0	$x \sin \theta$	$(h-y) \cos \theta$	$x \sin \theta + (h-y) \cos \theta$	$HA \cos \theta$	$[y \sin \theta + (h-y) \cos \theta] p$	N_0
①	+186,000	46.7	4.30	51.0	730	61200	61930
②	+430,000	35.0	14.30	49.3	880	51300	61900
③	+450,000	23.3	25.3	48.6	1050	58400	59450
④	+275,000	15.1	35.7	50.8	1130	61000	62130
⑤	+ 73,000	6.7	46.4	53.1	1270	63700	64970
⑥	- 73,000	1.6	53.4	55.0	1360	66000	67360
⑦	- 86,000						72250
⑧	- 82,000						72200
⑨	- 74,000						72060
⑩	- 60,000						71820
⑪	- 43,000						71530
⑫	- 0						70800

In this analysis the flexural and normal stresses were checked. The analysis shows that the maximum flexural stress is 25% of the ultimate flexural strength of the material and the normal tensile strength is 50% of the ultimate tensile strength of the material. Therefore, it is concluded that the external flange of the mold splice section possesses a safety factor of about 2 for the anticipated internal pressure.

The results of the analysis are shown graphically in Figure 6.

APPENDIX V (continued)

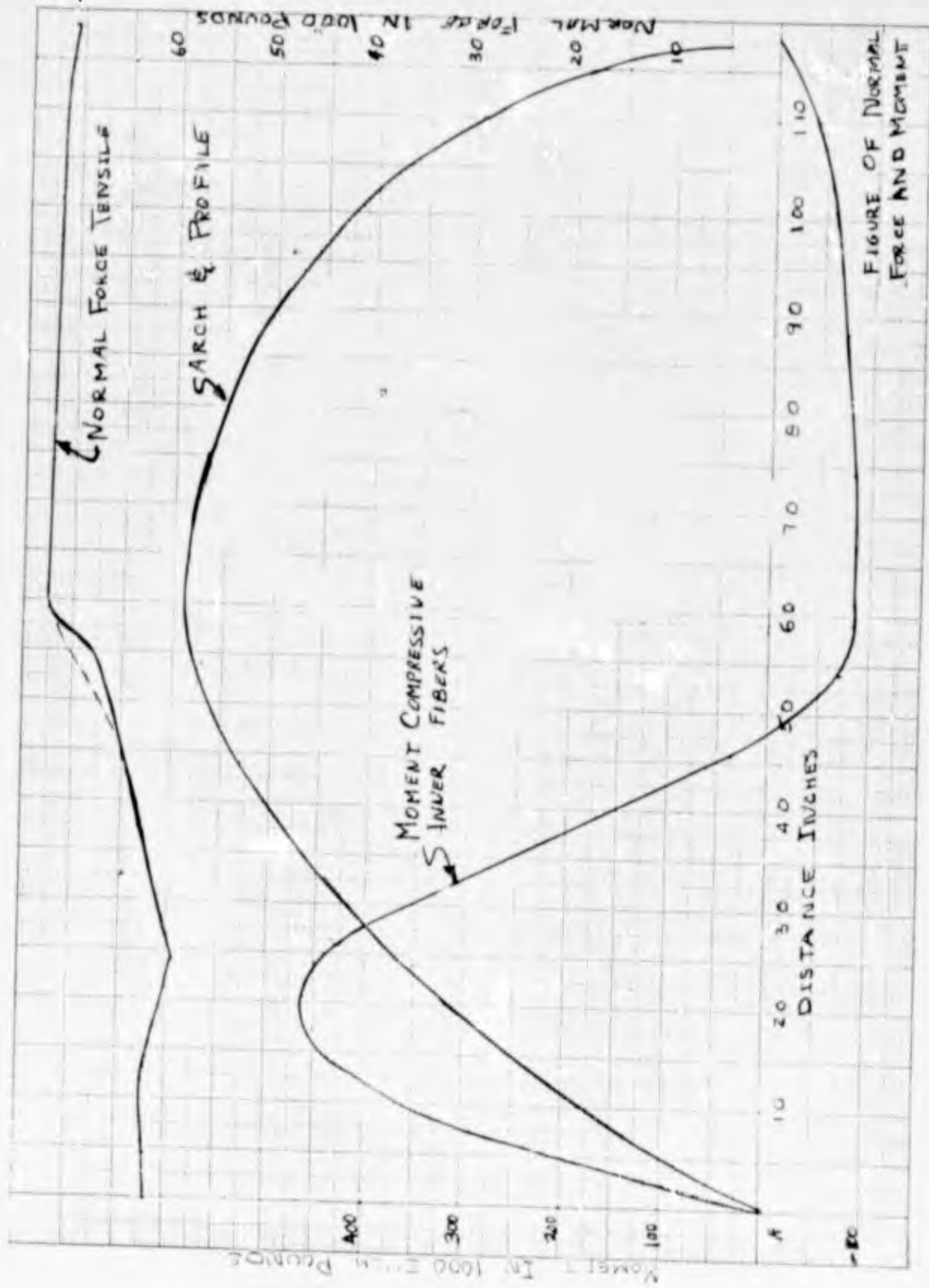


Figure 6

GRAPH OF MOMENT AND NORMAL FORCES

BLANK PAGE

APPENDIX VI
STRESS CALCULATIONS ON STEEL SEAMING FIXTURE

When looking at the action and reaction forces on the upper steel strongback section of the total seaming area it appears necessary to break the complex curvature into simple straight beams and assume that all joints are pivoted. This case, while not exact, permits calculations of stresses without using integration. These calculations will, in this case, indicate a more severe condition, and thus result in a structure superior to that obtained if integration formulas were used. This in turn gives a calculated safety factor which is greatly reduced from the actual safety factor present. Sections of the structure analyzed are shown below along with the calculation of the stress obtained in each section.

A cross section of the beam used in members Nos. 1, 2 & 3 is shown below.

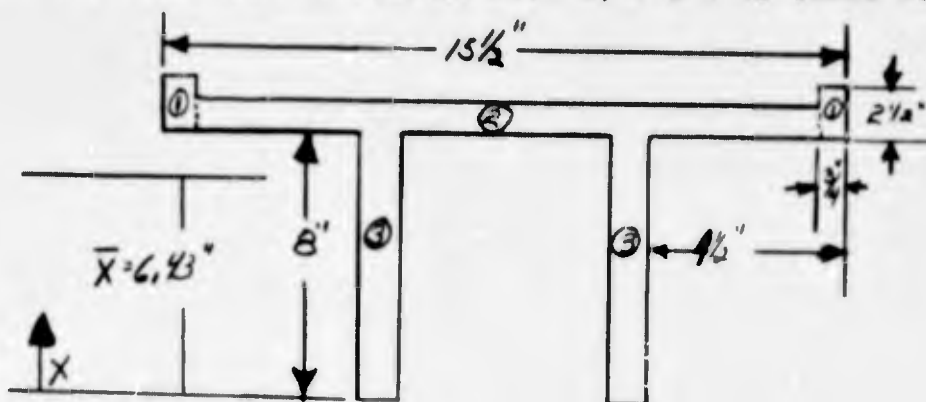


FIGURE 1

Obtaining physical properties of cross section:

Finding Center of Gravity:

(A)	Area	X	Ax	
(1)	3.75	9.25	34.6	
(2)	14.00	8.50	119.0	$\bar{X} = \frac{\sum Ax}{\sum A} = \frac{217.6}{33.75} = 6.45$
(3)	16.00	4.00	64.0	
	$\sum A=33.75$		$\sum Ax=217.6$	

APPENDIX VI (Continued)

Finding Moment of Inertia of Cross-Section

$$\begin{aligned}
 I_1 &= \frac{1}{12} b_1 h_1^3 + A_1 X_1^2 = \frac{1}{12} \times 1\frac{1}{2} \times (2\frac{1}{2})^3 + 3.75(9.25-6.45) = 1.96 + 10.50 \\
 &= 12.46 \text{ in}^4 \\
 I_2 &= \frac{1}{2} b_2 h_2^3 + A_2 X_2^2 = \frac{1}{2} \times \frac{14}{1} \times (1)^3 + 14 (8.50-6.45) = 1.17 + 28.70 \\
 &= 29.87 \text{ in}^4 \\
 I_3 &= \frac{1}{2} b_3 h_3^3 + A_3 X_3^2 = \frac{1}{2} \times 2 \times 8^3 + 16 (6.45 - 4.00) = 85.40 + 39.20 \\
 &= 124.60 \text{ in}^4 \\
 I_{\text{tot}} &= I_1 + I_2 + I_3 = 12.46 + 29.87 + 124.60 = 166.93 \text{ in}^4
 \end{aligned}$$

To find reactive forces R_1 & R_2 as indicated in the sketch.

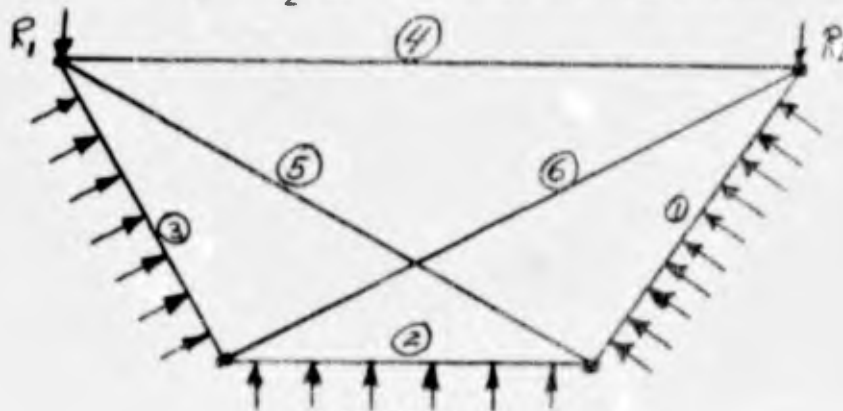


FIGURE 2

Member	Length
1	56.6"
2	58.0"
3	54.6"
4	118.0"
5	93.3"
6	105.2"

$$R_1 + R_2 = F_y = F (L_4)$$

$$R_1 = R_2$$

$$2R_1 = F \times L_4 = 1400 \times 118 = 165,000 \text{ lbs.}$$

$$R_1 = R_2 = \frac{165,000}{2} = 87,500\#$$

$$\begin{aligned}
 F &= 1400 \text{ lbs/in.} \\
 L_4 &= 118 \text{ in.}
 \end{aligned}$$

APPENDIX VI (Continued)

To find the maximum tension and compressive forces that could be obtained in this statically indeterminate structure, structural members Nos. 5 and 6 were removed one at a time and then replaced. A force polygon was constructed for each case and the forces obtained tabulated.

TABLE I
FORCE DETERMINATION

<u>Structural Member</u>	<u>Forces with Member #5 removed</u>	<u>Forces with Member #6 removed</u>	<u>Max F</u>
1	93,000 # comp	80,000 # comp	93,000 # C
2	93,000 # comp	60,000 # comp	93,000 # C
3	68,000 # comp	48,000 # comp	68,000 # C
4	4,000 # comp	20,000 # comp	20,000 # C
5	---	28,000 # comp	28,000 # C
6	33,000 # comp	---	33,000 # C

Sample Stress Analysis:

Member #1

$$\text{Stresses due to Compressive Forces} = \frac{F}{A}$$

$$\text{Stresses due to Bending Moments} = \frac{Mc}{I}$$

$$\text{Total Comp. Stress} = \frac{F}{A} + \frac{Mc}{I} = S_c$$

$$\text{where } M = Wx\frac{L}{2} - \frac{WxL^2}{4}$$

$$= Wx\frac{L^2}{4} - \frac{WxL^2}{8} = \frac{WL^2}{8}$$

- F(table I) = 93,000#
- A = 33.75 in²
- W = 1400 #/in
- L = 56.6"
- C_{comp} = 4.05"
- C_{ten} = 6.45
- I₁ = 166.93 in⁴

APPENDIX VI (Continued)

$$S_{comp} = \frac{93,000}{33.75} + \frac{1400 \times (56.6)^2}{8} \times \frac{4.05}{166.93}$$

$$= 2,260 + 13,600 = 15,860 \text{ psi}$$

$$S_{ten} = \frac{Mc}{I} - \frac{F}{A} = \frac{WL^2}{8} \times \frac{C_T}{I_1} - \frac{F}{A} = \frac{1400 \times (56.6)^2}{8} \times \frac{6.45}{166.93} - \frac{93,000}{33.75}$$

$$= 21,700 - 2,260$$

$$= 19,440 \text{ psi}$$

In the calculation of the safety factor the maximum tensile and compression strength of the steel was assumed to be 55,000 psi.

$$S.F. = \frac{\text{Ultimate Tensile or Comp.}}{\text{Actual Tensile or Comp.}}$$

$$S.F._T = \frac{55,000}{19,440} = 2.83$$

$$S.F._c = \frac{55,000}{15,860} = 3.47$$

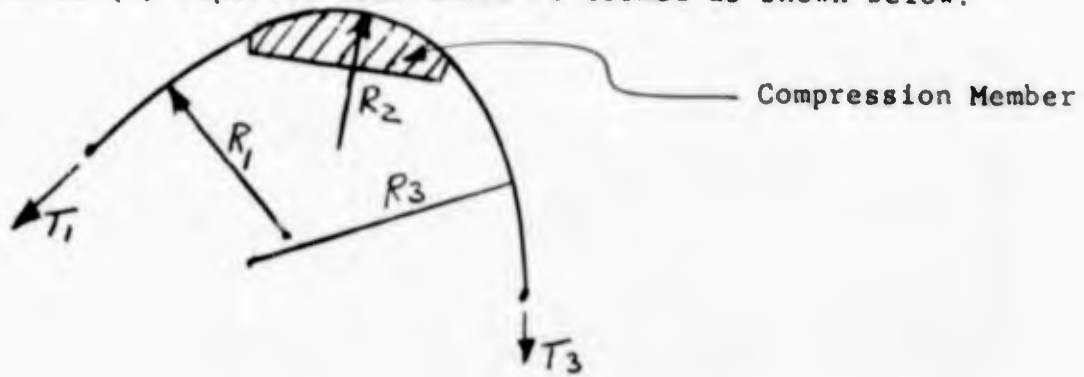
The stresses, lengths, loads, and safety factors for the individual members are tabulated below in Table II, showing the structure to be adequate.

TABLE II
PHYSICAL PROPERTIES OF STRONGBACK

Member	Fc (lbs)	A ₂ (in ²)	W (#/m)	L (in)	Cc (in)	C _T (in)	I (in ⁴)	S _c (psi)	S _T (psi)	<u>55,000</u> s _c	<u>55,600</u> s _t
1	93,000	33.75	1400	56.6	4.05	6.45	166.93	15,860	19,440	3.47	2.83
2	93,000	33.75	1400	58.0	4.05	6.45	166.93	16,510	20,440	3.32	2.69
3	68,000	33.75	1400	54.6	4.05	6.45	166.93	14,670	18,130	3.75	3.03
4	20,000	11.05	-	118.0	-	-	-	1,850	-	29	-
5	28,000	11.05	-	93.3	-	-	-	2,540	-	21	-
6	33,000	11.05	-	105.2	-	-	-	2,990	-	18	-

APPENDIX VII
PANEL FRICTION REQUIREMENTS

In determining the effectiveness of the compression member to maintain panel contour an analysis of tension loads had been accomplished. In this analysis it was assumed that three (3) separate arcs would be formed as shown below:



Thus, to determine loading on the panel during pressurization and the resultant components:

$$\frac{T_1 + T_3}{2} = NR_2 + PR_2$$

and: $T_1 - T_3 = NA$

also: $T_1 = PR_1$

$$T_2 = PR_2$$

$$T_3 = PR_3$$

Therefore: $PR_1 + PR_3 = 2R_2 (N+P)$

Thus: $\frac{PR_1 + PR_3}{2R_2} = N+P$

$$N = \frac{PR_1 + PR_3}{2R_2} - P$$

Where: $P =$ Internal Pressure

$T_1 =$ Tension, Upper

$T_2 =$ Tension, Middle

APPENDIX VII (Continued)

T_3 = Tension, Lower

R_1 = Radius, Upper

R_2 = Radius, Middle

R_3 = Radius, Lower

μ = Coefficient of Friction

N = Normal Force, psi

A = Area N acts over

If pure friction is assumed:

$$PR_1 - PR_3 = \left(\frac{PR_1 + PR_3}{2R_2} - P_1 \right) \mu A$$

$$R_1 - R_3 = \left(\frac{R_1 + R_3}{2R_2} - 1 \right) \mu \times A$$

$$\frac{R_1 - R_3}{R_1 + R_3} = \frac{1}{2R_2} - 1 \quad \mu$$

Analyzing the cross-section at each frame with their specific radii the following frictional requirements were determined necessary to prevent panel movement. (Table I)

APPENDIX VII (Continued)

TABLE I
FRictional REquirements

<u>Fr</u>	<u>R₁</u>	<u>R₂</u>	<u>R₃</u>	<u>R₁-R₃</u>	<u>R₁+R₃</u>	$\frac{\textcircled{1} R_1+R_3}{2R_2} - 1$	$\textcircled{2}$ <u>A</u>	$\textcircled{1} \times \textcircled{2}$	<u>μ</u>
7	102.5	23.1	61.5	41.0	164	2.55	29"	73.9	.555
8	88.5	25.7	70.5	18.0	159	2.10	31"	65.1	.277
9	83.8	27.5	74.5	9.3	158.3	1.88	34"	63.5	.146
10	74.5	30.1	79.0	4.5	153.5	1.53	36"	55.1	.082
11	68.5	33.7	78.7	10.2	147.2	1.19	38"	45.3	.225
12	63.0	36.5	83.0	20.0	146.0	1.00	41"	41.0	.488
13	60.5	40.0	85.5	25.0	146.0	0.83	43"	35.6	.702
14	58.8	42.5	85.5	26.7	144.3	0.70	45"	31.5	.849
15	52.5	44.0	85.0	32.5	137.5	0.56	48"	26.9	1.21
16	50.3	46.5	79.0	28.7	129.3	0.39	50"	19.5	1.47

From this it was determined the maximum coefficient of friction required was 1.47. With this in mind the problem at hand was to determine methods of attaining this. Several systems were evaluated against 35003 neoprene and included among others: (1) Exploded clay surface, (2) Extra Course Emery Cloth, (3) Resin Industrial Cloth Type 6 50X, (4) Carborundum LV, (5) Sandpaper 220A, 200C, 80 grit, 120 grit, #2 and 36X. Table II presents a comparison of various systems with respect to the actual coefficient of friction obtained. It can be seen, in analyzing these data that none of the evaluated system furnished the required strength, therefore an alternate idea had to be considered.

The second concept pursued was that of attaching a series of rubber biscuits to the panel surface. These in turn would mate with cavities in the compression member maintaining proper positioning of the panel. The first requirement was to determine the number of 2" diameter biscuits required per 3 inch width. The load exerted over this width

$$L = (R_1 - R_3) P \times 3$$

APPENDIX VII (Continued)

and the number of biscuits -

$$N = \frac{(R_1 - R_3) P \times 3}{4.90 \text{ in.}^2 \times 200}$$

where L = Load per 3" width

R₁ = Upper Radius

R₃ = Lower Radius

P = Internal Pressure

N = No. of Biscuits

4.90 in.² = Area/biscuit

200 lbs. = Max. load/in.²

From these equations Table III was generated showing the number of biscuits necessary at each frame.

APPENDIX VII (Continued)

TABLE II
FRICITION TESTS

<u>Material</u>	<u>Weight</u>	<u>Pull Required To Move</u>		<u>4 Coefficient of Friction</u>	
		Wet	Dry	Wet	Dry
Exploded Clay Surface	2.17		2.5		1.15
"	4.17		4.0		.96
"	6.17		6.25		1.01
"	7.17		7.25		1.01
"	8.50		8.50		1.00
"	10.00		10.00		1.00
Average Exploded Clay					1.02
Emery Cloth EC015	5.00		5.25		1.05
"	10.00		10.25		1.03
Average Emery Cloth					1.04
Resin Ind. Cloth Type 6 50X	5.00		5.00		1.00
"	10.00		10.00		1.00
Average Ind. Cloth					1.00
Carborundum LV	5.00		3.50		.70
"	10.00		8.00		.80
Average Carborundum LV					.75
Sandpaper 220A	5.00	-	6.50		1.3
" 280C	5.00	5.50	7.00	1.1	1.4*
" 80 Grit	7.00	7.50	7.50	1.07	1.07
" 120 Grit	4.00	-	4.50		1.12
" #2	4.00	-	3.75		.94
" 36X	4.00	-	4.25		1.06

*The sample with the largest coefficient of friction dry was tested under water to determine the friction characteristics under exact environmental conditions.

TABLE III
NO. OF BISCUITS REQUIRED

<u>Fr</u>	<u>R₁-R₃</u>	<u>(R₁-R₃)P</u>	<u>No. of Biscuits</u>
7	41.0	4,100	12.6
8	18.0	1,800	5.5
9	9.3	930	2.9
10	4.5	450	1.4
11	10.2	1,020	3.1
12	20.0	2,000	6.1
13	25.0	2,500	7.7
14	26.7	2,670	8.2
15	32.5	3,250	10.0
16	28.7	2,870	8.3

APPENDIX VII (Continued)

A sample biscuit construction was fabricated and tested. In one instance vertical cylindrical sections were evaluated as shown in Figure 1. Failure of this system was at the adhesive bond. A second system evaluated utilized tapered biscuits and yield results shown in Figure 2. A graph was plotted, as shown in Figure 3 displaying numbered required versus number attainable. It can be seen that at Frame 7 up to 7-1/2 the required exceeded the capacity. This coupled with the problem of notching the biscuits and recesses during compression member positioning prompted the evaluation of a more efficient approach.

The final concept evaluated and eventually adopted was that of cementing the panel to the sandblasted epoxy surface of the compression member. To determine the basic shear strength of a Code 369 -- cement bond. A sample bond of 35003 Neoprene to itself with a 2-3/4" x 3" bonding area was fabricated and tested. The results are shown in Figure 4. The ultimate shear strength of this sample, which failed at the cement bond in 339.5 lbs./in.². Calculation of shear strength necessary for the cement retention system is shown in Table IV. Data obtained assumes the entire compression member is bonded to the panel.

Thus: $T_1 - T_3 = S \times A$ and $T_1 = PR_1$, $T_3 = PR_3$

or, $PR_1 - PR_3 = SA$

and, $\frac{P}{A} (R_1 - R_3) = S$

APPENDIX VII (Continued)

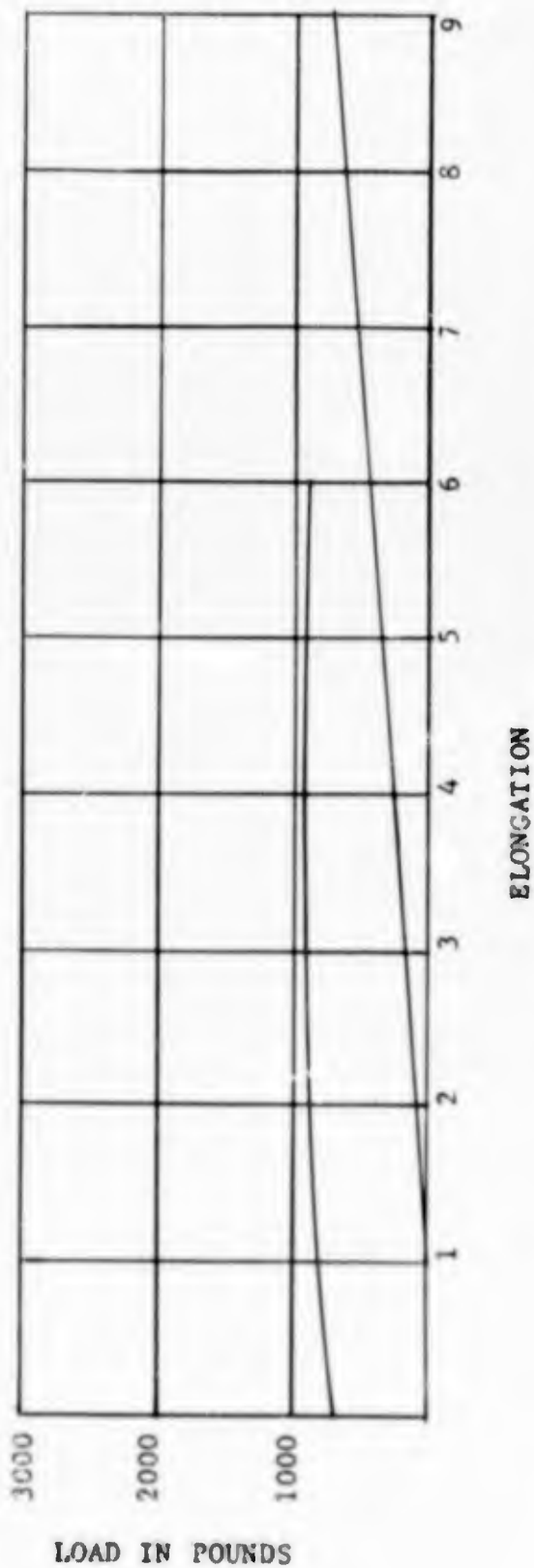


FIGURE 1
369 SHEAR TEST OF CYLINDRICAL BISCUITS

APPENDIX VI (Continued)

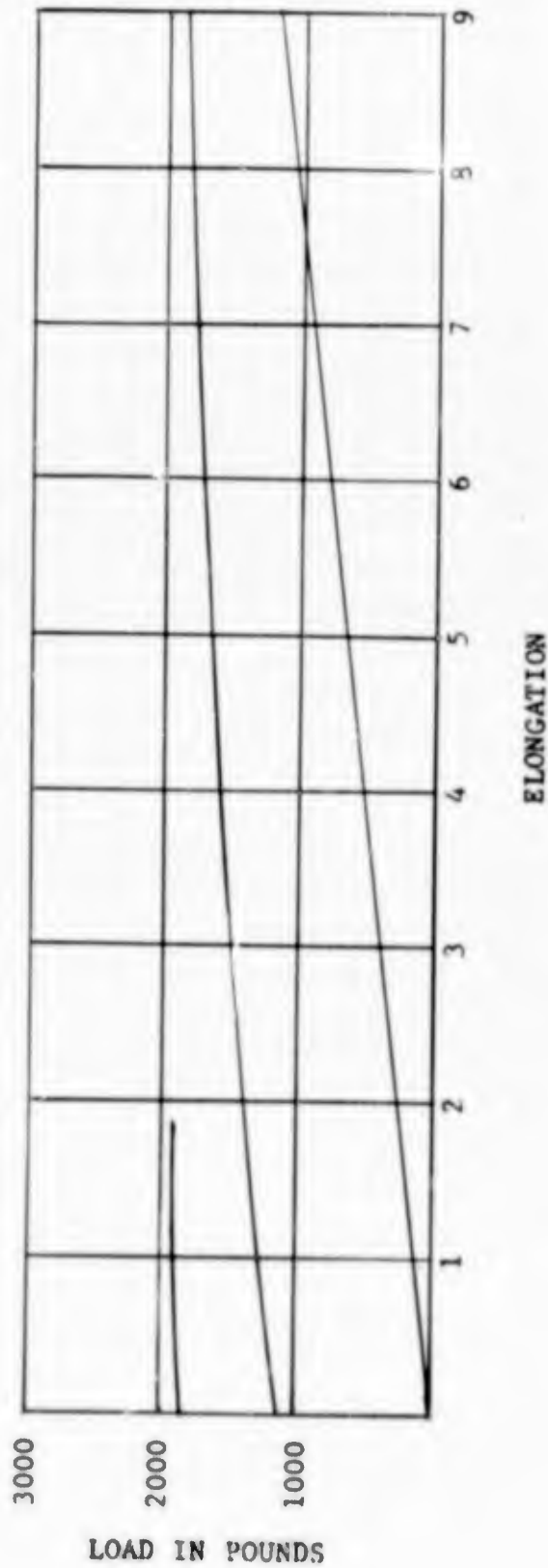
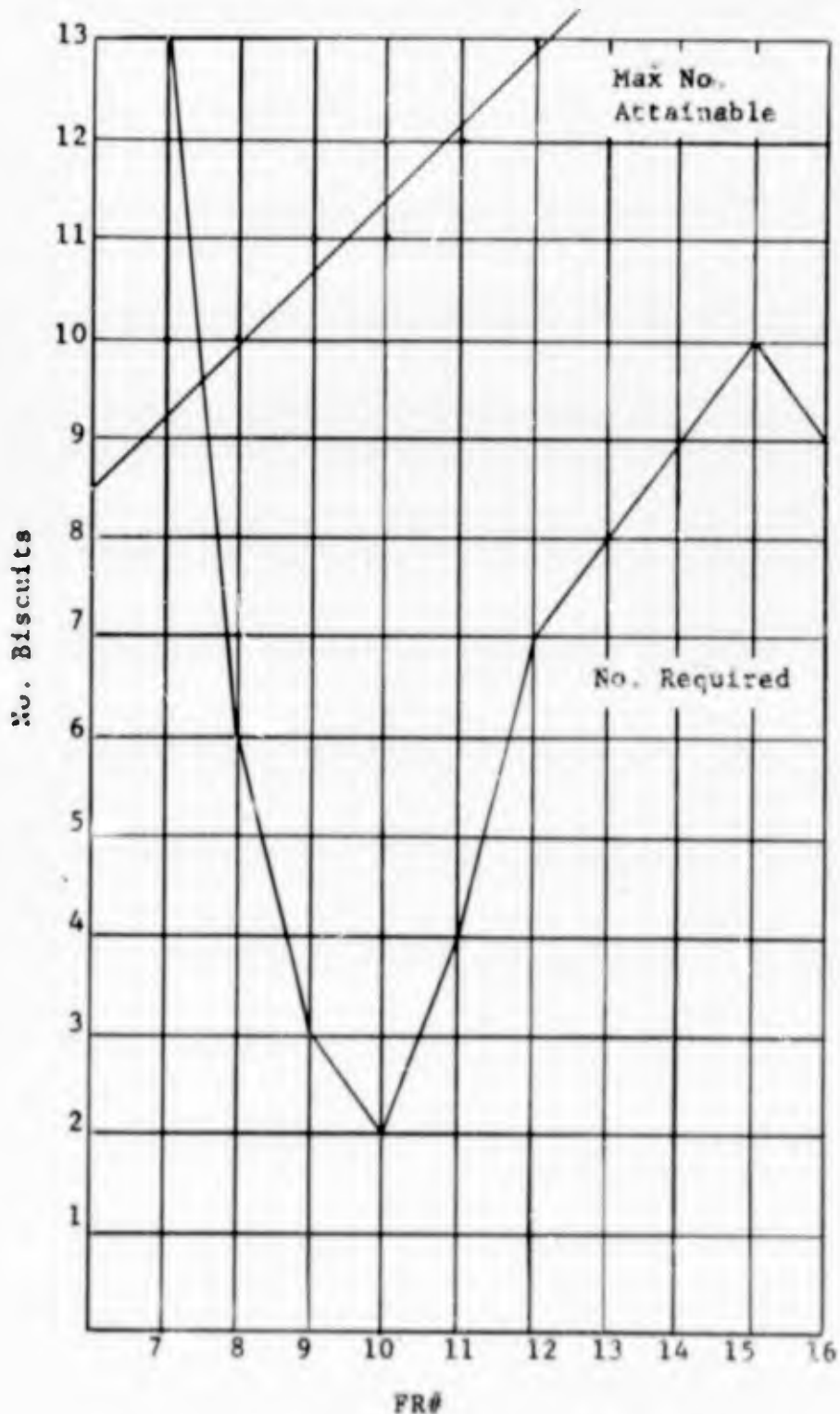


FIGURE 2
369 SHEAR TESTS OF TAPERED BISCUITS

APPENDIX VII (Continued)



FR	NO.	FR	NO.
7	13	13½	9
7½	11	13½	9
7½	9	13-3/4	9
7-3/4	7	14	9
8	6	14½	10
8½	5	14½	10
8½	5	14-3/4	10
8-3/4	4	15	10
9	3	15½	10
9½	3	15½	10
9½	3	15-3/4	10
9-3/4	3	16	9
10	2		
10½	3		
10½	3		
10-3/4	4		
11	4		
11½	5		
11½	6		
11-3/4	7		
12	7		
12½	8		
12½	8		
12-3/4	8		
13	8	Total 260	

FIGURE 3
 PLOT NO. BISCUITS REQUIRED/3 IN. WIDTH

APPENDIX VII (Continued)

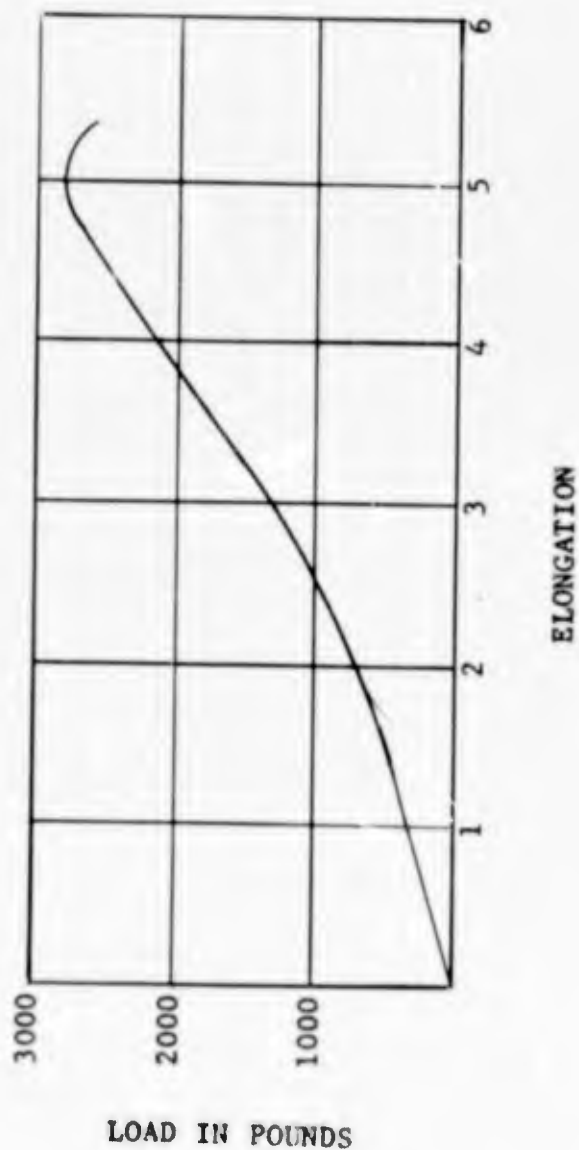


FIGURE 4
369 SHEAR TESTS 2-3/4" WIDTH X 3" LAP SPLICE

APPENDIX VII (Continued)

Where: P = Pressure
 A = Area
 R₁ = Upper Radius
 R₃ = Lower Radius
 T₁ = Upper Tension
 T₂ = Lower Tension
 S = Shear Strength required

TABLE IV

<u>Fr</u>	<u>R₁</u>	<u>R₃</u>	<u>R₁-R₃</u>	<u>A</u>	<u>P/A</u>	<u>S</u>	
7	102.5	61.5	41.0	29	3.45	143	Max. Shear Strength Req'd. for Cement 143 psi
8	88.5	70.5	18.0	31	3.23	58.1	
9	83.8	74.5	9.3	34	2.94	37.4	
10	74.5	79.5	4.5	36	2.78	12.5	
11	68.5	78.7	10.2	38	2.62	26.8	
12	63.0	83.0	20.0	41	2.44	48.7	
13	60.5	85.5	25.0	43	2.33	58.1	
14	58.8	85.5	26.7	45	2.22	59.3	
15	52.5	85.0	32.5	48	2.08	67.7	
16	50.3	79.0	28.7	50	2.00	57.3	

The maximum shear strength required for the cement is 143 psi. The maximum attainable is 339.5 psi. This system furnished the necessary strength and safety factor for retaining the panel in position during testing and was used during actual testing.

BLANK PAGE

Contract NObsr 89483
Serial No. SS041-001
Task 8156

Report No. 17
Phase I Interim Report
30 September 1964

APPENDIX VIII
MATHEMATICAL ANALYSIS

Consulting help from the Massachusetts Institute of Technology was sought for the development of membrane equations from which the following studies could be made on the acoustic window:

- (1) Effect of hydrodynamic forces.
- (2) Analysis of vibration characteristics.
- (3) Structural wave properties.

The several approaches presented by MIT to evaluate the effect of hydrodynamic forces on the window are included in this report. No formulas were submitted for the other two items.

Calculated results obtained through use of the MIT derivations with those obtained from BFG derivations were substantially comparable.

APPENDIX VIII (continued)
MEMBRANE ANALYSIS - CYLINDRICAL BEHAVIOUR

1. INTRODUCTION

We consider a cylindrical membrane (Fig. 1) supported along $a - a'$ and $b - b'$ which are parallel to the z axis. By cylindrical, we mean that the arc length of the membrane does not vary in the z direction. We restrict this analysis to the case of a normal pressure which also does not vary in the z direction. The behaviour of the membrane will be cylindrical, that is, independent of z , and we can work with a strip having a unit width (e.g. strip cd).

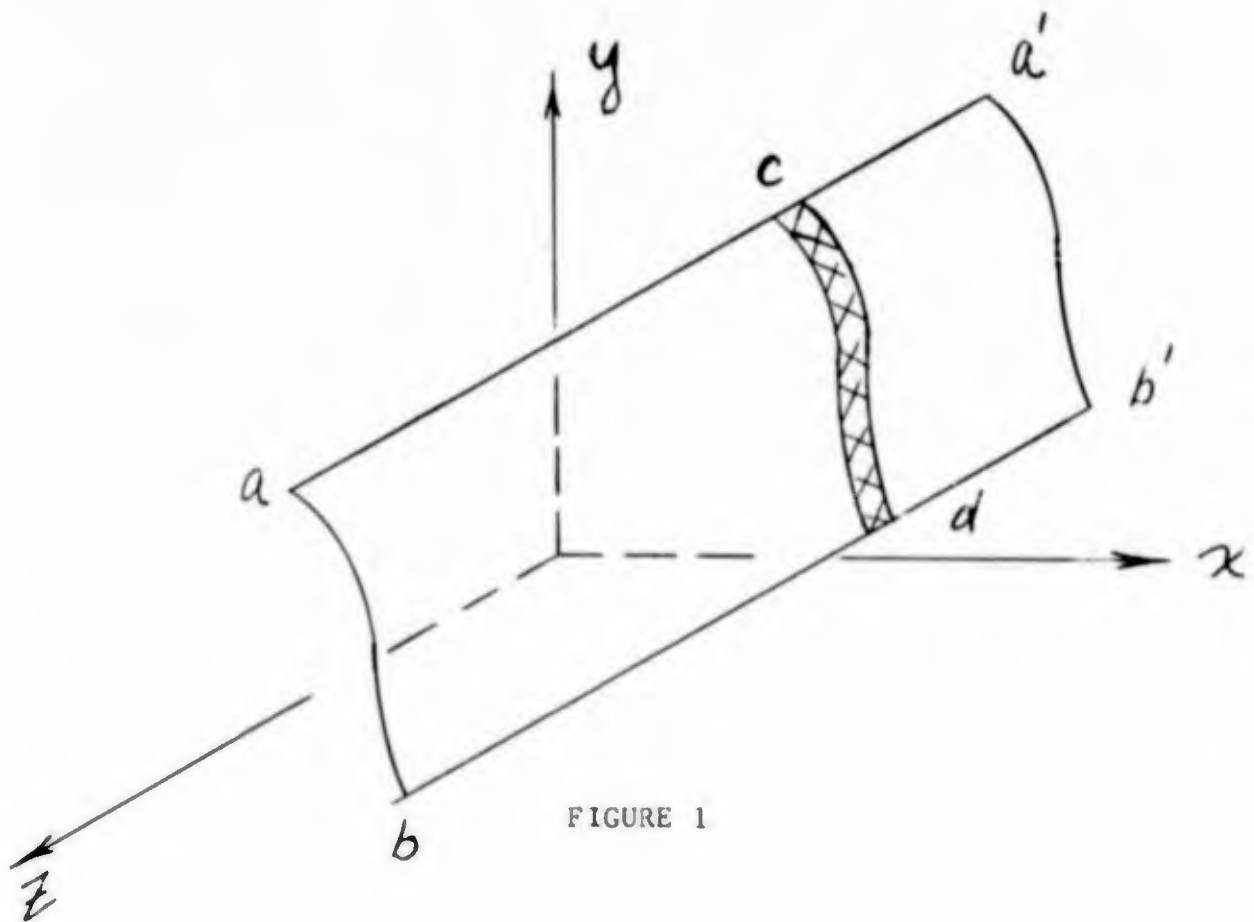


FIGURE 1

APPENDIX VIII (continued)

2. NOTATION AND GEOMETRIC RELATIONS

We introduce the following notation for the loaded membrane:

S = distance along curve

\vec{r} = position vector

\vec{t} = unit tangent vector in direction of increasing S

\vec{n} = unit normal vector, clockwise from \vec{t}

K = curvature

R = radius of curvature = $\frac{1}{K}$

T = tension per unit width

P = normal pressure, positive when in direction of \vec{n}

The positive directions are shown in Figure 2.

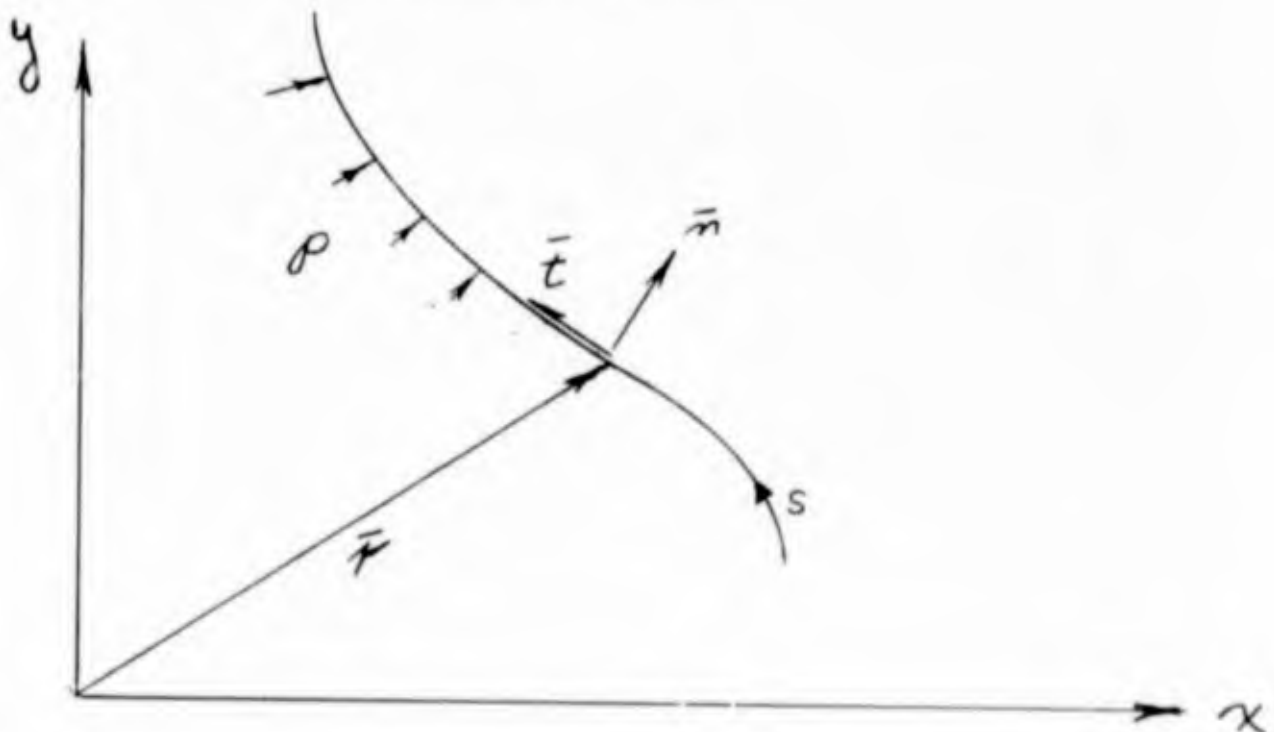


FIGURE 2

APPENDIX VIII (continued)

The tangent vector and curvature are defined

$$\bar{t} = \frac{d\bar{r}}{ds} \quad (2.1)$$

$$K = \frac{1}{R} = -\bar{n} \cdot \frac{d^2\bar{r}}{ds^2} = -\bar{n} \cdot \frac{d\bar{t}}{ds} \quad (2.2)$$

We have defined R such that, when R is positive the center of curvature is in the negative normal direction. Polar coordinates (r, θ) are the most convenient system for this problem. From figure 3,

$$\begin{aligned} \bar{r} &= x\bar{i} + y\bar{j} \\ \bar{i}_r &= \cos\theta\bar{i} + \sin\theta\bar{j} \\ \bar{i}_\theta &= -\sin\theta\bar{i} + \cos\theta\bar{j} \\ \bar{t} &= \sin\beta\bar{i}_r + \cos\beta\bar{i}_\theta \\ \bar{n} &= \cos\beta\bar{i}_r - \sin\beta\bar{i}_\theta \end{aligned} \quad (2.3)$$

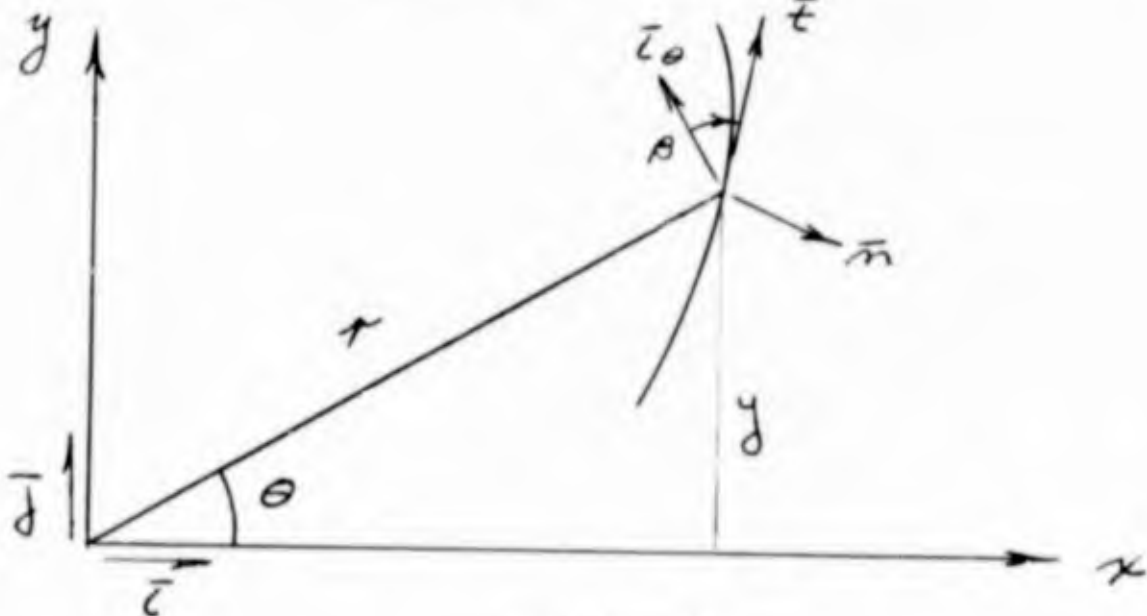
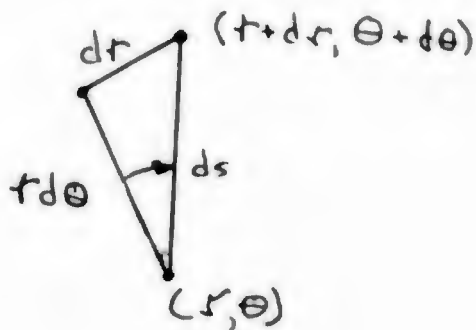


FIG. 3

APPENDIX VIII (continued)

The angle β is given by (see fig. 4):



$$\tan \beta = \frac{dr}{r d\theta} = \frac{1}{r} \left(\frac{dr}{d\theta} \right) \quad (2.4)$$

or

$$\sin \beta = \frac{dr}{ds} \quad (2.5)$$

The general expression for the curvature is:

$$\frac{1}{R} = \frac{d\theta}{ds} - \frac{d\beta}{ds} \quad (2.6)$$

When S is taken as the independent variable, (2.6) has the form.

$$\frac{1}{R} = \frac{\left[1 - \left(\frac{dr}{ds} \right)^2 \right]^{1/2}}{r} - \frac{\frac{d^2 r}{ds^2}}{\left[1 - \left(\frac{dr}{ds} \right)^2 \right]^{1/2}}$$

and θ is determined from

$$d\theta = \frac{1}{r} \left[1 - \left(\frac{dr}{ds} \right)^2 \right]^{1/2} ds$$

When θ is taken as the independent variable, we have

$$ds = \left\{ r^2 + \left(\frac{dr}{d\theta} \right)^2 \right\}^{1/2} d\theta$$

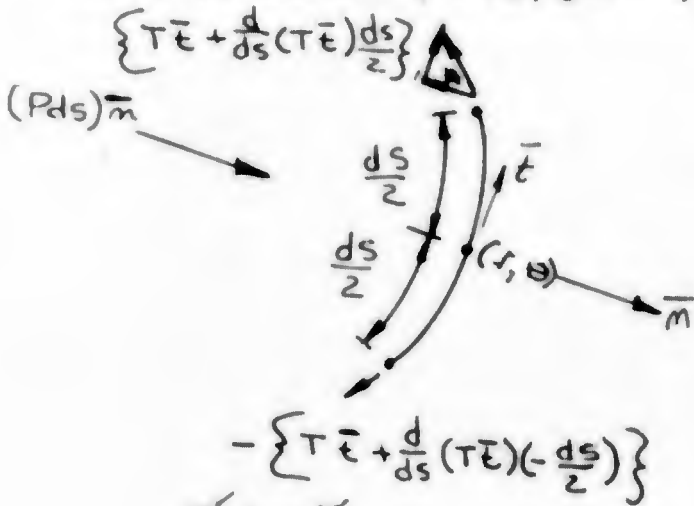
and

$$\frac{1}{R} = \frac{1}{\left[r^2 + \left(\frac{dr}{d\theta} \right)^2 \right]^{3/2}} \left\{ r^2 - r \frac{d^2 r}{d\theta^2} + 2 \left(\frac{dr}{d\theta} \right)^2 \right\}$$

APPENDIX VIII (continued)

Equilibrium Equations of Stress-Strain Relation

We consider a differential element of the deformed membrane. (Fig. 5). The membrane force vector has



the direction of the tangent vector, \bar{e} , and magnitude T . The external force vector is in the normal direction. The vector equilibrium equation is:

$$P\bar{m} + \frac{d}{ds}(T\bar{e}) = 0 \quad (3.1)$$

Expanding (3.1), we obtain the following scalar equilibrium equations:

$$\frac{dT}{ds} = 0 \quad (3.2)$$

$$P - \frac{1}{R}T = 0 \quad (3.3)$$

From Eq. 3.2, we obtain
 $T = \text{const.}$

Then, the second equation becomes

$$\frac{1}{R} = \frac{P}{T} \quad \text{where } T = \text{const.} \quad (3.4)$$

APPENDIX VIII (continued)

When $p = \text{const}$, the membrane deforms into a circular arc.

We consider next the stress-strain relation.

Let D be the extensional rigidity per unit width of the membrane. Let ΔS_0 be the initial length and ΔS the final length of an element. Then,

$$\Delta S = \left(1 + \frac{T}{D}\right) \Delta S_0 \quad (3.5)$$

Since T is constant, we can integrate (3.5) and obtain a relation between the initial and final lengths.

$$S = \left(1 + \frac{T}{D}\right) S_0 \quad (3.6)$$

Equations (3.4) and (3.6) are sufficient to determine the shape and tension. We consider first the case where θ is taken as the independent variable.

The boundary conditions are:

$$T = T_1 \quad \text{at } \theta = \theta_1 \quad (3.7)$$

$$T = T_2 \quad \text{at } \theta = \theta_2$$

Eqs. 3.4 and 3.6 have the form:

$$\frac{r^2 - r''r + 2r'^2}{[r^2 + r'^2]^{3/2}} = \frac{p}{T} \quad (3.8)$$

$$\int_{\theta_1}^{\theta_2} [r^2 + r'^2]^{1/2} d\theta = \left[1 + \frac{T}{D}\right] S_0 \quad (3.9)$$

where $()' = \frac{d}{d\theta}$ and $p = p(\theta)$

APPENDIX VIII (continued)

The two integration constants involved in the solution of the differential equation (3.8) and the constant, T , are determined from Eqs. 3.7 and 3.9. If S is taken as the independent variable, the equations are:

$$\frac{[1-\dot{\tau}^2]^{1/2}}{\tau} - \frac{\ddot{\tau}}{[1-\dot{\tau}^2]^{1/2}} = \frac{P}{T} \quad (3.10)$$

$$\tau = \tau_1 \text{ at } S = 0$$

$$\tau = \tau_2 \text{ at } S = \left[1 + \frac{T}{D}\right] S_0 \quad (3.11)$$

$$\theta_2 - \theta_1 = \int_0^{\left[1 + \frac{T}{D}\right] S_0} \frac{1}{\tau} [1-\dot{\tau}^2]^{1/2} dS \quad (3.12)$$

where $p = p(\tau)$

and $(\dot{\tau}) = \frac{d\tau}{dS}$

In this case, the three constants are determined from Eqs. 3.11 and 3.12.

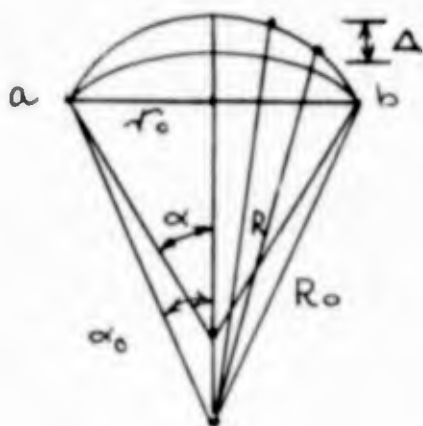
APPENDIX VIII (continued)

Uniform Normal Pressure Case

When the normal pressure is constant, the member deforms into an arc of a circle. The radius of curvature is

$$R = \frac{T}{p} = \text{const.} \quad (4.1)$$

where T is unknown. Consider the membrane supported at a, b , and let S_0 denote the initial arc length and R_0 the corresponding initial radius.



Integration of (4.1) results in

$$S = 2R\alpha \quad (4.2)$$

The boundary condition is $R \sin \alpha = r_0$ (4.3)

Finally, the stress-strain relation is

$$S = S_0 \left[1 + \frac{T}{D} \right] \quad (4.4)$$

There are four unknowns, namely, R, S, α , and T . We have four equations relating these unknowns, Eqs. 4.1 through 4.4

We consider first the case where $\frac{T}{D}$ is negligible with respect to unity. Then from 4.4,

$$S \approx S_0 \quad (4.5)$$

APPENDIX VIII (continued)

It follows from 4.2 and 4.3 that $R \approx R_0$ and $\alpha \approx \alpha_0$.
Finally,

$$T \approx R_0 \rho \quad (4.6)$$

The initial radius, R_0 , and central angle, α_0 , are

$$R_0 = \frac{S_0}{2\alpha_0} \quad (4.7)$$

where

$$\frac{\sin \alpha_0}{\alpha_0} = 2 \left(\frac{r_0}{S_0} \right) \quad (4.8)$$

To obtain a correction we substitute $T \approx R_0 \rho$ in the expression for S . Then

$$S \approx S_0 \left[1 + \frac{R_0 \rho}{D} \right] \quad (4.9)$$

$$\frac{\sin \alpha}{\alpha} \approx \frac{\sin \alpha_0}{\alpha_0} \frac{1}{1 + \frac{R_0 \rho}{D}} \quad (4.10)$$

$$R \approx \left\{ \frac{\alpha_0}{\alpha} \left[1 + \frac{R_0 \rho}{D} \right] \right\} R_0 \quad (4.11)$$

$$T \approx \left\{ \rho R_0 \right\} \left[\frac{\alpha_0}{\alpha} \left[1 + \frac{R_0 \rho}{D} \right] \right] \quad (4.12)$$

The quantity, $\frac{T}{D}$, must be small for engineering materials such as steel in order for the behaviour to be elastic. Also we assume that α_0 is of the order of unity, or equivalently, that S_0 is not of the order of R_0 .

APPENDIX VIII (continued)

We write

$$\alpha = \alpha_0 (1 + \epsilon) \quad (4.13)$$

and assume ϵ is a small w. r. to unity. Then

$$\sin \alpha \approx \sin \alpha_0 + \alpha_0 \epsilon \cos \alpha_0 \quad (4.14)$$

where we have taken

$$\cos \alpha_0 \epsilon \approx \epsilon$$

$$\sin \alpha_0 \epsilon \approx \alpha_0 \epsilon$$

Let us consider Eq. 4.10. Using 4.13 and 4.14,

$$\frac{\sin \alpha}{\alpha} \approx \frac{\sin \alpha_0 + \alpha_0 \epsilon \cos \alpha_0}{\alpha_0 (1 + \epsilon)} \approx \frac{\sin \alpha_0}{\alpha_0} \frac{1}{1 + \beta} \quad (4.15)$$

$$\text{where } \beta = \frac{R_0 P}{D} \ll 1$$

$$(4.16)$$

We solve Eq. 4.15 for ϵ .

$$\epsilon \approx \frac{\beta}{1 - \frac{\alpha_0 \cos \alpha_0}{\sin \alpha_0}} \approx \frac{R_0 P}{D} \frac{1}{1 - \frac{\alpha_0 \cos \alpha_0}{\sin \alpha_0}} \quad (4.17)$$

Now, Eqs. 4.11 & 4.12 can be written as

$$R \approx R_0 \left\{ \frac{\sin \alpha_0}{\sin \alpha} \right\} \quad (4.18)$$

$$T \approx (PR_0) \left[\frac{\sin \alpha_0}{\sin \alpha} \right]$$

But, from 4.14 and 4.17,

$$\frac{\sin \alpha_0}{\sin \alpha} \approx \frac{1}{1 + \epsilon \frac{\alpha_0 \cos \alpha_0}{\sin \alpha_0}} \approx \frac{1}{1 + \frac{\beta}{\frac{\sin \alpha_0}{\alpha_0 \cos \alpha_0} - 1}} \quad (4.19)$$

APPENDIX VIII (continued)

Finally

$$T \approx (PR_0) \left[\frac{1}{1 + \frac{\frac{R_0 P}{D}}{\alpha_0 \cos \alpha_0} - 1} \right] \quad (4.20)$$

$$R \approx R_0 \left[\frac{1}{1 + \frac{\frac{R_0 P}{D}}{\alpha_0 \cos \alpha_0} - 1} \right] \quad (4.21)$$

$$\alpha \approx \alpha_0 \left[1 + \frac{\frac{R_0 P}{D}}{1 - \frac{\alpha_0 \cos \alpha_0}{\sin \alpha_0}} \right] \quad (4.22)$$

Lastly, we determine the radial deflection at the mid point. This is given by (see Fig 6)

$$\Delta = -R_0 (1 - \cos \alpha_0) + R (1 - \cos \alpha) \quad (4.23)$$

Now for a small strain,

$$\cos \alpha \approx \cos \alpha_0 - \alpha_0 \epsilon \sin \alpha_0 \quad (4.24)$$

APPENDIX VIII (continued)

and then

$$\Delta \approx (1 - \cos \alpha_0)(R - R_0) + R(\alpha_0 t \sin \alpha_0)$$

$$\frac{\Delta}{R_0} \approx (1 - \cos \alpha_0) \left[\frac{\sin \alpha_0}{\sin \alpha} - 1 \right] + \alpha_0 t \sin \alpha_0$$

This reduces to:

$$\Delta \approx R_0 \left\{ (1 - \cos \alpha_0) \left[1 - \left(\frac{\frac{R_0 P}{D}}{1 - \frac{\alpha_0 \cos \alpha_0}{\sin \alpha_0}} \right) \left(\frac{\alpha_0 \cos \alpha_0}{\sin \alpha_0} \right) - 1 \right] + \alpha_0 \frac{\frac{R_0 P}{D} \sin \alpha_0}{1 - \frac{\alpha_0 \cos \alpha_0}{\sin \alpha_0}} \right\}$$

$$\text{Let } Z = \frac{\frac{R_0 P}{D}}{1 - \frac{\alpha_0 \cos \alpha_0}{\sin \alpha_0}} = \frac{\frac{R_0 P}{D} \sin \alpha_0}{\sin \alpha_0 - \alpha_0 \cos \alpha_0}$$

$$\begin{aligned} \Delta &= R_0 \left\{ (1 - \cos \alpha_0) \left[-Z \frac{\alpha_0 \cos \alpha_0}{\sin \alpha_0} \right] + Z \alpha_0 \sin \alpha_0 \right\} \\ &= R_0 \left\{ Z \left[- \frac{(1 - \cos \alpha_0) \alpha_0 \cos \alpha_0}{\sin \alpha_0} + \alpha_0 \sin \alpha_0 \right] \right\} \\ &= R_0 \left\{ Z \left[\frac{\alpha_0 \sin^2 \alpha_0 - (1 - \cos \alpha_0)(\alpha_0 \cos \alpha_0)}{\sin \alpha_0} \right] \right\} \\ &= R_0 \left\{ Z \left[\frac{\alpha_0 \sin^2 \alpha_0 - \alpha_0 \cos \alpha_0 + \alpha_0 \cos^2 \alpha_0}{\sin \alpha_0} \right] \right\} \end{aligned}$$

APPENDIX VIII (continued)

$$\Delta = R_0 \left\{ Z \left[\frac{\alpha_0 (1 - \cos \alpha_0)}{\sin \alpha_0} \right] \right\}$$

$$= R_0 \left\{ \frac{R_0 P \sin \alpha_0}{\sin \alpha_0 - \alpha_0 \cos \alpha_0} \left[\frac{\alpha_0 (1 - \cos \alpha_0)}{\sin \alpha_0} \right] \right\}$$

$$\Delta = \frac{R_0^2 P}{D} \left[\frac{\alpha_0 (1 - \cos \alpha_0)}{\sin \alpha_0 - \alpha_0 \cos \alpha_0} \right]$$

Approximate Solution - Non Uniform Pressure Case

We consider θ to be the independent variable and take the origin at the center of the circular arc corresponding to the undeformed length, s_0 . The supports are located at $\theta = \pm \theta_0$, $r = R_0$.

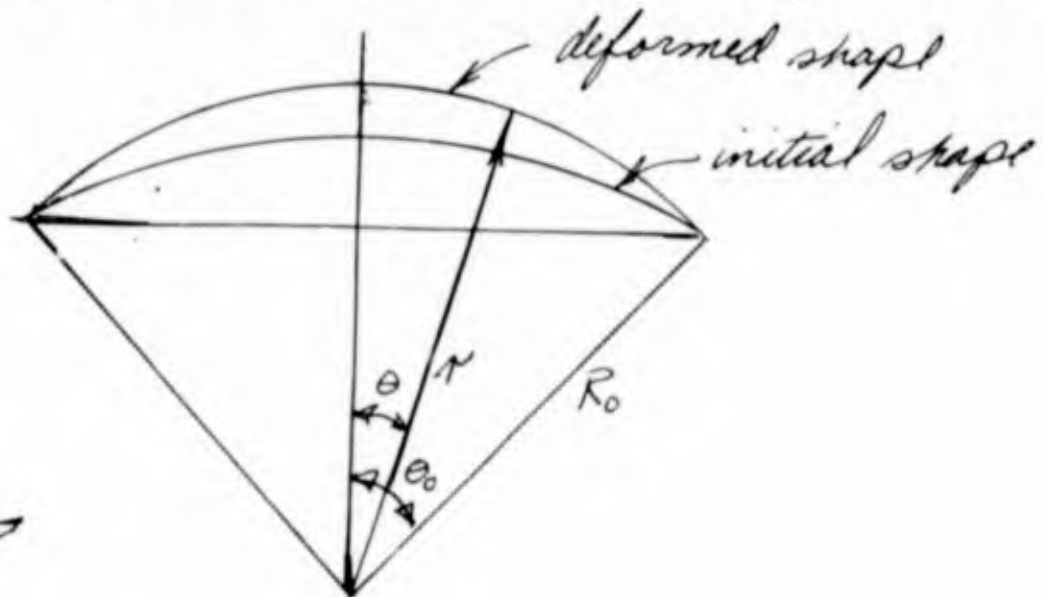


FIG. 7

APPENDIX VIII (continued)

The system of equations is
 $T = \text{const.}$

$$\frac{1}{R} = \frac{P}{T}$$

$$\frac{1}{R} = \frac{r^2 - r r'' + 2r'^2}{[r^2 + r'^2]^{3/2}} \quad \text{where } ()' = \frac{d}{d\theta} \quad (5.1)$$

$$S = \int_{-\theta_0}^{\theta_0} [r^2 + r'^2]^{1/2} d\theta = [1 + \frac{T}{\rho}] S_0$$

And the boundary conditions are

$$r = R_0 \quad \text{at } \theta = \pm \theta_0 \quad (5.2)$$

Now, we let

$$r = R_0(1 + \delta) \quad (5.3)$$

and consider δ small with respect to unity.

The expressions for R and S take the form

$$\frac{1}{R} = \frac{1}{R_0} \frac{(1 - 2\delta + \delta^2) - \delta''(1 + \delta) + 2(\delta')^2}{[1 + 2\delta + \delta^2 + (\delta')^2]^{3/2}} \quad (5.4)$$

$$S = R_0 \int_{-\theta_0}^{\theta_0} [1 + 2\delta + \delta^2 + (\delta')^2]^{1/2} d\theta \quad (5.5)$$

We note that $\delta' = \frac{d\delta}{d\theta}$ is approximately the angle between the tangents to the initial and deformed curves and therefore is a measure of the rotation of the tangent. Now, we assume δ and δ' are small w.r.t. to 1. Then using the expansion

APPENDIX VIII (continued)

$$(1+x)^n = 1 + nx + \frac{n(n-1)}{2!}x^2 + \dots \quad (5.6)$$

we have

$$\begin{aligned} [1 + \{2\delta + \delta^2 + \delta'^2\}]^{1/2} &\approx 1 + \delta + \frac{1}{2}(\delta^2 + \delta'^2) + \dots \\ [1 + \{2\delta + \delta^2 + \delta'^2\}]^{-3/2} &\approx 1 - 3\delta - \frac{3}{2}(\delta^2 + \delta'^2) + \dots \end{aligned} \quad (5.7)$$

Now we assume that

$$\begin{aligned} \delta^2 &\ll 1 \\ (\delta')^2 &\ll 1 \quad \delta\delta'' \ll 1 \end{aligned} \quad (5.8)$$

Then, Eqs 5.4 and 5.5 reduce to:

$$\frac{1}{R} = \frac{1}{R_0} [1 - \delta - \delta''] \quad (5.9)$$

$$S = 2R_0\theta_0 + R_0 \int_{-\theta_0}^{\theta_0} S d\theta = [1 + \frac{T}{D}] S_0 \quad (5.10)$$

Finally, the approximate system of equations is

$$S'' + S = 1 - \frac{R_0 P}{T} \quad (5.11)$$

$$S = 0 \text{ at } \theta = \pm \theta_0$$

$$\int_{-\theta_0}^{\theta_0} S d\theta = \frac{S_0}{R_0} \frac{T}{D} \quad (5.12)$$

We let

$$P = P_0 [1 + \bar{p}(\theta)] \quad (5.13)$$

APPENDIX VIII (continued)

Where P_0 is a constant and $|\bar{P}(\theta)|$ is small compared to unity. Also, we let

$$T = (R_0 P_0) \frac{1}{1+\tau} \quad (5.14)$$

where $|\tau|$ is small with respect to unity.

The equations take the form:

$$\delta'' + \delta = -\tau - (1+\tau)\bar{P} \quad (5.15)$$

$$\int_{-\theta_0}^{\theta_0} \delta d\theta = \frac{S_0 P_0}{D} \left[\frac{1}{1+\tau} \right] \quad (5.16)$$

$$\delta = 0 \text{ at } \theta = \pm \theta_0$$

The solution is:

$$\delta = -\tau + C_1 \cos \theta + C_2 \sin \theta - (1+\tau) S_p \quad (5.17)$$

where

$$S_p = -\cos \theta \int \bar{P}(\theta) \sin \theta d\theta + \sin \theta \int \bar{P}(\theta) \cos \theta d\theta \quad (5.18)$$

or alternately,

$$S_p = \int \bar{P}(\xi) \sin(\theta - \xi) d\xi \quad (5.19)$$

Equation (5.19) is more convenient for numerical integrations when $\bar{P}(\theta)$ is given in tabular form (we take the lower-limit as zero in this case).

The equations relating C_1 , C_2 , and τ are:

APPENDIX VIII (continued)

$$\begin{aligned}
 c_1 \cos \theta_0 + c_2 \sin \theta_0 &= \tau + (1 + \tau) [S_p]_{\theta = \theta_0} \\
 c_1 \cos \theta_0 - c_2 \sin \theta_0 &= \tau + (1 + \tau) [S_p]_{\theta = -\theta_0} \quad (5.20) \\
 \tau c_1 \sin \theta_0 - 2\theta_0 \tau - (1 + \tau) \int_{-\theta_0}^{\theta_0} S_p d\theta &= \frac{S_0 P_0}{D} \left[\frac{1}{1 + \tau} \right]
 \end{aligned}$$

Equations 5.20 reduce to

$$\begin{aligned}
 c_1 \cos \theta_0 &= \tau + \frac{1}{2} (1 + \tau) \{ [S_p]_{\theta = \theta_0} + [S_p]_{\theta = -\theta_0} \} \\
 c_2 \sin \theta_0 &= \frac{1}{2} (1 + \tau) \{ [S_p]_{\theta = \theta_0} - [S_p]_{\theta = -\theta_0} \} \\
 -\tau + c_1 \frac{\sin \theta_0}{\theta_0} - \left(\frac{1 + \tau}{2\theta_0} \right) \int_{-\theta_0}^{\theta_0} S_p d\theta &= \frac{P_0 P_0}{D} \left[\frac{1}{1 + \tau} \right] \\
 &\quad (5.21)
 \end{aligned}$$

We see from Eqs. 5.21 that c_2 vanishes when $p(\theta)$ is an even function of θ . Also, c_1 and τ do not involve $\bar{p}(\theta)$ when $\bar{p}(\theta)$ is an odd function of θ .

We write

$$\bar{p} = \bar{p}_E + \bar{p}_O \quad (5.22)$$

where \bar{p}_E is an even function of θ and \bar{p}_O is an odd function of θ . Then,

$$S_p = S_{p,E} + S_{p,O} \quad (5.23)$$

APPENDIX VIII (continued)

Equations 5.21 reduce to:

$$C_2 \sin \theta_0 = (1 + \tau) [S_{P,0}]_{\theta=\theta_0} \quad (5.24)$$

and

$$C_1 \cos \theta_0 = \tau + (1 + \tau) [S_{P,E}]_{\theta=\theta_0} \quad (5.25)$$

$$C_1 \frac{\sin \theta}{\theta_0} - \tau - \left(\frac{1 + \tau}{2\theta_0} \right) \int_{-\theta_0}^{\theta_0} S_{P,E} d\theta = \frac{R_0 P_0}{D} \left[\frac{1}{1 + \tau} \right]$$

∴ We will consider various pressure distributions.

Case A - Uniform Pressure

We take $\bar{p}(\theta) = 0$. Then, $S_p = 0$. Eqn 5.25

reduce to:

$$C_1 \cos \theta_0 = \tau \quad (5.26)$$

$$C_1 \frac{\sin \theta_0}{\theta_0} - \tau = \frac{R_0 P_0}{D} \left[\frac{1}{1 + \tau} \right]$$

Then, $C_1 = \frac{\tau}{\cos \theta_0} \quad (5.27)$

and

$$t \approx \frac{R_0 P_0}{D} \frac{1}{\frac{\sin \theta_0}{\theta_0 \cos \theta_0} - 1} \quad (5.28)$$

The expressions for τ and T are:

$$T = (R_0 P_0) \frac{1}{1 + \tau} \quad (5.29)$$

$$\tau = R_0 (1 + \delta) \text{ where } \delta = \tau \left\{ \frac{\cos \theta}{\cos \theta_0} - 1 \right\} \quad (5.30)$$

APPENDIX VIII (continued)

This solution agrees with the solutions obtained in section 4.

When $\theta_0 = \frac{\pi}{2}$, the solution is

$$\tau = 0$$

$$C_1 = \frac{\pi}{2} \left(\frac{R_0 P_0}{D} \right) \quad (5.31)$$

$$S = \frac{\pi}{2} \left(\frac{R_0 P_0}{D} \right) \cos \theta$$

$$T = R_0 P_0$$

Case B - Linear Variation In Pressure

We take

$$\bar{p}(\theta) = a \frac{\theta}{\theta_0} \quad (5.32)$$

where a is a constant. The particular solution is

$$S_p = a \frac{\theta}{\theta_0}$$

Now, C_1 and τ are given by Eqs. 5.27 and 5.28. The expression for C_2 follows from Eq. 5.24.

$$C_2 = a \frac{1 + \tau}{\sin \theta_0}$$

Finally, the solution for S is:

$$S = \tau \left\{ \frac{\cos \theta}{\cos \theta_0} - 1 \right\} + a (1 + \tau) \left\{ \frac{\sin \theta}{\sin \theta_0} - \frac{\theta}{\theta_0} \right\} \quad (5.34)$$

We consider τ to be negligible and take the solution as:

APPENDIX VIII (continued)

$$s \approx a \left\{ \frac{\sin \theta}{\sin \theta_0} - \frac{\theta}{\theta_0} \right\} \quad (5.35)$$

The derivatives are

$$s' \approx \frac{dr}{ds} \approx a \left\{ \frac{\cos \theta}{\sin \theta_0} - \frac{1}{\theta_0} \right\} \quad (5.36)$$

$$s'' = -a \frac{\sin \theta}{\sin \theta_0} \quad (5.37)$$

The slope is a maximum at $\theta = 0$ and is given by:

$$s'_{\max} \approx a \left[\frac{1}{\sin \theta_0} - \frac{1}{\theta_0} \right] \quad (5.38)$$

The deflection is a maximum at $\theta = \theta_m$ when

$$\cos \theta_m = \frac{\sin \theta_0}{\theta_0} \quad (5.39)$$

$$s_m = a \left\{ \frac{\sin \theta_m}{\sin \theta_0} - \frac{\theta_m}{\theta_0} \right\} \quad (5.40)$$

Results for various values of θ_0 are tabulated below:

θ_0	θ_m	s_m/a	s'_{\max}/a
15°	9°	0.003	0.04
30°	17°	0.018	0.09
45°	25.5°	0.041	0.14
60°	34°	0.078	0.20
75°	42.5°	0.134	0.27

APPENDIX VIII (continued)

Note that S is the relative change in the radius and S' is the rotation of the tangent (radians).

In the analysis, we have neglected S^2 , S'^2 , and SS'' with respect to unity. The results listed above indicate that these approximations are reasonable when a is of the order of unity. The limiting value of " a " will generally be determined by $S'm$.

Case C - General Pressure Distribution

We consider next the case where $\bar{p}(\theta)$ is given in tabular form. The particular solution, S_p , can be obtained by integrating the indefinite integral (Eq 5.19) numerically.

$$S_p(\theta) = \int_0^\theta \bar{p}(\xi) \sin(\theta - \xi) d\xi \quad (5.41)$$

Once $S_p(\theta)$ is known, the remaining integral,

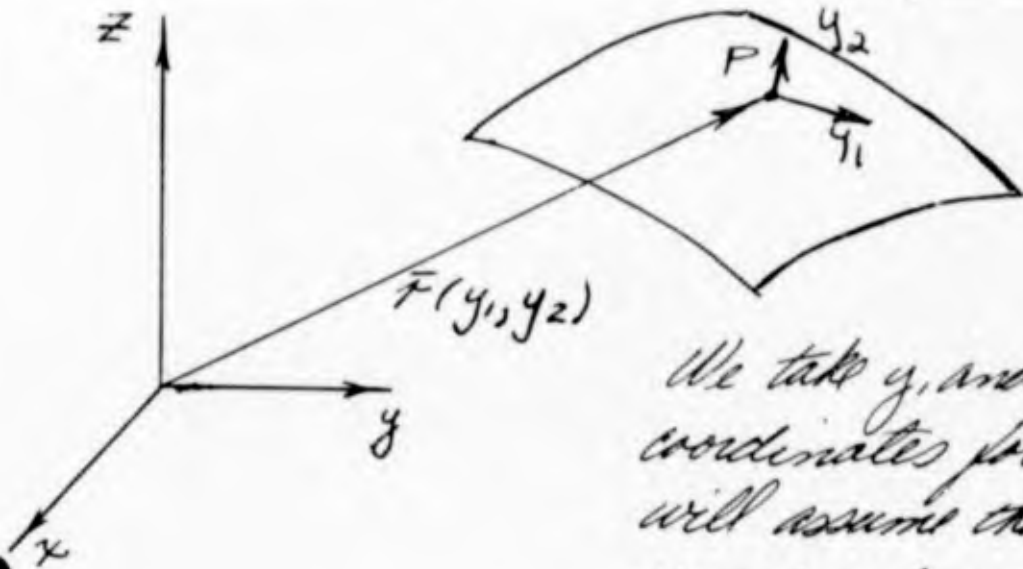
$$\int_{-\theta_0}^{\theta_0} S_p d\theta \quad (5.42)$$

can be readily determined and the constants C_1 , C_2 , and T can be found with Eqs 5.21. Simpson's rule can be used in the numerical integration. The determination of S_p and the evaluation of the integral can be combined in a single computer program.

APPENDIX VIII (continued)

Static Membrane Analysis
 (shallow shell theory)

1. Geometric Relations For Surface



We take y_1 and y_2 as curvilinear coordinates for the shell surface. We will assume that the coordinate lines, $y_1 = \text{const.}$ and $y_2 = \text{const.}$ are orthogonal. This requires

$$\frac{\partial \bar{r}}{\partial y_1} \cdot \frac{\partial \bar{r}}{\partial y_2} = 0 \quad (1)$$

where \bar{r} is the position vector to the surface. The first fundamental form for arc length reduces to:

$$dS^2 = \alpha_1^2 dy_1^2 + \alpha_2^2 dy_2^2 \quad (2a)$$

where

$$\alpha_1^2 = \frac{\partial \bar{r}}{\partial y_1} \cdot \frac{\partial \bar{r}}{\partial y_1} \quad (2b)$$

$$\alpha_2^2 = \frac{\partial \bar{r}}{\partial y_2} \cdot \frac{\partial \bar{r}}{\partial y_2}$$

APPENDIX VIII (continued)

The third Lamé parameter, $\alpha_{12} = \frac{\partial \bar{r}}{\partial y_1} \cdot \frac{\partial \bar{r}}{\partial y_2}$, is zero when the coordinate lines are orthogonal.

Using (2b), the unit tangent vectors and the normal vector are:

$$\bar{t}_1 = \frac{1}{\alpha_1} \frac{\partial \bar{r}}{\partial y_1} \quad (3)$$

$$\bar{t}_2 = \frac{1}{\alpha_2} \frac{\partial \bar{r}}{\partial y_2}$$

$$\bar{n} = \bar{t}_1 \times \bar{t}_2$$

We do not assume that the coordinate lines are lines of curvature. The differentiation formulas for the unit vectors have the form

$$\bar{t}_{j,j} = -\frac{\alpha_{j,k}}{\alpha_k} \bar{t}_k - \frac{\alpha_j}{R_{jj}} \bar{n} \quad (4a) \quad j \neq k$$

$j, k = 1, 2$

$$\bar{t}_{j,k} = \frac{\alpha_{k,j}}{\alpha_j} \bar{t}_k - \frac{\alpha_k}{R_{jk}} \bar{n} \quad (4b) \quad j \neq k$$

$j, k = 1, 2$

$$\bar{n}_{,j} = \frac{\alpha_j}{R_{jj}} \bar{t}_j + \frac{\alpha_j}{R_{jk}} \bar{t}_k \quad (4c) \quad j \neq k$$

$j, k = 1, 2$

where

$$\frac{1}{R_{jk}} = -\frac{1}{\alpha_j \alpha_k} \bar{n} \cdot \bar{r}_{,jk} \quad (4d)$$

APPENDIX VIII (continued)

and we have used the standard notation for partial differentiation for example, $\frac{\partial \bar{r}}{\partial y_2} = \bar{r}_{,2}$

With the above definition of R_{jk} , the second fundamental form for the surface takes the form:

$$d\bar{r} \cdot d\bar{n} = \frac{\alpha_1^2}{R_{11}} dy_1^2 + \frac{2\alpha_1\alpha_2}{R_{12}} dy_1 dy_2 + \frac{\alpha_2^2}{R_{22}} dy_2^2 \quad (5)$$

Finally, the three Gauss - Codazzi Relations which are actually continuity requirements for the surface are:

$$\alpha_j \left(\frac{1}{R_{jj}} \right)_{,k} - \alpha_k \left(\frac{1}{R_{jk}} \right)_{,j} = \alpha_{j,k} \left(\frac{1}{R_{kk}} - \frac{1}{R_{jj}} \right) + 2\alpha_{k,j} \frac{1}{R_{jk}} \quad (6a)$$

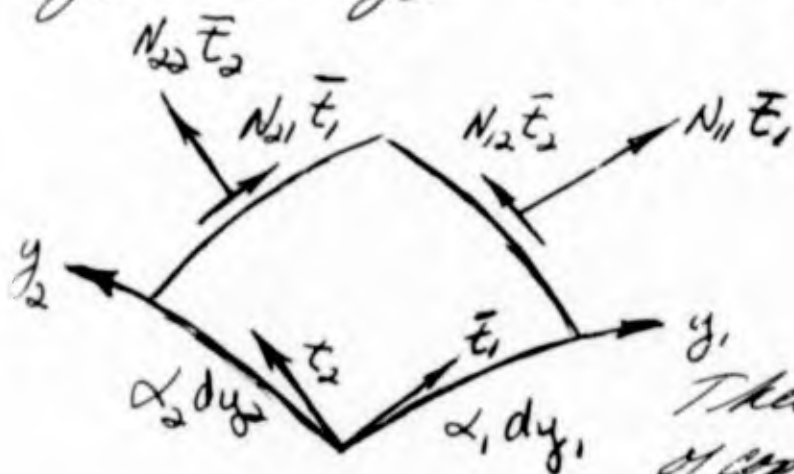
$$\alpha_1 \alpha_2 \left(\frac{1}{R_{12}} - \frac{1}{R_{11} R_{22}} \right) = \left(\frac{\alpha_{2,1}}{\alpha_1} \right)_{,1} + \left(\frac{\alpha_{1,2}}{\alpha_2} \right)_{,2} \quad (6b)$$

APPENDIX VIII (continued)

Equilibrium Equations

We consider an element of the surface bounded by the curves $y_1 = c_1$, $y_1 = c_1 + dy_1$, $y_2 = c_2$, $y_2 = c_2 + dy_2$. The arc lengths are $\alpha_1 dy_1$ and $\alpha_2 dy_2$.

We define \bar{N}_j as the stress resultant vector per unit width associated with the face whose normal acts in the \bar{t}_j direction.



These vectors are expressed in terms of components with respect to the \bar{t}_1, \bar{t}_2 directions.

Figure 2

$$\bar{N}_j = N_{j1} \bar{t}_1 + N_{j2} \bar{t}_2 \quad (5)$$

We define P as the external normal force per unit area, positive when in the positive normal direction. Summing up forces in the \bar{t}_1, \bar{t}_2 , and \bar{n} directions, we obtain the following system of 3 equilibrium equations.

$$\frac{\partial}{\partial y_1} (N_{11} \alpha_2) + \frac{\partial}{\partial y_2} (N_{21} \alpha_1) + N_{12} \alpha_{1,2} - N_{22} \alpha_{2,1} = 0 \quad (6a)$$

$$\frac{\partial}{\partial y_1} (N_{12} \alpha_2) + \frac{\partial}{\partial y_2} (N_{22} \alpha_1) + N_{21} \alpha_{2,1} - N_{11} \alpha_{1,2} = 0 \quad (6b)$$

$$\frac{N_{11}}{R_{11}} + \frac{N_{22}}{R_{22}} + \frac{1}{R_{12}} (N_{12} + N_{21}) = P \quad (6c)$$

APPENDIX VIII (continued)

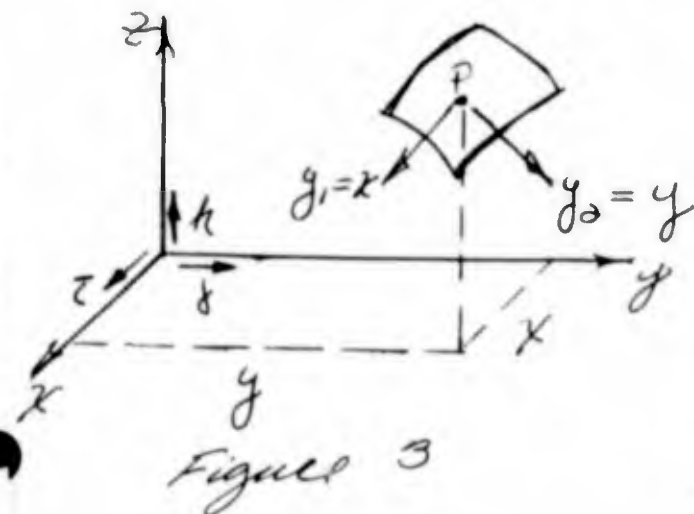
Consideration of the moment equilibrium of the element about the normal leads to the requirement that

$$N_{12} = N_{21} \quad (6d)$$

Therefore, there are three unknown stress resultants at a point N_{11} , N_{22} , and N_{12} . Equations (6) appear to be quite simple in form. However, in order to solve this system, the location of the surface must be known, that is, we must know α_s and $R_{j,k}$. In conventional thin shell theory, no distinction is made between the deformed and undeformed geometries. We will consider the case where the surface is shallow. In order to handle a non shallow surface, we must start with a non-orthogonal curvilinear coordinate system, and the equations are quite complex.

3 Specialization To Shallow Surfaces

We take the equations of the deformed surface as

$$z = Z(x, y) \quad (7)$$


The position vector to a point (x, y, z) is

$$r = x\bar{i} + y\bar{j} + z\bar{k} \quad (8)$$

where \bar{i} , \bar{j} , \bar{k} are unit vectors in the x , y , z directions. Now, we consider x and y to be the curvilinear coordinates.

APPENDIX VIII (continued)

$x = y_1, \quad y = y_2$ (9)
The Lamé parameters are

$$\alpha_1^2 = \frac{\partial \bar{r}}{\partial y_1} \cdot \frac{\partial \bar{r}}{\partial y_1} = 1 + z_{,x}^2$$

$$\alpha_2^2 = \frac{\partial \bar{r}}{\partial y_2} \cdot \frac{\partial \bar{r}}{\partial y_2} = 1 + z_{,y}^2 \quad (10)$$

$$\alpha_{12}^2 = \frac{\partial \bar{r}}{\partial y_1} \cdot \frac{\partial \bar{r}}{\partial y_2} = z_{,x} z_{,y}$$

When the surface is shallow,

$$z_{,x} \ll 1 \quad \text{and} \quad z_{,y} \ll 1$$

Therefore, we take

$$\alpha_1^2 \approx 1 \quad \alpha_2^2 \approx 1 \quad \alpha_{12} \approx 0 \quad (11)$$

and consider the coordinate directions to be orthogonal.

The unit tangent vectors are

$$\bar{t}_1 = \frac{1}{\alpha_1} \frac{\partial \bar{r}}{\partial y_1} \approx \bar{i} + z_{,x} \bar{k}$$

$$\bar{t}_2 = \frac{1}{\alpha_2} \frac{\partial \bar{r}}{\partial y_2} \approx \bar{j} + z_{,y} \bar{k}$$

Then, the normal vector is

$$\bar{n} = \bar{t}_1 \times \bar{t}_2 \approx \begin{vmatrix} \bar{i} & \bar{j} & \bar{k} \\ 1 & 0 & z_{,x} \\ 0 & 1 & z_{,y} \end{vmatrix} \approx -z_{,x} \bar{i} - z_{,y} \bar{j} + \bar{k} \quad (12)$$

APPENDIX VIII (continued)

Finally, the curvature terms, R_{jk} , reduce to:

$$\frac{1}{R_{11}} = -Z_{,xx}$$

$$\frac{1}{R_{22}} = -Z_{,yy} \quad (14)$$

$$\frac{1}{R_{12}} = -Z_{,xy}$$

We consider next the Gauss-Codazzi Equations. The first two are identically satisfied by (11) and (14). The third equation involves an error of the order of curvature squared and we have assumed this to be negligible. Therefore, the Gauss-Codazzi Equations are satisfied to the degree of our approximation.

We now examine the equilibrium equations. Taking $\alpha_1 = \alpha_2 = 1$ and $N_{12} = N_{21}$, these equations reduce to

$$\frac{\partial}{\partial x} N_{11} + \frac{\partial}{\partial y} N_{12} = 0 \quad (15a)$$

$$\frac{\partial}{\partial x} N_{12} + \frac{\partial}{\partial y} N_{22} = 0 \quad (15b)$$

$$N_{11} Z_{,xx} + 2N_{12} Z_{,xy} + Z_{,yy} N_{22} + P = 0 \quad (15c)$$

Equations 15 involve 4 unknowns,

N_{11} , N_{12} , N_{22} , and Z^2 . We can reduce these equations by introducing a stress function.

APPENDIX VIII (continued)

$$\begin{aligned} \text{Let } N_{11} &= \frac{\partial^2 F}{\partial y^2} = F_{,yy} \\ N_{22} &= \frac{\partial^2 F}{\partial x^2} = F_{,xx} \\ N_{12} &= -\frac{\partial^2 F}{\partial x \partial y} = -F_{,xy} \end{aligned} \quad (16)$$

With this definition of F , the first two equations are identically satisfied, and the third equation reduces to

$$z_{,xx} F_{,yy} - 2z_{,xy} F_{,xy} + z_{,yy} F_{,xx} + \rho = 0 \quad (17)$$

Finally, we obtain an additional equation involving z by assuming the shell is inextensible. Let A_0 be the surface area associated with the undeformed shell. The surface area element for the deformed position is given by

$$dA = \left| \frac{\partial \bar{r}}{\partial y_1} \times \frac{\partial \bar{r}}{\partial y_2} \right| dy_1 dy_2 \quad (18)$$

This reduces to

$$dA = \left\{ 1 + z_{,x}^2 + z_{,y}^2 \right\}^{1/2} dx dy \quad (19)$$

Assuming that $z_{,x}^2$ and $z_{,y}^2$ are small with respect to unity, we write (19) as

$$dA = \left\{ 1 + \frac{1}{2} (z_{,x}^2 + z_{,y}^2) \right\} dx dy \quad (20)$$

APPENDIX VIII (continued)

Finally, the inextensibility requirement takes the form

$$\int_x \int_y \left\{ 1 + \frac{1}{2} (z_{,x}^2 + z_{,y}^2) \right\} dx dy = A_0 \quad (21)$$

It remains to solve Eqs. (17) and (21) and satisfy the boundary conditions of z and F . We postpone further discussion of these equations until we have discussed the transformation law for the stress resultants.

4. Stress Resultant Transformation Law

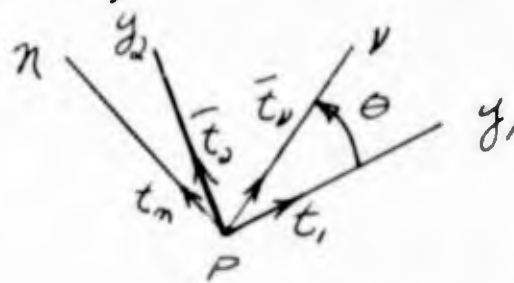
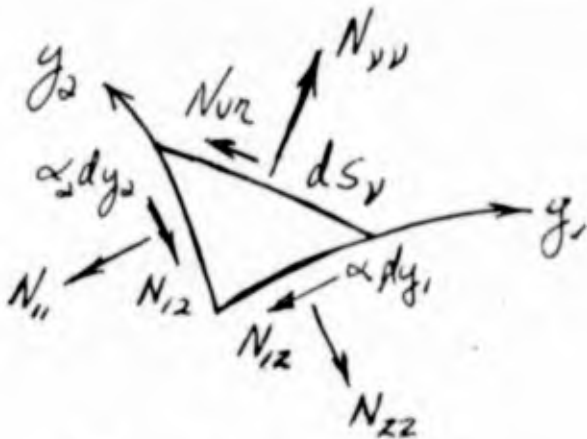


Figure 4.

for these directions be \bar{t}_v and \bar{t}_n . We want to determine the stress resultants per unit width, denoted by $N_{vv}, N_{vn} = N_{nv}, N_{nn}$, for these directions. The corresponding vectors are

$$\begin{aligned} \bar{N}_v &= N_{vv} \bar{t}_v + N_{vn} \bar{t}_n \\ \bar{N}_n &= N_{nv} \bar{t}_v + N_{nn} \bar{t}_n \end{aligned} \quad (22)$$

APPENDIX VIII (continued)

$$\begin{aligned} \bar{t}_v &= \cos \theta \bar{t}_1 + \sin \theta \bar{t}_2 \\ \bar{t}_n &= -\sin \theta \bar{t}_1 + \cos \theta \bar{t}_2 \end{aligned} \quad (23)$$

The transformation law, expressed in matrix form is *

$$\begin{bmatrix} N_{vv} & N_{vn} \\ N_{nv} & N_{nn} \end{bmatrix} = \begin{bmatrix} \cos \theta & \sin \theta \\ -\sin \theta & \cos \theta \end{bmatrix} \begin{bmatrix} N_{11} & N_{12} \\ N_{21} & N_{22} \end{bmatrix} \begin{bmatrix} \cos \theta & -\sin \theta \\ \sin \theta & \cos \theta \end{bmatrix} \quad (24)$$

Expanding, we have

$$\begin{aligned} N_{vv} &= N_{11} \cos^2 \theta + N_{22} \sin^2 \theta + 2N_{12} \sin \theta \cos \theta \\ N_{nn} &= N_{11} \sin^2 \theta + N_{22} \cos^2 \theta - 2N_{12} \sin \theta \cos \theta \\ N_{vn} &= N_{nv} = N_{12} (\cos^2 \theta - \sin^2 \theta) + \sin \theta \cos \theta (N_{22} - N_{11}) \end{aligned} \quad (25)$$

Once N_{11} , N_{22} , and N_{12} are known, we can find the stress resultants associated with any two orthogonal directions through the point.

* See "Matrix-tensor Methods in Continuum Mechanics",
- S.F. Borg, Van Nostrand Co., 1963.

APPENDIX VIII (continued)

Work sheet for page 34 and equilibrium equation 15.

$$\frac{\partial N_{11}}{\partial x} \Rightarrow T_V \cos \theta \sin \theta \frac{\partial \theta}{\partial x} + \cos^2 \theta \frac{\partial T_V}{\partial x}$$

$$+ \partial T_N \sin \theta \cos \theta \frac{\partial \theta}{\partial x} + \sin^2 \theta \frac{\partial T_N}{\partial x}$$

$$\frac{\partial N_{11}}{\partial x} = \sin \theta \cos \theta \frac{\partial \theta}{\partial x} (T_N - T_V) + \cos^2 \theta \frac{\partial T_V}{\partial x} + \sin^2 \theta \frac{\partial T_N}{\partial x}$$

By analogy

$$\frac{\partial N_{22}}{\partial y} = \sin \theta \cos \theta \frac{\partial \theta}{\partial y} (T_V - T_N) + \cos^2 \theta \frac{\partial T_N}{\partial y} + \sin^2 \theta \frac{\partial T_V}{\partial y}$$

also

$$\frac{\partial N_{12}}{\partial x} = (T_V - T_N) \cos \theta \sin \theta \frac{\partial \theta}{\partial x} + \frac{1}{2} \sin \theta \cos \theta \left(\frac{\partial T_V}{\partial x} - \frac{\partial T_N}{\partial x} \right)$$

$$\frac{\partial N_{12}}{\partial y} = (T_V - T_N) \cos \theta \sin \theta \frac{\partial \theta}{\partial y} + \frac{1}{2} \sin \theta \cos \theta \left(\frac{\partial T_V}{\partial y} - \frac{\partial T_N}{\partial y} \right)$$

Eq. 15a

$$\frac{\partial N_{11}}{\partial x} + \frac{\partial N_{12}}{\partial y} = 0$$

$$(T_V - T_N) \left\{ \cos \theta \sin \theta \frac{\partial \theta}{\partial y} - \sin \theta \cos \theta \frac{\partial \theta}{\partial x} \right\} + \frac{1}{2} \sin \theta \cos \theta \left(\frac{\partial T_V}{\partial y} - \frac{\partial T_N}{\partial y} \right) + \cos^2 \theta \frac{\partial T_V}{\partial x} + \sin^2 \theta \frac{\partial T_N}{\partial x} = 0$$

Eq. 15b

$$\frac{\partial N_{12}}{\partial x} + \frac{\partial N_{22}}{\partial y} = 0$$

$$(T_V - T_N) \left\{ \cos \theta \sin \theta \frac{\partial \theta}{\partial x} + \sin \theta \cos \theta \frac{\partial \theta}{\partial y} \right\} + \frac{1}{2} \sin \theta \cos \theta \left(\frac{\partial T_V}{\partial x} - \frac{\partial T_N}{\partial x} \right) + \sin^2 \theta \frac{\partial T_V}{\partial y} + \cos^2 \theta \frac{\partial T_N}{\partial y} = 0$$

End of work sheet

APPENDIX VIII (continued)

Now, let us take the ν and π directions to coincide with the principal directions of the wire reinforcement which are assumed to be orthogonal. We let

$$N_{\nu\nu} = T_{\nu} \quad N_{\pi\pi} = T_{\pi} \quad (26)$$

and take $N_{\nu\pi} = 0$. The quantity, T_{ν} , is the force per unit length due to the wires in the ν direction. If n_{ν} is the number of " ν " wires per unit length in the π direction, then the force in a " ν " wire is $\frac{T_{\nu}}{n_{\nu}}$. Similarly, the force in an " π " wire is $\frac{T_{\pi}}{n_{\pi}}$. This is illustrated in the sketch shown below.

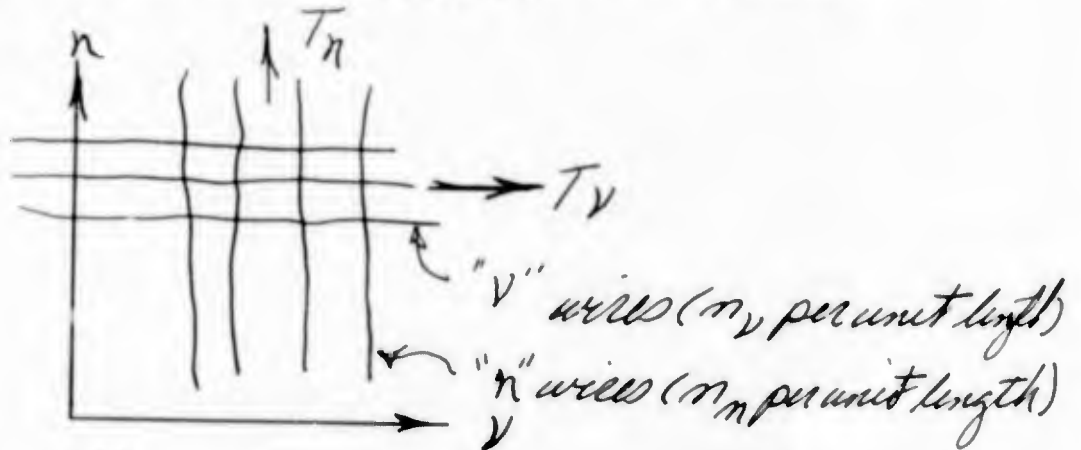


Figure 5

Using (26) and (25), we can express N_{11} , N_{12} and N_{22} in terms of T_{ν} , T_{π} , and θ where θ is the angle between the ν axis and the y_1 direction which corresponds to the direction of increasing χ (Refer to Figure 4)

$$\begin{aligned} N_{11} &= T_{\nu} \cos^2 \theta + T_{\pi} \sin^2 \theta \\ N_{22} &= T_{\nu} \sin^2 \theta + T_{\pi} \cos^2 \theta \\ N_{12} &= (T_{\nu} - T_{\pi}) \sin \theta \cos \theta = \frac{1}{2} (T_{\nu} - T_{\pi}) \sin 2\theta \end{aligned} \quad (27)$$

Note: To obtain (27) from (25), we interchange ν and π , π and y_2 , and take $N_{\nu\pi} = 0$ and $\theta = -\theta$.

APPENDIX VIII (continued)

We will now reconsider the equilibrium equations using the expansion for N_{11} , N_{12} , and N_{22}

5. Alternate System of Equations - Shallow Shell

We substitute for N_{11} , N_{22} , and N_{12} using (27) into the original equilibrium equations (see page 35), Eq. 15,

$$(T_1 - T_2) \left\{ \cos 2\theta \frac{\partial \theta}{\partial y} - \sin 2\theta \frac{\partial \theta}{\partial x} \right\} + \frac{1}{2} \sin 2\theta \left\{ \frac{\partial T_1}{\partial y} - \frac{\partial T_2}{\partial y} \right\} + \cos^2 \theta \frac{\partial T_1}{\partial x} + \sin^2 \theta \frac{\partial T_2}{\partial x} = 0 \quad (28a)$$

$$(T_2 - T_1) \left\{ \cos 2\theta \frac{\partial \theta}{\partial x} + \sin 2\theta \frac{\partial \theta}{\partial y} \right\} + \frac{1}{2} \sin 2\theta \left\{ \frac{\partial T_1}{\partial x} - \frac{\partial T_2}{\partial x} \right\} + \sin^2 \theta \frac{\partial T_1}{\partial y} + \cos^2 \theta \frac{\partial T_2}{\partial y} = 0 \quad (28b)$$

$$\left\{ T_1 \cos^2 \theta + T_2 \sin^2 \theta \right\} \frac{\partial^2 z}{\partial x^2} + \left\{ (T_1 - T_2) \sin 2\theta \right\} \frac{\partial^2 z}{\partial x \partial y} + \left\{ T_1 \sin^2 \theta + T_2 \cos^2 \theta \right\} \frac{\partial^2 z}{\partial y^2} + p = 0 \quad (28c)$$

We also have the inextensibility condition

$$\int_x \int_y \left\{ 1 + \frac{1}{2} \left(\frac{\partial z}{\partial x} \right)^2 + \frac{1}{2} \left(\frac{\partial z}{\partial y} \right)^2 \right\} dx dy = A_0 \quad (28d)$$

We have four equations relating unknowns

APPENDIX VIII (continued)

T_V , T_N , θ , and z . Note that θ is the angle between the coordinate line having the unit tangent vector, \bar{t}_1 , and the V direction.

6. Solutions of Equations 28

We assume $T_V = T_N = \text{constant} = C$. This leads to $N_{11} = N_{22} = C$ and $N_{12} = 0$. Equations 28c reduces to

$$\nabla^2 z = \frac{\partial^2 z}{\partial x^2} + \frac{\partial^2 z}{\partial y^2} = \frac{\rho}{C} \quad (29a)$$

where $\rho = \rho(x, y)$. Equation 28d remains the same,

$$\iint_{x, y} \left\{ 1 + \frac{1}{2} \left(\frac{\partial z}{\partial x} \right)^2 + \frac{1}{2} \left(\frac{\partial z}{\partial y} \right)^2 \right\} dx dy = A_0 \quad (29b)$$

It remains to solve Eqs (29a) and (29b) and satisfy the boundary conditions.

We consider the case where z is prescribed on the S boundaries. To solve the above system, we take a grid on the surface and replace the differential operators by finite difference operators. It is convenient to take constant intervals in the x and y directions although it is not necessary. We start by constructing a rectangular grid on the plane of the surface, that is, on the projection of the surface in the x - y plane. This is shown in Figure 6. This projection will be rectangular if the surface is bounded by planes perpendicular to the x - y plane.

APPENDIX VIII (continued)

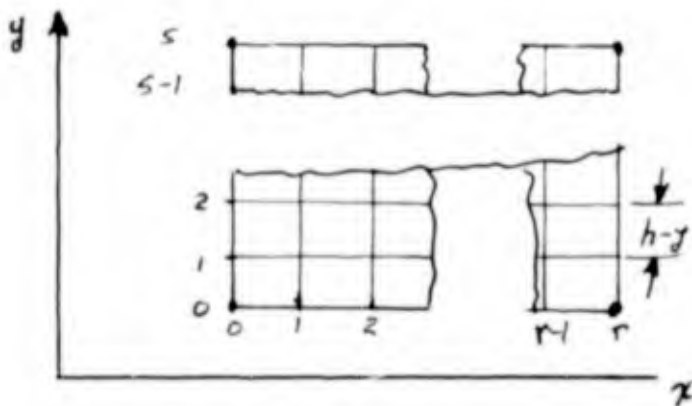


Figure 6.

directions, the partial derivatives at (n, m) reduce to (note: we are using central differences):

$$\left(\frac{\partial^2 z}{\partial x^2}\right)_{\substack{x=x_n \\ y=y_m}} = \frac{z(n+1, m) - 2z(n, m) + z(n-1, m)}{h_x^2} \quad (30a)$$

$$\left(\frac{\partial^2 z}{\partial y^2}\right)_{\substack{x=x_n \\ y=y_m}} = \frac{z(n, m+1) - 2z(n, m) + z(n, m-1)}{h_y^2} \quad (30b)$$

The differential equation for point (n, m) takes the form

$$z(n+1, m) + z(n-1, m) + [z(n, m+1) + z(n, m-1)] \left(\frac{h_x}{h_y}\right)^2 - 2z(n, m) \left[1 + \left(\frac{h_x}{h_y}\right)^2\right] = -\frac{h_x^2}{c} \rho(n, m) \quad (31)$$

and the boundary conditions are

$$\begin{aligned} \text{on } x=x_0 & \quad z(0, j) = f_1(0, j) & \quad j = 0, 1, 2, \dots, s \\ \text{on } y=y_0 & \quad z(k, 0) = g_1(k, 0) & \quad k = 0, 1, 2, \dots, n \end{aligned} \quad (32a)$$

APPENDIX VIII (continued)

$$\begin{aligned} \text{on } x = x_r \quad z(r, j) &= f_2(r, j) \quad j = 1, 2, \dots, 5 \\ \text{on } y = y_s \quad z(k, s) &= g_2(k, s) \quad k = 1, 2, \dots, r \end{aligned} \quad (32b)$$

where f_1, f_2, g_1, g_2 are given functions of x and y . Using difference operators, the equilibrium equation, (29a), is replaced by a set of $(r-2)(s-2)$ linear algebraic equations relating $z(m, m)$ where $m = 1, 2, \dots, r-1$ and $m = 1, 2, \dots, s-1$. The coefficient matrix is essentially quasi-diagonal and is particularly suited for iterative techniques such as relaxation.

The reduction of equations (29b) involves replacing integration by a summation. We note first that (29b) can be written in an alternate form, using Green's theorem. Green's Theorem reduces an area integral to a line integral around the boundary curve. If $\phi = \phi(x, y)$, then according to Green's Theorem,

$$\iint_A \left[\phi \nabla^2 \phi + \left(\frac{\partial \phi}{\partial x} \right)^2 + \left(\frac{\partial \phi}{\partial y} \right)^2 \right] dx dy = \oint_c \phi \frac{\partial \phi}{\partial n} ds \quad (33)$$

$$\text{where } \frac{\partial \phi}{\partial n} = l_y \frac{\partial \phi}{\partial x} + m_y \frac{\partial \phi}{\partial y} = \text{normal derivative}$$

and l_y, m_y are the direction cosines for the outward normal to the boundary curve with respect to the x and y directions. The positive direction for the line integration is taken as counter-clockwise.

APPENDIX VIII (continued)

The boundary curve for our problem consist of four straight lines parallel to either the x or y directions. Then, denoting the corner points by $A, B, C,$ and $D,$ we have

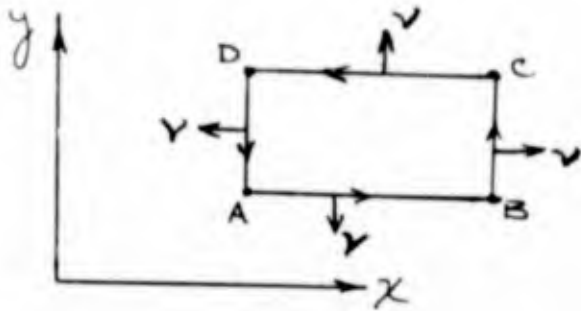


Figure 7

1) $A \rightarrow B$

$$l_y = 0 \quad m_y = -1$$

$$\frac{\partial z}{\partial n} = - \frac{\partial z}{\partial y}$$

2.) $B \rightarrow C$

$$l_y = +1 \quad m_y = 0$$

$$\frac{\partial z}{\partial n} = + \frac{\partial z}{\partial x}$$

3.) $C \rightarrow D$

$$l_y = 0 \quad m_y = +1$$

$$\frac{\partial z}{\partial n} = + \frac{\partial z}{\partial y}$$

4.) $D \rightarrow A$

$$l_y = -1 \quad m_y = 0$$

$$\frac{\partial z}{\partial n} = - \frac{\partial z}{\partial x}$$

Using $\nabla^2 z = -\frac{\rho}{c}$, we can write

$$\iint_{xy} \left[\left\{ \frac{\partial z}{\partial x} \right\}^2 + \left\{ \frac{\partial z}{\partial y} \right\}^2 \right] dx dy = \oint z \frac{\partial z}{\partial n} ds + \iint_A \frac{\rho}{c} dx dy \quad (34)$$

APPENDIX VIII (continued)

and the inextensibility requirement reduces to

$$\iint_A z \frac{\rho}{c} dx dy + \oint z \frac{\partial z}{\partial n} ds = 2(A_0 - A^*) \quad (35a)$$

$$\text{where } A^* = \iint_A dx dy \quad (35b)$$

It follows from Figure 6 that

$$A^* = r_s h_x h_y \quad (36)$$

We will use forward differences for the segments DA, AB, and backward segments for BC, CD.

1. DA

$$\left(\frac{\partial z}{\partial n}\right)_{0,j} = -\left(\frac{\partial z}{\partial x}\right)_{0,j} = -\frac{1}{h_x} \{z(1,j) - z(0,j)\}$$

$$\left(z \frac{\partial z}{\partial n}\right)_{0,j} = \frac{1}{h_x} \{f_1(0,j) - z(1,j)\} f_1(0,j)$$

$$ds = h_y \quad (37a)$$

$$j = 0, 1, 2, \dots, 5$$

2. AB

$$\left(\frac{\partial z}{\partial n}\right)_{k,0} = -\left(\frac{\partial z}{\partial y}\right)_{k,0} = -\frac{1}{h_y} \{z(k,1) - z(k,0)\}$$

$$\left(z \frac{\partial z}{\partial n}\right)_{k,0} = \frac{1}{h_y} \{g_1(k,0) - z(k,1)\} g_1(k,0)$$

$$(37b)$$

$$ds = h_x \quad k = 0, 1, 2, \dots, r$$

APPENDIX VIII (continued)

3 BC

$$\left(\frac{\partial z}{\partial n}\right)_{r,j} = \left(\frac{\partial z}{\partial x}\right)_{r,j} = \frac{1}{h_x} \{z(r,j) - z(r-1,j)\}$$

$$\left(z \frac{\partial z}{\partial n}\right)_{r,j} = \frac{1}{h_x} \{z(r,j) - z(r-1,j)\} f_2(r,j)$$

$$j = 0, 1, 2, \dots, 5 \quad (37c)$$

$$ds = h_y$$

4. CD

$$\left(\frac{\partial z}{\partial n}\right)_{k,s} = \left(\frac{\partial z}{\partial y}\right)_{k,s} = \frac{1}{h_y} \{z(k,s) - z(k,s-1)\}$$

$$\left(z \frac{\partial z}{\partial n}\right)_{k,s} = \frac{1}{h_y} \{z(k,s) - z(k,s-1)\} g_2(k,s)$$

$$k = 0, 1, 2, \dots, r \quad (37d)$$

$$ds = h_x$$

Using Eqs 37 and the trapezoidal rule, we have

$$\oint z \frac{\partial z}{\partial n} ds = \frac{1}{2} \frac{h_x}{h_y} \left[g_1(0,0) [g_1(0,0) - f_1(0,1)] + g_1(r,0) [g_1(r,0) - f_1(r,1)] \right]$$

$$+ \frac{h_x}{h_y} \sum_{k=1}^{k=r-1} g_1(k,0) [g_1(k,0) - z(k,1)]$$

$$+ \frac{1}{2} \frac{h_x}{h_y} \left[g_2(0,s) [g_2(0,s) - f_1(0,s-1)] + g_2(r,s) [g_2(r,s) - f_1(r,s)] \right]$$

APPENDIX VIII (continued)

$$\begin{aligned}
 & + \frac{h_x}{h_y} \sum_{k=1}^{k=r-1} g_2(k,s) [g_2(k,s) - z(k,s-1)] \\
 & + \frac{1}{2} \frac{h_y}{h_x} \left[f_1(0,0) [f_1(0,0) - g_1(1,0)] + f_1(0,s) [f_1(0,s) - g_2(1,s)] \right. \\
 & \quad \left. + f_2(r,0) [f_2(r,0) - g_1(r-1,0)] + f_2(r,s) [f_2(r,s) - g_2(r-1,s)] \right] \\
 & + \frac{h_y}{h_x} \sum_{j=1}^{j=s-1} \left\{ f_1(0,j) [f_1(0,j) - z(1,j)] \right. \\
 & \quad \left. + f_2(r,j) [f_2(r,j) - z(r-1,j)] \right\} \quad (38)
 \end{aligned}$$

We write (38) as

$$\oint z \frac{dz}{z} ds = A_1 - \frac{h_x}{h_y} B_1 - \frac{h_y}{h_x} B_2 \quad (39)$$

where

A_1 is a constant involving the products f g , and g g ,

$$B_1 = \sum_{k=1}^{k=r-1} \{ g_1(k,0) z(k,1) + g_2(k,s) z(k,s-1) \} \quad (40a)$$

$$B_2 = \sum_{j=1}^{j=s-1} \{ f_1(0,j) z(1,j) + f_2(r,j) z(r-1,j) \} \quad (40b)$$

APPENDIX VIII (continued)

We also use the trapezoidal rule to evaluate

$$\iint_A z \frac{\rho}{c} dx dy$$

This becomes

$$\iint_A z \rho dx dy = \frac{h_x h_y}{2} \left[\frac{1}{2} \left[\rho(0,0) g_1(0,0) + \rho(\tau,0) g_1(\tau,0) \right. \right. \\ \left. \left. + \rho(0,s) g_2(0,s) + \rho(\tau,s) g_2(\tau,s) \right. \right. \\ \left. \left. + \sum_{k=1}^{\tau-1} \rho(k,0) g_1(k,0) + \rho(k,s) g_2(k,s) \right] \right]$$

$$+ h_x h_y \left[\frac{1}{2} \sum_{j=1}^{s-1} \left\{ \rho(0,j) f_1(0,j) + \rho(\tau,j) f_1(\tau,j) \right\} \right. \\ \left. + \sum_{j=1}^{s-1} \sum_{k=1}^{\tau-1} \rho(k,j) z(k,j) \right] \quad (41)$$

We can write (40) as

$$\frac{1}{c} \iint_A z \rho dx dy = \frac{A_2}{c} + \frac{h_x h_y}{c} \sum_{j=1}^{s-1} \sum_{k=1}^{\tau-1} \rho(k,j) z(k,j) \quad (42)$$

where A_2 is a constant which involves only the boundary terms

APPENDIX VIII (continued)

The inoperational equation takes the form

$$\frac{A_2}{C} + \frac{h_x h_y}{C} B_3 + A_1 - \frac{h_x}{h_y} B_1 - \frac{h_y}{h_x} B_2 = 2(A_0 - A^*) \quad (43)$$

where

$$B_3 = \sum_{j=1}^{s-1} \sum_{k=1}^{r-1} P(k, j) z(k, j) \quad (44)$$

and B_1, B_2 are linear functions of z
 Now we write

$$z = z_n + \frac{1}{C} z_p \quad (45)$$

where

z_n is the homogeneous solution of $\nabla^2 z = 0$ which satisfies the boundary conditions.

z_p is the particular solution of $\nabla^2 z = -\rho$

If we substitute (45) in (43), we obtain a quadratic equation in C . The B_1, B_2, B_3 terms reduce to

$$\begin{aligned} B_3 &= B_{31} + \frac{1}{C} B_{32} \\ B_1 &= B_{11} + \frac{1}{C} B_{12} \\ B_2 &= B_{21} + \frac{1}{C} B_{22} \end{aligned} \quad (46)$$

where the B_{ij} terms involve z_n and z_p . Using (46), (43) takes the form

$$\begin{aligned} & C^2 \left\{ -2(A_0 - A^*) + A_1 - \frac{h_x}{h_y} B_{11} - \frac{h_y}{h_x} B_{21} \right\} \\ & + C \left\{ A_2 - \frac{h_x}{h_y} B_{12} - \frac{h_y}{h_x} B_{22} + B_{31} \right\} + h_x h_y B_{32} = 0 \quad (47) \end{aligned}$$

APPENDIX VIII (continued)

We determine z_n and z_p as follows. The finite difference equations are written for each interior point. The equations for points adjacent to the boundaries will involve the boundary values of z . If we let $\{z_i\}$ be the matrix of unknowns (z) the system of equations takes the form

$$[a_{ij}]\{z_i\} = -\frac{1}{2}\{P_i\} + \{\bar{z}_i\} \quad (48)$$

where the matrix, $\{\bar{z}\}$, involves the boundary values of z and $\{P_i\}$ is associated with the pressure loading. The homogeneous and particular solutions are

$$\{z_{n,i}\} = [a_{ij}]^{-1}\{\bar{z}_i\} \quad (49)$$

$$\{z_{p,i}\} = -[a_{ij}]^{-1}\{P_i\} \quad (50)$$

The problem reduces to determining $[a_{ij}]^{-1}$ which is of order $(7-1)(5-1)$.

APPENDIX VIII (continued)

Approximate Membrane Analysis

1. Method

The membrane is subdivided into curvilinear rectangular elements such as shown in Fig. 1. The internal forces acting on the sides of an element are replaced by their resultants as done in membrane theory. The force displacement relations are obtained from those of the membrane theory by considering each curvilinear element as a plane and by replacing the strains by the relative extensions and change of angle of the finite element.

With the above approximations two contiguous elements are considered as connected through a point to which the surface forces are applied. Writing the equilibrium of these joints results in stiffness equations that can be solved for the displacements.

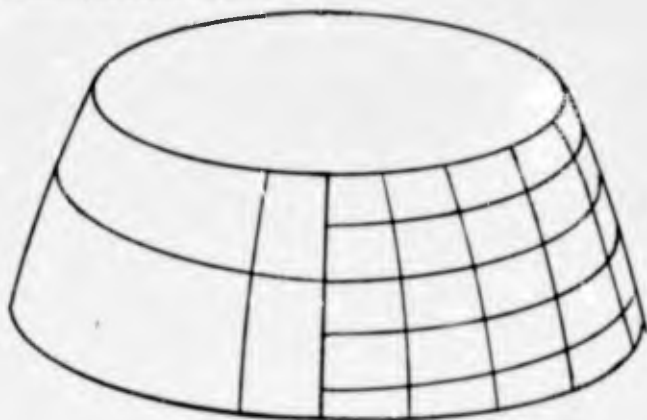


Figure 1.
Reduction to Finite
Elements

BLANK PAGE

APPENDIX VIII (continued)

2. Internal Forces

Fig. 2.a represents a plane rectangular element and the internal forces acting on it.

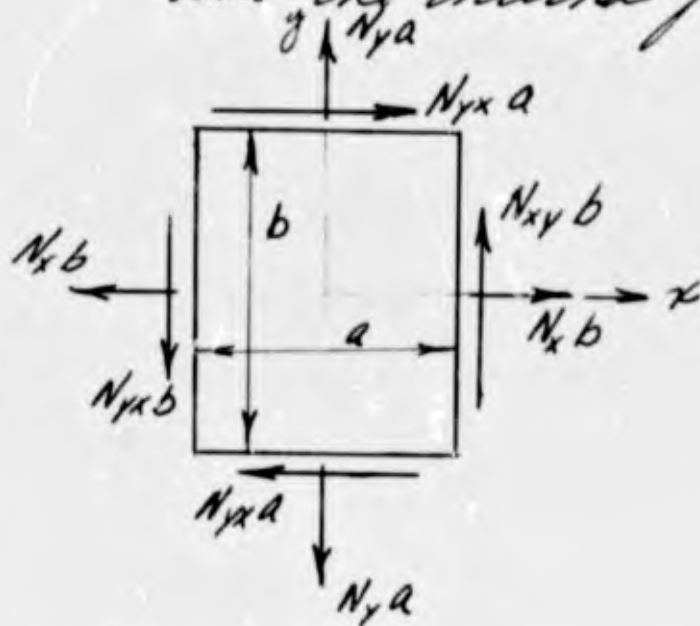


FIG. 2.a

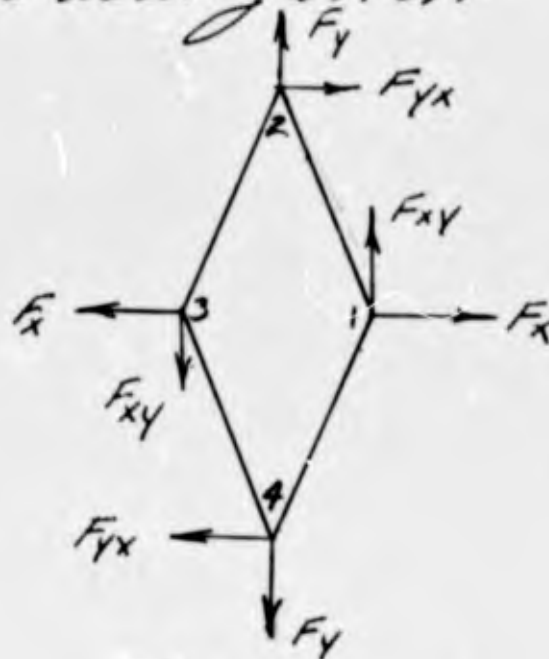


FIG. 2.b

Fig. 2b Represents the corresponding fictitious element where the internal forces are concentrated at points placed at the middle of the sides of the original element. We have.

$$\begin{aligned}
 F_x &= N_{xb} & , & & F_y &= N_{yb} \\
 F_{xy} &= N_{xy} b & , & & F_{yx} &= N_{yx} a \\
 N_{xy} &= N_{yx} & & & &
 \end{aligned}$$

①

APPENDIX VIII (continued)

When the numerical subscript refers to the joint and x or y refers to the direction. The force-displacement relations take the form

$$F_x = E_x h b \left(\frac{U_{1x} - U_{3x}}{a} + \gamma_x \frac{U_{2y} - U_{4y}}{b} \right)$$

$$F_{xy} = G h b \left(\frac{U_{1y} - U_{3y}}{a} + \frac{U_{2x} - U_{4x}}{b} \right) \quad (4)$$

$$F_{yx} = G h a \left(\frac{U_{1y} - U_{3y}}{a} + \frac{U_{2x} - U_{4x}}{b} \right)$$

$$F_y = E_y h a \left(\frac{U_{2y} - U_{4y}}{b} + \frac{\gamma_y}{a} \frac{U_{1x} - U_{3x}}{a} \right)$$

The matrix form of (4) is:

$$F = K U \quad (5)$$

where

$$F = \begin{bmatrix} F_x \\ F_{xy} \\ F_{yx} \\ F_y \end{bmatrix} \quad (6a)$$

$$U = \begin{bmatrix} U_{1x} \\ U_{1y} \\ U_{2x} \\ U_{2y} \\ U_{3x} \\ U_{3y} \\ U_{4x} \\ U_{4y} \end{bmatrix} \quad (6b)$$

B.F. Goodrich Aerospace and
 Defense Products

a Division of The B.F. Goodrich Company

APPENDIX VIII (continued)

3. Force Displacement Relations

The stress strain relations for an infinitesimal rectangular element are of the form

$$\begin{aligned}N_x &= E_x h (E_x + \nu_x E_y) \\N_y &= E_y h (E_y + \nu_y E_x) \\N_{xy} &= N_{yx} = G h w\end{aligned}$$

Where E_x, ν and G are Young's modulus, Poisson's ratio and the shear modulus, respectively. The subscript x and y account for a non isotropic material. The force displacement relations for the fictitious element are obtained by replacing the strains by relative extensions and change of angle of the finite element. Letting u denote a displacement we let

$$E_x = \frac{u_{1x} - u_{3x}}{a} \quad , \quad E_y = \frac{u_{2y} - u_{4y}}{b}$$

$$w = \frac{u_{1y} - u_{3y}}{a} + \frac{u_{2x} - u_{4x}}{b} \quad (3)$$

APPENDIX VIII (continued)

$$K = \begin{bmatrix} E_x h \alpha & 0 & 0 & E_x h \nu_x & -E_x h \alpha & 0 & 0 & -E_x h \nu_x \\ 0 & Gh \alpha & Gh & 0 & 0 & Gh \alpha & -Gh & 0 \\ 0 & Gh & Gh/\alpha & 0 & 0 & -Gh & -Gh/\alpha & 0 \\ E_y h \nu_y & 0 & 0 & E_y h/\alpha & -E_y h \nu_y & 0 & 0 & -E_y h/\alpha \end{bmatrix} \quad (6c)$$

$$\alpha = \frac{b}{a} \quad (6d)$$

Stiffness equations for the element can be obtained from the above by including the forces acting on joints 3 and 4. Also, in view of a transformation of coordinates from the local axis associated with an element to a global system of axis for the whole structure, we include the third component of the forces and displacements with regard to A z axis perpendicular to the element.

we let:

$$F_1 = \begin{bmatrix} F_x \\ F_{zy} \\ 0 \end{bmatrix} \quad F_2 = \begin{bmatrix} F_{yx} \\ F_y \\ 0 \end{bmatrix} \quad F_3 = -F_1 \quad F_4 = -F_2 \quad (7)$$

APPENDIX VIII (continued)

and

$$U_1 = \begin{vmatrix} U_{1x} \\ U_{1y} \\ U_{1z} \end{vmatrix} \quad U_2 = \begin{vmatrix} U_{2x} \\ U_{2y} \\ U_{2z} \end{vmatrix} \quad U_3 = \begin{vmatrix} U_{3x} \\ U_{3y} \\ U_{3z} \end{vmatrix} \quad U_4 = \begin{vmatrix} U_{4x} \\ U_{4y} \\ U_{4z} \end{vmatrix}$$

we can then write

$$\begin{vmatrix} F_1 \\ F_2 \\ F_3 \\ F_4 \end{vmatrix} = \begin{vmatrix} K_{11} & K_{12} & -K_{11} & -K_{12} \\ K_{21} & K_{22} & -K_{21} & -K_{22} \\ -K_{11} & -K_{12} & K_{11} & K_{12} \\ -K_{21} & -K_{22} & K_{21} & K_{22} \end{vmatrix} \begin{vmatrix} U_1 \\ U_2 \\ U_3 \\ U_4 \end{vmatrix} \quad (8)$$

(9)

where

$$K_{11} = \begin{vmatrix} E_x h \alpha & 0 & 0 \\ 0 & Gh \alpha & 0 \\ 0 & 0 & 0 \end{vmatrix} \quad K_{12} = \begin{vmatrix} 0 & E_x h \gamma_x & 0 \\ Gh & 0 & 0 \\ 0 & 0 & 0 \end{vmatrix}$$

$$K_{21} = \begin{vmatrix} 0 & Gh & 0 \\ E_y h \gamma_y & 0 & 0 \\ 0 & 0 & 0 \end{vmatrix} \quad K_{22} = \begin{vmatrix} Gh/\alpha & 0 & 0 \\ 0 & E_y h/\alpha & 0 \\ 0 & 0 & 0 \end{vmatrix}$$

(10)

APPENDIX VIII (continued)

Let T be the coordinate transformation matrix from the local system associated with an element to a global system. T is a 3×3 matrix whose Determination is discussed in (6). We use an asterisk for quantities referred to the global system. We have

$$F_i^* = T F_i \quad i = 1, 2, 3, 4$$

$$U_i^* = T U_i$$

or

$$U_i = T^{-1} U_i^* = T^t U_i^*$$

(11)

The stiffness equations for an element with regard to the global system are:

$$\begin{vmatrix} F_1^* \\ F_2^* \\ F_3^* \\ F_4^* \end{vmatrix} = \begin{vmatrix} K_{11}^* & K_{12}^* & -K_{11}^* & -K_{12}^* \\ K_{21}^* & K_{22}^* & -K_{21}^* & -K_{22}^* \\ -K_{11}^* & -K_{12}^* & K_{11}^* & K_{12}^* \\ -K_{21}^* & -K_{22}^* & K_{21}^* & K_{22}^* \end{vmatrix} \begin{vmatrix} U_1^* \\ U_2^* \\ U_3^* \\ U_4^* \end{vmatrix} \quad (12)$$

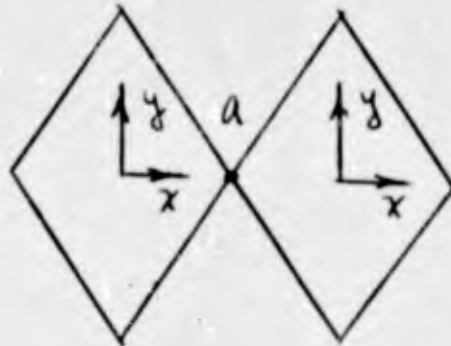
where

$$K_{ij}^* = T K_{ij} T^{-1} = T K_{ij} T^t$$

APPENDIX VIII (continued)

4) Equilibrium of the joints
each joint connects 2 elements in one of the
two ways as shown below:

joint type a



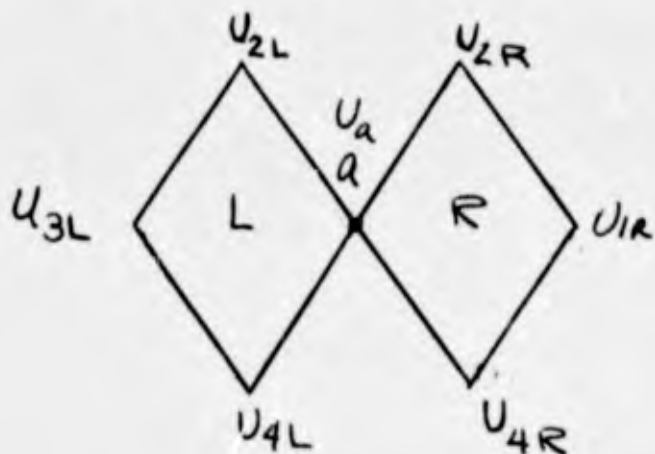
joint type b



APPENDIX VIII (continued)

Joint Type a

Let L refer to the element with respect to which joint a is joint # 1 and R refer to the element with respect to which joint a is joint # 3. Then, by superposition, the resultant of the internal forces acting on the elements at a is the sum of F_1^* of the element L and of F_3^* of the element R.



$$F_a^* = (K_{11L}^* + K_{11R}^*)U_a^* + K_{12L}^*U_{2L}^* - K_{11L}^*U_{3L}^* - K_{12L}^*U_{4L}^* \\ - K_{11R}^*U_{1R}^* - K_{12R}^*U_{2R}^* + K_{12R}^*U_{4R}^*$$

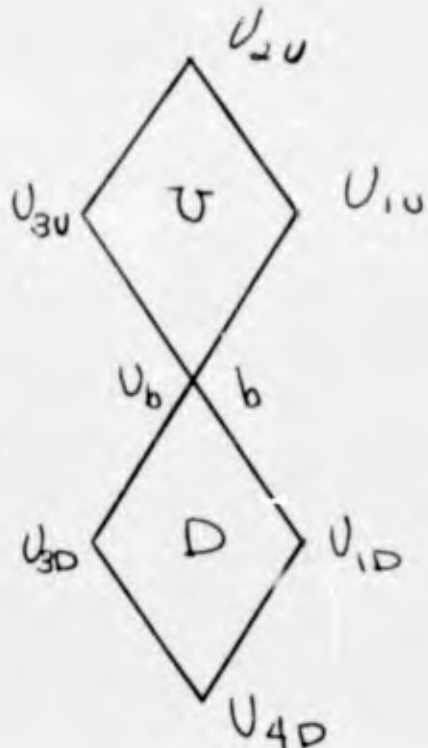
(13)

APPENDIX VIII (continued)

Joint type b

We let U and D refer to the elements with regard to which joint b has the numbers 1 and 2 respectively.

Then



$$F_b^* = (K_{20U}^* + K_{22D}^*) U_b^* - K_{21U}^* U_{1U}^* - K_{22U}^* U_{2U}^* + K_{21U}^* U_{3U}^* + K_{21D}^* U_{1D}^* - K_{21D}^* U_{3D}^* - K_{22D}^* U_{4D}^*$$

(14)

The equilibrium of joints a & b requires that F_a^* and F_b^* equal the external loads applied at joints a & b, respectively.

APPENDIX VIII (continued)

5) Stiffness of the Structure

The equilibrium of all the joints leads to a system of equations of the form

$$F_c^* = K_c^* U_c^* \quad (15)$$

Where F_c^* is the column matrix made of all the F_o^* 's and all the F_{85}^* . U_c^* is the column matrix of the displacement components of all the joints. K_c^* is the total stiffness matrix. It is convenient to imagine the total stiffness matrix as subdivided into square blocks, each a 3×3 matrix. The row and column index of each block refer then to two joints.

Development of total stiffness matrix by processing elements

Each element has 2 joints of type a and two joints of type b the contribution of one element to the total stiffness matrix is done as follows



APPENDIX VIII (continued)

add to block

K_{11}^*	11
K_{12}^*	12
$-K_{11}^*$	13
$-K_{12}^*$	14

add to block

K_{11}^*	33
$-K_{12}^*$	32
$-K_{11}^*$	31
K_{12}^*	34

add to block

K_{22}	22
K_{21}	21
$-K_{22}^*$	24
$-K_{21}^*$	23

add to block

K_{22}^*	44
$-K_{21}^*$	41
$-K_{22}^*$	42
K_{21}^*	43

see Fig. 3

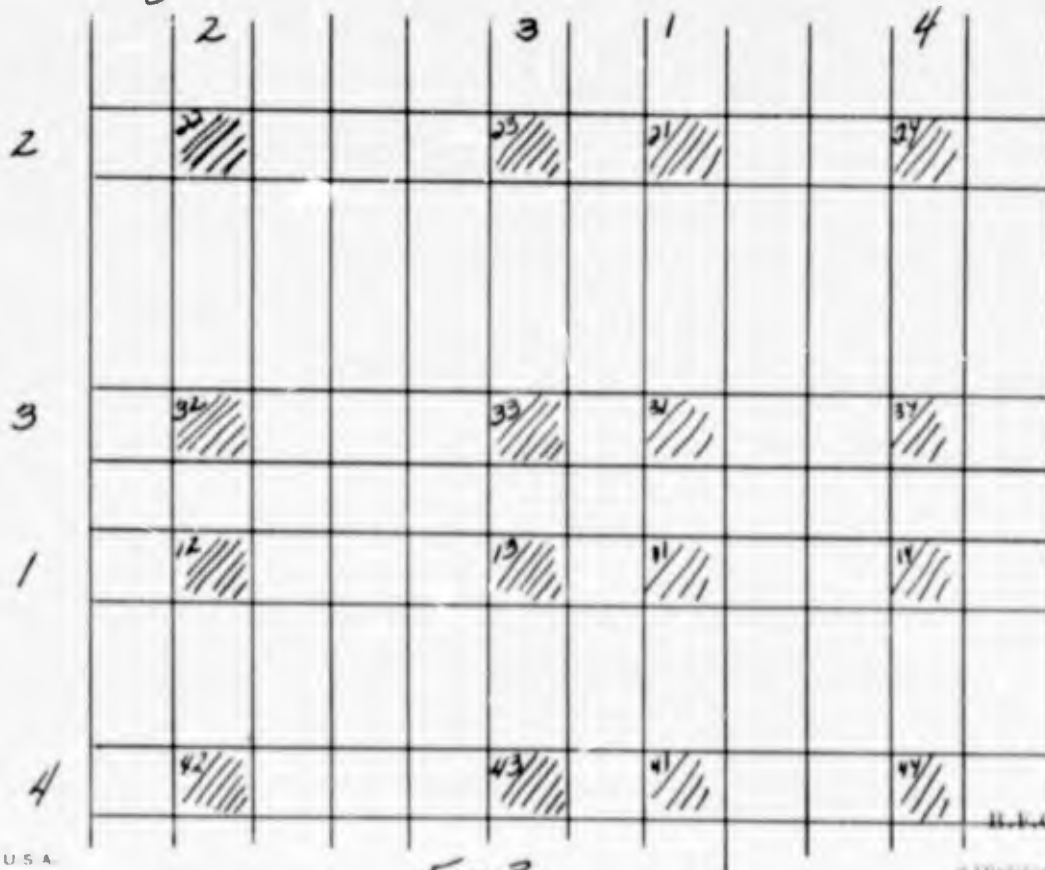


Fig 3

APPENDIX VIII (continued)

Note: In any one row of K_c^* there are only 7 non zero blocks corresponding to the joints of 2 contiguous elements. The block on the main diagonal is always non zero

K_c^* is not symmetric

6) Determination of the transformation matrix T

Consider any orthogonal system of axes with unit vectors $\bar{i}, \bar{j}, \bar{k}$ along the x, y, z axes and another system with unit vectors $\bar{i}^*, \bar{j}^*, \bar{k}^*$. A vector \bar{V} can be written -

$$\bar{V} = V_1 \bar{i} + V_2 \bar{j} + V_3 \bar{k} = \bar{V}_1^* \bar{i}^* + \bar{V}_2^* \bar{j}^* + \bar{V}_3^* \bar{k}^*$$

and

$$V_1^* = \bar{i}^* \bar{i} V_1 + \bar{i}^* \bar{j} V_2 + \bar{i}^* \bar{k} V_3$$

$$V_2^* = \bar{j}^* \bar{i} V_1 + \bar{j}^* \bar{j} V_2 + \bar{j}^* \bar{k} V_3$$

$$V_3^* = \bar{k}^* \bar{i} V_1 + \bar{k}^* \bar{j} V_2 + \bar{k}^* \bar{k} V_3$$

if we identify $\bar{i}, \bar{j}, \bar{k}$ with our local system and $\bar{i}^*, \bar{j}^*, \bar{k}^*$ with our global system then

$$T = \begin{matrix} \bar{i}^* \bar{i} & \bar{i}^* \bar{j} & \bar{i}^* \bar{k} \\ \bar{j}^* \bar{i} & \bar{j}^* \bar{j} & \bar{j}^* \bar{k} \\ \bar{k}^* \bar{i} & \bar{k}^* \bar{j} & \bar{k}^* \bar{k} \end{matrix}$$

APPENDIX VIII (continued)

Letting x_i, y_i, z_i be the global coordinates of joint # i of an element ($i=1, 2, 3, 4$) then

$$\bar{i}^* \bar{i} = \frac{x_1 - x_3}{a}$$

$$\bar{i}^* \bar{j} = \frac{x_2 - x_4}{b}$$

$$\bar{i}^* \bar{k} = \sqrt{1 - \left(\frac{x_1 - x_3}{a}\right)^2 - \left(\frac{x_2 - x_4}{b}\right)^2}$$

$$\bar{j}^* \bar{i} = \frac{y_1 - y_3}{a}$$

$$\bar{j}^* \bar{j} = \frac{y_2 - y_4}{b}$$

$$\bar{j}^* \bar{k} = \sqrt{1 - \left(\frac{y_1 - y_3}{a}\right)^2 - \left(\frac{y_2 - y_4}{b}\right)^2}$$

$$\bar{k}^* \bar{i} = \frac{z_1 - z_3}{a}$$

$$\bar{k}^* \bar{j} = \frac{z_2 - z_4}{b}$$

$$\bar{k}^* \bar{k} = \sqrt{1 - \left(\frac{z_1 - z_3}{a}\right)^2 - \left(\frac{z_2 - z_4}{b}\right)^2}$$



APPENDIX VIII (continued)

From their definitions a & b must satisfy the relations

$$a^2 = (x_1 - x_3)^2 + (y_1 - y_3)^2 + (z_1 - z_3)^2$$

$$b^2 = (x_2 - x_4)^2 + (y_2 - y_4)^2 + (z_2 - z_4)^2$$

The coordinates of the 4 joints are not arbitrary, requiring the diagonals of the element to intersect at their midpoints we must have:

$$\frac{x_1 + x_3}{2} = \frac{x_2 + x_4}{2}$$

$$\frac{y_1 + y_3}{2} = \frac{y_2 + y_4}{2}$$

$$\frac{z_1 + z_3}{2} = \frac{z_2 + z_4}{2}$$

and requiring them to be orthogonal we obtain

$$(x_1 - x_3)(x_2 - x_4) + (y_1 - y_3)(y_2 - y_4) + (z_1 - z_3)(z_2 - z_4) = 0$$

7) Boundary Conditions

We consider only the conditions of zero displacements at the boundary. Assume the joints are renumbered so that those at the boundary are last. The equation

$$K^* U^* = F^*$$

APPENDIX VIII (continued)

where the subscript t is deleted
can be partitioned in the form

$$\begin{vmatrix} K_{FF}^* & K_{FS}^* \\ K_{SF} & K_{SS} \end{vmatrix} \begin{vmatrix} U_F^* \\ U_S^* \end{vmatrix} = \begin{vmatrix} F_F^* \\ F_S^* \end{vmatrix}$$

where S refers to supports or joints
at the boundary and F refers to the
remaining joints.

The boundary conditions are -

$$U_S^* = 0$$

The displacements U_F^* are obtained by
solving

$$K_{FF}^* U_F^* = F_F^*$$

and the reactions F_S^* are then obtained
by computing

$$F_S^* = K_{SF} U_F^*$$

BLANK PAGE

H. Errata/Points of Clarification

1. Page 2 First Para. -

- 60" dome refers to the non-magnetic sonar dome, Model #CW177D/U with AN/UQS transducer.

- 100" pressurized rubber dome refers to the dome made for use with the AN/SQS-10 transducer on the USS Bronson. It was designated Model #CW-431(XN-1)/U.

2. Page 14 Para. 3 last sentence - service life should be testing.

Para. 3 add - This dome is still usable and was removed because the ship was placed in the F.R.A.M. program. This dome is in storage at USN/USL.

3. Page 42 last paragraph algebraically should be algebraically.

4. Page 91 First paragraph - Section I.C.J. should be I.10.C.

5. Page 174 First Paragraph - -4" WL should be -4' WL.

6. Page 187 First Paragraph - Appendix VI should be V.

7. Page 245 Table XXXIII Title - Dome should be Window.

8. Page 251 Table XXXIV Title - Domes should be Windows.

DL-5 Semi-Universal - \$450,000 should be \$150,000. This table indicates on a cost basis, for the first prototype window, the semi-universal concept is desirable. Also, considering a total of ten DL-5 and DLG-26 windows the added expense of designing another set of tooling for a DLG-26 window, additional space and facilities needed for two sets of tooling and handling expense of two separate windows instead of one indicates the semi-universal window is more desirable than the individually tailored ones.

9. Page 267, Figure 112 - The chock extension discussed is aft of the radial baffle and amounts to about 3". The reduction in critical scanning area is insignificant.

Contract NObsr 89483
Serial No. SS041-001
Task 8156

- 2 -

Report No. 17
Phase I Interim Report
30 September 1964

10. Page 268, Table XXXVII Stress Diagram of Window

Periphery - Calculated tensions based on a differential pressure of 40 psi.

11. Page 271, Figure 113 Schematic of Proposed Pressurization System - Available Water pressure source must have pressure equal to or higher than operational pressure within the dome.

BLANK PAGE